



# **Investigating Synaptonemal Complex Morphogenesis in Polyploid Wheat**

by  
Chiara Di Dio

Department of Genetics and Genome Biology  
University of Leicester

Thesis submitted to the University of Leicester  
for the degree of Doctor of Philosophy

January 2022

# Abstract

## Investigating Synaptonemal Complex Morphogenesis in Polyploid Wheat

Chiara Di Dio

The synaptonemal complex is a tripartite proteinaceous structure consisting of two filamentous lateral elements, joined by zipper-like transverse filaments and central elements that assemble to join homologous chromosomes and ensure recombination by formation of crossovers during meiotic prophase I. In polyploid wheat, components of the synaptonemal complex and its installation process are still elusive. The application of several distinct methodologies, such as Sanger sequencing, cloning and bioinformatics was conducted to analyse gene expression contribution and transcript variants for the *Triticum aestivum ASYNAPTIC 1 (ASY1)* and *ZYPPER-LIKE 1 (ZYP1)* genes. Mutant TILLING lines provided a valid strategy to functionally analyse *asy1* and *zyp1* and to characterize putative meiotic genes in polyploid wheat, identified via a computational screening.

Molecular analysis demonstrated a balanced expression level among the *ASY1* and *ZYP1* sub-genomes of hexaploid wheat, being also expressed in non-meiotic tissues, and uncovered the presence of de-novo transcript isoforms within their 3' UTRs. Cytological analysis revealed that *ASY1* is involved in chromosome homology search, since *asy1* hypomorphic mutants showed multivalent associations, and is required for formation of the obligate crossover, mirroring the *ph1* phenotype. Preliminary data of *zyp1* single knockouts suggested a conserved role of *ZYP1* in maintaining obligate crossovers, and in controlling the timing of synaptonemal complex assembly in tetraploid wheat. Furthermore, a wheat SWITCH1 (*SWI1*) orthologue was identified using co-expression bioinformatics tools. Lastly, a method to implement FISH-based single copy oligo-probes to discriminate individual wheat chromosomes was developed. This work provides advanced directions for studying meiosis in polyploid wheat, expanding the opportunities to manipulate crossovers and introgress agronomically important genes.

# Covid19 Impact Statement

To Whom It May Concern:

Following the ongoing outbreak of the Coronavirus 2019 (COVID-19), which was recently declared as pandemic by the World Health Organization, this research project was negatively impacted by the cumulative effects and uncertainties originated.

Several options direct to minimize and mitigate the impact to the overall project completion were evaluated and described in detail in this section.

Due to inability to access to the laboratory and greenhouses for 5 months (from March to August 2020), genotyping screening of single knock-out tetraploid TILLING lines of *TaASY1* and *TaZYP1* genes, generated by backcrossing individual lines with wild-type plants to unload the off-target mutations, were postponed until the return to the department (August 2020). Consumable shortages (mostly antibodies and mutant seeds for cytological work) and significant delays in lead times due to institutes/facilities closures across the countries, and above all, the impossibility to quantify the delay or compute the delivery of the materials and finances extension, further contributed to prolong the time required for the completion of the work. In pre-Covid19 situation, data collection and analysis of tetraploid wheat would have accomplished within December 2020 (9 months).

Additionally, genotyping screening of the double knockouts in *asy1* and *zyp1* tetraploid mutant lines and cytological investigation were postponed on August 2020 due to the closure of the department. In ideal situation, the timeframe to complete this analysis in tetraploid plants would require 3 or more weeks to identify the genotype by PCR screening, plus 5-6 weeks after sowing to immunolocalise the markers of the meiotic progress, and 6-7 weeks to fix the anthers and quantify the incidence of crossovers per meiocytes. Excluding any Covid19 constraints, the outcomes for this line were expected by June 2020, approximately.

The study of chromosome behaviour (non-homologous pairing) in *asy1* single knockout tetraploid mutant lines was mainly affected by 8-months delay in ordering and delivering laboratory materials (probes). Analogously, the delivery of *asy1* single knock-out hexaploid mutant line had a 3-months delay. Both mutant lines were ordered before the closure (March 2020). The outcomes for these studies were expected on August and September 2020, respectively.

Furthermore, due to travel disruptions, three secondments were affected. Training at industrial partner KWS Ltd, Cambridge (May 2020) was definitely cancelled. Proteomic assay of *TaASY1* and *TaZYP1* proteins programmed in partnership with the University of Birmingham over the second year (2019-2020) was substituted by the assessment of *TaASY1* and *TaZYP1* homoeologues expression level in hexaploid wheat through pyrosequencing, a well-defined approach used at INRA (partnership institute in France). Under the restricted circumstances, the collaboration with the INRA took place remotely, via Zoom platform, whose supervisor and PhD student provided assistance regarding the experimental materials and procedure (e.g. designing sub-genome specific primers). Although it was not possible to perform the pyrosequencing experiment scheduled by the end of the 2020, the experimental materials were at last used to set up the quantitative PCR experiment using the facility provided by the University of Leicester.

To mitigate data collection/analyses that were prevented by Covid-19, more emphasis was placed in theoretical aspects of the research topic, focusing on new questions and hypothesis, here elucidated by using bioinformatics tools (as described in Chapter 4), thereby analysing pre-existing publicly available data sets rather than generate more data in the laboratory.

As conclusive statement, I have appreciated the decision of the University of Leicester in considering the mentioned work suspension and delays as beyond my control, by accepting my request to extend the experimental period with original deadline of 36 months to 42 months, allowing me to complete the cytological studies of data generated using the bioinformatics approach (Chapter 4), in compliance with the updated terms of the project.

## Acknowledgements

Firstly, I would like to thank my supervisor Dr. James Higgins for granting me the opportunity to pursue this research project in his lab independently, whilst supporting me with excellent advice and guidance.

I am also grateful to the members of the Higgins' lab (Dr. Daisy Ogle, Dr. Martin France, Dr. Neelam Dave and Dr. Stuart Desjardins), to the PRP Professors Ed Louis and David Twell, for their impeccable suggestions and ideas, as well as to other colleagues and staff of the Department of Genetics and Genome Biology (long list) for sharing their lab experiences with me throughout the PhD time.

Special thanks must be given to Higgins' collaborators, whose include Dr. Kim Osman at University of Birmingham (UK), Dr. Veit Schubert at IPK (Gatersleben), Dr. Eric Jenczewski at INRA (France) and John Innes Centre at Norwich (UK) for their expertise and technical support, for the access to super-resolution microscope and other facilities, for seeds, and, not least, to the MEICOM network, who were and still are all kindly supportive.

Several other experts and organisations have also contributed to my professional and personal education by cooperating with me in non-scientific accomplishments, which include lab-based demonstrator, dissemination and outreach activities, where I was engaged during my PhD period.

Lastly, I would like to thank my parents (my boyfriend Lorenzo included) and all of my friends (le "ciofekine" Maria & Marta and Joana) for their support and kindness during the entire PhD path.

As conclusive thought, in parallel with the professional skills, this PhD fellow programme enhanced my personal qualities and provided me important "tools" to overcome my weaknesses.

# Table of Contents

<b>Chapter 1 .....</b>	1
<b>Introduction.....</b>	1
<b>1.1 Meiosis overview .....</b>	1
1.1.2 The molecular bases of meiotic recombination .....	5
1.1.3 The meiotic recombination pathways .....	8
1.1.4 Other factors regulating meiotic recombination .....	11
<b>1.2 The key SC components acting during the process of meiotic recombination in wheat .....</b>	13
1.2.1 <i>TaASY1</i> .....	15
1.2.2 <i>TaZYP1</i> .....	18
1.2.3 The regulation of SC in polyploidy wheat .....	19
1.2.3.1 The mechanism of chromosome pairing in polyploid wheat .....	20
1.2.3.2 The wheat transcriptome: a still unexplored research subject.....	25
<b>1.3 Wheat and Food Security.....</b>	27
<b>1.4 Project Aims .....</b>	29
<b>Chapter 2 .....</b>	31
<b>Investigating the gene regulatory sequences, splice variants and the meiotic function of wheat <i>ASY1</i>.....</b>	31
<b>2.1 Introduction.....</b>	31
<b>2.2 Materials and methods .....</b>	33
2.2.1 Plant materials and greenhouse conditions .....	33
2.2.2 Amplification of <i>TaASY1</i> .....	33
2.2.3 Proteomic validation of <i>TaASY1</i> protein .....	34
2.2.4 Cloning the full length coding region of <i>TaASY1</i> .....	38
2.2.5 Validation of <i>TaASY1</i> fragment insertion via colony PCR .....	40
2.2.6 Testing the efficiency of the designed <i>TaASY1</i> pyrosequencing primers .....	40
2.2.7 Quantitative PCR (qPCR) of <i>TaASY1</i> homoeologues.....	41
2.2.8 Cloning the untranslated regions (UTRs) of <i>TtASY1</i> .....	42
2.2.9 Identification of <i>asy1</i> TILLING lines in tetraploid and hexaploid wheat.....	43
2.2.10 Genotype screening of Kronos and Cadenza Parental (P) mutants.....	44
2.2.11 Crosses of Kronos Parental mutants .....	46
2.2.12 Genotyping of F1 mutants.....	47
2.2.13 Backcrosses of <i>asy1</i> Parents with tetraploid Kronos wild-type .....	47
2.2.14 Isolating pollen mother cells (PMCs) for metaphase I chromosome spreads ..	48

2.2.15 Immunolocalisation of PMCs .....	48
2.2.16 Statistics .....	52
<b>2.3 Results .....</b>	<b>54</b>
2.3.1 <i>TaASY1</i> is expressed in leaves and inflorescences of hexaploid <i>T. aestivum</i> cultivars Cadenza and Apogee .....	54
2.3.2 <i>TaASY1</i> homoeologues expression is likely redundant in reproductive and somatic tissues.....	56
2.3.3 A splice variant in <i>TaASY1-5B</i> cds ‘Apogee’ clone lacked the predicted acidic region of the protein .....	62
2.3.4 Identification of <i>TtASY1</i> 3’ UTR isoforms in germline DNA.....	65
2.3.5 Analysis of wheat <i>asy1</i> TILLING mutants .....	72
2.3.6 Cytological atlas of <i>asy1</i> single knockouts .....	78
2.3.7 <i>asy1</i> single KO displays multivalent interaction but reduced chiasmata .....	82
2.3.8 Cytological atlas of <i>asy1</i> double KO .....	84
2.3.9 <i>asy1</i> has a dosage dependent effect on homologous recombination.....	87
2.3.10 Fertility assessment .....	90
2.3.11 <i>asy1</i> single KO mutants exhibit a slight delay in spatio-temporal localization of ZYP1 .....	91
2.3.12 ASY1 is required for SC assembly .....	98
2.3.13 ASY1-ASY3 interaction may rely on ASY1 HORMA domain .....	100
2.3.14 ASY1 may interact with SMC3 to stabilise the SC at synapsis sites.....	102
2.3.15 ASY1 ensures obligate CO following the homologous pairing.....	105
2.3.16 ASY1 regulates proper homologous pairing in hexaploid wheat .....	106
<b>2.4 Discussion .....</b>	<b>110</b>
2.4.1 Molecular data overview.....	110
2.4.2 <i>TaASY1</i> sub-genome copies are not subjected to tissue-specific regulation in hexaploid <i>T. aestivum</i> .....	111
2.4.3 A rare alternative splicing event in hexaploid <i>T. aestivum</i> <i>TaASY1</i> .....	112
2.4.4 <i>De novo</i> <i>TtASY1</i> 3’ UTR isoforms are potentially expressed in tetraploid <i>T. turgidum</i> .....	113
2.4.5 Cytology data overview .....	114
2.4.6 <i>TtASY1</i> may fulfil interdependent meiotic functions in polyploid <i>T. turgidum</i> .....	115
2.4.7 SC assembly/disassembly is timely and spatially regulated by ASY1 in tetraploid <i>T. turgidum</i> .....	116
2.4.8 <i>TtASY1</i> controls proper chromosome pairing prior synapsis .....	117
2.4.9 ASY1-ASY3 interaction appears conserved in tetraploid wheat.....	119

2.4.10 ASY1 stabilises axial core formation in tetraploid wheat.....	120
2.4.11 ASY1 may act as a meiotic check-point in tetraploid <i>T. turgidum</i> .....	121
2.4.12 ASY1 has a conserved role in polyploid wheat.....	122
<b>2.5 Conclusions.....</b>	<b>123</b>
2.5.1 Molecular approach.....	123
2.5.2 Cytology approach .....	124
<b>Chapter 3 .....</b>	<b>125</b>
<b>Investigating the gene regulatory sequences, splice variants and the meiotic function of wheat <i>ZYP1</i>.....</b>	<b>125</b>
<b>3.1 Introduction.....</b>	<b>125</b>
<b>3.2 Materials and Methods .....</b>	<b>127</b>
3.2.1 Plant materials and greenhouse conditions .....	127
3.2.2 Amplification of <i>TaZYP1</i> .....	127
3.2.3 Proteomic validation of <i>TaZYP1</i> protein.....	128
3.2.4 Cloning the full length coding region of <i>TaZYP1</i> .....	128
3.2.5 Validation of <i>TaZYP1</i> fragment insertion via colony PCR.....	128
3.2.6 Testing the efficiency of the designed <i>TaZYP1</i> pyrosequencing primers.....	129
3.2.7 Quantitative PCR (qPCR) of <i>TaZYP1</i> homoeologues .....	129
3.2.8 Cloning the untranslated regions (UTRs) of <i>TaZYP1</i> .....	129
3.2.9 Identification of <i>zyp1</i> TILLING lines in tetraploid <i>T. turgidum</i> .....	130
3.2.2 Genotype screening of Kronos Parental mutants .....	132
3.2.3 Crosses of Kronos Parental mutants .....	133
3.2.4 Genotyping of F1 mutants.....	133
3.2.5 Backcrosses of <i>zyp1</i> Parents with tetraploid Kronos wild-type .....	133
3.2.6 Isolating pollen mother cells (PMCs) for metaphase I chromosome spreads ..	133
3.2.7 Immunolocalisation of PMCs .....	134
3.2.8 Statistics .....	134
<b>3.3 Results .....</b>	<b>134</b>
3.3.1 <i>TaZYP1</i> is expressed in leaves and inflorescences of hexaploid <i>T. aestivum</i> cultivars Cadenza and Apogee .....	134
3.3.2 <i>TaZYP1</i> homoeologues expression is likely redundant in reproductive and somatic tissues.....	135
3.3.3 The predicted <i>TaZYP1</i> cds isoforms in germline DNA .....	141
3.3.4 Analysis of wheat <i>zyp1</i> TILLING mutants .....	148
3.3.5 Cytological atlas of <i>zyp1</i> single knockouts .....	153
3.3.6 <i>zyp1</i> single KO exhibits loss of obligate CO .....	156

3.3.7 <i>zyp1</i> single KO preserves distal CO .....	158
3.3.8 Fertility assessment .....	161
3.3.9 Meiotic prophase I is delayed in <i>zyp1</i> single KO.....	161
3.3.10 Synapsis and desynapsis are disrupted in <i>zyp1</i> single KO .....	164
3.3.11 Recombination pathway is defective in <i>TtZYP1</i> lacking C-terminus.....	168
<b>3.4 Discussion .....</b>	<b>170</b>
3.4.1 Molecular data overview.....	170
3.4.2 Novel <i>TaZYP1</i> 3' UTR transcript variants were identified in meiotic tissues .	171
3.4.3 Cytology data overview .....	172
3.4.4 <i>TtZYP1</i> likely imposes Class I CO prior to SC formation and may be responsible of CO distribution in tetraploid <i>T. turgidum</i> .....	173
3.4.5 In tetraploid wheat, SC and CO are interdependent and rely on <i>TtZYP1</i> C-terminus.....	175
3.4.6 <i>TtZYP1</i> may favour centromeric CO in tetraploid <i>T. turgidum</i> .....	177
<b>3.5 Conclusions.....</b>	<b>178</b>
3.5.1 Molecular approach.....	178
3.5.2 Cytology approach .....	178
<b>Chapter 4 .....</b>	<b>180</b>
<b>Searching for SC central element gene candidate(s) in polyploid wheat using bioinformatics tools.....</b>	<b>180</b>
<b>4.1 Introduction.....</b>	<b>180</b>
<b>4.2 Materials and methods .....</b>	<b>183</b>
4.2.1 <i>TaZYP1</i> co-expression network with RNA-seq data from ExpVIP database ..	183
4.2.2 Alluvial diagram.....	184
4.2.3 Comparative analysis of CE orthologues from model organisms.....	185
4.2.4 Identification of tetraploid TILLING Lines .....	187
4.2.5 Genotype screening of single KO mutants.....	187
4.2.6 Isolating pollen mother cells (PMCs) for metaphase I chromosome spreads ..	188
4.2.7 Isolating pollen mother cells (PMCs) for metaphase I chromosome spreads ..	189
4.2.8 Statistics .....	189
4.2.9 Peptide antigens sequences for polyclonal antibody development .....	189
<b>4.3 Results .....</b>	<b>190</b>
4.3.1 <i>TaZYP1</i> co-expression sub-network screened seven uncharacterized genes with potential role in wheat meiosis.....	190
4.3.2 Analysis of TILLING mutants .....	191
4.3.3 <i>TaZYP1</i> is highly connected with genes having multiple meiotic roles in wheat .....	196

<b>4.4 Discussions .....</b>	198
4.4.1 WGCNA network as a promising method to unveil the evolutionary history of wheat CE .....	198
4.4.2 Preliminary data of candidate <i>SWI1</i> homologue in tetraploid wheat .....	200
4.4.3 <i>TaZYP1</i> is likely to play a more central role in meiotic recombination.....	202
<b>4.4 Conclusion .....</b>	204
<b>Chapter 5 .....</b>	206
<b>Application of chromosome-specific oligonucleotide probes for FISH karyotyping in <i>Triticum aestivum</i> .....</b>	206
<b>5.1 Introduction .....</b>	206
<b>5.2 Materials and methods .....</b>	209
5.2.1 Plant materials and growth conditions .....	209
5.2.2 Chromosome preparation for squashing technique .....	209
5.2.3 Chromosome preparation for dropping technique (Rodríguez-Domínguez et al., 2019).....	210
5.2.4 Chromosome preparation for streaming technique (Aliyeva-Schnorr et al., 2015).....	211
5.2.5 Evaluation of factors influencing the quality of mitotic chromosome spread in hexaploid <i>T. aestivum</i> landrace Chinese Spring.....	212
5.2.6 FISH procedure .....	213
<b>5.3 Results .....</b>	217
5.3.1 Comparative analysis of chromosome dispersion methodologies in tetraploid and hexaploid <i>Triticum</i> .....	217
5.3.2 Optimization of FISH protocol for MyTag oligo-probes .....	219
<b>5.4 Discussion .....</b>	228
5.4.1 Acetic acid clears the cytoplasm and improves chromosome dispersion in tetraploid and hexaploid <i>T. aestivum</i> .....	228
5.4.2 MyTag chromosome-specific oligo-probes likely form secondary structures in <i>T. aestivum</i> ‘Chinese Spring’ .....	231
<b>5.5 Conclusion .....</b>	234
<b>Chapter 6 .....</b>	235
<b>General conclusions .....</b>	235
<b>6.1 Introduction .....</b>	235
<b>6.2 ASY1 possesses a non-canonical gene expression pattern in polyploid wheat.</b>	236
<b>6.3 ASY1 is required for homology search in tetraploid wheat.....</b>	237
<b>6.4 ZYP1 is not exclusively expressed in meiotic tissues in polyploid wheat .....</b>	241
<b>6.5 In tetraploid wheat, SC and CO are interdependent and may rely on ZYP1 C-terminus .....</b>	242

<b>6.6 A novel meiotic gene candidate <i>SWI1</i> was identified in polyploid wheat with bioinformatics tools.....</b>	243
<b>6.7 An improved FISH-based oligo-probes protocol to discriminate individual sub-genomes in polyploid wheat .....</b>	243
<b>6.8 Research implication in Food Security .....</b>	244
<b>References.....</b>	246
<b>Appendices.....</b>	282

## List of Figures

Figure 1.1 Meiotic divisions I and II as observed in <i>Triticum aestivum</i> .....	4
Figure 1.2 Model of meiotic recombination with corresponding changes in chromosome structure. ....	7
Figure 1.3 The synaptonemal complex morphogenesis throughout leptotene and pachytene. ....	15
Figure 2.1 Schematic representation of wheat <i>ASY1-5A</i> and <i>ASY1-5B</i> coding regions and altered proteins from TILLING <i>ASY1</i> lines.....	44
Figure 2.2 Expression validation of <i>TaASY1</i> cDNA in hexaploid <i>T. aestivum</i> .....	55
Figure 2.3 Colony PCR of <i>TaASY1-5B</i> clone.....	57
Figure 2.4 Assessment of <i>TaASY1</i> homoeologues relative contribution in DNA coding region.....	58
Figure 2.5 Validation of pyrosequencing primer sets.....	61
Figure 2.6 Predicted protein coding annotation of <i>TaASY1</i> .....	62
Figure 2.7 A putative splice variant in <i>TaASY1-5B</i> cds ‘Apogee’ clone.....	63
Figure 2.8 The putative <i>TaASY1-5B</i> splice isoform identified in <i>T. aestivum</i> ‘Apogee’ clone.....	64
Figure 2.9 The predicted alternative protein of <i>TaASY1-5B</i> ‘Apogee’ clone. ....	65
Figure 2.10 Nested RACE PCR validates the expression of <i>TaASY1</i> UTRs in reproductive tissues.....	66
Figure 2.11 Multi sequence alignment of <i>TtASY1</i> 5’ UTR clones from tetraploid <i>T. turgidum</i> cv. Kronos with the genome reference.....	67
Figure 2.12 <i>TtASY1</i> 3’ UTR transcript variants with CPE <sub>1</sub> and CPE <sub>2</sub> sites.....	70
Figure 2.13 <i>TtASY1</i> 3’ UTR transcript variants.....	71
Figure 2.15 DNA coding region sequence of K0706 ( <i>asy1a</i> ) clone.....	74
Figure 2.16 DNA coding region sequence of K0157 ( <i>asy1b-1</i> ) clone. ....	75
Figure 2.17 DNA coding region sequence of K2071 ( <i>asy1b-2</i> ) clone. ....	76
Figure 2.18 DNA coding region sequence of C0971 ( <i>asy1 AAbbDD</i> ) clone. ....	77
Figure 2.19 Clustal Ω multiple alignments of protein sequence from WT and predicted <i>asy1</i> TILLING mutant lines.....	78
Figure 2.20 Cytological atlas of <i>asy1</i> single KO mutants. ....	80
Figure 2.21 Additional metaphase I phenotypes of <i>asy1</i> TILLING mutants. ....	81
Figure 2.22 <i>asy1</i> single KO mutants display altered chromosome configuration at metaphase I. ....	83
Figure 2.23 Schematic representation of the physical map of <i>T. aestivum</i> chromosome 5B.....	84
Figure 2.24 Cytological atlas of <i>asy1 Aabb</i> , <i>asy1 aabB</i> and <i>asy1 aabb</i> mutants. ....	86
Figure 2.25 Additional Metaphase I phenotypes in Kronos <i>asy1 Aabb</i> and <i>asy1 aabB</i> . ..	87
Figure 2.26 All <i>asy1</i> genotypes display increased severity in chiasmata frequency at metaphase I. ....	89

Figure 2.27 Meiotic prophase I progress of PMCs in <i>T. turgidum</i> cv. Kronos and <i>asy1</i> single KO mutants. ....	92
Figure 2.28 Immunolocalization of <i>TaASY1</i> and <i>AtZYP1</i> at meiotic leptotene stage in PMCs of WT Kronos and <i>asy1</i> single KO in A and B sub-genomes. ....	93
Figure 2.29 Localization of <i>TaASY1</i> and <i>AtZYP1</i> against a zygotene PMCs of WT and <i>asy1</i> single KO mutants. ....	94
Figure 2.30 PMC at zygotene stage in WT and <i>asy1a</i> mutant. ....	95
Figure 2.31 Analysis of synapsis monitored by <i>TaASY1</i> (green) and <i>AtZYP1</i> (red)... ...	96
Figure 2.32 Meiocytes of WT Kronos and <i>asy1a</i> mutant labelled with <i>TaASY1</i> (green) and <i>AtZYP1</i> (red) at diplotene stage.. ....	97
Figure 2.33 PMCs of WT Kronos and <i>asy1</i> single KO mutants at late diplotene. ....	98
Figure 2.34 Synapsis is defective in <i>asy1 aabB</i> .....	100
Figure 2.35 Localization of chromosome axes <i>TaASY1</i> (green), and <i>AtASY3</i> (red)..	102
Figure 2.36 ASY1 and SMC3 failed to localize on chromosome axes in <i>asy1 aaBb</i> during post-synapsis. ....	104
Figure 2.37 Analysis of meiotic DSBs formation using the anti- $\gamma$ H2AX antibody in male meiocytes in WT and <i>asy1 aabB</i> at leptotene stage.....	106
Figure 2.38 Cytological atlas of <i>asy1 AAbbDD</i> in hexaploid <i>T. aestivum</i> cv. Cadenza. ....	108
Figure 2.39 <i>asy1 AAbbDD</i> mutants display altered chromosome configuration at metaphase I. ....	110
 Figure 3.1 Schematic representation of <i>TtZYP1-2A</i> and <i>TtZYP1-2B</i> coding regions and altered proteins from TILLING <i>TaZYP1</i> lines. ....	131
Figure 3.2 Expression validation of <i>TaZYP1</i> cDNA in hexaploid <i>T. aestivum</i> .....	135
Figure 3.3 Colony PCR of <i>TaZYP1-2B</i> clone.....	136
Figure 3.4 Assessment of <i>TaZYP1</i> homoeologues relative contribution in DNA coding region. ....	137
Figure 3.5 Validation of pyrosequencing primer sets.....	140
Figure 3.6 Predicted protein coding annotation of <i>TaZYP1</i> ..	141
Figure 3.7 RACE PCR validates the expression of <i>TtZYP1</i> UTRs in reproductive tissues. ....	142
Figure 3.8 Multi sequence alignment of <i>TtZYP1</i> 5' UTR clones from tetraploid <i>T. turgidum</i> cv. Kronos with the genome reference.....	143
Figure 3.9 <i>TtZYP1</i> 3' UTR transcript variants with PAS <sub>1</sub> and PAS <sub>2</sub> sites. ....	146
Figure 3.10 <i>TtZYP1</i> 3' UTR transcript variants.....	147
Figure 3.11 Figure Western blot with <i>AtZYP1</i> antibody in hexaploid <i>T. aestivum</i> ... ...	148
Figure 3.12 DNA coding region sequence of K3331 ( <i>zyp1a-1</i> ) clone. ....	150
Figure 3.13 DNA coding region sequence of K3886 ( <i>zyp1a-2</i> ) clone. ....	151
Figure 3.14 DNA coding region sequence of K4200 ( <i>zyp1b</i> ) clone.....	152
Figure 3.15 Clustal Ω multi-alignments of protein sequence from WT and predicted <i>zyp1</i> TILLING mutant lines. ....	153
Figure 3.16 Cytological atlas of <i>zyp1</i> single KO mutants. ....	155
Figure 3.17 Additional metaphase I phenotypes of <i>zyp1</i> TILLING mutants.. ....	156

Figure 3.18 <i>zyp1</i> single KO mutants display altered chromosome configuration at metaphase I .....	157
Figure 3.19 Metaphase and anaphase I phenotypes of <i>zyp1 Aabb-1</i> mutant. ....	159
Figure 3.20 <i>zyp1</i> mutant genotypes display drastic changes in chromosome configuration at metaphase I. ....	160
Figure 3.21 Meiotic prophase I progress of PMCs in <i>T. turgidum</i> cv. Kronos and <i>zyp1</i> single KO mutants from pre-meiotic interphase to diplotene.....	162
Figure 3.22 Dual immunolocalization of <i>TaASY1</i> and <i>AtZYP1</i> at meiotic leptotene stage in PMCs of WT Kronos and <i>zyp1</i> single KO in A and B sub-genomes.....	163
Figure 3.23 Localization of <i>TaASY1</i> and <i>AtZYP1</i> against a zygotene PMCs of WT and <i>zyp1</i> single KO mutants. ....	165
Figure 3.24 Analysis of synapsis progress monitored by <i>TaASY1</i> (green) and <i>AtZYP1</i> (red) in <i>zyp1</i> meiocytes during pachytene, compared to the WT. (A-A3) WT Kronos. ....	166
Figure 3.25 Analysis of desynapsis monitored by <i>TaASY1</i> (green) and <i>AtZYP1</i> (red) in <i>zyp1</i> meiocytes during early diplotene, compared to the WT.....	167
Figure 3.26 Analysis of desynapsis monitored by <i>TaASY1</i> (green) and <i>AtZYP1</i> (red) in <i>zyp1</i> meiocytes during late diplotene, compared to the WT.....	168
Figure 3.27 Analysis of meiotic DSBs progression using the anti- <i>HvHEI10</i> antibody in male meiocytes in WT and <i>zyp1a-1</i> at pachytene stage. ....	170
 Figure 4.1 Workflow for data analysis to identify putative CE orthologue(s) in wheat.. ....	
.....	184
Figure 4.2 <i>TaZYP1</i> co-expression sub-network in hexaploid wheat. ....	190
Figure 4.3 Confirming the genotype of <i>cc1</i> , <i>cc2</i> and <i>cc3</i> TILLING mutants.....	193
Figure 4.4 Metaphase I spread of TILLING single KO mutants.....	195
Figure 4.5 Chromosome configuration analysis of CE candidate single KO mutants at metaphase I.. ....	195
Figure 4.6 Analysis of synapsis monitored by <i>TaASY1</i> (green) and <i>TtSWITCH1</i> (red) in Kronos WT meiocytes during zygotene. ....	196
Figure 4.7 The alluvial diagram of the wheat MG orthologues connected to <i>TaZYP1-2A</i> and 2D homoeologues.. ....	198
 Figure 5.1 Comparative evaluation of using three chromosome spreading techniques (dropping, streaming, squashing) in hexaploid <i>T. aestivum</i> landrace Chinese Spring. 213	
Figure 5.2 Oligo-probes used for FISH assay and MyTag oligo probes signal patterns in hexaploid <i>T. aestivum</i> ‘Chinese Spring’. ....	214
Figure 5.3 Workflow of the entire procedure used for testing <i>de novo</i> MyTag oligo probes in mitotic chromosomes of <i>T. aestivum</i> ‘Chinese Spring’.....	217
Figure 5.4 Qualitative evaluation of three spreading techniques (dropping, streaming, squashing) tested on mitotic chromosomes of <i>T. aestivum</i> ‘Chinese Spring’ . ....	218
Figure 5.5 FISH-Protocol 1 for detecting <i>T. aestivum</i> ‘ Chinese Spring’ homoeologous chromosomes from meristematic tissue using labeled synthetic oligo-probes.....	220

Figure 5.6 FISH-Protocol 2 for detecting *T. aestivum* ‘Chinese Spring’ homoeologous chromosomes from meristematic tissue using labeled synthetic oligo-probes..... 221  
 Figure 5.7 FISH-Protocol 3 for detecting *T. aestivum* ‘Chinese Spring’ homoeologous chromosomes from meristematic tissue using labeled synthetic oligo-probes..... 222  
 Figure 5.8 FISH-Protocol 4 for detecting *T. aestivum* ‘Chinese Spring’ homoeologous chromosomes from meristematic tissue using labeled synthetic oligo-probes..... 224  
 Figure 5.9 FISH-Protocol 5 for detecting *T. aestivum* ‘Chinese Spring’ homoeologous chromosomes from meristematic tissue using labeled synthetic oligo-probes..... 225  
 Figure 5.10 FISH result of individual MyTag oligo marking homoeologous chromosomes of *T. aestivum* ‘Chinese Spring’ .. ..... 227  
 Figure 5.11 FISH result of repetitive rDNA and MyTag oligo probes marking B chromosome in *T. aestivum* ‘Chinese Spring’ genome.. ..... 228

## List of Tables

Table 2.1 Solutions for Bradford Assay .....	36
Table 2.2 Solution for SDS-PAGE.....	37
Table 2.3 Solution for Western Blot .....	38
Table 2.4 Sub-genome specific primer sets for qPCR.....	41
Table 2.5 Sub-genome specific primers used to amplify <i>TaASY1</i> TILLING lines.. .....	46
Table 2.6 Solutions for immunolocalization experiment.....	52
Table 2.7 List of primary and secondary antibodies used in this project. ....	52
Table 2.8 Summary of metaphase I spread analysis comprising all <i>asy1</i> TILLING mutant genotypes. .....	90
Table 2.9 Seed-set score for Kronos TILLING lines.....	90
Table 3.1 Sub-genome specific primer sets for qPCR.....	130
Table 3.2 Sub-genome specific primers used to amplify <i>TtZYP1</i> TILLING lines.....	133
Table 3.3 Seed-set count for Kronos TILLING lines. ....	161
Table 4.1 Web resources used in this study.....	186
Table 4.2 Protein structure data of CE orthologues of model organisms. ....	186
Table 4.3 Summary of Kronos TILLING lines information from Ensembl Plants database. ....	187
Table 4.4 Subgenome specific primers used for wheat CE candidate(s) genotyping. .	188
Table 4.5 Peptide antigens sequences of ‘CC2’ used for protein immunolocalization.	189
Table 4.6 Supplementary data of <i>TaZYP1</i> sub-network results generated in Cytoscape 3.8.0 software. .....	191
Table 4.7 Data collection of wheat CE candidate genes identified by comparative analysis with known CE orthologues from model organisms.. .....	192
Table 4.8 Data for alluvial diagram. ....	197
Table 5.1 Representative panel of a starting FISH protocol.....	215
Table 5.2 Final protocol for mitotic chromosome preparation from meristematic tissue of three polyploid wheat genotypes. .....	219

## List of Abbreviations

- AS** Alternative Splicing  
**BSA** Bovine Serum Albumen  
**cds** coding region sequence  
**CE** Central Element  
**CO** Crossover  
**CPE** Cytoplasmic Polyadenylation Element  
**Ct** Cycle of threshold  
**cv** cultivar  
**DAPI** 4',6-diamidino-2-phenylindole  
**dHJ** Double Holliday Junction  
**DSB** Double Strand Break  
**FISH** Fluorescence In Situ Hybridisation  
**HORMA** HOP1–REV7–MAD2  
**HR** Homologous Recombination  
**IP** Immuno Precipitation  
**IWGSC** annotation International Wheat Genome Sequencing Consortium  
**KO** knock-out  
**LE** Lateral Element  
**M1** Metaphase I  
**NCO** Non-crossover  
**P adj** Adjusted P Value  
**PAS** PolyAdenylation Signals  
**PBS** Phosphate Buffered Saline  
**PFA** ParaFormAldehyde  
**Ph** Pair Homologous  
**PMC** Pollen Mother Cell  
**polyA** poly Adenilation  
**qPCR** Quantitative PCR  
**RACE** Rapid Amplification of cDNA Ends  
**SC** Synaptonemal Complex  
**SNP** Single Nucleotide Polymorphism

**SSC** Saline Sodium Citrate

**SSC** Saline-Sodium Citrate

**TF** Transverse Filament

**TILLING** Targeted Induced Local Lesions In Genomes

**UTR** UnTranslated Regions

**WGCNA** Weighted Gene Correlation Network Analysis

**WT** Wild Type

**ZMM** Zip Msh Mer

# **Chapter 1**

## **Introduction**

### **1.1 Meiosis overview**

Meiosis is a specific type of cell division that was selected in sexually reproducing eukaryotes to generate haploid gametes from diploid germ cells. Meiosis consists of a single round of DNA replication followed by two consecutive cell divisions referred to as meiosis I and meiosis II. The first division results in the exchange of genetic material and segregation of maternal and paternal chromosomes called homologous chromosomes, whereas the second division involves separation of sister chromatids to form haploid cells.

The process evolved before eukaryotic radiation over 1 billion years ago (reviewed by Lenormand et al., 2016), probably in early asexual unicellular organisms, and still persists to ensure genome stability, fertility and create genetic diversity. Evolutionally, two scenarios for this have been proposed. The first supposes that diploidy accidentally occurred by replication of the nuclear genome without subsequent cell division (endoreplication) (Szathmáry & Smith, 1995), and the return to haploidy occurred to correct this error. The second scenario assumes that the “ancient” meiosis evolved in response to the fusion of two haploid cells (syngamy), as in modern eukaryotic sexual life cycles. Syngamy may have been favoured because it allows recessive deleterious mutations to be masked in diploids (Szathmáry & Smith, 1995).

Today, it is known that this type of cell division is highly conserved across kingdoms (reviewed by Bomblies et al., 2015), yet the proteins that rule the different stages of meiosis are divergent at primary sequence level (reviewed by Bomblies et al., 2015). Adaptation phenomena have also determined timing and structures in which meiosis occurs.

In angiosperms, such as wheat, the germlines are not determined early during embryogenesis as in animals, but develop later in the specialized reproductive organs of the flower (Berger & Twell, 2011). Female meiosis occurs in the ovule, where a single diploid megasporangium undergoes meiosis to produce 4 haploid megasporangia.

Three of them abort, while one develops into the gametophyte containing the female gamete. Male meiosis occurs within the anther, a part of the male reproductive organ (stamen), and leads to the production of 4 haploid microspores from every single diploid pollen mother cell. Each microspore then divides mitotically to form a macrogametophyte or pollen grain (Berger & Twell, 2011).

Overall, each meiotic division comprises 4 stages, prophase, metaphase, anaphase, and telophase, whereas prophase I is further divided into 5 sub-stages (leptotene, zygotene, pachytene, diplotene, and diakinesis), defined cytologically through the study of changes in chromosome morphology and the behaviour of meiotic proteins (Figure 1.1). In hexaploid wheat cultivar Cadenza, immunocytology study showed that the whole meiotic process takes minimum 43 h, similarly to barley (Higgins et al., 2012; Osman et al., 2021); leptotene occupied approximately 17 h with zygotene to diplotene taking 16 h; diakinesis and the two meiotic divisions were completed within 3 h (Osman et al., 2021).

In leptotene (Greek; *thin threads*), individual chromosomes appear as long thin strands that have begun condensing. As chromosomes condense during early prophase, the sister chromatids become organized along axial elements (AEs). In most organisms, the interaction of DNA double strand breaks (DSBs) with matching sequences on the homologous chromosome brings the AEs of homologous chromosomes into alignment during early- to mid-leptotene. The sites of these interactions are visualized as ~400-nm inter axis bridges (Scott L. Page & Hawley, 2004). As leptotene proceeds, a small fraction of these bridges appear to mature into structures known as axial associations, which connect the paired lateral elements (LEs) (Scott L. Page & Hawley, 2004).

During zygotene (*paired threads*), these axial associations will eventually nucleate the formation of synapsis initiation sites between associated AEs. The AEs are thus incorporated into the synaptonemal complex (SC) structure as part of the LEs. The two homologous chromosomes being side by side and the chromosome pair at this stage is called a bivalent. In crop species, the telomeres are clustered in a region of the nuclear envelope to form a structure called the “bouquet”. When the bouquet is complete, chromosome synapsis starts (Bass et al., 2000). The telomere bouquet is thought to anchor the homologues ends in the nuclear membrane and help the homologues to find each other and pair (reviewed by Aguilar & Prieto, 2021).

At the onset of pachytene (*thick threads*), the chromosomes achieve a state known as synapsis, which refers to a tight continuous association along the chromosome length in which the four chromatids are aligned and held together by the SC (reviewed by Schwarzacher, 2003). In crops such as wheat, the alignment between homologous chromosomes starts at the telomeres and extends towards the centromere (Rabl orientation) (reviewed by Aguilar & Prieto, 2021). At this stage, the SC assembly consists of the paired LEs, which are connected by transverse filaments running between them. The assembly of the SC must be tightly regulated to ensure that it takes place only between pairs of homologous chromosomes and throughout their full lengths. Synapsis is completed when all the regions are expanded along the entire length of chromosomes. In most electron microscopy (EM) studies of the SC at pachytene, a central element appears as an electron-dense linear structure running down the centre of the SC (reviewed by Aguilar & Prieto, 2021).

Following pachytene, meiotic chromosomes undergo a phase of decondensation called diplotene (*two threads*), during which sister chromatid arms are held by cohesion complexes, while the SC disassembles and homologs often separate, except at chiasmata, the physical manifestations of reciprocal meiotic recombination events or CO (reviewed by Schwarzacher, 2003). From diplotene to diakinesis, chromosomes condense by a spiralling process, and discrete bivalent (homologous held by chiasmata) structures appear. Each bivalent is clearly observed as four separate chromatids, with each pair of sister chromatids linked at their centromeres and the non-sister chromatids linked by chiasmata (Kleckner, 1996).

The bivalents are maximally condensed at metaphase I and aligned onto the metaphase plate oriented by the spindle, allowing chiasma number estimation (Kleckner, 1996). At anaphase I sister chromatid arm cohesion from each pair of homologues is then released, allowing homologues to separate and segregate to opposite poles of the spindle (Kleckner, 1996). During telophase I, only one member of each pair of chromosomes arrives at each pole, and partially decondense (reviewed by Schwarzacher, 2003). There is no DNA replication and meiotic cells enter immediately into a mitotic-like second division. Briefly, at prophase II the DNA is not replicated, and the spindle starts to organize (Kleckner, 1996). The chromosomes align at the equatorial plate at metaphase II, then

sister chromatids migrate towards the opposite poles at anaphase II. At telophase II, one haploid set of chromosome reaches each pole and a tetrad of 4 haploid nuclei are formed. In the anthers of a flower, the four products of meiosis develop into pollen (Berger & Twell, 2011).

As anticipated, most of the crucial events of meiosis occur during prophase I, and despite species variability, meiotic processes generally include formation of programmed DNA double strand breaks (DSBs), assembly of SC, chromatin condensation and physical pairing of homologous chromosomes to allow recombination by crossover (CO) formation.

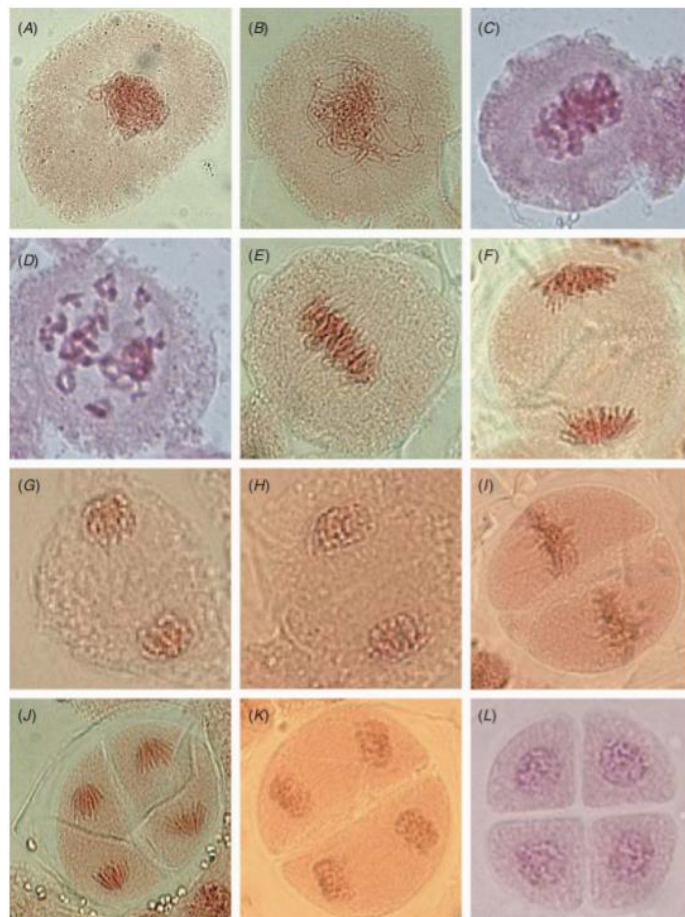


**Figure 1.1 Meiotic divisions I and II as observed in *Triticum aestivum*.** A–G) Prophase I is represented by its five sub-stages. At leptotene (not shown), chromatin starts to condense and the chromosomes are visible as long threads with the sister chromatids tightly associated together. A) During zygotene homologous chromosomes pair by means of the synaptonemal complex. B) In pachytene, the synaptonemal complex is fully formed and synapsis across the entire length of the homologues is completed. C) During diplotene homologues gradually separate, although still

holding each other at chiasmata points. D) At diakinesis each bivalent is clearly condensed and visible as four separate chromatids, with each pair of sister chromatids linked at their centromeres and the non-sister chromatids linked by chiasmata. E) During metaphase I chromosomes are aligned at the equatorial plate. F) At anaphase I the spindle separate sister chromatids to opposing pole. G) In telophase I only one member of each pair of chromosomes arrives at each pole and partially decondense. There is no DNA replication and cells enter immediately into the second division of meiosis. H–L) Panels illustrating the second meiotic division with H) representative of prophase II, where chromosomes decondense, I) being metaphase II, in which chromosomes align at the equatorial plate, J) anaphase II, where sister chromatids migrate towards the opposite poles entering in K) telophase II and finally forming L) four haploid cells or tetrad. Images were captured using light microscopy with 400X magnification (Able et al., 2009).

### 1.1.2 The molecular bases of meiotic recombination

At the molecular level, meiotic recombination is initiated by the formation of DNA Double-Strand Breaks (DSBs) (Figure 1.2), catalysed by SPORULATION-DEFICIENT 11 (SPO11), a highly conserved protein among eukaryotes with a sequence similarity to the A and B subunit of archaeal topoisomerase VI (TopVIA and TopVIB) (Bergerat et al., 1997; Keeney, 2008). While SPO11 is conserved across kingdoms, the accessory proteins required for its function vary. In *S. cerevisiae* there are at least nine other SPO11- or DSB-associated proteins, including MRE11, RAD50, XRS2, SKI8, REC102, REC104, REC114, MEI4, and MER2 (Neale et al., 2005). In plants, DSB-associated proteins include *AtPRD1*, *AtPRD2*, *AtPRD3*, *AtDFO*, *OsCRC1*, *OsSDS*, and *OsP31comet* (*OsBVF1*) (Nonomura et al., 2004; De Muyt et al., 2009; Zhang et al., 2012; Miao et al., 2013; Wu et al., 2015; Ji et al., 2016; Zhou et al., 2017). Mutants of *AtDFO* gene show defects in bivalent formation (homologous chromosomes linked by chiasmata) and meiotic univalent (Zhang et al., 2012), suggesting a potential meiotic role. *OsCRC1* (Central Region Component1), the rice ortholog of *S. cerevisiae* PCH2, is a central element component of the SC and interacts with ZEP1 (ortholog of *Arabidopsis* ZYP1), and it is also required for DSB formation (Miao et al., 2013), suggesting that the SC is important for both DSB formation and subsequent recombination. However, this is not the case for all known SC components or for all species. In yeast, it has been demonstrated that SPO11 catalysed DSBs are subject to negative feedback mechanisms, which inhibit the continued formation of DSBs in the presence of synapsed chromosomes (Carballo et

al., 2013; Thacker et al., 2014). In addition, this process involves the phosphorylation of REC114 by MEC1/TEL1 in response to DSB formation (Carballo et al., 2013). In the absence of these feedback mechanisms, cells experience higher levels of DSB formation (Thacker et al., 2014).

DSBs are processed by resection into 3' single-strand DNA ends by the MRX–N complex [MRE11–RAD50–XRS2 (NBS1)] and COM1 (SAE2) that may engage with either complementary sequences from homologous chromosomes or sister chromatids (reviewed by Wang & Copenhaver, 2018). In yeast, the MRX complex is also required for meiotic DSB formation (Neale and Keeney, 2005), contrary to *Arabidopsis*, where the AtMRE11 and AtRAD50 homologs are necessary for mitotic and meiotic repair and do not participate in DSB formation (Osman et al., 2011). A conserved ssDNA binding protein, replication protein A (RPA), binds 3' ends to protect them from degradation, remove secondary structures, and facilitate the loading of recombinases (reviewed by Wang & Copenhaver, 2018). Most eukaryotic organisms possess at least two structural and functional homologs of the bacterial RECA recombinase, RAD51 and DMC1, that have distinct functions (reviewed by Wang & Copenhaver, 2018). In *Arabidopsis*, a loss of function mutation in RAD51 leads to DNA fragmentation in meiocytes caused by an inability to repair SPO11 catalysed DSBs, compromised pairing and a complete lack of synapsis (Pradillo et al., 2012). Perturbing the function of *Dmc1* in both yeast and *Arabidopsis* leads to a complete absence of chiasmata and defective synapsis but does not result in chromosome fragmentation, suggesting that it is required for CO formation (Bishop et al., 1992; Couteau et al., 1999). *Drosophila* and *C. elegans*, which do not require the formation of crossovers for synapsis, do not have genes for DMC1 (reviewed by Wang and Copenhaver 2018).

Overall, DMC1 and RAD51 mediate invasion of the 3' ssDNA end into the double helix of the paired homologous chromosome to form a D-loop intermediate (Brown and Bishop 2014). At the 3' end, recombination-associated DNA synthesis anneal the D-loop to the second 3' end in a process called second-end capture. Additional DNA synthesis using the second 3' end, followed by ligation, yields an intermediate called a double Holliday junction (dHJ), which links the four DNA strands of two homologous chromosomes (Pyatnitskaya et al., 2019) (Figure 1.2).

The resolution of dHJs occurs by structure-specific endonucleases before the homologous

chromosomes segregate (anaphase I), which include MUS81–MMS4 (MUS81–EME1) [Methyl Methansulfonate, UV Sensitive 81–Methyl Methane Sulfonate Sensitivity 4 (Essential Meiotic Endonuclease 1)], SLX1–SLX4 (Synthetic lethal of unknown function), and YEN1 (GEN1) [Holliday junction resolvase YEN1 (Gen endonuclease homolog1)] (Schwartz & Heyer, 2011). The resolution of dHJs results as crossovers (COs) and non-crossovers (NCOs) (Allers & Lichten, 2001) (Figure 1.2). However, how the fate of a DSB is determined is still not fully understood, but it is thought that pro- and anti-CO pathways influence the repair outcome at DSB sites, and importantly, that several factors have been reported to define frequency and distribution of COs (Mercier et al., 2015).

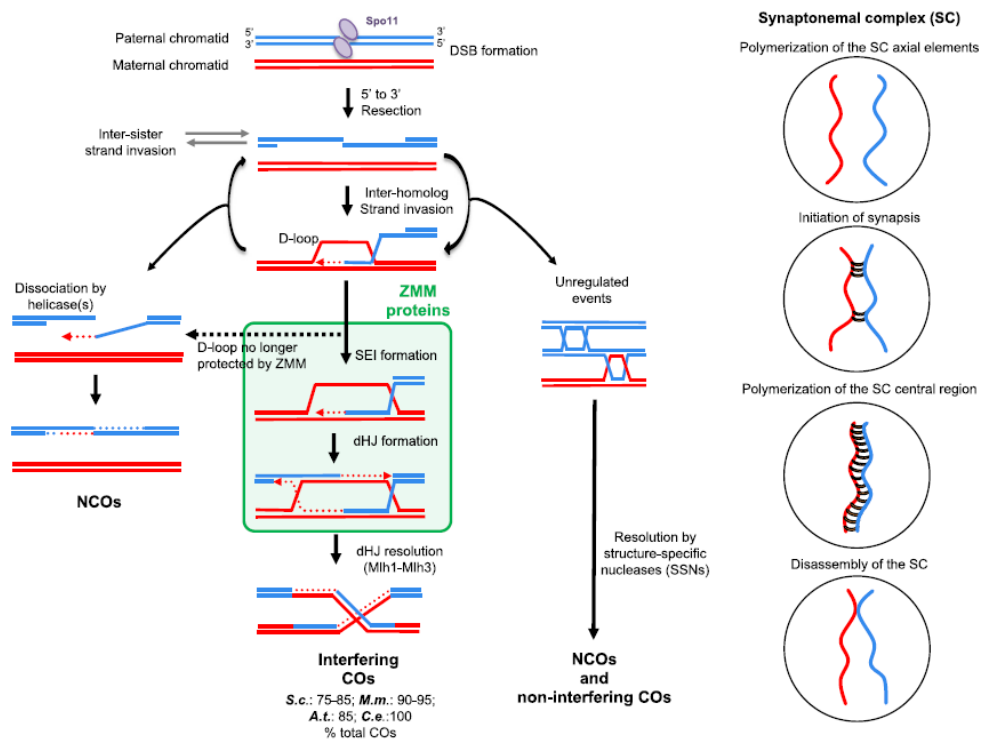


**Figure 1.2 Model of meiotic recombination with corresponding changes in chromosome structure.** Left: representation of the three main pathways of meiotic recombination. Parental double-stranded DNA molecules are depicted in blue and red. Dashed lines indicate newly synthesized DNA. Meiotic double-strand breaks (DSBs) formed by SPO11 can be repaired as two types of recombination products: crossovers (COs) and non-crossovers (NCOs), which correspond to DSB repair products with and without exchange of flanking sequences, respectively. COs produced by the ZMM (an acronym for Zip1-4, Msh4-5, Mer3, Spo16) pathway are formed via stabilized D-loop (the single-end invasion (SEI)) and double-Holliday-junction (dHJ) intermediates, and exhibit interference. Nevertheless, some CO-specific recombination

intermediates may be redirected towards NCO products following ZMM loading (dashed arrow). By contrast to ZMM-dependent COs, the non-interfering COs are randomly distributed along the chromosomes. Non-interfering COs are produced simultaneously with NCOs by the resolution by structure-specific nucleases of DNA intermediates that have escaped from helicases or ZMM activities. The estimated percentage of interfering COs over the total number of COs in different organisms is shown: *S.c. Saccharomyces cerevisiae*; *M.m. Mus musculus*; *A.t. Arabidopsis thaliana*; *C.e. Caenorhabditis elegans* (Serrentino and Borde 2012). The disassembly of DNA intermediates by helicase(s) leads to NCO products. Right: illustrations of the corresponding changes in chromosome structure are shown for a single pair of homologous chromosomes (red and blue lines) (Pyatnitskaya et al., 2019).

### 1.1.3 The meiotic recombination pathways

In eukaryotes, the regulation of frequency and distribution of COs at a whole-genome level relies upon various properties and conditions, such as interference, homeostasis and obligate CO.

- **Homeostasis** is a condition maintaining a stable number of COs even when DSB numbers are altered. In *S. cerevisiae*, *spo11* hypomorphic mutants decrease DSB frequency but do not cause a corresponding decrease in COs, up until a threshold (Martini et al., 2006). In maize (*Zea mays*), CO control is robust only to ensure one CO per chromosome pair. However, once this limit is reached, the CO number is linearly related to the DSB number (Sidhu et al., 2015).
- **Obligate CO or assurance** maintains the formation of at least one CO per homolog pair for the accurate segregation of homologous chromosomes (Jones & Franklin, 2006). Except for *S. cerevisiae*, where *mlh3* and *pch2* mutants appear to separate assurance from interference (Chakraborty et al., 2017), in *Arabidopsis* there is evidence that CO homeostasis, assurance, and interference are manifestations of a single underlying process (Knoll et al., 2012).
- **CO interference** is a phenomenon resulting in the non-random distribution of COs whereby the formation of one CO inhibits the formation of additional COs in adjacent regions, thus preventing clustering of COs (K. Wang et al., 2015). Although factors involved in this phenomenon are unclear, it has been suggested that a combination of physical stresses generated from the expansion and contraction of chromatin compressing the chromosome axis during prophase I,

combined with the diffusion of proteins along the axis, contribute to the establishment of an interfering signal (Wang et al., 2015; W. Zhang et al., 2018). In accordance with this model, components of the chromosome axis have been implicated in CO interference in budding yeast (L. Zhang et al., 2014), *Caenorhabditis elegans* (Libuda et al., 2013; Zhang et al., 2018), and *Arabidopsis* (Lambing et al., 2020a; Capilla-Perez et al., 2021; France et al., 2021). However, the chromosome axis in itself may not be sufficient to impose CO interference since axis is formed in *asy1* and *zyp1* mutant lines in which interference is lost (Lambing et al., 2020a; Capilla-Perez et al., 2021; France et al., 2021).

COs can be further categorized as being sensitive (**Class I**) or insensitive (**Class II**) to CO interference (reviewed by Lambing et al., 2017). In humans, mouse, *S. cerevisiae*, and plants, the majority of COs (70-85%) belong to Class I, which derived from the ZMM pathway. This includes a group of proteins, such as MSH4, MSH5, MER3, HEI10, ZIP4, SHOC1, PTD, as well as MLH1 and MLH3 in *Arabidopsis* (Börner et al., 2004). Current models suggest that this patterning could originate from the same process that is responsible for the obligatory CO (Wang et al. 2015). Several ZMM homologs have also been identified in rice, including ZEP1, ZIP4, MER3, MSH4, MSH5, and HEI10 (Wang et al., 2021). Analysis of *Tos17* insertion mutants of the rice *ZEP1* demonstrated that in common with other organisms, it is essential for SC formation and affects CO formation, suggesting a highly conserved mechanism of Class I CO formation among plant species. (Wang et al., 2010). However, rather than displaying a reduction in COs, analysis of the short arm of chromosome 11 revealed a more than threefold increase in COs in *zep1* mutants (Wang et al., 2010).

The Class II COs are rare, accounting for 10% to 20% of total COs (Berchowitz et al., 2007) and follow a different pathway, controlled by MUS81 (Berchowitz et al., 2007; Higgins et al., 2008). Additionally, an alternative CO pathway may exist beyond the Class I and II COs. Double mutants in both Class I and II factors, such as *msh4 mus81*, have a residual 5-10% of COs (Higgins et al., 2008), despite this mechanism is still unclear.

COs may also be subjected to a negative control. Based on evidence in yeast, most meiotic NCOs are thought to be generated by the synthesis dependent strand annealing (SDSA) pathway (reviewed by Lambing et al., 2017). SDSA follows the same initial steps as DSB

repair until second-end capture, when the invading strand instead dissociates, and the newly synthesized 3' DNA anneals to the initial single-strand 3' end. The recruitment of DNA synthesis and ligation in this case results in an NCO. Interestingly, in *Arabidopsis*, immunostaining analysis of DSB markers, such as  $\gamma$ H2A.X, RAD51, and DMC1, estimated that from the ~150–250 DSBs produced during meiosis, (reviewed by Lambing et al., 2017), only ~10 are repaired as COs, suggesting the presence of anti-CO factors that promote NCO formation. *Zmm* mutant recovery of fertility screens led to identification of three groups of anti-CO genes.

- First, the helicase FANCM and cofactors, MHF1 and MHF2, are thought to unwind post invasion intermediates to promote NCOs through the SDSA pathway (Crismani et al., 2012; Girard et al., 2014). In the *Arabidopsis* *fancm* mutant, CO frequency increases 3-fold compared with the wild type. These additional COs do not depend on ZMMs but require the MUS81 pathway, suggesting that, in the absence of FANCM, MUS81 repairs these intermediates and, as a result, generates extra class II COs.
- Second, the RTR complex, consisting of an RECQL helicase (a type IA topoisomerase) and the structural protein RMI1, is involved in the processing of DNA recombination intermediates in all eukaryotes (Mankouri & Hickson, 2007). In *Arabidopsis*, the *top3a-R640X* and the *recq4a recq4b* double mutation exhibit increases in CO frequency (Séguéla-Arnaud et al., 2015). Genetic analyses showed that both TOP3a and RECQL function independently of FANCM helicase, suggesting that several pathways actively limit CO formation, presumably by processing different intermediate substrates.
- Third, the AAA ATPase FIDGTIN-LIKE1 (*FIGL1*) also is an anti-CO protein that functions independently of FANCM (Girard et al., 2015). The observations of increased RAD51 foci and persistent DMC1 foci in the *figl1* mutant suggest that FIGL1 may control the dynamics of the two recombinases. Interestingly, the additional COs in these three groups of mutants are likely class II COs, because they depend on MUS81 and only show weak CO interference. Homologs of these anti-recombination factors have been also identified in crops. Current studies are investigating whether CO frequencies can be increased in crops by knocking down the anti-CO proteins. This subject is extensively reviewed by Kuo et al., (2021) and Wang et al., (2021).

#### 1.1.4 Other factors regulating meiotic recombination

In addition to homeostasis, assurance and interference, CO formation is also influenced by fine-scale features including allelic heterozygosity, chromatin accessibility, epigenetic modification, homology and ploidy level.

At a fine scale, COs usually form close to gene promoters and terminators in regions where DNA is accessible, also known as CO hotspots, and their level is influenced by epigenetic modifications (Wang and Copenhaver 2018). In *Arabidopsis* and maize, CO hotspots are closely associated with DSB hot spots, preferentially formed at specific region, such as active RNA Pol II transcription, low nucleosome density, DNA hypomethylated, transposable elements, and histone marks (H2A.Z and H3K4me3) (Choi et al., 2018). These regions/sequences are not conserved among plants. For instance, in maize, bread wheat and tomato, most DSBs are formed in repetitive DNA and only the DSBs that occur near genes with no hot spot are likely to contribute to CO formation (Demirci et al., 2017; Liu et al., 2010; Saintenac et al., 2009). Moreover, in *Arabidopsis* DSB hotspots are associated with AT-sequence richness (Choi et al. 2018), while in maize they are linked to a 20-bp-long GC-rich degenerate DNA sequence motif (He et al. 2017). This suggests that either there is a difference in the way the genic and epigenetics DSBs are formed or a difference in the way they are repaired (Blary and Jenczewski, 2019).

At a broader chromosomal scale, COs are distributed along the length of their chromosomes in a species-specific pattern. In *S. cerevisiae*, DSBs are thought to occur at DNA loops, along the chromosome axis (Borde & de Massy, 2013). Axis proteins, such as RED1, HOP1, and MEK1, and cohesin proteins, such as SCC1 and REC8, play a part in regulating CO frequency and distribution (Borde and de Massy 2013). In plants, a centromere-telomere gradient for CO frequencies exists. In distal euchromatic regions (that represents only ~ 20% of chromosome length) ~ 80% of COs form, while more centromeric regions are usually poor in COs, suggesting a specific role of chromatin feature in the recombination distribution (Demirci et al., 2017; Frédéric et al., 2014; Higgins et al., 2014; Lambing et al., 2017; Raz et al., 2021). This is very pronounced in the chromosome 3B of wheat, while in *Arabidopsis* and rice, CO frequency is more evenly distributed (Lambing et al., 2017), and in *Allium fistulosum*, it is even reversed. It

is known that in *Arabidopsis*, epigenetic marks, such as H3K9me2 and DNA methylation, suppress initiation of meiotic recombination in the centromeric and pericentromeric regions (Underwood et al., 2018). Meiotic-specific factors closely associated with recombination molecules are likely promising targets for control of the CO landscape. For example, components of the chromosome axis are involved in the decision between inter-sister and inter-homolog recombination and *Arabidopsis* ASY1 and ASY3 promote CO formation (Lambing et al., 2020a). *Arabidopsis* ASY1 ChIP sequencing revealed that ASY1 is enriched over the centromere-proximal regions, and a gradual reduction of ASY1 is associated with a remodelling of the COs from the centromere-proximal to the distal regions (Lambing et al., 2020a). It is speculated that the distal regions are crossover prone regions due to the early homologous pairing of the telomeres while the proximal regions are crossover prone due to the enrichment of ASY1 (Armstrong et al., 2001; Lambing et al., 2020a)

It is conceivable that COs are exclusively distal in cereals because the distal regions experience first the formation of DSBs and the pro-CO activity of ASY1 (Osman et al., 2021). In this context, it is important to remodel ASY1 on the chromosomes to achieve a remodelling of the CO landscape in cereals. Indeed, this can be achieved by increasing the temperature in barley (Higgins et al., 2012). The change of temperature reduces the polarization of axis formation, and ASY1 is detected more evenly on the chromosomes which is associated with an elevation of interstitial and centromere-proximal chiasmata (Higgins et al., 2012). However, this strategy may not be applicable to every crops, as seen in the observation that wheat recombination is only slightly and locally altered at high temperature (Coulton et al., 2020; Draeger et al., 2020).

Moreover, the mean number of COs per chromosome rarely exceeds three per bivalent, irrespectively of the chromosome size (Mercier et al. 2015), which it limits the opportunities for breeders to exploit the mechanism of meiotic recombination to combine desired traits. Also, it is known that in the vast majority of crop species, half of the identified Quantitative Traits Loci (QTLs) of interest for breeders are subjected to linkage disequilibrium, with direct consequences for genetic mapping Choulet et al. 2014). This process reduces the chance of increasing genetic diversity in these regions, and also decreases the chance of removing deleterious mutations which tend to accumulate in low recombining regions (Renaut & Rieseberg, 2015; Rodgers-Melnick et al., 2015).

## 1.2 The key SC components acting during the process of meiotic recombination in wheat

The SC is comprised of proteinaceous filaments (from Greek, *nēma*) in the state of tight pairing (*synapto*). Its macromolecular structure assembles between paired homologous chromosomes during early meiotic prophase and it is evolutionarily conserved among the vast majority of sexually reproducing eukaryotes from unicellular Protozoa, fungi, and algae to all vertebrates (reviewed by Penkina et al., 2002). This scaffold is required to stabilize homologous pairing interactions and promote interhomolog CO formation. COs not only produce genetic diversity among offspring, but in conjunction with sister chromatid cohesion, also provide essential physical attachments (chiasmata) between pairs of homologs, allowing for proper metaphase alignment and accurate segregation at meiosis I (reviewed by Gao and Colaiácovo, 2018). Without SC assembly or in case of alteration of its elements, interhomolog COs either fail to occur or are misregulated, suggesting a conserved function for the SC in promoting crossover formation (reviewed by Gao and Colaiácovo, 2018).

The basic three-dimensional macromolecular SC configuration (Figure 1.3) is overall conserved, consisting of two lateral elements (LEs) that assemble onto meiotic chromosome axes and flank a ~100 nm wide central region (CR) (reviewed by Gao and Colaiácovo, 2018). In most organisms, the central region consists of two subcomponents: the transverse filaments, that bridge the parallel homologous axes and the central element, located along the centre of the SC. The chromatin is organized into a series of loops that are tethered at their bases to the chromosome axes. Sister chromatids are closely held together by cohesins during early meiotic prophase I.

Notably, despite the conserved ultrastructure, evidence in model organisms, such as yeast, nematode, *Drosophila*, mammals, and *Arabidopsis*, suggest that SCs consist of proteins with diverged primary amino acid sequence (Zickler & Kleckner, 1999; Anuradha and Muniyappa, 2005). Thus, so far, the search of SC orthologues has been based on the characterization of certain protein structures and proprieties rather than by homology of

the full length sequence. For instance, many organisms contain conserved domains, such as the HORMA (HOP1–REV7–MAD2), which is predicted to form a globular structure that is involved in chromatin binding during the alignment of chromosomes (West et al., 2019). The HORMA domain is a common feature of the lateral element proteins HOP1/HIM-3, HTP-1, HTP-2, HTP-3/ASY1/HORMAD1 and HORMAD2 in *S. cerevisiae*, *C. elegans*, *A. thaliana* and *M. musculus*, respectively (Dobson et al., 1994; Schalk et al., 1999; Zetka et al., 1999; Caryl et al., 2000; Yuan, et al., 2000; Daniel et al., 2011; Hurlock et al., 2020). The transverse filament (TF) proteins, which include SYCP1 in Mammals, ZIP1 in *Saccharomyces cerevisiae*, C(3)G in *Drosophila melanogaster*, ZYP1 in *Arabidopsis thaliana* and six SYP(1-6) in *Caenorhabditis elegans*, share an extended central  $\alpha$ -helical domain, predicted to form coiled-coil structures, with a conserved organization pattern of N- and C-terminal regions, which is critical for the SC assembly and chiasmata formation (Meuwissen et al., 1992; Sym et al., 1993; Page and Hawley, 2001; Osman et al., 2006; Colaiacovo et al., 2003; MacQueen et al., 2002; Schild-Prufert et al., 2007; Smolikov et al., 2009; Smolikov et al., 2011; Gao & Colaiácovo, 2018). Similarly, the CE proteins are known to have  $\alpha$ -helical domains, which may organise into coiled-coil structures, except for *S. cerevisiae*, whose Ecm11 and Gmc2 do not contain any known protein domain (Humphryes et al., 2013). However, they share similar function with SYCE1, SYCE2, SYCE3 and TEX12 in mice and human (Costa et al., 2005; Hamer et al., 2006; Schramm et al., 2011), and with CONA and Corolla in *D. melanogaster* (Collins et al., 2014; Page et al., 2008).

In addition, some of these coiled-coil domain-containing proteins, such as SYCP1 and SYCP3 in mammals, SYP-1 in *Caenorhabditis elegans*, and Zip1 in budding yeast, can self-organize into higher-order structures in the absence of other SC proteins (reviewed by Gao and Colaiácovo, 2018), and may form the basic structural frame for SC assembly. Lastly, transverse filament proteins display conservation on how they are positioned or organized within the SC. For mouse SYCP1, yeast Zip1, fly C(3)G, worm SYP-1, and ZYP1 in *Arabidopsis* the N-terminal domain of the transverse filament protein is always located in the middle of the SC, while its C terminus is located next to the lateral elements (reviewed by Gao and Colaiácovo, 2018). Such a conserved organization pattern might be critical for the function of the SC. Many SC proteins also contain disordered or unstructured regions along their sequences. These regions, have been postulated to

promote protein–protein interactions and protein–nucleic acid interactions, as well as regulate protein lifetime (reviewed by Gao and Colaiácovo, 2018).

This thesis, focuses on wheat ASY1 and ZYP1, that will be introduced in the following paragraphs.

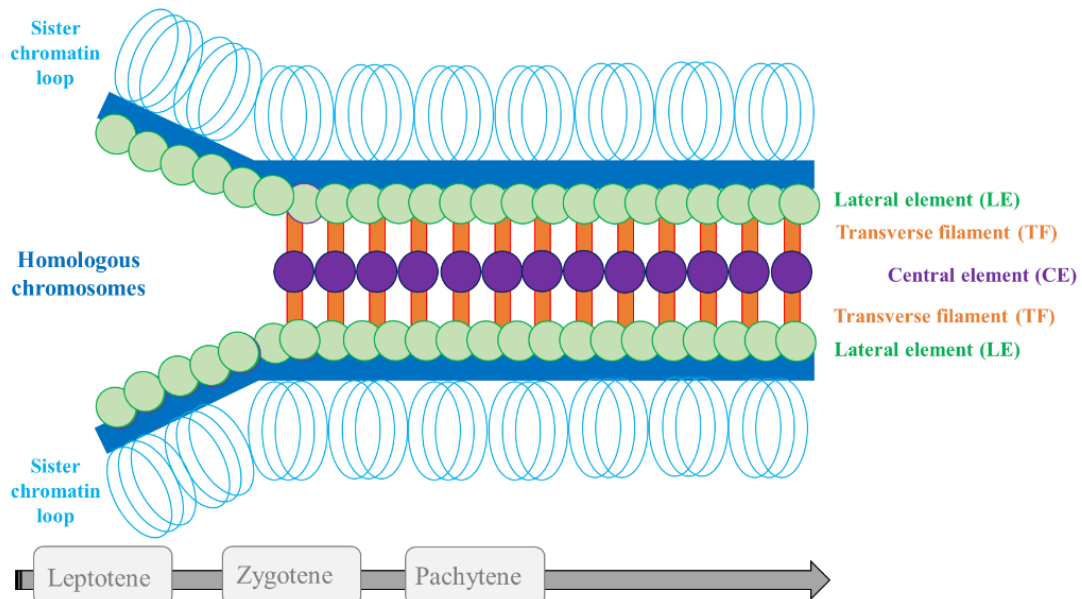


**Figure 1.3 The synaptonemal complex morphogenesis throughout leptotene and pachytene.** Sister chromatid loops on each homologous chromosome are represented in cyan, lateral elements (LEs) in green, central elements (CEs) in purple and transverse filaments (TFs) in orange. SC components progressively assemble among the homologous chromosomes. In the leptotene stage until zygotene, the lateral elements assemble and form the chromosome axis. In zygotene stage, LEs are connected by CEs and transverse TFs to form the SC. In the pachytene stage, the SC is fully assembled.

### 1.2.1 *TaASY1*

In *T. aestivum*, ASYNAPTIC 1 (ASY1) belongs to the HORMA (HOP1–REV7–MAD2) domain family, primarily involved in the chromosome axial elements morphogenesis during early stage of meiosis (Boden et al., 2007). Broadly, meiotic HORMADs are components of the meiosis-specific chromosome axis which promote DSB formation to allow the efficient pairing of homologous chromosomes. At the same time, HORMA domains (HORMADs) attenuate undesirable recombination between sister chromatids (reviewed by Rosenberg & Corbett, 2015). In organisms possessing a synaptonemal

complex, HORMADs support its formation, and depending on the organism, it may mount a checkpoint arrest when DSB repair is not completed or homologous chromosomes are not synapsed (Armstrong et al., 2002; Couteau & Zetka, 2005; Martinez-Perez & Villeneuve, 2005; Carballo et al., 2008; Daniel et al., 2011; Wojtasz et al., 2009; Kim et al., 2014; Rinaldi et al., 2017). However, several organisms have evolved species-specific features and functions.

Fungi have a single meiosis-specific HORMAD protein (HOP1) while mammals and plants express multiple paralogs (HORMAD1/2 and ASY1/2, respectively, and the nematode *C. elegans* has four (HIM-3, HTP-1, HTP-2, and HTP-3) (Caryl et al., 2000; Couteau & Zetka, 2005; Niu et al., 2005; Fukuda et al., 2012; Wojtasz et al., 2009). In fungi, plants, and mammals, the HORMAD is followed by several [S/T]Q residues representing potential Tel1/ATM-Rad3/Mec1/ATR phosphorylation sites, which enable meiotic HORMADs to act as structural adaptors for a meiotic checkpoint kinase cascade (Sanchez-Moran et al., 2007; Carballo et al., 2008; Daniel et al., 2011; Osman et al., 2018). Fungal HOP1 proteins also contain a centrally located CxxC Zn-finger motif which has been demonstrated to be important for *in vitro* DNA-binding of *S. cerevisiae* HOP1 (Hollingsworth et al., 1990; Tripathi et al., 2007).

Other diverged functions are reported among the different kingdoms. For example, in *S. pombe*, where the SC is absent, HOP1 has a major role in DSB formation, sister chromatid repair and promoting inter-homolog events, while in *S. cerevisiae* it is required for wild-type levels of meiotic recombination, for localization to meiotic chromatin and for homologous chromosome pairing (Hollingsworth & Byers, 1989; Latypov et al., 2010; Loidl et al., 1994). In yeast, HOP1 also acts downstream of DSB formation in promoting DMC1-dependent inter-homolog recombination by preventing DMC1-independent RAD51-driven recombination (Niu et al. 2005; Carballo et al. 2008). Interestingly, the genetic interaction of meiotic *Hormad* and *dmc1* genes generally does not show much conservation. In mouse both *Dmc1*<sup>-/-</sup> and *Hormad1*<sup>-/-</sup> single mutants undergo meiotic arrest at mid-pachytene, and so does the *Dmc1*<sup>-/-</sup> *Hormad1*<sup>-/-</sup> double mutant (Daniel et al. 2011), i.e., there is no reciprocal rescue as in *S. cerevisiae hop1<sup>Δ</sup> dmc1<sup>Δ</sup>*. In *Arabidopsis*, mutation of *asy1* or *dmc1* causes a strong reduction or absence of chiasmata, respectively, leading to fertility defects. However, *asy1 dmc1* double mutant and *dmc1* single mutant have the same phenotype (Sanchez-Moran et al. 2007). Thus,

contrarily to its orthologues, *AtASY1* is not required for DSB formation (Sanchez-Moran et al., 2007).

The four meiotic HORMA domain proteins in *C. elegans* (HIM-3, HTP-1, HTP-2, and HTP-3) have related but distinct functions. HTP-3 is required for axis localization of HIM-3, HTP-1, and HTP-2 (Goodyer et al., 2008; Severson et al., 2009), and its absence leads to failures in sister chromatid cohesion, chromosome segregation, homolog pairing, synapsis, and DSB formation (Goodyer et al., 2008). HIM-3 acts to promote arm cohesion within bivalents to stabilize chiasmata and establish a tension at the metaphase I plate, and it is required for homolog pairing and synapsis (Couteau & Zetka, 2005; Zetka et al., 1999). HIM-3 also promotes crossover formation by biasing recombination to the homolog instead of the sister chromatid, reflecting a conserved function in fungal and mammalian HORMA domain proteins (Zetka et al., 1999; Couteau et al., 2005; Martinez-Perez and Villeneuve, 2005; Niu et al., 2005; Wojtasz et al., 2009; Shin et al., 2010). HTP-1 and HTP-2 are highly similar to one another and appear to play partially overlapping roles. While *htp-2* mutants have no obvious meiotic defects, *htp-1* mutants exhibit extensive nonhomologous synapsis, suggesting a role in restricting SC assembly to occur between properly paired homologs (Couteau and Zetka, 2005; Martinez-Perez and Villeneuve, 2005), while loss of both paralogs results in severe abrogation of synapsis. These proteins also play a role in defining the pattern of cohesin removal during the meiotic divisions (Martinez-Perez et al., 2008).

In higher plants, ASY1 temporally associates with the meiotic chromosome axis and possess distinct functions (Armstrong et al., 2002; Cuacos et al., 2021). For instance, in *Arabidopsis* and *Brassica*, ASY1 proteins stabilise the axial core and ensure obligate CO, while in rice, the orthologous PAIR2 does not play a role in axial element formation, sister chromatid cohesion at centromeres or kinetochore assembly in meiosis I (Nonomura et al., 2006). Intriguingly, in mouse and *C. elegans*, the ASY1 orthologues are depleted from the synapsed chromosome axis, but reappear at diplotene (Zetka et al., 1999; Wojtasz et al., 2009; Shin et al., 2010). Therefore, the role of meiotic HORMA-domain proteins after desynapsis is still unclear. Overall, these disparate observations in various model organisms suggest that the genetic networks controlling DSB repair and CO formation, and how these processes are integrated with chromosome axis organization, have undergone considerable modifications during evolution.

### 1.2.2 *TaZYP1*

Numerous TF proteins (or ZYP1 orthologues) have been functionally characterized in *S. cerevisiae* (Zip1) (Sym et al., 1993), *Sordaria macrospora* (Sme4) (Espagne et al., 2011), *Mus musculus* (Sycp1) (de Vries et al., 2005; Qiao et al., 2012), *Drosophila* (C(3)G) (Page & Hawley, 2001), *Caenorhabditis elegans* (SYP1-6) (MacQueen et al., 2002; Colaiácovo et al., 2003; Smolikov et al., 2007; Hurlock et al., 2020; Zhang et al., 2020), and the plants *A. thaliana* (ZYP1, encoded by duplicated genes *ZYP1a* and *ZYP1b*) (Higgins et al., 2005), rice (ZEP1) (Wang et al., 2015; Wang et al., 2010), and barley (ZYP1) (Barakate et al., 2014). The current knowledge about the general organization of the ZYP1 orthologues in yeast, *C. elegans*, *Drosophila* and mammals relies on mutant analysis, genetic analysis and immunolocalization combined with electron microscopy or super-resolution microscopy studies (Dobson et al., 1994; Liu et al., 1996; Schmekel et al., 1996; Dong & Roeder, 2000; Anderson et al., 2005; Schild-Prüfert et al., 2011; Schücker et al., 2015; Hernández-Hernández et al., 2016). These conserved proteins first form parallel homodimers through their globular carboxyl-termini, organized in coiled-coil structure, which subsequently overlap in the central space of the SC, where they associate with the axial elements via their amino-termini, ensuring alignment and synapsis between homologous chromosomes.

Analysis of TF mutants showed that depletion of zipper-like proteins induce loss of synapsis, yet homologous chromosomes can still align, albeit at twice or more distance than in wild-type synapsed chromosomes (Sym et al., 1993; de Vries et al., 2005; Wang et al., 2010; Espagne et al., 2011). Zipper-like proteins have also been shown to be evolutionary required for most or all chiasmata formation in several species, such as *S. macrospora*, *Mus musculus*, *Drosophila*, *C. elegans*, and *Hordeum vulgare* (Sym et al., 1993; de Vries et al., 2005; Page & Hawley, 2001; MacQueen et al., 2002; Colaiácovo et al., 2003; Smolikov et al., 2007; Barakate et al., 2014; Börner et al., 2004). The *S. cerevisiae* Zip1 is one of the originally defined ZMM proteins required for class I CO formation. Interestingly, a separation-of-function allele of *ScZip1* (*zip1-N1*) is defective in tripartite SC assembly but makes class I COs (Voelkel-Meiman et al., 2016), suggesting that the Zip1 itself, rather than the tripartite SC, is a prerequisite for class I CO

formation in this species. Moreover, the effects of the single-allele mutation in such *S. cerevisiae* *zip1*-*N1* mutation (maintenance of class I COs), as well as in *C. elegans* *syp-1* (moderate COs decrease), was unexpectedly opposite compared to the null mutants, which displayed an increase of COs and attenuated interference (Libuda et al., 2013; Voelkel-Meiman et al., 2016). In plants, the function of ZYP1 during meiosis is species-specific. In *Arabidopsis thaliana*, ZYP1 RNA interference knock-down lines showed a minor decrease in chiasma number, with unregulated formation of multivalents and univalents (Higgins et al., 2005). Null *zyp1a* *zyp1b* double mutants also exhibited reduced chiasmata, but the crossover marker HEI10 and fluorescent pollen recombination analysis revealed an increase in CO formation as well as abolished CO interference and heterochiasmy (Capilla-Pérez et al., 2021; France et al., 2021). Similarly, in *Hordeum vulgare*, ZYP1 RNA interference knock-downs revealed a 25% chiasmata reduction when compared to the WT (Barakate et al., 2014). On the contrary, in *Oryza sativa*, homologous chromosomes in *zep1* mutants still align during prophase I but fail to form an SC and it displays an increased CO frequency and chiasma number, with reduced CO interference (M. Wang et al., 2010). *Zep1* mutants present reduced fertility due to effects downstream of meiosis, where ZEP1 is thought to be required for chromosome decondensation following the meiotic divisions, during early microsporogenesis (M. Wang et al., 2010). In rye, super-resolution microscopy (3D-SIM) investigations indicate that the dynamic behaviour of ZYP1 and other SC proteins, is involved in desynapsis and chromosome condensation for proper recombination and homolog separation (Hesse et al., 2019). The contrasting results from plants highlight the need for further study of this protein on a species-specific basis.

### 1.2.3 The regulation of SC in polyploidy wheat

The SC is a dynamic structure where its components undergo different types of modifications and changes throughout prophase I. The disassembly of the SC is also accompanied by changes in both chromosome compaction and composition and localization of additional proteins required for controlling the release of sister chromatid cohesion at meiosis I (chromosome remodelling) (reviewed by Penkina et al., 2002). Such changes in dynamic state during the assembly and disassembly of the SC are achieved through multiple layers of regulation. These processes are precisely coordinated with the

homologous recombination and may occur to some degree at transcriptional level. In polyploid species, such as wheat, the tight control of meiotic components is further complicated by its genome size. The next paragraphs will present some of the aspects that mainly contribute to the optimal organization of the SC in polyploid wheat.

#### 1.2.3.1 The mechanism of chromosome pairing in polyploid wheat

The study of meiosis in polyploid species began in 1929 (Newton & Darlington, 1929). Since then, an increasing number of publications have highlighted the important role of polyploidization (or whole genome duplication) in evolution and speciation, particularly in plants. All Angiosperms have polyploid ancestry and up to 25–30% of extant flowering plant species are polyploids (Alix et al., 2017). There are several routes leading to the formation of a polyploid individual, but the more likely mechanism operating is through the generation of unreduced gametes (reviewed by Svacina et al., 2020).

Polyploid species usually revert to a diploid state during evolution. The first part of this process, called cytogenetic diploidization, results in the formation of species, whose polyploid origin might be hidden by disomic inheritance and diploid-like meiosis. This step occurs rather rapidly after polyploid formation by establishment of genetic control mechanism or extensive chromosomal rearrangements.

For most species, a high level of ploidy has been the result of adaptive pressure in crop domestication and humankind has been using artificial polyploidization techniques and wide hybridization (introgression) as a tool for their breeding improvement (Salman-Minkov et al., 2016). Indeed, many important crops are autopolyploids that arose from within-species whole-genome duplications (e.g., potato, alfalfa, sugar cane) or allopolyploids, which have an interspecific hybrid origin (e.g., wheat, cotton, oilseed rape, coffee) (Jiao et al., 2011). Therefore, allopolyploids carry two (or more) full complements of chromosomes, each from a distinct progenitor genome, thus forming homoeologous subgenomes, which are differentiated based on variations in chromosome architecture, DNA sequences, and gene order. Nevertheless, chromosomes retain some degree of genetic affinity and thus share genomic synteny.

There are costs and benefits associated with allopolyploids (Comai, 2005). Firstly, it represents a significant evolutionary tool for improving possibilities of adaptation. For instance, the formation of allopolyploids disrupts self-incompatibility mechanisms that prevent self-pollination, enabling asexual reproduction (Comai 2005). This is an advantageous strategy because newly formed allopolyploid species are often reproductively isolated, thus self-compatibility provides a way to propagate the allopolyploid genome (Comai 2005). Allopolyploids exhibit heterosis, an enhanced growth vigour and an advantage in ecological adaptation compared to the diploid progenitors, enabling the hybrids to out-perform their progenitor species (Birchler et al., 2010). Gene redundancy (a strategy to mask deleterious alleles or an opportunity to better resist deleterious mutations and to diversify the extra copies of genes in subsequent evolution) and genome subfunctionalization (a neutral mutation process in which each paralog retains a subset of its original ancestral function) are other ways used by allopolyploids to out-compete their diploid progenitor species (Comai 2005). At the chromosomal level, the existence of extra chromosomal set(s) represents a significant fitness advantage for tolerating large rearrangements in the genome that would normally lead to fatal consequences in diploid progenitors. All these effects of polyploidization could additionally contribute to faster colonization of new niches, e.g., *T. aestivum* can grow in broad geographical areas and occupy a range of habitats (Feldman & Levy, 2005).

Another consequence of polyploidization is that it is initially accompanied by genetic changes and irregular meiosis, due to the presence of more than two identical homologs in autopolyploids, or very similar chromosomes (homoeologues) in allopolyploids. The genetic changes include epistasis, DNA loss, epigenetic changes (DNA methylation, histone modification, transposon suppression/release, small RNA-mediated gene silencing) homoeologous recombination, gene conversion and ectopic recombination may have negative aspects (Jackson & Chen, 2010; Liu et al., 2014).

When two diverged genomes merge into a single cell, duplicate copies of genes with similar or redundant functions may alter their gene expression patterns at different dimensions, including unequal parental contributions, transgressive upregulation or downregulation, silencing, altered expression times and locations, chromosome rearrangements (Yoo et al., 2013). The offspring produced may be aneuploid or have a different ratio of chromosomes than the parent, altering the chromosome dosage. Dosage

changes can involve duplication or deletion of whole chromosomes or as homoeologous non-reciprocal transpositions, leading to CO formation between homoeologous chromosomes and the use of homoeologous as a template for repair instead of the homolog (Gaeta & Chris Pires, 2010). Thus, one of the biggest challenges faced by a new polyploid, is how to manage the correct recognition, synapsis, recombination, and segregation of its multiple related chromosomes during meiosis, to produce balanced gametes.

During early meiotic prophase I in polyploid wheat, chromosome pairing starts with centromere associations (Bennett, 1979; Martinez-Perez et al., 2000). This is followed by the restriction of synapsis initiation between homoeologues, so that most of the pairing at zygotene is between homologous chromosomes. Telomeres aggregate on the nuclear envelope into Rabl configuration (Carl Rabl's theory), forming a cluster or bouquet (Fussell, 1987), facilitating homologous chromosome sorting and initiation of synapsis, yet the molecular mechanisms restricting the pairing to the true homologues is still unclear. After the formation of the telomere bouquet, SC formation is initiated near the telomeres during early prophase I, progressing lengthwise pairing as meiosis proceeds (Bass et al., 2000; Harper et al., 2004; Pernickova et al., 2019). Multiple homologs and homoeologues form multivalents at zygotene (Mason & Wendel, 2020; Svačina et al., 2020). This results in pairing configurations such as cross-structures, rings, and chains during metaphase (Rees, 1976; Sybenga, 2012). During zygotene, these presynaptic associations may progress into synaptic partner switches (Hobolth, 1981). Furthermore, recombination nodules are observed in synapsed regions between homoeologs (Hobolth, 1981), indicating the occurrence of strand invasion and potential CO formation between homoeologous chromosomes, although they do not progress as true COs (Jenkins & Rees, 1991). As cells enter pachytene, the number of synaptic partner switches declines, and almost all chromosomes show homologous synapsis by the end of pachytene (Holm, 1986).

Consequently, allopolyploid wheat exhibits homologous bivalent formations at metaphase I (Svačina et al., 2020). Recombination between homoeologous chromosomes could indeed homogenize the subgenomes, promoting further homoeologous CO, and it can eliminate the contribution of one parent in a genomic region, leading to gene dosage imbalance, aneuploid gametes and reduced fertility (Gaeta & Chris Pires, 2010).

Therefore, exclusive bivalent pairing at metaphase I is essential to ensure regular homologous segregation and consequently reproductive stability. Such diploid-like behavior is a result of genetic regulatory systems (reviewed in Jenczewski & Alix, 2004).

Notably, bivalent formation is accomplished by two complementary systems: in one system, the preferential pairing between homologues relies on the absence of homology between chromosomes from different subgenomes, which prevents their association during the early stages of meiosis, resulting in homologous pairing (see Svačina et al., 2020). In other words, the process of partner choice is mediated by a certain degree of sequence identity (homology). The second strategy implies a genetic control. In *Arabidopsis*, *Arabidopsis Histidine-Containing Phosphotransfer* (AHP2) is required for bivalent formation and for segregation of homologous chromosomes (Schommer et al., 2003). In rice, PAIR1 encodes a putative coiled-coil protein required for homologous pairing in meiosis (Nonomura et al., 2004). In polyploid wheat, the most important genetic regulation of homologous chromosome pairing control was first identified in 1957 and was termed as *Ph1* (pairing homoeologous 1) *locus*, which most likely arose during wheat polyploidization, rather than being passed down from a diploid ancestor (Okamoto, 1957; Riley & Chapman, 1958; Sears & Okamoto, 1958). Present on the long arm of chromosome 5B, the locus was shown to be primarily responsible for the strict diploid-like pairing as its absence resulted in higher order chromosome pairing associations at metaphase I of meiosis, likely due to the pairing among both homologous and homoeologous chromosomes (Okamoto, 1957). Thus, despite the high level of gene synteny and collinearity (a condition that could favour homoeologue recombination during meiosis and leads to aneuploidy), evidence suggests that polyploid wheat adopts a diploid-like behaviour during meiosis. Similar evidence has been reported for *Avena sativa* (Gauthier & McGinnis, 1968), *Festuca arundinacea* (Jauhar, 1975), *B. napus* (Jenczewski et al., 2003), and *Oryza sativa* (Nonomura et al., 2006). When pairing control genes are present in wheat (Holm, 1986), the proportion of multivalents at zygote is lower, indicating that the pairing control genes affect the assembly of initial synapsis and correct SCs among homoeologues, and that more than one gene contributes to allopolyploid diploidization.

Historically, *Ph1* was initially associated with a cluster of cyclin-dependent-like kinases (CDKs) on chromosome 5B interrupted by a block of heterochromatin (Greer et al., 2012;

Griffiths et al., 2006), and later reassociated with the meiotic phenotype of another candidate gene, *C-Ph1* (Bhullar et al., 2014). However, extensive analysis of RNA-seq data in wheat, wheat x rye hybrids and triticale with and without *Ph1*, indicated that the silenced *C-ph1* gene corresponded to a copy present on chromosome 5D, since the copy on chromosome 5B is not expressed at any meiosis stage (Martín et al., 2018). Recently, the *Ph1* locus was defined to a 70 Mb deletion region on chromosome 5B containing a duplicated 3B chromosome segment carrying the ZMM meiotic gene *ZIP4* and a heterochromatin tandem repeat block, inserted within a cluster of *CDK2-like* genes (Griffiths et al., 2006; Al-Kaff et al., 2008; Martín et al., 2014, Martín et al., 2017). The duplicated *ZIP4* gene (*TaZIP4-B2*) within this cluster is responsible for both promotion of homologous CO and restriction of homoeologous CO, as well as is involved in improved synapsis efficiency (Rey et al., 2017, Rey et al., 2018). This gene was proposed to be *Ph1*, as supported by the high level of homoeologous pairing found in the wheat - *Ae. Variabilis* hybrids of two *Tazip4-B2* TILLING mutants and one CRISPR mutant (Rey et al., 2017; Rey et al., 2018).

Another gene affecting chromosome behaviour during meiosis is called *Ph2* and it is located on the short arm of chromosome 3D but it exerts a weaker effect than does *Ph1* (Mello-Sampayo, 1971). The *Ph2* locus was found to be within a 14.3 Mb genomic gap, where the DNA mismatch repair protein *TaMSH7-3D*, was found within the deleted region (Serra et al., 2021). *TaMSH7-3D* is expressed in anthers at meiotic prophase I and it was noticed that the lack of functioning *TaMSH7-3D* in a hexaploid wheat x *Aegilops variabilis* hybrid, causes a 5.5-fold increase in chiasma frequency, thus, it is thought to play a role in recombination partner selection (homologous vs. homoeologous) by increasing the instability of homoeologous recombination.

The least effective regulator, *Ph3*, is located on the short arm of chromosome 3A (Driscoll, 1972). Overall, *ph* mutants typically display fewer ring bivalents (with two or more chiasmata) and more univalents, rod bivalents and multivalents when compared to the wild type during metaphase I of meiosis.

Lastly, the discovery of *TaZIP4-B2* and *TaMSH7-3D*, the two major genes governing homoeologous recombination in bread wheat, opened up the possibility of understanding their mechanism of action and interaction. Thus, combining both mutations may

eventually provide a way of increasing the effectiveness and simplicity of introducing wild related chromosomal regions into wheat, allowing the production of genetically distinct, attractive wheat cultivars (Serra et al., 2021).

### 1.2.3.2 The wheat transcriptome: a still unexplored research subject

In addition to whole genome duplication, genome regulatory mechanism such as alternative splicing (AS) is also widely accepted as a major mechanism for transcriptome plasticity and proteomic complexity during plant polyploidization (reviewed by Gao et al., 2021).

AS refers to a mechanism of post-transcriptional RNA processing whereby particular combinations of exons in a nascent transcribed pre-mRNA are either included or excluded to generate different mature mRNA splice isoform transcripts, resulting in multiple protein isoforms encoded by a single gene (Reddy et al., 2013). Short consensus sequences, the approximately nine nucleotide-long 5' splice site with a GU dinucleotide at the beginning of the intron, and the 3' splice site with an AG dinucleotide at the end of the intron and a region enriched in pyrimidines (C or U) located further upstream delimit the introns. In the process of alternative splicing, not every splice site is used during pre-mRNA maturation. Rather, exons can be removed together with flanking introns, designated exon skipping, or introns can stay in the pre-mRNA, designated intron retention. Using alternative 5' splice sites or alternative 3' splice sites variable portions of introns can be removed and variable portions of the exons remain in the mRNA. This variation in the splicing patterns entails major consequences for the resulting mRNA isoforms. The encoded proteins can be composed of distinct domains and thus have different functions (Nilsen & Graveley, 2010).

At the RNA level, alternative splice isoforms can be recognized as “aberrant” and removed via RNA decay pathways. Thus, variation in the sequence of alternative splice isoforms can lead to differences in quantitative changes in overall transcript levels, eventually affecting subcellular localization, stability, translatability, or regulation by microRNAs (miRNAs) (McGlincy & Smith, 2008).

At the post-transcriptional level, activation of stress tolerance mechanisms and timing of developmental transitions (seedling, flowering, boosting) involves *cis*- and *trans*-acting elements (Chaudhary et al., 2019; Petrillo et al., 2020). *Cis*-acting elements, which are generally present in untranslated regions (UTRs) of mRNAs, can regulate various mRNA properties like stability, transport and translation efficiency and also the functioning and sub-cellular localization of the translated proteins (Chaudhary et al., 2019; Petrillo et al., 2020). So far, a UTR length-dependent functional specialization of somatic genes is demonstrated in *Arabidopsis* (dicot) and rice (monocot). Nevertheless, UTR-based regulatory processes proposed for *Arabidopsis* genes may not hold true for rice. In both *Arabidopsis* and rice, distinct functional categories are enriched in genes with short (1–500 bp), medium (501–1,000 and 1,001–2,000 bp), and long (> 2,000 bp) UTRs, yet the functional enrichments within UTR length categories differ between the two models. For instance, genes with 5' or 3' UTRs in the 1 to 500-bp category mediate stress responses in *Arabidopsis*, but genes in this category mediate transport and metabolism in rice. Thus, the mechanism(s) connecting UTR length with gene expression is still an outstanding question, and possibly, existence of species-specific mechanisms are expected (Srivastava et al., 2018). Additionally, epigenetic features (chromatin modifications, nucleosome positioning, DNA methylation) modulated by environmental fluctuations, may influence the co-transcriptional splicing dynamics, with important consequence for plant/crop phenotypes (Chaudhary et al., 2019). However, limited information is available at the proteome level to fully understand the contribution of AS in plants.

In humans, over 95% of genes are alternatively spliced, while in plants, up to 70% of multi-exon genes undergo AS (Kim et al., 2007; Pan et al., 2008). Among all AS events, intron retention (IR) is the predominant process in plants (Drechsel et al., 2013), whereas exon-skipping (ES) is the major type in humans (Wang et al., 2008). AS has been studied in numerous economically valued grass species, including wheat (reviewed by Gao et al., 2021). However, although the AS of a homologue gene has been reported in wheat as earlier as 2003 (Bollig et al., 2003), to date, there are still only a few reports AS in wheat, especially using global expression profiling (Zhao et al., 2019). The reason behind this is that polyploid wheat shows high sequence similarity among subgenome homoeologues, making it difficult to distinguish and accurately assign splicing isoforms to their respective homoeologues. For instance, a global analysis of the regulation of AS in diploid grass and polyploid wheat grains revealed diversity in AS events not only between

the endosperm, pericarp and embryo overdevelopment, but also between sub-genomes (Gao et al., 2021).

## 1.3 Wheat and Food Security

The 1996 World Food Summit defines Food Security as “a condition existing when everyone has physical and economic access to sufficient, safe and nutritious food which meets their dietary needs for a healthy life” (World Food Summit, 1996). Over the 21st century, the Food system has been jeopardized by diverse drivers, namely demographic (growing population), ecological (climate change), economic and political (access, availability, utilization, stability of resources), which are all primarily sustained by crop production. Crop production is reliant on weather which can be unpredictable, most often associated with abiotic stress (increasing temperatures) and with more severe and frequent extreme weather events (e.g., droughts, floods, soil degradation) and changing agro-ecological conditions (e.g., declining land and water availability, crop seasons), but also with biotic stresses such as insects (Challinor et al., 2014; Deutsch et al., 2018). During the past century, an increasing pressure on food production and distribution, especially grains such as wheat, rice, and maize, has further led to the disruption of environmental resilience and narrowed the genetic diversity and adaptability of crop species. As consequence, future investments in cereal research are encouraged.

Wheat is the principal staple crop for an estimated 35% of the world population (IDRC 2010 - Miller, 2010). More than two-thirds of global wheat is used for food and one fifth is used for livestock feed. Wheat provides a national average of around 500 kcal of food energy and protein intake per capita per day (Acquino et al., 2009). Investments in novel wheat varieties resistant to diseases and pests, adapted to warmer temperatures, and which meet a sustainable intensification are suggested as strategies to improve global Food Security (Shiferaw et al., 2011).

Beyond its economic impact, wheat, as an allopolyploid, represents an excellent model organism for the study of chromosome pairing in allopolyploid during meiosis. The most common forms of domesticated wheat are tetraploid durum wheat (*Triticum turgidum* ssp. *durum* L.) and hexaploid bread wheat (*Triticum aestivum* L.). *Triticum aestivum* originated 500,000 years ago from the interspecific hybridization of two diploid

species, *T. urartu* (AA) and an unknown *Aegilops speltoides* species (BB), generating a tetraploid wheat (*T. dicoccoides*;  $2n = 4x = 24$ ; AABB), followed by domestication into *T. dicoccum* and *T. turgidum*. Later on, 10,000 years ago, *T. turgidum* hybridized with *A. tauschii* (DD), forming the allohexaploid wheat ( $2n = 6x = 42$ ; AABBDD (Matsuoka, 2011). As a result, Tetraploid and hexaploid wheat have large genomes, 12 and 16 Gbp respectively, which consist mostly (>85%) of repetitive elements. Typically, each gene exists as two (tetraploid wheat) or three (hexaploid wheat) copies. These closely related copies, known as homoeologous genes, are on average >95% similar across their coding regions and usually have a highly conserved gene structure (Martín et al., 2017a).

Nevertheless, the coexistence of diverged genomes is also structurally associated with ectopic non-homologous recombination (Martín et al., 2017b). As introduced earlier, wheat behaves as a diploid, with every chromosome synapsing and recombining only with its true homolog, and *Ph1* (Riley & Chapman, 1958) is the dominant locus primarily responsible for this phenotypic behaviour. *Ph1* inhibits introgression by suppressing COs between homoeologous chromosomes (Dhaliwal et al., 1977). It was first discovered by scoring the metaphase I phenotype of hexaploid wheat hybrids lacking the 5B whole chromosome, and this kind of deletion mutant was found to control correct pairing in wheat and its hybrids (Holm & Wang, 1988; Prieto et al., 2005). Wheat and wild relative hybrids have been widely used in breeding programs to introduce superior traits into wheat. Hybridisation between wheat and wild relatives (for example, rye or *Aegilops variabilis*) produces interspecific hybrids, containing haploid sets of wheat and wild relative homoeologous chromosomes, but exhibiting virtually no COs during meiosis. Thus, successful introgression is limited by the low frequency of homoeologous CO between wheat and wild relative chromosomes. However, in *Ph1* deleted wheat-rye hybrids, an average of 7 COs per cell is observed (Sears, 1977). Since the historical *Ph1* deletion mutant in Chinese Spring was CS *ph1b* (Sears, 1977), further deletion mutants of the *Ph1* locus characterised by reduced homologous COs and increased homoeologous recombination events at meiotic metaphase I were subsequently created and studied (Roberts et al., 1999; Al-Kaff et al., 2008; Martín et al., 2014; King et al., 2017).

In addition, as in most crop species, in polyploid wheat the extremely low frequency and uneven distribution of meiotic recombination events along chromosomes (Mercier et al., 2015) hampers opportunities for plant breeders to break linkage drag and exploit the

desired pool of genes. The combination of these factors has, for a long time, restricted the development of genomics tools in wheat and other crops with large genomes (Svačina et al., 2020). Recent advances in sequencing technologies and bioinformatics tools have aided to overcome these difficulties, and there are now a wide range of resources available for genomic analysis in wheat, including high-throughput genotyping, genome editing and genomic selection (Borrill et al., 2019). The speed of wheat research has also been limited by its relatively long generation time, which ranges from four to six months depending on the requirement of cold periods (vernalisation) to induce flowering. Again, recent advances in the use of controlled growth conditions, such as speed breeding, have radically changed these timeframes (Watson et al., 2018). Speed breeding can achieve up to 6 generations per year for spring wheat (*T. aestivum*) and durum wheat (*T. durum*). The use of supplemental lighting in a glasshouse environment and light-emitting diode (LED) supplemental lighting allows rapid generation cycling through single seed descent and potential for adaptation to larger-scale crop improvement programs, saving costs (Watson et al., 2018). Wheat has now become a tractable system for translational, comparative and functional genomics (Borrill et al., 2019).

## 1.4 Project Aims

The stabilization of diverged sub-genomes and the mechanism controlling inter-homolog bias in polyploid wheat was studied in the present research project through a combination of molecular, cytological and bioinformatics methodologies with the aim to obtain evidence of how meiotic recombination is established in wheat and in which ways these outcomes may be potentially served for breeding purposes.

**Aim 1:** Determine the relative sub-genome expression contribution of two SC genes, *ASY1* and *ZYP1*, in both meiotic and non-meiotic tissues in hexaploid *Triticum* cultivars. Once the transcript level was determined via cloning, sequencing and qPCR assays, the incidence of alternative spliced isoforms within the coding regions and untranslated regions of reproductive tissues and their gene regulatory sequences were examined.

**Aim 2:** Determine the meiotic role of the target SC genes (*ASY1* and *ZYP1*) by identifying and validating novel *asy1* and *zyp1* TILLING mutant lines for individual sub-genome. To uncover the possible association between *ASY1* and *ZYP1* with SC assembly and chiasma frequency and distribution, cytological analysis of chromosome

configuration and monitoring of SC dynamics from male meiocytes in *asy1* and *zyp1* single knockout lines during prophase I were carried out. CO markers detected via fluorescent microscopy were used to evaluate this possibility. Specifically, in respect to ASY1, to confirm the *ph1b* phenocopy (homoeologues recombination) obtained with previous *TaASY1* RNAi knockdown lines (reduced expression) (Boden et al., 2009), the initial cytological characterization of the *asy1* single knockout mutants was accompanied by the generation of a full knock-out gene by crossing individual TILLING lines. Regarding ZYP1, the absence of a functional study of this protein in wheat and the evidence of a putative role in Class ICO and the non-random CO distribution from closely related species such as barley (Barakate et al 2014), led to the hypothesis of a conserved role of ZYP1 in wheat, which was elucidated in detail here identifying and crossing uncharacterized TILLING lines.

**Aim 3:** The search for putative central element proteins in polyploid wheat was performed using the wheat co-expression network data (Alabdullah et al., 2019) coupled with a comparative analysis of known orthologues from model organisms via bioinformatics sources. This was followed by a cytological approach intended to verify the meiotic function of the selected wheat CE candidates.

**Aim 4:** Develop a protocol for employing FISH-based single copy oligo-probes capable of discriminating individual wheat chromosomes for karyotyping *Triticum aestivum* and for the study of chromosome pairing in polyploid wheat.

# **Chapter 2**

## **Investigating the gene regulatory sequences, splice variants and the meiotic function of wheat ASY1**

### **2.1 Introduction**

In *Triticum aestivum*, the ASY1 protein is a component of the meiotic chromosome axis, highly expressed in anthers at prophase I of meiosis (Boden et al., 2007). *TaASY1* possesses an open reading frame of 1764 bp, which encodes a predicted protein of 588 amino amino acids (MW 66.3 kDa) (Boden et al., 2007). Wheat ASY1 shares significant sequence similarity to PAIR2 from *Oryza sativa* (80%), ASY1 from *Arabidopsis thaliana* (53.8%) and *Brassica oleacea* (51.2%), and to a lesser extent, HOP1 from yeast (*ScHOP1* 16.5%), HIM3 from *C. elegans* and HORMAD1/2 from mouse (Zetka et al., 1999; Nonomura et al., 2006; Boden et al., 2007; Wojtasz et al., 2009; Caryl et al., 2003). Crucially, it contains a conserved N-terminal HORMA domain, whose level of identity between the HORMA domains from *TaASY1* compared to *OsPAIR2*, *AtASY1*, *BoASY1* and *ScHOP1* are significant (Boden et al., 2007). Furthermore, *TaASY1* is composed of 22 exons and 21 introns and is greater than 6.5 Kb in length. Southern blot analysis in hexaploid wheat has shown that *TaASY1* is mapped to chromosomes of Group 5 with a single copy of this gene on each of the three sub-genomes A, B and D (Boden et al., 2007). Interestingly, the rice orthologue, PAIR2, is mapped to Chromosome 9, and the long arm of rice 9 shows conservation of gene order with wheat chromosome Group 5. Wheat ASY1 lacks the Zinc finger motif present in HOP1, but carries a SWIRM domain (SWI3, RSC8 and MOIRA), a small alpha-helical domain of about 85 amino acid residues, containing a helix-turn helix motif that may bind to DNA. This is also found in many chromosomal proteins involved in chromatin modification or remodelling (Qian et al., 2005). Recently, super-resolution 3D Structured Illumination Microscopy (3D-SIM) analysis revealed that in wheat and barley, ASY1 play a major role in chromosome axis remodelling during meiosis I (Colas et al., 2017). Further details are discussed below.

In hexaploid wheat, the first attempt to understand the role of *TaASY1* relied on RNAi knockdown lines (Boden et al., 2009), where the reduced expression of *TaASY1* generated

high levels of multiple chromosome associations at metaphase I, implying homoeologues recombination at the expense of homologous association (Boden et al., 2009), representing a phenocopy of wheat chromosome pairing *ph1b* (Sears, 1977). Nevertheless, how homoeologous interactions were excluded from the meiotic recombination pathway in wild-type polyploid wheat and whether *TaASY1* may represent a true candidate for *Ph1* locus, remains unsolved.

Crucially, when a gene is knocked-down, a residual level of its product may still be retained. Therefore, the persistence of the *TaASY1* protein in RNAi lines, whilst at lower levels, may limit complete understanding of its function. This was suspected in *Taasy1* RNAi lines by Boden et al. (2009), where the remaining *TaASY1* protein immuno-detected in the mutants perhaps allowed a partial stabilization of the chromosome axis, buffering the phenotype effect of the mutation. Hence, to definitively characterize the biological function of *TaASY1*, a cytological assessment of a complete removal of the protein was evaluated as an alternative approach in this work.

The use of the recent advances in wheat genetic resources, particularly the availability of the TILLING EMS mutant collection, allowed the identification of novel *asy1* mutant lines (Uauy et al., 2009; Krasileva et al., 2017). Here, the genotype of *asy1* single knock-out mutant plants was confirmed by PCR and Sanger sequencing and an *asy1* full knock-out was achieved by crossing homozygous plants for single allele mutation. Chromosome configuration and SC protein dynamics of mutant male meiocytes during prophase I were investigated with microscopy and immuno-cytological techniques in both *asy1* single and complete knock-out plants.

Prior to the cytological analysis of the selected *asy1* TILLING lines, this project first intended to elucidate the relative gene expression level among the *TaASY1* homoeologues during meiosis. As previously mentioned, the co-existence of diverged sub-genomes in polyploid wheat, is not obvious (Svačina et al., 2020). The stabilization process following the wheat polyploidization may have led to modifications in the expression of *TaASY1* homoeologues during meiosis. Therefore, an initial examination of this process was accomplished by comparing patterns of expression in somatic and meiotic tissues through the combination of cloning and sequencing strategies.

The occurrence of alternative splicing was hypothesised to be one mechanism to strictly control the transcript level of *TaASY1* and related meiotic recombination processes. In this respect, evidence from yeast and mammal models support high levels of male germline spliced variants, proposed to modulate trans-meiotic differentiation (Schmid et al., 2013; Juneau et al., 2007; Naro et al., 2017). Therefore, to assess the incidence of alternative spliced isoforms in polyploid wheat during meiosis, the full length of *TaASY1*, including the UTRs, were cloned and the expression of transcript variants were examined within reproductive tissues of polyploid wheat cultivars. Different molecular methods and data are compared and discussed herein.

## 2.2 Materials and methods

### 2.2.1 Plant materials and greenhouse conditions

Kronos and Cadenza wild type and TILLING mutant seeds ‘K0706’, ‘K0157’ and ‘K2071’ (see paragraph 2.2.9) were sown in 3 cm<sup>2</sup> welled trays and transferred to 9 cm<sup>2</sup> pots once germinated. Plants were grown in soil-based compost (Levington Advance Pot and Bedding M1 Compost) under greenhouse conditions with photoperiod of 16h days light cycle at constant temperature of 22°C (day)/16°C (night), and relative humidity ~60%. Plants were monitored daily and watered regularly.

### 2.2.2 Amplification of *TaASY1*

The *Triticum aestivum* genome assembly initially used was TGACv1 (The Genome Analysis Centre) (Kersey et al., 2018), which was built on the landrace Chinese Spring, and hosted on public domain database Ensembl Plants (EMBL-EBI) (<http://plants.ensembl.org>). *TaASY1* nucleotide reference sequences were therefore downloaded from Ensembl Plants under the accession numbers:

TRIAE\_CS42\_5AL\_TGACv1\_376268\_AA1234690

TRIAE\_CS42\_5BL\_TGACv1\_405487\_AA1328460

TRIAE\_CS42\_5DL\_TGACv1\_434593\_AA1438460

Primer pairs used for the amplification of *TaASY1* genes were designed by aligning the reference sequences of *T. aestivum* ‘Chinese Spring’ using Omega Clustal W. Total RNA was extracted from hexaploid wheat *T. aestivum* cv. Cadenza and Apogee inflorescences

at meiosis stage (6-7 weeks old) and flag leaf Zadoks' stage 11 (Zadoks et al., 1974) using ISOLATE II RNA Mini Kit (catalog number 52071; Bioline). cDNA synthesis protocol was followed using Tetro cDNA Synthesis Kit (catalog number: 65042; Bioline), and the product was quantified using Nanodrop 2000. Following cDNA synthesis, polymerase chain reactions (PCR) were performed using RedTaq (catalog number 21108; Bioline). Reaction mixture (20 $\mu$ l) contained 10  $\mu$ l of 10X RedMix (*Taq* polymerase), 1  $\mu$ l of 10  $\mu$ M forward primer, 1  $\mu$ l of 10  $\mu$ M reverse primer and 1  $\mu$ l of 1ng – 1 $\mu$ g cDNA template and 8  $\mu$ l deionised water. Oligonucleotides used for the isolation of *TaASY1* were:

TaASY1cDNAF = 5'-CCTATTCCCTGAGAAGTAC-3'

TaASY1cDNAR = 5'-TCACTGAAGACATGGCAATT-3'

The reaction was initiated with a denaturation step at 93°C for 2 minutes, followed by 35 cycles of 93°C for 30 seconds, annealing at 58°C for 45 seconds, with one cycle of 72°C for 3 minutes, and a final extension at 72°C for 10 minutes. Post PCR reactions were analysed by gel electrophoresis (1% agarose gel) and visualised using ethidium bromide and a UV transilluminator.

### 2.2.3 Proteomic validation of *TaASY1* protein

Western blot analysis of wheat *TaASY1* protein was conducted on wild type *T. aestivum* cv. Cadenza. Firstly, Bradford assays were conducted to determine protein concentration for the equal loading of protein samples destined for Western analysis. Quadruplicates of Bovine Serum Albumin (BSA) dilution series were prepared with concentrations of 0, 10, 50, 100 $\mu$ g BSA using Bio-Rad Protein Assay Standard II, lyophilised BSA, diluted in sterile deionised water. 200 $\mu$ l of Bradford reagent (Bio-Rad) was added to 800 $\mu$ l of each sample of the dilution series and incubated for 5 minutes at room temperature. All protein samples were isolated from fresh anthers in presence of IP-non-denaturing buffer (Table 2.1) and then quantified using a spectrophotometer at an absorbance wavelength of 595 nm. Values obtained for both the standard and protein samples were used to generate a standard curve, with the prediction of the concentration of the protein samples based on their recorded absorbance readings: 1) 0  $\mu$ g, 2) 1.115 Abs = 10 $\mu$ g, 3) 1.823 Abs= 50 $\mu$ g, 4) 1.979 Abs= 100 $\mu$ g.

Subsequently, protein samples were prepared for electrophoresis in reactions containing the same concentration of proteins (50  $\mu$ g) with Final Sample Buffer (Table 2.2). For this

analysis, proteins were extracted from fresh anthers (n=10) at zygotene stage (typically 0.8mm). The anthers (100mg approximately) were treated with 100 $\mu$ l Final Sample Buffer (0.5M Tris pH 6.8, 2% SDS, 10% Glycerol,  $\beta$ -mercaptoethanol, 0.001% Bromophenol blue, 1 tablet of phosphatase inhibitors cOmplete EDTA-free (Roche)), ground in 1.5ml tube using a yellow tip to lyse the cell walls and then denatured at 99°C for 10 minutes. The sample were then centrifuged at 16,000 g for 30 seconds to pellet the insoluble debris before loading 35 $\mu$ l of sample for SDS PAGE (according to the Bio-Rad manual, with conditions as follows: 50V for 10 minutes, 100V (stacking gel) for 20 minutes and 200V (resolving gel) for ~60 minutes).

Upon completion of migration, proteins were transferred to a 0.22  $\mu$ m immunoblot nitrocellulose membrane (BioRad) and fixed in methanol for 15 seconds, then placed in a container with transfer buffer. Eight sheets of Whatman paper (Fisher Scientific) were cut to the size of the membrane and soaked in transfer buffer for two minutes. The gel was briefly rinsed with distilled water before being transferred to the electroblotting apparatus, set to run at 100V for 1 hour and 15 minutes. After that, one gel was stained in 0.1% Brilliant Blue R250 (Sigma) with gentle agitation at room temperature for 1 hour, which was followed by a de-stain treatment in a fixing solution of 20% methanol, 7% glacial acetic acid diluted in sterile deionised water; the second gel was placed in a tray containing cold transfer buffer (25mM Tris-Base pH 8.5, 0.2M Glycine, 20% Methanol) and the immunoblot nitrocellulose membrane (BioRad) for 10 minutes. The proteins were run for 1 hour at constant ~400 mA.

Once electroblotting was completed, the membrane was immediately immersed and incubated in blocking solution, 5% skimmed milk powder w/v in 1X PBS/Tween20 (0.1% Tween20) (Table 2.3) at 4°C overnight with gentle agitation on rocker. Afterwards, primary antibody incubations were conducted in 10ml of 1:5000 dilution of primary antibodies in blocking solution. The ASY1 guinea pig polyclonal primary antibody raised against the wheat *TaASY1* HORMA domain (Desjardins et al., 2020b) was used. Membrane was sealed on a plastic container with the primary antibody and allowed to incubate at room temperature for 60 minutes with gentle agitation. Washing with 1X PBS/Tween20 was following performed 3 times for 5 minutes each with gentle agitation. The secondary IgG antibody, a goat anti-guinea pig Horseradish Peroxidase (HRP) conjugated (ab6908), was then added at a 1:2000 dilution in blocking solution and left to

incubate at room temperature for 60 minutes with gentle agitation. Washing with 1X PBS/Tween20 was following performed 3 times for 5 minutes each with gentle agitation. Detection for western was carried out using EZ-ECL kit (abcam), applied onto the membrane for 2 to 5 minutes and the outcomes were acquired by SynGene (geneflow) machine.

<b>IP-buffer (non-denaturing)</b>	<b>stock concentration</b>	<b>200ml</b>	<b>10ml</b>	<b>MW</b>
20 mM Tris-HCl, pH 7.5	1 M	4 ml	0.02g	121
150 mM NaCl	5 M	6 ml	0.09g	58
10% glycerol	87%	23 ml	1.5ml	-
2 mM EDTA	0.5 M	0.8 ml	0.007g	372

**Table 2.1 Solutions for Bradford Assay.**

<b>4X Final Sample Buffer</b>	<b>V=8ml</b>
0.5M Tris pH=6.8	0.5ml
10% SDS	1.6ml
Glycerol	0.8ml
B-mercaptoethanol	0.4ml
0.05% Bromophenol blue	0.004g
ddH <sub>2</sub> O	4.5ml
add 1 tablet cOmplete EDTA-free (Roche)	
<b>10% resolving gel V=15ml for 2gels</b>	<b>10% stacking gel V=10ml for 2 gels</b>
Water 6.1ml	Water 6.1ml
Tris-HCl 3.75ml	Res-HCl 2.5ml
10% SDS 0.150ml	10% SDS 0.100ml
Acrylamide 5.0ml	Acrylamide 1.2ml
15% APS 0.075ml	15% APS 0.050ml
TEMED 0.015ml	TEMED 0.010ml
<b>Coomassie stain</b>	<b>V=200ml</b>
0.1% Brilliant Blue R250	0.2g

45% Methanol	90ml
45% Glacial acetic acid	90ml
ddH <sub>2</sub> O	20ml
<b>De-stain</b>	V=500ml
20% Methanol	100
7% Glacial acetic acid	35
ddH <sub>2</sub> O	365
<b>1X Resolving buffer</b>	V=500ml
1.5M Tris-Base pH=8.8	90g
ddH <sub>2</sub> O	Up to V
<b>1X Stacking buffer</b>	V=500ml
0.5M Tris-Base pH=6.8	30g
ddH <sub>2</sub> O	Up to V
<b>5X Running buffer</b>	V=800ml
1.5% Tris-Base pH=8.3	12g
7.2% Glycine	57.6g
0.5% SDS	4.0g
<b>Transfer buffer</b>	V=1L
25mM Tris-Base pH=8.5	3g
0.2M Glycine	15g
20% Methanol	200ml

**Table 2.2 Solution for SDS-PAGE.**

<b>Phosphate-buffered saline (1X PBS)</b>	<b>V = 500ml</b>
PBS (100X)	10 preprepared tablets
ddH <sub>2</sub> O	499.5ml

<b>PBS-T</b>	V= 500ml
1X PBS	499.5ml
0.1% Tween20	0.5ml
<b>Blocking solution</b>	V= 10ml
1X PBS	10ml
5% Bovine Serum Albumen (BSA)	0.5g
<b>Primary antibodies</b>	V= 10ml
Anti-ASY1 guinea pig	1:5000 dilution
Anti-ZYP1 rabbit	1:5000 dilution
Blocking solution	0.998ml
<b>Secondary antibodies</b>	V= 10ml
Goat anti-guinea pig Alexa Fluor 488	1:2000 dilution
Goat anti-rabbit Texas Red 568	1:2000 dilution
Blocking solution	0.998ml

**Table 2.3 Solution for Western Blot.**

#### 2.2.4 Cloning the full length coding region of *TaASY1*

To obtain the full length of *TaASY1* genes, PCR was performed on synthesised cDNA using Q5® High-Fidelity DNA Proofreading Polymerase (catalog number M0491; NEB) with the following primer set:

ASY1cDNAF1 = 5'-ATGGCTCAGAACGACGAAGGA-3'

ASY1cDNAR1 = 5'-CTTGAAACTTGTGAAGATAG-3'

Reaction mixture (25 µl) contained 5 µl of 5X Q5 Reaction Buffer, 0.5 µl of 10 mM dNTPs, 1.25 µl of 10 µM Forward Primer, 1.25 µl of 10 µM Reverse Primer, 1 µl of DNA Template, 0.25 µl of Q5 High-Fidelity DNA Polymerase, 5 µl of 5X Q5 High GC Enhancer and 10.75 µl of Nuclease-Free Water. The reaction was initiated with a denaturation step at 98°C for 2 minutes, followed by 35 cycles of 98°C for 10 seconds, annealing at 58°C for 45 seconds, one cycle of 72°C for 3 minutes, with a final extension

at 72°C for 10 minutes. Post PCR reactions were analysed by gel electrophoresis (1% agarose gel) and visualised using ethidium bromide and a UV transilluminator.

Subsequently, PCR amplicons were ligated into pDrive vector with PCR Cloning Kit (catalog number: 231122; Qiagen). Ligation reaction was left in water bath (~16°C) overnight. Transformation was performed with ligation mixture and *E. coli* strain DH5α competent cells by following standard transformation protocol (catalog number: 18263-012; Life Technologies) with minor variations, e.g. 4 µl of ligation mixture was added to competent cells, instead of 1µl as per the protocol.

Transformed cells were selected for culturing in ~5ml liquid LB broth with agar (Lennox) (15g/L Agar, 10g/L Tryptone, 5 g/L Yeast Extract, 5 g/L NaCl) containing ampicillin (100 µg/ml) as a selective agent. An additional selection reagent was added, including 5-bromo-4-chloro-3-indolyl-β-D-galactopyrano-side (X-gal, 50 µl of 40mg/ml X-gal in dimethyl formamide), which allowed for blue/white selection of colonies that contained pDrive vector and the respective coding sequence insert. Cells were left to grow in an orbital shaker at 200 rpm (37°C) overnight. After that, selected white colonies were plated out onto agar plates and left overnight at 37°C. The cultures were used for plasmid extraction following protocol in Plasmid DNA Mini Kit (catalog number: D6942-00; Omega Biotek). Extracted DNA was quantified using Nanodrop 2000 (Thermo Scientific) and Sanger sequenced by Eurofins GATC Biotech Company using the M13F primer 5'-CAGGAAACAGCTATGAC-3' for the full length *TaASY1* genes. Returned sequences were compared to the *in silico* obtained sequencing using Basic Local Alignment Search Tool (BLAST, NCBI) for determining orthologous sequence similarity.

Coding region sequences of individual homoeologous gene were analysed using Clustal Omega (EMBL-EBI) (Sievers et al., 2011), while ExPASy (SIB) (Gasteiger et al., 2003) was used to translate wheat nucleotide sequences. Using the predicted translation of the open reading frame for each of the three genes, the ExPasy Translate Tool website was utilised to identify amino acids. When the reference genome sequence of hexaploid wheat landrace Chinese Spring with 21 chromosomal assembly and gene was presented by IWGSC annotation [International Wheat Genome Sequencing Consortium (IWGSC) v1.0] (Appels et al., 2018), the updated accession number TraesCS5A02G286500, TraesCS5B02G285800 and TraesCS5D02G294100 retrieved from public domain database Ensembl Plants (EMBL-EBI) were later used to analyse the predicted alternative isoforms.

### 2.2.5 Validation of *TaASY1* fragment insertion via colony PCR

White colonies were screened via colony PCR for the presence of the coding sequences of each *TaASY1* homoeologous (from independent transformation reactions). Sub-genome specific oligonucleotides used for the isolation of the *TaASY1-5B* were:

ASY1B\_F = 5'-GCAGAAGTCACTCCTGAC-3'

ASY1B\_R = 5'-TCAGATAACTGACCAGG-3'

Each colony PCR mixture (20 µl) contained 10 µl of 2X RedMix (Bioline), 1 µl of 10 µM forward primer, 1 µl of 10 µM reverse primer and 8 µl deionised water. Using a sterile pipette tip, individual white colonies were selected from plates and dipped into single 20 µl PCR mixture before being placed into 5 ml liquid aliquots of LB/Ampicillin (100 µg/ml as selective agent) for overnight growth and generation of stocks.

PCR was initiated with a denaturation step at 93°C for 5 minutes, followed by 35 cycles of 93°C for 30 seconds, annealing at 58°C for 45 seconds, single cycle of 72°C for 3 minutes, with a final extension at 72°C for 10 minutes. Post PCR reactions were analysed by gel electrophoresis (1% w/v agarose gel) and visualised using ethidium bromide and a UV transilluminator. Plasmid DNA was isolated from positive liquid cell cultures as mentioned previously with Plasmid DNA Mini Kit (catalog number: D6942-00; Omega Bioteck), to provide a template for sequencing reactions and analysis of the coding regions of the target genes. The reference nucleotide sequences (Chinese Spring) retrieved from Ensembl Plants (<https://plants.ensembl.org/index.html>) were aligned with the clones. Omega Clustal W (<https://www.ebi.ac.uk/Tools/msa/clustalo/>) was used as a tool for the comparison alignment of nucleotide sequences of the gene of interest. The Neighbour-joining phylogenetic trees generated as output from a multiple sequence alignment, allowed the identification of the sub-genome origin.

### 2.2.6 Testing the efficiency of the designed *TaASY1* pyrosequencing primers

Total RNA was extracted from hexaploid *Triticum aestivum* cv. Cadenza inflorescence using isolate II RNA mini kit (Bioline) and cDNA was synthesised with the Tetro cDNA synthesis kit (Bioline). The coding region sequences of each sub-genome were aligned by Omega Clustal W software. The sequencing primers were positioned within a short sequence (> 200 bps) flanked by a single SNP that discriminates the distinct

homoeologues (e.g. A vs B+D, B vs A+D and D vs A+B). Primer pairs that are consensus between the different copies were designed using PyroMark Assay Design Software 2.0 (Qiagen, INRA). Pyrosequencing assay was developed by the PyroMark Analysis Software (Qiagen, INRA). The high scoring primer combinations that were developed for amplification of *TaASY1* homoeologues were validated by gradient PCRs using RedTaq (catalog number 21108; Bioline). The reaction was initiated with a denaturation step at 93°C for 2 minutes, followed by 40 cycles of 93°C for 20 seconds,  $\Delta T_m$  between 58°C-70°C for 45 seconds for each primer set (Table 2.4), a single cycle at 72°C for 30 seconds, and a final extension at 72°C for 60 seconds. Once the optimal annealing temperature for each primer combination was defined, the fragments were then PCR-amplified in a final reaction volume of 20  $\mu$ L and check off target amplifications, applying the above mentioned cycling conditions. Generated amplicons were visualized on 2% agarose gel that was subjected to electrophoresis at 100 V for 60 minutes, using a low molecular weight DNA ladder (NEB #B7025).

<b>Primer sets</b>	<b>Oligonucleotide sequence 5' → 3'</b>	<b>T<sub>a</sub> (°C)</b>	<b>Size (bp)</b>
ASY1 A+B vs D_F	ATGCCCATGGATGCTGAAT	66	106
ASY1 A+B vs D_R	TATGTGAGAAGGAGGAAGGCC		
ASY1 A+D vs B_F	ACGCACTTCCAATGGATTATGTGA	67	67
ASY1 A+D vs B_R	TTCAGGGCAAGCTTGATGG		
ASY1 B+D vs A_F	AGCTACCCAACACAAACGG	64	55
ASY1 B+D vs A_R	AACATGAGTCGCACAGGGA		

**Table 2.4 Sub-genome specific primer sets for qPCR.**

## 2.2.7 Quantitative PCR (qPCR) of *TaASY1* homoeologues

The experimental conditions set up to measure *TaASY1* homoeologous expression levels were:

- 1 experimental factor = hexaploid WT *T. aestivum* cv. Cadenza
- 3 conditions = sub-genome specific primer sets (A+B vs D, A+D vs B, B+D vs A)
- 4 biological samples = four cDNA synthesised from total RNA four Cadenza WT individuals

- 3 biological replicates = three replicates each cDNA sample ( $3 \times 4 = 12$  samples)

The reaction mix based on standard volume of 20 $\mu$ l included 10 $\mu$ l of 2X SensiFAST SYBR® No-ROX (Bioline, BIO-98020), 0.8 $\mu$ l each of 10 $\mu$ M forward and reverse primers (Table 2.4), 1 $\mu$ l of cDNA template and water up to volume. The reaction was suitable for the 3-step cycling, consisted in an initial denaturing cycle at 95°C for 2 minutes, followed by forty cycles of 95°C for 5 seconds with annealing occurring at 60°C for 10 seconds; final extension was set at 72°C for 15 seconds.

## Statistics

The Ct means (Cycle of threshold = expression intensity) of 3 technical replicate values from the 4 independent cDNA biological samples of each sub-genome specific primer set were calculated and normalized to eliminate technical variability between experiments. Differential expression among the homoeologues was quantified comparing the normalized Ct values ( $\Delta Ct$ ) of all independent biological sample (cDNA) means between the biological conditions (sub-genomes) and standard deviation, by selecting individual sub-genome as reference. The expression ratio, known as fold change ( $2^{-\Delta Ct}$ ), was also determined for statistics significance.

### 2.2.8 Cloning the untranslated regions (UTRs) of *TtASY1*

Total RNA of tetraploid *T. turgidum* cv. Kronos was isolated from manually dissected ovaries and anthers, reverse transcribed to single-strand cDNA with the GeneRacer kit (Invitrogen). The 5' and 3' ends of *TaASY1* cDNA were amplified by PCR utilising Platinum Taq DNA Polymerase High Fidelity (Thermo Fisher Scientific) in accordance with the GeneRacer kit manual (Invitrogen). cDNA synthesis was primed using the GeneRacer® Oligo dT primer which includes the oligo dT sequence and target sequences for the GeneRacer® 3' along with the 5' Primers and the GeneRacer® 3' and 5' Nested Primers.

The first reaction used the following external primers to amplify the 5' UTR:

ASY1utrR1 5' = 5'-GGACCCAAGCAGGACTCCCACAAGCAA-3'

GeneRacer™ 5' = 5'-GCACGAGGACACTGACATGGACTGA-3'

An aliquot of this reaction was used as a template in the second PCR with specific nested oligonucleotides previously designed to amplify the 5' UTR, which are:

ASY1utrR2 5' Nested = 5'-CCCTGTGCGACTCATGTTCATTGCAA-3'

GeneRacer<sup>TM</sup> 5' Nested = 5'-GGACACTGACATGGACTGAAGGAGTA-3'

Similarly, to amplify the 3' UTR, the following primers were used during the first reaction:

ASY1utrF2 3' = 5'-GCAGGTCAAGCGCCAGAAGTCCTA-3'

GeneRacer<sup>TM</sup> 3' = 5'-GCTGTCAACGATACTGCTACGTAACG-3'

Primers used in the second cycle were:

ASY1utrF1 3' Nested = 5'-GGACCCAAGCAGGACTCCCACAAGCAA-3'

GeneRacer<sup>TM</sup> 3' Nested = 5'-CGCTACGTAACGGCATGACAGTG-3'

Cycling conditions were in accordance to the manufacturer's instruction, with minor modifications: annealing temperature at 68°C with extension time of 30 seconds for the first reaction and annealing temperature at 65°C with extension time of 30 seconds for Nested PCR. Amplicons were purified using E.Z.N.A.<sup>®</sup> Cycle Pure Kit (Omega Bio-tek). Sanger sequencing was performed by Eurofins GATC Biotech Company. Omega Clustal W was used for the comparison alignment of nucleotide sequences of the gene of interest.

## 2.2.9 Identification of *asy1* TILLING lines in tetraploid and hexaploid wheat

Wheat TILLING (Targeted Induced Local Lesions In Genomes) lines [*Triticum turgidum durum* cv. Kronos (2n=4x=14) and cv. Cadenza (2n=6x=21)] were screened by BLAST search on Wheat TILLING database (<http://www.wheat-tilling.com/>) (Krasileva et al., 2017). Accession number TraesCS5A02G092700 (*TtASY1-5A*) and TraesCS5B02G045200 (*TtASY1-5B*) were used. From tetraploid cv. Kronos, three TILLING lines carrying a STOP codon mutation were identified: K0706 (*TtASY1-5A*), K0157 (*TtASY1-5B*) and K2071 (*TtASY1-5B*); from hexaploid cv. Cadenza, one EMS-induced line was selected: C0971 (*TaASY1-5B*).

K0706 has a putative mutation at the splice donor site in the codon AGG of exon 7, which should change in AGA, causing the retention of intron number 8 and the introduction of a premature STOP codon. The truncated transcript is expected to preserve the HORMA domain (residues 1-232) (Figure 2.1). K0157 has a predicted CAG to TAG mutation within exon 10, thereby resulting in a premature STOP codon, which may lead to a truncated ASY1 transcript, albeit expected to maintain the HORMA domain (Figure 2.1). Similarly, K2071 has TGG to TGA mutation in the exon 2, which is predicted to result in a premature STOP codon, and the expected product should also lose 24 amino acid

residues from the HORMA domain (Figure 2.1). Lastly, C0971 has a putative SNP that affects the first nucleotide of the 3' intron acceptor site in the **ATA** codon (exon 14), predicted to create a premature STOP codon downstream, which would be translate into a partially functional protein, consisting of HORMA and coiled coil domains, but lacking the closure-binding motif (Figure 2.1).

Seeds of the identified TILLING lines were obtained from [www.SeedStor.ac.uk](http://www.SeedStor.ac.uk) and purchased from John Innes Centre (JIC), Norwich, UK. The presence of mutations in the coding sequences was confirmed for the individual TILLING lines by Sanger-sequencing and genotyping using SNP-specific primers calibrated by gradient PCR, as described in the following paragraph.

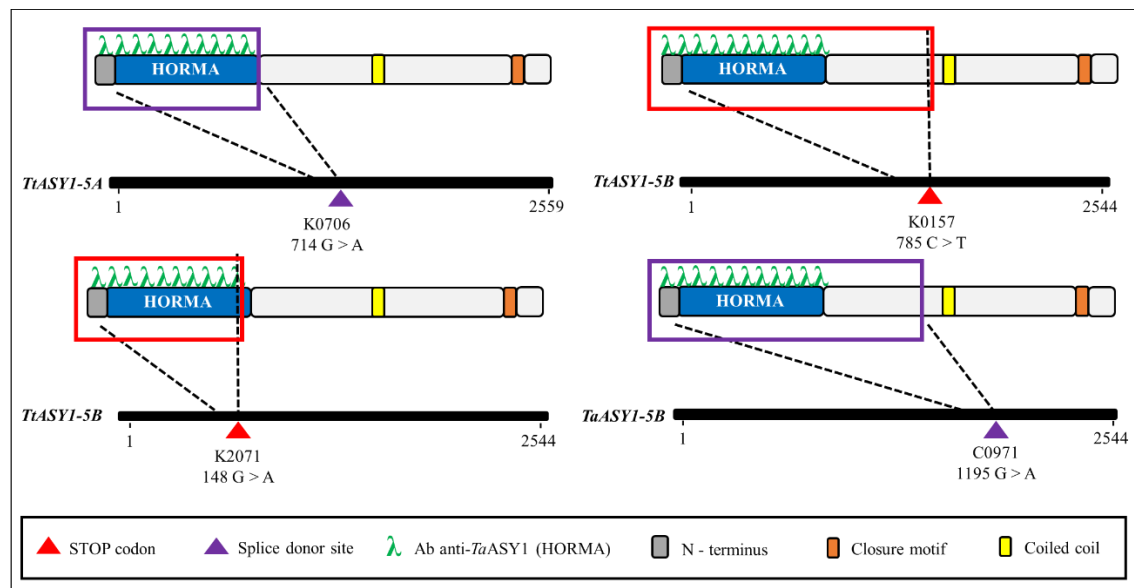


**Figure 2.1 Schematic representation of wheat *ASYI-5A* and *ASYI-5B* coding regions and altered proteins from TILLING *ASYI* lines.** Black bars depict wheat *ASYI* homoeologous genes with TILLING mutation site (SNP), nucleotide change and nucleotide position. Two lines with predicted splice donor site mutation and two lines with premature STOP codons were selected: K0706 (714 G > A, V 231 > STOP), K0157 (785 C > T, Q 307 > STOP), K2071 (148 G > A, W 156 > STOP) and C0971 (1195 G > A, P 254 > STOP). Truncated *ASYI* proteins with the HORMA domain (blue rectangle) antibodies against *TaASYI* ( $\lambda$ , in green) binding onto the N-terminus (grey rectangle), coiled coil residues (yellow) and closure motif (orange) are represented above each gene (rectangular inserts). Legend is located at the bottom.

## 2.2.10 Genotype screening of Kronos and Cadenza Parental (P) mutants

Total genomic DNA was isolated from *T. turgidum* cv. Kronos and cv. Cadenza flag leaf tissue (~500mg) at GS11 stage (Zadoks et al., 1974) using DNeasy® Plant Mini Kit (catalog number 69104; Qiagen) and DNA concentration was quantified using Nanodrop 2000 (Thermo Scientific). Gradient PCR was used to calculate the  $\Delta T_m$  of designed TILLING line genomic primers on wild-type Kronos (Table 2.5); 0.5 $\mu$ l of each genomic forward and reverse primer was used. PCR cycle: denaturation at 94°C for 30 seconds; annealing at 45°C-65°C for 45 seconds for Kronos *asy1* mutants and 60°C-68°C for 45 seconds for Cadenza *asy1* mutant; extension at 72°C for 40 seconds; 35 cycles. Subsequently constant PCR at optimum annealing temperatures carried out for each mutant: annealing at 48.5°C, 59°C, 54° and 60°C for K0706, K0157, K2071 and C0971 respectively; Wild-type Kronos A and B were used as controls.

The DNA concentration was quantified using Nanodrop 2000 (Thermo Scientific). Amplicons were then purified using E.Z.N.A.® Cycle Pure Kit (Omega Bio-tek). Where necessary, gel extractions were performed by cutting the correctly sized band out of the agarose gel (using a blue light box) and gel excisions were purified using the Gel Extraction Kit (Monarch). Ligations were performed into the pDrive vector (Qiagen), using Qiagen PCR cloning kit (incubated overnight at 16°C). Transformations were performed into DH5 $\alpha$  competent *E. coli* cells (Thermo Fisher Scientific). Plasmid extractions were performed using the E.Z.N.A. Plasmid Mini-Kit I (Omega Bio-tek). Sanger sequencing using forward genomic primer of corresponding genes (Table 2.5) was performed by Eurofins Genomics, GATC Lightrun Sequencing services. Screening of SNP (point mutation induced by EMS treatment) in the sequence was detected using Chromas Lite 2.0 and Clustal Omega (EMBL-EBI).

<b>Subgenome Specific Primers</b>	<b>Oligonucleotide sequence 5' → 3'</b>
ASY1gDNAaF	GCTGTTCTGATTCTGTCAC
ASY1gDNA5aR	CATGGTTAGACATACTGTAT
K0706wt	GACTTTACGGACACCGAGG
K0706alt	GACTTTACGGACACCGAGA
K0706common	CGCAGATGTGGTCTATATCC
ASY1gDNA5bF3	ATGTCTGTACCGTATTTGT
ASY1gDNA5bR3	GTTTCTGGGCTGCTATTA

K0157wt	AGATGGAAATTGCAAAGGTC
K0157alt	AGATGGAAATTGCAAAGGTT
K0157common	TGTGTAAACAGACCATGC
ASY1gDNA5bF	GGCACTAGGTCAGGATCGG
ASY1gDNA5bR	ACGTGTAGCGTATTAAGTTG
K2071wt	CCAGGAGGTTGATTGATTGG
K2071alt	CCAGGAGGTTGATTGATTGA
K2071common	ATGGCCTCATAAAGTGAAGG
gASY1B_Cadenza_F	ATGCTGTTAACAAAGGTCAAG
gASY1B_Cadenza_R	GTAGCTAAGCTTCAGGG
C0971wt	GTACCGTCCTTAAACCC TTG
C0971alt	ATACCGTCCTTAAACCC TTG
C0971common	CAAGTTTCTGGGCTGCTAT

**Table 2.5 Sub-genome specific primers used to amplify *TaASY1* TILLING lines.** Genomic primers (green) were used to validate the mutation via Sanger-sequencing.

### 2.2.11 Crosses of Kronos Parental mutants

Tetraploid Kronos wheat approximately ~50cm in height at GS55 (Zadoks et al., 1974), having the head just protruding from the flag leaf were chosen for emasculation. Firstly, the anthers' developmental stage was verified. If the anthers were small and green with a tight stigma, emasculation can be performed. On the contrary, if the anthers started to become slightly yellow, hand heat could speed up their maturation with pollen spilling by the time the whole spike was being emasculated. Consequently, self-pollination may occur. Spikelets from the same inflorescence that were sterile were removed. The florets in the centre of each spikelet, which develop asynchronously to the outer florets, were also removed. The selected spikelets were emasculated by removing sepals, petals, stamen and the three anthers of each floret, using watch-makers forceps, leaving only the gynoecia.

Separate plants at GS59 (Zadoks et al., 1974), which corresponds to the complete emergence of the inflorescence from the flag leaf, were selected as male. Mature, yellow anthers were then used to pollinate the developed stigma of the emasculated spikelets by

rubbing one against the other. Spikelets with feathered stigmata, which is a too advanced stage for emasculation, were excluded from pollination. Both pollen and stigma have to reach the proper developmental stage for an efficient pollination. Stigma receptiveness can be checked daily after emasculation; it is usually mature two or three days after emasculation. A mature stigma is feathered compared to an immature one which is tightly curled up. Pollen maturity is reached when the anthers start to turn yellow and be slightly rounded.

The receptor plants were labelled with a crossing tag (genotype, date, etc.) and the emasculated ears were covered with a crossing bag to avoid any cross-pollination; pollinated donor was also bagged. Seeds from the resulting pollination were collected and subjected to PCR-based genotyping, after they turned from green to light brown, at around 4 weeks. Homozygous individuals for mutation (K0706 *asy1a* × K0157 *asy1b-1* and K0706 *asy1a* × K2071 *asy1b-2*) were crossed, while heterozygous individuals from F1 (AaBb) were self-pollinated in parallel to create an F<sub>2</sub> population segregating for the mutation (double KO aabb). A wild-type line was also included as controls.

### 2.2.12 Genotyping of F1 mutants

The genotype of Kronos F1 mutants derived from single knock-out crosses was confirmed through PCR with designed mutant primers (Table 3.1). Gradient PCR was used to identify the annealing temperature ( $\Delta T_m$ ) that the primers would no longer work to give a band on wild-type Kronos; these were 65.8°C (K0706wt and common primers), 63.9°C (K0706alt and common primers), 61.2°C (K0157wt and common primers), 64.4°C (K2071wt and common primers) and 64°C (C0971wt and common primers). Subsequently, all samples were confirmed to be homozygous/heterozygous for corresponding point mutation, using Chromas Lite 2.0 software.

### 2.2.13 Backcrosses of *asy1* Parents with tetraploid Kronos wild-type

Following the non-mendelian segregation of the F<sub>2</sub> segregants from *asy1-b1* × *asy1a* cross (K2071 × K0706 TILLING lines), one backcross with Kronos WT was performed for *asy1b-1* (K0157 line) in order to decrease the secondary mutation load.

## 2.2.14 Isolating pollen mother cells (PMCs) for metaphase I chromosome spreads

Meiotic metaphase I cells were isolated after 6-7 weeks in tetraploid *T. turgidum* cv. Kronos and after 12-13 weeks in hexaploid cv. Cadenza under these conditions. Wheat inflorescences were collected by removing the covering leaves. Immature wheat inflorescences (1.5-2.0 cm) at the booting stage GS39 (Zadoks *et al.*, 1974), ~42 days post-sowing were harvested and placed on a moist 9 cm filter paper in a 9 cm petri dish. Early anthers (0.5–1.5 mm length) from the inflorescence were dissected with watchmaker's forceps and a fine mounted needle, and placed in 1 ml of ethanol:acetic acid (3:1) fixative at room temperature. The fixative solution was replaced after 1 h and again at the end of the day for at least 3 days. The anthers were transferred to an embryo dish, the fixative was removed and the sample was washed with 1 ml of 0.01M citrate buffer (pH 4.5) 4 times for 5 minutes each. After removing the final wash, 1 ml of enzyme solution (1% w/v pectolyase, 1% w/v cellulase) was added (Table 3.2), and the sample was incubated at 37°C for 60 minutes and then the digestion was stopped by removing the enzyme solution and replacing it with 1 ml of ice-cold sterile distilled water. At this stage, the anthers were sorted by size, using a calibrated eyepiece graticule. Approximately 6 anthers of the same size were transferred onto a slide, with a minimum amount of water, and quickly macerated with a mounted needle. 10 µl of 70% acetic acid was added to the material and placed on a 45°C hot plate. The anthers were spread horizontally with a mounted needle. Another 10µl of 70% acetic acid was added and slides were left for 45 seconds. 200µl of room temperature 3:1 fixative was applied to the slide with a pipette by forming a circle around the drop of acetic acid, as the droplet is repelled by it. Another 200µl was added, this time onto the drop, and the excess was allowed to drain off the slide. Slides were then dried using a standard commercial hairdryer. Slides were stained with 10 µl DAPI (4',6-diamidino-2-phenylindole) (10ng/ml in Vectashield) and coverslips (24 x 40 mm) placed on top. Chromosome spreads were imaged from wild type (n = 50) and mutants (n = 50 each line) using Nikon NiE epifluorescence microscope in conjunction with NIS-Elements software. This protocol can be found in Desjardins *et al.*, 2020a.

## 2.2.15 Immunolocalisation of PMCs

Wheat plants going through meiosis are 5-6 weeks old in tetraploid and ~11-12 weeks in hexaploid, still containing the inflorescence in the flag sheath leaf during the wheat booting stage. A slightly swollen area (boot) indicates the position of the spike that is ~3–4.5 cm during meiosis I. For better consistency between samples, only primary tillers were used. Inflorescences were collected from mutant and wild-type plants of *Triticum durum* cv. Kronos and/or Cadenza placed in a 9 cm Ø petri dish on a piece of wet filter paper to prevent drying. Anthers from 3-4 inflorescences were dissected for each mutant using a watchmaker's forceps and a fine mounted needle under a dissecting microscope, equipped with a calibrated graticule such that 10 bars were equal to 1mm (using a ruler placed on the objective). For attaining synchronized male meiocytes from anthers in different meiotic stages, including pre-meiotic (G2) and prophase I sub-stages (leptotene, zygotene, pachytene, diplotene, diakinesis), up to 10 anthers were sorted by size using the MeioCapture method (Shunmugam et al., 2018) and immediately placed in a drop of extraction buffer on a cavity slide (Table 2.6). The anthers were cut transversely with a razor blade and the meiocytes were squeezed out with a thick mounted needle. 6 ml of water and 6 ml of digestion medium were added to digest the cell walls of the meiocytes, then incubated at 37°C for 2 min in a closed moist container to prevent drying out of cells. Material was transferred to a clean Superfrost Plus glass slide (Fisher Scientific, Suwanee, GA, USA) where 10µl of 1% Lipsol detergent was applied to degrade cell membranes and aid spreading of the cells (optimum Lipsol concentrations lie between 1 and 2%; early stages, such as G2 and leptotene, are more suited to 1.5–2%). Following, the sample was fixed by applying 20µl of 4% paraformaldehyde to the cells (pH 8.0 and stored at 4°C) under a fume hood, and leaving to dry for at least 1 hour. Paraformaldehyde was made to cover the whole surface of the material, using a pipette tip. After drying, slides were given a brief rinse in sterile, distilled water for ~two seconds, before washing 3 times in 1 x phosphate buffered saline (PBS) containing 0.1% Triton for 5 minutes per wash, at room temperature. After washing, 50µl of blocking solution (1% bovine serum albumin (BSA) in PBS) was applied to each slide, covered with a piece of Parafilm (~2cm x 3cm) and incubated at room temperature for 10 minutes. Primary antibodies were diluted in blocking solution (two antibodies per slide, mixed together with blocking solution). Specially, the ASY1 guinea pig polyclonal primary antibody raised against the wheat *TaASY1* HORMA domain, 1:500 (Desjardins et al., 2020b) and the *AtZYP1* rat or rabbit polyclonal antibody raised against *Arabidopsis*, 1:500 (Higgins et al., 2005; Osman et al., 2018) were used to localise PMCs (Table 2.7). Other antibodies and the relative dilutions

used in this project are the following: anti-rat ASY3, 1:500 (Ferdous et al., 2012a), anti-SMC3, 1:500 (Ferdous et al., 2012b) and anti-HsyH2A.X rabbit, 1:500 (Merck). Parafilm coverslips were removed from slides using watch-makers forceps and 50 $\mu$ l of primary antibody solution was applied to each slide and covered with a fresh piece of Parafilm. Slides were then incubated in a humid chamber with damp tissue paper to prevent drying out at 37°C for 30 min or overnight (approximately 15- 18 hours) at 4°C. Parafilm coverslips were then removed as before, and slides were washed in a Coplin jar in PBS containing 0.1% Triton, 2 times for 5 minutes per wash. Secondary antibodies goat anti-guinea pig conjugated to Alexafluor 488 (abcam) and/or goat anti-rabbit/rat conjugated to Texas Red 568/Cy3 594 (Vector Laboratories/ Jackson Immuno Research), were diluted in blocking solution (1:200 ratio each). 50 $\mu$ l of the secondary antibody mix was applied to the slides, and incubated in the dark, at room temperature for 30 minutes. Slides were washed another 2 times in PBS/Triton before draining and counter-staining with 10 $\mu$ l DAPI in Vectashield (10ng/ml). Coverslips (24 x 40 mm) were then placed on top and slides were viewed with a Nikon NiE epifluorescence microscope equipped with filters for DAPI, FITC and Texas Red. Meioocytes were imaged using specific exposure times from wild type ( $n = 20$ ) and mutants ( $n = 20$ ) using and processed with the public domain program NIS Element Viewer. Counts were performed using NIS software and chiasmata frequency significance ( $P_{adj} < 0.001$ ) was established using pairwise Wilcoxon sum rank test in R 3.6.1 software. The adjustment methods include the Bonferroni correction. This protocol can be found in Desjardins et al., 2020a.

Alternatively, due to the difficulty to stage PMCs extracted from the anthers of *asy1* double KO plants, a different technique was used to analyse this genotype. Anthers were treated according to the metaphase I spread protocol described in section 2.2.14. After that, slides were dried out at room temperature for 10 minutes before boiling them in 10 mM of tri-sodium citrate (citrate buffer pH = 7.0 adjusted with citric acid granules) (Table 2.6) in microwave for 45 seconds. Subsequently, samples were permeabilized in cold 1X PBS/0.1% Triton for 10 minutes. Lastly, slides were treated with blocking solution for 10 minutes, before being incubated with the desired antibody combination, as described above.

<b>Fixative solution</b>	v/v
--------------------------	-----

three parts of absolute ethanol to one part of acetic acid fixative	
<b>Citrate buffer (0.01 M) pH 4.5</b>	V= 10ml
0.1 M sodium citrate	445µL
0.1 M citric acid	555µL
ddH <sub>2</sub> O	9 ml
<b>Enzyme solution</b>	V= 333µL aliquot
1% cellulose	
1% pectolyase	
0.01 M citrate buffer, pH 4.5	
WS: 333µL enzyme solution+667µL 0.01M citrate buffer	
<b>Meiocyte extraction medium</b>	V= 100ml
0.1 M sodium citrate	4.45ml
0.1 M citric acid	5.55ml
ddH <sub>2</sub> O	90 ml
Dilute 2:1 working concentration with sterile deionized water	
<b>Digestion medium</b>	V= 1ml aliquot
sucrose	0.375g
polyvinylpyrrolidone (MW 40,000; Sigma Aldrich)	0.25g
ddH <sub>2</sub> O	25ml
<b>Spreading medium</b>	
1% Lipsol (SciLabware Ltd., Stone, Staffordshire, UK)	
ddH <sub>2</sub> O	
<b>Paraformaldehyde fixative</b>	
paraformaldehyde (EM grade)	4g
ddH <sub>2</sub> O	100ml

1 M NaOH	4 drops
filtering through Whatman paper and adjust the pH to 8.0	
<b>Phosphate-buffered saline (1X PBS)</b>	V= 500ml
PBS (100X)	10 preprepared tablets
ddH <sub>2</sub> O	499.5ml
<b>PBST</b>	V= 500ml
1X PBS	499.5ml
0.1% Triton X-100	0.5ml
<b>Blocking solution</b>	V= 10ml
1X PBS	10ml
5% Bovine Serum Albumen (BSA)	0.5g

**Table 2.6 Solutions for immunolocalization experiment.**

Primary antibodies	Diluted in blocking solution (v/v)
Guinea pig $\alpha$ ASY1 (Desjardins et al., 2020b)	1:500 dilution
Rabbit $\alpha$ ZYP1 (Osman et al., 2018)	1:500 dilution
Rat $\alpha$ ZYP1 (Higgins et al., 2005)	1:500 dilution
Rat $\alpha$ ASY3 c	1:500 dilution
Rat $\alpha$ SMC3 (Ferdous et al., 2012b)	1:500 dilution
Rabbit $\alpha$ $\gamma$ H2AX (Merck)	1:500 dilution
Secondary antibodies	Diluted in blocking solution (v/v)
Goat $\alpha$ guinea pig 488 (Abcam)	1:200 dilution
Goat $\alpha$ rabbit 594 (Vector Laboratories)	1:200 dilution
Goat $\alpha$ rat Cy3 (Jackson Immuno Research)	1:200 dilution

**Table 2.7 List of primary and secondary antibodies used in this project.**

## 2.2.16 Statistics

### Chiasmata count

Initially, the mean and standard deviation values of rod bivalents, multivalents and univalents at meiotic metaphase I between Kronos WT and the *asy1* mutant lines were recorded. After that, all data involving multiple comparisons underwent a broad statistical assessment using a Kruskal–Wallis one-way analysis of variance in R 3.6.1 software to verify that there were statistically significant differences ( $\alpha < 0.05$ ) between data sets within one experiment. All direct one-on-one statistical comparisons between Kronos WT (control) and *asy1* single KO mutant (experimental variables) data were performed using Wilcoxon rank sum test adjusted with Bonferroni correction method in R 3.6.1 software to determine the significant differences among the mean number of chiasmata per nucleus occurring between Kronos WT and *asy1* single KO mutants. Both Kruskal–Wallis and Mann–Whitney U tests are non-parametric and therefore do not assume normal distribution of data points within a data set. Data were tested against the null hypothesis ( $H_0$ ) that the mean number of chiasmata per nucleus (median change) between Kronos WT and each mutant genotype was unchanged, and that the sets of data were independent. The null hypothesis was tested for 95% confidence interval for the difference in means where the cut-off point ( $\alpha$  level) is equal to 0.05. The  $P\text{-}adj$  represents the probability of error involved in rejecting the null hypothesis. If  $P\text{ adj} > \alpha$  level, the null hypothesis is not rejected, and the mean chiasma of Kronos WT is not significantly different from the mean chiasma of each mutant genotypes. However, if  $P\text{ adj} < \alpha$  level, the null hypothesis is rejected and the mean chiasma of Kronos WT is not equal to the mean chiasma of each mutant genotypes.

Data presented as violin plot with included box-and-whisker plots were produced in ggplot2 package using the geom\_violin() function with its standard settings. The lower and upper ‘hinges’ of the box represent the first and third quartile, respectively, and the black bar within the box indicates the median (=second quartile). The ‘whiskers’ represent the minimum and maximum of the range, unless they differ by more than 1.5 times the interquartile distance from the median. In the latter case, the borders of the 1.5 times interquartile distance around the median are indicated by the ‘whiskers’ and values outside this range (‘outliers’) are shown as open circles.

### **$\gamma$ H2AX foci count**

The  $\gamma$ H2AX foci were scored with Fiji - ImageJ software using the function ‘Count Nuclear Foci’. The optimal value making each nucleus as single region was chosen and

the noise tolerance was adjusted with ‘Find Maxima’ tool. Nuclei were measured with ‘Analyze Particles’. A nucleus size discrimination of over >200 pixel was set to exclude particles that weren’t nuclei. The output from ‘overlay outlines’ was checked for accuracy of the process. A two sample *t*-test was performed in R 3.6.1 software to verify the significant differences among the mean number of  $\gamma$ H2AX foci per nucleus occurring between Kronos WT and *asy1 aabB*. A two-sample *t*-test was applied to define the statistical significance between WT and *asy1 aabB* mutant in R 3.6.1 software.

### Segregants distribution from the backcrossed plants

Following the backcross with the WT, *asy1* mutant plants heterozygous for A and B sub-genomes (AaBb x AaBb) were self-pollinated and the resulting segregation ratio of the F<sub>2</sub> offspring was calculated using the chi square ( $\chi^2$ ) distribution in Microsoft Excel with the formula  $\chi^2 = \sum \frac{(O-E)^2}{E}$ , where *O* is the observed value and *E* represents the expected value. Data were tested against the H<sub>0</sub> that each allele of *asy1* mutants was independently assorted, according to Mendel’s laws. The number expected in each category (genotypes) was predicted from the results of the Punnett square.

The null hypothesis claimed that there was no significant difference between the expected and observed result, and it was tested for 95% confidence interval ( $\alpha = 0.05$ ). The degree of freedom (Df) and  $\chi^2$  distribution table were used to determine the critical value (cv). The Df was calculated by subtracting “1” from the total number of each genotypes. If the calculated  $\chi^2 > cv$ , the null hypothesis is rejected, otherwise, if  $\chi^2 \leq cv$ , the null hypothesis cannot be rejected, indicating statistical significance.

## 2.3 Results

### 2.3.1 *TaASY1* is expressed in leaves and inflorescences of hexaploid *T. aestivum* cultivars Cadenza and Apogee

Before undertaking the targeted induced lesion in genomes (TILLING) mutant analysis, the expression contribution of *TaASY1* homoeologues in hexaploid *T. aestivum* during meiosis were assessed. First expression of *TaASY1* was validated, so total RNA from inflorescences (Figure 2.2 a) and flag leaves (Figure 2.2 b) was extracted from two distinct cultivars, Cadenza and Apogee, reverse-transcribed into cDNA and amplified via

conventional PCR using gene-specific primers, designed within consensus sequences identical for all sub-genomes (Figure 2.2 a). The results show a band of ~2500 bps in reproductive and somatic tissues of both cultivars (Figure 2.2 a, b).

<b>a</b>	TRIAE_CS42_5AL	ACTCGCTGTTCTAACAGGAATTGCTCCGGATTGCTATATACAAACATCAGCTACATCA	293
	TRIAE_CS42_5BL	ACTCGCTGTTCTAACAGGAATTGCTCCGGATTGCTATATACAAACATCAGCTACATCA	206
	TRIAE_CS42_5DL	ACTCGCTGTTCTAACAGGAATTGCTCCGGATTGCTATATACAAACATCAGCTACATCA	287
	*****	*****	*****
		ASY1cDNAF	
	TRIAE_CS42_5AL	GAGGCCTATTCCCTGAGAAGTACTTCATGATAAGTCTGTTCCGGCACTAGAGATGAAGA	353
	TRIAE_CS42_5BL	GAGGCCTATTCCCTGAGAAGTACTTCATGATAAGTCTGTTCCGGCACTAGAGATGAAGA	266
	TRIAE_CS42_5DL	GAGGCCTATTCCCTGAGAAGTACTTCATGATAAGTCTGTTCCGGCACTAGAGATGAAGA	347
	*****	*****	*****
	TRIAE_CS42_5AL	GGAAGTCTCTGGCTGGCGAAGAGTCGATGTGCATGCCGACAAGCGGACCAGGAAGGCCA	1904
	TRIAE_CS42_5BL	GGAAGTCTCTGGCTGGCGAAGAGTCGATGGGCACGCCGACAAGCGGACCAGGAAGACCA	1826
	TRIAE_CS42_5DL	GGAAGTCTCTGGCTCGCGAAGAGTCGATGTGCACGCCGACAAGCGGACCAGGAAGACCA	1907
	*****	*****	*
		ASY1cDNAR	
	TRIAE_CS42_5AL	GCATGGTGAAGGAGCCGATCCTCCAGCAGGTCAAGCGC CAGAAGTCTTAGTTCA GTGA-G	1963
	TRIAE_CS42_5BL	GCATGGTGAAGGAGCCGATCCTCCAGCAGGTCAAGCGCCAGAAGTCTTAGTTCA GTGGG	1886
	TRIAE_CS42_5DL	GCATGGTGAAGGAGCCGATCCTCCAGCAGGTCAAGCGCCAGAAGTCTTAGTTCA GTGA-G	1966
	*****	*****	*

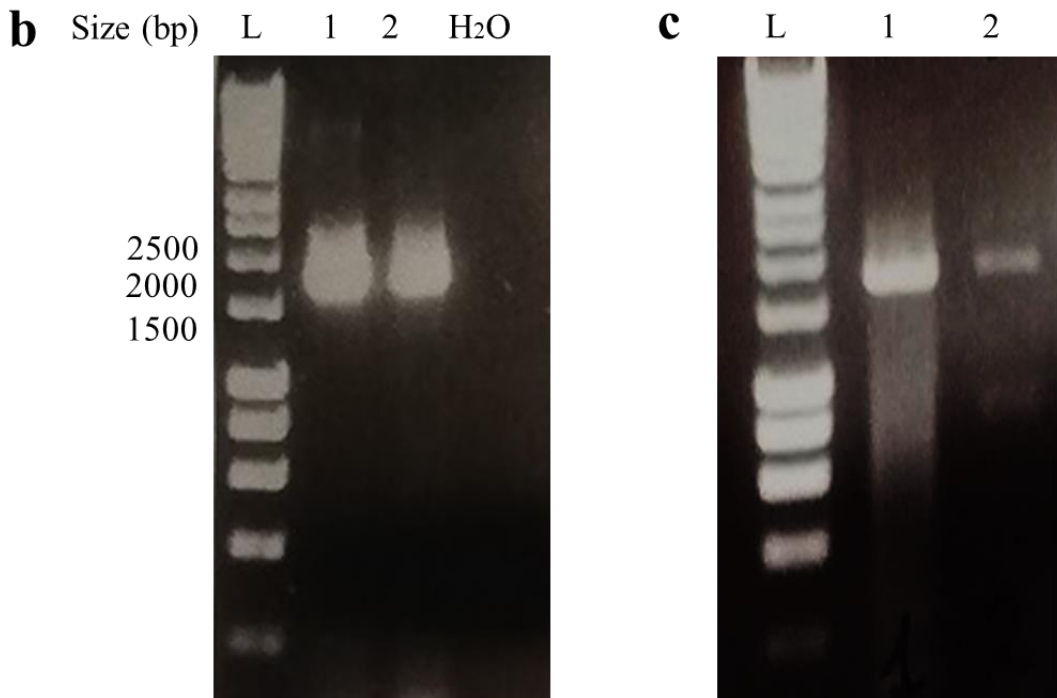


**Figure 2.2 Expression validation of *TaASY1* cDNA in hexaploid *T. aestivum*.** a) Multiple sequence alignment among the coding region sequences of *TaASY1* A, B and D sub-genomes from Chinese Spring reference. Forward and reverse primers are highlighted in yellow. b) *TaASY1* coding region amplicons of *T. aestivum* cvs. Apogee and Cadenza from inflorescence and c) from flag leaf using gene specific primers. L = DNA ladder; 1 = lane for Apogee cDNA; 2 = lane for Cadenza cDNA; H<sub>2</sub>O = negative control. Coding region primers, with consensus sequences for all sub-genomes, were used.

### 2.3.2 *TaASY1* expression from sub-genomes is likely to be redundant in reproductive and somatic tissues

In hexaploid *T. aestivum*, *TaASY1* homoeologues are located within chromosomes 5A, 5B and 5D. At the coding DNA sequence and amino acid levels, *TaASY1-5A* (TraesCS5A02G092700) showed 95% identity and similarity to *TaASY1-5B* (TraesCS5B02G098800), 97 and 96% identity and similarity to *TaASY1-5D* (TraesCS5D02G105000), respectively, whereas *TaASY1-5B* has 96 and 94% identity and similarity to *TaASY1-5D*, respectively (data retrieved from Ensembl Plants database). In order to compare the relative expression of *TaASY1* homoeologues, total RNA samples were collected from anthers of hexaploid *T. aestivum* cvs. Cadenza and Apogee possessing wild-type genotypes at the late leptotene-early zygotene stage (according to the anther size) and reverse-transcribed into cDNA.

To amplify *TaASY1* transcripts from A, B and D sub-genomes in an unbiased manner, primers were designed within cDNA region sharing 100% sequence similarity, thereby the proportion of the resulting clones represented the relative amount of each sub-genome expression (Figure 2.3 a). Thus, the full length *TaASY1* coding region (cds) was cloned and Sanger sequenced. A colony PCR screening was additionally executed to confirm the amplification of specific sub-genome ASY1 transcripts. In designing primers for specific sub-genomes, splice variants were not considered. An example is illustrated in Figure 2.3 b: the *TaASY1-5B* cDNA clone (Figure 2.3 b) was detected using B sub-genome specific primers (Figure 2.3 a) prior  $\Delta T_m$  optimization, and the *TaASY1-5A* cDNA clone previously sequenced was included as negative control.

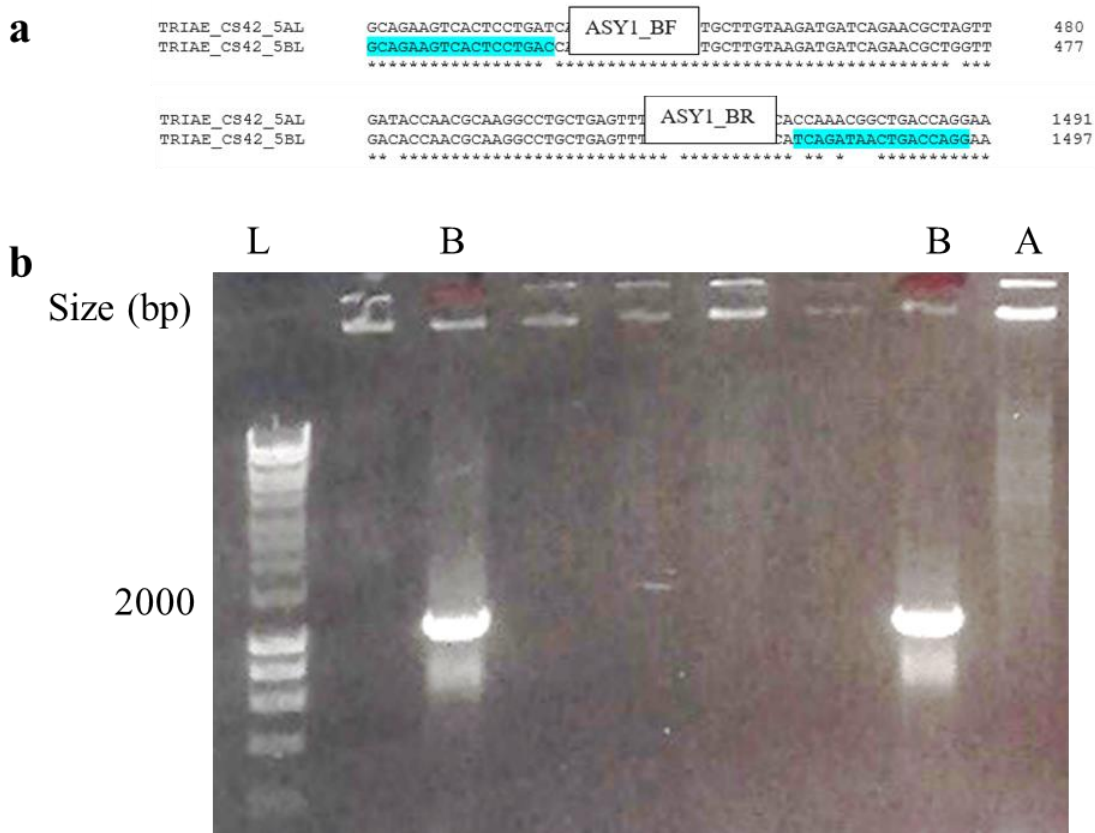


**Figure 2.3 Colony PCR of *TaASY1-5B* clone.** a) Multiple sequence alignment between the coding region sequences of *TaASY1* A and D sub-genomes from Chinese Spring reference. Forward and reverse primers are highlighted in sky blue. b) *TaASY1-5B* cds clone. L = DNA ladder; B = *TaASY1-5B* clone; A = *TaASY1-5A* clone used as negative control. Coding region primers, sub-genome specific, were used.

From *TaASY1* cds cloning analysis differential expression among the *TaASY1* homoeologues. Indeed, 90% of *TaASY1* clones sequenced (n=19) belonged to the A sub-genome, while only 10% of clones (n=19) expressed the B and D sub-genomes (5% B and 5% D) (Figure 2.4 a). This result suggested a possible A sub-genome dominance, in apparent antagonism with the RNA-Seq data from Wheat Expression Browser (expVIP) (<http://www.wheat-expression.com/>) (Figure 2.4 b). A more rigorous examination led to interpret the results obtained with the two methods (cloning and RNA-seq from expVIP) as equivalent. Comparing the Transcripts Per Million (TPM) and standard error of the mean (SEM) values of four representative RNA-seq datasets, emerged a relevant biological variability, which fits with the cloning data (this study). Therefore, to better estimate the homoeologous expression level of *TaASY1*, a pyrosequencing assay at INRA (France) as secondment was planned. Nevertheless, due to COVID lockdown travel

restrictions, this analysis was not possible and therefore an alternative qPCR approach was adopted, with primer sets designed by PyroMark Assay Design Software 2.0 (Qiagen, INRA).

a	<i>TaASYI</i> cds clones (n=19)	<i>TaASYI</i> -5A	<i>TaASYI</i> -5B	<i>TaASYI</i> -5D
		90%	5%	5%

b	<i>TaASYI</i> homoeologues relative contribution in DNA coding region	<i>TaASYI</i> -5A	<i>TaASYI</i> -5B	<i>TaASYI</i> -5D
	spike, reproductive, none, other (n=76)	2.18 ± 0.88	0.91 ± 0.50	2.05 ± 0.81
	spike, reproductive, none, Chinese Spring (n=16)	1.68 ± 1.01	0.32 ± 0.17	1.72 ± 0.67
	spike, reproductive, none, Azhurnaya (n=33)	2.68 ± 1.05	1.51 ± 0.92	2.43 ± 1.15
	leaves/shoots, vegetative, none, Azhurnaya (n=24)	<b>1.69 ± 0.95</b>	<b>1.40 ± 0.86</b>	<b>1.41 ± 1.08</b>

**Figure 2.4 Assessment of *TaASYI* homoeologues relative contribution in DNA coding region.** a) Proportion of *TaASYI* sub-genomes from cds clones expressed in percentage. b) Predicted gene expression level of A, B and D homoeologues of *TaASYI* from publicly available RNA-Seq data. The table shows a predicted differential expression among *TaASYI* homoeologues. The relative proportion of *TaASYI*-5A, *TaASYI*-5B and *TaASYI*-5D homoeologues were calculated in sixteen reproductive tissue sample of *T. aestivum* ‘Chinese Spring’ normalized via TPM method. Data retrieved from Wheat expVIP database. TPM= transcripts per million; SEM= standard error of the mean; n= number of observations; None = wild-type plants. Green colour= RNA-seq data from vegetative samples.

First of all, primer pairs flanking a single SNP that discriminates the different *TaASYI* copies (e.g. A+B vs D, A+D vs B and B+D vs A) and with high score values were prioritised and tested by conventional PCR (Figure 2.5 a-c). PCR products amplified by *TaASYI* A+B vs D, *TaASYI* B+D vs A and *TaASYI* A+D vs B primer sets had a predicted size of 106, 55 and 150 bps, respectively (Figure 2.5 d). Subsequently, the expression level of each *TaASYI* homoeologous combination was compared and quantified on four cDNA extracted from four wild-type Cadenza individual with a qPCR assay.

The above results from Wheat ExpVIP database and cloning were comparable with the qPCR data, which ultimately revealed that *TaASYI* homoeologues were redundant at gene expression level (Figure 2.5 e), therefore there was no obvious upregulation of the *TaASYI*-5A transcript, as instead detected with the cloning approach.

**a**

Primer Set 1 F1R1 $T_a = 66$ , 106bp			Score: 91 Quality: High		
Primer	Id	Sequence	Nt	Tm, °C	%GC
PCR	F1	ATGCCCATGGATGCTGAAT	19	70.2	47.4
PCR	R1	TATGTGAGAAGGAGGAAGGCC	21	69.5	52.4
Sequencing	S1	TGGATGGAGAAAGGTGT	17	53.7	47.1
Target Polymorphisms	Position1				
Sequence to Analyze	GCACTAGAGATGAAGATTAAGAAGCTGATGCCCATGGATGCTGAATCCAGGAGGTTGATT GATTGGATGGAGAAAGGTGTC/TTATGATGCCTACAAAAGAAATATCTCAAGACCCCTT CTCTCTGTATATGTGAGAAGGAGGAAGGCC				

ASY1_5AL_cds	ASY1_A+B vs D_F	CCAGGAGGTTGATTGGATGGAGAAAGGTGTC	CATGAT	240
ASY1_5BL_cds		CCAGGAGGTTGATTGGATGGAGAAAGGTGTC	CATGAT	237
ASY1_5DL_cds	ASY1_A+B vs D_R	ATGCCCATGGATGCTGAATGGAGAAAGGTGTC	CATGAT	240
		*****	*****	*****
ASY1_5AL_cds		GCCTTACAAAAGAAATATCTCAAGACCCCTCTCTCTG	ASY1_A+B vs D_R	GC
ASY1_5BL_cds		GCCTTACAAAAGAAATATCTCAAGACCCCTCTCTCTG		GC
ASY1_5DL_cds		GCCTTACAAAAGAAATATCTCAAGACCCCTCTCTCTG	TATGTGAGAAGGAGGAAGGC	300
		*****	*****	*****

**b**

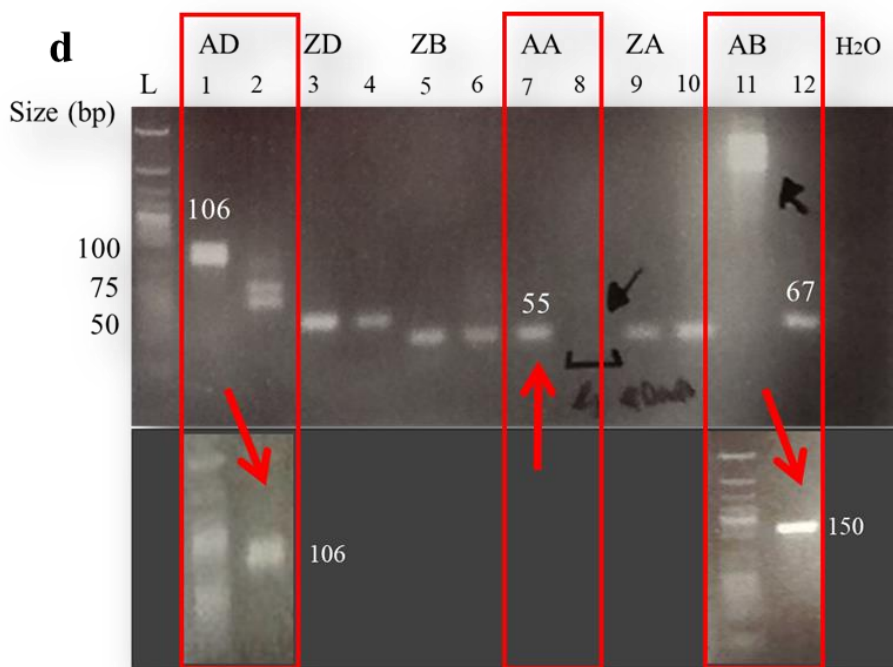
Primer Set 1 F1R1 $T_a=67$ , 67bp			Score: 95 Quality: High		
Primer	Id	Sequence	Nt	Tm, °C	%GC
PCR	F1	ACGCACTTCCAATGGATTATGTGA	24	73.5	41.7
PCR	R1	TTCAGGGCAAGCTTGATGG	19	71.2	52.6
Sequencing	S1	CCAATGGATTATGTGACT	18	50.4	38.9
Target Polymorphisms	Position1				
Sequence to Analyze	ATGAAGGCATTATACCACGCACCTCCAATGGATTATG TGACTGTAGCTAACGCTTCAGGGCAAGCTTGATGGCGAAGCCAACCAGA				

ASY1_5AL_cds	ASY1_A+D vs B_F	TGACATAGCT	ASY1_A+D vs B_R	1251
ASY1_5BL_cds	TTATACCACTTCACATGGATTATGTGAC	AGCTAACGCTTCAGGGCAAGCTTGAT		1257
ASY1_5DL_cds	TTATACCACTTCACATGGATTATGTGAC	AGCTAACGCTTCAGGGCAAGCTTGAT		1260
	*****	*****	*****	*****
ASY1_5AL_cds	GGCGAAGCCAACCAGAGCACAGTCGGAAGTTGATGGACAAATGGTGCAGATGGATAC		1311	
ASY1_5BL_cds	GGCGAAGCCAACCAGAGCACAGTCGGAAGTTGATGGACAAATGGTGCAGATGGATAC		1317	
ASY1_5DL_cds	GGCGAAGCCAACCAGAGCACAGTCGGAAGTTGATGGACAAATGGTGCAGATGGATAC		1320	
	*****	*****	*****	*****

**c**

Primer Set 1 FIR1, T <sub>a</sub> =64, 55 bp			Score: 91 Quality: High		
Primer	Id	Sequence	Nt	T <sub>m</sub> , °C	%GC
PCR	F1	AGCTACCCCAACACAAACGG	20	71.1	55.0
PCR	R1	AACATGAGTCGCACAGGGAA	19	69.3	52.6
Sequencing	S1	TCCCTGTGCGACTCATGTT	18	52.3	33.3
Target Polymorphisms	Position1				
Sequence to Analyze		ATGATTGAAGAGTATGCCTTCTCATTAGCTACCCAAACACAAACGGGGAGGAA GTTG CAATGAACATGAGTCGCACAGGGAGCAAAAAGAATAGTGCACATTCAAGTC AATGCA AGCAGAAGTCACTCTGA			

ASY1\_5AL\_cds      CCAATGATTGAAGAGTATGCCTTCTCATTAGCTACCCAAACACAAACGGGGAGAAGTT      360  
ASY1\_5BL\_cds      CCCATGATTGAAGAGTATGCCTTCTCATTAGCTACCCAAACACAAACGGGGAGAAGTT      357  
ASY1\_5DL\_cds      CCAATGATTGAAGAGTATGCCTTCTCATTAGCTACCCAAACACAAACGGGGAGAAGTT      360  
\*\* \*\*\*\*\*  
ASY1\_5AL\_cds      GCAATGACATGAGTCGCACAGGGAGCAAAAAGAATAGTGCACATTCAAGTC AATGCA      420  
ASY1\_5BL\_cds      GCAATGACATGAGTCGCACAGGGAGCAAAAAGAATAGTGCACATTCAAGTC AATGCA      417  
ASY1\_5DL\_cds      GCAATGACATGAGTCGCACAGGGAGCAAAAAGAATAGTGCACATTCAAGTC AATGCA      420  
\*\*\*\*\*



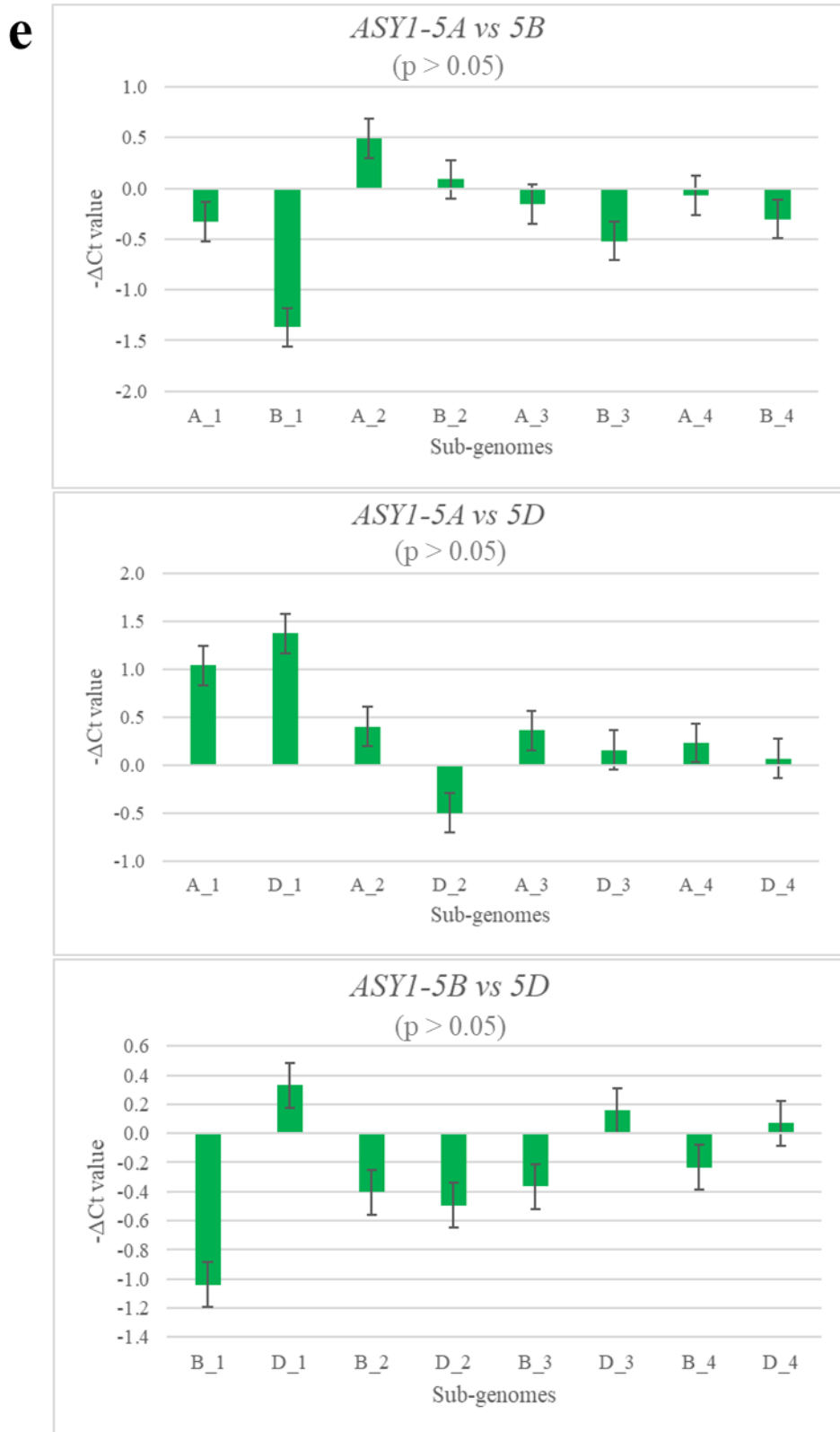


**Figure 2.5 Validation of pyrosequencing primer sets.** a) *TaASY1* with identical A and B homoeologous sequences, but with a SNP in D genome (A+B vs D). b) *TaASY1* with conserved A and D homoeologous sequences, but with a SNP in B genome (A+D vs B). c) *TaASY1* with identical B and D homoeologous sequences, but with a SNP in A genome (B+D vs A). SNPs are

indicated in purple. d) PCR results of predicted *TaASY1* amplicon combination sizes (red arrows). L = DNA marker; odd numbers (1, 3, 5, 7, 11) = Cadenza cDNA; even numbers (2, 4, 6, 8, 12) = Kronos cDNA; AD = *TaASY1* A+B vs D; AA = *TaASY1* B+D vs A; AB = *TaASY1* A+D vs B; H<sub>2</sub>O = negative control. e) qPCR results showing equal contribution of each *TaASY1* sub-genomes. ZA, ZB, ZD refer as to *TaZYP1* data (see Chapter 3). Error bars represent the standard deviation of three technical replicates. P values for statistical significance are shown in brackets.

### 2.3.3 A splice variant in *TaASY1-5B* cds ‘Apogee’ clone lacked the predicted acidic region of the protein

Another relevant mechanism that is known to be involved in several regulatory aspect of gene expression is the alternative splicing (AS). The aim of this study was to explore the presence of potential AS events of *TaASY1* cds in hexaploid *T. aestivum* cvs. Cadenza and Apogee. This approach consisted of cloning the full-length coding sequences of *TaASY1* genes and compare with the alternative isoforms currently predicted on Ensembl Plants database (Figure 2.6). As previously showed in Figure 2.2, no more than a single band appeared from the amplification of cDNA using gene-specific primers.

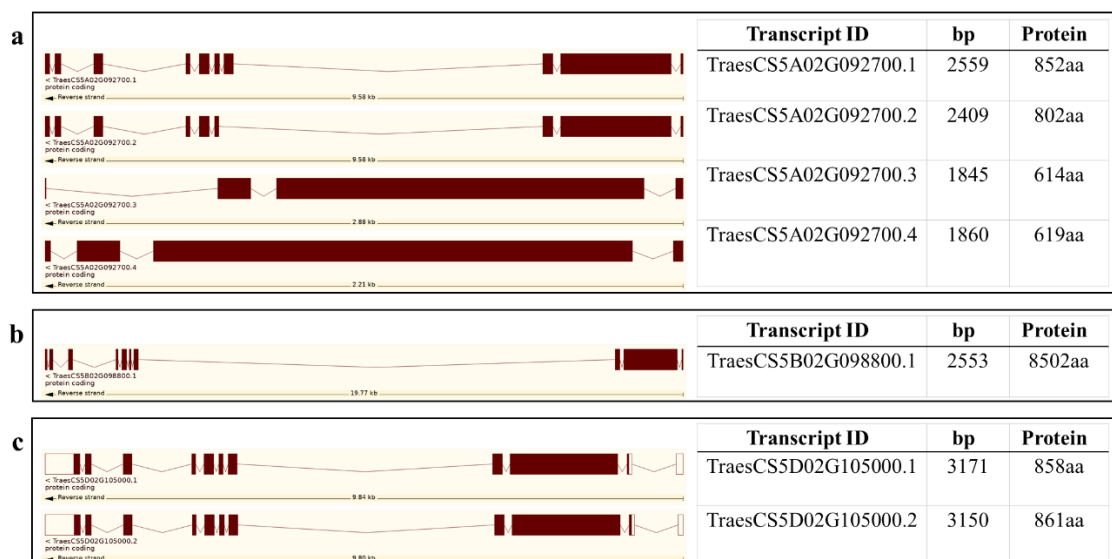


**Figure 2.6 Predicted protein coding annotation of *TaASY1*.** a) *TaASY1-5A* with 4 transcripts (splice variants) b) *TaASY1-5B* with 1 transcript, c) *TaASY1-5D* with 2 transcripts. Transcripts are drawn as boxes (exons) and lines connecting the boxes (introns). Filled boxes represent coding sequence and unfilled boxes (or portions of boxes) represent untranslated regions (UTR). Genes annotated with high confidence by IWGSC method. Data source: Ensembl Plants.

Intriguingly, a candidate splice variant in *TaASY1-5B* cds cloned in Apogee was identified with the multi-alignment analysis of the cloned sequences. The complete sequence of this *TaASY1-5B* Apogee clone was 100% identical to the B genomic sequence of the reference Chinese Spring (Figure 2.7), apart from a suspect non-canonical splicing event at the 5' splice donor site that might have occurred.

complete_36JA09 TRIAE_CS42_5BL_cds	TATGATGATGCCACACCTGAGGATTACGAGCCTCCCTTCTTTAAGGGTTGTGCTGAGAAT TATGATGATGCCACACCTGAGGATTACGAGCCTCCCTTCTTTAAGGGTTGTGCTGAGAAT *****	595 600
complete_36JA09 TRIAE_CS42_5BL_cds	GAAGCCGTAATATATGGAAACAAGAACCCCTTGAGAAGA GAAGCCGTAATATATGGAAACAAGAACCCCTTGAGAAGATGGGAAGTGGGAATGTCAATAGC *****	648 660
complete_36JA09 TRIAE_CS42_5BL_cds	AAGCATCTTGTGTTAGCTTGAAAGGTTAAGAGTGTGCTTGATCCATGTGATGCTAATGAT *****	648 720
complete_36JA09 TRIAE_CS42_5BL_cds	GCTAACACGTGATGATGACAAGATGAGCTGGGTCGTGAGTCAGACCAAGATAATGATT *****	648 780
complete_36JA09 TRIAE_CS42_5BL_cds	TCCGACACCGAGGTTGCCCRCTCTGAGTGGATCGTTACGTCGTTGCTCCTAATGATGGA *****	648 840
complete_36JA09 TRIAE_CS42_5BL_cds	CAACTCAGAAGATGAAACTCAAAGATGCTGCTCATGAG AATTGCAAAGGTCAAGAGGGTACAAACTCAGAAGATGAAACTCAA-GATGCTGCTCATGAG *****	673 900
complete_36JA09 TRIAE_CS42_5BL_cds	GAAGAGCTAACAGCTCAAGTAAGAGCATGGATATGCTCAAGAGACATGGGTACTGTTAAT GAAGAGCTAACAGCTCAAGTAAGAGCATGGATATGCTCAAGAGACATGGGTACTGTTAAT *****	733 960

**Figure 2.7 A putative splice variant in *TaASY1-5B* cds ‘Apogee’ clone.** The alignment of *TaASY1-5B* cds ‘Apogee’ clone with the B gDNA reference sequence (accession number: TRIAE\_CS42\_5BL\_TGACv1\_405487\_AA1328460) shows a putative isoform resulting from a non-canonical splicing event at the 5' splice donor site (purple).

To further investigate the origin of this isoform, a nucleotide multi-alignment including the B region and genomic reference sequences, along with the Apogee cds clone was performed (Figure 2.8). The putative splice variant had the exon number 7 partially truncated (Figure 2.8). Canonical mature protein-coding mRNA includes a 5' cap, 5' UTR, coding region, 3' UTR, and poly(A) tail. Coding regions begin with the start codon and end with a terminal (nonsense) codon. Here, the putative splice variant had the exon number 7 partially truncated, due to a leaky termination codon **TAA>GAA** within the intron 7 (data derives from the genomic reference sequence), it completely missed the exon 8 (exon skipping), and lacked 61 nucleotides upstream of exon 9 (Figure 2.8). As a consequence, the resulting alternative transcript was predicted to encode a shorter protein

of 515 amino acids, compared to the reference (591 aa), lacking the terminal 79 amino acid residues of the acidic region, as predicted by ExPASy translate tool (Figure 2.9).

ref_5B_genomic complete_36JA09 ref_5B_cds	E7 AACAAGAACCCCTGAAAGATG <b>GAA</b> GTGGGGAAATGTCATAGCAAGCATCTTG ATATGGAAACAAGAACCCCTGAAAGATG <b>TG</b> <b>ATATGGAAACAAGAACCCCTGAAAGATGAAAGTGGGGAAATGTCATAGCAAGCATCTTG</b> *****	3960 648 672
ref_5B_genomic complete_36JA09 ref_5B_cds	TTAGCTTGAAGGTGAGTGGAAATTACAGCATCTGTCCAGAATTCTGTTGGGTCTTT <b>TTAGCTTGAAG</b> ----- E8	4020 648 685
ref_5B_genomic complete_36JA09 ref_5B_cds	TGATCAATTCTCATGTTGCTTGTGTTATGCAGGTTAAGAGTGTCCCTGATCCATGTGA ----- <b>GTAAAGAGTGTCCCTTGATCCATGTGA</b> -----	4080 648 710
ref_5B_genomic complete_36JA09 ref_5B_cds	TGCTAATGATGCTAACAGTGTGATGACAAGATGAGCTGGTCGTGAGTCAGACCAAGA ----- <b>TGCTAATGATGCTAACAGTGTGATGACAAGATGAGCTGGTCGTGAGTCAGACCAAGA</b> -----	4140 648 770
ref_5B_genomic complete_36JA09 ref_5B_cds	TAATGATTTCGGACACCGAGGTAAAGGCCAAAGAAAATCAGATAACTGATAGTTCACT ----- <b>TAATGATTTCGGACACCGAG</b> -----	4200 648 821
ref_5B_genomic complete_36JA09 ref_5B_cds	AACATTATCTTAGTTGCTCTTTTTGGTTATGGACATGTTGACCTCCCTTTGCAT ----- -----	4260 648 821
ref_5B_genomic complete_36JA09 ref_5B_cds	GAAAATGTCGTACCGTATTTGTTCTTTGTAATCTAAAGTATTCCCTGACATTAC ----- ----- E9	4320 648 821
ref_5B_genomic complete_36JA09 ref_5B_cds	ATAATCCCTGATTCTATTAGGTCGCCCATCTGAAGTGGATCGTTACGTCGTTGCTCCTA ----- ----- <b>GTTCGCCCATCTGAAGTGGATCGTTACGTCGTTGCTCCTA</b> -----	4380 648 821
ref_5B_genomic complete_36JA09 ref_5B_cds	ATGGTAACATTATTCCATGATGCTCTCATTTATTAAATATTTGGTCTAAATATACTT ----- <b>ATGGTAACATTATTCCATGATGCTCTCATTTATTAAATATTTGGTCTAAATATACTT</b> -----	4440 648 821
ref_5B_genomic complete_36JA09 ref_5B_cds	GCTACAACAGATGAAATTGCAAAGGTCAAGGTGGTACAAACTCAGAAAGTCAGTTATTG ----- <b>GCTACAACAGATGAAATTGCAAAGGTCAAGGTGGTACAAACTCAGAAAGTCAGTTATTG</b> -----	4500 648 821
ref_5B_genomic complete_36JA09 ref_5B_cds	GTTCAAGAGAGCTTATTGCTCTCACATACAGTATATGTTACATGCAGACG ----- <b>GTTCAAGAGAGCTTATTGCTCTCACATACAGTATATGTTACATGCAGACG</b> -----	4560 648 827
ref_5B_genomic complete_36JA09 ref_5B_cds	TGGTCTATGTCGTTGTTGCTCTTCTAATT <b>TC</b> ATATATTACAGATGAAACTCAA-G ----- <b>CA</b> ACTCAGAAGATGAAACTCAAAG ----- * ***** * -----	4620 659 886

**Figure 2.8 The putative *TaASY1-5B* splice isoform identified in *T. aestivum* ‘Apogee’ clone.**

The multi-alignment shows the presence of alternative nonsense codon TAA > GAA in intron 7 (red triangle) and a non-canonical TC dinucleotide at 5' splice acceptor site within the intron 9 (red triangle). Genomic and coding region nucleotide sequences derive from Chinese Spring reference are highlighted in black and orange, respectively. Coding region sequence from Chinese Spring Exon 7 and exon 9 (E = exon) lacking 45 and 61 nucleotides respectively (dashes), and exon 8 skipping (dashes) are illustrated.

ref_5B	MVMAQKTKEAEITEQDSLLLTRNLLRIAIYNISYIRGLFPEKYFNDKSVPALEMKIKKLM	60
apogee_5B	MVMAQKTKEAEITEQDSLLLTRNLLRIAIYNISYIRGLFPEKYFNDKSVPALEMKIKKLM	58
	*****	*****
ref_5B	PMDAESRRLIDWMEKGVYDALQQKYLKTLLFCICEKEEGPMIEEYAFSFSPNTNGEEVA	120
apogee_5B	PMDAESRRLIDWMEKGVYDALQQKYLKTLLFCICEKEEGPMIEEYAFSFSPNTNGEEVA	118
	*****	*****
ref_5B	MNMSRTGSKKNSATFKSNAAEVTPDQMRSACKMIRTLVSLMRTLDDQMPPEERTILMKLLY	180
apogee_5B	MNMSRTGSKKNSATFKSNAAEVTPDQMRSACKMIRTLVSLMRTLDDQMPPEERTILMKLLY	178
	*****	*****
ref_5B	YDDATPEDYEPPFFKGCAENEAVNIWNKNPLKMEVGNVNSKHLVLALKVKSVLDPAND	240
apogee_5B	YDDATPEDYEPPFFKGCAENEAVNIWNKNPLK <span style="color:red">-OTQKM-</span>	216
	*****	:: :
ref_5B	ANSDDDKMSLGR <span style="background-color:skyblue">ESDQDN</span> DISDTEVRSEVDRYVVAPNDGNCKG <span style="background-color:skyblue">QS</span> GTN <span style="background-color:blue">SE</span> DETQDAHE	300
apogee_5B	- <span style="color:red">-----</span> KLKDAHE	224
	*****	:: :*****
ref_5B	EELTAQVRAWICSRDMGTVNASDVLSNYPDISLEMVEDILERLLKDGLLSRAGKDGYAVN	360
apogee_5B	EELTAQVRAWICSRDMGTVNASDVLSNYPDISLEMVEDILERLLKDGLLSRAGKDGYAVN	284
	*****	*****
ref_5B	KVTDPKTPYIKKEKEVAMHNVTPTEGTKNNNDTVMYMKALYHALPMDYVTVAKLQGKLDG	420
apogee_5B	KVTDPKTPYIKKEKEVAMHNVTPTEGTKNNNDTVMYMKALYHALPMDYVTVAKLQGKLDG	344
	*****	*****
ref_5B	EANQTTVRKLM <span style="background-color:skyblue">DKMVQDGYI</span> KNSGNRRLG <span style="background-color:blue">KAVI</span> HSEVTNRKLL <span style="background-color:blue">EIKK</span> I <span style="background-color:blue">LE</span> VD <span style="background-color:blue">I</span> D <span style="background-color:blue">MA</span> ID	480
apogee_5B	EANQTTVRKLM <span style="background-color:skyblue">DKMVQDGYI</span> KNSGNRRLG <span style="background-color:blue">KAVI</span> HSEVTNRKLL <span style="background-color:blue">EIKK</span> I <span style="background-color:blue">LE</span> VD <span style="background-color:blue">I</span> D <span style="background-color:blue">MA</span> ID	404
	*****	*****
ref_5B	TNARPAEFDRRDHQITDQEMKDGSTNGRFQSVGSDLTRTRELPEQQQNKKDPSRTPTSNR	540
apogee_5B	TNARPAEFDRRDHQITDQEMKDGSTNGRFQSVGSDLTRTRELPEQQQTNKDPSRTPTSNR	464
	*****	*****
ref_5B	ESATSLES <span style="background-color:skyblue">GVLGQRIRKSLAGEE</span> SMGTPDKTRKTS <span style="background-color:blue">MVKE</span> PI <span style="background-color:blue">LQQVKRQKS</span>	591
apogee_5B	ESATSLES <span style="background-color:skyblue">GVLGQRIRKSLAGEE</span> SMC <span style="background-color:blue">MPDKR</span> TRKAS <span style="background-color:blue">MVKE</span> PI <span style="background-color:blue">LQQVKRQKS</span>	515
	*****	*****

**Figure 2.9 The predicted alternative protein of *TaASY1-5B* ‘Apogee’ clone.** ExPASy translate tool prediction of a 515 aa-protein from *TaASY1-5B* Apogee clone (apogee\_5B), compared to the 591 aa of the reference (ref\_5B), missing 79 amino acid residues of the acidic region (aquamarine). HORMA domain sequence is also highlighted in sky blue. Red dashes indicate the missing amino acids of Apogee clone and red letters depict the diverged amino acids.

### 2.3.4 Identification of *TtASY1* 3' UTR isoforms in germline RNA

To monitor if any *TtASY1* 5' and/or 3' UTR transcripts were expressed in reproductive structures containing germline tissues of tetraploid *T. turgidum* cv. Kronos, total RNA was isolated from dissected ovaries and anthers, reverse-transcribed into cDNA with gene specific primers (covering the exon adjacent to the untranslated regions) and amplified via a nested RACE PCR (Figure 2.10). *TtASY1* 5' UTR PCR products were 200 bp from ovary and 300 bp from anther samples (Figure 2.10 a, b). In addition, at least 2 products

were amplified in *TtASY1* 3' UTR from ovaries (approximately 400 and 500 bp) and 3 products from anthers (roughly 400, 600 and 800 bp) (Figure 2.10 c).

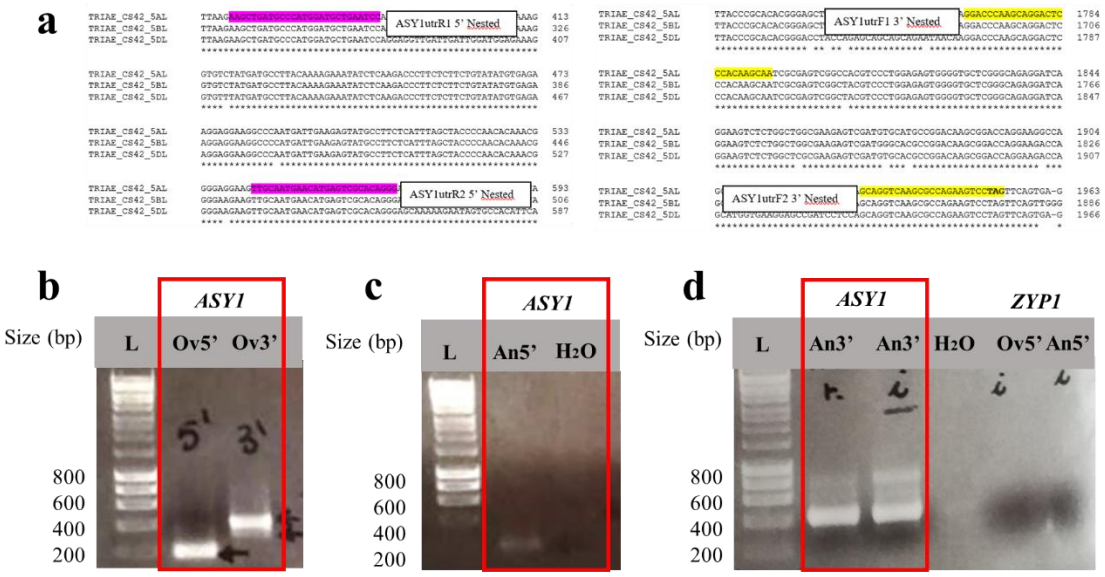


**Figure 2.10 Nested RACE PCR validates the expression of *TtASY1* UTRs in reproductive tissues.** a) Multiple alignment among the genomic reference sequence of *TtASY1* sub-genomes showing the nested 5' (pink) and 3' (yellow) UTR primers. b) Visualisation of 5' and 3' UTR amplicons from ovary tissue by gel electrophoresis following the second amplification with nested PCR primers (red). c) 5' and d) 3' UTR amplicons from anther tissue by gel electrophoresis following the second amplification with nested PCR primers (red); water was used as negative control. L = DNA ladder; Ov = ovary; An = anther; H<sub>2</sub>O = negative control; unboxed lanes= *TtZYP1* analysis (refers to Chapter 3).

To characterize the *TtASY1* UTRs, RACE PCR gene amplicons were cloned, Sanger sequenced and aligned to the reference genome TGACv1 annotation using the bioinformatics Omega Clustal W tool for comparison analysis between the reference sequence and the novel UTR sequences. Following the latest wheat genome annotation, Sanger sequencing results were also mapped to the reference wheat genome, IWGSC v1.0 (Appels et al., 2018) (Figure 2.2). Here, no 5' UTR sequence was identified either in anthers or in ovaries, as instead expected from Ensembl Plants database (Figure 2.11).

**a**

96HE15	CGACTGGAGCACGAGAACACTTGACATGGCTCAGAAGACGAAGGAGGCCGAGATCACGGAG	60
96HE14	CGACTGGAGCACGAGGACACTGACATGGCTCAGAAGACGAAGGAGGCCGAGATCACGGAG	60
96HE19	CGACTGGAGCACGAGGACACTTGACATGGCTCAGAAGACGAAGGAGGCCGAGATCACGGAG	60
96HE20	CGACTGGAGCACGAGGACACTTGACATGGCTCAGAAGACGAAGGAGGCCGAGATCACGGAG	60
96HE16	CGACTGGAGCACGAGGACACTTGACATGGCTCAGAAGACGAAGGAGGCCGAGATCACGGAG	60
96HE17	CGACTGGAGCACGAGGACACTTGACATGGCTCAGAAGACGAAGGAGGCCGAGATCACGGAG	29
96HE22	ASY1 5' Nested R1 CTGACATGGAC-----TGAAGGAGTAGAAAAGAA CTGACATGGAC-----TGAAGGAGTAGAAAAGAA	35
	*****	*** * ***
96HE15	CAGGACTCGCTGTTCTAACAAAGGAATTGCTCCGGATTGCTATATACAAACATCAGCTAC	120
96HE14	CAGGACTCGCTGTTCTAACAAAGGAATTGCTCCGGATTGCTATATACAAACATCAGCTAC	120
96HE19	CAGGACTCGCTGTTCTAACAAAGGAATTGCTCCGGATTGCTATATACAAACATCAGCTAC	120
96HE20	CAGGACTCGCTGTTCTAACAAAGGAATTGCTCCGGATTGCTATATACAAACATCAGCTAC	120
96HE16	CAGGACTCGCTGTTCTAACAAAGGAATTGCTCCGGATTGCTATATACAAACATCAGCTAC	120
96HE17	GACTTACGGACACCAGAACGAATTGCTCCGGATTGCTATATACAAACATCAGCTAC	89
96HE22	GACTTACGGACACCAGAACGAATTGCTCCGGATTGCTATATACAAACATCAGCTAC	95
	**	**** *****
96HE15	ATCAGAGGCCTATTCCCTGAGAAGTACTTCATGATAAGTCTGTTCCGGACTAGAGATG	180
96HE14	ATCAGAGGCCTATTCCCTGAGAAGTACTTCATGATAAGTCTGTTCCGGACTAGAGATG	180
96HE19	ATCAGAGGCCTATTCCCTGAGAAGTACTTCATGATAAGTCTGTTCCGGACTAGAGATG	180
96HE20	ATCAGAGGCCTATTCCCTGAGAAGTACTTCATGATAAGTCTGTTCCGGACTAGAGATG	180
96HE16	ATCAGAGGCCTATTCCCTGAGAAGTACTTCATGATAAGTCTGTTCCGGACTAGAGATG	180
96HE17	ATCAGAGGCCTATTCCCTGAGAAGTACTTCATGATAAGTCTGTTCCGGACTAGAGATG	149
96HE22	ATCAGAGGCCTATTCCCTGAGAAGTACTTCATGATAAGTCTGTTCCGGACTAGAGATG	155
	*****	*****
96HE15	AAGATTAAGAACCTGATGCCCATGGATGCTGAATCCAGGAGGTTGATTGATGGATGGAG	240
96HE14	AAGATTAAGAACCTGATGCCCATGGATGCTGAATCCAGGAGGTTGATTGATGGATGGAG	240
96HE19	AAGATTAAGAACCTGATGCCCATGGATGCTGAATCCAGGAGGTTGATTGATGGATGGAG	240
96HE20	AAGATTAAGAACCTGATGCCCATGGATGCTGAATCCAGGAGGTTGATTGATGGATGGAG	240
96HE16	AAGATTAAGAACCTGATGCCCATGGATGCTGAATCCAGGAGGTTGATTGATGGATGGAG	240
96HE17	AAGATTAAGAACCTGATGCCCATGGATGCTGAATCCAGGAGGTTGATTGATGGATGGAG	209
96HE22	AAGATTAAGAACCTGATGCCCATGGATGCTGAATCCAGGAGGTTGATTGATGGATGGAG	215
	*****	*****

**b**

	ASY1 5' Nested R1	
TRIAE_CS42_5AL_cdna ASY1K.F52F	-----CCTCTCTCTCTCTCTCCCACCCCTCCACGCCGCACACAACAC 51 CTGAGCACGAGAACACTTGATGACGAAGGAGGCCGAGATCACGGAGCAGACTC 60	
TRIAE_CS42_5AL_cdna ASY1K.F52F	ACGCCCACCAGG-----GCGGCAAAATGGTGAGTT-----CCCGCGC 93 GCTGTTCTAACAGGAATTGCTCCGGATTGCTATATACAAACATCAGCTACATCAGAGG 120	
TRIAE_CS42_5AL_cdna ASY1K.F52F	CCCCGCCCCGCCCCCGCCCTCA-TCCCGTGGTTGCGCCGCCGTGCC---TTCCCG 148 CCTATTCCCTGAGAAGTACTTCATGATAAGTCTGTTCCGGACTAGAGATGAAGATTAA 180	
TRIAE_CS42_5AL_cdna ASY1K.F52F	CATGCTAACGGCGCCCGTGCCTTCTCCGGTGGATCAGGGTATGGCTCAGAACAGC 208 GAAGCTGATGCCCATGGATGCTGAATCCTCGACTGGAGCACGAGGACACTGACATGGACG 240	
TRIAE_CS42_5AL_cdna ASY1K.F52F	AAGGAGGCGGAGATCACGGAGCAGGACTCGCTGCTTCTAACAGGAATTGCTCCGGATT 268 AAGGAGGCGGAGATCACGGAGCAGGACTCGCTGCTTCTAACAGGAATTGCTCCGGATT 300	
TRIAE_CS42_5AL_cdna ASY1K.F52F	GCTATATACAAACATCAGCTACATCACAGGGCTATTCCCTGAGAAGTACTTCATGATAAG 328 GCTATATACAAACATCAGCTACATCACAGGGCTATTCCCTGAGAAGTACTTCATGATAAG 360	
TRIAE_CS42_5AL_cdna ASY1K.F52F	TCTGTTCCGGCACTAGAGATGAAGATTAAGAAGCTGATGCCCATGGATGCTGAATCCAGG 388 TCTGTTCCGGCACTAGAGATGAAGATTAAGCTGATGCCCATGGATGCTGAATCCAGG 420	
	OligoRNA RACE	

**Figure 2.11 Multi sequence alignment of *TtASY1* 5' UTR clones from tetraploid *T. turigidum* cv. Kronos with the genome reference. a) Clone sequences derived from anthers; b) clone sequences derived from ovaries. Primer labels used are indicated in text boxes and primer sequences are highlighted in the respective colour. Start codon ATG is highlighted in yellow.**

Instead, more than two sequences were found in *TtASY1* 3' UTR, whose clone ASY1K.M317 had the predicted 3' UTR sequence from TGACv1 annotation (Figure 2.12 b). The alternative 3' UTR spliced isoforms showed two *novel cis*-acting regulatory sequence elements, namely Cytoplasmic Polyadenylation Element (CPE) sites: TTTAT, located at 240 nucleotides downstream of the STOP codon TTG (Figure 2.12 a, highlighted in green) and TTTTAAT, placed at 322 nucleotides downstream of the STOP codon and 80 nucleotides downstream of the previous CPE (Figure 2.12 b, highlighted in yellow). To simplify, from now on, TTTAT sequence will be named CPE<sub>1</sub> and TTTTAAT will be referred to as CPE<sub>2</sub>. From this analysis, four distinct categories of 3' UTR alternative isoforms could be discriminated based on the number of CPE sites: transcript variants with both CPE<sub>1</sub> and CPE<sub>2</sub>, transcript variants with either CPE<sub>1</sub> or CPE<sub>2</sub> and transcript variants lacking both CPE sites.

ASY1K.M317F	TTGGTAGCAAAACGTAACGAGAGAGACTTGTGCCCCCCCCTGAGACGTGTTG	TTTGAT
TRIAE_CS42_5AL_TGACv1.1	TTGGTAGCAAAACGTAACGAGAGAGACTTGTGCCCCCCCCTGAGACGTGTTG	TTTGAT
ASY1K.F38F	TTGGTAGCAAAACGTAACGAGAGAGACTTGTGCCCCCCCCTGAGACGTGTTG	TTTGAT
ASY1K.M316F	TTGGTAGCAAAACGTAACGAGAGAGACTTGTGCCCCCCCCTGAGACGTGTTG	TTTGAT
ASY1K.F34F	TTGGTAGCAAAACGTAACGAGAGAGACTTGTGCCCCCCCCTGAGACGTGTTG	TTTGAT
ASY1K.F32F	TTGGTAGCAAAACGTAACGAGAGAGACTTGTGCCCCCCCCTGAGACGTGTTG	TTTGAT
ASY1K.F31F	TTGGTAGCAAAACGTAACGAGAGAGACTTGTGCCCCCCCCTGAGACGTGTTG	TTTGAT
ASY1K.M312F	TTGGTAGCAAAACGTAACGAGAGAGACTTGTGCCCCCCCCTGAGACGTGTTG	TTTGAT
ASY1K.M31F	TTGGTAGCAAAACGTAACGAGAGAGACTTGTGCCCCCCCCTGAGACGTGTTG	TTTGAT
ASY1K.M311F	TTGGTAGCAAAACGTAACGAGAGAGACTTGTGCCCCCCCCTGAGACGTGTTG	TTTGAT
ASY1K.M321F	TTGGTAGCAAAACGTAACGAGAGAGACTTGTGCCCCCCCCTGAGACGTGTTG	TTTGAT
ASY1K.F312F	TTGGTAGCAAAACGTAACGAGAGAGACTTGTGCCCCCCCCTGAGACGTGTTG	TTTGAT
ASY1K.M34F	TTGGTAGCAAAACGTAACGAGAGAGACTTGTGCCCCCCCCTGAGACGTGTTG	TTTGAT
ASY1K.F33F	TTGGTAGCAAAACGTAACGAGAGAGACTTGTGCCCCCCCCTGAGACGTGTTG	TTTGAT
*****		
ASY1K.M317F	GTGGGTGCTCACGCCATGGTTTAATGATGTAICTATTGAACCTCTGTACTGAGCAG	360
TRIAE_CS42_5AL_TGACv1.1	GTGGGTGCTCACGCCATGGTTTAATGATGTAICTATTGAACCTCTGTACTGAGCAG	360
ASY1K.F38F	GTGGGTGCTCACGCCATGGTTTAATGATGTAICTATTGAACCTCTGTACTGAGCAG	312
ASY1K.M316F	GTGGGTGCTCACGCCATGGTTTAATGATGTAICTATTGAACCTCTGTACTGAGCAG	310
ASY1K.F34F	GTGGGTGCTCACGCCATGGTTTAATGATGTAICTATTGAACCTCTGTACTGAGCAG	317
ASY1K.F32F	GTGGGTGCTCACGCCATGGTTTAATGATGTAICTATTGAACCTCTGTACTGAGCAG	312
ASY1K.F31F	GTGGGTGCTCACGCCATGGTTTAATGATGTAICTATTGAACCTCTGTACTGAGCAG	312
ASY1K.M312F	GTGGGTGCTCACGCCATGGTTTAATGATGTAICTATTGAACCTCTGTACTGAGCAG	312
ASY1K.M31F	GTGGGTGCTCACGCCATGGTTTAATGATGTAICTATTGAACCTCTGTACTGAGCAG	312
ASY1K.F35F	GTGGGTGCTCACGCCATGGTTTAATGATGTAICTATTGAACCTCTGTACTGAGCAG	312
ASY1K.M318F	GTGGGTGCTCACGCCATGGTTTAATGATGTAICTATTGAACCTCTGTACTGAGCAG	346
ASY1K.M320F	GTGGGTGCTCACGCCATGGTTTAATGATGTAICTATTGAACCTCTGTACTGAGCAG	333
ASY1K.M38F	GTGGGTGCTCACGCCATGGTTTAATGATGTAICTATTGAACCTCTGTACTGAGCAG	348
ASY1K.M36F	GTGGGTGCTCACGCCATGGTTTAATGATGTAICTATTGAACCTCTGTACTGAGCAG	348
ASY1K.M35F	GTGGGTGCTCACGCCATGGTTTAATGATGTAICTATTGAACCTCTGTACTGAGCAG	348
ASY1K.M311F	GTGGGTGCTCACGCCATGGTTTAATGATGTAICTATTGAACCTCTGTACTGAGCAG	342
ASY1K.M321F	GTGGGTGCTCACGCCATGGTTTAATGATGTAICTATTGAACCTCTGTACTGAGCAG	348
ASY1K.F312F	GTGGGTGCTCACGCCATGGTTTAATGATGTAICTATTGAACCTCTGTACTGAGCAG	348
ASY1K.M34F	GTGGGTGCTCACGCCATGGTTTAATGATGTAICTATTGAACCTCTGTACTGAGCAG	360
ASY1K.F33F	GTGGGTGCTCACGCCATGGTTTAATGATGTAICTATTGAACCTCTGTACTGAGCAG	348
*****		
ASY1K.M317F	CGATGATCGCGC-----	372
TRIAE_CS42_5AL_TGACv1.1	CGATGATCGCGC-----	372
ASY1K.F38F	-----	312
ASY1K.M316F	-----	310
ASY1K.F34F	-----	317
ASY1K.F32F	-----	312
ASY1K.F31F	-----	312
ASY1K.M312F	-----	312
ASY1K.M31F	-----	312
ASY1K.F35F	-----	312
ASY1K.M318F	-----	346
ASY1K.M320F	-----	333
ASY1K.M38F	-----	348
ASY1K.M36F	-----	348
ASY1K.M35F	-----	348
ASY1K.M311F	-----	342
ASY1K.M321F	-----	348
ASY1K.F312F	-----	348
ASY1K.M34F	CGAT-----	364
ASY1K.F33F	-----	348
*****		
TRIAE_CS42_5BL_TGACv1.1	CTTGGTAGCAAACGTAACGAGAGAGACTTGT-----CCCCCTGAGACGTGTTGTTG-----	230
ASY1K.M319F	CTTGGTAGCAAACGTAACGAGAGAGACTTGT-----CCCCCTGAGACGTGTTGTTGTTCA	234
ASY1K.F36F	CTTGGTAGCAAACGTAACGAGAGAGACTTGT-----CCCCCTGAGACGTGTTGTTGTTCA	234
ASY1K.F39F	CTTGGTAGCAAACGTAACGAGAGAGACTTGT-----CCCCCTGAGACGTGTTGTTGTTCA	234
ASY1K.F37F	CTTGGTAGCAAACGTAACGAGAGAGACTTGT-----CCCCCTGAGACGTGTTGTTGTTCA	234
ASY1K.M33F	CTTGGTAGCAAACGTAACGAGAGAGACTTGTGCCCCCCCCTGAGACGTGTTG-----TTTA	237
*****		
TRIAE_CS42_5BL_TGACv1.1	-----	230
ASY1K.M319F	TGATGTTGTTCACTGGAGACTGTACTGTGAGGCCACTTTGCTGAATGATGAAACGT	294
ASY1K.F36F	TGATGTTGTTCACTGGAGACTGTACTGTGAGGCCACTTTGCTGAATGATGAAACGT	294
ASY1K.F39F	TGATGTTGTTCACTGGAGACTGTACTGTGAGGCCACTTTGCTGAATGATGAAACGT	294
ASY1K.F37F	TGATGTTGTTCACTGGAGACTGTACTGTGAGGCCACTTTGCTGAATGATGAAACGT	294
ASY1K.M33F	TGATGTTGTTCACTGGAGACTGTGACC-----GAGGCCACTTTGCTGAATGCTGAAACGT	295
*****		
TRIAE_CS42_5BL_TGACv1.1	-----	230
ASY1K.M319F	AACATGTTGTTACATGATGATCATCGTTG-----GTTGCTCACGCCAATGACGGTCGG	350
ASY1K.F36F	AACATGTTGTTACATGATGATCATCG-----TGGGTGCTCACGCCAATGACGGTCGG	334
ASY1K.F39F	AACATGTTGTTACATGATGATCATCG-----TGGGTGCTCACGCCAATGACGGTCGG	309
ASY1K.F37F	AACATGTTGTTACATGATGATCATCG-----TGGGTGCTCACGCCAATGACGGTCGG	309
ASY1K.M33F	AGCAATGTTGTTACATGATGATCATCGC-----CATGGTTTAATGATGATCATTTG-----	343
*****		
TRIAE_CS42_5BL_TGACv1.1	---- 230	
ASY1K.M319F	CGC 353	
ASY1K.F36F	---- 334	
ASY1K.F39F	---- 309	
ASY1K.F37F	---- 309	
ASY1K.M33F	---- 343	

**Figure 2.12 *TtASY1* 3' UTR transcript variants with CPE<sub>1</sub> and CPE<sub>2</sub> sites.** a) CPE<sub>1</sub> sequence TTTAT is highlight in green. b) CPE<sub>2</sub> sequence TTTTAAT is highlight in yellow. Clones are aligned with A reference (5A\_TGACv1.1). The clone ASY1K.M317 is the predicted 3' UTR sequence from TGACv1 annotation (red). c) Clones aligned with B reference (5B\_TGACv1.1). ASY1K.F = *TaASY1* clone sequence from Kronos (K) ovary (F = female) is highlight in pink; ASY1K.M = *TaASY1* clone sequence from Kronos (K) anther (M = male) is highlight in sky blue.

Unexpectedly, from this approach it emerged that the 3' polyA tail of *TtASY1* contained an additional G nucleotide (10%, n = 24) (Figure 2.13), albeit no distinct pattern was observed in polyA tail length and nucleotide composition in relation to the CPE sequences. The *TtASY1* 3' UTR sequences are listed in Appendix (Table S1).

In total, nine *TtASY1* 3' UTR isoforms were identified in tetraploid *T. turgidum* cv. Kronos reproductive tissues (ovaries and anthers), based on two parameters: presence/absence of CPE sequences and nucleotide length. The results are illustrated in Figure 2.13 a.

Considering both CPE categories and nucleotide length, two 3' UTR variants from A sub-genome were common in the reproductive tissues tested: v1 (variant 1: 348 bps, containing CPE<sub>1</sub>, CPE<sub>2</sub> and polyA tail of 24 adenosines) and v2 (variant 2: 312 bps, possessing CPE<sub>1</sub> only and polyA tail of 24 adenosines) (Figure 2.13 b).

Taking into account their frequency among the A and B sub-genomes, in ovaries, v2 was the major isoform, especially in A clones (57%, n = 7), but it was totally absent in B clones, albeit the sample size of the latter was extremely small (n = 3). v1 appeared in 29% of A clones (n = 7). The remaining 14% (n = 7) were represented by v3, a transcript of 317 nucleotides lacking the CPE2 sequence. In respect to the ovary B clones, three different 3' UTR isoforms were found (n = 3), all lacking the CPE sequences (Figure 2.13 b). Interestingly, v5, a variant of 309 bps (n = 3), was not detected in anther sample, and had a G nucleotide within the polyA tail (Figure 2.13 b).

In anthers, v4 included a set of 3' UTR isoforms possessing a wider length variability in the CPE<sub>1</sub> + CPE<sub>2</sub> category was identified (Figure 2.12 a), and it was the most abundant

from the A sub-genome (50%, n = 12) (Figure 2.12 b). The anther counterpart of v1 accounted for 33% (n = 12), while v2 represented the minority, with 17% (n = 12) (Figure 2.13 b). From B sub-genome, two variants differing in nucleotide length and CPE content were found (n = 2).

<b>TtASYI 3'UTR CPE sites (n=24)</b>	<b>F (bp + polyA)</b>	<b>M (bp + polyA)</b>
CPE <sub>1</sub> + CPE <sub>2</sub>	<b>348 + 27</b> <b>348 + 24</b> 333 + 28 <b>348 + 26</b> <b>348 + 23</b> <b>348 + 25</b> 342 + 20 <b>348 + 25</b> 364 + 23	372 + 27 346 + 35 333 + 28 <b>348 + 26</b> <b>348 + 23</b> <b>348 + 25</b> 342 + 20 <b>348 + 25</b> 364 + 23
CPE <sub>1</sub>	317 + 20 <b>312 + 41</b> <b>312 + 28</b> <b>312 + 18</b> <b>312 + 23</b>	<b>312 + 26</b> 310 + 29 <b>312 + 19</b>
CPE <sub>2</sub>		343 + 25 *
absent	334 + 26 * <b>309 + 20 *</b> <b>309 + 23 + G *</b>	353 + 16 * <b>309 + 23 + G *</b>

<b>TtASYI-5A</b>		
→ v1: 348 bp <u>TGA</u> TTCAGTG <b>TTTAT</b> <b>TTTTAAT</b> <b>AAAAAAAAAAAAAAA</b> <b>AAAAAAAAAAA</b>	29% (n=7)	
→ v2: 312 bp <u>TGA</u> TTCAGTG <b>TTTAT</b> <b>TTTTAAT</b> <b>AAAAAAAAAAA</b> <b>AAAAAA</b>	57% (n=7)	
→ v3: 317 bp <u>TGA</u> TTCAGTG <b>TTTAT</b> <b>TTTTAAT</b> <b>AAAAAAAAAAA</b> <b>AAAAAA</b>	14% (n=7)	
→ v1: 348 bp <u>TGA</u> TTCAGTG <b>TTTAT</b> <b>TTTTAAT</b> <b>AAAAAAAAAAA</b> <b>AAAAAA</b>	33% (n=12)	
→ v2: 312 bp <u>TGA</u> TTCAGTG <b>TTTAT</b> <b>TTTTAAT</b> <b>AAAAAAAAAAA</b> <b>AAAAAA</b>	17% (n=12)	
→ v4: 333-372 bp <u>TGA</u> TTCAGTG <b>TTTAT</b> <b>TTTTAAT</b> <b>AAAAAAAAAAA</b> <b>AAAAAA</b>	50% (n=12)	

<b>TtASYI-5B</b>		
v5: 309 bp <u>TGA</u> TTCAGTT <b>TTTTAAT</b> <b>AAAAAAAAAAA</b> <b>GAAAAAA</b>	33.3% (n=3)	
v6: 309 bp <u>TGA</u> TTCAGTT <b>TTTTAAT</b> <b>AAAAAAAAAAA</b> <b>AAAAAA</b>	33.3% (n=3)	
v7: 334 bp <u>TGA</u> TTCAGTT <b>TTTTAAT</b> <b>AAAAAAAAAAA</b> <b>AAAAAA</b>	33.3% (n=3)	
v8: 343 bp <u>TGA</u> TTCAGTT <b>TTTTAAT</b> <b>AAAAAAAAAAA</b> <b>AAAAAA</b>	100% (n=2)	
v9: 353 bp <u>TGA</u> TTCAGTT <b>TTTTAAT</b> <b>AAAAAAAAAAA</b>	100% (n=2)	

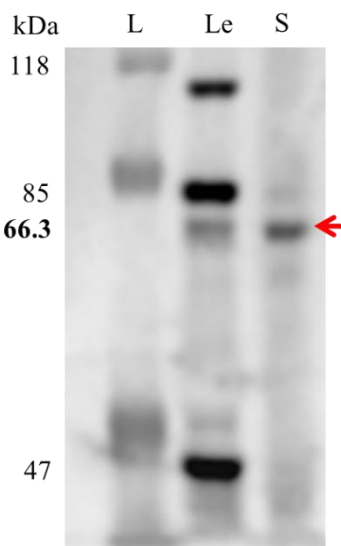
  

Legend:   anther     ovary     CPE<sub>1</sub>     CPE<sub>2</sub>

**Figure 2.13 *TtASY1* 3' UTR transcript variants.** a) Table recording the CPE categories identified in ovary (F) and anther (M) samples. Length in bps and the number of adenoses within the polyA tail are also indicated. Asterisk (\*) refers to the B sub-genome cloned. G (red) depicts

the guanosine presents in the polyA tail. b) 3' UTR clone sequences from ovaries (pink background) and anthers (sky blue background) of *TtASY1-5A* and *TtASY1-5B*. v1-9 = nine splice variants, in grey = STOP codon (TGA) followed by seven nucleotide of the splice variant, CPE sites (when present), polyA tail in purple, frequency expressed in percentage and the total clone number in brackets are on the left side; Legend is located at the bottom.

The expected translated product of the *ASY1* gene of 66.3 kDa was confirmed by Western Blot using *TaASY1* (HORMA domain) antibody (Desjardins et al., 2020b) (Figure 2.14). Note, other non-specific bands are also detected (Figure 2.14).



**Figure 2.14** Western blot with *TaASY1* antibody in hexaploid *T. aestivum*. Red arrow points to a product with the expected MW of *TaASY1* protein (66.3 kDa). L = DNA ladder; Le = leaf; S = spike.

### 2.3.5 Analysis of wheat *asy1* TILLING mutants

Sanger sequencing confirmed the predicted SNP mutation in the respective *ASY1* sub-genomes of the four TILLING lines selected and PCR-based genotyping allowed screening of the desired genotypes for this study. PCR primer sets flanking the corresponding SNP site were designed to individually amplify *ASY1-5A* and *ASY1-5B*. In tetraploid cv. Kronos, homozygous individuals aaBB (single KO in A sub-genome) and AAbb (single KO in B sub-genome) were found in K0706 (*asy1 aaBB*), K0157 (*asy1 AAbb-1*) and K2071 (*asy1 AAbb-2*), respectively. Analogously, in hexaploid cv. Cadenza, homozygous individuals AAbbDD were identified in C0971 (*asy1 AAbbDD*). To

simplify, from now on tetraploid *asy1 aaBB* and *asy1 AAbb* genotypes will be referred to as *asy1a* and *asy1b*, respectively, according to the expected mutant alleles in A or B subgenome.

To verify the consequence of the mutation at the transcript level, the DNA coding region of each *asy1* mutant was cloned and sequenced. Segregating WT plants originated from EMS mutagenesis were also used as a control to exclude that the *asy1* phenotype could derive from background mutations which may form during the TILLING process. As expected from the *in-silico* prediction, in K0706 (*asy1a*) clone, a G to A transition at nucleotide 714 affected the splice donor site at 5'end of the DNA coding region, which led to the use of a downstream splice site. This resulted in a frame-shift and thereby created a premature in-frame STOP codon, predicted to generate a truncated, partially non-functional *TtASY1-5A* protein lacking of major functional domains, such as the coiled-coil and the closure motif domains at the C-terminal, indispensable to interact with the lateral element partner (Figure 2.15). Similarly, in both K0157 (*asy1b-1*) and K2071 (*asy1b-2*) clones, a C to T transition at nucleotide position 785 and a G to A transition at nucleotide 148, respectively, determined the formation of a premature STOP codon mutation, TAG and TGA, respectively, resulting in a predicted truncated *TtASY1-5B* protein, missing the coiled coil and the closure motif domains (Figure 2.16 and Figure 2.17, respectively). Moreover, in K0157 line, 75 residues of the HORMA domain were absent from the final transcript. Finally, In C0971 (*asy1 AAbbDD*) clone, a codon change **GTA → ATA** at nucleotide 1195 altered the splice donor site at 5'end of the DNA coding region, introducing a frame-shift modification, which generated a premature in-frame STOP codon (TGA). In this case, the *TaASY1-5B* protein was predicted to be in part unable to bind with the axial elememts, due to the loss of the functional closure motif (Figure 2.18). In all mutants, the antibodies anti-*TaASY1* (HORMA) used in this analysis, could still bind to the nonsense proteins, which indeed conserved the HORMA domain residues. A summary of the predicted consequences into each *asy1* mutant transcript derived from the EMS treatment are shown in Figure 2.19.

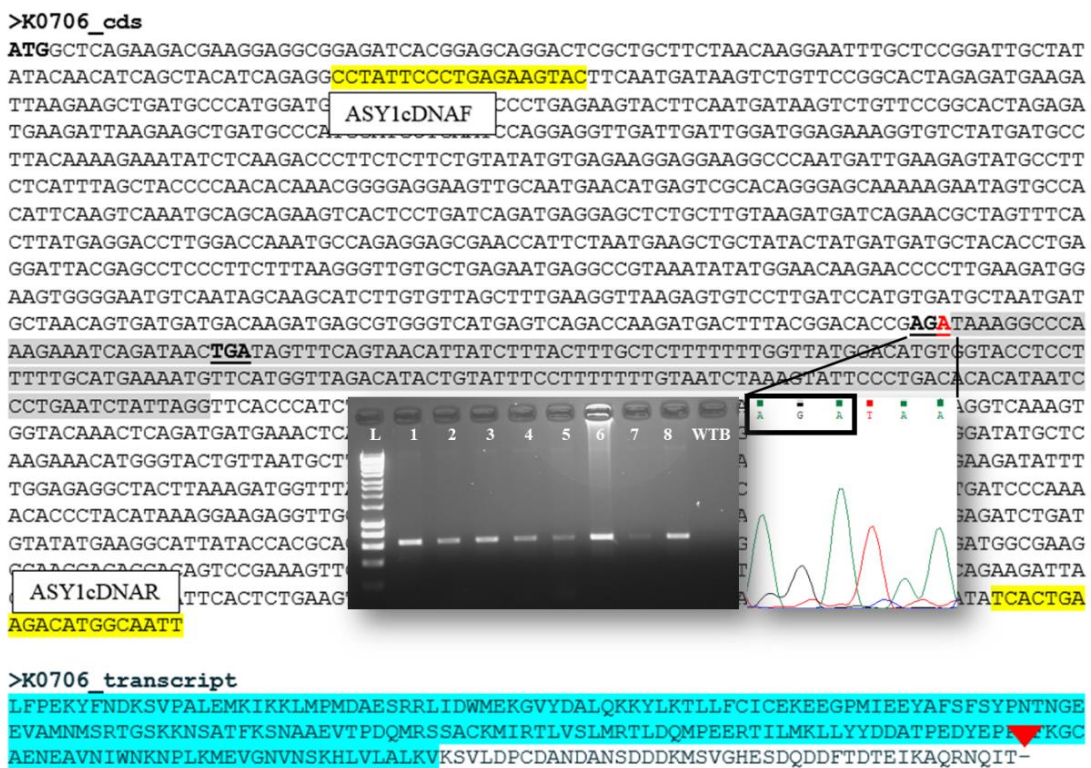


**Figure 2.15 DNA coding region sequence of K0706 (*asy1a*) clone.** Splice donor site mutation AG|GT → AG|AT between exon 8 and exon 9, causing the retention of intron 8 at nucleotide position 714 (highlighted in grey) and predicted to generate a premature STOP codon TGA downstream is shown. Left insert represents the 600 bps PCR amplicons amplified by primer pairs specific for *TtASY1-5A* (L= DNA ladder; 1-8= *asy1a* cDNA clones; WTB = wild type Kronos B clone previously sequenced), while the insert on the right illustrates the sequence trace of the mutation site (image from Chromas Lite). Forward and reverse primers amplifying *ASY1* coding region sequence are labelled in yellow. The predicted translation product in reading frame 1 exemplifies the consequence of the TILLING mutation, a premature STOP codon (red triangle), in the respect of HORMA domain (highlighted in blue). Transcript sequence was retrieved from UniProtKB database.

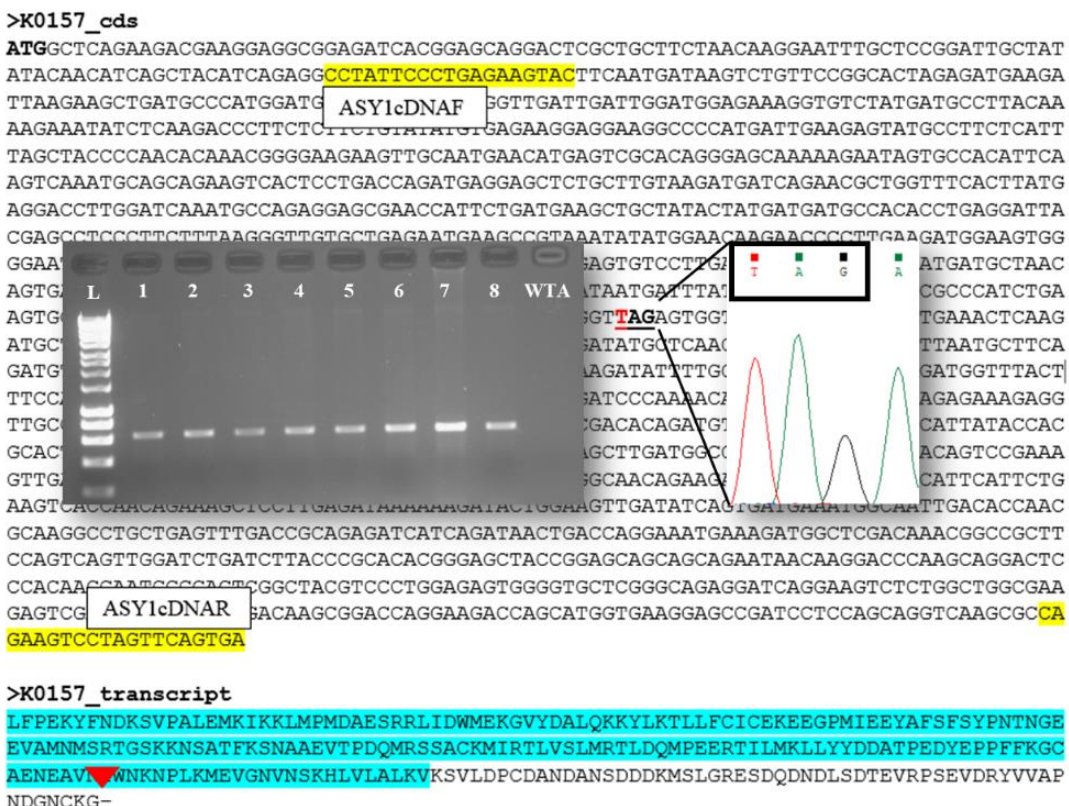


**Figure 2.16 DNA coding region sequence of K0157 (*asy1b-1*) clone.** The translation CAG → TAG at nucleotide position 785, causing a premature STOP codon TGA downstream is represented. Left insert shows the 600 bps PCR amplicons amplified by primer pairs specific for *TtASY1-5B* (L= DNA ladder; 1-8= *asy1b-1* cDNA clones; WTA = wild type Kronos A clone previously sequenced), while the insert at the right illustrates the sequence trace of the STOP codon mutation (image from Chromas Lite). Forward and reverse primers amplifying ASY1 coding region sequence are labelled in yellow. Translated protein (5'3' Frame 1 below) shows the premature STOP codon (red triangle) and the HORMA domain (highlighted in blue). Transcript sequence was retrieved from UniProtKB database.

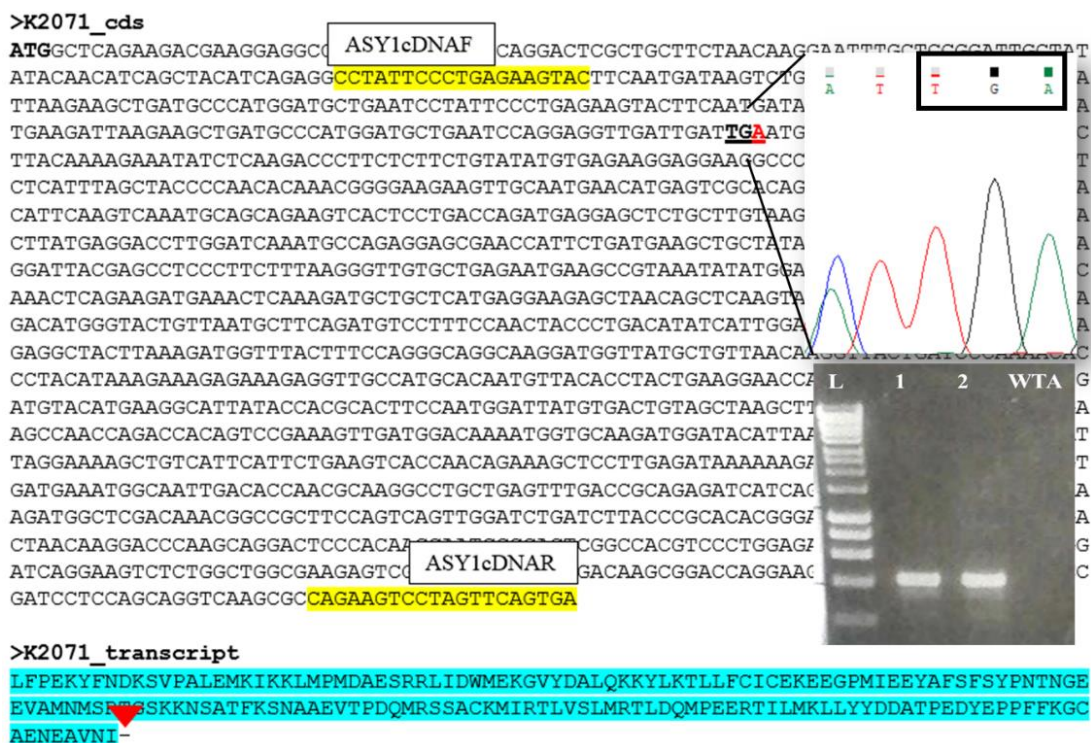


**Figure 2.17 DNA coding region sequence of K2071 (*asy1b-2*) clone.** The translation TGG → TGA at nucleotide position 148, causing a premature STOP codon (TGA) is exemplified. Top insert shows the sequence trace of the STOP codon mutation (image from Chromas Lite), while the insert at the bottom illustrates the 400 bps PCR amplicons amplified by primer pairs specific for *TtASY1-5B* (L= DNA ladder; 1, 2= *asy1b-2* cDNA clones; WTA= wild type Kronos A clone previously sequenced). Forward and reverse primers amplifying *ASY1* coding region sequence are labelled in yellow. Translated protein (5'3' Frame 1 below) shows the STOP codon (red triangle) and the HORMA domain (highlighted in blue), missing 24 amino acid residues. Transcript sequence was retrieved from UniProtKB database.

**Figure 2.18 DNA coding region sequence of C0971 (*asy1 AAbbDD*) clone.** Splice donor site mutation **GTA → ATA** between exon 8 and exon 9, causing the retention of intron 9 at nucleotide position 1195 (highlighted in grey), predicted to generate a premature STOP codon TGA downstream, is represented. Left insert shows the 400 bps PCR amplicon amplified by primer pairs specific for *TaASY1-5B* (L= DNA ladder; 1= *asy1 AAbbDD* cDNA clone; WT= wild type Cadenza clone previously sequenced), while the insert on the right illustrates the sequence trace of the mutation site (image from Chromas Lite). Forward and reverse primers amplifying *ASY1* coding region sequence are labelled in yellow. Translated protein (5'3' Frame 1 below) shows the STOP codon (red triangle) and HORMA domain (highlighted in blue). Transcript sequence was retrieved from UniProtKB database.

K0706	<b>LFPEKYFNDKSVP</b> ALEMKIKKLMPMDAESRRILIDWMEKGVYDALQKKYLKTLLFCICEKE	60
ASY1_WT	LFPEKYFNDKSVP <b>ALEMKIKKLMPMDAESRRILIDWMEKGVYDALQKKYLKTLLFCICEKE</b>	60
K0157	LFPEKYFNDKSVP <b>ALEMKIKKLMPMDAESRRILIDWMEKGVYDALQKKYLKTLLFCICEKE</b>	60
C0971	LFPEKYFNDKSVP <b>ALEMKIKKLMPMDAESRRILIDWMEKGVYDALQKKYLKTLLFCICEKE</b>	60
K2071	LFPEKYFNDKSVP <b>ALEMKIKKLMPMDAESRRILIDWMEKGVYDALQKKYLKTLLFCICEKE</b>	60
	*****	
K0706	EGPMIEEYAFSFSYPTNGEEVAMNMSRTGSKKNSATFKSNAAEVTPDQMRSACKMIRT	120
ASY1_WT	EGPMIEEYAFSFSYPTNGEEVAMNMSRTGSKKNSATFKSNAAEVTPDQMRSACKMIRT	120
K0157	EGPMIEEYAFSFSYPTNGEEVAMNMSRTGSKKNSATFKSNAAEVTPDQMRSACKMIRT	120
C0971	EGPMIEEYAFSFSYPTNGEEVAMNMSRTGSKKNSATFKSNAAEVTPDQMRSACKMIRT	120
K2071	EGPMIEEYAFSFSYPTNGEEVAMNMSRTGSKKNSATFKSNAAEVTPDQMRSACKMIRT	120
	*****	
K0706	LVSIMRTLDQMPEERTILMKL <sup>LYDDA</sup> T PEDYEPPFFKGCAENEAVNIWNKNPLKMEVGN	180
ASY1_WT	LVSIMRTLDQMPEERTILMKL <sup>LYDDA</sup> T PEDYEPPFFKGCAENEAVNIWNKNPLKMEVGN	180
K0157	LVSIMRTLDQMPEERTILMKL <sup>LYDDA</sup> T PEDYEPPFFKGCAENEAVNIWNKNPLKMEVGN	180
C0971	LVSIMRTLDQMPEERTILMKL <sup>LYDDA</sup> T PEDYEPPFFKGCAENEAVNIWNKNPLKMEVGN	180
K2071	LVSIMRTLDQMPEERTILMKL <sup>LYDDA</sup> T PEDYEPPFFKGCAENEAVNIWNKNPLKMEVGN	168
	*****	
K0706	VNSKHLVLALKVKSVDPCDANDANSDDDKMSVGHESDQD-DFTDTEIKAQRNQIT	235
ASY1_WT	VNSKHLVLALKVKSVDPCDANDANSDDDKMSVGHESDQD-DFTDTEVHPSEVDRYVAP	239
K0157	NDGNCKG	247
C0971	NDGNCKG <b>QSGTNSEDETQDAAHHEELTAQVR</b> AWICSRNMGTVNASDVL <sup>S</sup> NYPDISLEMVE	300
K2071	-----	168
	-----	
K0706	-----	235
ASY1_WT	NDGNGK <b>CQSGTNSDDETQDAAHHEELTAQVR</b> AWICSRNMGTVNASDVL <sup>S</sup> NYPDISLEMVE	299
K0157	NDGNCKG	247
C0971	NDGNCKG <b>QSGTNSEDETQDAAHHEELTAQVR</b> AWICSRDNGTVNASDVL <sup>S</sup> NYPDISLEMVE	300
K2071	-----	168
	-----	
K0706	-----	235
ASY1_WT	DILERL <b>LKDGLLSRAGKDGYAVNKITDPKTPYIKE--EVAMHNVS</b> PTEGTKNNSGDLMYM	357
K0157	-----	247
C0971	DILERL <b>LKDGLLSRAGKDGYAVNKVTDPKTPYIKKEKEVAMHNVT</b> PTEGTKNNNDTDVMM	360
K2071	-----	168
	-----	
K0706	-----	235
ASY1_WT	KALYHALPMDYVTIAKLQ <b>GKLDGEANQSTVRKLM</b> DKMVQDG <sup>I</sup> YIKNSGNRRLGKAVIHSEV	417
K0157	-----	247
C0971	KIPSINP	367
K2071	-----	168
	-----	
K0706	-----	235
ASY1_WT	TNRK <b>LLEIKKILEVDITEDMAI</b>	439
K0157	-----	247
C0971	-----	367
K2071	-----	168

**Figure 2.19 Clustal Ω multiple alignments of protein sequence from WT and predicted asy1 TILLING mutant lines.** The alignment shows the corresponding position of the amino acid (in bold) affected by EMS treatment (red triangles). K0706= *asy1a*; K0157= *asy1b-1*; K2071= *asy1b-2*; C0971= *asy1 AAbbDD*; ASY1\_WT= protein sequence of ASY1 wild-type.

### 2.3.6 Cytological atlas of *asy1* single knockouts

To determine the possible cytological consequence of the truncated ASY1, chromosome spread of pollen mother cells isolated from ethanol:acetic acid fix anthers and DAPI

staining of the chromatin of WT control and *asy1* single knockout (KO) were assessed during the sub-stages of the first meiotic prophase using the MeioCapture method (Shunmugam et al., 2018) (Figure 2.20). Early prophase I (leptotene) looked similar between the WT (Figure 2.20 A) and *asy1* single mutants (Figure 2.20 A-M), where unpaired chromosomes appeared as thin treads. However, from zygotene to diplotene, thicker regions of unpaired chromosomes were predominant in all *asy1* genotypes (Figure 2.20 F-P). Occasionally, small fragments were observed in *asy1b-2* at zygotene and diplotene (Figure 2.20 N, P, arrows), which, at these stages, could be caused by variable structural organization of chromatids, due to insufficiency of ASY1. Chromosome thickness and stickiness, indicative of chromosome alignment failure, persisted in diakinesis (Figure 2.20 E1-M1), so that most of chromosomes cluster together at metaphase I.

During metaphase I, 14 ring bivalents, each one forming at least 2 chiasmata, were clearly observed in tetraploid WT (Figure 2.20 A1) and organised onto the equatorial plate (Figure 2.20 B1, blue insert depicts the ring shape, red crosses represent two COs), so that chromosomes segregated regularly and equally to the opposite poles during anaphase I (Figure 2.20 C1), thereby forming balanced tetrads (Figure 2.20 D1). Dissimilarly, in *asy1* single KO mutants, metaphase I chromosomes were found mostly as rod bivalents (Figure 2.20 F1, blue insert depicts the rod shape, where maximum 1 CO is formed, represented as a red cross), but also as unpaired univalents (Figure 2.20 J1, arrows), or tetravalents (Figure 2.20 F1, N1, stars), that resulted in chromosome missegregation (Figure 2.20 G1, circles) and chromosome bridges (Figure 2.20 K1, O1, arrows) at anaphase I, as well as unbalanced tetrads with micronuclei (derived from lagging chromosomes) (Figure 2.20 H1, arrow) or triads (Figure 2.20 L1, P1).

Less frequent phenotypes (4%, n = 50) were also detected at metaphase I in *asy1* single mutants with this analysis (Figure 2.21). Typically, chromosomes were sticky (Figure 2.21 A-C) and organised in clusters (Figure 2.21 A1-C1), an unusual configuration never observed in any WT meiocytes here. Nevertheless, there is a high probability that the infrequent phenotypes were basic artefacts due to fixed materials improperly spread. Confidently, all single KO mutants manifested a consistent phenotype.

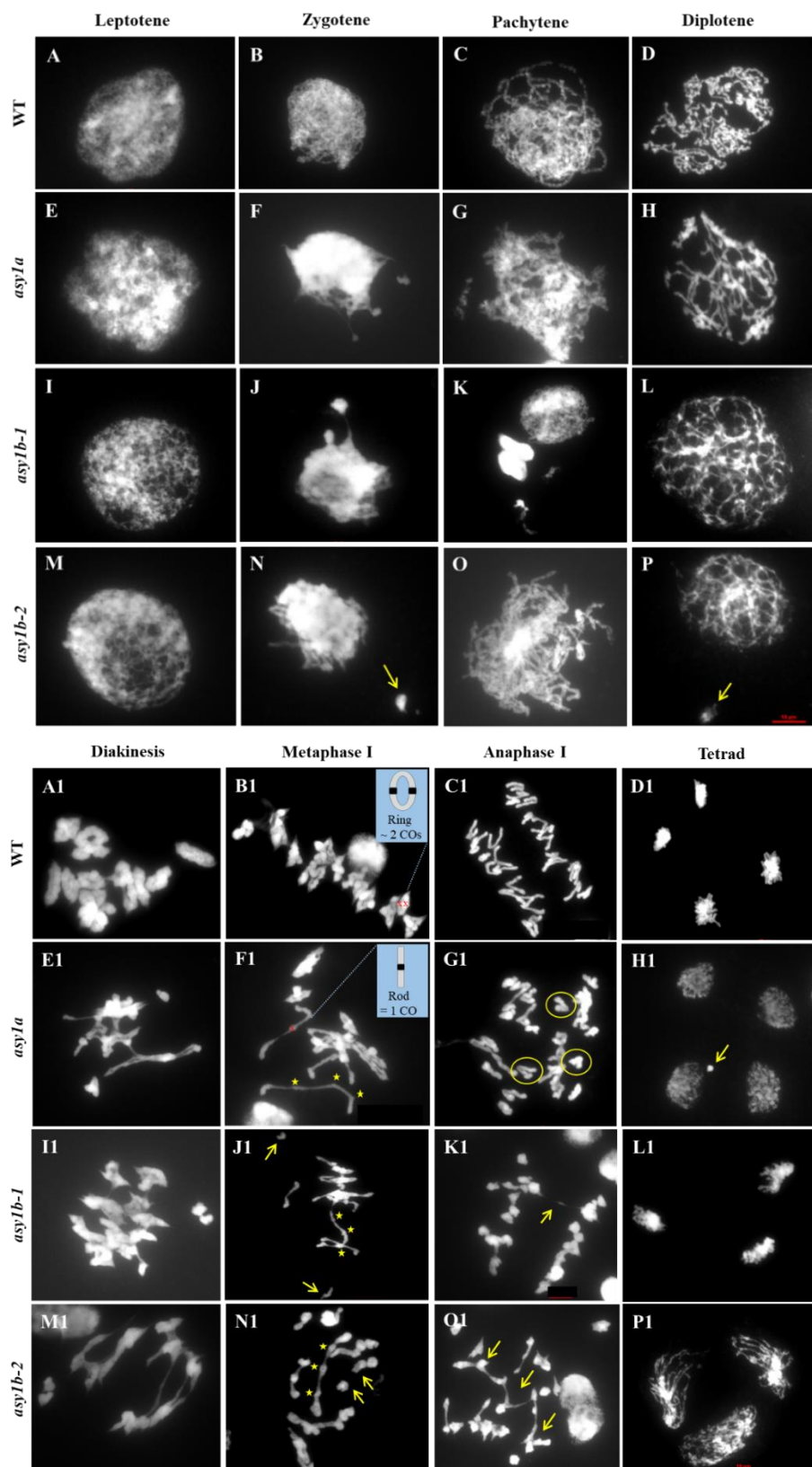


**Figure 2.20 Cytological atlas of *asy1* single KO mutants.** (A-P) Upper panel: male germ cells of WT Kronos at (A) leptotene, (B) zygote, (C) pachytene, (D) diplotene were compared with male germ cells from *asy1a*, *asy1b-1* and *asy1b-2* at (E, I, M) leptotene, (F, J, N) zygote, (G, K, O) pachytene and (H, L, P) diplotene stages. (A-M) Leptotene appeared similar in all genotypes

analysed. (N) At zygotene, *asy1b-2* showed the first sign of disorder (arrow). (G-O) During pachytene, *asy1a* and *asy1b* showed thicker chromatin (unpaired regions), extended until diplotene (H-P). (A1-P1) Lower panel: male germ cells of WT Kronos at (A1) diakinesis, (B1) metaphase I, (C1) anaphase I, (D1) tetrad stages were compared with male germ cells from *asy1a*, *asy1b-1* and *asy1b-2* at (E1, I1, M1) diakinesis, (F1, J1, N1) metaphase I, (G1, K1, O1) anaphase I and (H1, L1, P1) tetrad stages. In the WT: (A1) fourteen ring bivalents at diakinesis, linearly oriented on the equatorial plate (B1). (C1, D1) Balanced anaphase and tetrads, respectively. In *asy1a* and both *asy1b* lines: (E1-M1) Chromatin stickiness at diakinesis (F1) Prevalence of rod bivalents (arrow), tetravalent formation (F1, N1, stars indicating chiasma points) and univalents (J1, arrows) at metaphase I. (G1) Univalent mis-segregation (circles) and chromosome bridges at anaphase I (K1, O1, arrows). (H1) Unbalanced tetrads (arrow) or triads (L1, P1). DNA is counterstained with DAPI and shown in grey. Scale bars = 10  $\mu$ m.

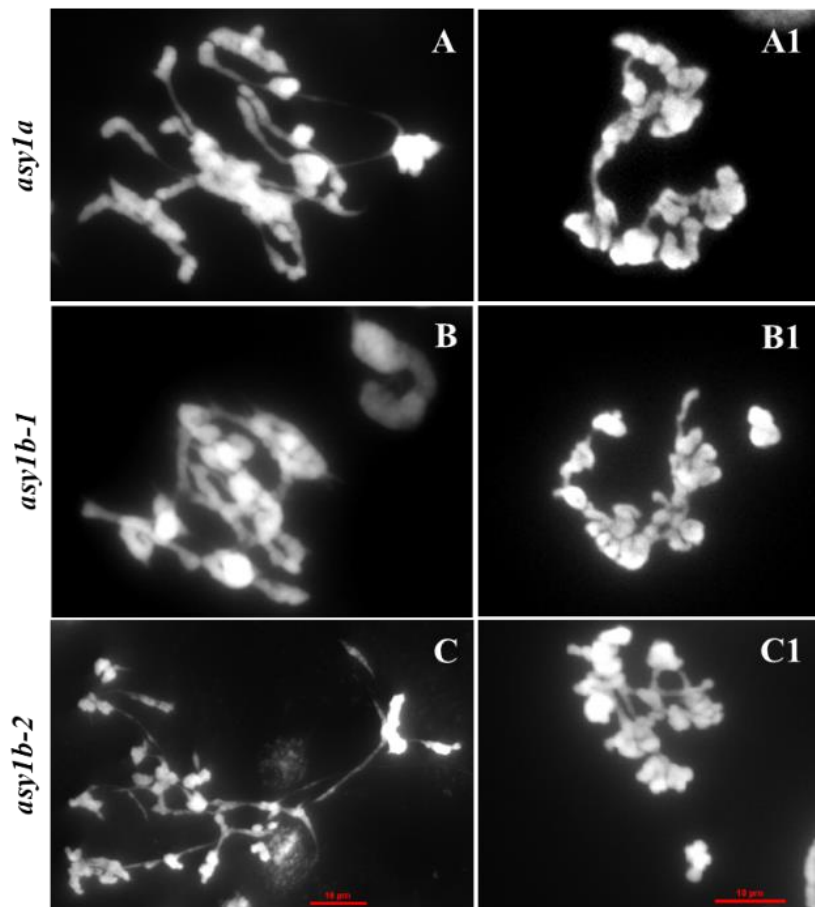


**Figure 2.21 Additional metaphase I phenotypes of *asy1* TILLING mutants.** (A-C) Chromosome stickiness and (A1-C1) chromosome clusters were typical of all genotypes. DNA is counterstained with DAPI and shown in grey. Scale bars = 10  $\mu$ m.

### 2.3.7 *asy1* single KO displays multivalent interaction but reduced chiasmata

The number of chiasmata in the WT genotype ranged from 21 to 30 per nucleus with the mean frequency of  $26.14 \pm 2.18$  ( $n = 50$ ) (Figure 2.22 a), consistent with the CO numbers (mean = 26.22) estimated in the same species by Desjardins et al., (2020b). In *asy1a*, significantly fewer chiasmata were observed compared to the WT, ranging from 16 to 27 per nucleus with a mean of  $22.44 \pm 2.79$  ( $n = 50$ ) (Figure 2.22 a), and a decrease of ring bivalents ( $9.12 \pm 2.45$ ,  $n = 50$  versus  $11.24 \pm 1.66$ ,  $n = 50$  WT), was observed ( $P < 0.01$ ). Similarly, *asy1b-1* and *asy1b-2* exhibited  $22.48 \pm 2.80$  and  $22.58 \pm 2.44$  chiasmata per nucleus (both  $n = 50$ ), respectively, with a prevalence of rod bivalents ( $3.50 \pm 2.14$  and  $3.74 \pm 1.59$ , respectively,  $n = 50$  versus  $2.6 \pm 1.67$ ,  $n = 50$  observed in the WT) rather than ring bivalents ( $P < 0.01$ ) (Figure 2.22 b). Reduced chiasma values for all *asy1* single KO lines were not significantly different (pairwise Wilcoxon rank sum test,  $P_{adj} > 0.05$ ,  $n = 50$  *asy1a*,  $n = 50$  *asy1b-1* and  $n = 50$  *asy1b-2*), rather they significantly differed from the WT (pairwise Wilcoxon rank sum test,  $P_{adj} < 0.001$ ,  $n = 50$  each single *asy1a/b* lines and  $n = 50$  WT) (Figure 2.22 c). All mutants exhibited a ~6-fold increase of univalents (Figure 2.22, bar chart), which reflected in approximately 15% reduction in chiasmata per nucleus in *asy1a* and *asy1b*. Multiple chromosome interactions, prevalently tetravalents (6-8%,  $n = 50$ ), were also common in the three lines evaluated (Figure 2.22 a). Chiasma count datasets are provided in Appendix (Table S2).

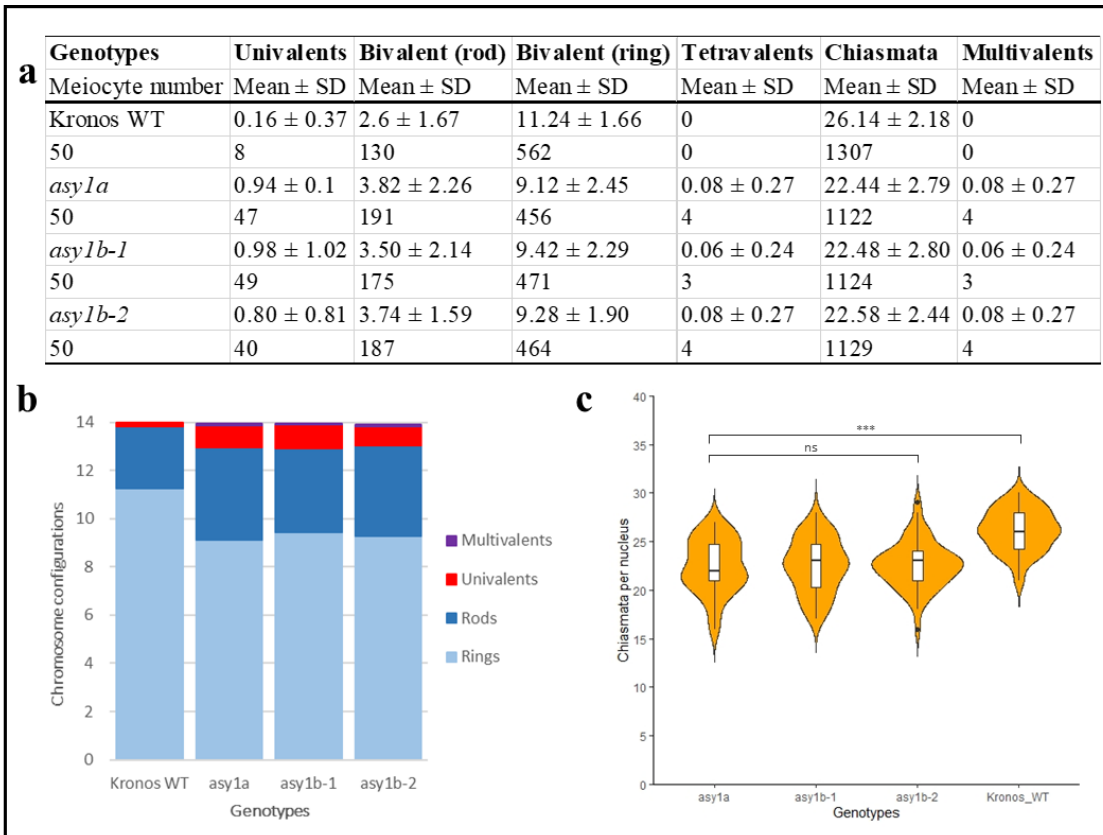


**Figure 2.22** *asy1* single KO mutants display altered chromosome configuration at metaphase

I. a) Table summarising: average, standard deviation (SD), range of bivalents, univalents, multivalents and chiasmata per male meiocyte in Kronos WT and TILLING lines analysed. n = number of meiocytes; minimum two independent plants per genotype. b) Bar chart illustrates the mean values of rings bivalents (sky blue), rods bivalents (dark blue), univalents (red) and multivalents (purple) per cells among WT and *asy1* single mutants. Legend is on the right. c) Violin plot exemplifies chiasmata frequency per male meiocyte. ns= not significant; asterisks indicate significant difference by pairwise Wilcoxon rank sum test (\*\* P adj < 0.001). The adjustment methods include the Bonferroni correction.

Notably, these data resemble the *ph1b* phenotypes (Sears, 1977). Hence, it was hypothesised that *ASY1-5B* may have been included within the *ph1b* region originally deleted (Sears, 1977). Deletion analyses of *Ph1 locus* have identified a list of candidate genes within the *ph1b* mutant (Griffiths et al., 2006; Al-Kaff et al. 2008). This list in fact contains uncharacterized genes, which may include *ASY1-5B* (Figure 2.23). Therefore, the genetic map of the wheat chromosome 5B (long arm) was investigated using Ensembl Plants database and it revealed that *ASY1-5B* was outside the defined 2.5 Mb of the *Ph1 locus* (Griffiths et al., 2006) and close to *ZIP4-5B* (Figure 2.23).

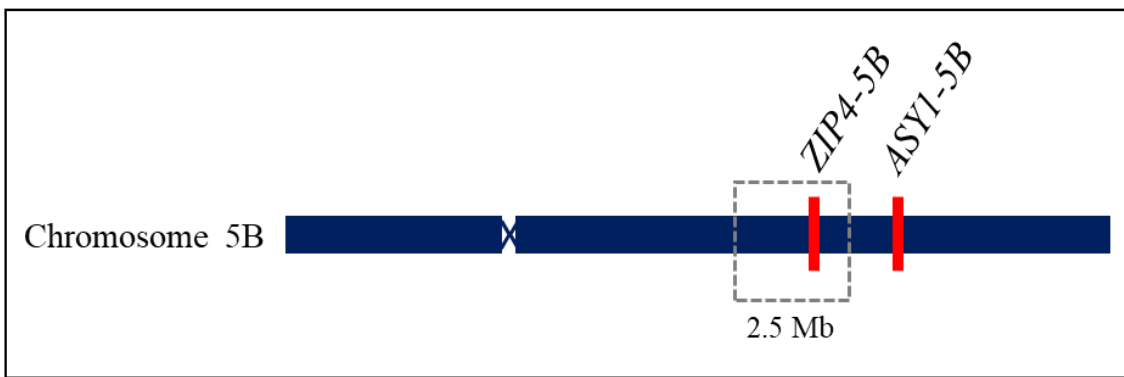


**Figure 2.23 Schematic representation of the physical map of *T. aestivum* chromosome 5B.**  
The *TaASY1-5B* homoeologous is mapped outside the 2.5 Mb deletion region of the *Ph1* locus (dashed rectangle) (Griffiths et al., 2006), but it is ~34 Mb close to *TaZIP4-5B*.

### 2.3.8 Cytological atlas of *asy1* double KO

The generation of *asy1* double KO was only achieved from the *asy1-b2* x *asy1a* cross (K2071 x K0706 TILLING lines). Instead, for *asy1b-1* (K0157 line), one backcross to the WT were performed in order to abolish the secondary mutation load manifested in form of non-mendelian segregation among the F<sub>2</sub> segregants from *asy1-b1* x *asy1a* cross (K2071 x K0706 TILLING lines). Unexpectedly, despite the backcross, the PCR-based genotyping and the Chi-square ( $\chi^2$ ) showed that the F<sub>2</sub> generation's segregates were subjected to Mendel's law of independent assortment (the alleles of two or more different genes are sorted into gametes independently of one another). The result of the Chi-square is provided in Appendix (Table S3). In addition, a large reduction in fertility was found among segregating families, supporting the idea that the mutation load was not removed despite the backcross, hence, the resulting phenotype was independent from *TtASY1* and therefore not suitable for the analysis.

Therefore, the project was mainly focused on the *asy1 aabb* genotype generated from the *asy1b-1* x *asy1a* cross (K2071 x K0706 lines). Unfortunately, due to the unpredicted difficulty to stage male meiocytes from plants carrying *asy1* double KO (aabb) mutation, resulted mostly asynchronous and with developmental defects (premature senescence), it was decided to add *asy1* triple allele mutant genotypes (Aabb and aabB) to expand this analysis.

First, as previously, chromosome spreads from fixed anther samples were used to record meiotic stages where chromosome behaviour becomes aberrant in *asy1 Aabb*, *asy1 aabB*

and *asy1 aabb* genotypes (Figure 2.24). Here, male germ cells were completely asynchronous, making challenging the identification of the correct meiotic stages when associated to the corresponding anther size. The first sign of disorder appeared early, during leptotene (Figure 2.24 A-G). At zygotene, SC failed to form between most homologous chromosomes (Figure 2.24 B-E, arrows) or possibly in any, as in *asy1* null mutants (Figure 2.24 H). Synapsis and chiasma formation was impaired (Figure 2.24 C, F, arrows), and it was not possible to find any meiocytes at pachytene and diplotene stages in *asy1* double mutants (Figure 2.24 I, P), therefore cells with complete synapsis were never observed. Chromosomes did not pair properly in *asy1 Aabb*, *asy1 aabB* at diplotene (Figure 2.24 J, M). Chromosome configurations were irregular in these genotypes, including univalents at metaphase I (Figure 2.24 K, starts), precocious chromatid separation or monad (Figure 2.24 N, arrow), and rarely, chromosome interlocks (Figure 2.24 N, circle), and multivalents (Figure 2.25), all together resulting in the asynchronous chromosome segregation during anaphase I (Figure 2.24 L O, arrows) and a subsequent semi-fertile phenotype (Table 2.8). Specifically, a ~64% decrease of fertility was recorded in these lines (Table 2.8). Intuitively, a more extreme condition was observed in *asy1 aabb* at metaphase I, where only univalents were present (Figure 3.10 Q), which continually led to lagging chromosomes during anaphase I (Figure 2.24 R, arrows) and complete sterility (no seed was produced) (Table 2.8).

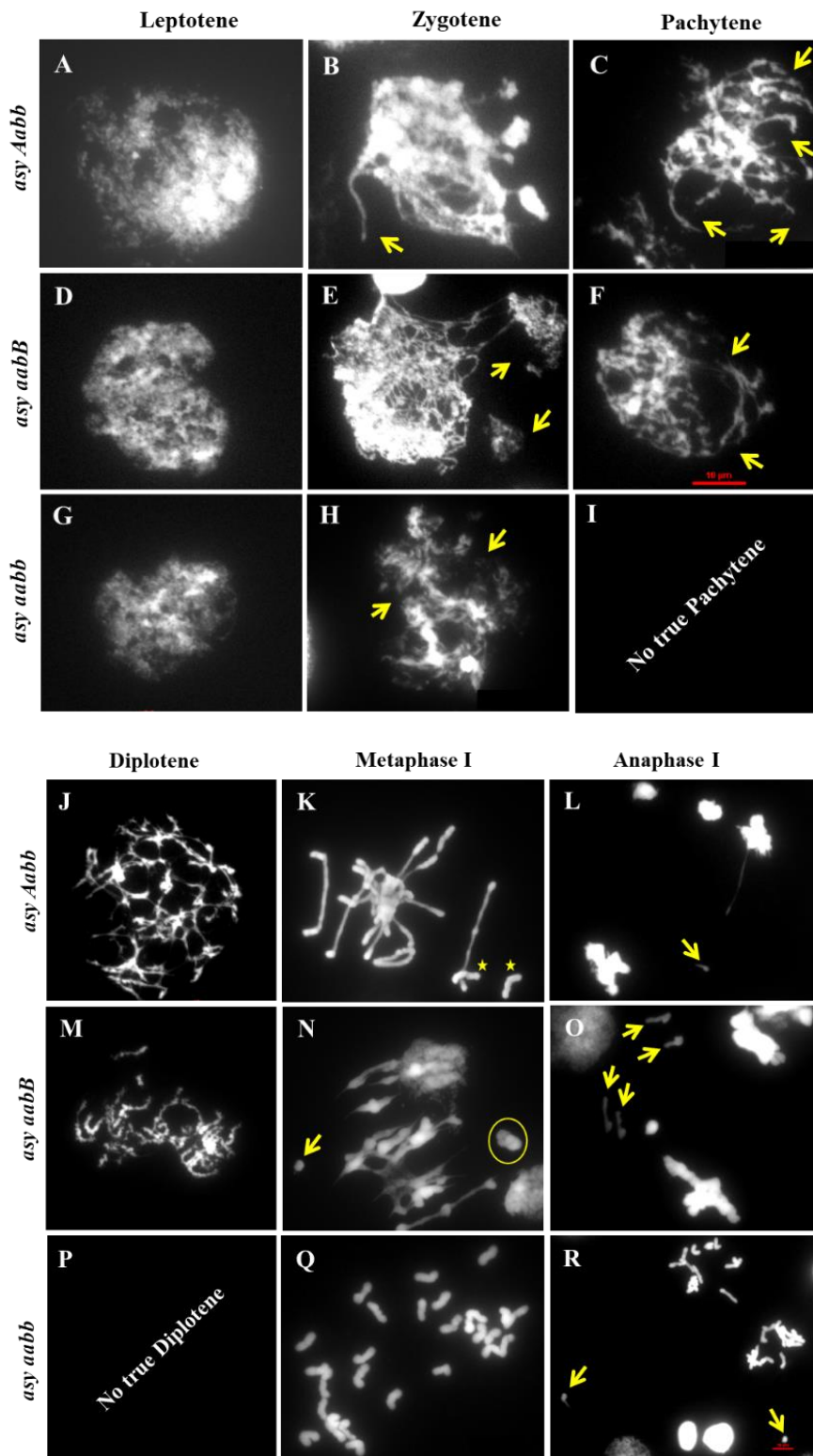


**Figure 2.24 Cytological atlas of *asy1 Aabb*, *asy1 aabB* and *asy1 aabb* mutants.** (A-I) Upper panel: male germ cells from leptotene to pachytene. (A-G) In all *asy1* mutants, chromatin appeared already disorganized at leptotene. (B-H) Zygote-like stage in *asy1 Aabb*, *asy1 aabB* and *asy1 aabb*, respectively, showing SC disruption (arrows). (C-I) Asynapsed sites in *asy1 Aabb* and *asy1 aabB* meiocytes (arrows) at pachytene-like stage. No meiocyte was correlated to

pachytene in *asy1* null mutants. (J-R) Lower panel: male germ cells from diplotene to anaphase I. (J-P) Diplotene was very similar to pachytene stage, where chromatin appeared progressively thicker and disassemble (unpaired regions), and it was not detected in *asy1 aabb*. (K, N) Metaphase I in *asy1 Aabb*, *asy1 aabB* showing univalents (K, starts), monad (N, arrow), chromosome interlock (N, circle). (Q) Twenty-eight univalents were present in all *asy1 aabb* meiocytes. (L-R) Lagging chromosomes migrating outside the pole during anaphase I (arrows). DNA is counterstained with DAPI and shown in grey. Scale bars = 10  $\mu$ m.

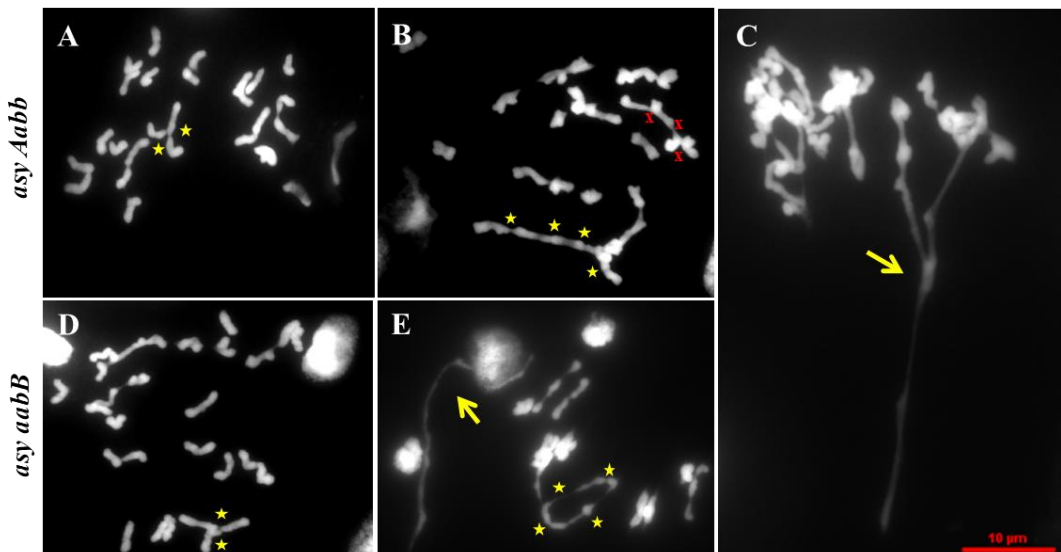


**Figure 2.25 Additional Metaphase I phenotypes in Kronos *asy1 Aabb* and *asy1 aabB*.** (A-C) *asy1 Aabb*. (D-E) *asy1 aabB*. (A, D) Trivalents (stars). (B) Tetravalent (red crosses) and pentavalent (stars) (C) Multivalent (arrow). (E) Tetravalent (stars) and multivalent (arrow). DNA is counterstained with DAPI and shown in grey. Scale bars = 10  $\mu$ m.

### 2.3.9 *asy1* has a dosage dependent effect on homologous recombination

CO formation was reduced, but not abolished in *asy1* single mutants. As expected, in *asy1 Aabb*, a significant increase of rod bivalents per nucleus ( $6.18 \pm 4.29$ , n = 50) at the expense of ring bivalents were observed, compared with *asy1b-1* and *asy1b-2* ( $3.50 \pm 2.14$  and  $3.74 \pm 1.59$ , n = 50 each line) (Figure 2.26 a), and the incidence of unpaired chromosomes (univalents) (Figure 2.26 a). Likewise, *asy1 aabB* rod bivalents ( $6.30 \pm 4.22$ , n = 50) prevailed over ring bivalents (56-57% reduction), with numerous univalents formed at metaphase I ( $3.56 \pm 5.27$ , n = 50), compared to the single mutants *asy1a* ( $3.82 \pm 2.26$ , n = 50); univalents also increased ~4-fold (Figure 2.26 a). All together, these data coincided with a significant 33-34% reduction in chiasmata per nucleus in *asy1 Aabb* and

*asy1 aabB*, respectively (Figure 2.26 b), from ~22 COs every fifty cells in *asy1* single mutants to ~15 COs in the triple mutants. Multivalents also increased compared to the single KO genes ( $0.18 \pm 0.48$ ,  $n = 50$ ) (Figure 2.26 a). As a result, *TaASY1-5A* and *TaASY1A-5B* triple allele mutants induced an apparent 2.25-fold increase in homoeologous recombination, although this would need to be confirmed with either molecular or cytological markers.

When compared to the WT, *asy1 Aabb* and *asy1 aabB* genotypes showed an additive effect of *TtASY1* in respect of chiasma frequency. Indeed, in *asy1 Aabb*, there was significant deviation in numbers of ring bivalents ( $11.24 \pm 1.66$ ,  $n = 50$  versus  $4.04 \pm 3.71$ ,  $n = 50$ , in the WT) and chiasmata ( $26.14 \pm 2.18$ ,  $n = 50$  versus  $15.14 \pm 8.40$ ,  $n = 50$ , in the WT) (Figure 2.26 c). Analogously, in *asy1 aabB*, a drop in ring bivalent mean number ( $3.80 \pm 3.57$ ,  $n = 50$ ) and consequently in chiasmata ( $14.58 \pm 8.16$ ,  $n = 50$ ) were observed (Figure 2.26 a). In other words, *asy1 Aabb* and *asy1 aabB* had approximately 42-43% less chiasmata per nucleus in comparison with the WT plants (Figure 2.26 b). There was also an 18% increase of multivalents, prevalently tetravalents, in the two genotypes evaluated (Figure 2.26 b). Lastly, from fifty *asy1 aabb* cells analysed, all cells showed 28 univalents (Figure 2.26 a), which led to a complete abolishment of the obligate chiasma and sterility (Figure 2.26 b). The whole metaphase I spread comparative analysis including all *asy1* TILLING mutant genotypes and the corresponding data values are summarised in Table 2.8. Chiasma count data sets are provided in Appendix (Table S4).

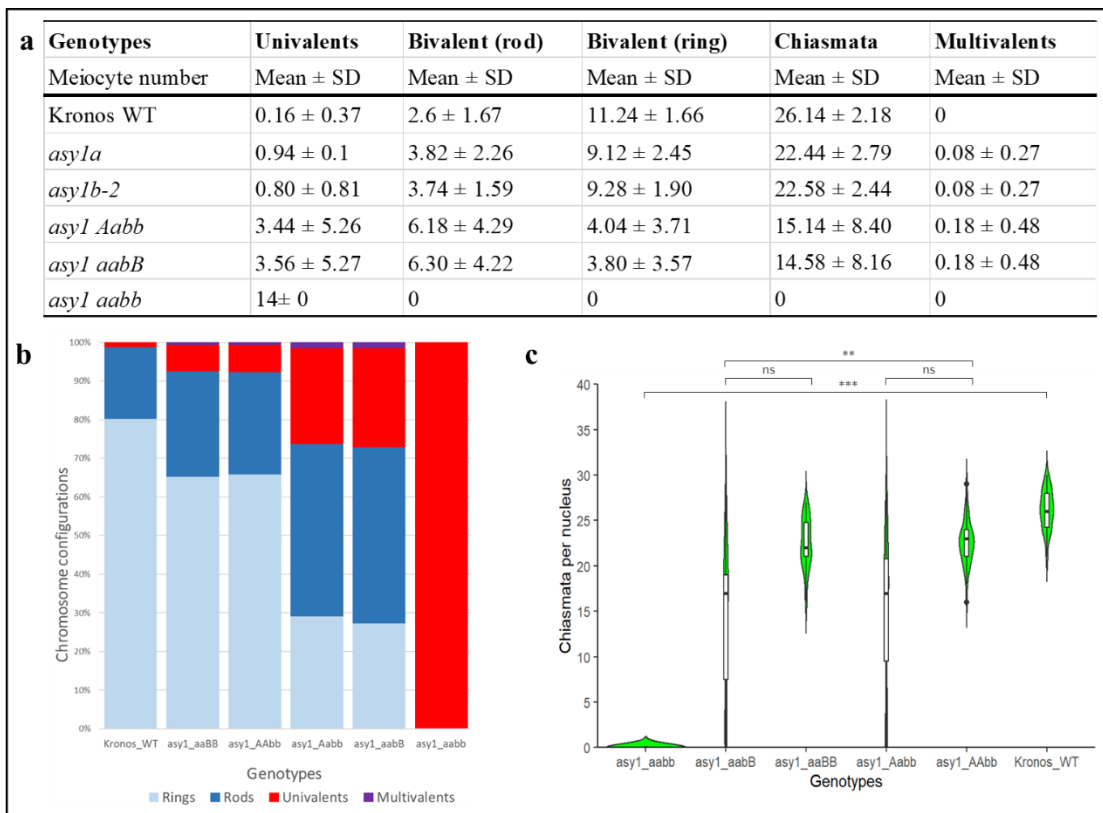


**Figure 2.26 All *asy1* genotypes display increased severity in chiasmata frequency at metaphase I.** a) Table summarises: average, standard deviation (SD), range of bivalents, univalents, multivalents and chiasmata per male meiocyte in Kronos WT and TILLING lines analysed. n = number of meiocytes; minimum two independent plants per genotype. b) Bar chart illustrates the mean values of rings bivalents (sky blue), rods bivalents (dark blue), univalents (red) and multivalents (purple) per cells among WT and *asy1* single mutants. Legend is at the bottom. c) Violin plot exemplifies chiasmata frequency per male meiocyte. Significant differences are indicated by pairwise Wilcoxon rank sum test (Signif. codes: 0 ‘\*\*\*’ 0.001 ‘\*\*’ 0.01 ‘\*’ 0.05 ‘.’ 0.1 ‘ ’ 1). The adjustment methods include the Bonferroni correction.

<b>Genotypes</b>	<b>Univalents</b>	<b>Rods</b>	<b>Rings</b>	<b>Multivalents</b>	<b>Chiasmata</b>	<b>Fertility</b>
<i>Kronos WT</i>	-	-	-	-	-	-
<i>asy1a</i>	6 fold rise	1.3 fold rise	18% drop	6-8% rise	15% drop	25% drop
<i>asy1b-1</i>	6 fold rise	1.3 fold rise	18% drop	6-8% rise	15% drop	21% drop
<i>asy1a-b2</i>	6 fold rise	1.3 fold rise	18% drop	6-8% rise	15% drop	35% drop
<i>asy1 Aabb</i>	4 fold rise s	1.6 fold rise s	56-57% drop s	2 fold rise s	42-43% drop s	64% drop
<i>asy1 aabB</i>	4 fold rise s 21.5% wt	1.6 fold rise s 24% wt	56-57% drop s 63% wt	2.25 fold rise s 15% rise wt	33.35% drop s 42-43% drop wt	64% drop
<i>asy1 aabb</i>	100%	0	0	0	0	100% drop
<i>asy1 AAbbDD</i>	6 fold rise	1.2 fold rise	6% drop	6% rise	5% drop	-

**Table 2.8 Summary of metaphase I spread analysis comprising all *asy1* TILLING mutant genotypes.** *asy1* single KO data were compared with WT data, while *asy1* triple allele mutant data were compared with WT and *asy1* single KO data. wt= wild type; s= single KO. Fertility data expressed in percentage are also shown in the last column on the right.

### 2.3.10 Fertility assessment

To assess whether meiotic chromosome abnormalities caused by *asy1* were associated with changes in fertility, seeds were scored from Kronos segregating WT and *asy1* mutants. In Kronos WT, the average number of seeds per inflorescence from the primary tiller was 22 seeds (n = 3), while in all *asy1* mutants, fertility was largely compromised. In *asy1* single KO mutants, the seed sets were significantly reduced by 25%, 21% and 35% in *asy1a*, *asy1b-1* and *asy1b-2* respectively, compared to WT (Table 2.9). In *asy1 Aabb* and *asy1 aabB* only one inflorescence was fertile, and finally, *asy1 aabb* had completely sterile anthers. Consistently, a ~64% decrease of fertility was recorded in *asy1 Aabb* and *asy1 aabB* mutants (Table 2.9).

<b>Genotype</b>	<b>Plant 1</b>	<b>Plant 2</b>	<b>Plant 3</b>	<b>Average ± SD</b>
Kronos WT	24	24	18	22 ± 3.46
<i>asy1a</i>	22	16	12	16.6 ± 5.03
<i>asy1b-1</i>	20	18	14	17.3 ± 3.05
<i>asy1b-2</i>	18	14	10	14 ± 4
<i>asy1 Aabb</i>	8	0	0	8 ± 4.62
<i>asy1 aabB</i>	8	0	0	8 ± 4.62
<i>asy1 aabb</i>	0	0	0	0 ± 0

**Table 2.9 Seed-set score for Kronos TILLING lines.** Counts for both segregating WT and allelic mutants of *asy1* seeds extracted from the primary inflorescences of three distinct individuals were recorded. Seven genotypes, WT control included, have been analysed.

### 2.3.11 *asy1* single KO mutants exhibit a slight delay in spatio-temporal localization of ZYP1

To determine if the loss of a single *TtASY1* gene would still allow its localization on chromosome axes to correctly form the SC, the dynamics of the chromosome axis marker *TaASY1* (Sanchez-Moran et al., 2007) and the transverse filament protein, *AtZYP1* (Higgins et al., 2005) were cytologically monitored in tetraploid *T. turgidum* cv. Kronos during prophase I (Figure 2.27). Since the *asy1* single KO mutants were predicted to retain the HORMA domain, the antibodies anti-*TaASY1* (HORMA) used in this work should still localise onto the chromatin of all mutants if the HORMA domain is sufficient for the protein to localise. However, the protein would be expected to be non-functional and downstream effects would be observed.

Kronos meiocytes were staged according to anther length and the size of the anthers correlated to individual meiotic stage (MeioCapture method) (Shunmugam et al., 2018), as shown in Figure 2.27 in brackets. In WT, at early stage of G2 (0.6 mm), ASY1 was detected as numerous foci distributed throughout the nucleus (Figure 2.27), which then formed short linear stretches during the onset of leptotene (0.7 mm) (Figure 2.27 A1), similarly to *Arabidopsis*, *Brassica* and *Oryza*, ASY1/PAIR2 (Armstrong et al., 2002; Sanchez-Moran et al., 2007, Nonomura et al., 2006). At this stage, ZYP1 formed distinctive axis-associated foci at specific sites, where the SC begins to assemble along both homologs. During zygotene (0.8 mm) (initiation of SC assembly and chromosomes synapses), ASY1 signals were entirely linearized and ZYP1 signals gradually extended until pachytene (0.9 mm) (Figure 2.27 A2). As synapsis progressed, ASY1 signals became discontinuous with varying intensities near the nucleolus (unstained circular body within each meiocyte), consistent with observations in *Arabidopsis* that the nucleolar organizing regions do not undergo synapsis (Sims et al., 2021), while ZYP1 signal elongation, marking the synapsis regions, continued throughout the nucleus between homologous chromosomes (Figure 2.27 A3) until homologous chromosomes completed synapsis. By diplotene (1.0 mm) (initiation of SC disassembly and chromosomes desynapsis), ASY1 underwent partial degradation resulting in fragmented ASY1 threads which progressively remodelled into coiled structures that resemble polycomplexes

(Lambing et al., 2015) (Figure 2.27 A4), and ZYP1 signals were no longer detectable. Considering the nucleous size (smaller than 10 $\mu$ m) of *asy1* mutants, it is more likely that these are apoptotic cells (Figure 2.27 B4-D4).

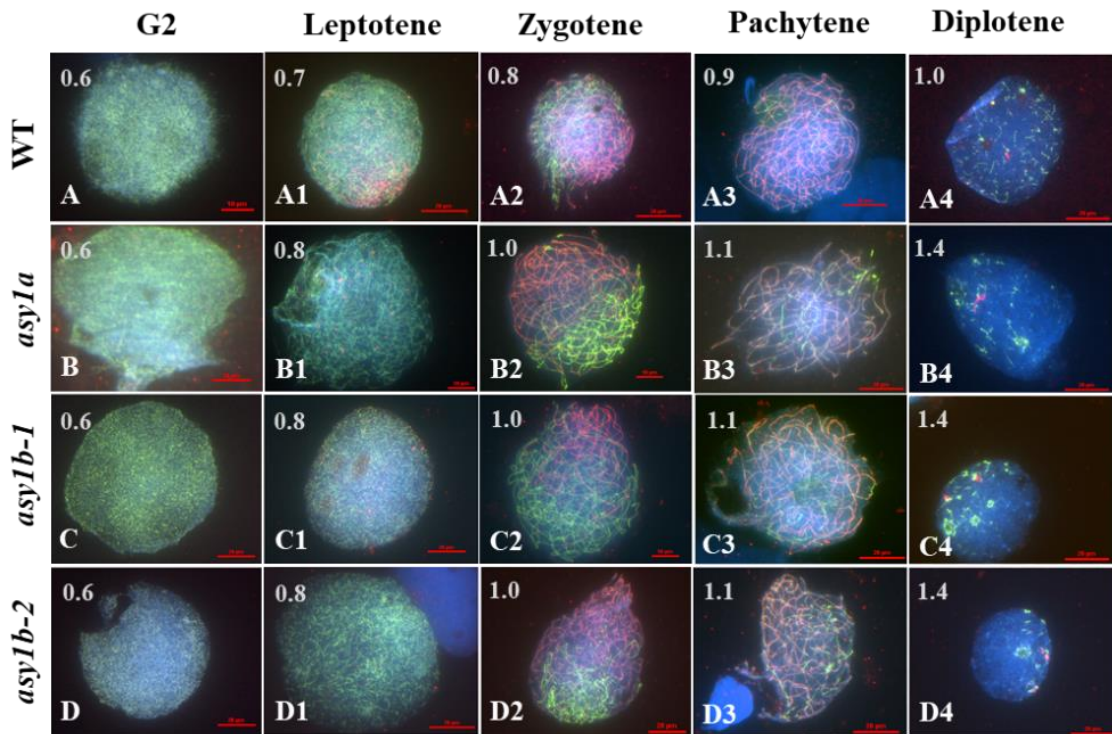


**Figure 2.27 Meiotic prophase I progress of PMCs in *T. turgidum* cv. Kronos and *asy1* single KO mutants.** (A-D4) Chromosome axes were marked with ASY1 (green), transverse filaments connecting homologous chromosomes were detected via ZYP1 (red), and chromatin was counterstained in DAPI (blue). Anthers ranging from 0.6 to 1.4 mm in length, shown on the top left of each image, corresponds to distinct meiotic sub-stages. (A-D) Pre-meiotic G2. (A1-D1) Leptotene. (A2-D2) Zygote. (A3-D3) Pachytene. (A4-D4) Diplotene-like. (B-B4) *asy1a*, (C-C4) *asy1b-1*, and (D-D4) *asy1b-2* mutants exhibited slightly delay during meiotic prophase I in comparison with the WT (A-A4). In all images, the nucleolar region is represented as an unstained circular body within the PMCs. Scale bar = 10 and 20  $\mu$ m.

In *asy1a* and *asy1b*, axis formation marked by ASY1 (green) initiated normally at pre-meiosis/G2 stage, when the anthers measured 0.6 mm, as in WT (Figure 2.28 B-D). ASY1 polymerization was indistinguishable with the WT until leptotene (Figure 2.28 B1-D1), however ZYP1 became visible later (Figure 2.28 B1-D1), when the anthers reached 0.8 mm (versus 0.7 mm in WT). In these mutants, ASY1 resulted in a WT-like phenotype, while ZYP1 appeared as foci or short stretches.

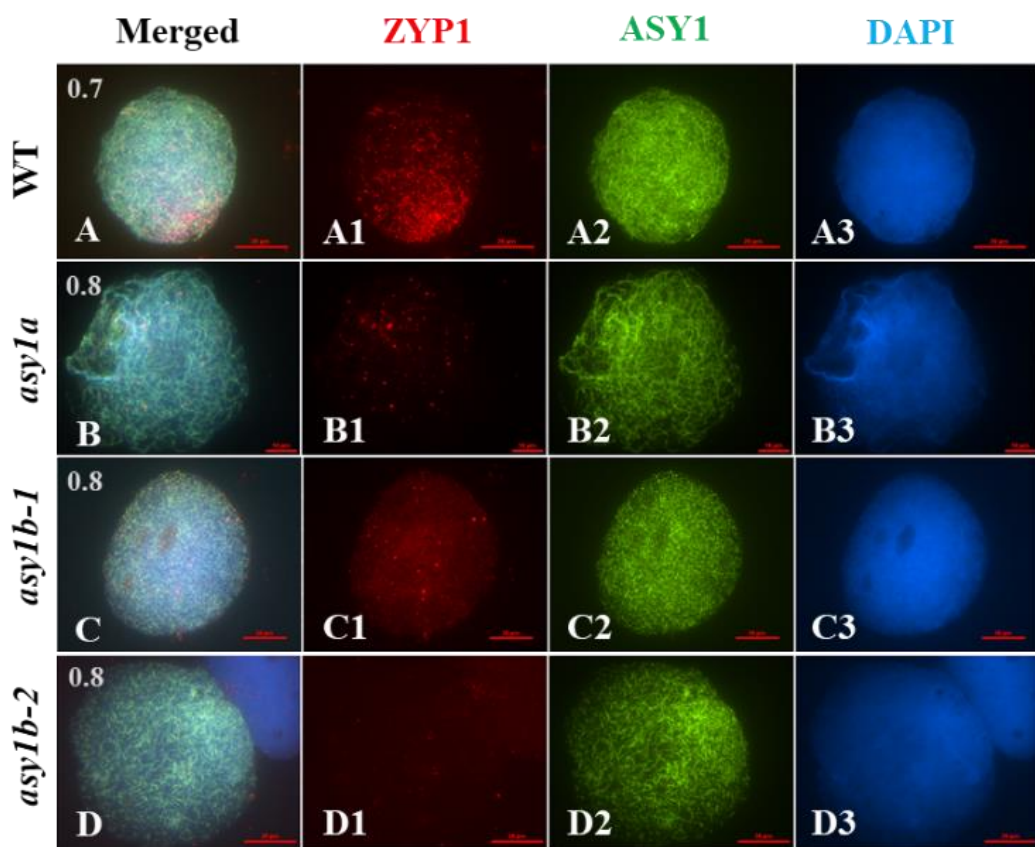


**Figure 2.28 Immunolocalization of *TaASY1* and *AtZYP1* at meiotic leptotene stage in PMCs of WT Kronos and *asy1* single KO in A and B sub-genomes.** (A-A3) WT Kronos. (B-B3) *asy1a*. (C-C3) *asy1b-1*. (D-D3) *asy1b-2*. (A-D) merged images of (A1-D1) transverse filament ZYP1 (red), (A2-D2) chromosome axis ASY1 (green) and (A3-D3) chromatin counter-stained with DAPI (blue). (A1) At leptotene, ZYP1 begin to linearize in WT, but not in *asy1* single mutants (B1-D1), where ZYP1 signals still appear as punctuate foci in the nuclei. (A2) WT axial elements were marked by continuous ASY1 labelling (green), as in all *asy1* single mutants (B2-D2). Anthers size (mm) are indicated on the top left of each merged image. Scale bar = 10 and 20  $\mu$ m.

As zygotene progressed, homologous chromosomes failed to pair, as indicated by altered ASY1 labelling (Figure 2.29 B2-D2, arrows). At this stage, ZYP1 never completely linearized (Figure 2.29 B1-D1). In addition, it is common to see small portions of isolated ASY1 signals (Figure 2.30 A1, dashed square insert) marking asynapsed sites, and occasionally chromosome interlocks (Figure 2.30 A2, dashed circle insert), indicating that SC formation is largely impaired/disorganized. Possibly, the search for the correct homologous chromosome in *asy1* single mutants was temporally

compromised. As a consequence, the SC structure appeared dissociated at pachytene (1.1 mm), as reflected by incomplete ZYP1 polymerization (discontinuous ZYP1 signal), demonstrating that homologous chromosome possibly did not fully synapse (Figure 2.31 B1-C1, dashed inserts).

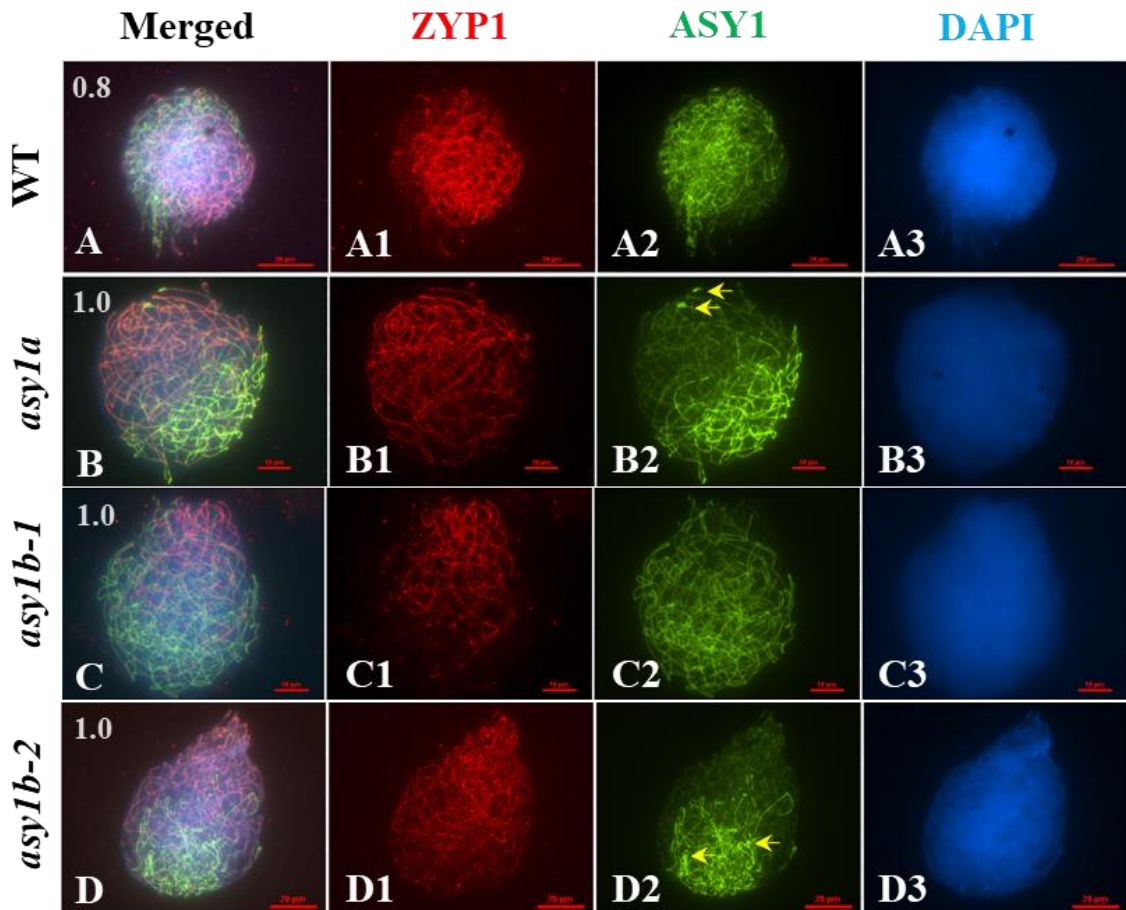


**Figure 2.29 Localization of *TaASY1* and *AtZYP1* against a zygotene PMCs of WT and *asy1*single KO mutants.** (A-A3) WT Kronos. (B-B3) *asy1a*. (C-C3) *asy1b-1*. (D1-D3) *asy1b-2*. (A-D) merged images of (A1-D1) transverse filament *AtZYP1* (red), (A2-D2) chromosome axis ASY1 (green) and (A3-D3) chromatin counter-stained with DAPI (blue). (A1) In WT, ZYP1 (red) is fully linearized at synapsis points. (B1-D1) In *asy1* single KO mutants, synapsis seems to start normally, but the polymerization of ZYP1 appears to be compromised. (A2) In WT, SC connects homologous chromosomes, while in *asy1* mutants, small portion of SC showed isolated ASY1 (green) signals, marking asynapsed sites (B2-D2). Anther sizes (mm) are indicated on the top left of each merged image. Scale bar = 10 µm (shorter red bar) and 20 µm (longer red bar).

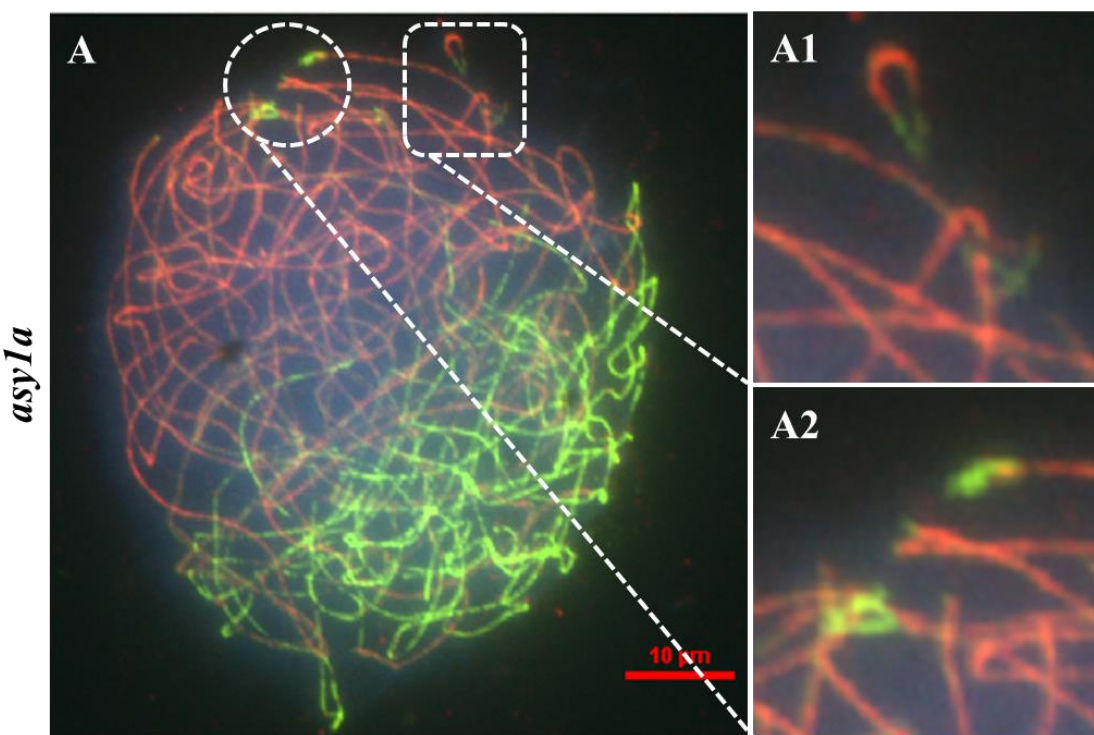


**Figure 2.30** PMC at zygotene stage *asy1a* mutant. A) Immunostaining of *AtZYP1* protein (red), *TaASY1* protein (green) in an *asy1a* nucleus, depicting an example of un-synapsed meiotic chromosomes. Signal fragmented coincides with desynapsis of the chromosomal axes. (A1) The tripartite structure of SC appears interrupted. (A2) Homolog chromosomes forming entanglement (interlock). Scale bars 10  $\mu$ m.

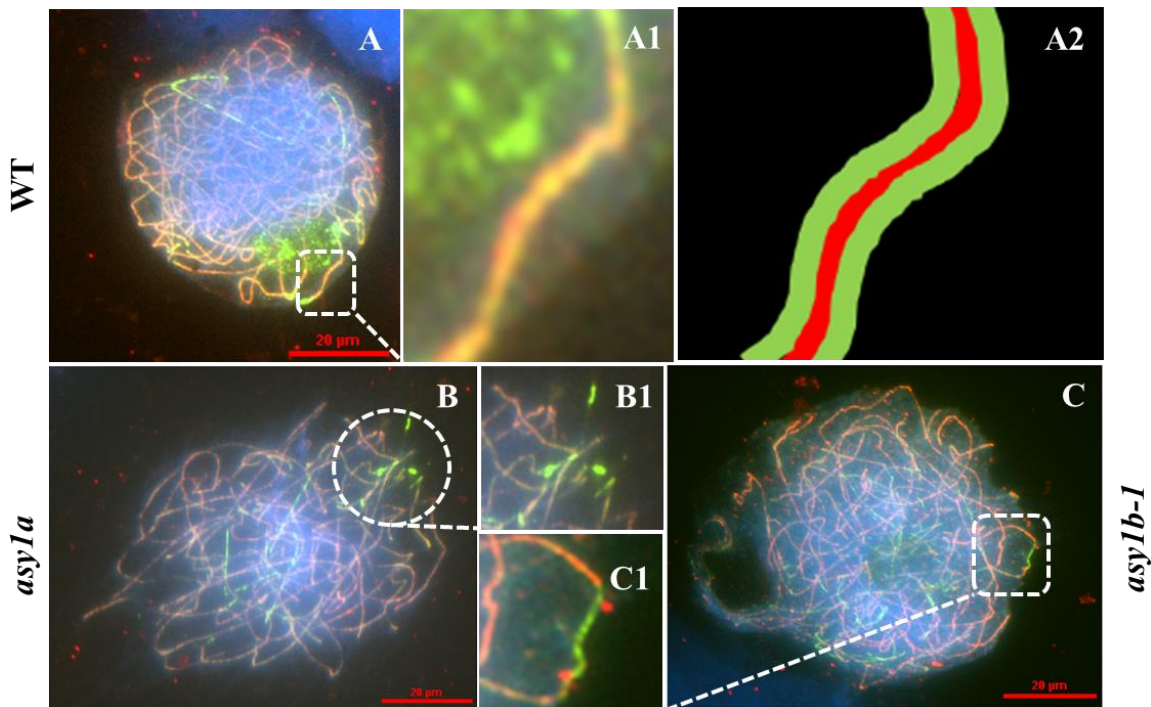


**Figure 2.31 Analysis of synapsis monitored by *TaASY1* (green) and *AtZYP1* (red).** (A) WT Kronos, (B) *asy1a* and (C) *asy1b-1* meiocytes at pachytene stage. (A) Synapsis is complete at pachytene with both *TaASY1* (green) and *AtZYP1* (red) overlapping. (A1) Detail of the tripartite structure of SC in the WT. (A2) Cartoon of axial element *TaASY1* (green) and transverse filament *AtZYP1* (red) in WT. (B1-C1) Absence of tripartite structure in *asy1a* and *asy1b-1*, respectively. Chromatin was counter-stained in DAPI (blue). Scale bar = 20  $\mu$ m.

At diplotene (1.4 mm), ASY1 and ZYP1 did not reduce into short fragments, but appeared as distinct foci (Figure 2.31). ASY1 proteins did not normally degrade, but remained in excess forming polycomplexes (chromatin regions with more intense ASY1 signal) (Figure 2.32), until later stage (Figure 2.33) as result of synapsis failures, or possibly meiocytes underwent apoptosis.

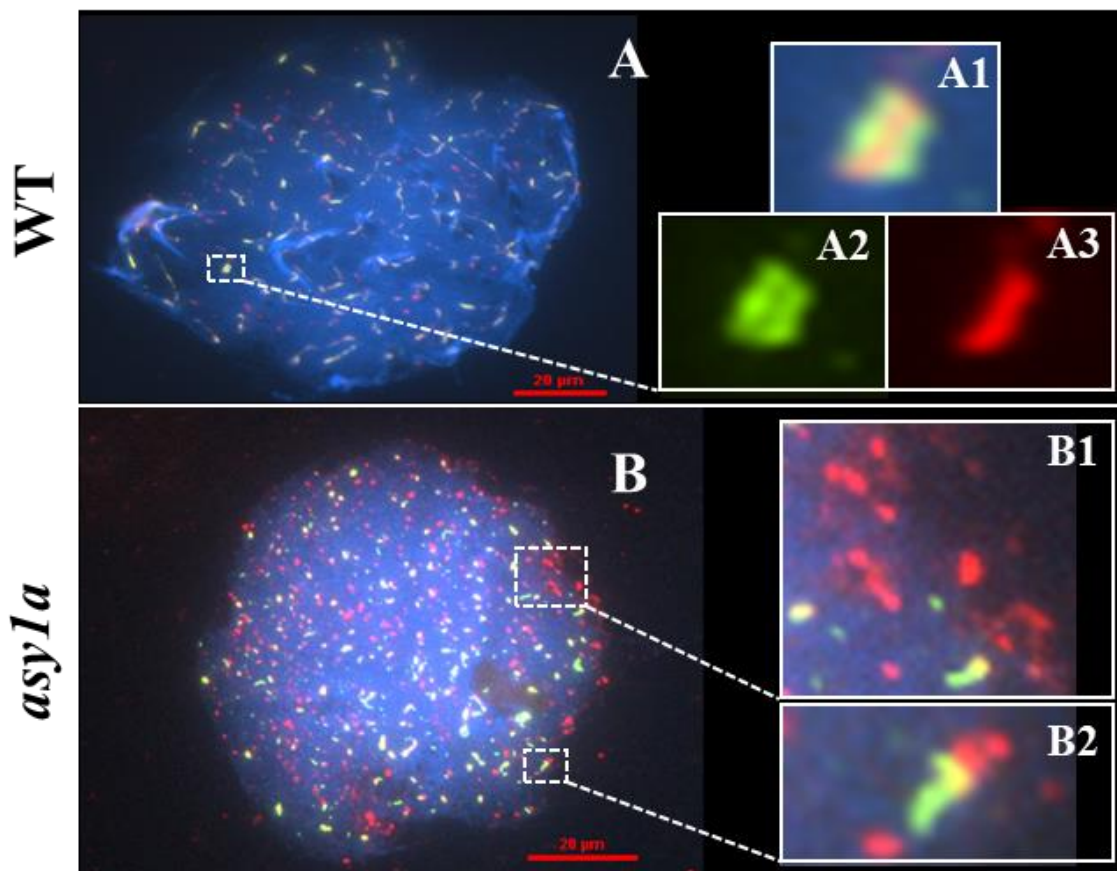


**Figure 2.32 Meiocytes of WT Kronos and *asy1a* mutant labelled with *TaASY1* (green) and *AtZYP1* (red) at diplotene stage.** (A) WT meiocyte showing normal SC disassembly, with (A1) the residual tripartite structure composed of (A2) short stretches of lateral element ASY1 and (A3) transverse element ZYP1 becoming fragmented, coinciding with desynapsis of the chromosomal axes. (B) *asy1a* meiocyte, with (B1-B2) punctate SC components. Chromatin was counter-stained in DAPI (blue). Scale bar = 20  $\mu$ m.

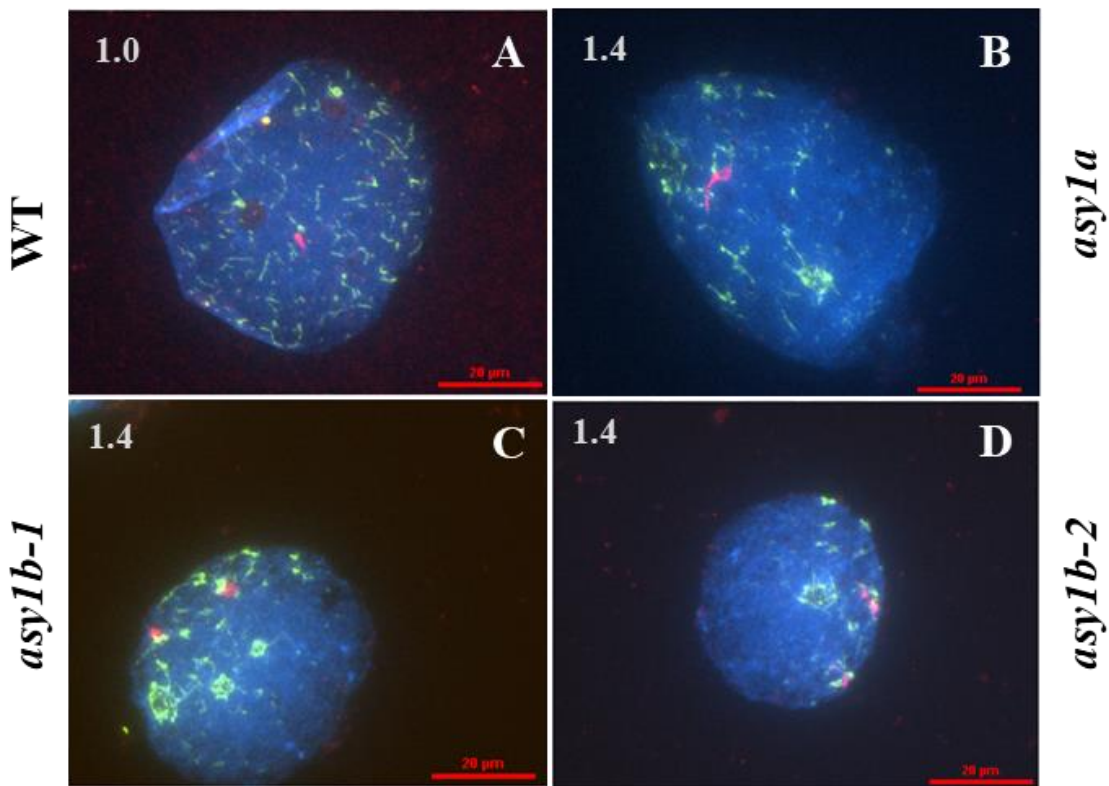


**Figure 2.33 PMCs of WT Kronos and *asy1* single KO mutants at late diplotene.** (A) WT, (B) *asy1a*, (C) *asy1b-1*, (D) *asy1b-2*. (A-D) Immunolocalization of *TaASY1* (green) and *AtZYP1* (red). (A) In WT, ASY1 form polycomplexes, which further aggregate and polarized in *asy1* mutants (B-D). Chromatin was counterstained in DAPI (blue). Anthers size (mm) are indicated on the top left of each image. Scale bar = 20  $\mu$ m.

### 2.3.12 ASY1 is required for SC assembly

Given the loss of spatio-temporal coordination in localizing the transverse filament protein ZYP1 in *asy1* mutants lacking functional sub-genome gene copies, triple *asy1* mutants heterozygous in B allele (aabB) were investigated for effect on SC morphogenesis. Previous inspection of DAPI-stained chromosome spread preparations from male meiocytes suggested chromosome axis formation was abnormal in *asy1 aabB* mutant. The SC morphogenesis in *asy1 aabB* was analysed cytologically using anti-*TaASY1* and anti-*AtZYP1* antibodies (Figure 2.34). Comparing with the single KO mutants, this phenotype was difficult to stage since the lack of an obvious correspondence between the anther size and the meiotic phases. Moreover, the reduced sample size (low germination rate) and premature senescence of the ears, where only the first tiller fully developed, negatively contributed to identify the exact collecting time of the sample. A variation from the conventional immunostaining technique was also performed to extract

and preserve the integrity of the male meiocytes of these genotypes. Ethanol-based fixed material (3:1 ethanol:acetic acid), subjected to heat treatment in microwave as described in Materials and methods, paragraph 2.2.15, was preferred to analyse the behaviour of target meiotic markers in *asy1 aabB*.

Overall, at early stages, ASY1 (green) localised to chromosome axes as discontinuous signals (Figure 2.34 D2), with no ZYP1 loading (Figure 2.34 D3-F3). Loss of the SC protein ZYP1 resulted in the expected failure to form SC. Zygote was largely perturbed, characterized by polycomplexes, indicating that ASY1 was not loaded in all chromosomes (Figure 2.34 E2). The polycomplexes persisted through pachytene-like (Figure 2.34 F2), and might result from the inability of the truncated ASY1 protein to resolve multiple axial element associations that have been observed in this mutant, and that are confidently thought to lead to multivalents at metaphase I (Holm & Wang, 1988). Insufficient ASY1 synthesis had obvious consequence for chromatin condensation at later stages, as no meiocyte in TILLING *asy1 aabB* nuclei were identified at diplotene/diakinesis. Evidently, the fragmentation of the ASY1 signal reflects a role of this protein as structural component of axial and lateral elements, which serves as a scaffold for the structural organization of chromatids, whose exact dosage is finely regulated to form the SC and ultimately sustain CO events.

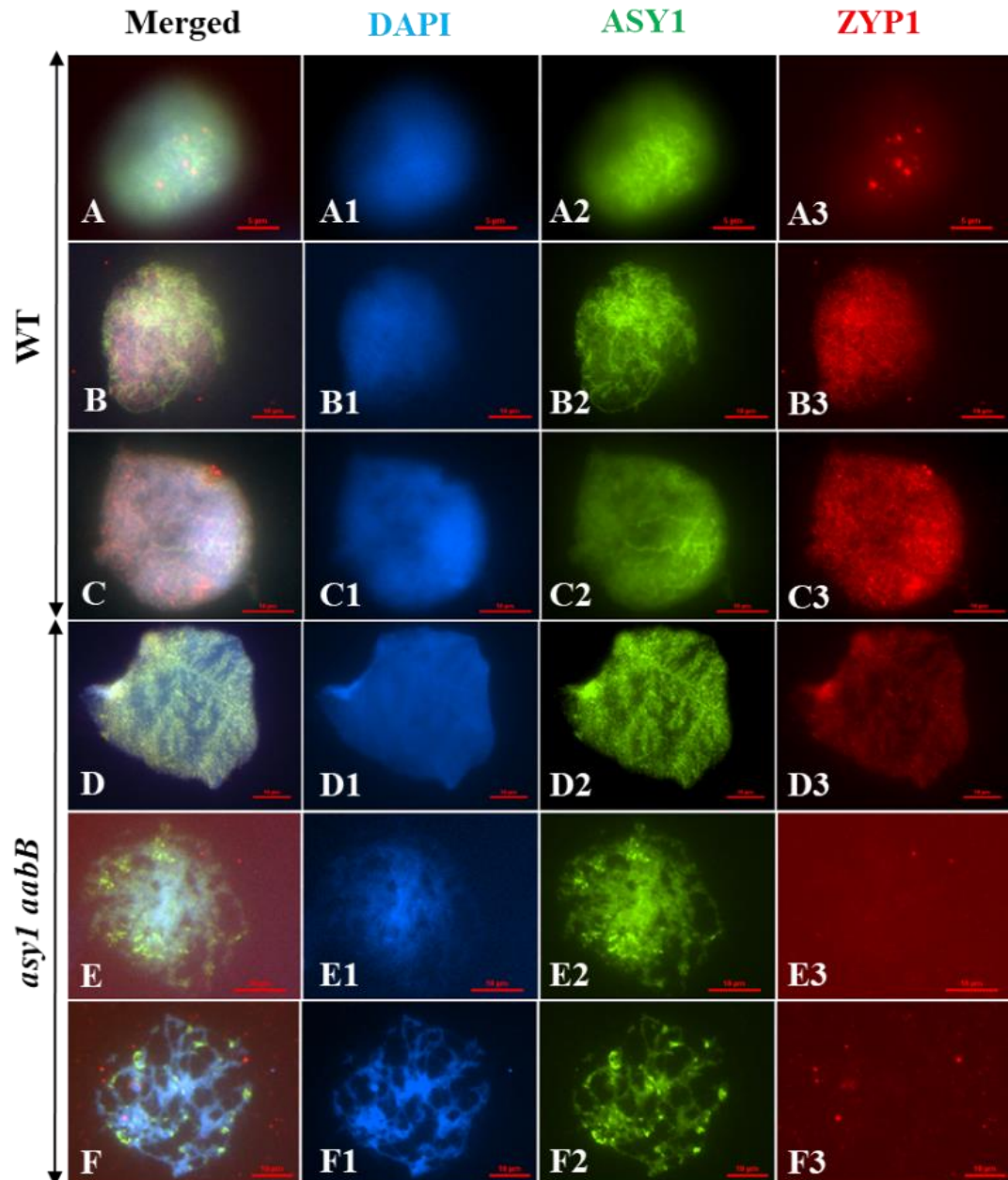


**Figure 2.34 Synapsis is defective in *asy1 aabB*.** (A-F) merged images of (A1-F1) chromatin counter-stained with DAPI (blue), (A2-F2) chromosome axis *TaASY1* (green), and (A3-F3) transverse filament *AtZYP1* (red). (A, D) Leptonene. (B, E) Zygotene. (C, F) Pachytene in WT and *asy1 aabB*, respectively. (D3-F3) ZYP1 was not detected in any meiotic stages, while ASY1 was unevenly distributed at leptotene (D2) and persisted during zygotene (E2) and pachytene-like (F2), forming polycomplexes in asynapsed regions. DNA is counterstained with DAPI and shown in blue. Scale bar = 10μm.

### 2.3.13 ASY1-ASY3 interaction may rely on ASY1 HORMA domain

The development of chromosome axis formation during meiotic prophase I was followed by co-immunolocalization of *TaASY1* (Sanchez-Moran et al., 2007) and the coiled-coil

protein *AtASY3* (Ferdous et al., 2012a) in *asy1 Aabb* (Figures 2.35). Fixed material (3:1 ethanol:acetic acid) via the antigen rescue through microwaving immunostaining conditions was utilised. In WT, at early leptotene, ASY1 and ASY3 co-localized, appearing as punctate foci throughout the nucleus (Figure 2.35) until zygotene, when they both linearized over the entire length of all chromosomes. During diplotene, ASY3, reduced to numerous foci overlapping ASY1, while ASY1 persisted as loop-like structures until later stage (Figure 2.35). This is consistent with the *asy1* mutant in *Arabidopsis* and *Brassica rapa*, where ASY3 loading was independent of ASY1 (Sanchez-Moran et al., 2007; Cuacos et al., 2021) and in the *asy1 Aabb* mutants, ASY3 proteins still loaded onto the chromosomes (Figure 2.35). At leptotene, both proteins appeared less linear and patchier than WT, reflecting the reduced ASY1 abundance in this mutant. Moreover, from leptotene to zygotene, one or two fragments were observed in most of the meiocytes analysed (Figure 2.35 D2, D3, E2, E3, white circles), probably caused by disorganised SC in absence of the full polymerization of ASY1 or they could be unspecific cytoplasmatic staining or technical artefacts formed during sample preparation. It was difficult to detect meiocytes at pachytene, due to a poor availability of the anthers, or possibly meiotic axes were not always completely established, leading to poor SC installation (Figure 2.35). At diplotene, ASY1 appeared polarized and aggregated near the nucleolus as disordered treads of different intensities, instead of forming loop-like structures, while ASY3 formed polycomplexes (Figure 2.35). This outcome potentially highlights a major role of ASY1 in SC axis organization, whose integrity may rely on ASY1-ASY3 bonds, whereby synapsis is successfully installed.

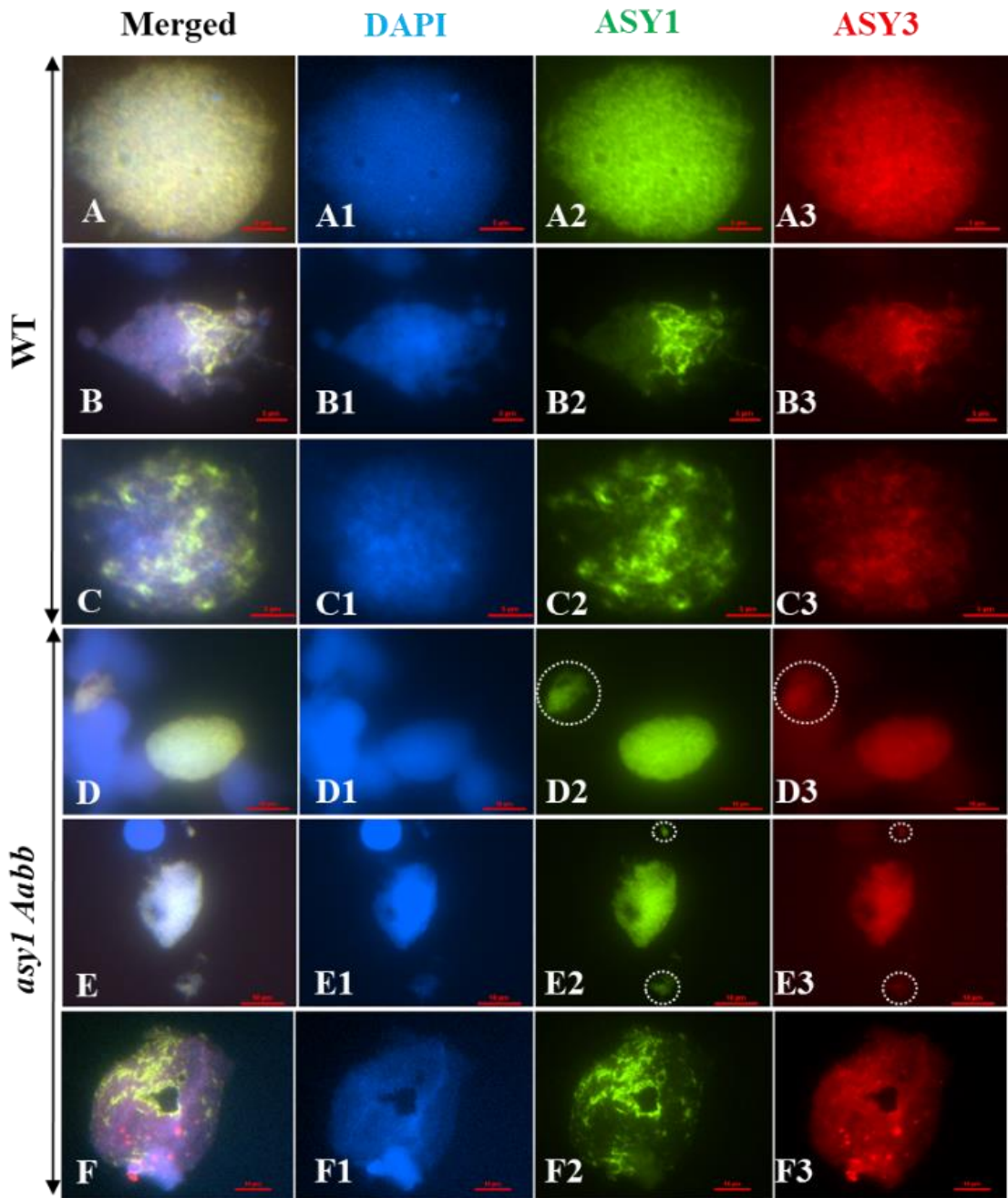


**Figure 2.35 Localization of chromosome axes *TaASY1* (green), and *AtASY3* (red).** Chromatin stained in DAPI. in *asy1 Aabb*. Chromatin stained in DAPI. (A-F) merged images of (A1-F1) chromatin counter-stained with DAPI (blue), (A2-F2) chromosome axis *TaASY1* (green), and (A3-F3) transverse filament *AtASY3* (red). (A, D) Leptotene. (B, E) Zygote. (C, F) Pachytene in WT and *asy1 Aabb*, respectively. (D2-E3) Fragments (circles) during zygote and pachytene-like. DNA is counterstained with DAPI and shown in blue. Scale bar = 10 $\mu$ m.

### 2.3.14 ASY1 may interact with SMC3 to stabilise the SC at synapsis sites

The defect in chromosome segregation observed during anaphase I in *asy1 aabB*, led to an investigation into the interaction of *TaASY1* (Sanchez-Moran et al., 2007) with the

cohesin protein *AtSMC3* (Ferdous et al., 2012b). Immunolocalization of these proteins were performed on fixed anther samples (3:1 ethanol:acetic acid) followed by antigen rescue (Figure 2.36). In WT, at early leptotene, ASY1 and SMC3 co-localized, appearing as punctuate signals throughout the nucleus (Figure 2.36 A-A3). At zygotene, both proteins formed continuous thread-like signals along the chromosomes (Figure 2.36 B-B3), similar to *Arabidopsis thaliana* (Ferdous et al., 2012) and *Brassica rapa* (Cuacos et al., 2021). During late pachytene, ASY1 and SMC3 appeared as numerous foci widely distributed throughout the nucleus (Figure 2.36 C-C3). In conformity with data of *Arabidopsis* and *Brassica rapa* *asy1* mutants, where cohesins appeared normal along the chromosome axes (Sanchez-Moran et al., 2007; Cuacos et al., 2021), in wheat *asy1 aabB* mutants, cohesin axial core did not seem to be perturbed, although formed a different pattern. In this species, ASY1 and SMC3 signals appeared discontinuous at leptotene (Figure 2.36 D-D3), and did not co-localized over the entire meiotic process. At zygotene-like, ASY1, together with SMC3, did not localize to the axis as in WT, and their signals progressively reduced as discrete spots (Figure 2.36 E-E3). During pachytene-like, the loading of ASY1 was severely compromised, forming prematurely polycomplexes compared to the WT, demonstrating that ASY1-independent axes formation were insufficient to support normal SC organization. At this point, SMC3 vanished prematurely (Figure 2.36 F-F3). Later stages were not found or ASY1 was absent in this genotype.

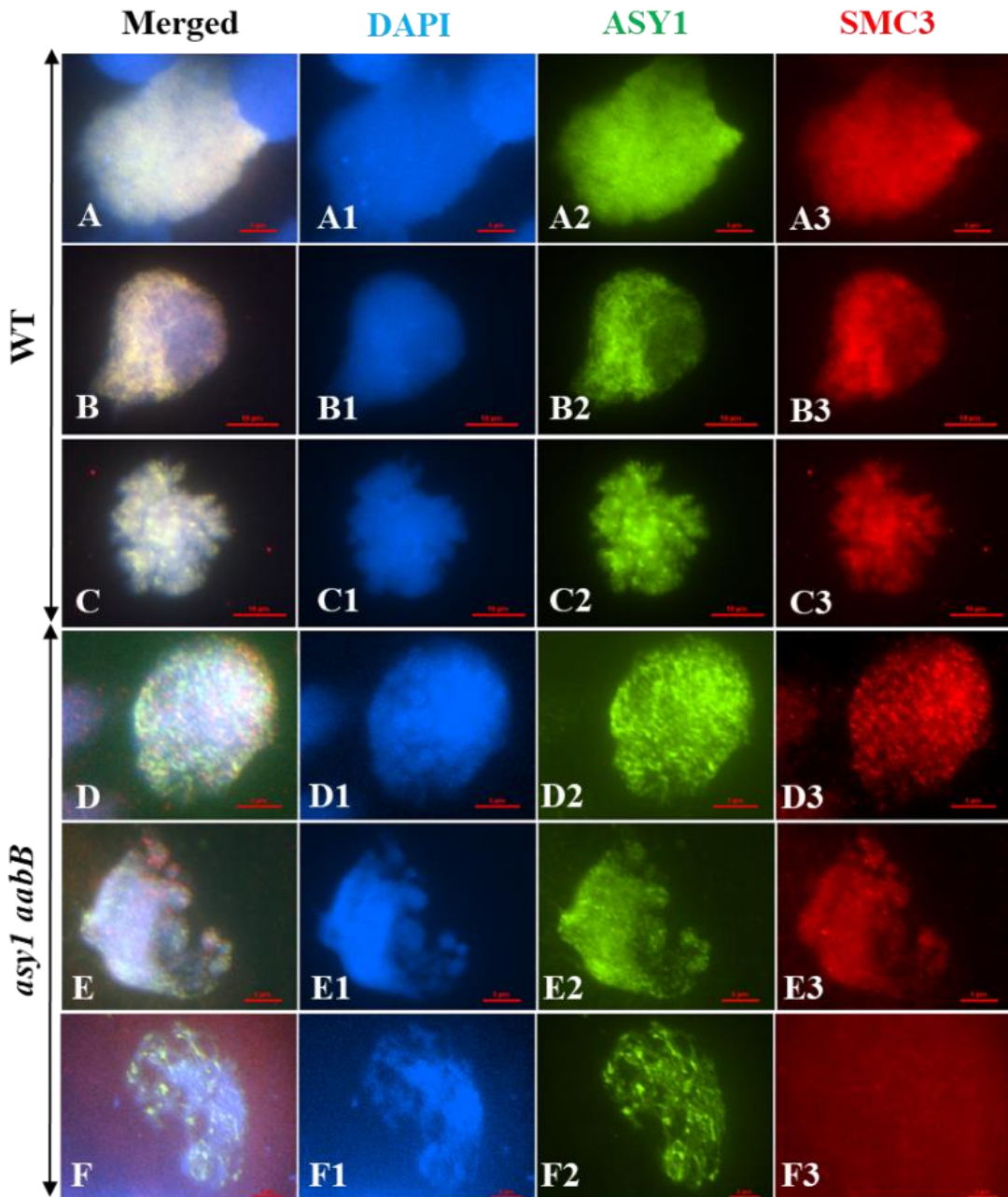


**Figure 2.36 ASY1 and SMC3 failed to localize on chromosome axes in *asy1 aabB* during post-synapsis.** (A-F) merged images of (A1-F1) chromatin counter-stained with DAPI (blue), (A2-F2) chromosome axes *TaASY1* (green), and (A3-F3) transverse filament *AtSMC3* (red). (A, D) Leptotene. (B, E) Zygote and Zygote-like respectively. (C, F) Pachytene in WT and *asy1 aabB*, respectively. (A2-A3) In WT, ASY1 and SMC3 co-localized and began to polymerize as numerous foci, which gradually linearized at zygote (B2-B3) and aggregated at late pachytene-early diplotene (C2-C3). (D2-E2) In defective *asy1 aabB*, ASY1 formed foci in leptotene-zygote-like cells and aggregated in late pachytene cells (F2). (D3-E3) SMC3 did not co-localize with chromosome axis and failed to be loaded in late pachytene stage (F3). DNA is counterstained with DAPI and shown in blue. Scale bars =10 $\mu$ m.

### 2.3.15 ASY1 ensures obligate CO following homologous pairing

To verify whether the reduction of chiasmata in *asy1 aabB* was caused by defects in DSB formation, the number of  $\gamma$ H2AX foci were monitored in wild type and *asy1 aabB* fixed meiocytes ('microwave' immunostaining). Immunolocalization of antibodies against  $\gamma$ H2AX, the phosphorylated form of H2AX that marks DSBs, have been extensively used to infer the number of breaks based on the number of foci observed in the nuclei at early prophase I (Sanchez-Moran et al., 2007; Ferdous et al., 2012; Higgins et al., 2012). The coiled-coil protein ASY3 has also been used as ASY1-independ marker for early prophase I chromosomes (Ferdous et al., 2012) in *asy1* triple (hypomorphic) mutant heterozygous for B copy. As in the previous analysis, loading of ASY3 (green) on meiotic chromosomes in *asy1 aabB* was also compared with the WT (Figure 2.37 A2, B2). This was correlated to a difference in number of  $\gamma$ H2AX (red) foci between WT ( $1341 \pm 20.8$ ,  $n = 20$ ) (Figure 2.37 A3) and *asy1 aabB* mutants ( $717 \pm 14.7$ ,  $n = 20$ ) (Figure 2.37 B3) during leptotene, corresponding to almost 50% DSB number decrease in *asy1 aabB*. A two-sample *t*-test confirmed that there was statistically significant difference between WT and *asy1 aabB* mutant ( $P < 0.001$ ). The full data set of foci counts is recorded in Appendix (Table S5).

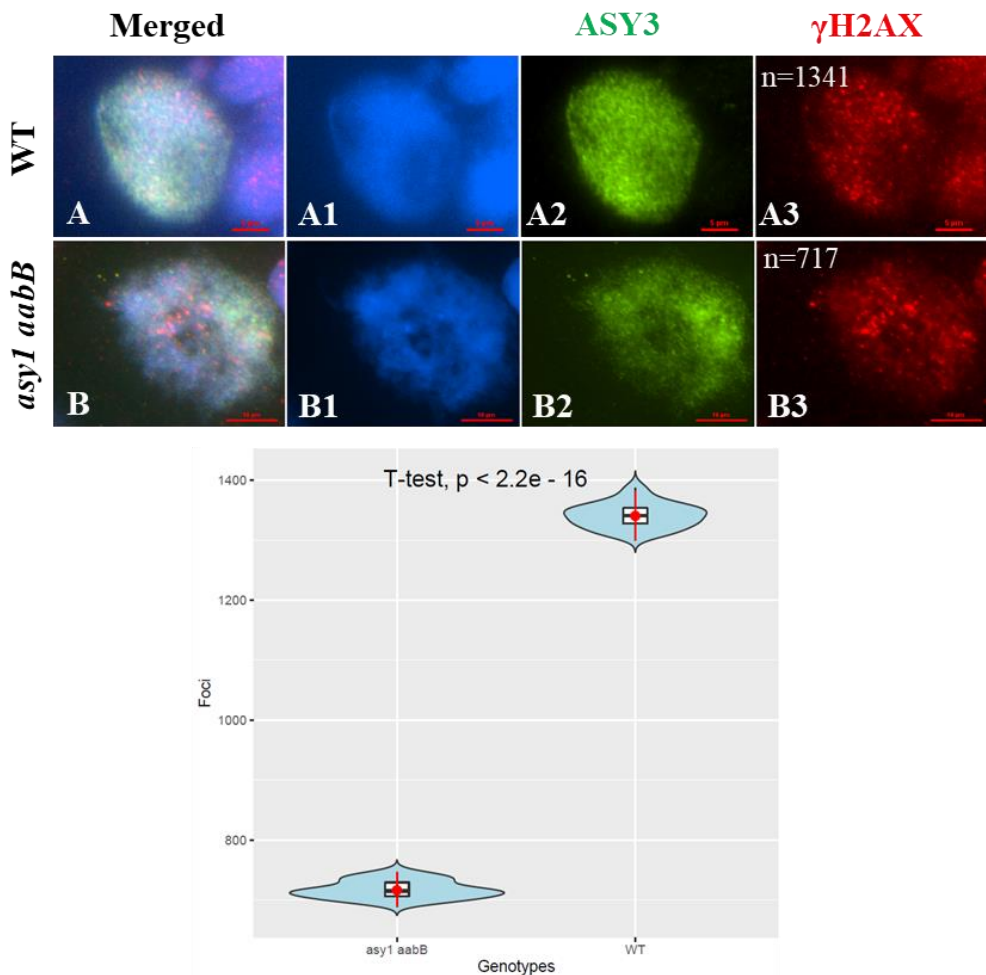


**Figure 2.37 Analysis of meiotic DSBs formation using the anti- $\gamma$ H2AX antibody in male meiocytes in WT and *asy1 aabB* at leptotene stage.** (A-B) merged images of (A1-B1) chromatin counter-stained with DAPI (blue), (A2-B2) chromosome axis *AtASY3* (green), and (A3-B3) early meiotic recombination events marked by  $\gamma$ H2AX (red). (A3-B3) In both,  $\gamma$ H2AX appeared as numerous foci at DSB sites. (A3) WT meiocyte with 1341 foci. (B3) *asy1 aabB* meiocyte with 717 foci. Data are presented as violin plots. Results of the two-sample *t*-test are shown ( $P < 0.001$ ). Scale bars = 5 and 10  $\mu$ m.

### 2.3.16 ASY1 regulates proper homologous pairing in hexaploid wheat

To validate the outcomes from tetraploid wheat, a cytological atlas was used to investigate meiotic prophase I in hexaploid *T. aestivum* cv. Cadenza and *asy1 AAbbDD* TILLING mutant (Figure 2.38). As shown in tetraploid wheat, at leptotene WT and *asy1 AAbbDD* were apparently identical (Figure 2.38 A, B). Zygote differed in hexaploid *asy1*, where chromatin appeared thicker than in WT (Figure 2.38 C, D). Synapsis did not always occur in *asy1* (Figure 2.38 F, arrows) and it appeared incomplete at diplotene (Figure 2.38 H).

At diakinesis, 21 bivalents, mostly rings (Figure 2.38 I), formed at least two chiasmata per meiocytes during metaphase I in WT (Figure 2.38 K), whereas reduction in chiasma formation was already evident in *asy1*, represented as univalents during diakinesis (Figure 2.38 J, yellow arrow) and at metaphase I (Figure 2.38 L). Univalent formation at diakinesis can be caused by a failure of homology recognition and/or synapsis, or the inability to mature recombination intermediates into stable chiasmata. To discriminate between these possibilities, analysis of chromosome pairing at leptotene/zygotene and pachytene nuclei by fluorescence in situ hybridization (FISH) would be necessary. Fragments were also present at early stages (Figure 2.38 J, blue arrows). Multivalent interactions, such as tetravalents (Figure 2.38 M, stars), chromosome clusters (Figure 2.38 N, arrow), chromosome interlocks (Figure 2.38 O, star) and fragments (Figure 2.38 O, arrow), were also common in *asy1 AAbbDD*, which generated defective anaphase I (Figure 2.38 P).

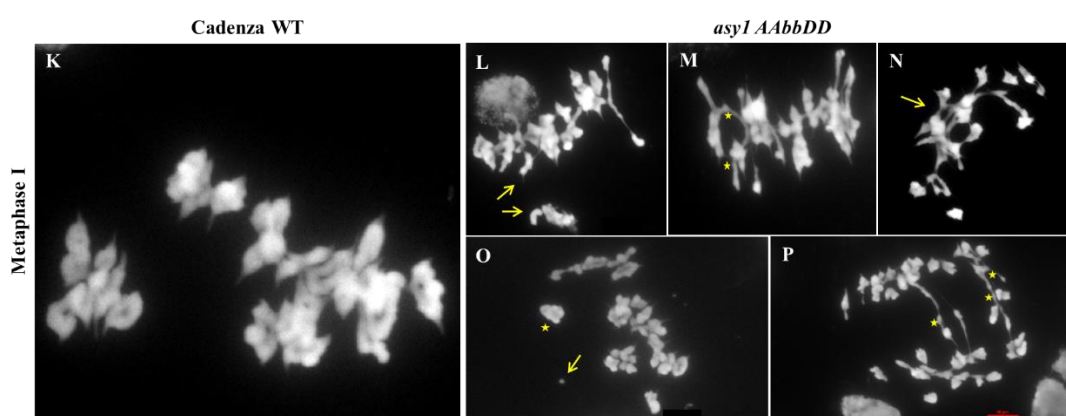
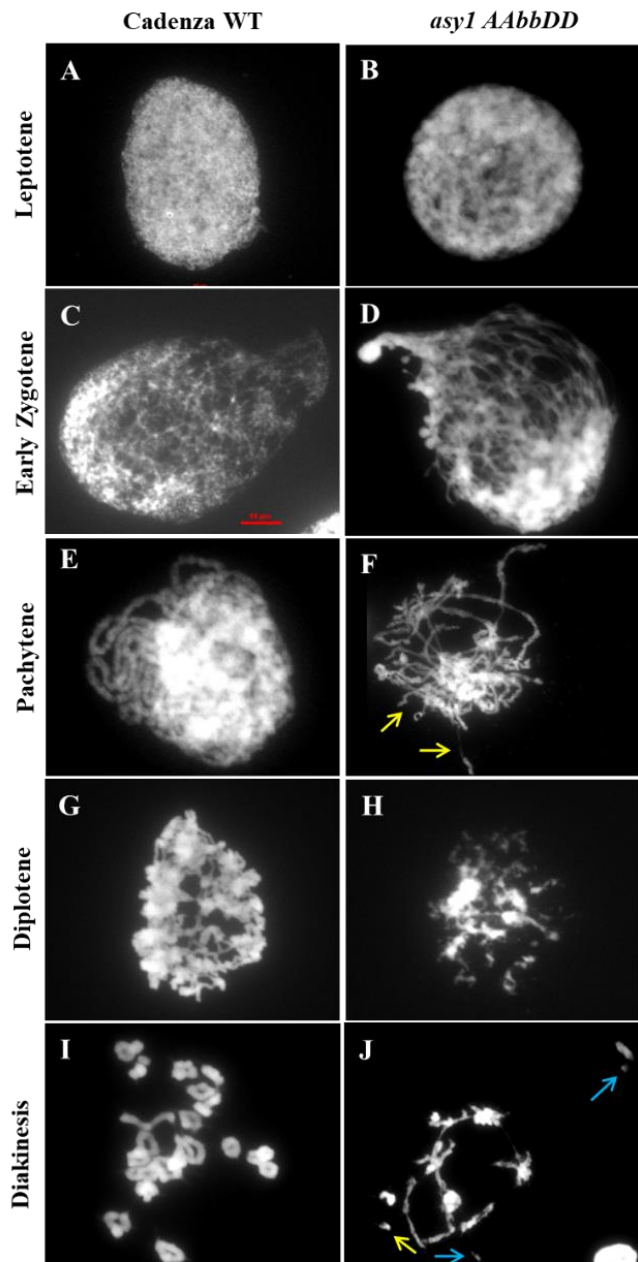


**Figure 2.38 Cytological atlas of *asy1 AAbbDD* in hexaploid *T. aestivum* cv. Cadenza.** Upper panel: (A, I) WT. (B-J) *asy1 AAbbDD*. (A, B) Leptotene, (C, D) zygote, (E, F) pachytene, (G, H) diplotene, (I, J) diakinesis. Lower panel: (K-P) Metaphase I. Yellow arrows and stars indicate specific cytological features. Red scale bar is present in panel D and P.

H) diplotene, (I, J) diakinesis. Lower panel: metaphase I in WT (K) and *asy1 AAbbDD* (L-P). In *asy1 AAbbDD*: (F) Asynased regions during pachytene (arrows). (J) Univalents (yellow arrow) and small fragment (blue arrows) already formed at diakinesis and frequently present in PMCs at metaphase I, as showed by yellow arrows (L). (M) Tetravalent, (N), chromosome clusters (O), interlock (start) and fragment (arrow), (P) chromosome lagging (stars) during segregation process occurring at anaphase I. DNA is counterstained with DAPI and shown in grey. Scale bars = 10  $\mu\text{m}$ .

Furthermore, the different meiotic chromosome configurations for each meiocyte were scored. In tetraploid TILLING mutants, changes in ASY1 gene dosage generated a decrease in CO frequency and a different level of multiple chromosome associations (Figure 2.39 a). Similarly, chiasma values for the hexaploid TILLING line and WT were significantly different (two-sample *t*-test,  $P < 0.001$ ,  $n = 50$  *asy1 AAbbDD* and  $n = 50$  Cadenza WT) (Figure 2.36 c). In detail, the mean number of chiasmata for PMCs in Cadenza WT was  $39.48 \pm 1.55$  ( $n = 50$ ) (Figure 2.39 a), consistent with Osman et al., data:  $41.8 \pm 0.28$  ( $n = 64$ ) (Osman et al., 2021). Contrastingly, in *asy1 AAbbDD*, the chiasma number was significantly reduced ( $37.42 \pm 3.54$ ,  $n = 50$ ), as shown from the rise of rod bivalents per nucleus ( $3.02 \pm 2.24$ ,  $n = 50$ ) ( $P < 0.001$ ) compared to the WT Cadenza ( $2.44 \pm 1.43$ ,  $n = 50$ ). This was at the expense of ring bivalents (6% drop,  $n = 50$ ) and the higher incidence of univalents increased ~6-fold (Figure 2.39 b), as in tetraploid *asy1* single KO TILLING lines. Three tetravalents out of fifty male meiocytes were detected in this line ( $0.06 \pm 0.24$ ,  $n = 50$ ), corresponding to a comparable 6% increase of multivalent formation detected in tetraploid *asy1* single KO lines. Overall, there was only a 5% reduction of CO number, compared to the 15% reduction resulted from the tetraploid TILLING lines evaluated previously. No further conclusion may be drawn regarding the supposed discrepancies in chiasma frequency between the tetraploid and hexaploid wheat TILLING mutants, since only one hexaploid mutant line versus three tetraploids were evaluated in this study. Data set of chiasma counts are provided in Appendix (Table S6).

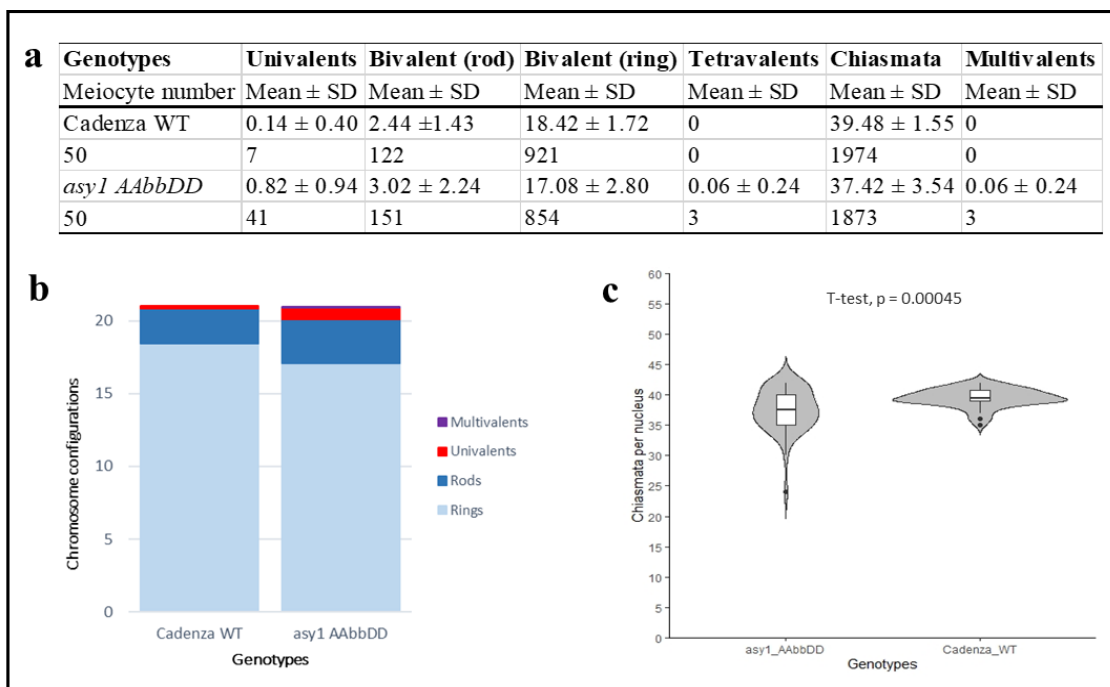


**Figure 2.39** *asy1 AAbbDD* mutants display altered chromosome configuration at metaphase

I. a) Table summarising: average, standard deviation (SD), range of bivalents, univalents, multivalents and chiasmata per male meiocyte in Cadenza WT and the TILLING line analysed. n = number of meiocytes; minimum two independent plants per genotype. b) Bar chart illustrates the mean values of rings bivalents (sky blue), rods bivalents (dark blue), univalents (red) and multivalents (purple) per cells among WT and *asy1 AAbbDD* mutants. Legend is on the right. c) Violin plot exemplifies chiasmata frequency per male meiocyte. Results of the two-sample t-test are shown ( $P < 0.001$ ).

## 2.4 Discussion

### 2.4.1 Molecular data overview

The results of *TaASY1* gene expression analysis in meiotic and non-meiotic tissues of hexaploid *T. aestivum* revealed a significant balanced expression among the sub-genome copies, as also verified with the downstream cytology analysis of *asy1* TILLING mutants in A or B copy (*asy1* single KOs were partially functional). Cloning and Sanger sequencing methods used for identifying alternative splicing events and interpreting the outcomes were highly sensitive and reliable. No supplementary analysis was initiated to corroborate the hypothesis of a regulatory function of the *TaASY1* 3' UTR isoforms in gene expression during meiosis.

## 2.4.2 *TaASY1* sub-genome copies are not subjected to tissue-specific regulation in hexaploid *T. aestivum*

The apparent contrasting results of the cloning method with the tissue-specific RNA-seq datasets (Wheat Exp VIP db), qPCR and cytology evidence from *asy1* TILLING mutant phenotypes regarding the assessment of the individual sub-genome contribution within the *TaASY1* coding region, may have arisen due to the intrinsic biological variability and from the small clone sample size examined (~20 clones). A further explanation in support of these data may be found in the absence of a tissue specific gene expression regulation highlighted in *TaASY1* using these molecular methods. Indeed, the *TaASY1* coding region appeared to be equally expressed in both leaf and inflorescence tissues evaluated (Figure 2.1). The direct deduction would be that wheat meiotic genes such as *TaASY1* (and *TaZYP1*, as discussed in Chapter 3) are also expressed in somatic tissues. Interestingly, the ASY1 protein extracted from leaves in this study had the same size band as anthers, further suggesting that the ASY1 protein is also expressed in leaves. The other bands detected were probably aspecific, due to the nature of the antibody. This polyclonal antibody was raised against a recombinant protein comprising amino acids residues 422-845 of *ZYP1b* from *Arabidopsis* bud cDNA (Higgins et al., 2005). About the timing and whether *TaASY1* is activated and functional in non-meiotic tissues is still for debate.

Fascinating evidence reinforcing the above hypothesis derives from a wheat co-expression analysis of Alabdullah et al. (2019) and an unpublished wheat meiotic transcriptome work of Jiang et al. (in preparation). For instance, from co-expression analysis of the ZMM meiotic recombination gene *TaZIP4*, the authors obtained evidence of a different homoeologous expression profile between the three *TaZIP4* homoeologues on group 3 chromosomes (TraesCS3A02G401700, TraesCS3B02G434600 and TraesCS3D02G396500). These were strongly connected to the largest meiosis-related module (gene with meiotic function), and the *TaZIP4* copy responsible for *Ph1* phenotype (TraesCS5B02G255100), did not cluster in the same meiotic module, being expressed in most non-meiotic tissues (Martín et al., 2017; Martín et al., 2018; Rey et al., 2018; Alabdullah et al., 2019). Similar findings were obtained with *TaZYP1-2B* (TraesCS2B02G338300) retrieved from the same co-expression network data (Alabdullah et al., 2019). A detailed discussion of this result is found in Chapter 3. Unsurprisingly, in 2022, Jiang and collaborators discovered alternative isoforms in

polyploid wheat, possessing identical expression patterns in both vegetative and reproductive tissues. Thus, antagonistically to *A. thaliana*, in which meiotic genes are tightly regulated in reproductive tissues, it seems that in polyploid *T. aestivum* a different, unknown mechanism has evolved to control the gene expression. Some hypotheses are discussed in the next paragraph 2.4.3.

This current work has confirmed that cloning and RNA-seq represent unbiased and reliable molecular methods to measure the gene expression pattern in polyploid wheat. Hence, the biological variability observed in these data may rely on other factors, such as sensitivity of technical procedure, specificity and efficiency of calibrated sub-genome specific primer design, or environmental conditions. Lastly, as assumed, a qPCR assay using sub-genome specific primers, effectively allowed a sensitive and valid measurement of gene expression level, confirming a balanced expression of *TaASY1* sub-genome copies in hexaploid *T. aestivum*.

#### 2.4.3 A rare alternative splicing event in hexaploid *T. aestivum* *TaASY1*

The use of the cloning method in this study was intended to obtain the sequences of the three sub-genome ASY1 copies, as well as identify splice variants. The multi-alignment analysis of the *TaASY1* cloned sequences uncovered a putative splice variant in *TaASY1-5B* of Apogee, differing in the presence of a non-canonical splicing event at the 5' TC splice donor site. Nevertheless, since such non-canonical 5' splice donor site has not been recorded in any other clones, it is more likely that this variant is rare, although may play an unknown role. In line with this assumption, previous work in plants reported that the proportion of non-canonical splice sites, other than the canonical splice site GT-AG, is around or below 2% (Burset et al., 2000; Kupfer et al., 2004; Pucker & Brockington, 2018). Non-canonical splice site combinations can be divided into major non-canonical GC-AG and AT-AC combinations and the minor non-canonical splice sites, which are all other dinucleotide combinations at the terminal intron positions. The combined frequency of all minor non-canonical splice site combinations is low, e.g., 0.09% in plants (Pucker & Brockington, 2018). The robustness of these data is further supported by Jiang et al. (2022), who prevalently identified splice switches, rather than splice variants in polyploid wheat.

#### 2.4.4 *De novo* *TtASY1* 3' UTR isoforms are potentially expressed in tetraploid *T. turgidum*

The cloning and sequencing strategies allowed identification of nine putative *TtASY1* 3' UTR isoforms, whose only clone ASY1K.M317 had the predicted 3' UTR reference sequence. Furthermore, the cloning approach unmasked the presence of specific regulatory regions within the 3' UTR variants, the CPE sequences, which might be a relevant source for future work. CPEs are essential for polyadenylation and polyadenylation-dependent translation of mRNA during oocyte maturation in *Xenopus laevis* (Sheets et al., 1994) and are critical for oocyte maturation as blocking this process inhibits progress into meiosis (Sheets et al., 1994). The poly(A) tails are not static, rather, they are dynamically regulated during development and cell cycle (Subtelny et al., 2014; Kappel et al., 2015; Eichhorn et al., 2016; Lim et al., 2016; Morgan et al., 2017). Previous work has focused on measuring the poly-A tail length via Illumina sequencing, revealing that poly-A tail regulation is a major mechanism controlling gene expression (F. Yang et al., 2020). For example, in *Drosophila*, *Xenopus* and zebrafish, poly-A tail lengths are carefully regulated during early development (Eichhorn et al., 2016; Lim et al., 2016; Morgan et al., 2017). Hence, it is tempting to speculate that in tetraploid wheat the frequency of *cis*-acting sequence elements, regardless or not of their link with the different poly-A tail composition and reproductive tissues, may vary during meiosis to promote changes in protein abundance or, not mutually exclusively. It is also plausible that G-tailed mRNAs might constitute to specific subcellular location for transcriptional element(s) in *TtASY1* gene.

So far, due to the small sample size tested, the existence of any meiotic tissue-specific selection for the expression of a certain *TtASY1* 3' UTR variants, above all in respect to the polyA tail nucleotide composition remains unexplored. The G-residues in the poly(A) tail detected in 10% of *TtASY1* 3' UTR transcripts were previous discovered in humans and *Arabidopsis thaliana* poly(A) tails (Lim et al., 2018). In both species, the role of G-content in regulating translational efficiency through a conserved family of RNA binding proteins, termed cytoplasmic poly(A)-binding proteins (PABs) using next-generation genome tools, was demonstrated (Sachs et al., 1987; Deo et al., 1999; Sladic et al., 2004). In tetraploid *T. turgidum*, all it is known so far from this work is the apparent lack of a distinct pattern between the polyA tail length and guanosine percentage correlated to the

CPE sequences. Whether such association is appropriate or functional during meiosis, requires to be investigated.

In respect of the approach utilised for this analysis, since the cloning and sequencing methods of the full length *TaASY1* coding sequences was proved to be accurate and reliable, it is unlikely that the remaining group of isoforms identified was the result of sequencing errors. Therefore, the possibility of novel isoforms which may be translationally activated/silenced during meiotic division process, was speculated. In this context, it has to be mentioned that, as for the coding region analysis, the primer designing procedure for the UTR investigation did not include the transcript variant reference sequences. Thus, in order to analytically and accurately corroborate the hypothesis of *de novo TtASY1* 3' UTR isoforms, a quantitative PCR experiment may be designed. Furthermore, in support of these undescribed 3' splice variants data, a recent work recorded a series of unannotated isoform switching (differential transcript usage) in male meiocytes of polyploid wheat, timely isolated during prophase I, which could potentially include those found in the present project (Jian et al., 2021, under review). The phenomenon of the isoform switching, could have an impact in driving protein level changes during meiosis, favouring adaptive functionality of target genes (Cheng et al., 2018).

In perspective, intriguing questions can be addressed in regards to these findings: Does the guanosine content within the polyA tail of *TtASY1* has any significant effect on the mRNA stability (degradation or protection from deadenylation process)? Does the polyA tail nucleotide composition has changed during evolution or following the polyploidization process in wheat? Do these features affect the binding of any regulatory element(s)? Are those sequences target of polyA-binding proteins? Future research will be needed to elucidate the importance of these regulatory features in polyploid wheat.

#### 2.4.5 Cytology data overview

Cytological analyses of metaphase I chromosomes demonstrated that knock-out of single *TtASY1-5A* or *TtASY1A-5B* copies induced a substantial change in chiasma frequency combined with a slight increase in putative homoeologous recombination. Clearly, these

data demonstrate that individual *TtASY1-5A* and *TtASY1-5B* copies are functionally redundant in tetraploid *T. turgidum*, and all *asy1* single KO mutants manifested a consistent phenotype. Exacerbated consequences observed in *asy1* triple allele mutants further validate the additive effect of the gene copies. Minor aberrant consequences, such as chromosome fragmentation, entanglements and unbalanced chromosome segregation, explained the reduced fertility in *asy1* mutants. In line with this statement, immunolocalization data revealed a progressive disruption of synaptic elements, which severely compromise chromosome pairing and segregation among the *asy1* mutant genotypes evaluated. More relevant, the ASY1 loading onto the chromosome axes was temporally perturbed throughout the prophase I (based on the anther size staging), with important effects on SC stability, leading simultaneously to unpaired chromosomes and promiscuous chromosome interactions.

Additionally, as expected, the phenotype of these *asy1* TILLING lines resembles what previously observed in the *Taasy1<sup>RNAi</sup>* mutants (Boden et al., 2009). Indeed, when *TaASY1* was depleted in hexaploid wheat, a degree of homoeologous synapsis established. Following the results of this analysis, where a single *asy1* KO already provoked a significant effect on chromosome pairing, it can be inferred that ASY1 may act early during the process of synapsis, ensuring the choice of homologous chromosomes and avoiding homoeologous interactions.

Preliminary findings in hexaploid *T. aestivum* cv. Cadenza of a single KO *TaASY1* in B genome (C0971 TILLING line), further support the potential role of *TaASY1* in inter-homologous recombination bias, recapitulating the *Taasy1<sup>RNAi</sup>* phenotype (Boden et al., 2009). A comprehensive discussion of the cytology results is described in the following paragraphs.

#### 2.4.6 *TtASY1* may fulfil interdependent meiotic functions in polyploid *T. turgidum*

DAPI staining analysis of *asy1* mutants allowed monitoring of the origin and fate of defective chromosome behaviour within male meiocytes. Distinctly, the metaphase I spread analysis of all *asy1* TILLING genotypes revealed a consistent phenotype, marked

by a gradual increase of severity in terms of chromosome configuration (univalent pairs, rod bivalents rather than rings and multivalents) and fertility rate, as well. Collectively, when compared to the WT, *asy1* partial-loss-of-function had an additive effect of *ASY1* in respect of chiasma frequency. In other words, these data clearly showed a dosage sensitivity of *ASY1* in regards to chiasma regulation, consistent with its ortholog in *Arabidopsis* (Lambing et al., 2020).

Moreover, reduced viability of germ cells associated with aberrant chromosome orientation (detected at anaphase I, together with chromosome lagging and missegregation) is a typical phenotype of *ASY1* orthologous mutants reported in considerable number of organisms, such as *S. cerevisiae*, *C. elegans*, *A. thaliana*, and *M. musculus* (Zetka et al., 1999; Nonomura et al., 2006; Sanchez-Moran et al., 2007; Carballo et al., 2008; Rinaldi et al., 2017). However, further experiments are required to accurately quantify the proportion of viable and non-viable grains, for example by performing a pollen viability test (such as Alexander staining of pollen) on wheat *asy1* mutants, and to ideally validate *ASY1* role in univalent behaviour (anaphase I) by using centromere FISH probes to discriminate chromosome break points.

More importantly, the fact that it was possible to note that the chromosome flaws in *asy1* remained unsolved at later meiotic stages, provided a determinant starting point for the interpretation of the following data and for downstream management of experimental validations or choice of alternative approaches.

#### 2.4.7 SC assembly/disassembly is timely and spatially regulated by *ASY1* in tetraploid *T. turgidum*

Co-immunolocalization data involving *TaASY1* and *AtZYP1* antibodies in *asy1* single KO showed evidence of first sign of failure in *ASY1*-*ZYP1*-axis association and defective synapsis. In the selected *asy1* TILLING mutants, the interactive HORMA domain at N-terminus of the truncated *ASY1* protein should still guarantee the *ZYP1* binding. Surprisingly, the *ASY1* HORMA antibody used in this study detected a disorganised SC structure, having incomplete *ZYP1* polymerization in *asy1* single KO and totally absence of *ZYP1* loading in *asy1* triple allele mutants. Whether it corresponded to altered *ZYP1*

expression or not remains unknown. Surely, such defects were responsible of the rise in univalents and homoeologous recombination, unveiled with the previous chromosome spreading method. Taking in account the parallelism with the *Taasy1* RNAi (Boden et al., 2009), it can be argued that synapsis failure in *asy1* TILLING mutants may have more presumably been caused by erroneous search for the correct homologous. A detailed discussion to support this hypothesis is provided in the next paragraph 2.4.8.

#### 2.4.8 *TtASY1* controls proper chromosome pairing prior synapsis

As previously mentioned in the Introduction (Chapter 1), the coexistence of multiple, genetically closely related sub-genomes in allopolyploid wheat is maintained by a genetic barrier created against these chromosomes (homoeologous) that favours only the recombination occurring between homologous chromosomes during the first meiotic division (Sears et al., 1952; Riley & Chapman, 1958; Sears & Okamoto, 1958). Such barrier is thought to be established by two distinct loci, *Ph1* and *Ph2* (Sears, 1952; Riley, R. & Chapman, 1958; Mello-Sampayo, 1971). From early studies in hexaploid wheat, the altered localization of *TtASY1* in *ph1b* and the high levels of multiple chromosome associations in *Taasy1*<sup>RNAi</sup> knockdown mutants at metaphase I suggested a *Ph1*-dependent control of *ASY1* in terms of homologous chromosome pairing (Boden et al., 2009), yet the exact mechanism of action is still undetermined. Accordingly, in *asy1* KO mutants generated through TILLING (this study), changes in protein dosage may be responsible for promiscuous chromosome interactions, which may compromise proper chromosome partner choice. Importantly, following the increasing availability of specific molecular markers and the completion of the wheat genome assembly, it is now known that wheat *ASY1-5B* lies outside the 2.5 Mb deletion region of *Ph1* locus (Griffiths et al., 2006).

An alternative causative factor involved in chromosome pairing control is thought to be linked to the chromatin condensation. In *Arabidopsis*, there is evidence that *AtASY1* structurally alters the heterochromatin condensation along the chromosome axes to impede sister chromatids DSB repair via sister chromatids (Sanchez-Moran et al., 2007). In *ph1b*, the up-regulation of *TtASY1* was potentially caused by chromatin remodeling (Holm and Wang, 1988; Prieto et al., 2004, Boden et al., 2009). Likewise, in *asy1*

TILLING mutants analysed here, truncated or null ASY1 protein may re-allocate SC components for effect of chromatin alteration, with consequence on chromosome alignment. To prove the robustness of one or the other hypothesis, it would be necessary to consider the interplay between chromosome condensation and SC organization.

As stated earlier, in a wild-type tetraploid and hexaploid wheat genotypes, chromosome pairing begins amongst homoeologues, which initially cluster together via centromeres during anther development (pre-meiosis) (Martinez-Perez et al., 2000). By the start of the telomere bouquet, heterochromatin decondenses, leading to chromosome elongation and sister chromatid separation, resulting in a marked increase of homologous interactions (Martínez-Pérez et al., 1999; Prieto et al., 2005; Colas, 2008). Therefore, the multiple associations are resorted prior synapsis (Martinez-Perez et al., 2003; Sepsi et al., 2017; Osman et al., 2021). At later stage, chromosomes de-sort and pairing is completed. Intuitively, the centromere associations need to be resorted pre-meiotically, before SC assembly.

In the *asy1* TILLING lines evaluated in this study, albeit centromere behaviour was not investigated, the disruption of the SC components (interaction and/or polymerization) caused by ASY1 deficiency represented the main findings. At the onset of meiosis, the binding of ZYP1 onto the homologous chromosomes in tetraploid *asy1* resulted temporally delayed, possibly due to these structural changes, which in turn destabilises the proteinaceous components of the SC so that chromosomes, lacking a solid scaffold, cluster together and recombination proceeds between homoeologues instead of their counterparts. Failure of homologous recognition and synapsis may also contribute to the formation of univalents already at diakinesis, as consequence of unsolved DSB repair, and decrease CO frequency, as indicated by the reduced frequency of H2AX in *asy1 aabB*. A similar strategy was found in budding yeast, where HOP1 orthologous promotes inter-homolog recombination by preventing DMC1-independent RAD51-driven recombination to repair downstream DSB events (Niu et al., 2005; Carballo et al. 2008). Such evidence better supports the hypothesis that ASY1 may fulfil a meiotic control on homology searching along the axial element via stable strand invasion prior alignment and synapsis, thus, less likely it may be involved in modulating chromatin condensation.

To corroborate this hypothesis, a FISH assay using wheat centromere specific probes on chromosome spread sample could be planned in future. Alternatively, since the incidence of ectopic non-homologous recombination in *asy1* mutants, the high frequency of univalent may be consequent to unregulated CO interference designation mechanism. For instance, it was noticed that meiocytes having multivalent formed with uneven chromosome pair number (e.g. trivalent), were usually associated to unpaired univalent. Virtually, the maturation of intra-homologous crossovers potentially determines the suppression of inter-homologous crossovers, which, yet not necessarily implies a reduction in chiasma frequency, may lead to non-homologous univalent formation. In *A. thaliana*, immunolocalization of MLH1 onto *asy1* mutants, positively revealed that CO interference is a mechanism mediated by ASY1 (Lambing et al., 2020). The same analysis could confirm this hypothetical conserved role of ASY1 in polyploid wheat.

#### 2.4.9 ASY1-ASY3 interaction appears conserved in tetraploid wheat

Dual immunolocalization analysis of ASY1 and ASY3 in tetraploid wheat *asy1 Aabb* mutant revealed a conserved interactive role of these axial element proteins with *Arabidopsis* and *Brassica rapa* (Sanchez-Moran et al., 2007; Cuacos et al., 2021). Furthermore, the observation that in WT plants ASY1 and the coiled-coil ASY3 remain bound to the chromosome core after desynapsis but are defective in tetraploid *asy1 Aabb* mutants is suggestive of a later function of wheat ASY1.

The hypothesis that ASY1 plays a central role in SC disassembly might be further corroborated by its interaction with PCH2, whose interactions appeared to be dispensable to the structure of the axial elements in tetraploid wheat. As other HORMAD proteins previously described, ASY1 possesses a HORMA domain at the N-terminus and a closure motif at the C-terminus. In unsynapsed chromosomes, ASY1 proteins assume a so-called self-closed state (HORMA domain fold itself with its closure motif), functionally required to block the binding of their HORMA domain with the closure motifs of the linker proteins, such as ASY3, whereby, during synapsis, ASY1 unblock this bond to connect with ASY3. The conformational conversion from a self-closed to the unlocked state is mediated by the conserved AAA<sup>+</sup> ATPase PCH2/TRIP13 protein (Rosenberg & Corbett, 2015; Ye et al., 2017; West et al., 2018; Yang et al., 2020). Nevertheless, in a context

where ASY1 lacks its own closure motif, but saves the HORMA domain, as in these TILLING mutants, it is obvious that the interaction with ASY3 is preserved, while the removal of ASY1 along the chromosomes after synapsis would be perturbed. Consistent with this mode of action, in *asy1 Aabb* mutant, ASY1 and ASY3 polycomplexes formed at diplotene are likely due to the inability of PCH2 to intervene for removing the excess of truncated ASY1, arising from the constant unlocked state. Thus, it is reasonable to speculate that ASY1 without its own closure motif may interfere with the progression of the desynapsis process. Thus, it seems that the nuclear localization of ASY1 and its binding partner ASY3 relies on the existence of both HORMA domain and closure-motif, which together with PCH2, are essential to assure the progress of meiosis. However, additional experiments are required to study in depth the precise regulation of ASY1-ASY3 and ASY1-PCH2 dynamics on the chromosome axis in wheat.

#### 2.4.10 ASY1 stabilises axial core formation in tetraploid wheat

Simultaneous immunolocalization data of *AtSMC3* and ASY1 in tetraploid *T. turgidum* *asy1 aabB* showed that the cohesin axial core was not perturbed at zygotene-pachytene transition, in compliance with *asy1* mutant of *A. thaliana* and *B. rapa*, where cohesins were present as normal along the chromosome, yet the signal appeared discontinuous and faint (Sanchez-Moran et al., 2007; Cuacos et al., 2021). Nonetheless, it is more likely that the abnormal phenotype was caused by technical artefacts.

More relevant, although major alterations in the distribution of SMC3 were observed along the chromosomes in *asy1 aabB* (fragments), SMC3 was still found to associate during early stage of the first meiotic division, highlighting the critical role of ASY1 in SC morphogenesis, which it might be potentially extended during desynapsis in sister chromatid cohesion and homologous chromosome disjunction. Consistent with this interpretation, a significant frequency of nondisjunction events recovered from fixed *asy1 aabB* meiocytes could originate from the missegregation of exchange chromosomes at anaphase I, as previously recorded in *Ph1*, HIM-3 and HORMAD1 (Zetka et al., 1999; Couteau & Zetka, 2005; Martinez-Perez & Villeneuve, 2005; Martinez-Perez et al., 2008; Boden et al., 2009; Daniel et al. 2011). Therefore, as yeast and mammal orthologues, wheat ASY1 localises on desynapsed chromosomes to presumably stabilise sister

chromatid cohesion and promote chromosome segregation at the first meiotic division, potentially through the mediation of mechanical expansion stress (Kleckner et al., 2004). In future research, FISH experiment using centromere-specific probe to examine the centromere cohesion status in tetraploid *asy1* meiocytes, could reveal whether cohesion-deficiency, here manifested as fragments, was caused by defective SMC3-ASY1 interaction or, more likely, derive from disorganised SC due to the partial loss of ASY1, thereby demonstrating a role for ASY1 in chiasma junction.

#### 2.4.11 ASY1 may act as a meiotic check-point in tetraploid *T. turgidum*

Incomplete data from the *asy1* double KO (null mutants) was obtained from the TILLING lines selected. Metaphase I spread experiment on fixed *asy1* double KO segregants generated by crossing K2071 and K4200 lines, showed asynaptic chromosomes and it was not possible to find any meiocytes at pachytene and diplotene stages. Attempts to immunolocalize ASY1-independent meiotic markers, such as ASY3 or SMC3, in *asy1 aabb* during meiotic prophase I was extremely challenging, due to the difficulty to stage male meiocytes, resulted mostly asynchronous and with drastic morphological and genetic defects (premature senescence, low viability, semi-sterility). In order to preserve the integrity of the male meiocytes of this genotype, an ethanol-based fixed material (3:1 ethanol:acetic acid) using the ‘microwave’ immunostaining technique was preferred. Nevertheless, the microwave immunostaining, successfully used for the remaining *asy1* mutant genotypes, did not produce viable results. Such condition induced to hypothesise that presumed failure in immunostaining experiments using meiotic markers (data not recorded), accidentally interpreted as technical issues, were, in fact, true consequence of a meiotic arrest. A separate work in mouse *hormad1<sup>-/-</sup>* single and double mutants reports that the germline cells defective or lacking HORMAD1 were able to programme a meiotic arrest at mid-pachytene stage (Daniel et al., 2011). Thus, it is tempting to speculate that tetraploid wheat ASY1 may create a check-point arrest when homologous chromosomes do not synapse, a common strategy observed in its mammal orthologous. However, these data remain unproven.

In respect to the second TILLING independent line K0157 carrying a mutation in B sub-genome, unexpectedly, despite a single round of backcross with WT plant (note, K0706

having a mutation in A sub-genome was also backcrossed with WT), the F<sub>2</sub> generations were again subjected to a non-medielian segregation, as showed by PCR-based genotyping. The presumed genotypes of the segregants screened were inadvertently interpreted as non-mendelian (disproved by the chi square test) on the strength of inefficiency during the PCR genotyping, which could be typically resulted from a suboptimal PCR conditions (e.g. ΔT<sub>m</sub>) coupled with imprecise sub-genome specific primers designation. Indeed, each group of primer sets testing the effects of the predicted nonsense mutation were designed to be specific for the target sub-genome, thereby the efficiency was simultaneously dependant onto their sequences (sequences detrimental to primer design, i.e. containing a G quartet, palindromic sequences, were ruled out) and onto the level of similarity among the ASY1 sub-genomes at the coding DNA sequence level. In view of their high nucleotide similarity (95-97%) (data retrieved from Ensembl Plants database), the specificity of the primer sets to individual sub-genome was extremely debatable. These features led to include *asy1* triple allele mutant genotypes (Aabb and aabB) from K2071 x K0706 cross in this work. For these genotypes, again, plants showed developmental defects and low germination rate, therefore the microwave immunostaining was used to compensate the poor materials yielded from the crossing. In this respect, it is worth to clarify that here the diffuse appearance of the WT nuclei is probably caused by the heat treatment which could contribute to alter the morphological conformation of histone proteins (not demonstrated).

In perspective, an improved genotyping approach would be sequencing PCR products, which may overcome the technical concerns encountered in this work.

#### 2.4.12 ASY1 has a conserved role in polyploid wheat

As conclusive observation, the preliminary metaphase I data from hexaploid wheat detected only a 5% reduction of CO number, compared to the 15% drop resulted from the tetraploid TILLING lines evaluated previously, and 6% rise of multiple chromosome interactions, as in tetraploid. No further conclusion may be proposed regarding the supposed discrepancies in chiasma frequency between the tetraploid and hexaploid wheat TILLING mutants, since only one hexaploid mutant lines versus three tetraploid lines were evaluated in this study. In general, all stages of meiotic prophase examined in hexaploid wheat appeared undistinguishable with the tetraploid species, corroborating an

intra-specific role of ASY1 at different ploidy level. Beyond this, again, there is a strong correlation with the meiotic phenotype of *Taasy1*<sup>RNAi</sup> mutant (Boden et al., 2009).

In future research, due to the presence of multiple gene copies in hexaploid species, it may be convenient to generate a full *TaASY1* KO ideally through the implementation of CRISPR/Cas9 genome editing, which, by targeting multiple homoeologue alleles simultaneously, could accelerate the process of functional gene validation (Li et al., 2021). Achieving a comprehensive knowledge of this protein has the ultimately aim to integrate mutant version of *TaASY1*, enhancing breeding strategies direct to commercial wheat varieties.

## 2.5 Conclusions

### 2.5.1 Molecular approach

The major findings derived from the molecular analysis was the validation of a balanced expression of *TaASY1* homoeologues in hexaploid *T. aestivum*, whilst “buffered” by an intrinsic biological variability. The implementation of cloning and next-generation sequencing unveiled non-canonical expression patterns of *TaASY1*, being also expressed in non-meiotic tissue, although the analysis of the cloning data was not extended to a systematic investigation on a large number of samples and mutants.

In future, the purpose may be to quantify the alternative 3' UTR isoforms and correlate the CPE sequences to 3' UTR isoforms. Further experiments are required to shed light on the wheat *ASY1* regulatory mechanism during meiosis. For example, it could be possible to estimate alteration in mRNA stability through measure its enrichment with quantitative PCR. It will be also interesting to analyse the composition of poly(A) tail in other conditions, such as meiotic stages or environments. Functional analysis of the putative isoforms and their regulatory elements may be undertaken with genome editing and cytology technologies. Such work will lead to a future direction for the ultimate understanding of poly(A)-tail-mediated regulation of *TtASY1* gene expression, offering unexplored opportunity to manipulate meiotic recombination rates, accelerating the development of superior germplasm for crop breeding (Stapley et al., 2017).

## 2.5.2 Cytology approach

Following the evaluation of *TaASY1* homoeologous expression level, the cytology study showed that the precise dosage of *TtASY1* in tetraploid wheat may be required to efficiently modulate the homology search at site of synapsis. This would be required as a precondition to discriminate the correct chromosome partner prior to synapsis and ensure SC integrity during the first meiotic division, which are ultimately critical to preserve fertility in polyploid wheat. Moreover, the wider effects of *asy1* TILLING mutants on the mechanism of meiotic recombination could be explained by the fact that this protein may be involved in multiple interdependent processes, such as SC assembly/disassembly and homoeologous recombination (alignment and CO) suppression.

The discovery of similar behaviour with *ph1* in both tetraploid and hexaploid wheat will integrate *ASY1* mutants within cereal breeding programmes worldwide and enable more opportunities of alien introgression with wild wheat relatives into wheat elite. This in turn will have the potential to expand the genetic diversity available in the *Triticeae* tribe, where especially common wheat represents one of the three major food crops important for world food security.

# **Chapter 3**

## **Investigating the gene regulatory sequences, splice variants and the meiotic function of wheat ZYP1**

### **3.1 Introduction**

In *Triticum aestivum*, ZIPPER-LIKE 1 (ZYP1) conserves the structural organization typical of the TF proteins (Khoo et al., 2012). Generally, all TFs are thought to be evolved to coordinate distinct but related meiotic functions, such as CO control and/or SC installation (Meuwissen et al., 1992; Sym et al., 1993; Page & Hawley, 2001; MacQueen et al., 2002; Osman et al., 2006; Smolikov et al., 2007; Smolikov et al., 2009; Schild-Prüfert et al., 2011; Gao & Colaiácovo, 2018).

In hexaploid *T. aestivum* ‘Chinese Spring’, the full-length 2592 bps coding sequence of *TaZYP1* was isolated using a combination of standard and 3' RACE PCR techniques and encodes a protein product of 863 aa in length with a predicted MW of 98.541 kDa and a pI equal to 6.4. The predicted *TaZYP1* amino acid sequence shares high levels of conservation with its homologues in close relative species, such as 80% identity with *Oryza sativa* ZEP1 (Wang et al., 2010). However, the level of sequence conservation was reduced when compared with the *Arabidopsis* homologues, *AtZYP1b* (40% similarity), *AtZYP1a* (39% similarity) (Higgins et al., 2005) and only while 36 – 40% similarity with the corresponding proteins of *S. cerevisiae* ZIP1 (Sym et al., 1993), Mammalian SYN1/SCP1 (Meuwissen et al., 1992), *C. elegans* SYP-1 and SYP-2 (MacQueen et al., 2002; Colaiacovo et al., 2003), *Drosophila melanogaster* and C(3)G (Page and Hawley et al., 2001). Southern blot analysis hexaploid wheat showed that the *TaZYP1* gene is located on chromosome group 2 with a copy on the A, B and D genome respectively, and subsequent quantitative Real-Time PCR profiling showed that *TaZYP1* was highly expressed during pre-meiotic interphase (Khoo et al., 2012). A supplemental quantitative analysis on *TaZYP1* was performed in *ph1b* mutant, where its expression was instead slightly elevated (Khoo et al., 2012).

When forming TF, wheat *TaZYP1* exhibits remarkable structural conservation with its orthologues. The general organization is composed of a long coiled-coil motif flanked by globular N- and C-terminal domains. The length (70–90 nm) of the coiled-coil motif largely determines the width (100 nm) of SC (Anuradha and Muniyappa, 2005). Especially, amino acid sequence analysis revealed that both the N- and C-terminal regions of *TaZYP1* (aa positions 1- 68 and 723-863 respectively) have high pI values of 10.22 and 10.05. In addition, 18.75% of the C-terminus consisted of arginine and lysine residues. A putative DNA-binding S/TPXX motif was also found within this region (aa positions 761 to 764), which may interact with DNA during the formation of the SC (Khoo et al., 2012). 3-dimensional protein modelling predicted that the central region of *TaZYP1* forms a coiled-coil domain structure from aa position 69 to 722 (Khoo et al., 2012).

The immunolocalization profiles of *TaZYP1* during meiosis has been recently monitored in hexaploid wheat cv. Cadenza (Osman et al., 2021). *TaZYP1* signal first appears as small foci during leptotene, as in *Arabidopsis* and rice, and contrarily to rye, in which it is represented as short linear tracts (Higgins et al., 2005; Mikhailova et al., 2006; Wang et al., 2010). From zygotene, *TaZYP1* signal starts to lengthen until pachytene, when it fully linearizes. At diplotene, *TaZYP1* profile reverses, so that it progressively shortens and vanishes at diakinesis, except for rice ZEP1, which instead reloads twice onto decondensed chromatin after the diakinesis stage of prophase I (during the prophase II and telophase II stages) (Higgins et al., 2005; Mikhailova et al., 2006; Wang et al., 2010). Additionally, the localization profiles of *TaZYP1* during meiosis was assessed in *ph1b* and *Taasy1* lines, where the authors found a delay in *TaZYP1* elongation until pachytene and persistence of a more intense signal in diplotene meiocytes (Khoo et al., 2012).

So far, studies on WT *TaZYP1* in *T. aestivum* has revealed its DNA-binding capabilities *in vitro* (Khoo et al., 2012) and has elucidated its spatio-temporal localisation profile during the early stages of meiosis through the use of polyclonal anti-*TaZYP1* antibody on WT meiocytes, *ph1b* and four *Taasy1* mutants (Khoo et al., 2012), thus not considering any mutant version of this protein. Thus, the intent of this project was mainly to functionally investigate *TtZYP1* mutants in tetraploid wheat. The approach used involved the identification of TILLING mutant lines carrying a single knocked-out gene from tetraploid *T. turgidum* cv. Kronos. The hypothetical conserved function of wheat ZYP1

in CO was addressed by immuno-localising the HEI10 Class I CO marker on fixed male nuclei.

Furthermore, likewise *TaASY1* genes, the meiotic transcriptome and the mechanisms regulating the meiotic recombination has remained largely unexplored in wheat. Thus, as previously planned and accomplished for the study of *TaASY1* genes, a preliminary molecular analyses to assess the gene expression contribution of *TaZYP1* homoeologues and the potential presence of alternative spliced isoforms were carried out. Relevant outcomes and future directions are discussed in detail in this chapter.

## 3.2 Materials and Methods

### 3.2.1 Plant materials and greenhouse conditions

Kronos wild-type and TILLING plants were grown in soil-based compost (Levington Advance Pot and Bedding M1 Compost) under greenhouse conditions with photoperiod of 16h days light cycle at constant temperature of 22°C (day)/16°C (night), and relative humidity ~60%. Plants were monitored daily and watered regularly.

### 3.2.2 Amplification of *TaZYP1*

*TaZYP1* nucleotide reference sequences of *T. aestivum* ‘Chinese Spring’ were downloaded from Ensembl Plants (EMBL-EBI) database under the accession numbers:

TRIAE\_CS42\_2AL\_TGACv1\_096047\_AA0316910

TRIAE\_CS42\_2BL\_TGACv1\_131351\_AA0426540

TRIAE\_CS42\_2DL\_TGACv1\_158639\_AA0523770

The procedure for the amplification of *TaZYP1* is described in Chapter 2, paragraph 2.2.2.

Oligonucleotides used for the isolation of the *TaZYP1* genes were:

ZYP1F3 = 5'-TCGATGGGTTCCGATCTCTC-3'

ZYP1R2 = 5'-CCAAATGCATAAGGGTCATCAG-3'

The reaction was initiated with a denaturation step at 93°C for 2 minutes, followed by 35 cycles of 93°C for 30 seconds, annealing at 65° for 45 seconds, with a single cycle of 72°C for 3 minutes, ending at 72°C for 10 minutes. Post PCR reactions were analysed by

gel electrophoresis (1% agarose gel) and visualised using ethidium bromide and a UV transilluminator.

### 3.2.3 Proteomic validation of *TaZYP1* protein

Western blot analysis was performed as in Chapter 2, paragraph 2.2.3, here using the primary *AtZYP1* rabbit polyclonal antibody raised against *Arabidopsis* C-terminus domain, 1:5000 dilution (Higgins et al., 2005; Osman et al., 2018) and a goat anti-rabbit Horseradish Peroxidase (HRP) conjugated (ab6908), 1:2000 dilution, as secondary IgG antibody (Table 2.3).

### 3.2.4 Cloning the full length coding region of *TaZYP1*

To obtain the full length of *TaZYP1* genes, a PCR were performed on synthesised cDNA using Q5® High-Fidelity DNA Proofreading Polymerase (catalog number M0491; NEB) using the cDNA primer set:

ZYP1F3 = 5'-TCGATGGGTTCCGATCTCTC-3'

ZYP1R2 = 5'-CCAAATGCATAAGGGTCATCAG-3'

The PCR reaction for *TaZYP1* genes was initiated with a denaturation step at 98°C for 2 minutes, followed by 35 cycles of 98°C for 10 seconds, annealing at 65° for 45 seconds, one cycle of 72°C for 3 minutes, with a final extension at 72°C for 10 minutes. PCR amplicons were then cloned and sequenced as described in Chapter 2, paragraph 2.2.4.

The primers used for Sanger sequencing (Eurofins GATC Biotech Company) were:

M13F = 5'-CAGGAAACAGCTATGAC-3'

M13R = 5'-GTAAAACGACGGCCAGT-3'

ZYP1intF2 = 5'-GATAAAGAGCATGCATCAATG-3'

The updated accession number TraesCS2A02G340400, TraesCS2D02G318100 and TraesCS2B02G338300 retrieved from public domain database Ensembl Plants (EMBL-EBI), IWGSC assembly (Appels et al., 2018), were later used to analyse the predicted alternative isoforms.

### 3.2.5 Validation of *TaZYP1* fragment insertion via colony PCR

Sub-genome specific oligonucleotides used for screening PCR clones of *TaZYP1-2B* were:

ZYP1B\_F = 5'-CAAGCTGAGAAGAGCAAT-3'

ZYP1B\_R = 5'-TTTAGCAGCTTGTGGCT-3'

PCR was initiated with a denaturation step at 93°C for 5 minutes, followed by 35 cycles of 93°C for 30 seconds, annealing at 65° for 45 seconds, one cycle of 72°C for 3 minutes, with a final extension at 72°C for 10 minutes. Post PCR reactions were analysed by gel electrophoresis (1% w/v agarose gel) and visualised using ethidium bromide and a UV transilluminator. Plasmid DNA was isolated from positive liquid cell cultures as mentioned previously with Plasmid DNA Mini Kit (catalog number: D6942-00; Omega Bioteck), to provide a template for sequencing reactions and analysis of the coding regions of the target genes. The reference nucleotide sequences (Chinese Spring) were aligned with the clones. Omega Clustal W was used as a tool for the comparison alignment of nucleotide sequences of the gene of interest. The Neighbour-joining phylogenetic trees generated as output from a multiple sequence alignment, allowed the identification of the sub-genome origin.

### 3.2.6 Testing the efficiency of the designed *TaZYP1* pyrosequencing primers

*TaZYP1* pyrosequencing primers were designed as reported in Chapter 2, paragraph 2.2.6 and validated by gradient PCRs using RedTaq (catalog number 21108; Bioline). The reaction was initiated with a denaturation step at 93°C for 2 minutes, followed by 40 cycles of 93°C for 20 seconds,  $\Delta T_m$  between 64°C-74°C for 45 seconds, a single cycle at 72°C for 30 seconds for each primer set (Table 3.1), and a final extension at 72°C for 60 seconds. Once the optimal annealing temperature for each primer combination was defined, the fragments were then PCR-amplified in a final reaction volume of 20 µL and check off target amplifications, applying the above mentioned cycling conditions. Generated amplicons were visualized on 2% agarose gel that was subjected to electrophoresis at 100 V for 60 minutes, using a low molecular weight DNA ladder (NEB #B7025).

### 3.2.7 Quantitative PCR (qPCR) of *TaZYP1* homoeologues

Experimental conditions, qPCR reaction and statistics employed to measure *TaZYP1* homoeologous expression levels were identical of those established for *TaASY1*, previously described in Chapter 2, paragraph 2.2.7.

### 3.2.8 Cloning the untranslated regions (UTRs) of *TaZYP1*

The study of *TaZYP1* UTRs was carried out as in Chapter 2, paragraph 2.2.8.

The first reaction used the following external primers to amplify the 5' UTR:

ZYP1utrR1 5' = 5'-TTCCAGCTTGCCGAGGAATCATGC-3'

GeneRacer™ 5' = 5'-GCACGAGGACACTGACATGGACTGA-3'

The successive reaction used the following internal primers:

ZYP1utrR 5' Nested = 5'-GACTTCACTGAAGCCTGCTCCTTGA-3'

GeneRacer™ 5' Nested = 5'-GGACACTGACATGGACTGAAGGAGTA-3'

Similarly, to amplify the 3' UTR, the following primers were used during the first reaction:

ZYP1utrF1 3' = 5'-GAGAGGCTGTCGTCGCTCAGACA-3'

GeneRacer™ 3' = 5'-GCTGTCAACGATAACGCTACGTAACG-3'

Primer used in the second cycle were:

ZYP1utrF2 3'Nested = 5'-CCAGGTCCAGGT CCTGAGACCAA-3'

GeneRacer™ 3' Nested = 5'-CGCTACGTAACGGCATGACAGTG-3'

Cycling conditions were in accordance to the manufacturer's instruction, with minor modifications: annealing temperature at 68°C with extension time of 30 seconds for the first reaction and annealing temperature at 65°C with extension time of 30 seconds for Nested PCR. Amplicons were purified using E.Z.N.A.® Cycle Pure Kit (Omega Bio-tek). Sanger sequencing was performed by Eurofins GATC Biotech Company. Omega Clustal W was used for the comparison alignment of nucleotide sequences of the gene of interest.

Primer sets	Oligonucleotide sequence 5' → 3'	T <sub>a</sub> (°C)	Size (bp)
ZYP1 A+B vs D_F	GCATGCATCAATGTCAAGTCA	66	75
ZYP1 A+B vs D_R	TACTATGGAATGGTCCAAGAGGA		
ZYP1 A+D vs B_F	GCAGGTTGACACACAAAGAAAAACA	67.8	52
ZYP1 A+D vs B_R	AGCTCCGCAGTGTCTTGATGA		
ZYP1 B+D vs A_F	GAGAACAAAGCGAGAATCTGAGAGG	67.8	45
ZYP1 B+D vs A_R	GTCTTAAGGAGGAACATGCCG		

**Table 3.1 Sub-genome specific primer sets for qPCR.**

### 3.2.9 Identification of *zyp1* TILLING lines in tetraploid *T. turgidum*

Wheat TILLING (Targeted Induced Local Lesions In Genomes) lines [*Triticum turgidum durum* cv. Kronos (2n=4x=14)] were screened by BLAST search on Wheat TILLING database (<http://www.wheat-tilling.com/>), (Krasileva et al., 2017). Accession number

TraesCS2A02G340400 (*TtZYP1-5A*) and TraesCS2B02G338300 (*TtZYP1-5B*) were used. From tetraploid cv. Kronos, three TILLING lines carrying a STOP codon mutation were identified: K3331 (*TtZYP1-5A*), K2886 (*TtZYP1-5A*) and K4200 (*TtZYP1-5B*). K3886 has a putative mutation at the splice donor site in the codon **CAG** of the exon 16, which should change in **TAG**, causing the introduction of a premature STOP codon. The truncated transcript is expected to preserve the coiled-coil domain and DNA-binding S/TPXX motif (Figure 3.1). Similarly, K3331 has a predicted **CAG** to **TAG** mutation within the exon 16, thereby resulting in a premature STOP codon, which may lead to a truncated ASY1 transcript, lacking of a large portion of the coiled-coil structure (Figure 3.1). Lastly, in K4200, the EMS treatment is expected to generate a **CAG** to **TAG** change in the exon number 5, developing a predicted premature STOP codon, albeit expected to mostly maintain the coiled-coil domain (Figure 3.1).

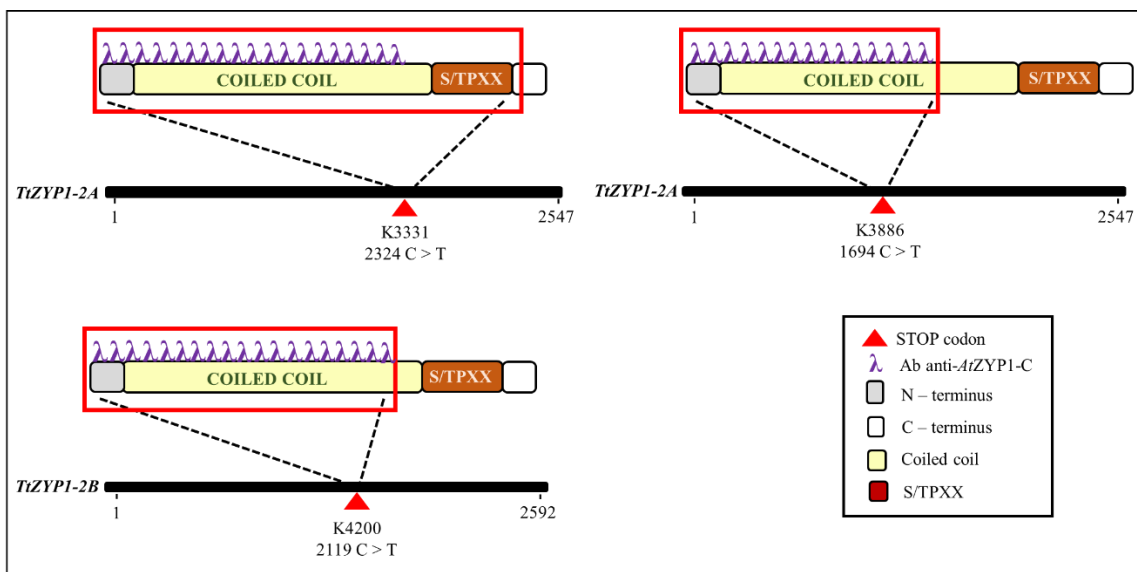


**Figure 3.1 Schematic representation of *TtZYP1-2A* and *TtZYP1-2B* coding regions and altered proteins from TILLING *TaZYP1* lines.** Black bars depict *TaZYP1* homoeologous genes with TILLING mutation site (SNP), nucleotide change and nucleotide position. Three lines with predicted premature STOP codons were identified: K3331 (2324 C > T, Q 774 > STOP), K3886 (1694 C > T, Q 564 > STOP) and K4200 (2119 C > T, Q 706 > STOP). Truncated ZYP1 proteins with the coiled coil domain (yellow) antibodies against *AtZYP1-C* terminus ( $\lambda$ , in purple) binding onto the N-terminus (grey), DNA-binding S/TPXX motif (brown) and C-terminus (white) are represented above each gene (rectangular inserts). Legend is located at the bottom right.

Seeds of the identified TILLING lines were obtained from [www.SeedStor.ac.uk](http://www.SeedStor.ac.uk) and purchased from John Innes Centre (JIC), Norwich, UK. The presence of mutations in the coding sequences was confirmed for the individual TILLING lines by Sanger-sequencing and genotyping using SNP-specific primers calibrated by gradient PCR, as described in Chapter 2, paragraph 2.2.10.

### 3.2.2 Genotype screening of Kronos Parental mutants

The genotyping procedure of Kronos Parental TILLING mutants has been previously described in Chapter 2, paragraph 2.2.10. Gradient PCR was used to calculate the  $\Delta T_m$  of designed TILLING line genomic primers on wild-type Kronos (Table 3.2) 0.5 $\mu$ l of each genomic forward and reverse primer was used. PCR cycle: denaturation at 94°C for 30 seconds; annealing at 59°C-68°C for 45 seconds for Kronos *zyp1* mutants; extension at 72°C for 40 seconds; 35 cycles. Subsequently constant PCR at optimum annealing temperatures carried out for each mutant: annealing at 60.1°C, 61.0°C and 66.4°C for K3331, K3886 and K4200 respectively; Wild-type Kronos A and B were used as controls.

Subgenome Specific Primers	Oligonucleotide sequence 5' → 3'
ZYP1gDNAaF1	GTAGAGTGTAGAACTGTAGG
ZYP1gDNAaR1	CCATGCTATCTGAAGGCTA
K3331wt	GAAGGTAGAGAAAGCAAGTC
K3331alt	GAAGGTAGAGAAAGCAAGTT
K3331common	CCAATCTCTAATCAAATCTTACTGA
ZYP1gDNAaF2	GTTCATCTCATAATTAACTTGTAGG
ZYP1gDNAaR2	GTATTGGTTCCTGGATGA
K3886wt	AGTTGTCACTCAGAAATGATC
K3886alt	AGTTGTCACTCAGAAATGATT
K3886common	TTACTTTGTTACTACTCTAGTG
ZYP1gDNA5bF	GAAGAAGATTGTCAGAAACTT
ZYP1gDNA5bR	TTCTTAACATGCTTGCCG
K4200wt	CAGTTACAGTGGAAAGTGATGGG
K4200alt	TAGTTACAGTGGAAAGTGATGGG
K4200common	AGGTGTTTGAATGCGTCAGG

**Table 3.2 Sub-genome specific primers used to amplify *TtZYP1* TILLING lines.** Genomic primers (green) were used to validate the mutation via Sanger-sequencing.

### 3.2.3 Crosses of Kronos Parental mutants

The crossing procedure of Kronos Parental TILLING mutants has been previously described in Chapter 2, paragraph 2.2.10.

For *zyp1* analysis, homozygous individuals for mutation (K3331 *zyp1a-1* × K4200 *zyp1b* and K3886 *zyp1a-2* × K4200 *zyp1b*) were crossed, while heterozygous individuals from F1 (AaBb) were self-pollinated in parallel to create an F<sub>2</sub> population segregating for the mutation (double KO aabb). A wild-type line was also included as controls.

### 3.2.4 Genotyping of F1 mutants

The genotype of Kronos F<sub>1</sub> mutants derived from single KO crosses was confirmed through PCR with designed mutant primers (Table 4.1). Gradient PCR was used to identify the annealing temperature ( $\Delta T_m$ ) that the primers would no longer work to give a band on WT Kronos; these were 60.1°C (K3331wt and common primers), 61.0°C (K3886alt and common primers), 61.2°C (K0157wt and common primers) and 66.4°C (K4200wt and common primers). Subsequently, all samples were confirmed to be homozygous/heterozygous for corresponding point mutation, using Chromas Lite 2.0 software.

### 3.2.5 Backcrosses of *zyp1* Parents with tetraploid Kronos wild-type

Following the non-mendelian segregation of the F<sub>2</sub> segregants from both crosses (K3331 and K3886 x K4200 TILLING lines), one backcross with Kronos WT were performed for *asy1a-1* (K3331 line) and *asy1a-2* (K3886 line) in order to decrease the secondary mutation load.

### 3.2.6 Isolating pollen mother cells (PMCs) for metaphase I chromosome spreads

Protocol and reagents used for metaphase spread experiments have been previously described in Chapter 2, paragraph 2.2.14.

### 3.2.7 Immunolocalisation of PMCs

Protocol and reagents used for immunolocalization experiments have been previously described in Chapter 2, paragraph 2.2.15.

### 3.2.8 Statistics

Chiasma frequency and recombination foci count differences were tested for significance as described in Chapter 2, paragraph 2.2.16.

## 3.3 Results

### 3.3.1 *TaZYP1* is expressed in leaves and inflorescences of hexaploid *T. aestivum* cultivars Cadenza and Apogee

As previously shown for *TaASY1* in Chapter 2, to quantify the relative contributions of *TaZYP1* homoeologues in hexaploid *T. aestivum*, their expression in inflorescences (Figure 3.2 a) and leaves (Figure 3.2 b) of Cadenza and Apogee was validated by using RT-PCR on cDNA with gene-specific primers. The results show a band of ~2800 bps in meiotic and non-meiotic tissues of both cultivars (Figure 3.2).

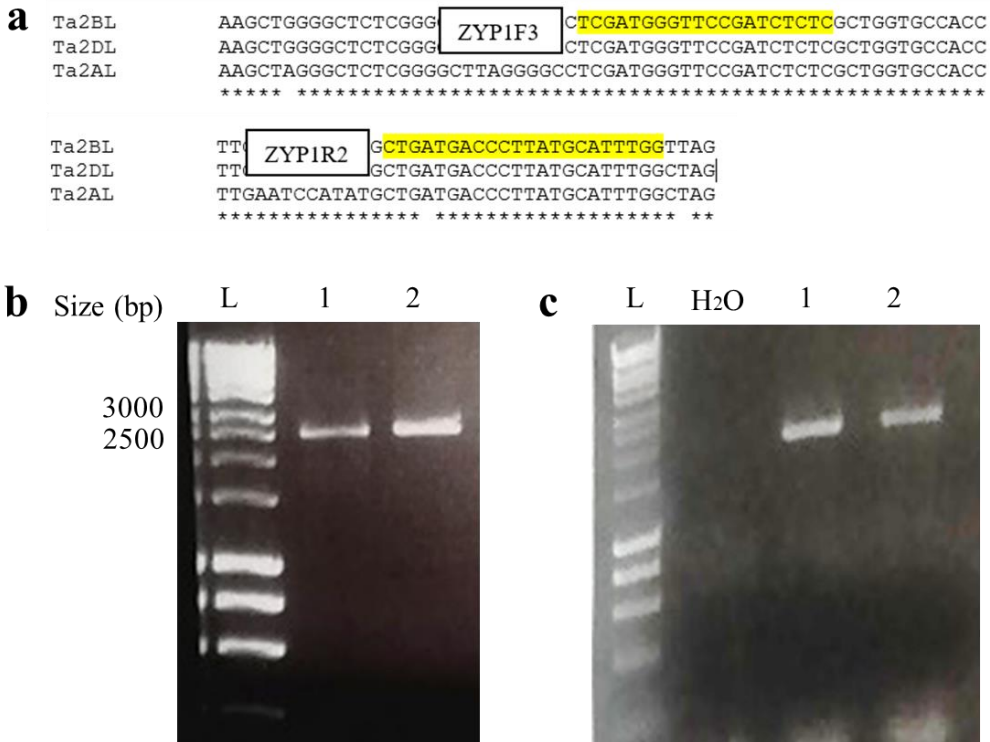


**Figure 3.2 Expression validation of *TaZYP1* cDNA in hexaploid *T. aestivum*.** a) Multiple sequence alignment among the coding region sequences of *TaZYP1* A, B and D sub-genomes from Chinese Spring reference. Forward and reverse primers are highlighted in yellow. *TaZYP1* coding region amplicons of *T. aestivum* cvs. Apogee and Cadenza from b) inflorescence and c) flag leaf using gene specific primers. L = DNA ladder; 1 = lane for Apogee cDNA; 2 = lane for Cadenza cDNA.

### 3.3.2 *TaZYP1* homoeologous gene expression is likely redundant in reproductive and somatic tissues

In hexaploid *T. aestivum*, *TaZYP1* homoeologues are located on chromosomes 2A, 2B and 2D. At the coding DNA sequence and amino acid levels, *TaZYP1-2A* (TraesCS2A02G340400) showed 99 and 98% identity and similarity to both *TaZYP1-2B* (TraesCS5B02G098800) and *TaZYP1-2D* (TraesCS5D02G105000), respectively, likewise, *TaZYP1-5B* shares 99 and 98% identity and similarity to *TaZYP1-2D*, respectively (data retrieved from Ensembl Plants database). To compare the relative expression of *TaZYP1* homoeologues, total RNA samples were collected from inflorescences of hexaploid *T. aestivum* cvs. Cadenza and Apogee. To unbiased amplify *TaZYP1* transcripts from A, B and D sub-genomes, primers were designed within cDNA region sharing 100% sequence similarity, thereby the proportion of the resulting clones represented the relative amount of each sub-genome expression (Figure 3.3 a). Thus, the

full length of *TaZYP1* cds was cloned and Sanger sequenced. A colony PCR screening was performed to confirm the amplification of specific sub-genome ZYP1 transcripts. In designing primers for specific sub-genomes, splice variants were not considered. An example is illustrated in Figure 3.3 b. Here, the *TaZYP1-2B* clone derived from  $\Delta T_m$  optimization of B sub-genome specific primers using a *TaZYP1-2A* clone as negative control previously sequenced.

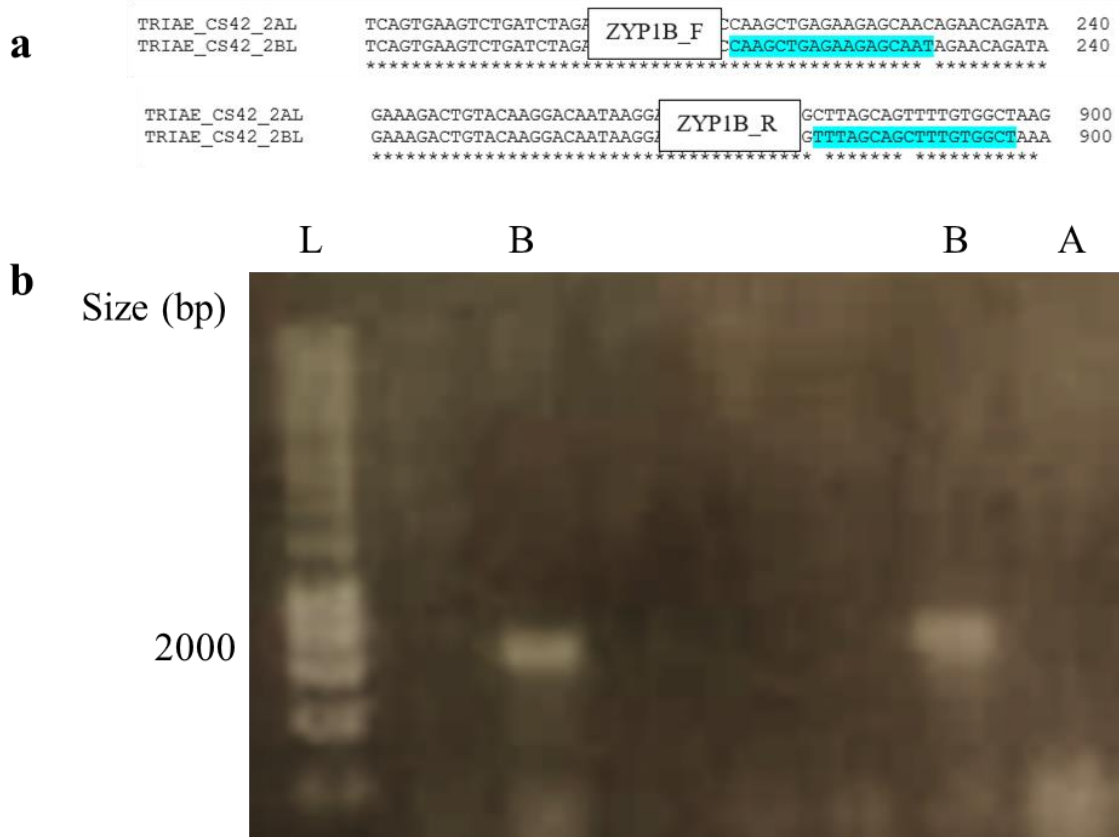


**Figure 3.3 Colony PCR of *TaZYP1-2B* clone.** a) Multiple sequence alignment between the coding region sequences of *TaZYP1* A and D sub-genomes from Chinese Spring reference. Forward and reverse primers are highlighted in sky blue. b) *TaZYP1-2B* cds clone. L = DNA ladder; B = *TaZYP1-2B* clone; A = *TaZYP1-2A* clone used as negative control. Green colour= RNA-seq data from vegetative samples.

From the analysis of *TaZYP1* cds clones emerged that 75% of *TaZYP1* clones sequenced (n=20) belonged to the A sub-genome, 20% of clones (n=20) expressed the B sub-genome and only 5% of clones (n=20) expressed the D sub-genome, suggesting differential expression level among the sub-genomes and, importantly, possible dominance of the A sub-genome (Figure 3.4 a). Intriguingly, the RNA-Seq data from Wheat Expression

Browser (expVIP) (<http://www.wheat-expression.com/>), showed a high variability in expression among the *TaZYP1* homoeologues, as indicated by TPM and SEM values of three representative datasets (Figure 3.4 b). Thus, to better measure the homoeologous expression level of *TaZYP1* genes a qPCR experiment was implemented, as for the *TaASY1* genes (see Chapter 2).

a	<i>TaZYP1</i> cds clones (n=20)	<i>TaZYP1-2A</i>	<i>TaZYP1-2B</i>	<i>TaZYP1-2D</i>
		75%	20%	5%
b	<u>Wheat Exp Vip Datasets</u> (TPM ± SEM)	<i>TaZYP1-2A</i>	<i>TaZYP1-2B</i>	<i>TaZYP1-2D</i>
	spike, reproductive, none, other (n=76)	0.84 ± 0.28	0.96 ± 0.40	0.58 ± 0.20
	spike, reproductive, none, Chinese Spring (n=16)	2.31 ± 2.13	2.31 ± 2.0	1.13 ± 0.79
	<b>spike, reproductive, none, Azhurnaya (n=33)</b>	<b>2.23 ± 1.06</b>	<b>1.78 ± 0.57</b>	<b>1.13 ± 0.33</b>

**Figure 3.4 Assessment of *TaZYP1* homoeologues relative contribution in DNA coding region.** a) Proportion of *TaZYP1* sub-genomes from cds clones expressed in percentage. b) Predicted gene expression level of A, B and D homoeologues of *TaZYP1* from publicly available RNA-Seq data. The table shows a predicted sub-genome dominance of *TaZYP1-2B*. The relative proportion of *TaZYP1-2A*, *TaZYP1-2B* and *TaZYP1-2D* homoeologues were calculated in sixteen reproductive tissue sample of *T. aestivum* ‘Chinese Spring’ normalized via TPM method. Data retrieved from Wheat expVIP database. TPM= transcripts per million; SEM= standard error of the mean; n= number of observations; None = wild-type plants.

Primer pairs flanking a single SNP that discriminates the different *TaZYP1* copies (e.g. A+B vs D, A+D vs B and B+D vs A) and with high score values were prioritised and tested by conventional PCR (Figure 3.5 a-c). PCR products amplified by *TaZYP1* A+B vs D, *TaZYP1* B+D vs A and *TaZYP1* A+D vs B primer sets had a predicted size of 75, 45 and 52 bps, respectively (Figure 3.5 d). Subsequently, the expression level of each *TaZYP1* homoeologous combination was compared and quantified on four cDNAs from four wild-type Cadenza individuals with a qPCR assay.

Both the above results from Wheat ExpVIP database and cloning fitted with the qPCR data, which ultimately revealed that *TaZYP1* homoeologues were redundant at gene expression level (Figure 3.5 e), therefore there was no significant upregulation of *TaZYP1-2A* transcript, as instead detected with the cloning approach.

**a**

Primer Set 1 F1R1, T <sub>a</sub> =66, 75 bp			Score: 98 Quality: High		
Primer	Id	Sequence	Nt	Tm, °C	%GC
→ PCR	F1	GCATGCATCAATGTCAAGTCA	21	69.7	42.9
↔ PCR	R1	TACTATGGAATGGTCCAAGAGGA	23	68.7	43.5
→ Sequencing	S1	TGTCAAGTCATGTCGC rc= GCGACATGACTTGAC	16	51.5	50.0
Target Polymorphisms	Position1				
Sequence to Analyze		TTTGTGGCTAAAGTAGCTGAGCTAGATAAAGAGCATGCATCAATGTCAAGTCATGTCGCCAGATTGCTTCT TCATTTGATAAGTACTATGGAATGGTCCAAGAGGAAGACTGCTGATAACAAGATCTGCTAAGGACAAA			

ZYP1_2AS_cds	GTAGCTGAGCTAGATAAAGA	TCATGTCGTAGATTGCTTCT	960
ZYP1_2BS_cds	GTAGCTGAGCTAGATAAAGA	TCATGTCGTAGATTGCTTCT	960
ZYP1_2DS_cds	GTAGCTGAGCTAGATAAAGAGCATGCATCAATGTCAAGTCATGTCGCAGATTGCTTCT	960	
	*****	*****	
ZYP1_2AS_cds	TCATTTGATAAGTACTA	AAACTGCTGATAACAAGATCTGCT	1020
ZYP1_2BS_cds	TCATTTGATAAGTACTA	AAACTGCTGATAACAAGATCTGCT	1020
ZYP1_2DS_cds	TCATTTGATAAGTACTATGGAATGGTCCAAGAGGAAGACTGCTGATAACAAGATCTGCT	1020	
	*****	*****	

**b**

Primer Set 1 F1R1, T <sub>a</sub> =67.8, 45 bp			Score: 96 Quality: High		
Primer	Id	Sequence	Nt	Tm, °C	%GC
→ PCR	F1	GAGAACAAAGCGAGAACATGAGAGG	24	71.8	50.0
↔ PCR	R1	GTCTTAAGGAGGAACATGCCG	21	69.9	52.4
→ Sequencing	S1	CCTTAAGACGCATCAA rc= TTGATGCGTCTTAAGG	16	50.0	43.8
Target Polymorphisms	Position1				
Sequence to Analyze		CTCTATAAGGAAATGGAGCACAAATGCAACGAAAAGATATTAGAGAACAGCGAGAACATGAGAGGTGCTTGTGCT GTCTTAAGGAGGAACATGCCGAGTGGTGGCAAGAATTCAACAGGATAAA			

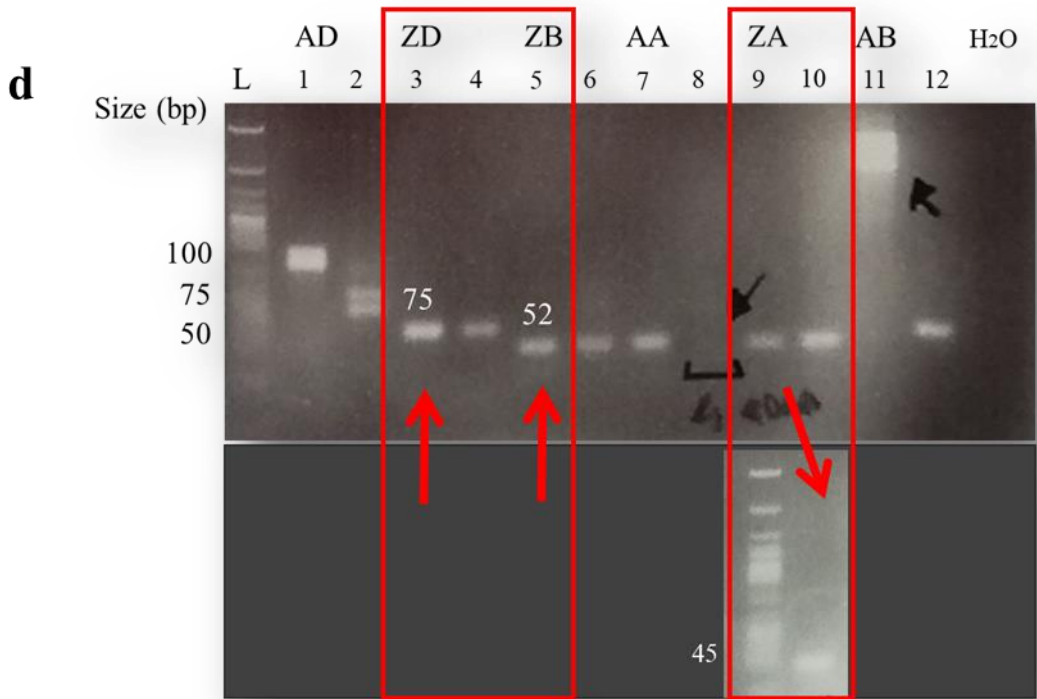
ZYP1_2AS_cds	AACGAAAAGATATTAGAGAACAGCGAGAACATGAGAGGTGCTTGATGCGTCTTAACCGAG	1860
ZYP1_2BS_cds	AACGAAAAGATATTAGAGAACAGCGAGAACATGAGAGGTGCTTGATGCGTCTTAACCGAG	1860
ZYP1_2DS_cds	AACGAAAAGATATTAGAGAACAGCGAGAACATGAGAGGTGCTTGATGCGTCTTAACCGAG	1860
	*****	*****
ZYP1_2AS_cds	GAACATGCCGAGTGGTGGCAAGAACAGGATAACGAGCTTAAGGAATCAACTCTT	1920
ZYP1_2BS_cds	GAACATGCCGAGTGGTGGCAAGAACAGGATAACGAGCTTAAGGAATCAACTCTT	1920
ZYP1_2DS_cds	GAACATGCCGAGTGGTGGCAAGAACAGGATAACGAGCTTAAGGAATCAACTCTT	1920
	*****	*****

**c**

Primer Set 1 F1R1, T <sub>m</sub> =67.8, 52 bp			Score: 100 Quality: High		
Primer	Id	Sequence	Nt	T <sub>m</sub> , °C	%GC
PCR	F1	GCAGGTTGACACACAAGAAAAACA	24	72.3	41.7
PCR	R1	AGCTCCGCAGTGTCTTGATGA	22	73.4	50.0
Sequencing	S1	ACACAAGAAAAACAGATCA	19	50.5	31.6
Target Polymorphisms	Position1				
Sequence to Analyze		CTGCACAGCGAGATTGCTAACGCGTACCGAGGTTGACACACAAGAAAAACAGATCAGCGAGCTCCGCAG TGGTCTTGATGAGAACAGTTGATATTTCCTTGATGAGAAAG			

↓

ZYP1_2AS_cds	CGTGACCA	ZYP1 A+D vs B_F	AAAACAGATCAGTGA	ZYP1 A+D vs B_R		1500
ZYP1_2BS_cds	CGTGACCA	CCAGGTTGACACACAAGAAAAACA	GATCAGCG	AGCTCCGCAGTGTCTTGAT		1500
ZYP1_2DS_cds	CGTGACCA	CAGGTTGACACACAAGAAAAACAGATCAGTGA	GAGCTCCGCAGTGTCTTGAT			1500
	*****	*****	*****	*****		*****
ZYP1_2AS_cds	GAGAAGGAACAGTTGATATTCTCTGTAGAAAGAGAGAAGAGTTGGAGGAACAAAAG					1560
ZYP1_2BS_cds	GAGAAGGAACAGTTGATATTCTCTGTAGAAAGGGAGAAGAGTTGGAGGAACAAAAG					1560
ZYP1_2DS_cds	GAGAAGGAACAGTTGATATTCTCTGTAGAAAGAGAGAAGAGTTGGAGGAACAAAAG					1560
	*****	*****	*****	*****		*****



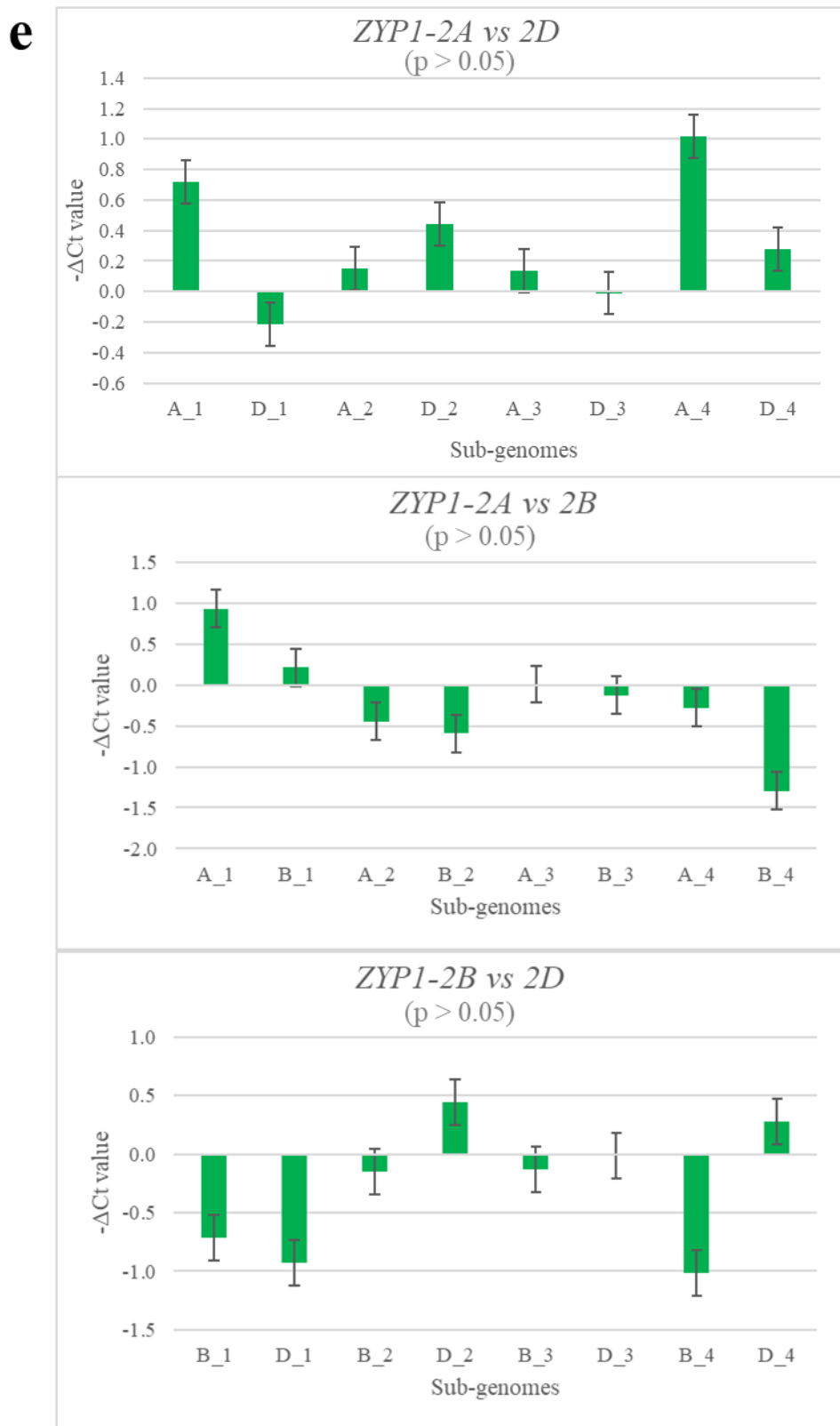


**Figure 3.5 Validation of pyrosequencing primer sets.** a) *TaZYP1* with identical A and B homoeologous sequences, but with a SNP in D genome (A+B vs D). b) *TaZYP1* with conserved A and D homoeologous sequences, but with a SNP in B genome (A+D vs B). c) *TaZYP1* with identical B and D homoeologous sequences, but with a SNP in A genome (B+D vs A). d) PCR

results of predicted *TaZYP1* amplicon combination sizes (red arrows). SNPs are indicated in purple. L = DNA marker; odd numbers (1, 3, 5, 7, 11) = Cadenza cDNA; even numbers (2, 4, 6, 8, 12) = Kronos cDNA; ZD = *TaZYP1* A+B vs D; ZB = *TaZYP1* A+D vs B; ZA = *TaZYP1* B+D vs A; H<sub>2</sub>O = negative control. e) qPCR results showing balanced contribution of each *TaZYP1* sub-genomes. Error bars represent the standard deviation of three replicates. P values for statistical significance are shown in brackets.

### 3.3.3 The predicted *TaZYP1* cds isoforms in germline DNA

The full length of *TaZYP1* cds genes from *T. aestivum* cvs. Cadenza and Apogee were cloned and the alternative isoforms currently predicted on Ensembl Plants database (Figure 3.6) were inspected, as previously described in Chapter 2. With this approach, no AS was detected in the *TaZYP1* cds genes. Accordingly, the initial amplification of *TaZYP1* cDNA using gene-specific primers, only displayed a single PCR product of 2800 bps (Figure 3.2).

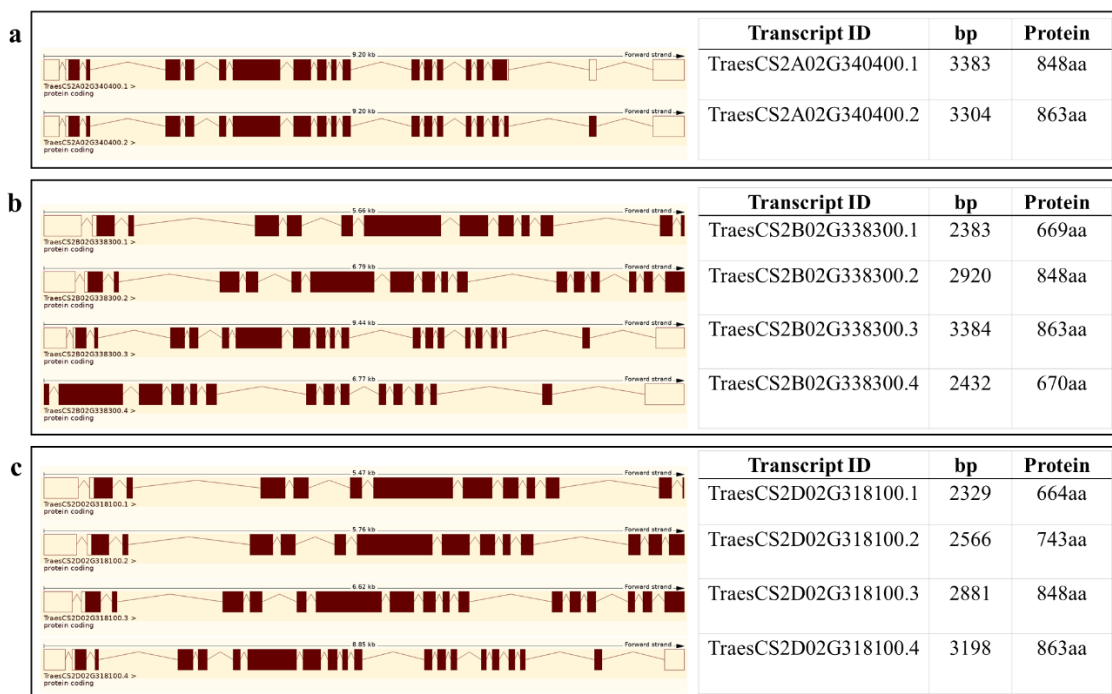


**Figure 3.6 Predicted protein coding annotation of *TaZYP1*.** a) *TaZYP1-2A* with 2 transcripts (splice variants), b) *TaZYP1-2B* with 4 transcripts, c) *TaZYP1-2D* with 4 transcripts. Transcripts are drawn as boxes (exons) and lines connecting the boxes (introns). Filled boxes represent coding sequence and unfilled boxes (or portions of boxes) represent UnTranslated Regions (UTR). Genes annotated with high confidence by IWGSC method. Data source: Ensembl Plants.

### 3.3.4 Identification of *TtZYP1* 3' UTR isoforms in reproductive tissues

The study of untranslated regions in *TtZYP1* began with the synthesis of first-strand cDNA from total RNA of tetraploid *T. turgidum* cv. Kronos, isolated from dissected ovaries and anthers, amplified with gene specific primers (covering the exon adjacent to the untranslated regions) via a nested RACE PCR (Figure 3.7 a). Two 5' UTR products with lengths equal to 300 and 600 bp were amplified in *TtZYP1* 5' UTR from ovary and anther samples, respectively (Figure 3.7 b), corresponding to the predicted 5' UTR from wheat genome annotation, IWGSC v1.0 (Appels et al., 2018). Two identical-size *TtZYP1* 3' UTR products in both ovaries and anthers (300 and 400 bp) were also observed (Figure 3.6 b), diversely from the RefSeqv1.0 annotation (Figure 3.7 c).

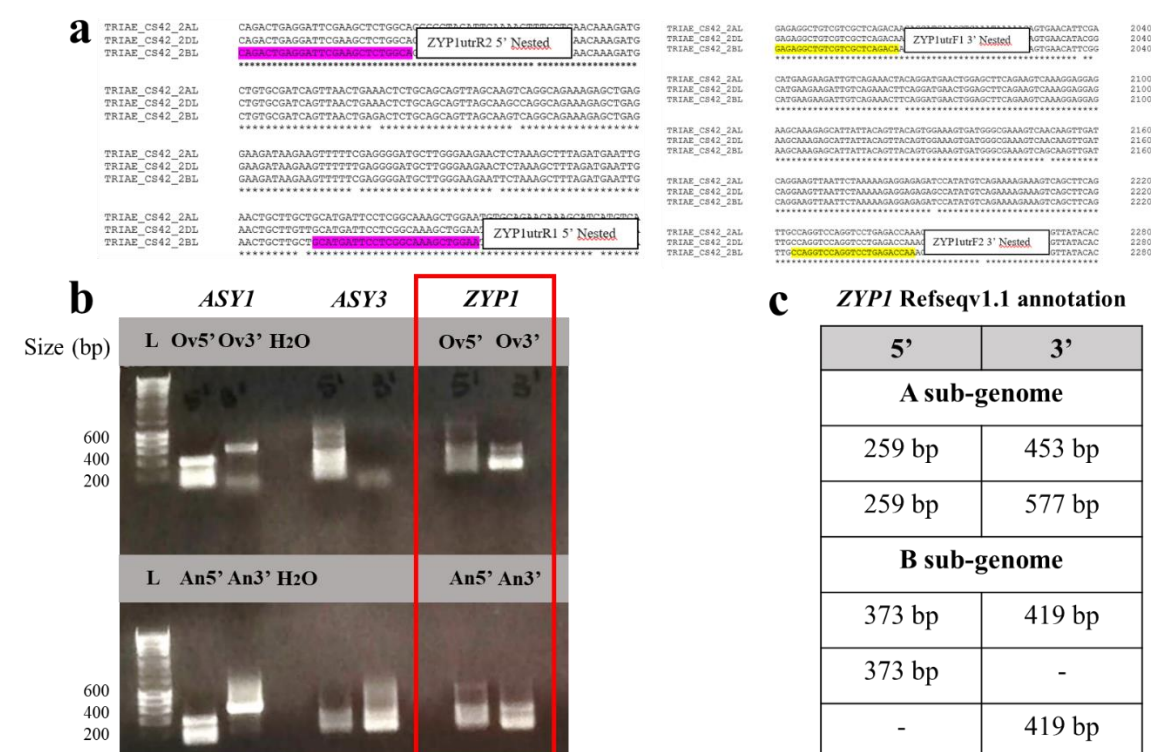


**Figure 3.7 RACE PCR validates the expression of *TtZYP1* UTRs in reproductive tissues.** a) Multiple alignment among the genomic reference sequence of *TtZYP1* sub-genomes showing the nested 5' (pink) and 3' (yellow) UTR primers. b) Visualisation of 5' and 3' UTR amplicons by gel electrophoresis following the second amplification with nested PCR primers (red). c) UTR isoforms data from Ensembl Plants database. Length are indicated in base pair (bp). L = DNA ladder; Ov = ovary; An = anther; H<sub>2</sub>O = negative control.

To characterize the *TtZYP1* UTRs, RACE PCR gene amplicons were cloned, Sanger sequenced and aligned to the reference genome TGACv1 annotation with the

bioinformatics Omega Clustal W tool for comparison analysis between the reference and the novel UTR sequences. Contrarily to what predicted on Ensembl Plants database, no *TtZYP1* 5' UTR transcript was found either in ovary or in anther samples (Figure 3.8). Following the latest wheat genome annotation, Sanger sequencing results were also mapped to the wheat reference genome, IWGSC v1.0 (Appels et al., 2018) (Figure 3.6).

OligoRNA RACE		
ZYP1.F51	-----	CGACTGGAGCACGA 14
ZYP1.F54	-----	0
ZYP1.F58	-----	CGACTGGAGCACGA 14
ZYP1.F6	-----	CGACTGGAGCACGA 14
ZYP1.F57	-----	CGACTGGAGCACGA 14
cZYP1A	ATGCAGAAGCTAGGGCTCTCGGGCTTAGGGCCTCGATGGTTCCGATCTCTCGCTGGT	60
cZYP1B	ATGCAGAAGCTGGGCTCTCGGGCTTAGGGCCTCGATGGTTCCGATCTCTCGCTGGT	60
ZYP1.F51	GGACACTGACATGGACTGAAGGAGTAG----AAAAGAGGCTGAAGA-----	56
ZYP1.F54	-----	0
ZYP1.F58	GGACACTGACATGGACTGAAGGAGTAGAAACCAAAGAGGCTGAAGA-----	60
ZYP1.F6	GGACACTGACATGGACTGAAGGAGTAGAAACCAAAGAGGCTGAAGA-----	60
ZYP1.F57	GGACACTGACATGGACTGAAGGAGTAGAAACCAAAGAGGCTGAAGA-----	60
cZYP1A	GCCACCTCTACGGCTGGGAAGGCCACGAACCCCAAGCCCTCGTCGGATGCTGGAGGTAGC	120
cZYP1B	GCCACCTCTACGGCTGGGAAGGCCACGAACCCCAAGCCCTCGTCGGATGCTGGAGGTAGC	120
ZYP1.F51	-----	ACTCTGGCAGCAGGCT 72
ZYP1.F54	-----	0
ZYP1.F58	-----	ACTCTGGCAGCAGGCT 76
ZYP1.F6	-----	ACTCTGGCAGCAGGCT 76
ZYP1.F57	-----	ACTCTGGCAGCAGGCT 76
cZYP1A	ACATACGGGAGCTTCGCCAACCTTAAGATCACAGCAGAGAAATTAGTCAGGAGCAGGCT	180
cZYP1B	ACATACGGGGCTTCGCCAACCTTAAGATCACAGCAGAGAAATTAGTCAGGAGCAGGCT	180
 <b>ZYP1utrR 5' Nested</b>		
ZYP1.F51	ATA-----	75
ZYP1.F54	-----	0
ZYP1.F58	ATA-----	79
ZYP1.F6	ATA-----	79
ZYP1.F57	ATA-----	79
cZYP1A	TCAGTGAAGTCTGATCTAGAAATGGCGCATACCAAGCTGAGAAGAGCAACAGAACAGATA	240
cZYP1B	TCAGTGAAGTCTGATCTAGAAATGGCGCATACCAAGCTGAGAAGAGCAATAGAACAGATA	240

**Figure 3.8 Multi sequence alignment of *TtZYP1* 5' UTR clones from tetraploid *T. turgidum* cv. Kronos with the genome reference.** Clones derive from ovary tissue. Primers used are indicated in text boxes. Start codon ATG is highlighted in yellow.

Instead, seven alternative *TtZYP1* 3' UTR spliced isoforms were collectively found in tetraploid *T. turgidum* cv. Kronos reproductive tissues (ovaries and anthers), of which, only the clones ZYP1.M32 and ZYP1.M33 aligned with 172 nucleotides to the 3' UTR transcript of wheat reference genome, IWGSC v1.0 (Appels et al., 2018) (Figure 3.9 c). The alternative 3' UTR spliced isoforms had two undescribed regulatory sequences, termed PolyAdenylation Signals (PAS): AAATAAAA and AAATAAAAA, both located at 227 nucleotides downstream the STOP codon (Figure 3.9 a). For simplicity, AAATAAAA

sequence will be re-named PAS<sub>1</sub> and AAATAAAAA will be referred to as PAS<sub>2</sub>. From this analysis, two distinct categories of 3' UTR alternative isoforms could be discriminated based on the number of PAS sequences: transcript variants with PAS<sub>1</sub> and transcript variants with PAS<sub>2</sub>, whose transcript sequence of each category mostly share identical nucleotide length. The overall results are illustrated in Figure 3.10 a.



**Figure 3.9 *TtZYP1* 3' UTR transcript variants with PAS<sub>1</sub> and PAS<sub>2</sub> sites.** a) PAS<sub>1</sub> sequence AAATAAA is highlight in green, while PAS<sub>2</sub> motif is highlight in yellow. b) Clones are aligned with A reference. c) Clones aligned with B reference. The clones ZYP1.M32 and ZYP1.M33 are the predicted 3' UTR variants from IWGSC RefSeqv1.1 annotation. ZYP1.F = *TtZYP1* clone sequence from ovary (F = female) is highlight in pink; ZYP1.M = *TtZYP1* clone sequence from anther (M = male) is highlight in sky blue.

Surprisingly, 42% of the resulting 3' polyA tail of *TtZYP1* ( $n = 19$ ) contained additional G nucleotide (Figure 3.10), albeit no distinct pattern was observed in polyA tail length and nucleotide composition in relation to the PAS sequences. The *TtZYP1* 3' UTR sequences are listed in Appendix (Table S7).

Considering both PAS sequence types and nucleotide lengths, only one 3' UTR variants from A sub-genome were common in the reproductive tissues tested, which is v1 (variant 1): 395 bps, containing PAS<sub>1</sub> sequence and polyA tail of 21 adenosines and 3 guanosines (Figure 3.10 b).

Taking into account their frequency among the A and B sub-genomes, in anther, the v1 was the most frequent in the A clones (72%,  $n = 7$ ), but it was totally absent in B clones, albeit the sample size of the latter was extremely small ( $n = 2$ ). Less frequent were v2 and v3, each accounting for 14% among the A clones ( $n = 7$ ), differing for their PAS sequences (Figure 3.10 b). Moreover, these variants did not contain any G within the polyA tail. In B clone anthers ( $n = 2$ ), v7 had the shortest 3' UTR transcript (247 bps) with a long polyA tail, consisted of 32 adenosines and 4 guanosines (Figure 3.10 b).

In the ovary counterparts, two 3' UTR isoforms were equally expressed (40%,  $n = 10$ ): v1 and v5. They were similar in size (395 and 407 bps respectively) and in polyA tail-G content, but differed in PAS sequences (v1 had PAS<sub>1</sub>, while v5 had PAS<sub>2</sub>). The remaining alternative transcripts v4 and v6 represented only a minor part of the total (10%,  $n = 10$ ) and were longer in nucleotides (613-623 bps) and polyA tail, especially v6 (Figure 3.10 b).

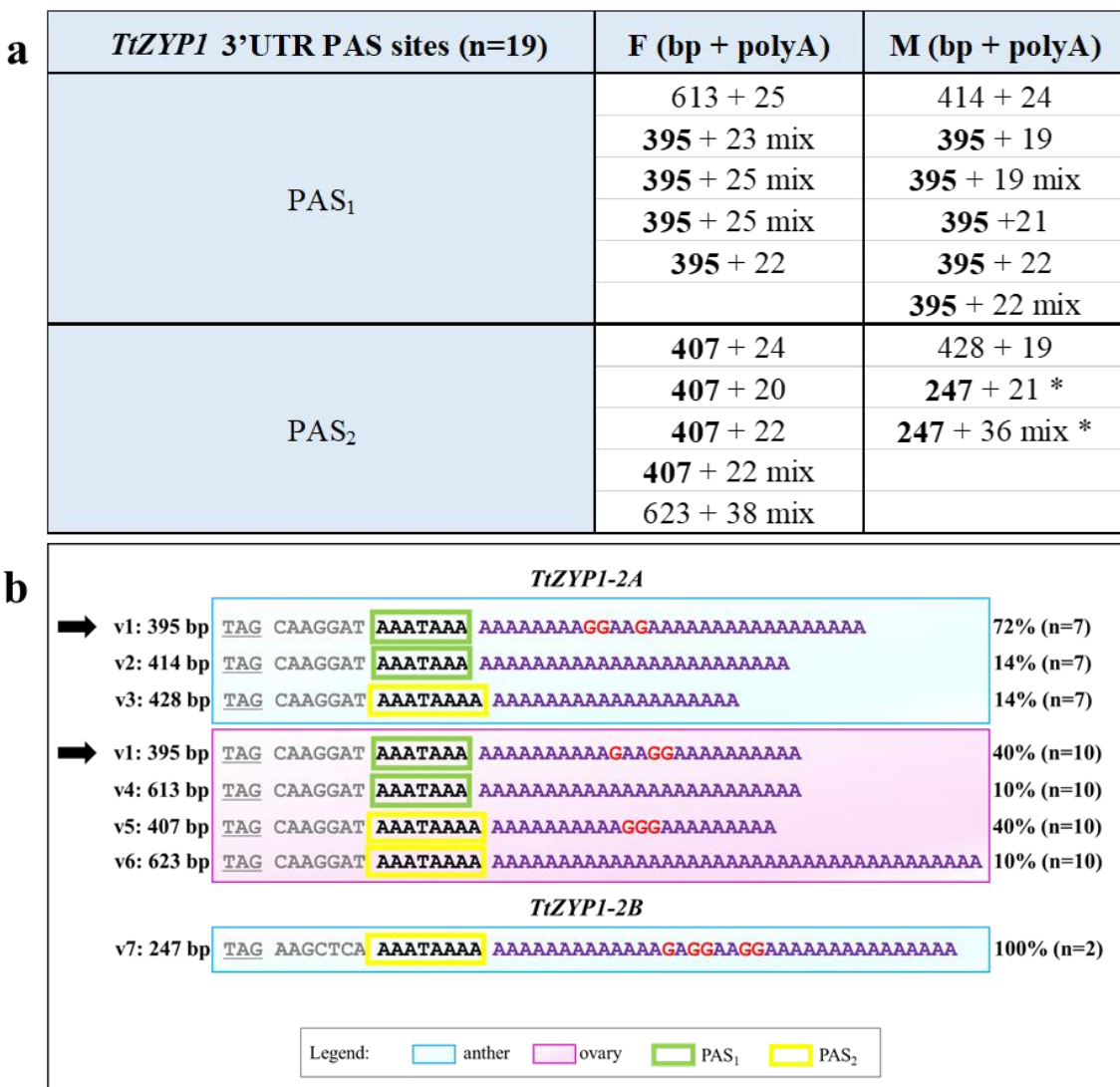


**Figure 3.10 *TtZYP1* 3' UTR transcript variants.** a) Table recording the PAS sequences identified in ovary (F) and anther (M) samples. Length in bps and the number of adenosine and/or guanosines within the polyA tail are also indicated. Asterisk (\*) refers to the B sub-genome cloned; “mix” refers to the simultaneous adenosine and guanosine occurrence in the polyA tail. b) 3' UTR clone sequences from ovaries (pink background) and anthers (sky blue background) of *TtZYP1-2A* and *TtZYP1-2B*. v1-7 = seven splice variants, in grey = STOP codon (TAG) followed by seven nucleotide of the splice variant, PAS sequences (when present), polyA tail in purple, frequency expressed in percentage and the total clone number in brackets are on the left side; Legend is located at the bottom.

The predicted translated product of 98.541 kDa was only detected in leaves, but not in inflorescences (Figure 3.11). Here, the Western blot assay revealed the presence of two proteins with MW equal to 85 and ~75 kDa within the spike specific for ZYP1 antibody, but this does not necessarily imply that these proteins are ZYP1 (Figure 3.11). The

difficulty encountered to extract wheat ZYP1 was more likely due to its poor solubility, being incorporated between two densely organized lateral elements. This is being suggested for spikes versus leaves.

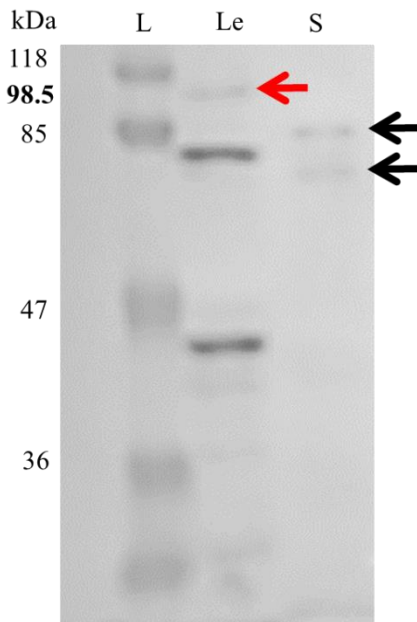


**Figure 3.11 Figure Western blot with *AtZYP1* antibody in hexaploid *T. aestivum*.** A protein of the expected size for *TaZYP1* protein of 98.5 kDa extracted from leaves (Le) is pointed with a red arrow. Black arrows show two proteins with MW equal to 85 and ~75 kDa detected using *AtZYP1* antibody raised against rabbit. L = DNA ladder; Le = leaf; S = spike.

### 3.3.4 Analysis of wheat *zyp1* TILLING mutants

Sanger-sequencing confirmed the predicted SNP mutation in the respective *TtZYP1* sub-genomes of the three TILLING lines identified and PCR-based genotyping allowed to screen the intended genotypes for this study. PCR primer pairs flanking the corresponding SNP site were designed to individually amplify *TtZYP1-2A* and *TtZYP1-2B*. In tetraploid cv. Kronos, homozygous individuals aaBB (single KO in A sub-genome) were found in K3331 (*zyp1 aaBB-1*) and K3886 (*zyp1 aaBB-2*), while homozygous individuals AAbb (single KO in B sub-genome) were found in K4200 (*zyp1b*). For simplification, from now on tetraploid *zyp1 aaBB* and *zyp1 AAbb* genotypes will be referred to as *zyp1a* and *zyp1b*, respectively, according to the expected mutant alleles in A or B subgenome.

To confirm the presence of the predicted mutation within the coding region of *TtZYP1* genes, the coding DNA sequence of each *zyp1* single KO mutant was cloned and

sequenced, as previously described in Chapter 2. As predicted *in-silico*, in K3331 (*zyp1a-1*) clone, a C to T transition at nucleotide 2324 in the **CAG** codon, determined the formation of a premature in-frame termination codon **TAG**, resulting in a predicted truncated *TtZYP1-2A* protein, missing 14 aa residues of coiled coil domain, DNA-binding S/TPXX motifs and the C-terminus (Figure 3.12). Similarly, in K3886 (*zyp1a-2*) clone, a C to T transition at nucleotide position 1694 in the **CAG** codon, introduced a premature STOP codon **TAG**, resulting in a predicted nonsense *TtZYP1-2A* protein, which, beyond the C-terminus, lacked 196 amino acid residues of the coiled coil domain (Figure 3.13). Lastly, in K4200 (*zyp1b*) clone, a codon change **CAG** → **TAG** at nucleotide 2119, generated a premature termination of the *TtZYP1-2B* transcript, predicted to be partially functional, due to the loss of 54 residues dispensable to form functional coiled-coil structure and the C-terminal (Figure 3.14). In all mutants, the antibodies anti-*AtZYP1* (N-terminal, residue 1-416) used in this analysis, could still bind to the truncated proteins, which indeed conserved greatly the coiled coil domain. A summary of the predicted consequences into each *zyp1* mutant transcript derived from the EMS treatment is described in Figure 3.15.

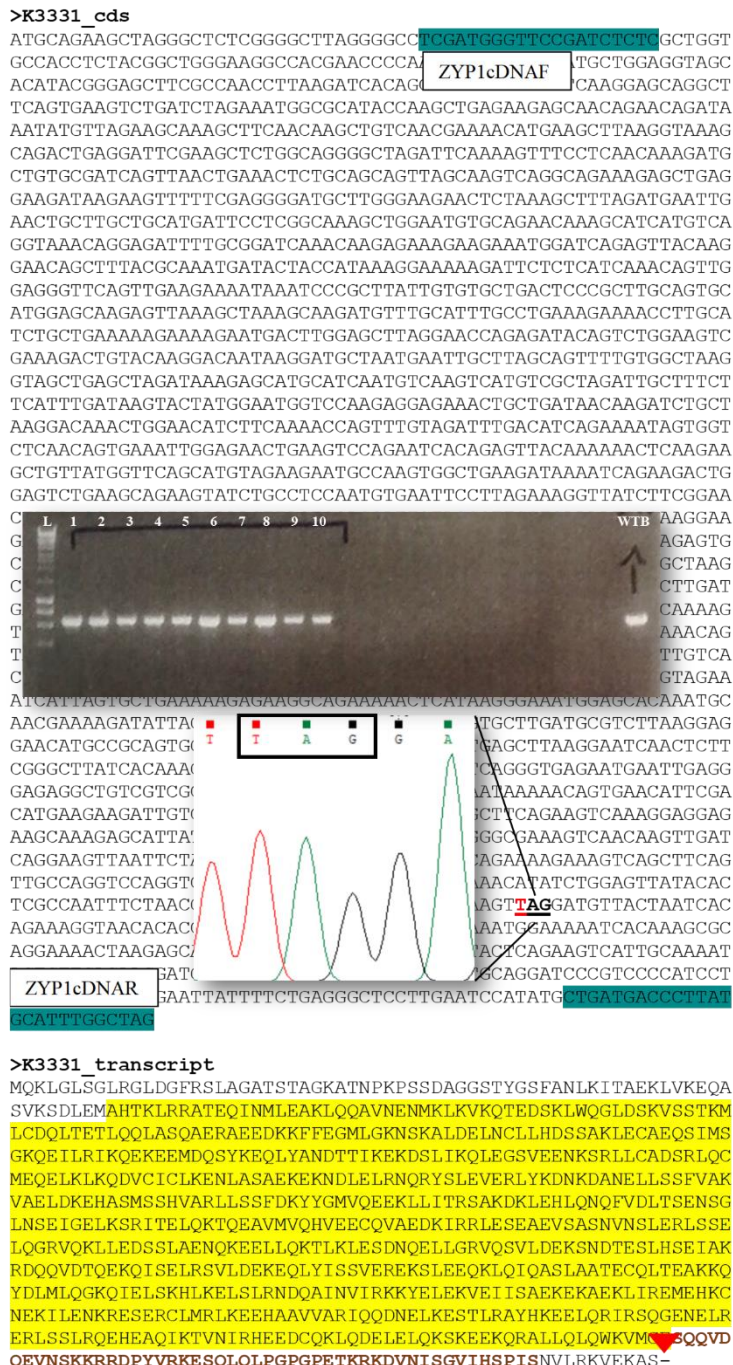


**Figure 3.12 DNA coding region sequence of K3331 (*zyp1a-1*) clone.** The translation CAG → TAG at nucleotide position 2324, causing a premature termination of the transcript is represented. Top insert represents the 500 bps PCR amplicons amplified by primer pairs specific for *TtZYP1-2A* (L= DNA ladder; 1-10= *zyp1a-1* cDNA clones; WTB = wild type Kronos B clone previously sequenced), while the insert at the bottom illustrates the sequence trace of the mutation site (image from Chromas Lite). Forward and reverse primers amplifying ZYP1 coding region sequence are labelled in aquamarine. Translated protein (5'3' Frame 1 below) shows the premature STOP codon (red triangle), the coiled coil domain (highlighted in yellow) and the DNA-binding S/TPXX motif (brown). Transcript sequence was retrieved from UniProtKB database.

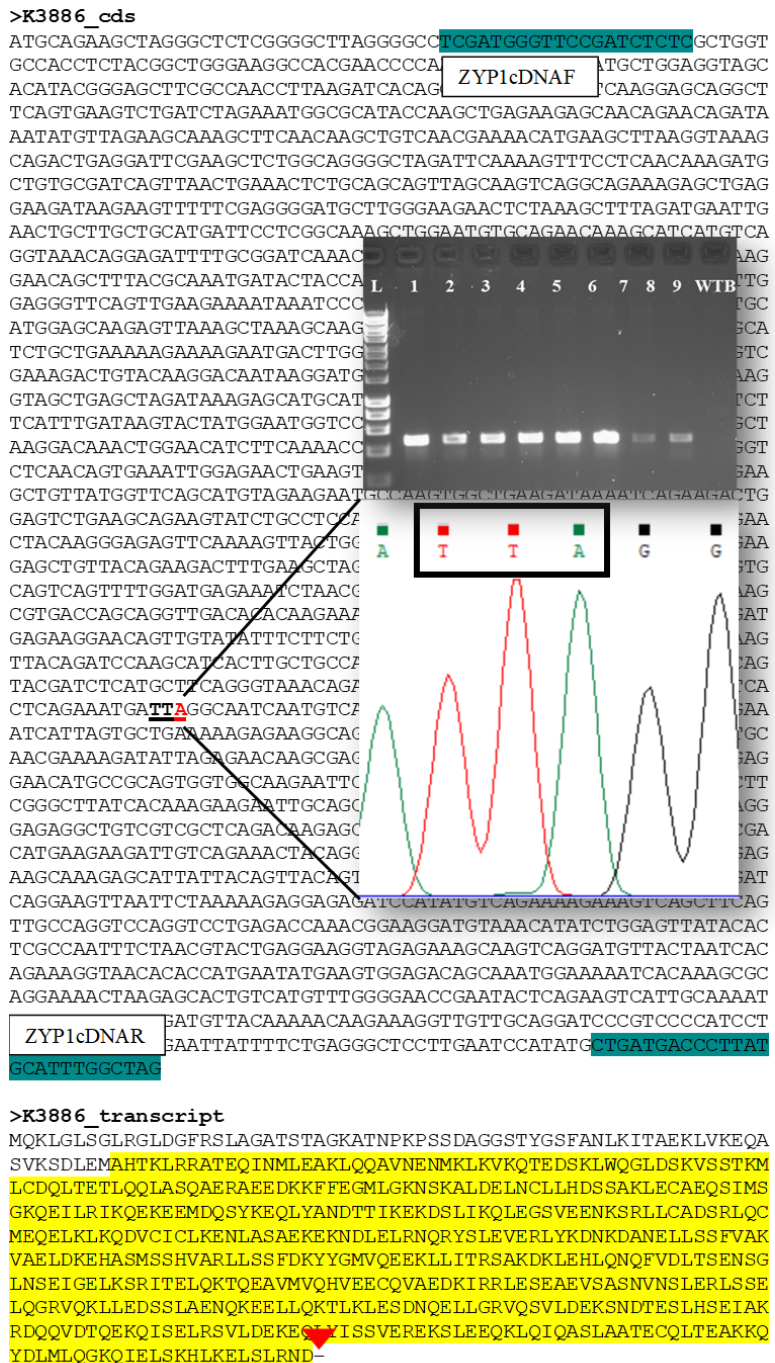


**Figure 3.13 DNA coding region sequence of K3886 (*zyp1a-2*) clone.** The translation CAG → TAG at nucleotide position 1694, causing a premature termination of the transcript is exemplified. Top insert represents the 500 bps PCR amplicons amplified by primer pairs specific for *TtZYP1-2A* (L= DNA ladder; 1-9= *zyp1a-2* cDNA clones; WTB = wild type Kronos B clone previously sequenced), while the insert at the bottom shows the sequence trace of the mutation site (image from Chromas Lite). Forward and reverse primers amplifying ZYP1 coding region sequence are labelled in aquamarine. Translated protein (5'3' Frame 1 below) shows the premature STOP codon (red triangle) and the coiled coil domain (highlighted in yellow). Transcript sequence was retrieved from UniProtKB database.

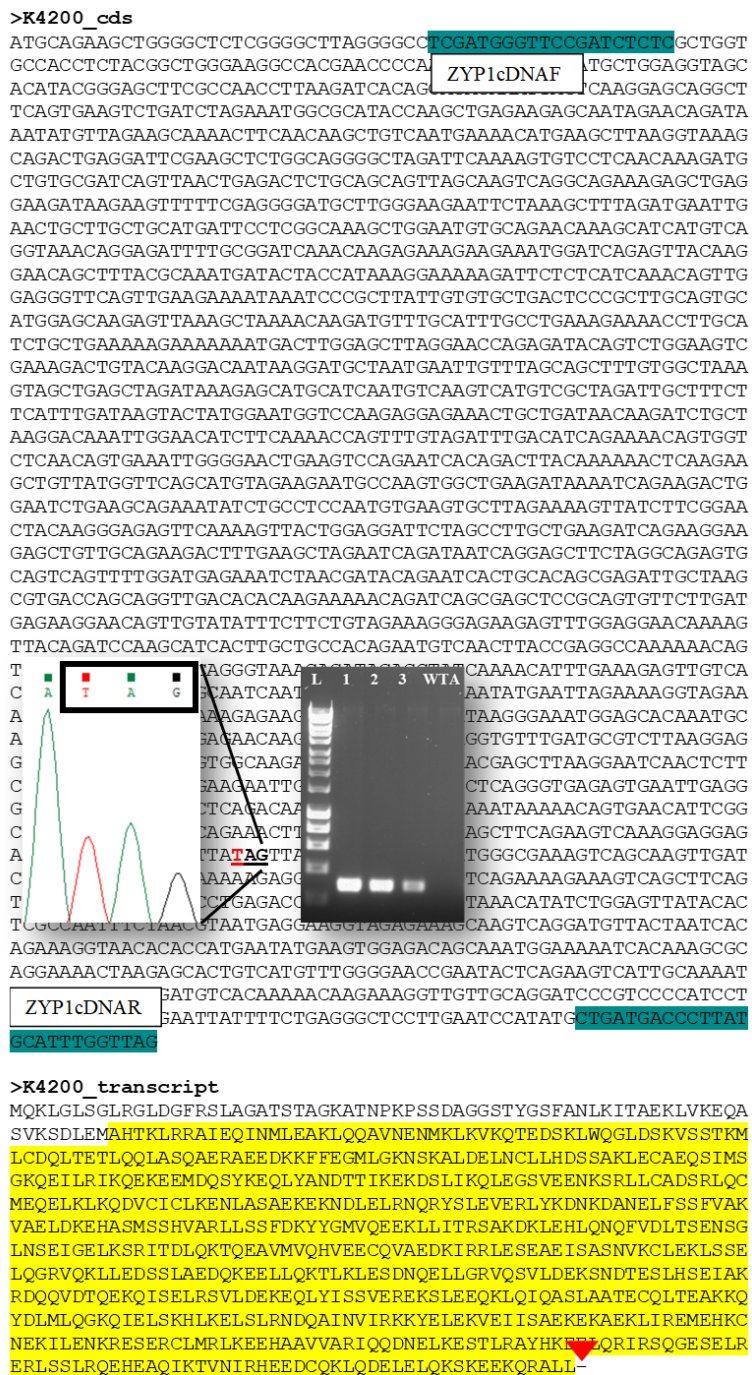


**Figure 3.14 DNA coding region sequence of K4200 (zyp1b) clone.** The translation CAG → TAG at nucleotide position 2324, causing a premature termination of the transcript is depicted. Right insert represents the 300 bps PCR amplicons amplified by primer pairs specific for *TtZYP1-2B* (L= DNA ladder; 1-3= *zyp1b* cDNA clones; WTA = wild type Kronos A clone previously sequenced), while the insert on the left illustrates the sequence trace of the mutation site (image from Chromas Lite). Forward and reverse primers amplifying ZYP1 coding region sequence are labelled in aquamarine. Translated protein (5'3' Frame 1 below) shows the premature STOP codon

(red triangle) and the coiled coil domain (highlighted in yellow). Transcript sequence was retrieved from UniProtKB database.

K4200	RDQQVDTQEKKQISELRSVLDEKEQLYISSVEREKSLEEQKLQIQA S LAATECQLTEAKKQ	540
K3886	RDQQVDTQEKKQISELRSVLDEKEQLYISSVEREKSLEEQKLQIQA S LAATECQLTEAKKQ	540
K3331	RDQQVDTQEKKQISELRSVLDEKEQLYISSVEREKSLEEQKLQIQA S LAATECQLTEAKKQ	540
WT	RDQQVDTQEKKQISELRSVLDEKEQLYISSVEREKSLEEQKLQIQA S LAATECQLTEAKKQ	540
	*****	*****
K4200	YDLMLQGKQIELSKHLKELSLRND <b>Q</b> AINVIRKKYELEKVEII SAEKEKAELIREMEHKC	600
<b>K3886</b>	<b>YDLMLQGKQIELSKHLKELSLRND-</b>	564
K3331	YDLMLQGKQIELSKHLKELSLRND <b>Q</b> AINVIRKKYELEKVEII SAEKEKAELIREMEHKC	600
WT	YDLMLQGKQIELSKHLKELSLRND <b>Q</b> AINVIRKKYELEKVEII SAEKEKAELIREMEHKC	600
	*****	*****
K4200	NEKILENKRESERCLMRLKEEHAAVVARIQ <b>Q</b> QDNELKESTLRAYH KEELQRIRSQGESELR	660
K3886	-----	564
K3331	NEKILENKRESERCLMRLKEEHAAVVARIQ <b>Q</b> QDNELKESTLRAYH KEELQRIRSQGENELR	660
WT	NEKILENKRESERCLMRLKEEHAAVVARIQ <b>Q</b> QDNELKESTLRAYH KEELQRIRSQGENELR	660
	*****	*****
<b>K4200</b>	ERLSSLRQEHEAQIKTVNIRHEEDCQKLQDELELQKSKEEKQRALL- -----	706
K3886	-----	564
K3331	ERLSSLRQEHEAQIKTVNIRHEEDCQKLQDELELQKSKEEKQRALLQLQW KVMGESQQVD	720
WT	ERLSSLRQEHEAQIKTVNIRHEEDCQKLQDELELQKSKEEKQRALLQLQW KVMGESQQVD	720
	-----	-----
K4200	-----	706
K3886	-----	564
<b>K3331</b>	<b>QE</b> VNSKKRDPYVRKESQLQLP GP PETKRKDVNISGVIVHSPI SNVLRKVEKAS-----	774
WT	QE VNSKKRDPYVRKESQLQLP GP PETKRKDVNISGVIVHSPI SNVLRKVEKASQDV TNH	780
	-----	-----
K4200	-----	706
K3886	-----	564
K3331	-----	774
WT	RKVTHHEYEVETANGKITKRRKT KSTVMFGEPTQKSLQNTVDK DVTKTRKVAGSRPH	840
	-----	-----
K4200	-----	706
K3886	-----	564
K3331	-----	774
WT	ANIGELFSEGSLNPYADD PYAFG	863

**Figure 3.15 Clustal Ω multi-alignments of protein sequence from WT and predicted *zyp1* TILLING mutant lines.** The alignment shows the corresponding position of the amino acid (in bold) affected by EMS treatment in each line (red triangles). K4200= *zyp1b*; K3331= *zyp1a-1*; K3886= *zyp1a-2*; WT= protein sequence from Kronos wild-type.

### 3.3.5 Cytological atlas of *zyp1* single knockouts

As previously for *asy1* mutants (Chapter 2), a meiotic atlas was used to detect chromosome organization of three independent TILLING lines of *zyp1* single KO and compared to the WT (Figure 3.16). Synchronised male meiocytes were identified by MeioCapture method (Shunmugam et al., 2018). DAPI stained images revealed no obvious difference between WT and *zyp1* mutants from leptotene to diplotene stages (Figure 3.16 A-P). Morphologically, in all leptotene nuclei examined, unpaired

chromosomes appeared as thin threads, while synapsed chromosomes thickened and fully synapsed at pachytene. However, mutants exhibited aberrant chromosome behaviour during diakinesis. During this stage, 14 ring bivalents were clearly distinguishable in WT (Figure 3.16 A1), but rather stickiness and entangled mass of chromatin (interlock) were recorded in *zyp1* mutants (Figure 3.16 E1-M1). Consistently, at metaphase I, 14 homologous chromosomes condensed normally and paired as ring bivalents at the equatorial plate in WT genotype (Figure 3.16 B1), while increasing number of rod bivalents (Figure 3.16 F1, arrows) or even unpaired chromosomes were detected in *zyp1* lines (Figure 3.16 J1-N1, circles), indicating a failure to form COs. Less frequent sticky chromosomes, perhaps interlocks, were also observed in *zyp1a-2* and *zyp1b* at metaphase I ( $n = 2$ ,  $n = 1$  respectively) (Figure 3.17 B, C).

As meiosis progressed to anaphase I, chromosome rearrangement was aberrant (Figure 3.16 G1) and homologues failed to migrate regularly to opposite poles as in WT (Figure C1). Rare events of unbalanced tetrad (Figure 3.16 H1, arrows show lagging chromosomes) with occasional fragments were typical of *zyp1* (Figure H1, circle), but not for WT (Figure 3.16 D1). As a consequence, seed set decreased in *zyp1* mutants (Table 3.3).

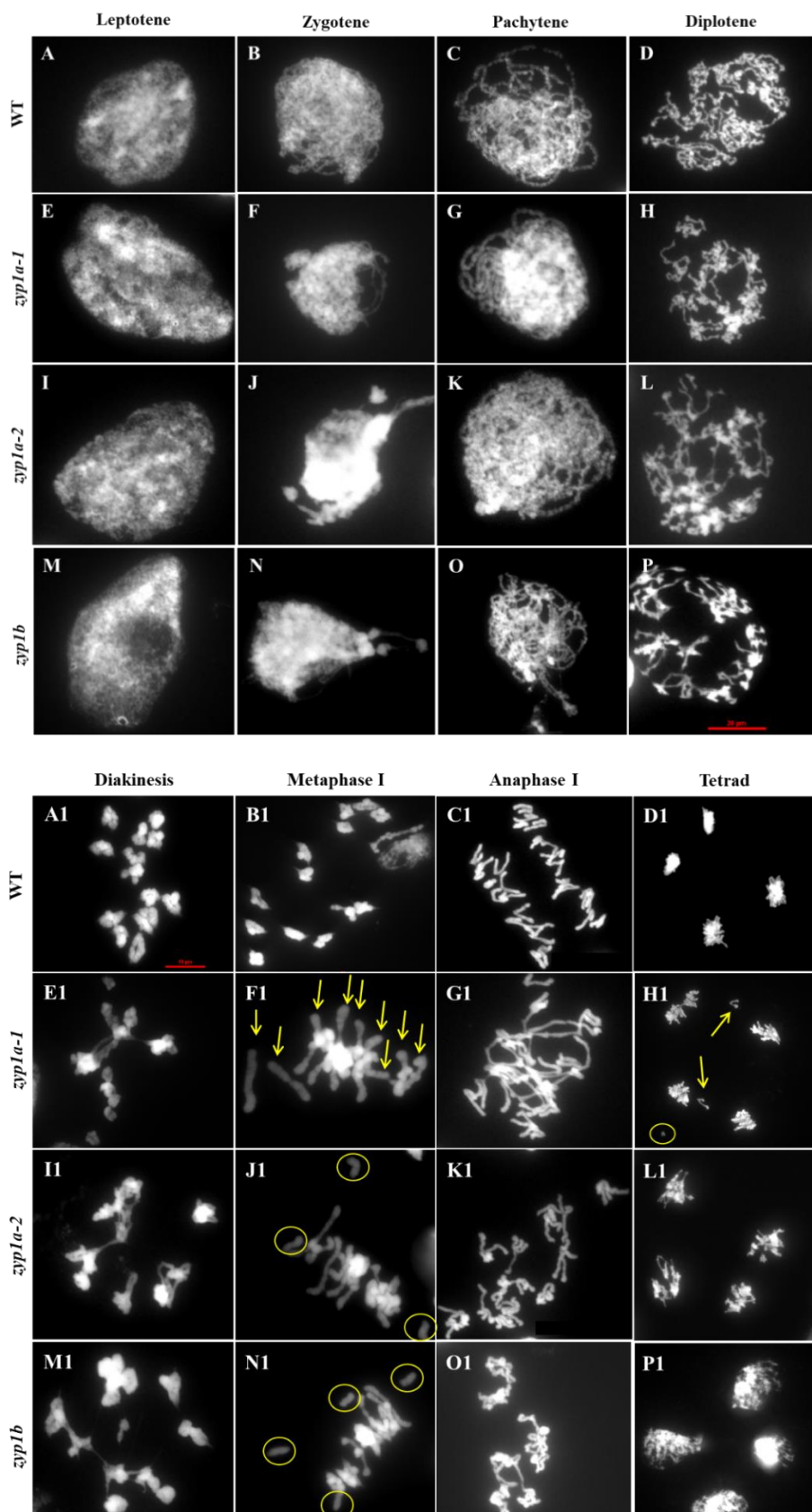


**Figure 3.16 Cytological atlas of *zyp1* single KO mutants.** (A-P) Upper panel: male germ cells of WT Kronos at (A) leptotene, (B) zygote, (C) pachytene, (D) diplotene were compared with male germ cells from *zyp1a-1*, *zyp1a-2* and *zyp1b* at (E, I, M) leptotene, (F, J, N) zygote, (G,

K, O) pachytene and (H, L, P) diplotene stages. (A-P) From leptotene to diplotene all genotypes analysed appeared similar, forming normal chromosomes. (A1-P1) Lower panel: male germ cells of WT Kronos at (A1) diakinesis, (B1) metaphase I, (C1) anaphase I, (D1) tetrad stages were compared with male germ cells from *zyp1a-1*, *zyp1a-2* and *zyp1b* at (E1, I1, M1) diakinesis, (F1, J1, N1) metaphase I, (G1, K1, O1) anaphase I and (H1, L1, P1) tetrad stages. In the WT: (A1) fourteen ring bivalents at diakinesis, regularly oriented on the equatorial plate (B1). (C1, D1) Normal segregation at anaphase and balanced tetrads, respectively. In both *zyp1a* lines and *zyp1b* line: (E1-M1) Chromosome interlocks at diakinesis (F1) Prevalence of rod bivalents (arrow) and univalents (J1, N1 circles) at metaphase I. (G1) Chromosome bridges and (K1, O1) nondisjunction at anaphase I. (H1) Chromosome lagging (arrows) and fragment (circle) in *zyp1a-1* at tetrad stage. (L1, P1) WT-like tetrad in *zyp1a-2* and *zyp1b* respectively. DNA is counterstained with DAPI and shown in grey. Scale bars = 10  $\mu$ m upper panel and 20  $\mu$ m lower panel.

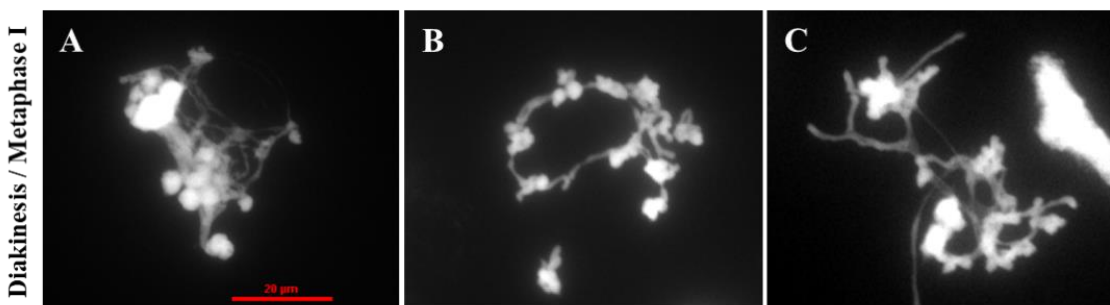


**Figure 3.17 Additional metaphase I phenotypes of *zyp1* TILLING mutants.** (A) Chromosome stickiness in *zyp1a-1* at diakinesis I and (B-C) chromosome interlocks in *zyp1a-2* and *zyp1b* respectively during metaphase I. DNA is counterstained with DAPI and shown in grey. Scale bars = 20  $\mu$ m.

### 3.3.6 *zyp1* single KO exhibits loss of obligate CO

To further investigate the CO patterning in *zyp1*, chiasma frequency and distribution was assessed during metaphase I. Kronos WT segregants showed mostly 14 ring bivalents ( $11.24 \pm 1.66$ , n = 50) with a mean of  $26.14 \pm 2.18$  chiasmata calculated in fifty cells (Figure 3.18 a). The mean number of ring bivalents decreased in all *zyp1* lines with an average of 9 rings per meiocyte ( $9.16 \pm 2.02$  in *zyp1a-1*,  $8.2 \pm 1.98$  in *zyp1a-2* and  $10.04 \pm 1.93$  in *zyp1b*) versus a mean of  $11.24 \pm 1.66$  occurred in the WT (Figure 3.18 a). On the contrary, rod bivalent in *zyp1* lines increased greatly ( $4.02 \pm 1.76$  in *zyp1a-1*,  $4.48 \pm 1.71$  in *zyp1a-2* and  $3.4 \pm 1.70$  in *zyp1b*) compared to the WT ( $2.6 \pm 1.67$ ) (Figure 3.18

a). Dissimilarly from WT, where univalents rarely formed ( $0.16 \pm 0.37$ ,  $n = 50$ ), *zyp1* meiocytes also contained unpaired chromosomes ( $0.84 \pm 0.89$  in *zyp1a-1*,  $1.32 \pm 1.33$  in *zyp1a-2* and  $0.56 \pm 0.70$  in *zyp1b*), corresponding to 5-fold rise in *zyp1a-1*, 8-fold rise in *zyp1a-2* and 3.5-fold rise in *zyp1b*, in comparison with the WT (Figure 3.18 a). A low frequency of multivalent interaction was typical of *zyp1* mutants, registered in on average 1.5 out of 50 cells each line (Figure 3.18 a). Lastly, the reduced chiasma values for both *zyp1a* lines ( $22.3 \pm 2.57$  and  $20.88 \pm 2.91$  chiasmata per cell for *zyp1a-1* and *zyp1a-2*, respectively,  $n = 50$  each) and *zyp1b* line ( $22.48 \pm 2.35$ ,  $n = 50$ ) were not significantly different (Wilcoxon rank sum test,  $P_{adj} > 0.05$ ,  $n = 50$ ) (Figure 3.18 c). The complete datasets for chiasma counts are in the Appendix (Table S8).

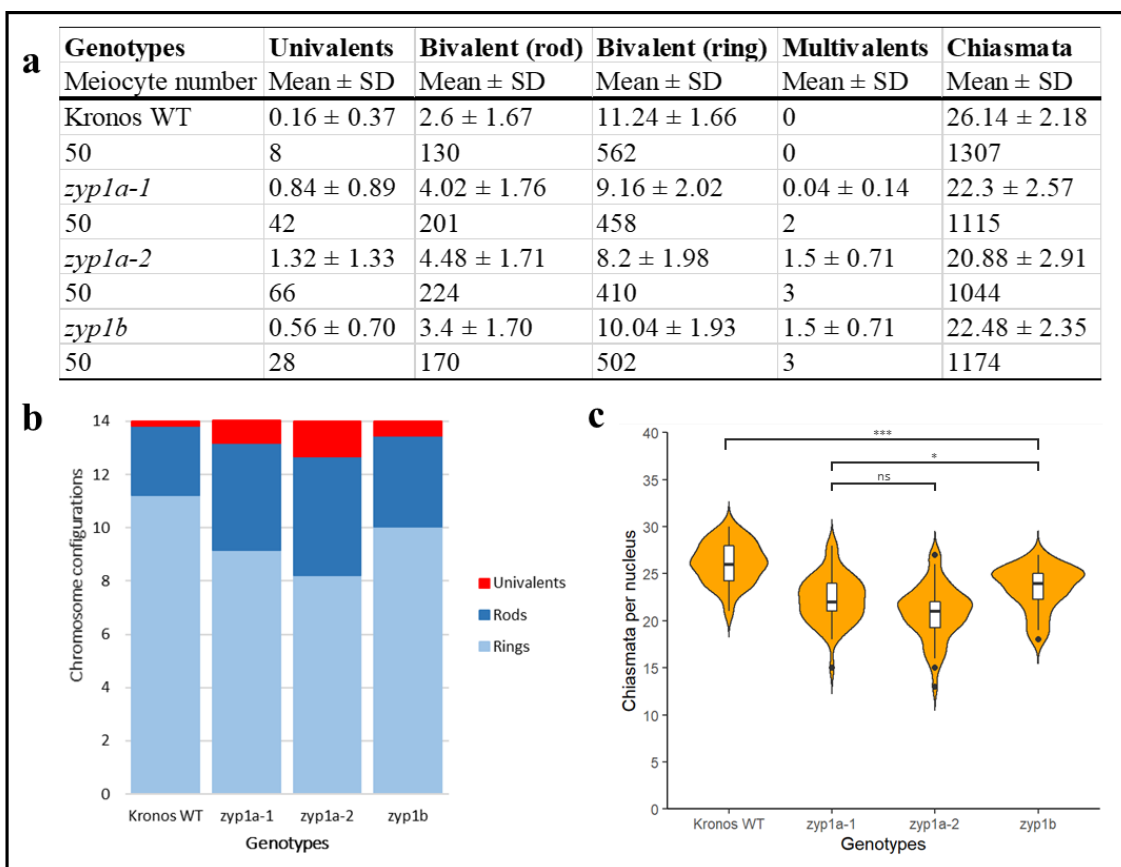


**Figure 3.18 *zyp1* single KO mutants display altered chromosome configuration at metaphase**  
**I.** a) Table summarising: average, standard deviation (SD), range of bivalents, univalents, multivalents and chiasmata per male meiocyte in Kronos WT and TILLING lines analysed.  $n$  = number of meiocytes; minimum two independent plants per genotype. b) Bar chart illustrates the mean values of rings bivalents (sky blue), rods bivalents (dark blue), univalents (red) and multivalents (purple) per cells among WT and *zyp1* single mutants. Legend is on the right. c) Violin plot exemplifies chiasmata frequency per male meiocyte. ns= not significant; asterisks

indicate significant difference by pairwise Wilcoxon rank sum test (\*\*\*)  $P_{adj} < 0.001$ ). The adjustment methods include the Bonferroni correction.

### 3.3.7 *zyp1* single KO preserves distal CO

To verify if CO patterning along chromosomes in *zyp1* mutants changed like its closely related species barley, the distribution of COs was also investigated. Concurrently, the F<sub>2</sub> segregants, which would include the *zyp1* double KO genotype, were genotyped. Notably, whilst subjected to the same controlled greenhouse conditions, Kronos WT plants exhibited normal vegetative growth and development, whereas F<sub>2</sub> plants homozygous for any of the SNPs of both TILLING lines crossed, showed poor germination rate and premature senescence. From both crossed lines, a non-mendelian segregation was hypothesised. Therefore, to overcome this inconvenience, both *zyp1a* lines were backcrossed once with WT plants. Nevertheless, germination rates remained constantly lower than in WT, especially among the genotypes produced from K3886 line (*zyp1a-2*). From four starting *zyp1* homozygous individuals aaBB crossed with the WT, twenty-five seeds were produced, where only six out of twenty-five germinated. Viability was also affected, since all seeds presented extremely slow growth and died 14 days after germination. The backcrossed involved the other *zyp1a* line, K3331, had a single-KO-like yield, yet with fewest seed sets per floret. The result of the chi square ( $\chi^2$ ) did not prove any significant difference between the observed genotypes and those expected under Mendel's law (see Appendix, Table S9). Thus, only the triple allele *zyp1 Aabb-1* mutant instead of double KO genotype *zyp1 aabb*, was considered reliable and utilized for the CO patterning analysis (Figure 3.19).

In *zyp1 Aabb-1*, meiosis appeared aberrant, presenting sticky chromosomes at diakinesis I (Figure 3.19 A) and univalents at metaphase I (Figure 3.19 B), which led to the formation of small fragments (3 events in 20 meiocytes) (Figure 3.19 C) and missegregation at anaphase I (2 events in 20 meiocytes) (Figure 3.19 D). The cytological manifestation of COs, chiasmata, were interpreted according to the bivalent shapes at metaphase I, which allowed the determination of their relative position along chromosomes, classified as telomeric (near the telomeres), sub-telomeric (toward the sub-telomeric regions) and interstitial (close the centromeres) (Sybenga, 1975) (Figure 3.20 a). In the WT, the vast majority of chiasmata were telomeric (57%, n = 1307), followed

by 31% interstitial and the remaining 12% were centromeric (Figure 3.20 a'). From the Table in Figure 3.18 a', it is evident that this proportion was maintained in *zyp1* with a single knocked-out copy ( $n = 1115$  in *zyp1a-1*,  $n = 1042$  in *zyp1a-2* and  $n = 1164$  in *zyp1b*), and in *zyp1 Aabb-1*, since recombination predominantly occurred distally (59%,  $n = 549$ ), although a slight increase of CO (31%,  $n = 549$ ) was recorded in centromeric regions (Figure 3.20 b). The complete dataset for CO distribution is in the Appendix (Table S10).

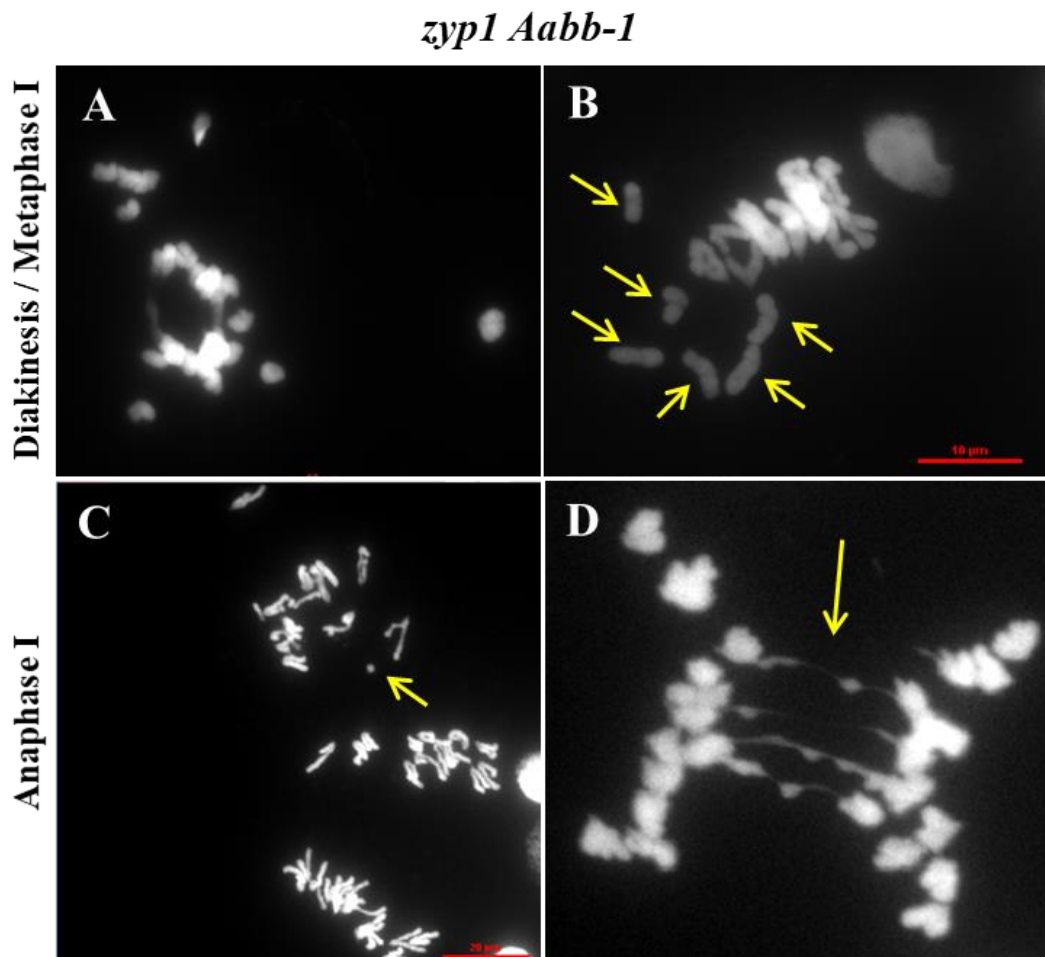


**Figure 3.19 Metaphase and anaphase I phenotypes of *zyp1 Aabb-1* mutant.** A) Chromosome stickiness at Diakinesis I. B) Three univalent pairs at Metaphase I (arrows). C) Fragments (arrow), D) chromosome lagging (arrows) and missegregation at Anaphase I. DNA is counterstained with DAPI and shown in grey. Scale bars = 10 and 20  $\mu$ m.

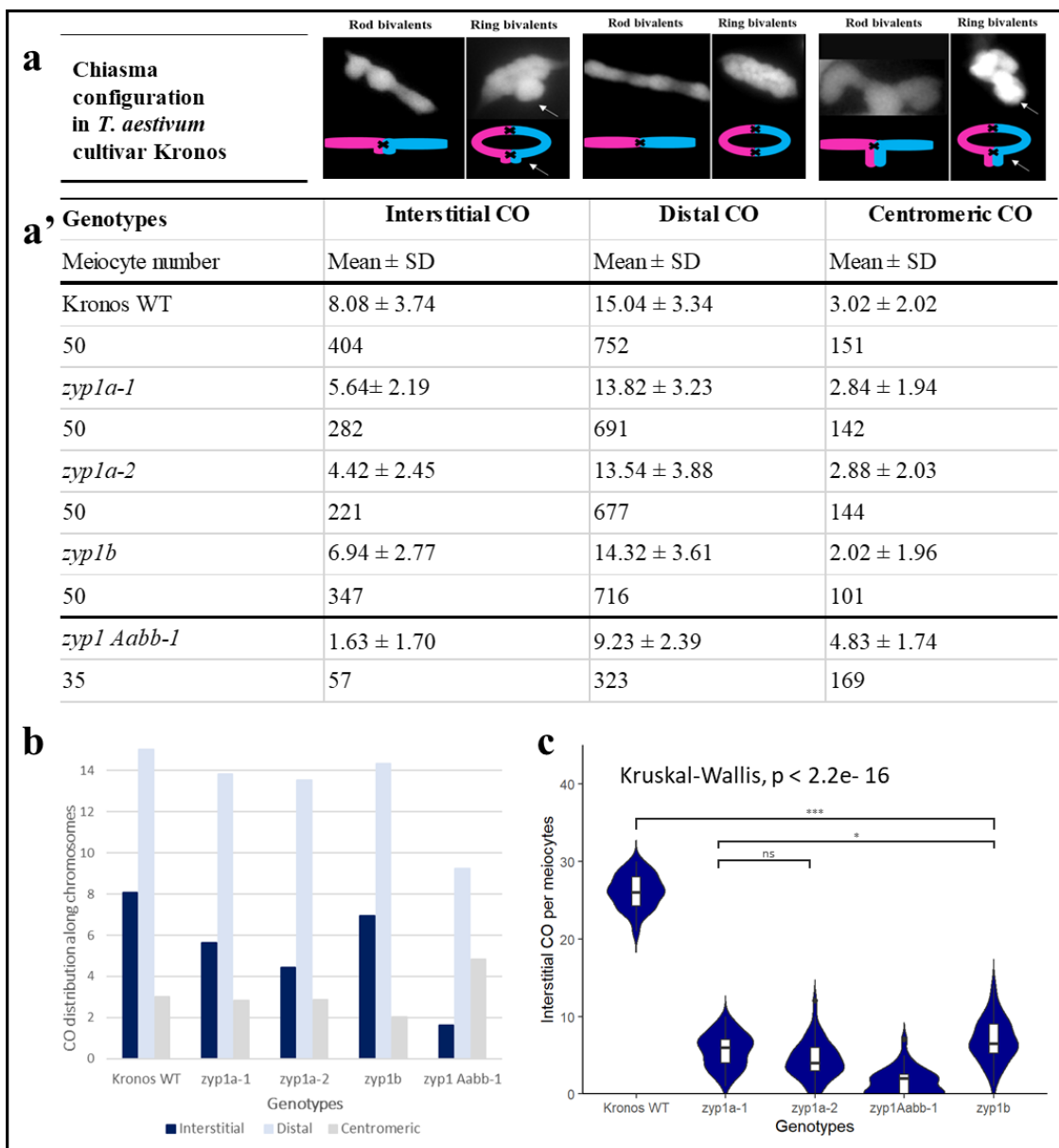


**Figure 3.20 *zyp1* mutant genotypes display drastic changes in chromosome configuration at metaphase I.** a) Cartoon of chiasma configuration of *T. turgidum* cv. Kronos. Panel depicts bivalent shapes (ring and rod) at metaphase I, including point of chiasmata (black crosses) and its position (centromeric, interstitial and distal, indicated with white arrows) along the homologous chromosomes (blue and pink colour). a') Table summarising: average, standard deviation (SD), range of bivalents, univalents, multivalents and chiasmata per male meiocyte in Kronos WT and *zyp1* mutant genotypes analysed. n = number of meiocytes; minimum two independent plants per genotype. b) Bar chart illustrates the mean values of rings bivalents (sky blue), rods bivalents (dark blue), univalents (red) and multivalents (purple) per cells among WT and *zyp1* *zyp1* mutant genotypes. Legend is on the right. c) Violin plot exemplifies chiasmata frequency per male meiocyte. Significant difference tested by pairwise Kruskal-Wallis test is shown ( $P \text{ adj} < 0.001$ ).

### 3.3.8 Fertility assessment

As for *asy1* mutants in Chapter 2, seeds from Kronos segregating WT and *zyp1* mutants were manually scored. Preliminarily, in Kronos WT, the average number of seeds per inflorescence from the primary tiller was 22 seeds ( $n = 3$ ), while in *zyp1* single KO mutants the seed sets were significantly reduced (Table 3.3). Indeed, there were a 25%, 36% and 32% fertility reduction in *zyp1a-1*, *zyp1a-2* and *zyp1b*, respectively (Table 3.3).

Genotype	Plant 1	Plant 2	Plant 3	Plant 4	Average $\pm$ SD
<b>Kronos WT</b>	24	24	22	18	22 $\pm$ 2.83
<b><i>zyp1a-1</i></b>	24	22	16	4	16.5 $\pm$ 9
<b><i>zyp1a-2</i></b>	16	14	14	12	14 $\pm$ 1.63
<b><i>zyp1b</i></b>	22	20	14	4	15 $\pm$ 8.08

**Table 3.3 Seed-set count for Kronos TILLING lines.** Counts for both segregating WT and in the allelic mutants of *zyp1* extracted from the primary inflorescences of three distinct individuals were recorded. Four genotypes, WT control included, have been analysed.

### 3.3.9 Meiotic prophase I is delayed in *zyp1* single KO

To identify any meiotic defect in the spatio-temporal dynamics of ZYP1 in the three *T. turgidum* cv. Kronos TILLING lines screened, immunocytology with antibodies raised against *TaASY1* (Desjardins et al., 2020b) and *AtZYP1* (Higgins et al., 2005) was performed (Figure 3.21). Synchronised Kronos meiocytes were staged according to the anther length by MeioCapture method (Shunmugam et al., 2018), as for the previous *asy1* analysis (see Chapter 2). Immunolocalisation data showing the progression of ASY1 and ZYP1 loading in Kronos WT were consistent with the previous analysis on hexaploid *T. aestivum* cv. Chinese Spring and Cadenza (Khoo et al., 2012; Osman et al., 2021). Here, ASY1 and ZYP1 first appeared as faint punctate foci onto the same regions of the chromatin simultaneously during leptotene, albeit they never co-localise with one other (Figure 3.21 A). As meiosis progressed into zygotene, ZYP1 formed short linear tracts (Figure 3.21 A1), which lengthened and condensed at pachytene (Figure 3.21 A2), mirroring the condensation of the chromatin. Here, the ZYP1 signal appeared on regions of chromatin only after *TaASY1* first appeared within those regions and only lengthened into those regions after ASY1 signal was unloaded. At the onset of diplotene, low residual

levels of ZYP1 signal were observed (Figure 3.21 A3), which completely dissipate during late diplotene (Figure 3.21 A4).

Unsurprisingly, the temporal localisation of ZYP1 among all *zyp1* mutants differed significantly from the WT. At leptotene, ZYP1 installation starts when the anthers are 0.7 mm long in WT (Figure 3.21 A), while in *zyp1* mutants, ZYP1 elongation is visible when the anthers reach 1.0 mm (Figure B1-D1). At WT zygotene (0.8 mm), homologous chromosomes pair in most of the meiocytes, as indicated by ASY1 and ZYP1 labelling, but not in *zyp1* zygotene (Figure 3.21 B1-D1), where the search for the correct homologous is largely delayed (1.05 mm) due to the truncated ZYP1. Pachytene is the stage of the synapsis for definition, clearly visible in WT in 1.0 mm anthers (Figure 3.21 A2). However, no fully synapsed in *zyp1* mutant nuclei was observed in 1.0 - 1.1 mm anthers (Figure 3.21 B2-D2). WT diplotene is common in anthers long 1.0 – 1.1 mm (Figure A3-A4), but not in any *zyp1* mutants, where diplotene meiocytes did not form until anther reached 1.2 - 1.4 mm (Figure 3.21 B3-D3 and B4-D4), confirming that the meiotic prophase I as a whole was timely affected. Further details are illustrated in the following Figures and discussed below.

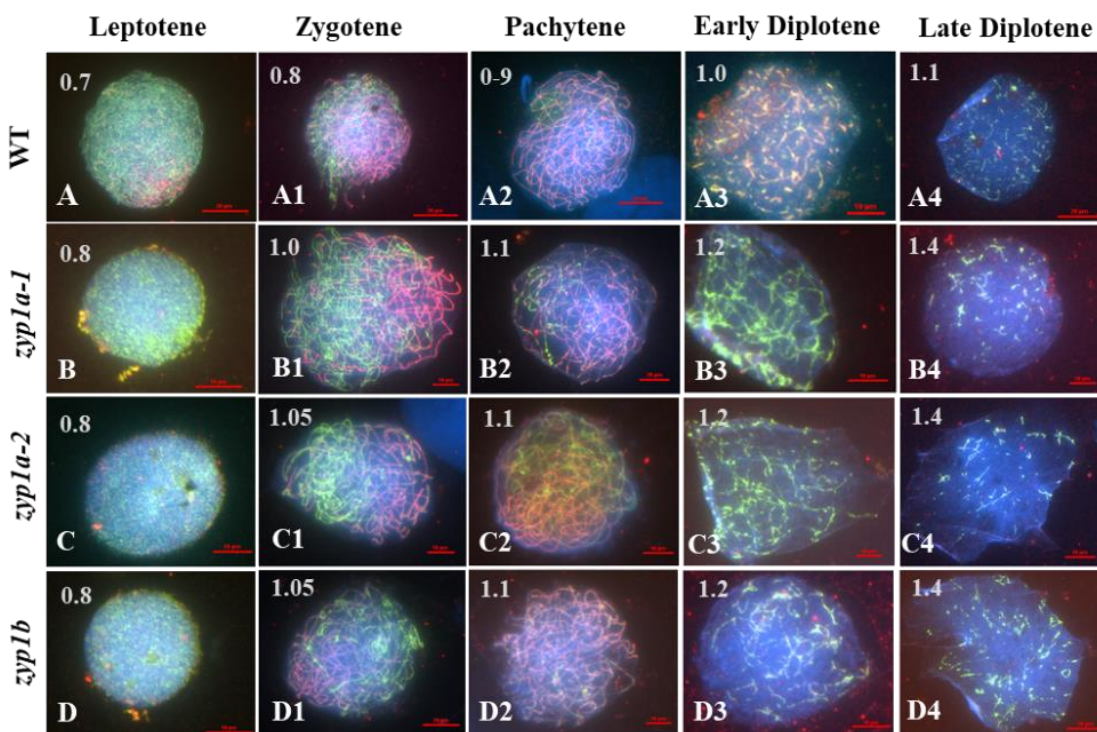


**Figure 3.21 Meiotic prophase I progress of PMCs in *T. turgidum* cv. Kronos and *zyp1* single KO mutants from pre-meiotic interphase to diplotene.** (A-D4) Chromosome axes were

marked with ASY1 (green), transverse filaments connecting homologous chromosomes were detected via ZYP1 (red), and chromatin was counterstained in DAPI (blue). Anthers ranging from 0.7 to 1.4 mm in length were specifically correlated to the meiotic prophase I sub-stages, and are here shown on the top left of each image. (A-D) Leptotene. (A1-D1) Zygote. (A2-D2) Pachytene. (A3-D3) Early Diplotene. (A4-D4) Late Diplotene. (B-B4) *zyp1a-1*, (C-C4) *zyp1a-2*, and (D-D4) *zyp1b* mutants exhibited a considerable delay throughout the entire meiotic prophase I in comparison with the WT (A-A4). In all images, the nucleolar region is represented as an unstained circular body within the PMCs. Scale bar = 10 and 20  $\mu$ m.

In all *zyp1* single KO mutants, ASY1 was still faithfully loaded onto the chromatin in a pattern similar to the WT until late leptotene (Figure 3.22 B2-D2). Instead, ZYP1 loading was largely delayed since the beginning of the leptotene, here started when the anthers reached 0.8 mm (Figure 3.22 B1-D1), and not in 0.7 mm as frequently occurs in the WT (Figure 3.22 A1).

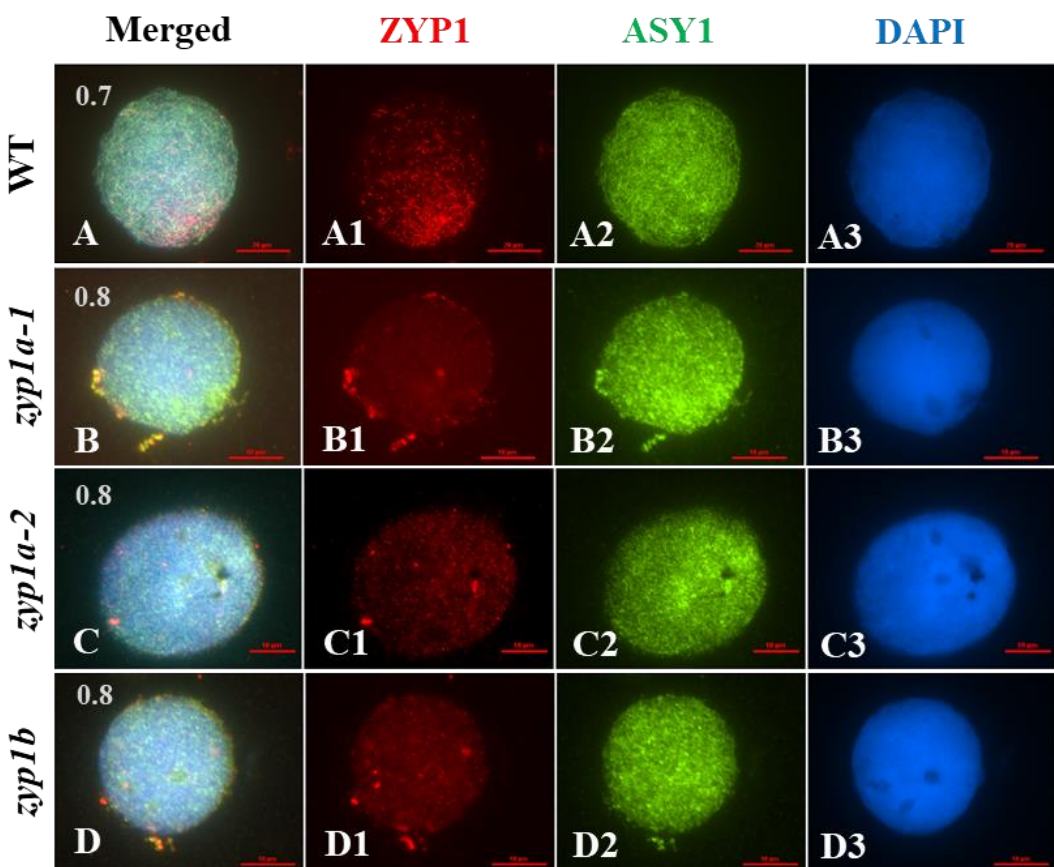


**Figure 3.22 Dual immunolocalization of *TaASY1* and *AtZYP1* at meiotic leptotene stage in PMCs of WT Kronos and *zyp1* single KO in A and B sub-genomes. (A-A3) WT Kronos. (B-B3) *zyp1a-1*. (C-C3) *zyp1a-2*. (D-D3) *zyp1b*. (A-D) merged images of (A1-D1) transverse filament ZYP1 (red), (A2-D2) chromosome axis ASY1 (green) and (A3-D3) chromatin counter-**

stained with DAPI (blue). (A1) At leptotene, ZYP1 began to linearize in WT, but not in *zyp1* single mutants (B1-D1), where ZYP1 signals appeared as large and unpolarised foci in the nuclei. (A2) WT axial elements were marked by continuous ASY1 labelling (green), as in all *zyp1* single KO (B2-D2). Anthers size (mm) are indicated on the top left of each merged image. Scale bar = 10 and 20  $\mu\text{m}$ .

### 3.3.10 Synapsis and desynapsis are disrupted in *zyp1* single KO

During zygotene, the SC forms between the aligned pairs of homologous chromosomes in a WT context (Zickler & Kleckner, 1999; (Scott L. Page & Hawley, 2004). However, this was not the case of the *zyp1* lines examined in this study. The development of the SC was less obvious, since most of ASY1 still polymerized, therefore the chromosomes could align, but ZYP1 failed to properly elongate between the axial elements, appearing with a diffuse and discontinuous signal, possibly due to the loss of the C-terminus (Figure 3.23 B1-D1). This situation led ASY1 to reorganize itself along the SC structure as it assembles (Figure 3.23 B2-D2). While remodelling, ASY1 assumed a spiral-like shape and formed polycomplexes, suggesting that ASY1 remodelling is perturbed (Figure 3.23 B2-D2, dashed inserts). The irregular reshaping of the axes, however, led most of the meiocytes to progress prematurely into the diplotene, as the phenotype suggests, indicating that SC assembly was spatially and temporally disrupted.

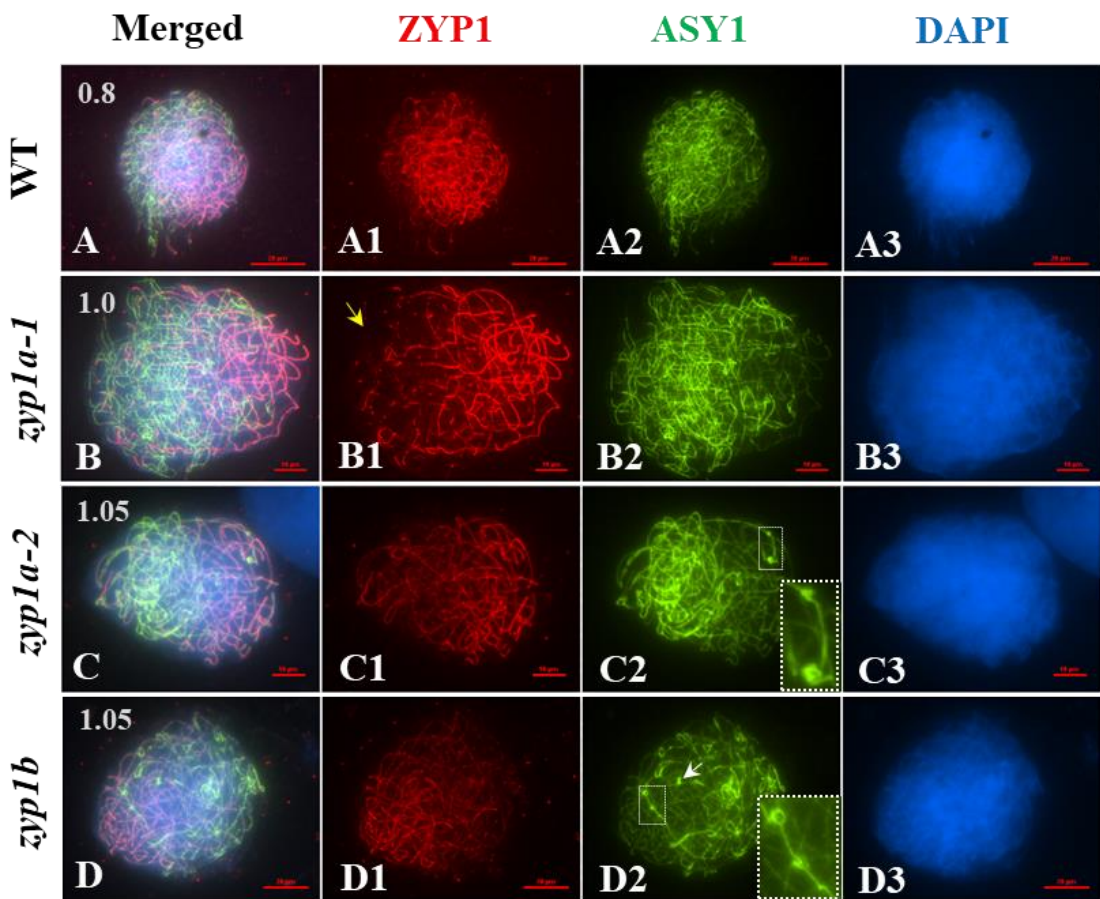


**Figure 3.23 Localization of *TaASY1* and *AtZYP1* against a zygotene PMCs of WT and *zyp1* single KO mutants.** (A-A3) WT Kronos. (B-B3) *zyp1a-1*. (C-C3) *zyp1a-2*. (D1-D3) *zyp1b*. (A-D) merged images of (A1-D1) transverse filament AtZYP1 (red), (A2-D2) chromosome axis ASY1 (green) and (A3-D3) chromatin counter-stained with DAPI (blue). (A1) In WT, ZYP1 (red) is fully linearized at synapsis points. (B1-D1) In *zyp1* single KO mutants, the polymerization of ZYP1 is incomplete, leaving a certain amount of protein isolated, visualised as red spots rather than linear threads (B1, arrow). (A2) In WT, clearly ASY1 lengthened in chromatin region before ZYP1 linearized, while in *zyp1* mutants, ASY1 aggregates in a spiral shape throughout the nucleus (dashed rectangle, arrow), forming interlocks and progressing prematurely into diplotene (C2-D2). Anthers size (mm) are indicated on the top left of each merged image. Scale bar = 10 and 20  $\mu$ m.

As synapsis progressed in *zyp1* mutants, ASY1 polycomplexes persisted (Figure 3.24 B2, D2) and ZYP1 never fully linearized at pachytene (Figure 3.24 B1, D1).

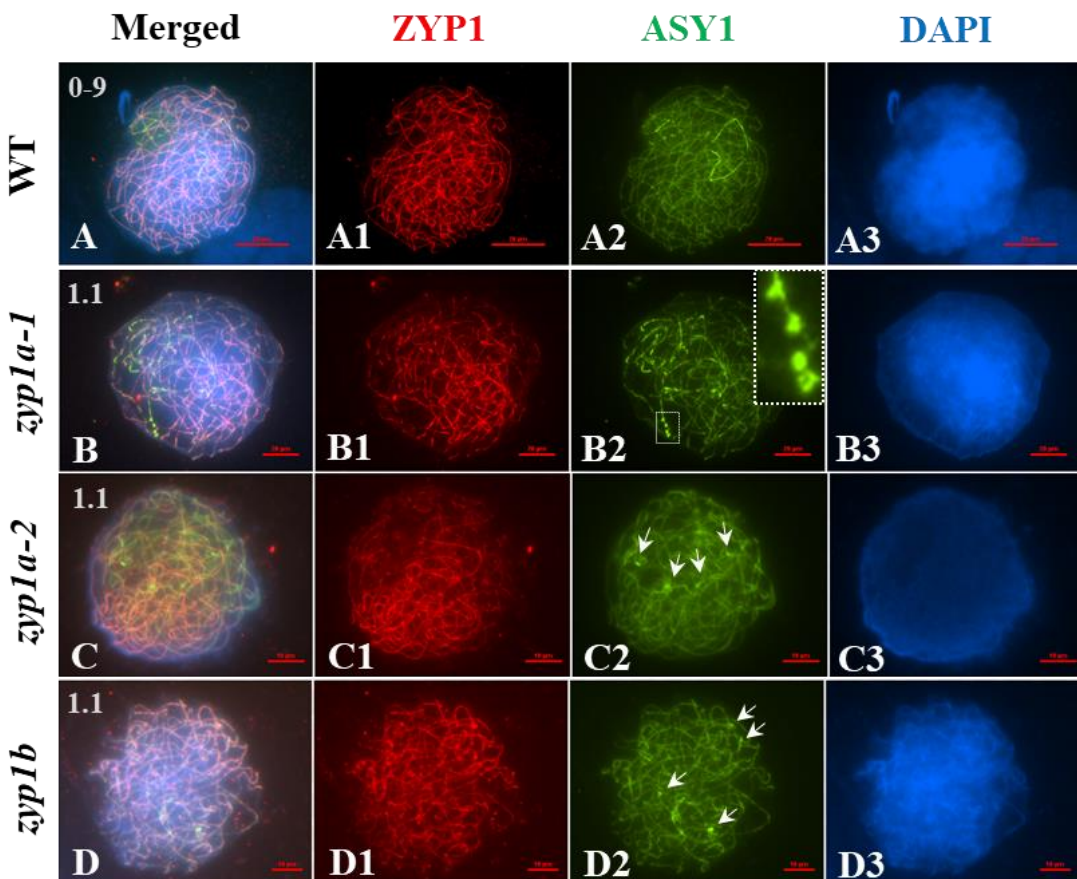


**Figure 3.24 Analysis of synapsis progress monitored by *TaASY1* (green) and *AtZYP1* (red) in *zyp1* meiocytes during pachytene, compared to the WT. (A-A3) WT Kronos. (B-B3) *zyp1a-1*. (C-C3) *zyp1a-2*. (D1-D3) *zyp1b*. (A-D) merged images of (A1-D1) transverse filament AtZYP1 (red), (A2-D2) chromosome axis ASY1 (green) and (A3-D3) chromatin counter-stained with DAPI (blue). (A1-A2) Synapsis is complete: ZYP1 (red) fully lengthened after ASY1 (green) was unloaded. (B1-D1) In *zyp1* single KO mutants, ZYP1 did not totally linearized, and the signal appeared faint and punctuate. (B2-D2) Dashed insert and arrows display ASY1 polycomplexes already visible at this stage. Anthers size (mm) are indicated on the top left of each merged image. Scale bar = 10 and 20  $\mu$ m.**

Desynapsis was also followed in *zyp1* mutants. At the onset of diplotene, contrarily to the WT (Figure 3.25 A1), ZYP1 was not present (Figure 3.25 B1, D1). This was instead accompanied by an abundance of ASY1 polycomplexes (Figure 3.25 B2, D2), which persisted until later stage (Figure 3.26 B2, D2).

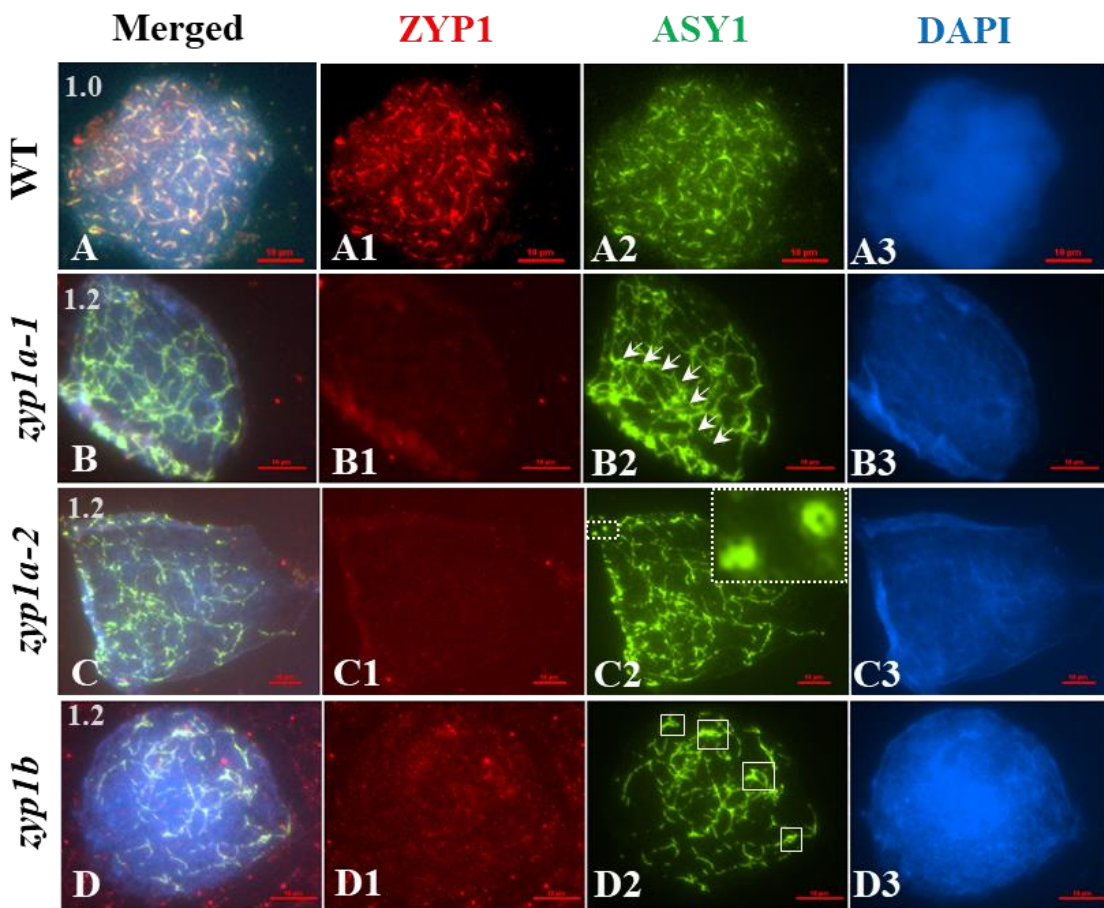


**Figure 3.25 Analysis of desynapsis monitored by *TaASY1* (green) and *AtZYP1* (red) in *zyp1* meiocytes during early diplotene, compared to the WT. (A-D3) WT Kronos. (B-B3) *zyp1a-1*. (C-C3) *zyp1a-2*. (D1-D3) *zyp1b*. (A-D) merged images of (A1-D1) transverse filament AtZYP1 (red), (A2-D2) chromosome axis ASY1 (green) and (A3-D3) chromatin counter-stained with DAPI (blue). (A1-A2) SC starts to disassemble: ZYP1 (red) and ASY1 (green) progressively and simultaneously shortened. (B1-D1) In *zyp1* single KO mutants, ZYP1 did not persisted until this stage, while (B2-C2) ASY1 extensively aggregated as spiral-like structure (arrows and inserts) in both *zyp1a* lines. (D2) ASY1 polycomplexes already visible in *zyp1b* at this stage (rectangles). Anthers size (mm) are indicated on the top left of each merged image. Scale bar = 10 and 20  $\mu$ m.**

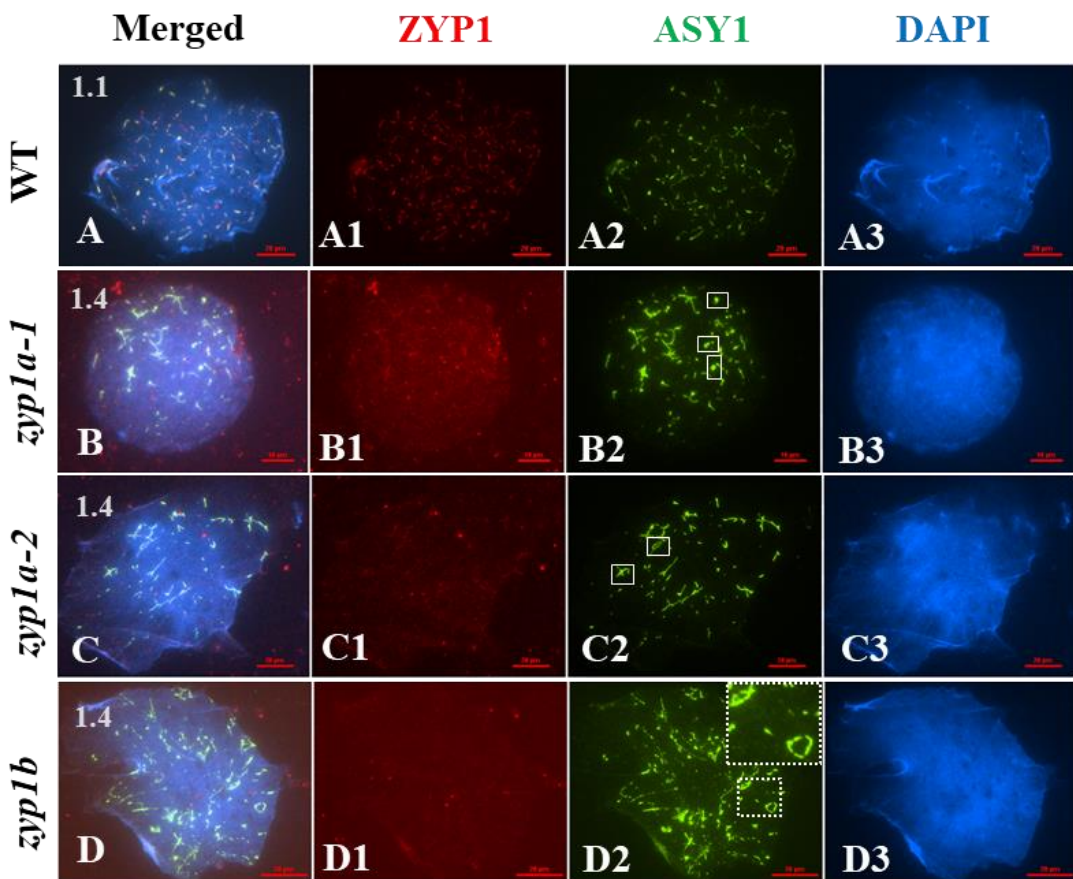


**Figure 3.26 Analysis of desynapsis monitored by *TaASY1* (green) and *AtZYP1* (red) in *zyp1* meiocytes during late diplotene, compared to the WT. (A-A3) WT Kronos. (B-B3) *zyp1a-1*. (C-C3) *zyp1a-2*. (D1-D3) *zyp1b*. (A-D) merged images of (A1-D1) transverse filament AtZYP1 (red), (A2-D2) chromosome axis ASY1 (green) and (A3-D3) chromatin counter-stained with DAPI (blue). (A1-A2) SC totally disassembled: both ZYP1 (red) and ASY1 (green) signals become faint. (B1-D1) In *zyp1* single KO mutants, ZYP1 was not observed, while (B2-D2) ASY1 signal displayed stronger signal in all *zyp1* lines (rectangles). (D2) Dashed insert shows the persistence of spiral-like structure during SC desegregation in *zyp1b* line. Anthers size (mm) are indicated on the top left of each merged image. Scale bar = 10 and 20  $\mu$ m.**

### 3.3.11 Recombination pathway is defective in *TtZYP1* lacking C-terminus

Preliminary data on chiasma frequency in *zyp1* single KO provided an estimate of the total number of COs per meiocyte. Since the visualization of chiasmata was not always obvious in chromosome spread preparations (COs occurring on overlapped chromosomes may be underestimated), to better understand the number of interfering class I COs and their progression during meiotic prophase I, a co-immunolocalization of the class I CO

marker *HvHEI10* (Desjardins et al., 2020a) together with *AtZYP1* antibody (Higgins et al., 2005) was performed using the antigen rescue through microwaving immunostaining conditions. HEI10 is a member of the Zip3/HEI10 family of proteins thought to possess SUMO/ubiquitin E3 ligase activity (Chelysheva et al., 2012; Wang et al., 2012). In *A. thaliana* and *S. macrospora*, Zip3/HEI10 marks Class I CO sites and smaller axis-associated foci have been shown to emerge during late prophase I (Chelysheva et al., 2012; (De Muyt et al., 2014).

In the respect of the SC structure at pachytene, WT HEI10 foci were small and widely associated to the transverse filaments marked by ZYP1 in tetraploid wheat (Figure 3.27 A), whereas, in *zyp1a-1* meiocytes, HEI10 foci appeared morphologically larger and slightly closer each other along the transverse filament (Figure 3.27 B). The mean number of recombination events were estimated and tested for significant differences between the two genotypes (Figure 3.27, violin plot). In thirty WT nuclei, a mean of  $28.8 \pm 2.8$  HEI10 foci were scored, whereas there were on average  $23.13 \pm 3.9$  ( $n = 30$ ) exchanges per meiocytes in *zyp1a-1* single KO, corresponding to 19.34% DSBs being not repaired. Two sample *t*-test confirmed that WT and *zyp1a* mutant values are significantly different ( $P < 0.001$ ) (Figure 3.27, violin plot). The dataset for HEI10 foci count is in Appendix (Table S11).

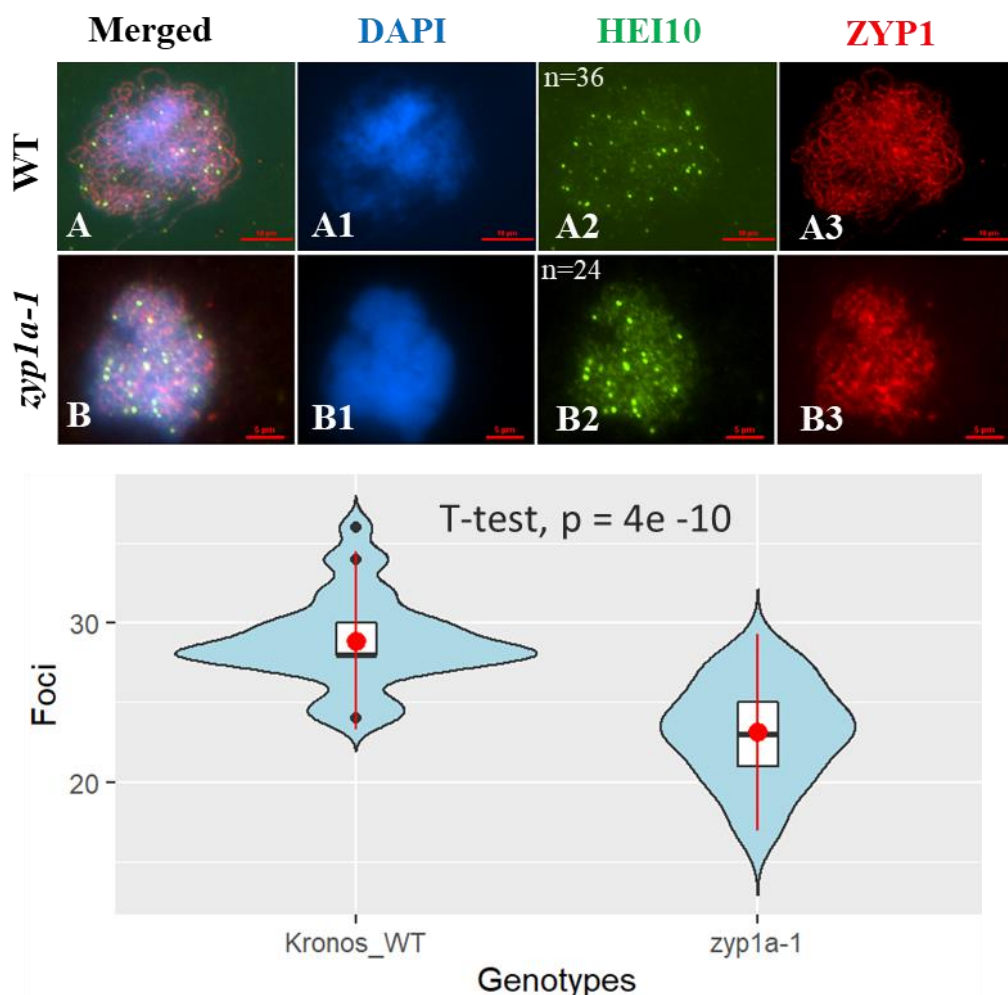


**Figure 3.27 Analysis of meiotic DSBs progression using the anti-*HvHEI10* antibody in male meiocytes in WT and *zyp1a-1* at pachytene stage.** (A-B) merged images of (A1-B1) chromatin counter-stained with DAPI (blue), (A2-B2) *HvHEI10* (green), and (A3-B3) transverse filament marker ZYP1 (red). (A2) WT meiocytes with 36 HEI10 foci. (B2) *zyp1a-1* meiocyte with 24 HEI10 foci. Data presented as violin plots. Result of the *t*-test is shown ( $P < 0.001$ ). Scale bars = 5 and 10  $\mu$ m.

## 3.4 Discussion

### 3.4.1 Molecular data overview

The main results of *TaZYP1* gene expression analysis in somatic and reproductive tissues of hexaploid *T. aestivum* revealed a significant balanced expression among the sub-genome copies, as verified with the cytology analysis of *zyp1* TILLING mutants in A or B copy (*zyp1* single KOs were partially functional). Cloning and Sanger sequencing

methods used for identifying alternative splicing events and interpreting the outcomes were highly sensitive and reliable. The potential regulatory function of the *TtZYP1* 3' UTR isoforms in gene expression during meiosis remains to be evaluated.

### 3.4.2 Novel *TaZYP1* 3' UTR transcript variants were identified in meiotic tissues

From the *TtZYP1* 3' UTR splice variant investigation, only clones ZYP1.M32 and ZYP1.M33 shared the predicted 3' UTR reference sequence. As for the coding region analysis, the primer designing strategy for unveiling *TtZYP1* UTR variants did not map to the reference transcript variant sequences. Nevertheless, the five remaining transcript variants identified displayed a high level of similarity and a typical common features recorded in 3' UTR transcripts (e.g. PAS sequences) (Srivastava et al., 2018), which strongly support the reliability of the outcomes.

Considering the sequence analysis, cloning data also revealed the presence of proper regulatory PAS sequences within the 3' UTR variants, despite the sample size tested ( $n = 19$ ) was inadequate to propose a meiotic tissue-specific expression contribution of a certain or all *TtZYP1* 3' UTR variants. Furthermore, the discovery of guanosine(s) in the polyA tail of *TtZYP1* 3' UTR isoforms, occurring in high frequency (42%,  $n = 19$ ), might conceal crucial mechanism to modulate the gene expression. The function of G-content within the poly(A) tail in regulating translational efficiency was previously demonstrated in human and *Arabidopsis thaliana* transcriptomes (Sachs et al., 1987; Deo et al., 1999; Sladic et al., 2004; Lim et al., 2018). In addition, the use of different polyadenylation sites processing an mRNA in multiple isoforms that generally differ in their 3' UTR length, has been found to play essential roles of increasing transcriptome diversity and regulating gene expression profiles (Shi, 2012; Tian & Manley, 2017). Genome-wide identification of polyA motifs has been recorded in plants (Zhu et al., 2020). Generally, PAS sequences can affect the mRNA stability, translation, cellular localizations to regulate gene functions (Shi, 2012; Xing & Li, 2011). In tetraploid *T. turgidum* (this study), the fact that there was no correlation between the polyA tail features (length and G%) with the PAS sequences, did not exclude a theoretical (speculative) interplay. Unfortunately, this work did not cover the functional analysis, which may be proposed for future studies, such as constructing *TtZYP1* mutant lines lacking their PAS sequence(s) or measuring the

abundance of the various 3' UTR isoforms. Additionally, the newest development of several computational tools and databases (extensively reviewed in Zhang et al., 2021) to detect PAS sequences will enrich our knowledge on their function, their impact on meiosis, and potentially wide open the possibility of manipulating one or more isoforms in e.g. breeding programme.

As speculated for *TaASY1* (Chapter 2), the *TtZYP1* 3' UTR transcripts found may influence mRNA stability or abundance, thereby gene expression regulation, prior their G percentage within the polyA tail and signify changed during evolution or following the polyploidization process in wheat. Therefore, further experiments are required to fully understand the composition of poly(A) tail in reproductive tissues or meiotic stages.

### 3.4.3 Cytology data overview

DAPI stained analysis of metaphase chromosome configuration during the first meiotic division clearly demonstrated that the chemically-induced knock-out of single *TtZYP1-2A* or *TtZYP1-2B* copies alter the CO landscape in tetraploid *T. turgidum*, and the individual allelic genes are functionally redundant, as manifested by the consistent phenotypes of all *zyp1* lines examined. The incapability to generate a complete *zyp1* KO led to include the analysis of *zyp1 Aabb-1* genotype. Preliminary data from *zyp1* triple allele mutation potentially confirmed a telomere-led distribution of recombination events in tetraploid *T. turgidum*, similar to findings in *Arabidopsis* and barley *zyp1* RNAi lines findings (Higgins et al., 2005; Barakate et al 2014).

The dynamism of ASY1 and ZYP1 along the chromosomes of mutant plants showed synaptic regions and occasional chromosome clustering and fragment formations. Desynapsis was also perturbed, possibly as consequence of unsynchronised ZYP1 loading amid the chromosome axis since pre-synapsis. Thus, this preliminary work categorically demonstrated that ZYP1 is dispensable for normal SC elongation and for assuring Class I CO events, confirmed by the slight reduction of HEI10 marker in *zyp1a-1* mutant. As hypothesised, these data further suggest that CO in tetraploid wheat is SC-dependent and timely regulated. Ultimately, these finding highlight a conserved role of *TtZYP1* in Class I CO designation among plants.

### 3.4.4 *TtZYP1* likely imposes Class I CO prior to SC formation and may be responsible of CO distribution in tetraploid *T. turgidum*

Preliminary cytological analysis of *zyp1* single KO in A and B sub-genomes generated in tetraploid *T. turgidum* cv. Kronos via EMS treatment, revealed a conserved role of *TtZYP1* in Class I CO control. The reduction of 10-20% in chiasma event was mostly attributed to an increased occurrence of rod bivalents and unpaired chromosomes detected at metaphase I in each *zyp1* lines, which was comparable to *Arabidopsis* (20% decrease of COs) and barley ZYP1 RNAi lines (reduced expression led to 25% drop of COs) (Higgins et al., 2005; Barakate et al 2014). This discovery is also comparable to the decrease in CO events reported in their defective *Drosophila* and mouse orthologues (Page et al., 2001; de Vries et al., 2005). In line with these findings, both *TtZYP1* homoeologues showed functional redundancy, possibly correlated with their equal gene expression, based upon quantitative PCR performed over this project.

Subsequently, data from *HvHEI10* foci count at pachytene stage strongly corroborate the behaviour of hypomorphic *zyp1a-1* in regards to chiasma frequency, yet how COs, in their totality, progress to the later stages of prophase I in tetraploid wheat is unknown. According to the *HvHEI10* data, CO were reduced by 19.34% ( $n = 50$ ) in *zyp1a-1*, which is consistent with the data acquired at the metaphase I in the same line using the chromosome spreading technique, meaning that the remaining DSBs were resolved in this genotype. Recently, the proportion of Class I COs in WT hexaploid wheat cv. Cadenza was determined by Osman et al. (2021), who counted  $41.3 \pm 1.1$  *HvHEI10* foci in twenty cells scored. The discrepancy of the WT outcomes on *HvHEI10* foci between Cadenza ( $n = 41$  foci, Osman et al. 2021) and Kronos ( $n = 26$  foci, this study) may be due to the different sample preparation. Whilst the protocol included the same antibody and buffers, the heat treatment (antigen rescue technique) may have altered the binding site for the epitope, which could further explain the change in foci morphology. Similar effect was obtained in WT genotype and with the analysis *asy1* triple allele mutant described in Chapter 2. Hence, larger and diffuse foci appeared close each other and were underestimated. Consistently, *AtZYP1* and DAPI signals appeared equally diffuse. Secondary, the possibility that the mean of COs may be slightly lower in tetraploid species than hexaploid cannot be ruled out. That said, the CO reduction in *zyp1a-1* mutant remains valid. To overcome this limit, other recombination proteins may be employed for this

purpose, such as the MutL mismatch repair proteins MLH3 and MLH1 (Phillips et al., 2013; Cannavo et al., 2020; Kulkarni et al., 2020).

Alternatively, a loss of interference-sensitive COs could be speculated to explain the morphology changes of the *HvHEI10* foci. This is indeed a common feature of diverse mutated version of ZYP1 orthologues generated in other eukaryotes, included *Poaceae* such as rice and barley (Wang et al., 2010; Barakate et al 2014). Nevertheless, only one mutant line was considered for this count, therefore, to strengthen the powerful of the data, the utilization of MutL mismatch repair proteins or a spatial measurement among the SC components could be more informative. In case of confirmation, these data could be of remarkable interest for breeding application.

Intriguingly, cytological data detected a low incidence of minor meiotic aberration, such as chromosome interlocks, chromosome lagging and fragments. Formerly, *Arabidopsis ZYPI* RNAi knockdown gene and super-resolution microscopy analysis in *Arabidopsis* CRISPR/Cas9 *zyp1* highlighted the presence of entanglements (Higgins et al., 2005; France et al., 2021). In addition, spatial measurement using super-resolution microscopy revealed that such interlock formation was associated with a distance variation between the co-aligned homologues (France et al., 2021). In future, super-resolution microscopy may also be a useful approach to unveil the nature of the metaphase chromosome interlocks observed in *zyp1* mutants here. For now, taking in account the large size of wheat chromosome, as well as the low occurrence of this defect, it is more likely that chromosome entanglements observed in these *zyp1* lines evaluated are the result of artefacts deriving from the spreading technique.

Taken together, these data also explained the reduced fertility in the TILLING genotypes tested. These are preliminary data, and as such, need to be accurately validate in future, for instance, via a pollen viability test, such as Alexander staining of pollen (Alexander, 1969). In general, reduced fertility rate were also common in rice, barley and *Arabidopsis* carrying mutation in ZYP1 orthologues (Wang et al., 2010; Barakate et al., 2014; France et al 2021; Capilla-Pérez et al., 2021). Therefore, the reduced fertility in *zyp1* lines is presumably based on defective CO formation/synapsis. Supplementary evidence of this were found with the immunolocalization of ASY1 and ZYP1, supposed to verify the

dynamism of target SC elements when lacking a single copy of ZYP1. The results of this study are discussed in details in the next paragraph below.

### 3.4.5 In tetraploid wheat, SC and CO are interdependent and rely on *TtZYP1* C-terminus

The lack of the C-terminus in the final ZYP1 product of *zyp1a* and *zyp1b* TILLING lines identified in tetraploid *T. turgidum* in this study, largely impacted the spatial localization of ZYP1 and ASY1 along the chromosome axes. Moreover, the additional lack of 196 amino acid residues of the coiled coil domain in *zyp1a-2* TILLING line, apparently not showing any distinct phenotype compared with the remaining two lines, is suspected to have a more important role in SC assembly. For instance, previous data in *S. cerevisiae* *zip1* mutants has shown that deletions including the coiled coil significantly impact the width of the SC. Recently, *zyp1* null mutants in *Arabidopsis* confirmed that the entire removal of the TF protein induced instability to the SC structure, above all along the axial elements (Tung & Roeder, 1998; Capilla-Perez et al., 2021; France et al., 2021). Hence, ideally, a complete *zyp1* KO in tetraploid wheat achievable with the identification of a different TILLING line or by using a different genome editing approach would validate this supposition in polyploid wheat.

Intriguingly, co-immunolocalization analysis of ZYP1 and ASY1 in *zyp1* single KO lines showed that deletion of *TtZYP1* C-terminus presumably altered the exact timing of two dynamic events, namely centromere clustering and ASY1/PCH2 system, as previously reported by Sепси et al. (2017).

#### 1) *TtZYP1* coordinates SC installation prior to synapsis in tetraploid *T. turgidum*

In wheat-rye and oat-maize hybrids, observations on centromere and chromosome pairing revealed that centromere clustering coincides with the initial formation of SC axial elements during meiotic leptotene, and is temporally tightly followed by the formation of the telomere bouquet (Maestra et al., 2002; Sепси et al., 2017). In accordance with other studies, the location of synapsis (initiation and elongation) are spatiotemporally separated (Higgins et al., 2012): sub-telomeric synapsis occurs at the leptotene-zygotene transition, while elongation of interstitial synapsis emerged at mid-zygotene at multiple points of the chromosome arms. The initiation and release of individual centromeres from the clusters coincides with the emergence of sub-telomeric synapsis (ZYP1) during which no linear

or punctate ZYP1 co-localise with the centromeres (Sepsi et al., 2017). Curiously, in *zyp1 Aabb-1* a major effect was observed during mid-zygotene, when interstitial COs occur, resulting in chiasmata reduction. However, as anticipated earlier, these are preliminary results that need to be validated ideally with a full KO gene.

Notably, *zyp1* single KO mutant meiocytes formed at early meiotic prophase I stage, had commonly larger ZYP1 foci, compared to the faint signals exhibited in the WT, and did not show the polar orientation typical of the WT-telomere organization (Sepsi et al., 2017), rather, ZYP1 proteins appeared widely dispersed throughout the nucleus. Such a phenotype was independent of the A or B copy that was knocked-out, and crucially, it is more severe than the ones tracked in *ph1b* mutants and barley *HvZYP1<sup>RNAi</sup>*, in which the delay did not start before late zygotene (Khoo et al., 2012; Higgins et al., 2012). This evidence led to speculate an additional key role of ZYP1 during pre-synapsis in tetraploid wheat.

## **2) *TtZYP1* may mediate ASY1/PCH2 localization in tetraploid *T. turgidum***

The formation of ASY1 polycomplexes at the zygotene-diplotene transition in *zyp1* single KO mutants, was interpreted as an attempt of ASY1 to remodel along the chromatin axes, and its persistence at later stages suggested a defect in unloaded system. Clearly, the faint and diffuse ZYP1 signal, that mirrors the insufficient protein required for SC installation, coupled with the intensification of ASY1 signal, which possibly reflects the accumulation of stalled proteins, led to a disfavoured condition for chromosomes to synapse. Prospectively, it could be hypothesised that a complete knockout of *TtZYP1* may lead to more severe consequences, primarily asynapsis or meiotic arrest. Consistently, deletion analysis of *S. cerevisiae zip1* showed that null mutants, whilst formed full-length axial elements, failed to synapse their homologs (Sym et al., 1993; Nag et al., 1995). Similar SC alterations were also observed In *Drosophila c(3)g* and mouse *syp1* mutants (Hall, 1972; MacQueen et al., 2002).

A possibility may be that ASY1 polycomplexes originated from the lack of protein removal normally operated by PCH2. In this context, the impossibility to connect with ZYP1, may leave dissociated ASY1 being dispersed throughout the nucleus, which ultimately justifies the intensification of ASY1 signal detected in this stage. Indeed, it is known that both association and dissociation of ASY1 with homologous axes require

ZYP1 localization (Lambing et al., 2015; Balboni et al., 2020). Moreover, the ASY1 coiled structures has been recently found in early diakinesis wild-type rye meiocytes, investigated using 3D-SIM (Hesse et al., 2019). In rye, spiral-like structures are established by the accumulation of separate ASY1 threads around a ZYP1 core possibly to stabilize recombination sites at chromosome arms and counteract the tension for premature separation throughout diakinesis. Here, ASY1 spiral-like structures formed only partially (ZYP1 was totally absent) during SC disassembly and persisted in *zyp1* single KO at higher level compared to the WT, as demonstrated from the larger foci and increased signal intensity of ASY1. The limited resolving power of a fluorescence microscopy might have concealed informative details concerning the binding propriety between the transverse element ZYP1 and axial-associated ASY1 in the altered forms of *zyp1*, lacking the S/TPXX motif at C-terminus. Nevertheless, the evidence of incomplete synapsis in concomitant with the lack of ASY1 depletion operated by PCH2 in *zyp1* mutants, demonstrated a conserved role of ZYP1 in synapsis (linked to ASY1) and possibly desynapsis (linked to PCH2) completion among plants (Lambing et al., 2015; Balboni et al., 2020). Data from the *ZYP1* co-expression network also included PCH2 in the same co-expression module (full dataset from alluvial diagram), suggesting a hypothetical interplay between ZYP1-PCH2 in wheat.

### 3.4.6 *TtZYP1* may favour centromeric CO in tetraploid *T. turgidum*

In this work, a complete ZYP1 knockout was unfortunately not achieved. An attempt to remove possible off-target mutations within the *zyp1* TILLING lines identified and genotyped for K3886 line (*zyp1a-2*) did not change the fate in recovery of *zyp1* null mutants, either because there were not enough backcross generations or that somehow ZYP1 is required for normal plant development. Alternatively, the PCR genotyping strategy could be at fault and null mutants were not detected with this approach. This could be due to primer designing inaccuracy when it comes to discriminate SNP amid nucleotide sequences with a high level of similarity, as in the case of *ZYP1* homoeologues. Alternative genotyping approach would be sequencing PCR products, as discussed in Chapter 2.

Relatively to *zyp1* single KOs and *zyp1 Aabb-1* derived from the second backcross involving K3331 line (*zyp1a-1*), the analysis of CO patterning did not reveal any

significant modification in chiasma distribution, since chiasmata predominantly occurred distally as in WT at the expense of proximal regions, suggesting that ZYP1 is not involved in CO distribution. Nonetheless, it is worth to note that in *zyp1* *Aabb-1* a slight increase of centromeric CO was detected. This is in line with the *zip1* mutant in yeast where COs are increased in pericentromeric regions (S. Y. Chen et al., 2008; Vincenten et al., 2015), corroborating the hypothesis of a conserved CO placement among eukaryotes. However, these finding are still preliminary, since either A or B alleles remained functional in the TILLING lines analysed, thereby the consequence of the mutation might be potentially buffered by the presence of the wild-type homoeologous, as largely demonstrated for other species possessing a polyploidy genome (Chen et al., 2012; Kashtwari et al., 2019). For instance, in tetraploid *T. turgidum* MSH4, a mismatch repair protein belonging to the MutSy complex, and importantly, a meiosis-specific ZMM protein, when single homozygous recessive mutation for A and B subgenomes were induced, the authors did not register any remarkable effect in comparison with the fully knock-out mutants (Desjardins et al., 2020a). Such evidence definitely corroborate the mild phenotype observed so far in *zyp1*.

## 3.5 Conclusions

### 3.5.1 Molecular approach

The major findings of this work was the validation of a balanced expression of *TtZYP1* homoeologues in hexaploid *T. turgidum*. Surprisingly, widespread non-adenosine residues within the body of many poly(A) tails were detected. Therefore, Sanger sequencing enabled to detect isoform-specific poly (A) tails in *TtZYP1* 3' UTR, revealing that the composition of poly(A) tails is far more complex than what initially supposed. More mechanisms of poly(A) tail modification and regulation need to be experimentally investigate on a larger sample size and mutant lines.

### 3.5.2 Cytology approach

Cytology studies demonstrated that SC assembly has to be spatially and temporally regulated in tetraploid wheat and that ZYP1 may fulfil a remarkable role at multiple stages of synaptic process in this species. More relevant, considering the similarity with barley and the conserved role of its orthologues in coordinating the recombination pathway, it would be interesting to further test the CO pattern in *zyp1* null mutant in future, in view

of eventual application in plant breeding programmes, such as to unlock chromosome regions normally deprived of crossover (cold spot).

# **Chapter 4**

## **Searching for SC central element gene candidate(s) in polyploid wheat using bioinformatics tools**

### **4.1 Introduction**

During the prophase stage of meiosis I, the elaborate SC structure assembles onto the chromosomes to stabilize the pairing interactions between the homologues (synapsis), promote crossover formation, regulate cessation of DNA double-strand break (DSB) and ensure accurate meiotic chromosome segregation (reviewed by Lenormand et al., 2016). As anticipated in Chapter 1, the SC has been observed in a wide range of sexually reproductive organisms, from yeast to human (reviewed by Lenormand et al., 2016). In all cases, it adopts a remarkably conserved tripartite ribbon-like organization, consisting of lateral elements (LEs) that holds the sister chromatids of the homologues together, a central element (CE) along the midline and an array of transverse filaments (TFs) that interconnect the LEs generating a zipper- like structure (reviewed by Gao and Colaiácovo, 2018).

In model organisms, such as yeast, nematode, *Drosophila*, mammals, and *Arabidopsis*, SCs are similar in general morphology (Zickler & Kleckner, 1999), but differ in ultrastructure and consist of proteins with diverged primary amino acid sequence (Anuradha & Muniyappa, 2005). For instance, many organisms contain conserved features, such as an HORMA domain within their LE proteins and an extended central  $\alpha$ -helical domain, mostly organising into coiled-coil structures in their TF and CE proteins (reviewed in Gao & Colaiácovo, 2018; West et al., 2019). Thus, the search of SC orthologues has been based on the characterization of certain protein structures rather than by homology of the full length sequence.

In plants, no CE orthologues have been identified yet, although so far all studies were based on amino acid sequence similarity (Grishaeva & Bogdanov, 2014). Curiously, the appearance of CE proteins was evolutionarily concomitant with genome complication,

typical of higher Metazoa, including plants (Grishaeva & Bogdanov, 2014). Hence, it was hypothesised that wheat may have evolved one or more CE components.

To address this assumption, putative CE orthologue(s) were searched within the newly annotated wheat transcriptome by screening uncharacterised meiotic genes that may interact with TF *TaZYPI* homoeologues, based on their co-expression (Alabdullah et al., 2019). Gene expression data are generated either by microarray or RNA sequencing (RNA-seq). Considering the major benefits of RNA-seq over microarray (higher accuracy for low-abundance transcripts, higher resolution for identifying tissue-specific expression, for discriminating expression profiles of closely related paralogues, improved statistical power (van Dam et al., 2018), as well as the recent release of high-quality reference sequences in wheat (Adamski et al., 2020; Hassani-Pak et al., 2021), the latest RNA-seq datasets from wheat available from public data sources, were used for this purpose (Pearce et al., 2015; Borrill et al., 2016; Ramírez-González et al., 2018; Alabdullah et al., 2019).

In plant biology, gene network analysis of transcriptomics data has proven to be an effective strategy for identification of candidate genes (Serin et al., 2016). One method to infer gene function from gene expression data obtained from RNA-seq technology is the Weighted Gene Co-expression Network Analysis (WGCNA), an approach that constructs networks of genes upon the assumption that co-activated genes across a group of samples are functionally related. A typical co-expression network construction and analyses can be described with the following steps (reviewed by van Dam et al., 2018):

- 1) Firstly, individual relationships between genes are defined based on correlation measures between each pair of genes (Song et al., 2012). These relationships describe the similarity between expression patterns of the gene pair across all the samples. The correlation values are commonly scaled between 0 and 1 so that values  $< 0.5$  indicate negative correlation and values  $> 0.5$  indicate positive correlation.
- 2) Secondly, co-expression associations are used to construct a network, represented as a gene– gene similarity matrix where each node represents a gene and each edge represents the presence and the strength of the co-expression relationship

(Song et al., 2012). The connections are also quantified in weight values between 0 and 1 that indicate the strength of co-regulation between the genes.

- 3) Thirdly, a clustering technique is used to group genes with similar expression patterns across multiple samples to produce modules (groups of strongly co-expressed genes). The resulting modules often represent biological processes and they can subsequently be interpreted by functional enrichment analysis, a method to identify and rank overrepresented functional categories in a list of genes (reviewed by van Dam et al., 2018). The most widely used clustering package for co-expression analysis is Weighted Gene Correlation Network Analysis (WGCNA) (Zhang & Horvath, 2005). It constructs co-expression modules using hierarchical clustering on a correlation network created from expression data (Langfelder & Horvath, 2008). Hierarchical clustering iteratively divides each cluster into sub-clusters to create a tree with branches representing co-expression modules. Modules are then defined by cutting the branches at a certain height.

In wheat, previously, Ramírez-González et al., (2018) defined sets of co-expressed modules of candidate meiotic genes (MGs) and orthologues of known MGs using co-expression network analysis and orthology informed approaches from RNA-Seq samples, which were later employed to build a WGCNA network (Alabdullah et al., 2019). The construction of the MG co-expression network allowed the identification of other genes with hypothetical roles in meiosis, which represent key candidates to be functionally validated via reverse genetics approaches (Alabdullah et al., 2019).

Here, the WGCNA network created by Alabdullah et al., (2019) was used to identify novel CE candidate genes in polyploid wheat, with the TF *TaZYPI* homoeologues (*TaZYPI-2A* and *TaZYPI-2D*) as main genes (or hub genes) of the network. The co-expression network was additionally employed to facilitate the discovery of wheat orthologues of known MGs connected with *TaZYPI* to gain further insights on *TaZYPI* role during meiosis. The studies have been performed at bioinformatics level, using a combination of RNA-seq data publicly available and online resources.

Since the lack of *in silico* TILLING line mutants of the putative candidate genes identified from the former analysis, it was not possible to validate their function, therefore, a

comparative analysis was conducted. Here, specific biochemical features, conserved domains and meiotic tissue-specific gene expression of *Triticum aestivum* and *Arabidopsis* homologues, were considered. *Arabidopsis*, although more distantly related (separated from wheat by ~200 million years of evolution) than rice, represents the best model in plant studies, possessing the most well developed genome functional annotation. Ultimately, candidate wheat CE orthologues were investigated for a meiotic role by cytological examination of chromosome spreads of male meiocytes in tetraploid wheat cv. Kronos TILLING mutant lines, with a single KO gene.

## 4.2 Materials and methods

### 4.2.1 *TaZYP1* co-expression network with RNA-seq data from ExpVIP database

The WGCNA network constructed by Alabdullah et al., (2019), publicly available on ExpVIP database (<http://www.wheat-expression.com/>), was used to identify putative CE orthologue(s) in wheat from uncharacterized genes connected to *TaZYP1* homoeologues. The workflow for this analysis is described in Figure 4.1. First of all, *TaZYP1-2A* (TraesCS2A02G340400) and *TaZYP1-2D* (TraesCS2D02G318100) were selected as “guide genes” to construct a subnetwork containing only the genes strongly connected to many orthologues of MGs with various meiotic functions. According to Ramírez-González et al., (2018) data, *TaZYP1-2A* homoeologue was clustered in Module 2, the largest meiosis-related module, while *TaZYP1-2D* homoeologue was clustered in Module 19, which grouped non-meiotic genes. Instead, *TaZYP1-2B* homoeologue (TraesCS2B02G338300) belonged to Module 0, which contained all genes unassigned to any module into the network. Therefore, *TaZYP1-2B* homoeologue was excluded in this analysis, and only the genes listed in Module 2 and 19 were considered. Edge files created with gene annotation for the target modules were used to cluster previously uncharacterized meiotic genes within these modules, ranked based on the strength of the connection (weight values). The subnetwork complexity (n= 3,940 genes) was reduced using an edge weight > 0.1. Data, containing candidate gene IDs, *TaZYP1* homoeologues, Gene Ontology (GO) annotation and weighed values, were filtered in R Studio software 1.3.9. Cytoscape 3.8.0 software (Shannon et al., 2003) was used to visualize the network and to show connections between genes. Thereby, statistics were calculated and added as

attributes to the nodes or edges in Cytoscape. The attributes include the “degree” (the number of connections of a node) and “GO terms” (biological function associated to highly connected nodes). Each gene ID linked to *TaZYP1* homoeologues was individually blasted on KnetMiner database (Hassani-Pak et al., 2021) to gain additional biological function information from *Arabidopsis* homologues. Finally, the candidate gene IDs were blasted on Wheat-TILLING database (<http://www.wheat-tilling.com/>) for functional analysis.

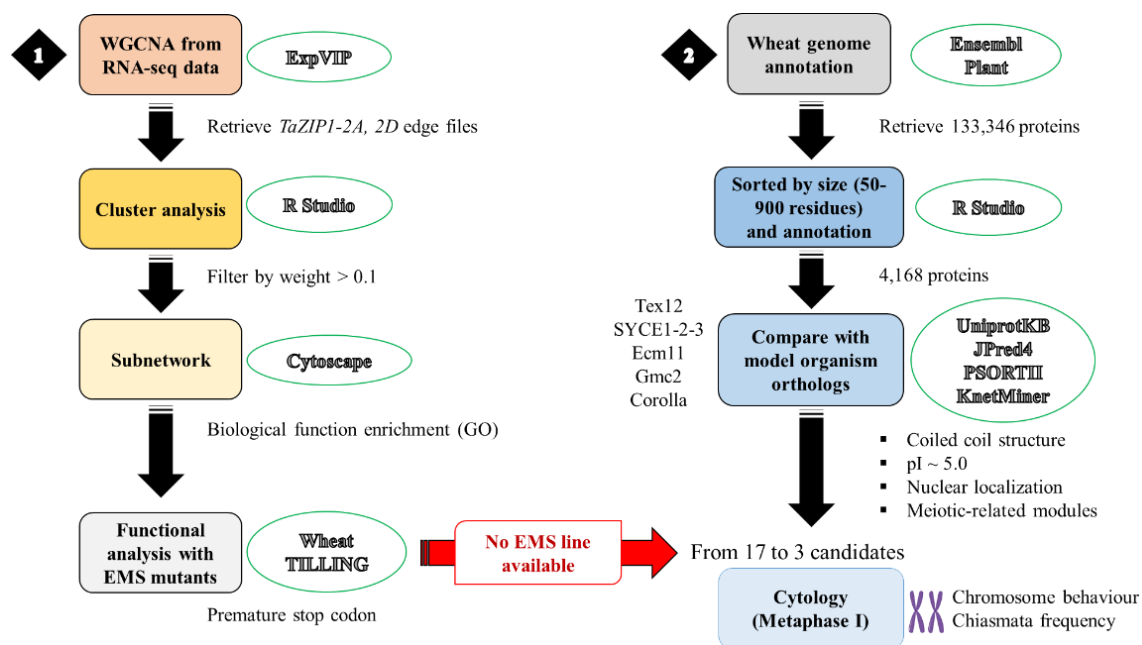


**Figure 4.1 Workflow for data analysis to identify putative CE orthologue(s) in wheat.** CE candidate(s) were connected with wheat *TaZYP1* homoeologues, using RNA-seq data from ExpVIP database and comparative analysis through web sources. 1) Data processing and co-expression sub-network generation; 2) online resources refer to the identification of putative CE genes by comparative examination. Square boxes represent procedures and approaches used. Green outline circles represent tools. Black arrows correspond to direct steps.

#### 4.2.2 Alluvial diagram

An auxiliary use of the WGCNA (Alabdullah et al., 2019) was to gain insights on *TaZYP1* function, when connected to the wheat orthologues of known meiotic genes (MGs) from the co-expressed network. To identify novel interacting partners from wheat itself, edge files of *TaZYP1-2A* and *TaZYP1-2D* modules were merged with the GO terms and filtered by weight to rank the strongest connected genes. The top 30 genes with the highest

connection were selected (weight >0.1). The output containing *ZYP1* gene homoeologues, gene IDs and expected annotation was loaded on RAWGraphs 2.0 (<https://app.rawgraphs.io/>) to create an alluvial diagram.

#### 4.2.3 Comparative analysis of CE orthologues from model organisms

The workflow for the comparative analysis is described in Figure 4.1.2. Firstly, the entire *Triticum aestivum* transcriptome annotation was downloaded as a FASTA file from Ensembl Plants database (<https://plants.ensembl.org/wheat>). Briefly, data, containing 133,436 amino acid sequences, were sorted by size (a mean amino acid number of 65-900 residues, within the range size of the orthologues isolated in model species) (Table 4.2) and annotation via Microsoft Excel spreadsheet (total= 4,168 protein sequences), and then processed into the format required in R Studio software 1.3.9 (<https://www.r-project.org/>). At this stage, this list of proteins was ranked according to data retrieved from web resources used to predict protein structures, domains, functions and tools for sequence similarity retrieval and tissue-specific gene expression databanks (Table 4.1). Public dataset with putative MGs from Module 2 were retrieved from expression browser publicly available (Alabdullah et al., 2019) (wheat eFP browser, [http://bar.utoronto.ca/efp\\_wheat/cgi-bin/efpWeb.cgi](http://bar.utoronto.ca/efp_wheat/cgi-bin/efpWeb.cgi)) and merged with 4,168 proteins in R Studio. Wheat Expression Browser powered by ExpVIP (<http://www.wheat-expression.com/>) and KnetMiner ([https://knetminer.org/Triticum\\_aestivum/](https://knetminer.org/Triticum_aestivum/)) databases were also referred to discriminate proteins grouped in co-expressed meiotic-related module, expression profile (spike/reproductive tissues) and GO terms. The output included 1,086 amino acid sequences and relative annotation, further screened by considering other common features of CE orthologues from model organisms (Table 4.2). Accordingly, only proteins having a predicted coiled coil structure were considered (n=36 candidates). Data were retrieved from Jpred4 and PSORTII. Subcellular localization (nuclear) and isoelectric point (pI) (Sanchez-Moran et al., 2008) stored in ExPASy database ([https://web.expasy.org/compute\\_pi/](https://web.expasy.org/compute_pi/)) were also prioritised (n= 17 candidates). Finally, a total of 3 candidates, TraesCS5B02G024200, TraesCS7B02G143500 and TraesCS3A02G081400, with a length comprising between 117-364 residues, a predicted coiled coil structure, and an isoelectric point (pI) next to 5.0 were selected for downstream analyses (Table 4.3 a). To determine whether the three hypothetical candidate genes were

involved in meiosis, reverse genetics approach using ethyl methanesulphonate (EMS) mutagenised wheat lines was chosen. *In silico* -homozygous mutant alleles predicted to carry a premature stop codon on single subgenome for each of the three candidates were identified (see paragraph below) and retrieved online from Wheat-TILLING database (<http://www.wheat-tilling.com/>) (Table 4.3 b).

Resources	Information	URL	References
<b>UniProtKB</b>	Sequence	<a href="http://www.uniprot.org/">http://www.uniprot.org/</a>	(“UniProt: the universal protein knowledgebase in 2021.,” 2021)
<b>BLAST</b>	Sequence	<a href="http://blast.ncbi.nlm.nih.gov/">http://blast.ncbi.nlm.nih.gov/</a>	(“Database resources of the National Center for Biotechnology Information.,” 2018)
<b>JPred4</b>	Structure	<a href="http://www.compbio.dundee.ac.uk/www-jpred/">http://www.compbio.dundee.ac.uk/www-jpred/</a>	(Drozdetskiy et al., 2015)
<b>PSORTII</b>	Subcellular localization	<a href="https://psort.hgc.jp/form2.html">https://psort.hgc.jp/form2.html</a>	(Nakai & Horton, 1999)
<b>Ensembl Plants</b>	Wheat genome annotation	<a href="https://plants.ensembl.org/Triticum_aestivum/Info/Index">https://plants.ensembl.org/Triticum_aestivum/Info/Index</a>	(Howe et al., 2020)
<b>ExpVIP</b>	Expression level EMS population	<a href="http://www.wheat-expression.com/">http://www.wheat-expression.com/</a>	(Ramírez-González et al., 2018)
<b>KnetMiner</b>	Gene network	<a href="https://knetminer.com/">https://knetminer.com/</a>	(Hassani-Pak et al., 2021)

**Table 4.1 Web resources used in this study.**

Orthologue IDs	Helix structure length	Coiled coil length	Subcellular localization	Isoelectric point (pI)
Tex12 ( <i>Homo/Mus</i> )	123/123	31	nuclear	5.22/5.22
SYCE1 ( <i>Homo/Mus</i> )	351/329	166	nuclear	5.89/5.98
SYCE2 ( <i>Homo/Mus</i> )	218/171	59	nuclear	5.57/5.11
SYCE3 ( <i>Homo/Mus</i> )	88/88	34	nuclear	4.53/4.66
Ecm11 ( <i>S.cerevisiae</i> )	302	41	nuclear	8.21
Gmc2 ( <i>S.cerevisiae</i> )	188	33	nuclear	4.79

**Table 4.2 Protein structure data of CE orthologues of model organisms.** Data were retrieved from online databanks: UniProtKB (orthologs ID, helix length, coiled coil domain length), PSORTII (subcellular localization) and ExPASy (pI).

#### 4.2.4 Identification of tetraploid TILLING Lines

Wheat TILLING (Targeted Induced Local Lesions In Genomes) lines [*Triticum turgidum durum* cv. Kronos ( $2n=4x=14$ )] were identified on Wheat TILLING database (<http://www.wheat-tilling.com/>): Kronos4243 AAbb (TraesCS5B02G024200), Kronos2901 (TraesCS7B02G143500) AAbb and Kronos3182 aaBB (TraesCS3A02G081400, TraesCS3A02G081400). Seeds were obtained from [www.SeedStor.ac.uk](http://www.SeedStor.ac.uk) and purchased from John Innes Centre (JIC), Norwich, UK (Krasileva et al., 2017). Kronos2901 AAbb, located on chromosome 7B, carried a **TCA** to **ACA** mutation, predicted to result in a premature stop codon at 227 nucleotide position. Kronos4243 AAbb, located on chromosome 3B, had an **GGT** to **AGT** mutation at 273 cDNA position, which were predicted to cause a truncated protein due to a premature stop codon. Kronos3182 aaBB, located on chromosome 3A, carried a **CCA** to **TCA** stop codon mutation at nucleotide position 160. The presence of premature stop codon mutations per individual TILLING lines was confirmed by genotyping using SNP-specific primers calibrated by gradient PCR (Table 4.3). To simplify, Kronos2901, Kronos4243 and Kronos3182 will be renamed *cc1*, *cc2* and *cc3* respectively from now on.

Gene scaffold	TILLING lines	Rename	wt	alt	cDNA position	Consequence
TraesCS7B02G143500	K2901	<i>cc1</i>	G	<b>A</b>	227	Stop gained
TraesCS5B02G024200	K4243	<i>cc2</i>	G	<b>A</b>	273	Stop gained
TraesCS3A02G081400	K3182	<i>cc3</i>	C	<b>T</b>	160	Stop gained

**Table 4.3 Summary of Kronos TILLING lines information from Ensembl Plants database.**

#### 4.2.5 Genotype screening of single KO mutants

The genotyping procedure of Kronos Parental TILLING mutants has been previously described in Chapter 2, paragraph 2.2.10. Gradient PCR was used to calculate the  $\Delta T_m$  of designed TILLING line genomic primers (Table 4.4) on wild-type Kronos; 0.5 $\mu$ l of each genomic forward and reverse primer was used. PCR cycle: denaturation at 94°C for 30 seconds; annealing at 60°C-68°C for 45 seconds for each mutant; extension at 72°C for 40 seconds; 35 cycles. Subsequently constant PCR at optimum annealing temperatures was carried out for each mutant: annealing at 63°C, 64°C and 64°C for K4243, K2901 and K3182 respectively. Wild type Kronos A and B were used as controls. The DNA concentration was quantified using Nanodrop 2000 (Thermo Scientific). Amplicons were then purified using E.Z.N.A.® Cycle Pure Kit (Omega Bio-tek) and Sanger sequencing

using forward genomic primer of corresponding genes was performed by Eurofins. Screening of SNP (point mutation induced by EMS treatment) in the sequence was detected using Chromas Lite 2.0 and Clustal Omega (EMBL-EBI).

Genotyping Primers	Oligonucleotide sequence 5' → 3'	T <sub>a</sub> (°C)
K2901gen7bF	<b>TGAAAGTTGAAACGTGTGG</b>	62
K2901gen7bR	<b>GGTGTACTACAGGTGCCA</b>	
K2901wt	CCGTGCAATTCAGCCTGC	64
K2901alt	CCGTGCAATTCAGCCTGT	
K2901common	GGACATTTAACATGGCATGCTA	
K4243gen5bF	<b>CTGGTTGAATTGTTGTCTCC</b>	62
K4243gen5bR	<b>ACAGCCTCATACTTCTCCTG</b>	
K4243wt	TGATTGGTAAAACTCAGATGTACC	63
K4243alt	TGATTGGTAAAACTCAGATGTACT	
K4243common	CGAATGGCAAGCTGGAGC	
K3182gen3aF	<b>GCAACATGCTCTACAACCGAG</b>	63
K3182gen3aR	<b>GCAGCGACAGATGAACTAA</b>	
K3182wt	CTTCATCGCGCCCATCTGG	64
K3182alt	CTTCATCGCGCCCATCTGA	
K3182common	TCATCTGTCCGGTTGCTGAA	

**Table 4.4 Subgenome specific primers used for wheat CE candidate(s) genotyping.**

Genomic primers (green) were used to validate the mutation via Sanger-sequencing.

#### 4.2.6 Isolating pollen mother cells (PMCs) for metaphase I chromosome spreads

Protocol and reagents used for metaphase spread experiments have been previously described in Chapter 2, paragraph 2.2.14.

#### 4.2.7 Isolating pollen mother cells (PMCs) for metaphase I chromosome spreads

Protocol and reagents used for immunolocalization experiments have been previously described in Chapter 2, paragraph 2.2.15.

#### 4.2.8 Statistics

Chiasma frequency and recombination foci count differences were tested for significance as described in Chapter 2, paragraph 2.2.16.

#### 4.2.9 Peptide antigens sequences for polyclonal antibody development

The protein sequence of CC2 (TraesCS5B02G024200) was BLASTed in *Arabidopsis* proteome via Ensemble Plant database (<https://plants.ensembl.org>) to obtain its accession ID (AT5G51330), following used in UniProtKB (<https://www.uniprot.org/uniprot>) and TAIR10 *Arabidopsis* databases (<https://www.arabidopsis.org>) to retrieve additional information about putative GO function and to localise the tissue-specific gene expression of the *Arabidopsis* homologous, respectively. The CC2 *Arabidopsis* homologous corresponds to the gene *SWI1*, highly expressed in meiotic tissue (bud) and coding for SWITCH1, known to be involved in meiotic sister chromatid cohesion and reciprocal meiotic recombination in *Arabidopsis* (Yang et al., 2019; Mahesh et al., 2021). Once confirmed the meiotic role of the *Arabidopsis* orthologous, two immunogenic peptide consensus sequences, identical for all homologues and long approximately 17-24 amino acid residues, were designed for CC2 homologue candidate (Table 4.5). The peptides were synthesised in rat and conjugated to KLH carrier protein for polyclonal antibody production by Gemini Biosciences Ltd company. Antibodies raised against CO markers are available at Dr. James Higgins' laboratory (University of Leicester).

Gene ID	Arabidopsis Accession ID	Peptide Sequences
TRAESCS5B02G024200	AT5G51330	a. KRGDPVSADGYALKAKMQVEE b. QVEELTKELAGVKRHMQQLV

**Table 4.5 Peptide antigens sequences of ‘CC2’ used for protein immunolocalization.**

## 4.3 Results

### 4.3.1 *TaZYP1* co-expression sub-network screened seven uncharacterized genes with potential role in wheat meiosis

The co-expression sub-network built from *TaZYP1-2A* and *TaZYP1-2D* homoeologues (Figure 4.2) contained 7 uncharacterized genes with putative meiotic-related roles, thus potential CE candidates in wheat, and 1 gene connected to *TaZYP1-2A* homoeologous, predicted to play a non-meiotic function, which are listed and supplementary described in Table 4.6.

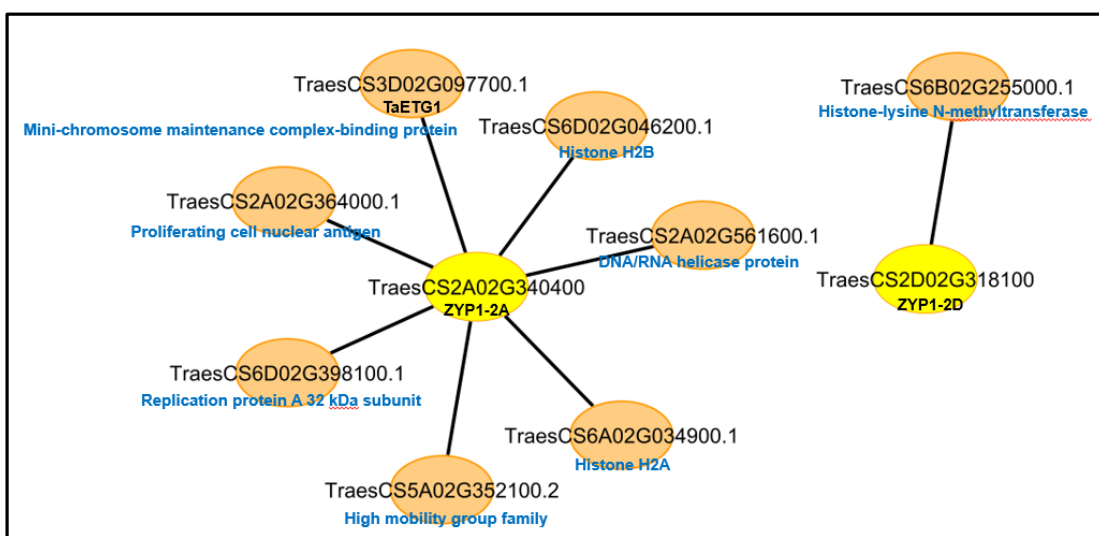


**Figure 4.2** *TaZYP1* co-expression sub-network in hexaploid wheat. This subnetwork was constructed using *TaZYP1-2A* and *TaZYP1-2D* homoeologues as hub genes from module 2 and 19, respectively. Edge weight > 0.15 was used as a threshold to visualize genes in the subnetwork using Cytoscape 3.8.0 software.

<i>T. aestivum</i> gene IDs	<i>Arabidopsis</i> gene IDs	UniProtKB annotation	GO – biological process
<i>TraesCS2A02G561600</i>	<i>AT5G63950</i>	<i>CHR24</i>	Probable chromatin remodeling factor that regulate homologous recombination (HR) and non-homologous recombination (NHR) (Shaked et al., 2006)
<i>TraesCS5A02G352100</i>	<i>AT1G20693</i>	<i>HMGB2</i>	Chromatin assembly or disassembly (phosphorylation activity) (Stemmer et al., 2003)
<i>TraesCS2A02G364000</i>	<i>AT2G29570</i>	<i>PCNA2</i>	DNA replication (Anderson et al., 2008), mismatch repair, and resolution of double Holliday junction (dHJ) in CO (Gaudet et al., 2011; Kulkami et al., 2020)
<i>TraesCS6A02G034900</i>	<i>AT5G02560</i>	<i>HTA12</i>	Heterochromatin organization (Yelagandula et al., 2014)
<i>TraesCS6D02G046200</i>	<i>AT3G45980</i>	<i>H2B</i>	Nucleosome assembly, DNA methylation control (Sridhar et al., 2007)
<i>TraesCS6B02G255000</i>	<i>AT1G04050</i>	<i>SUVR1</i>	Inactive histone-lysine methyltransferase involved in transcriptional gene silencing and chromatin remodelling (Dou et al., 2014)
<i>TraesCS3D02G097700</i>	<i>AT2G40550</i>	<i>ETG1</i>	Regulator of DNA replication. Required for sister chromatid cohesion (Takahashi et al., 2010)
<i>TraesCS6D02G398100</i>	<i>AT4G34270</i>	<i>TIP41L</i>	Regulation of phosphoprotein phosphatase activity (Gaudet et al., 2011)

**Table 4.6 Supplementary data of *TaZYP1* sub-network results generated in Cytoscape 3.8.0 software.** Sources: Ensembl Plants, KnetMiner and UniProtKB databases. GO terms information were retrieved from literature searches.

#### 4.3.2 Analysis of TILLING mutants

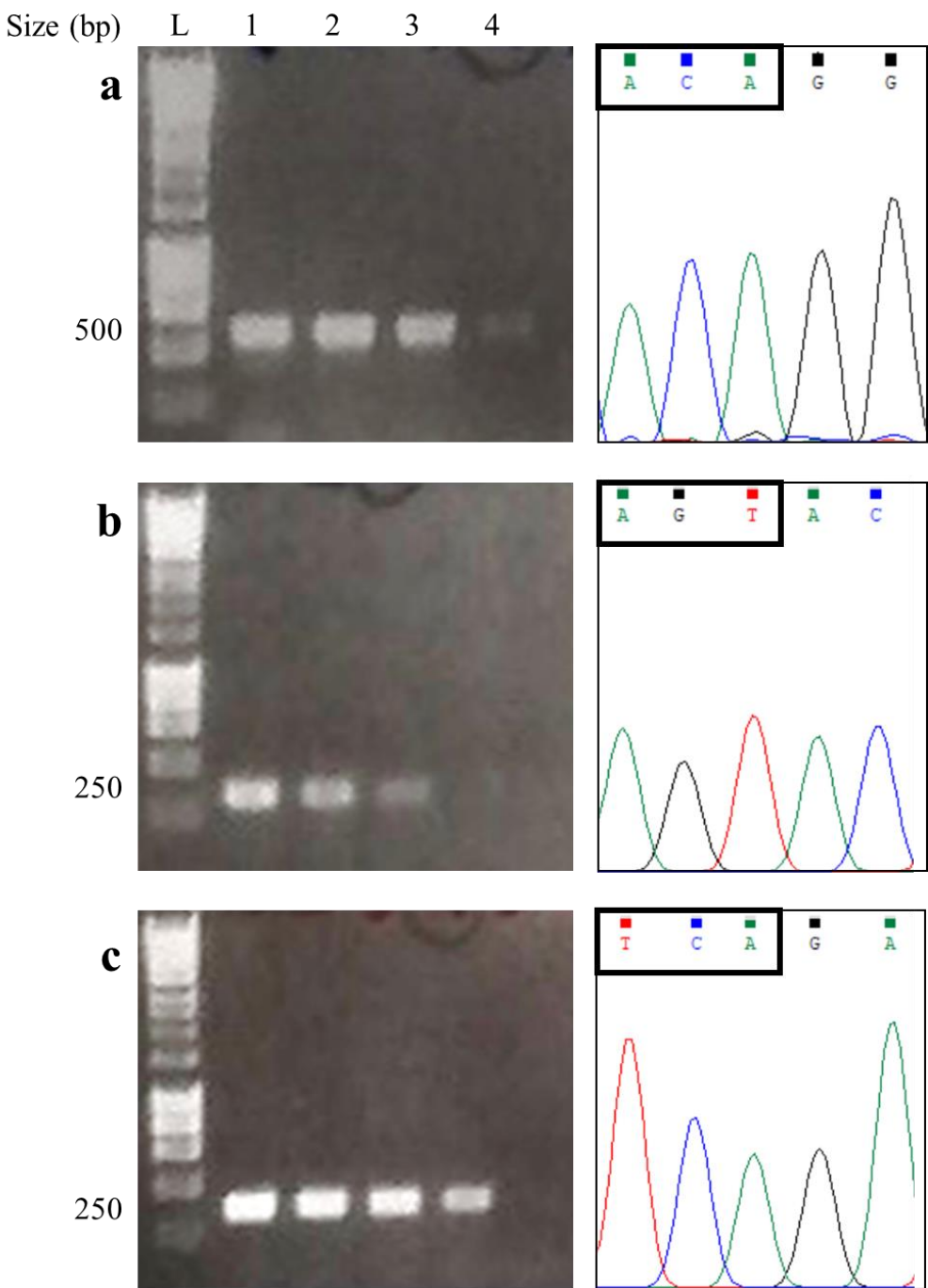
Due to the lack of wheat TILLING lines for any of the CE gene candidates detected from the *TaZYP1* co-expression network, web resources were then used as alternative approach to gain supplementary data to identify putative CE orthologue(s) in wheat transcriptome. The comparative analysis identified three candidate genes, here called *CC1*, *CC2*, *CC3*, presenting a predicted coiled-coil domain in their protein structure (Table 4.7). Interestingly, *CC2* and *CC3* were expected to be expressed in reproductive tissues (spike), while *CC1* in vegetative tissue (leave/shoots) (Table 4.7). To validate their meiotic role, *cc1*, *cc2*, *cc3* single KO gene of TILLING K2901 AAbb, K4243 AAbb and Kronos3182 aaBB, respectively, were selected and genotyped by PCR and sequencing (Figure 4.3). Once confirmed the presence of the predicted stop codon mutation within the DNA coding region, the phenotype of mutant plants was analysed cytologically (Figure 4.4).

<b>a</b>	<b>Gene candidates</b>	<b>Prot Length</b>	<b>Jpred4 domain</b>	<b>PSORTII CC length</b>	<b>PSORTII Subcell loc</b>	<b>pI ExPASy</b>
	<i>CC1</i>	117	coiled coil (CC)	49-89	47.8 %: nuclear	6.45
	<i>CC2</i>	228	coiled coil (CC)	17-125	73.9 %: nuclear	4.81
	<i>CC3</i>	364	coiled coil (CC)	35-168	65.2 %: nuclear	5.48

<b>b</b>	<b>Gene candidates</b>	<b>KnetMiner Module 2</b>	<b>ExpVIP</b>	<b>ID GO (Alabdullah et al., 2019)</b>	<b>Pfam ID</b>
	<i>CC1</i>	Histone H3-R2 Methylation	leaves/shoots	GO:0005737	NA
	<i>CC2</i>	VPS60-1 vacuolar transport	spike	GO:0030968	PF03357
	<i>CC3</i>	Histone H3-R2 Methylation	spike	NA	NA

**Table 4.7 Data collection of wheat CE candidate genes identified by comparative analysis with known CE orthologues from model organisms.** Kronos TILLING mutant lines (in brackets), secondary structure prediction, tissue-specific gene expression and pI are predicted from various web sources, such as Ensembl Plants, Jpred4, PSORTII, ExPASy, KnetMiner, ExpVIP and Pfam databanks. CC: coiled coil prediction accuracy >82 (Drozdetskiy et al., 2015).



**Figure 4.3 Confirming the genotype of *cc1*, *cc2* and *cc3* TILLING mutants.** a-c) Left inserts show the gradient PCR used to calculate the  $\Delta T_m$  of designed *cc1*, *cc2* and *cc3* TILLING primers on Kronos WT: 500, 250 and 250 bps PCR amplicons amplified by primer pairs specific for 7B, 5B and 3A genome of *cc1* (TraesCS7B02G143500), *cc2* (TraesCS5B02G024200) and *cc3* (TraesCS3A02G081400), respectively are presented. Right inserts illustrate the sequence trace of the translations TCA → ACA, GGT → AGT and CCA → TCA detected in *cc1*, *cc2* and *cc3*, respectively (images from Chromas Lite). L= DNA ladder; 1-4= wild type Kronos previously sequenced.  $\Delta T_m = 62\text{-}68^\circ\text{C}$ , where 1= 62.1°C, 2= 62.4°C, 3= 63.2°C, 4= 64.3°C.

In general, all mutant plants showed a pleiotropic phenotype, such as bent tillers, reduced plant height, delay flowering and sterility. Analysis of chromosome spread at meiotic metaphase I from male meiocytes revealed a wild-type phenotype (Figure 4.4 a) of *cc1*, displaying predominantly ring bivalents (Figure 4.4 b), while *cc2* and *cc3* exhibited an increase of rod bivalents and unpaired chromosomes (Figure 4.4 c, d). Specifically, in *cc1*, rings prevailed on rods ( $P \text{ adj} > 0.05$ ) and it had less than 1% of univalent pairs ( $P \text{ adj} > 0.05$ ) (Figure 4.5 a, b), maintaining unaltered the obligate chiasma per meiocyte ( $n = 50$ ) ( $P \text{ adj} > 0.05$ ) (Figure 4.5 a, b). Inconsistently, *cc1* TILLING plants ( $n = 10$ ) were sterile (under greenhouse conditions). Germination rate of this line was also low ( $n = 3/10$ ), therefore possibly the phenotype may be the result of off-target mutations accumulated during the mutagenesis process of TILLING method, which is a very common phenomenon, as well as, the main drawback in the context of such technology (Blary & Jenczewski, 2019). *cc2* differed slightly in number of COs events ( $n = 50$ ) ( $P \text{ adj} < 0.05$ ), resulting from a 7% decrease of ring bivalents ( $n = 50$ ) (Figure 4.5 a, b). Indeed, the mutant displayed  $2.08 \pm 1.41$  ( $n = 50$ ) mean rod bivalents per meiocyte at metaphase I, in comparison with  $0.08 \pm 0.27$  ( $n = 50$ ) rod bivalents observed in wild type (Figure 4.5) ( $P \text{ adj} < 0.01$ ). This change probably led to complete infertility of the plants analysed ( $n = 10$ ). *cc3* showed the greatest effect on meiotic recombination, compared to the other mutant lines and the wild type (Figure 4.5 a, b). This is due to the rise of the incidence of univalents ( $P \text{ adj} < 0.05$ ) and rod bivalents ( $P \text{ adj} < 0.01$ ) detected during metaphase I (Figure 4.5 b, c). In *cc3*,  $0.3 \pm 0.46$  ( $n = 50$ ) univalents per meiocyte were observed, compared with  $0.08 \pm 0.27$  ( $n = 50$ ) in the wild type (Figure 4.5) ( $P \text{ adj} < 0.01$ ), which may explain the lack of fertility of the plants analysed ( $n = 10$ ). Moreover, on average, *cc3* exhibited  $1.92 \pm 1.26$  ( $n = 50$ ) rod bivalents per nucleus, a minor change compared to  $1.28 \pm 1.38$  ( $n = 50$ ) rod bivalents in wild type, whereas, together with univalents, contributes to the 8% reduction in chiasmata per meiocyte, from  $26.56 \pm 1.4$  in the wild type ( $n = 50$ ) to  $24.48 \pm 1.51$  ( $n = 50$ ) in *cc3* (Figure 4.5 a, b) ( $P \text{ adj} < 0.01$ ). Statistically, all single KO mutants were different from wild-type (WT), in terms of frequency of chiasmata, rod bivalents rather than ring bivalents, and univalent pairs (pairwise Wilcoxon rank sum test,  $P \text{ adj} > 0.05$ ) (Figure 4.5 b). The full data sets list can be found in Appendix (Table S12).

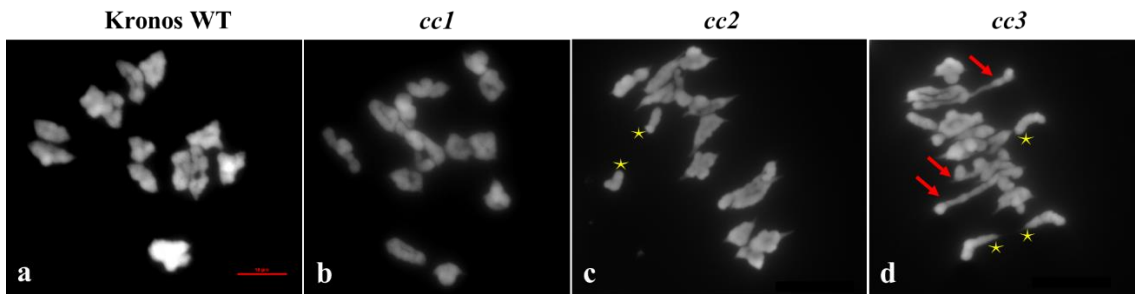


**Figure 4.4 Metaphase I spread of TILLING single KO mutants.** a) Kronos WT exhibits ring bivalents at meiotic metaphase I. b) *cc1* mutant shows a wild-type phenotype, characterized by ring-shaped chromosomes. c) *cc2* and d) *cc3* display univalent pairs (yellow stars) and mainly rod-shaped chromosomes (red arrows). Sample were stained in DAPI. Scale bar 10  $\mu$ m.

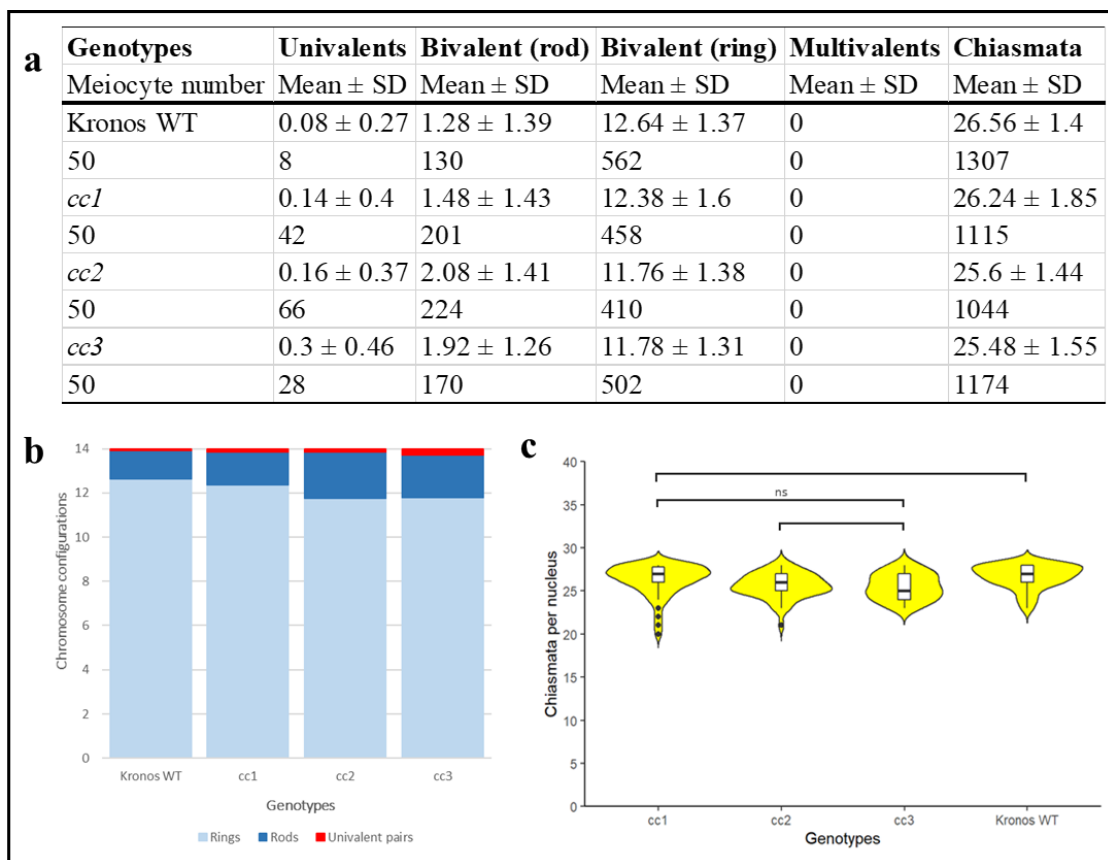


**Figure 4.5 Chromosome configuration analysis of CE candidate single KO mutants at metaphase I.** a) Table summarising: average, standard deviation (SD), range of bivalents, univalents, multivalents and chiasmata per male meiocyte in Kronos WT and TILLING lines analysed. n = number of meiocytes; minimum two independent plants per genotype. b) Bar chart illustrates the mean values of rings bivalents (sky blue), rods bivalents (dark blue) and univalents (red) per meiocytes among WT and TILLING single mutants. Legend is at the bottom. c) Violin

plot exemplifies chiasmata frequency per male meiocyte. ns= not significant; asterisks indicate significant difference by pairwise Wilcoxon rank sum test (Significant codes: 0 ‘\*\*\*’ 0.001 ‘\*\*’ 0.01 ‘\*’ 0.05 ‘ns’ 0.1 ‘ ’). The adjustment methods include the Bonferroni correction.

After that, the localization of CC2 candidate (homologous of *Arabidopsis SWI1*) within male meiocytes was further investigated in tetraploid wheat.. In *Arabidopsis*, *SWI1* is highly expressed in meiotic tissue (bud) and its product SWITCH1 mediates meiotic sister chromatid cohesion and reciprocal recombination during meiosis (Yang et al., 2019; Mahesh et al., 2021). Triple-immunolocalization analysis using antibodies anti-ASY1, -ZYP1 and -SWITCH1 were carried out on Kronos WT male meiocyte during zygotene to verify the predictive wheat SWITCH1 protein function. As showed in Figure 4.6, the candidate wheat SWITCH1, clearly co-localised with ASY1 onto the chromatin on WT meiocytes, confirming its activity during meiosis.

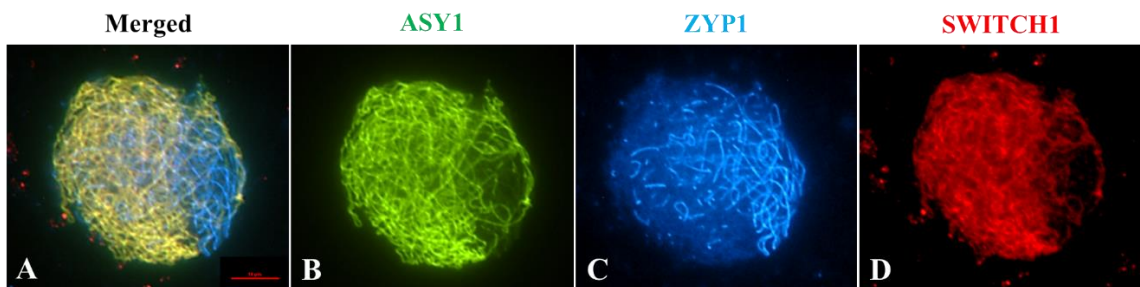


**Figure 4.6 Analysis of synapsis monitored by *TaASY1* (green) and *TtSWITCH1* (red) in Kronos WT meiocytes during zygotene.** (A) merged images of (B) chromosome axis *TaASY1* (green), (C) transverse filament *AfZYP1* (blue), and (D) candidate *SWITCH1* (red), unambiguously attached to the chromatin on WT meiocytes. Scale bar = 10  $\mu$ m.

#### 4.3.3 *TaZYP1* is highly connected with genes having multiple meiotic roles in wheat

The alluvial diagram (Figure 4.7) generated from the merged functional annotation data of *TaZYP1-2A* and *TaZYP1-2D* homoeologues co-expressed modules and wheat orthologues of known MGs (Table 4.8), revealed that *TaZYP1* was mainly connected to genes involved in several meiotic functions, which can be grouped as follow:

##### 1) DSB repair (*TaH2AX*, *TaMSH7*, *TaHOP2*, *TaRPA1a*)

- 2) Sister chromatin cohesion** (*TaESP*, *TaETG1*, *TaSMC2*, *TaSGO1*, *TaMis12a*)
- 3) CO formation and distribution** (*TaFANCM*, *TaEME1B*, *TaRecQ-7*, *TaAKR1*, *TaKIN1*)
- 4) Meiotic progression and meiotic entry** (*TaAM1*, *TaCDC45*, *TaMEI1*, *TaPS1*, *TaCYCA1*).

ZYPI_homoeologue	Gene_name	Expected_function
<i>TaZYP1-2A</i>	<i>TaETG1</i>	Sister chromatid cohesion establishment
<i>TaZYP1-2A</i>	<i>TaSMC2</i>	condensin complex (homologous chromosome segregation)
<i>TaZYP1-2A</i>	<i>TaETG1</i>	Sister chromatid cohesion establishment
<i>TaZYP1-2A</i>	<i>TaCDC45</i>	Meiotic entry
<i>TaZYP1-2A</i>	<i>TaCDC45</i>	Meiotic entry
<i>TaZYP1-2A</i>	<i>TaCDC45</i>	Meiotic entry
<i>TaZYP1-2A</i>	<i>TaSMC2</i>	condensin complex (homologous chromosome segregation)
<i>TaZYP1-2A</i>	<i>TaMSH7</i>	DSB repair
<i>TaZYP1-2A</i>	<i>TaSYN3</i>	Sister chromatid cohesion
<i>TaZYP1-2A</i>	<i>TaH2AX</i>	DSB repair
<i>TaZYP1-2A</i>	<i>TaH2AX</i>	DSB repair
<i>TaZYP1-2A</i>	<i>TaSGO1</i>	Centromeric cohesion protection
<i>TaZYP1-2A</i>	<i>TaETG1</i>	Sister chromatid cohesion establishment
<i>TaZYP1-2A</i>	<i>TaPS1</i>	Meiotic cell cycle control
<i>TaZYP1-2A</i>	<i>TaCYCA1</i>	Meiotic cell cycle control
<i>TaZYP1-2A</i>	<i>TaCYCA1</i>	Meiotic cell cycle control
<i>TaZYP1-2A</i>	<i>TaSYN3</i>	Sister chromatid cohesion
<i>TaZYP1-2A</i>	<i>TaEME1B</i>	Class II CO pathway
<i>TaZYP1-2A</i>	<i>TaRecQ-7</i>	Involved in gene conversion, increase GC and CO frequency
<i>TaZYP1-2A</i>	<i>TaPS1</i>	Meiotic cell cycle control
<i>TaZYP1-2A</i>	<i>TaSYN3</i>	Sister chromatid cohesion
<i>TaZYP1-2A</i>	<i>TaMSH7</i>	DSB repair
<i>TaZYP1-2A</i>	<i>TaFANCM</i>	Anti-CO activity
<i>TaZYP1-2A</i>	<i>TaMis12a</i>	Sister kinetochore association at meiosis I
<i>TaZYP1-2A</i>	<i>TaMEI1</i>	Meiotic entry
<i>TaZYP1-2A</i>	<i>TaSGO1</i>	Centromeric cohesion protection
<i>TaZYP1-2A</i>	<i>TaESP</i>	Sister chromatid cohesion release
<i>TaZYP1-2A</i>	<i>TaHOP2</i>	SPO 11 -inducedand IH bias DSB repair
<i>TaZYP1-2A</i>	<i>TaCDC45</i>	Meiotic entry
<i>TaZYP1-2A</i>	<i>TaH2AX</i>	DSB repair
<i>TaZYP1-2A</i>	<i>TaPS1</i>	Meiotic cell cycle control
<i>TaZYP1-2D</i>	<i>TaAM1</i>	Prophase I progression (Leptotene–zygotene transition)
<i>TaZYP1-2D</i>	<i>TaKIN-1</i>	Regulation of synapsis and CO distribution
<i>TaZYP1-2D</i>	<i>TaAXRI</i>	Regulation of CO distribution
<i>TaZYP1-2D</i>	<i>TaRPA1a</i>	DSB repair
<i>TaZYP1-2D</i>	<i>TaRPA1a</i>	DSB repair

**Table 4.8 Data for alluvial diagram.** Only the top 30 genes strongly connected with ZYPI homoeologues were considered (weight > 0.1).

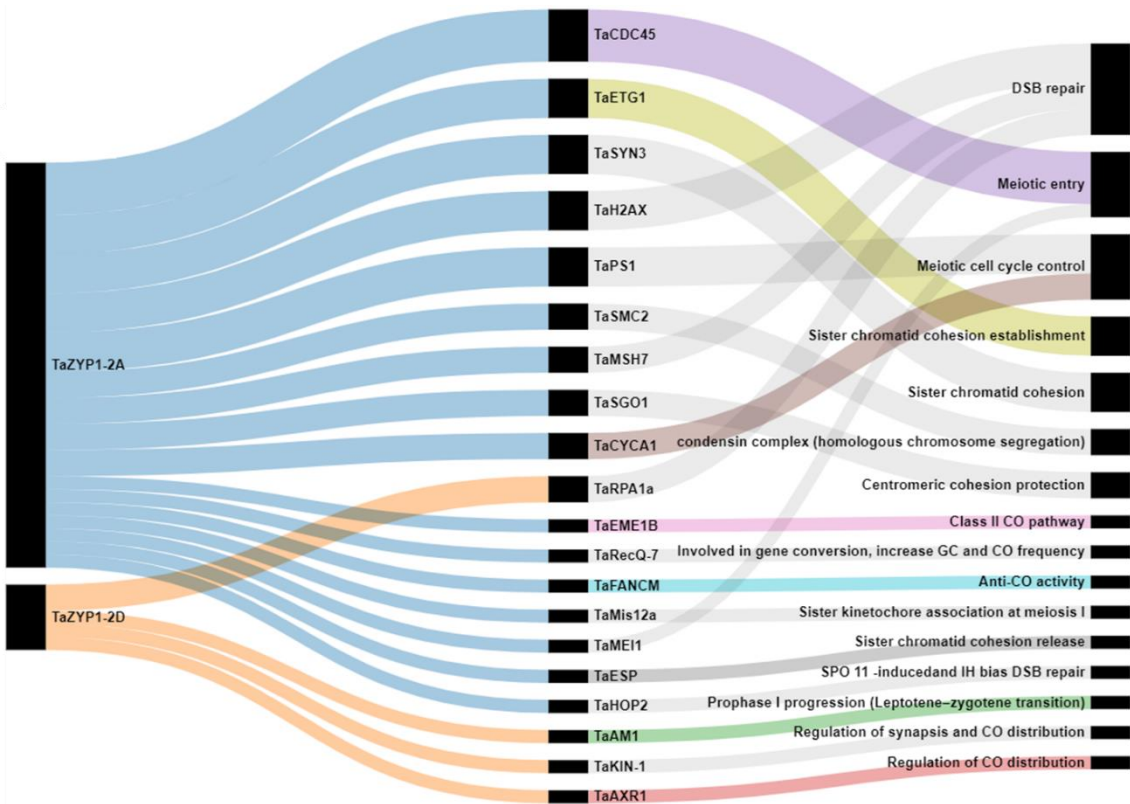


**Figure 4.7 The alluvial diagram of the wheat MG orthologues connected to *TaZYP1-2A* and *2D* homoeologues.** Edge weight > 0.1 was used as threshold to visualize connected genes. Black bars indicate the number of homoeologous for each connected gene. Blocks represent clusters of nodes, and stream fields between the blocks represent changes in the composition of these clusters over time. The height of a block represents the size of the cluster and the height of a stream field represents the size of the components contained in both blocks connected by the stream field.

## 4.4 Discussion

### 4.4.1 WGCNA network as a promising method to unveil the evolutionary history of wheat CE

From this network, the best CE candidate was expected to be *TraesCS5A02G352100* (High mobility group B protein 2, *HMGB2*), a putative meiotic gene highly connected to *TaZYP1-2A* homologue (weight > 0.15), whose transcript was predicted to be involved in chromatin assembly/disassembly via phosphorylation events in *Arabidopsis* and maize (Stemmer et al., 2003). More broadly, in previous works, posttranslational modification of the SC has been reported as a major aspect of its regulation, especially phosphorylation (Fukuda et al., 2012; Jordan et al.,

2012<sup><https://www.ncbi.nlm.nih.gov/pmc/articles/PMC5800814/></sup> - bib24; Leung et al., 2015; Gao et al., 2016; Nadarajan et al., 2017). For instance, proteomic studies in *Brassica oleracea* revealed that phosphorylated *BoASY1* and *BoASY3* (LE) play a role in establishing protein-protein interaction during prophase I of meiosis (Osman et al., 2018). In yeast, phosphorylation of TF Zip1 regulates the crossover/noncrossover decision during meiosis (Chen et al., 2015). Interestingly, in *Caenorhabditis elegans*, phosphorylated SYP-1 (CE) facilitates the progression of meiotic prophase and is required for the disassembly of SC components and meiotic chromosome segregation in late prophase (Sato-Carlton et al., 2018). Mammalian SYCP1 (TF) also contains several phosphorylation sites, which might be important for SC assembly (Meuwissen et al., 1992). Deficiency of each known SC protein abrogates synapsis, DSB resolution and crossover formation, resulting in complete male/female infertility for SYCP1 and CE proteins (de Vries et al., 2005; Bolcun-Filas et al., 2007; Bolcun-Filas et al., 2009; Hamer et al., 2008; Schramm et al., 2011; Yuan et al., 2000; Yang et al., 2006).

Unfortunately, no mutant line for TraesCS5A02G352100 (*HMGB2*) gene has been produced yet among wheat TILLING collection to functionally validate the hypothetical CE role of such gene in tetraploid wheat. Nevertheless, this was not the only obstacle derived from this study. The initial approach to identify CE orthologue(s) in polyploid wheat was based upon the use of RNA-seq datasets derived from wheat anther samples previously utilised to assess the homoeologous expression patterns of meiotic genes according their differential expression level (Alabdullah et al., 2019). The first limit encountered was related to the distinct categorization of the individual *TaZYP1* homoeologues, which did not cluster into the same meiotic module. This is the case of *TaZYP1-2B* homoeologue, grouped in a non-meiotic module (Module 0), which also included some other essential functionally characterized meiotic genes, such as *ASY1* and *DMC1* (Boden et al., 2007; Boden et al., 2009; Devisetty et al., 2010). A plausible explanation upon this data may reflect the differential expression profile of such genes, being involved in non-meiotic process, likewise observed in other wheat homoeologue genes expressed both in meiotic and somatic tissues (Martín et al., 2017; Rey et al., 2017; Rey et al., 2018). Therefore, exclusive expression during meiosis may not be the most appropriate criterion for classifying meiotic genes. Examining expression patterns of known meiotic genes may be of help in identifying better criteria.

Furthermore, RNA-seq data processed by Alabdullah et al., 2019, although deriving from a large sample size (17 anther samples), did not include a gene expression level throughout the different stages of meiosis, which may be relevant for the exact estimation of genes expressed only in specific sub-stages of meiotic process. In fact, CE orthologues are known to localise between the axial element of the SC at prophase I sub-stages of meiosis. Another argument may be that these genes might not be highly regulated in wheat. Thus, when RNA-seq samples for specific meiotic stages in wheat will be available, a more accurate assignment of these meiotic genes in the network will be eventually achieved.

The remaining genes highly co-expressed with *TaZYP1* (weight > 0.15) were categorised as non-meiotic genes, thereby involving somatic pathways (TraesCS6D02G398100, similar to *AtTIP41*) and sister chromatid cohesion during mitosis (TraesCS3D02G097700, also known as *TaETG1*) (Punzo et al., 2018; Takahashi et al., 2010), perhaps due to a potential role of *TaZYP1* in development process(es), as stated earlier, for its dual expression activity in meiotic and non-meiotic tissues. However, further studies are needed to test this hypothesis.

#### 4.4.2 Preliminary data of candidate *SWI1* homologue in tetraploid wheat

The comparative analysis of fully characterised CE orthologues from model species, based on the principle that proteins constituting the SC display conserved features, such as predicted secondary structure (e.g. coiled coil domain as interaction motif) and function (assembly and synapsis) among eukaryotes (Moens, 1984; Zickler & Kleckner, 1999), led to the identification of three CE candidate genes in wheat (*CC1*, *CC2* and *CC3*). Their transcripts were predicted to have features observed in other CE orthologues, such as a coiled-coil domain, an isoelectric point ~5, a nuclear localization (> 65%) and a tissue-specific expression in spike, which suggest a role in meiotic recombination, except for *CC1*, which was predicted to be predominantly expressed in leaves and EMS mutant analysis of chromosomes at metaphase I revealed a wild type phenotype. Instead, preliminary data of single KO gene of *cc2* and *cc3* in tetraploid wheat, displayed a distinct phenotype, characterised by modest crossover disruption (7% and 8%, respectively) during meiotic metaphase I, infertility and pleiotropic effects. These data are consistent with mammalian *syce2* and *tex12* mutants, which exhibited deficiency of CO formation

and complete male/female infertility for CE proteins (de Vries et al., 2005; Bolcun-Filas et al., 2007; Bolcun-Filas et al., 2008; Hamer et al. 2008; Schramm et al., 2011; Yuan et al., 2000; Yang et al., 2006).

Although being premature, the cytological phenotypes defined from these preliminary data (occurrence of univalents at meiotic metaphase I and complete sterility), highlighted a potential CO assurance-related function of *CC2* and *CC3* genes in tetraploid wheat, especially *CC2/SWII*. Excitingly, triple-immunolocalization analysis including SC markers and SWITCH1 on Kronos WT male meiocyte unequivocally validated wheat SWITCH1 as promising candidate. In *Arabidopsis*, SWITCH1 is required for meiotic chromosome organization including maintenance of sister chromatid cohesion in prophase I of meiosis (Yang et al., 2019; Mahesh et al., 2021).

Nevertheless, at least two considerations must be taken in account. Firstly, data have not yet been supported by a full knockout mutation of the gene, which may unveil a more severe mutant phenotype. Indeed, only the effect of single KO homoeologous gene copy was evaluated, and, as known, in polyploid species genome redundancy promotes a “buffering” effect in which the deleterious alleles are masked by the extra copies of WT alleles. Thus, the duplicated genes offer a protective effect against single-locus deleterious mutations, as already demonstrated for wheat *TtMSH4* (Desjardins et al., 2020a). For a complete gene knockout, plant lines carrying mutations of each of the homoeologues separately must be combined by a series of crossings, which is labour intensive and time-consuming. At this stage, a complementary experiment that may aid to fill the gap on their function in CO pathway would be cytologically immunolocalise the candidate proteins with CO Class I markers, such as HEI10 (Chelysheva et al., 2012) during meiosis. Furthermore, the use of protein markers, such as presence of double-strand break (DSBs) ( $\gamma$ -H2AX), homologous recombination (DMC1) and sites of crossing-over (MLH1) (Hunter & Borts, 1997; Mahadevaiah et al., 2001) may be employed to monitor the dynamism of the wheat CE protein candidates, and eventually confirm their role in CO processing and synapsis propagation.

The second consideration relied on the choice to restrict the searching for specific features in wheat proteome, which may have consequently ruled out other equally suitable candidates. For example, the presence of a coiled-coil domain may also occur in many

non-meiotic proteins. Besides, there is evidence in *ScEmc11* and *ScGmc2* that the presence of the alpha helix structure does not form any coiled coil domain (Humphryes et al., 2013), yet still these proteins play a critical role in SC morphogenesis, as seen in other known CE proteins (Costa et al., 2005; Hamer et al., 2006; Page et al., 2008; Schramm et al., 2011; Collins et al., 2014). This should not surprise, considering the evolutionary history of the CE orthologues. CE proteins arose relatively recently, in parallel to the evolution of early eukaryotes, therefore they may be more variable in structure and function (Grishaeva & Bogdanov, 2014). Thus, it may be reasonable to expect that wheat may have evolved an independent structure of SC proteins, with a divergent protein-protein interaction mechanism to link LE and ensure proper chromosome alignment and synapsis.

Alternatively, it is possible that other element(s) of the SC in wheat might act as a CE functional homologue. This hypothesis is supported by the fact that *CeSYP* proteins, initially thought to be TF components, were then reclassified as CE proteins for their function in assembly/disassembly of SC (Hurlock et al., 2020).

Lastly, the low germination rate and the sterility of the *cc1* TILLING plants was presumably due to off-target mutations accumulated during the mutagenesis process of TILLING method (Blary & Jenczewski, 2019), while the same phenotype exhibited by the remaining wheat candidates analysed (*cc2/swi1* and *cc3*) may be caused by the emergence of univalents. Thus, it would be interesting to confirm the dual role of CC2/SWITCH1 in CO control and fertility, and further analyse CC3.

**4.4.3 *TaZYP1* is likely to play a more central role in meiotic recombination**  
The alluvial diagram allowed to discover the existence of additional meiotic roles of *TaZYP1*, taking in account annotated wheat meiotic genes, being highly co-expressed with *TaZYP1* homoeologues.

According to this data, a putative function of *TaZYP1* in DSB repair was hypothesised. Consistently, studies on yeast (*Zip1*), barley (*ZYP1*) and mouse (*SYCP1*) orthologues have suggested that these proteins are required for proper DSB processing at late meiotic stages (Börner et al., 2004; Barakate et al., 2014; de Vries et al., 2005). In yeast *zip1* null

mutants showed defects in the progression from DSBs to the single end invasions (SEIs), double Holliday junctions (dHJs), and CO formation, thereby Zip1 fulfils its role namely in the early step of meiotic recombination, before an intact SC structure is formed (Börner et al. 2004). Interestingly, the gene *TraesCS2A02G364000* from the initial *TaZYP1* co-expression subnetwork, showed similarity to proliferating cellular nuclear antigen (PCNA), a multifunctional protein originally identified as an auxiliary protein of DNA polymerase delta, involved in the control of eukaryotic DNA replication (Anderson et al., 2008), and recently, in other nuclear activities, such as double Holliday junction resolution in mismatch repair (Gaudet et al., 2011) and CO (Kulkarni et al., 2020). In human, PCNA is important for crossover-biased resolution by the implication of MutL $\gamma$  complex (Kulkarni et al., 2020). In *Arabidopsis*, the mismatch-recognition polypeptide *AtMSH7* (MutS $\gamma$  heterodimers) retains a putative proliferating-cell nuclear antigen (PCNA)-interaction domain in its N-terminus, thought to suppress inter-species crosses, by antagonizing CO formation between homoeologous chromosomes (Wu et al., 2003). As in *Arabidopsis*, also hexaploid wheat *TaMSH7-3D* gene, located within *Ph2* locus, and *TaZIP4-B2* gene, in the *Ph1* locus, are responsible for promotion of homologous CO and restriction of homoeologous CO (Serra et al., 2021; Rey et al., 2017, Rey et al., 2018). From the previous network (this study), another gene co-expressed with *TaZYP1* that was also predicted to maintain the recombination occurring between homologous rather than non-homologous (Shaked et al., 2006), was *TraesCS2A02G561600* (chromatin remodeling 24, *CHR24*), a probable chromatin remodeling factor. Intriguingly, histone genes, such as *TraesCS6A02G034900* (histone H2A, *HTA12*) (Yelagandula et al., 2014), *TraesCS6D02G046200* (histone *H2B*) (Sridhar et al., 2007), and *TraesCS6B02G255000* (probable inactive histone-lysine N-methyltransferase, *SUVRI*) possibly required for methylation control and chromatin remodelling (Han et al., 2014), were predicted to co-express with *TaZYP1* and previously connected to *TaZIP4* (Alabdullah et al., 2019). In hexaploid wheat, it has been observed that the process of homolog recognition is associated with major changes in chromosome chromatin structure, suggesting that changes in chromatin structure may be involved in the homolog recognition process and synapsis initiation (Prieto et al., 2005). Chromatin and histone H1 phosphorylation are also known to be involved in premeiotic replication event ruled by the *CDK2*-like gene cluster and promote synapsis efficiency in wheat (Greer et al., 2012; Rey et al., 2018).

The alluvial diagram also reported association between *TaZYP1* and wheat orthologues of genes known to be involved in the control of meiotic CO formation and distribution such as *TaFANCM*, *TaEME1B*, *TaRecQ-7*, *TaAKR1* and *TaKINI* (Mercier et al., 2015). This suggests that *TaZYP1* may have a role in CO pathway regulation in wheat. Consistent with this prediction, it is already known that in *C elegans* and *S cerevisiae*, the *SYP1* and *ZIP1*, respectively, contributes to maintain class I CO and CO interference by stabilizing the alignment of homologous chromosomes during the formation of SC (Mlynarczyk-Evans & Villeneuve, 2017; Chen et al., 2015). Similarly, in barley and *Arabidopsis*, *ZYP1* mediates CO interference and it is required for CO assurance (Barakate et al., 2014; Capilla-Pérez et al., 2021; France et al., 2021). Contrarily, zebrafish TF SYCP1, is not required for the progression of DSBs into CO, but it has conserved the homologous alignment function (Imai et al., 2021).

Lastly, genes controlling meiotic progression (*TaAMI*) and meiotic entry (*TaCDC45*, *TaMEII*, *TaPS1*, *TaCYCA1*) were associated to wheat *ZYP1*. In line with these data, it is well known that in budding yeast *ZIP1* is involved in meiotic recombination checkpoint pathway (Acosta et al., 2011); in plants, such as barley and *Arabidopsis*, Barakate et al., (2014) and both Capilla-Pérez et al. (2021) and France et al. (2021), respectively, demonstrated the importance of *ZYP1* in timing the meiotic stages; in maize, *am1*-mutants showed transcriptional mis-regulation of several meiotic genes, including *ZYP1* (Nan et al., 2011).

Certainly, the role of wheat *ZYP1* in CO pathway and cell development predicted by this study still need to be investigated in the future. It would be interesting to understand whether *TaZYP1* may play a role in DSB initiation, or an additive role in wheat inter-homologous bias and in meiotic progress through the aid of cytological techniques.

## 4.4 Conclusions

In this work, a wheat gene co-expression network was used to identify CE protein(s) in wheat by targeting the TF *TaZYP1* homoeologues as hub genes. From this analysis, the function of TraesCS5A02G352100 and TraesCS2A02G364000, a predicted factor controlling chromatin changes via phosphorylation activity and a PCNA factor responsible of CO resolution, respectively, have not been explored yet, due to the lack of

mutant variants. The extensive literature on the role of phosphorylation in regulating SC assembly in most CE proteins, as well as on the meiotic recombination-related events, render both genes suitable meiotic candidates to be analysed ideally through the use of reverse genetics and cytology technologies.

In this preliminary study, cytological data have demonstrated that, while CC1 is not required for meiotic recombination in tetraploid wheat, CC2 and CC3 may be essential for Class I CO pathway, especially CC2/SWITCH1. Excitingly, triple-immunolocalization analysis with SC markers and SWITCH1 on Kronos WT male meiocyte categorically localised SWITCH1 at synapsis sites during meiotic prophase I. Future mutant analysis of *SWI1* may specifically confirm the mechanism of action or timing in polyploid wheat.

Since the growing positive impact of RNA-seq in many wheat research topics, primarily attributed to the decreased costs of large-scale gene expression profiling, shortly this methodology, by extending the sample size and including staged meiotic samples, may become more suitable for future analysis.

To conclude, these findings illustrated the tremendous benefits of the newly *in silico* prediction tools, increasingly convenient and widely applicable in routine laboratory-based analysis, and it promoted novel and intriguing questions about the role of wheat *ZYP1* in both meiotic and somatic pathways.

# **Chapter 5**

## **Application of chromosome-specific oligonucleotide probes for FISH karyotyping in *Triticum aestivum***

### **5.1 Introduction**

*Triticum aestivum* or common wheat is an allopolyploid species originated from two distinct interspecific hybridizations that resulted in the development of cultivated tetraploid *Triticum turgidum* ssp. *durum* and hexaploid *Triticum aestivum*, from three related diploid species (Marcussen et al., 2014). Wheat cultivars, as other member of Poaceae family, are worldwide utilised for food and feed production due to their outstanding adaptability to colonize a wide range of habitats and for possessing key agronomical traits (Feldman & Levy, 2005; Dubcovsky & Dvorak, 2007; FAOSTAT, 2021).

Besides its economic impact, wheat is also an excellent model organism for speciation and meiosis studies. Polyploidy in wheat is followed by diploidization, so that the chromosome pairs maintain a disomic inheritance. Generally, this event evolves rapidly after polyploidization, usually by extensive chromosomal rearrangements, but in wheat, diploidization arose via a genetic control mechanism (*Ph loci*) among the chromosome partners, which enhanced adaptation and fitness (Feldman and Levy, 2005; Dubcovsky and Dvorak, 2007). Intriguingly, humankind has been artificially manipulating this phenomenon (polyploidization), extending gene introgression with their wild relatives as a tool for breeding and crop improvement.

An efficient and powerful tool for understanding species-specific genomic architecture and organization, as well as to shed light on cross-species homology requires the construction of chromosome karyotypes, achievable through the use of fluorescent *in situ* hybridization (FISH) or genomic *in situ* hybridization (GISH) techniques (Lysak et al., 2001; Danilova et al., 2014; Tiwari et al., 2014). The first FISH karyotype of common wheat landrace Chinese Spring was developed using tandem repeats of ribosomal DNA

(rDNA) as probes, such as pAs1, pSc119.2, 5S rDNA, 45S rDNA, pTa535, pTa713 (Mukai et al., 1993). Later, other microsatellites enabled the identification of individual wheat chromosomes based on their distinctive FISH patterns (Komuro et al., 2013). Bacterial artificial chromosome (BAC)-based FISH analysis has been able to differentiate A, B, and D sub-genomes of common wheat (P. Zhang et al., 2004). FISH technology has also been widely used to analyze the chromosomes of hybrids between wheat and its wild relatives (Mirzaghaderi et al., 2014; Tang et al., 2014; Delgado et al., 2017).

In the past decade, in addition with the development of DNA sequencing and synthesis technologies, a new generation of FISH techniques, called oligonucleotide fluorescence *in situ* hybridization (oligo-FISH), which utilizes single-copy oligonucleotides (oligos) as FISH probes, has been established. Oligo-FISH probes provide certain advantages over conventional probes derived from rDNA, BAC sequences, or repetitive sequences (Han et al., 2015; do Vale Martins et al., 2019; Braz et al., 2020). For instance, whilst rDNA and other tandemly repeated sequences can generate strong FISH signals, they are not suitable for comparative cytogenetic studies because of their abundance and divergence among different species (Fukui et al., 1994; Badaeva et al., 1996; Kato et al., 2004). Thus, repetitive DNA probes are not suitable for detecting chromosome homoeology, unless applied in chromosome pairing analysis. Probes designed from large-insert genomic clones such as BACs generate strong background signals because of the mass of repetitive sequences in the genome, especially in those large complex plant genomes (Janda et al., 2006; Suzuki et al., 2012). In contrast, synthetic oligo probes derived from a single copy region of genome allow for hybridization to precisely defined targets without the interference of repetitive sequences, and are easy to maintain. Lastly, while oligo probes designed for tandem repeats (SSR or non-SSR) and genome-specific repetitive sequences of wheat developed for the non-denaturing FISH (ND-FISH) technology has the advantage of identifying chromosomes or specific segments in genome (Cuadrado et al., 2009; Cuadrado & Jouve, 2010; Fu et al., 2015; W. Jiang et al., 2021), the comparatively low cost to synthesize a pool of short oligo probes has provided a new and affordable method to develop chromosome-specific painting and enabled more application scenarios (Han et al., 2015; Jiang, 2019)

So far, successful applications of FISH by oligo painting have been reported for several commercial plant species, including cucumber (*Cucumis sativus*) (Han et al., 2015), strawberry (*Fragaria x ananassa*) (Qu et al., 2017), sugarcane (*Saccharum officinarum*) (Meng et al., 2018), potato (*Solanum tuberosum*) (Braz et al., 2018), banana (*Musa*) (Šimoníková et al., 2019), maize (*Zea mays*) (Albert et al., 2019; do Vale Martins et al., 2019), rice (*Oryza sativa*) (X. Liu et al., 2020), and poplar (*Populus*) (Xin et al., 2020). Recently, Song et al. (2020) built a chromosome 4D specific library for FISH painting based on the reference genome sequences of common wheat (IWGSC, 2018) and its D genome donor *Aegilops tauschii* (Luo et al., 2017).

In this chapter, the use of novel single-oligo FISH probes (MyTag), chromosome-specific for hexaploid *T. aestivum* ‘Chinese Spring’, was tested as promising and efficient tool to accurately karyotype wheat chromosomes among the three distinct sub-genomes, and ultimately, unveil the genetic mechanism underlying the behaviour of homoeologous chromosomes following its diploidization. The features of these specific probes would accelerate future study of meiotic gene candidate(s) implied in this process, among the others, wheat ASY1, which seems to be functionally active during homologous pairing, as showed and discussed in Chapter 3. At the same time, their first application with this project, required scrupulous adjustments to the sample type (mitotic chromosomes from meristematic roots) and methodology (FISH) compared to the conventional probes, e.g. tandem repeat rDNA probes used as control.

Intuitively, the preliminary phase was creating a good chromosome spread to allow the access and penetration of MyTag probes within individual sub-genome specific targets. Briefly, the technique to use for meristematic chromosome preparation in both tetraploid and hexaploid wheat was identified by critical comparative analysis of previous published methods (squashing, streaming, dropping), before a direct bench-top assay. Physical and chemical variables known to affect chromosome dispersion and morphological integrity were tailored in the form of alternative protocols, according to the ploidy level of the species. The results obtained from the three spreading methods were compared and discussed in paragraph 5.4.1 Subsequently, the favourable conditions for the FISH-based single copy oligo-probes method were developed following the analogous strategy:

literature search, experimental validation, data interpretation. An extensive discussion of the approach employed and suggestions on future improvements are reported herein.

## 5.2 Materials and methods

### 5.2.1 Plant materials and growth conditions

Root meristematic protoplasts were obtained from seedling in tetraploid *Triticum turgidum* cv. Kronos and hexaploid *Triticum aestivum* cv. Cadenza and landrace Chinese Spring. Only healthy seeds were considered in this experiment. The method used to check for seed viability was the water test. Simply, seeds were placed in a container with tap water for 15 minutes. Seeds that sank were still viable, whereas seeds that floated (due to lack of viable embryos or nutrient stores) were discarded. Up to 20 seeds were germinated on two layers of moist filter paper in a Petri dish under dark conditions for 2 days at 22-24°C. Primary roots with length of 0.8-1.0 cm in Kronos, 1.0-1.5 cm in Cadenza and 0.8-2.5 cm in Chinese Spring were cut off by using a fine forceps.

### 5.2.2 Chromosome preparation for squashing technique

**Metaphase arrest:** Meristematic tissues were treated with ice-cold water by immersing maximum 20 roots in a 25 ml glass bottle containing cold tap water into crushed ice-water for 20 (Kronos), 24 (Cadenza) or 25 (Chinese Spring) hours to synchronize and arrest the metaphases.

**Fixation:** Water was replaced by ethanol: acetic acid (3:1) fixative to fix the roots at room temperature for 2 days. Roots were stored in a freshly prepared ethanol: acetic acid (3:1) fixative at 4 °C until use. Using forceps, 10-20 roots were placed on filter paper to remove the fixative, transferred into a watch glass and washed with 0.01 M citrate buffer (0.01 M citric acid + 0.01 M sodium citrate, pH 4.8) twice for 5 min.

**Enzyme treatment:** Before the enzyme treatment, the root tips were washed in 0.01 M citrate buffer three times for 5 minutes each. After fixation, meristematic tissues became whiter than the remaining part of the roots. Based upon this change, roots were easily dissected to remove undesired non-meristematic tissue using a razor blade. Up to 20 root tips were incubated in 1 ml enzyme mixture composed by 2% cellulose (w/v) (Cellulase

Onozuka R-10, 10,000 units g/L; Duechafa Biochemie) and 1% pectolyase (w/v) (Pectolysase Y-23,>1,000 units per gram, MP Biomedicals) diluted in 0.01 M citrate buffer at 37 °C for about 65 (Kronos), 70 (Cadenza) or 75 min (Chinese Spring) to soften the plant tissue in a watch glass. The enzymatic digestion time was adjusted according to the root diameter, other than the species. The enzyme mixture was stored at -20 °C and reused up to three times.

**Post-enzyme treatment:** The enzyme solution was carefully discarded with a narrow bore plastic pipette and the root tips were washed with 3 ml 0.01 M citrate buffer twice. Individual digested meristems were transferred with a fine Pasteur pipette onto a clean polysine slide, ensuring to remove the excess of enzyme buffer. A drop of 60% glacial acetic acid (10µl) was added onto the root tip. As sample, individual tip meristem was rapidly macerated with a tungsten needle and covered with 18 x 18 mm cover glass, lightly tapping (squashed) to allow chromosomes to spread. The slides were then sit on hotplate at 50°C for 1 minute to clear the cytoplasm. Next, the slide was inverted and pressed gently onto a double layer of tissue paper, thereby the quality of the chromosome spread was examined using a phase-contrast microscope. If all chromosome complements appeared intact, well-condensed, not overlapped and without any cytoplasm, then sample was considered suitable for FISH. In case of insufficient digestion of the meristems, the sample were returned to the incubation step and the digestion was extended until completion. Lastly, good slides were frozen thoroughly by dipping in liquid nitrogen for few seconds, the cover glass was flicked off with a blade and the preparation was slowly air-dried at room temperature overnight before storing them in a slide box at -20 °C until required.

### 5.2.3 Chromosome preparation for dropping technique (Rodríguez-Domínguez et al., 2019)

**Metaphase arrest, fixation, enzyme treatment:** The preparation of cell suspension for dropping technique followed the same procedure of the squashing method until the enzyme digestion (see above paragraph 5.2.2).

**Post-enzyme treatment:** Here, tip meristems were subjected to a further post-enzymatic treatment. In this case, tip meristems were rapidly placed in 96% ethanol solution and macerated by pipetting in a watch glass until creating a protoplast suspension.

Subsequently, the solution of protoplasts was transferred in a clean 1.5 ml microcentrifuge tube and washed with 96% ethanol three times at maximum speed for five minutes each in a microcentrifuge. The pellet was re-suspended and then centrifuged in 60% glacial acetic acid. Finally, the cell suspension was cleared by adding 20–100 µl of fix 1:3 (ethanol:acetic acid) depending on cell concentration. Approximately 7 µl of cell suspension was dropped onto a clean polysine slide at 20 cm distance under a vertical laminar flow hood to facilitate the spreading. The protoplasts can be stored in solution at –20° C. Lastly, good slides were stored in a dry place at room temperature until use.

#### 5.2.4 Chromosome preparation for streaming technique (Aliyeva-Schnorr et al., 2015)

**Metaphase arrest and fixation:** The preparation of mitotic chromosomes for stream technique was subjected to identical metaphase arrest and fixation procedures as in squashing and dropping techniques describes previously (see paragraphs 5.2.2 and 5.2.3).

**Enzyme treatment:** Here the enzyme mixture contained 0.7% cellulase (Onozuka R-10, Duechela Biochemie), 0.7% cellulose (Sigma-Aldrich), 1% pectolyase (Y23, MP Biomedicals) and 1% cytohelicase (Sigma-Aldrich) diluted in 0.01 M citrate buffer.

**Post-enzyme treatment:** The enzyme was removed by pipetting and the root tips were washed with 5 ml 0.01 M citrate buffer twice to replace the residual enzyme. Followed a wash step in 1 ml of 96% ethanol in the same watch glass. Ethanol was replaced with freshly prepared fixative (1:3 ethanol:acetic acid), and root meristems were centrifuge at max speed twice. After that, supernatant was discarded and pellet was re-suspended and transferred to a clean 2 ml micro-centrifuge tube. Pellet was further disintegrated by pipetting vigorously throughout the column. According to the concentration of cell suspension, 10-15 µl fixative per root tip was added. At this point, sufficient polysine slides were immerged in ice-cold tap water in the fridge for 30 min. Meanwhile, two layers of water-soaked paper tissue were placed on a hot plate at 50 °C. Once the hot plate reached the desired temperature, cooled slides were placed on the top of the moist paper tissue and 7-10 µl of cell suspension were dropped from a distance of 20 cm. Immediately, 10 µl of acetic acid-ethanol mixture were pipetted on the same place of cell suspension, leaving the slides on the hot plate for additional 2 min. Slides were finally dried out on

the hot plate in absence of wet tissues for 1 min and checked for the quality of the chromosome spread by using a phase-contrast microscope. Good slides were stored in 96% ethanol in a Coplin jar at -20 °C.

### 5.2.5 Evaluation of factors influencing the quality of mitotic chromosome spread in hexaploid *T. aestivum* landrace Chinese Spring

To obtain high quality metaphase chromosomes from hexaploid *T. aestivum* ‘Chinese Spring’ root tips, the three spreading techniques commonly used for wheat or its closer relatives described in paragraphs 5.2.2, 5.2.3 and 5.2.4 were evaluated for their efficiency. Mitotic metaphase chromosomes derived from hexaploid *T. aestivum* ‘Chinese Spring’ root tips were prepared according to the three spreading techniques (dropping, streaming, squashing) described in the previous paragraphs of this chapter. The outcomes were compared using at least 20 roots for each slide preparation and 50 slides each method. All samples were observed under a phase-contrast microscope. Four distinct phenotypes were detected throughout the experimental procedures, which were used as standard to evaluate the condition of metaphase cells and elect the optimal preparation to use for downstream experiments, FISH in this case. The “standard” phenotypes were classified as phenotype 1, phenotype 2, phenotype 3 and phenotype 4, according their percentage of overlapped chromosomes, number of metaphase cells and presence/absence of cytoplasm (Figure 5.1). More specifically, fixed meristematic cells with completely overlapping chromosomes with a frequency of less than 5 mitotic metaphases I and abundant cytoplasm, were classified as phenotype 1; cells containing less than 5 mitotic metaphases I, abundant cytoplasm, but 50% overlapping chromosomes were defined as phenotype 2; cells having 25% overlapping chromosomes, more than 5 mitotic metaphases I, and free from cytoplasm, were categorized as phenotype 3; lastly, cells containing only 10% overlapping chromosomes, more than 5 mitotic metaphases I, and dissolved/hydrolyzed cytoplasm belonged to phenotype 4 and were considered the most suitable for FISH assay.

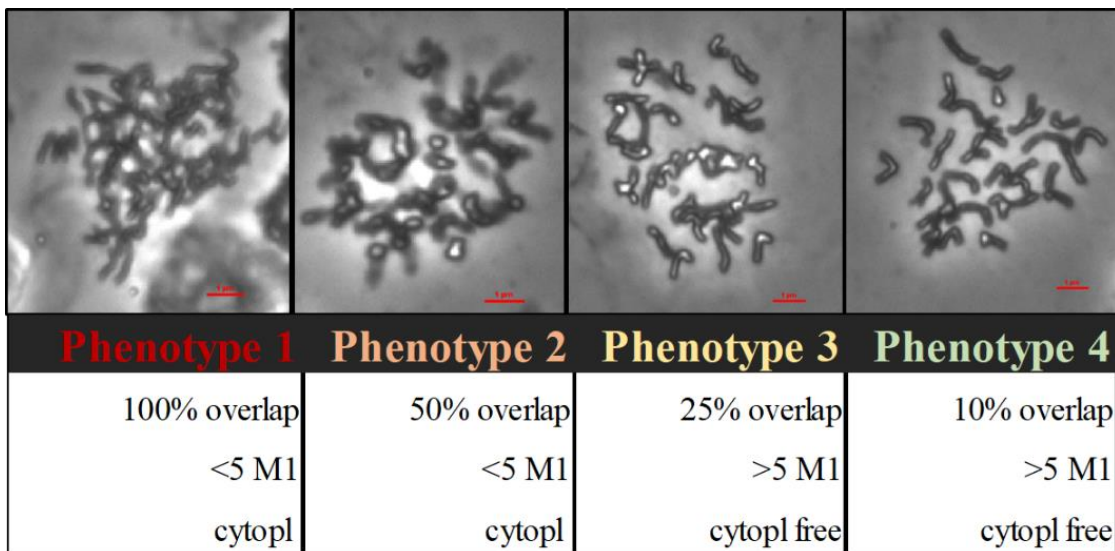


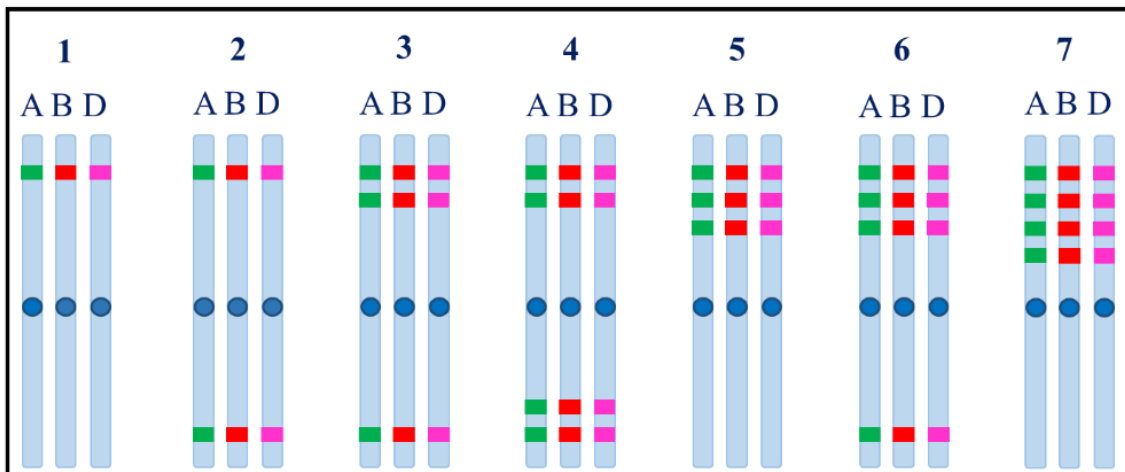
**Figure 5.1 Comparative evaluation of using three chromosome spreading techniques (dropping, streaming, squashing) in hexaploid *T. aestivum* landrace Chinese Spring.** Four metaphase phenotypes of Chinese Spring was evaluated qualitatively. A total of 50 slides per spreading technique were used. The images show the distinct phenotypes observed under phase-contrast microscope with the corresponding descriptions below (percentage of overlapped chromosomes, number of metaphase cells and presence/absence of cytoplasm). Scale bar = 1  $\mu$ m.

### 5.2.6 FISH procedure

**Probes:** Figure 5.2 shows the different oligodeoxyribonucleotide probes used for FISH analysis in hexaploid *T. aestivum* cv. Chinese Spring, control (repetitive rDNA) and MyTag, both directly labeled with fluorophores and the chromosome indexing of MyTag oligo probes. Alexa 488-labeled probes included repetitive sequence Oligo-pSc119.2-2 (Tang et al., 2014) and MyTag (B); Oligo-pTa794-1, a *Bam*HI fragment of the 5S rDNA, that has a 120-bp coding sequence for the 5S rRNA gene and the intergenic spacers isolated from *Triticum aestivum* L. (Gerlach & Dyer, 1980) and MyTag (B) were labeled with Texas Red and Atto 550, respectively; lastly, Oligo-pTa71-2, a 9-kb plasmid fragment of common wheat containing the coding sequences for the 18S, 5.8S, and 25S rRNA genes and the intergenic spacer sequences of *Triticum aestivum* (Gerlach & Bedbrook, 1979) and MyTag (D) were both labeled in Cy5. MyTag oligo probes were synthesized and supplied by Daicel Arbor Biosciences Company (USA), while control probes were available at Higgins' Lab. The 43-oligonucleotide sequences of MyTag (A), (B) and (D) and their GC contents and homology level were not provided, while the oligonucleotide sequences of repetitive rDNA probes were the following:

- Oligo-pSc119.2-2 5'-[488] TTCCA CGATT GACGA TTCCG GGGGT GCGTT TACGT GTCCG TCGTC -3'
- Oligo-pTa794-1 5'-[Tx Red] YRGA GTTC TGAT GGGA TCCG GTGC TTTA GTGY TGST ATGA TCGCA -3'
- Oligo-pTa71-2 5'-[Cy5] GGGCA AAACC ACGTA CGTGG CACAC GCCGC GTA -3'

Sub-genomes	Probes (fluorophore)	
	Control	MyTag
A	Oligo-pTa794-1 (Texas Red)	A (Alexa 488)
B	Oligo-pSc119.2-2 (488)	B (Atto 550)
D	Oligo-pTa71-2 (647)	D (Atto 647N)

**Figure 5.2 Oligo-probes used for FISH assay and MyTag oligo probes signal patterns in hexaploid *T. aestivum* ‘Chinese Spring’.** Upper panel: control oligo probes includes the tandem repeat rDNA probes Oligo-pTa794-1, Oligo-pSc119.2-2 and Oligo-pTa71-2; MyTag includes the single-oligo probes A, B and D. Fluorophore labels are indicated in brackets. Lower panel: predicted locations of MyTag oligo-FISH signals on 21 homoeologous chromosomes of Chinese Spring. Oligos were selected from a total of 63 chromosomal regions (21 green, 21 red and 21 yellow). The 21 homoeologous chromosomes can be distinguished from each other based on number and location of the green/red/magenta signals.

The selection and dosage of reagents used to develop a novel FISH protocol suitable for MyTag oligo probes are listed in Table 5.1.

FISH conditions		Protocol X
Pre-hybridization	<b>Sample</b>	Meristematic root tips
	<b>Fixation</b>	EtOH:Acetic-acid 3:1 for 48h
	<b>Preparation</b>	Dropping
	<b>Permeabilization</b>	HCl (0.01 M), 1 min + RNase (100µg/ml) 37°C, 60 min
	<b>Proteinase</b>	Pepsine (0.5 µg/ml), 10 min
	<b>Post-fixation</b>	Formaldehyde (4%), 10 min
Hybridization	<b>Probe type</b>	43 nucleotides (oligo-nucleotides)
	<b>Reagents (based on stringency)</b>	Probes (10 - 15 pmol) Formamide (70 - 50 - 30 - 0%) Dextran sulfate (10%) SSC (2 - 6X) Salmon sperm DNA (1 µg/µl) EDTA (10 mM) 10% SDS glycerol (18%) or Q5 enhancer
	<b>Denaturation (°C)</b>	62 - 85 for 3 -10 min or sequential
	<b>Incubation (°C)</b>	37 or 42
	<b>Time (hours)</b>	2h or Overnight
	<b>Initial washes</b>	<b>High stringency:</b> Formamide (50 - 25 - 0%), SSC (0.1X) 40°C, 3 x 5 min <b>Low stringency:</b> SSC (4 - 2X) RT, 3 x 5 min
	<b>Final washes</b>	<b>High stringency:</b> SSC (0.1X)/Tween 20 (0.2%) RT, 2 x 2 - 5 min <b>Low stringency:</b> SSC (2 - 4X)/Tween 20 (0.2%) RT, 2 x 2- 5 min
Post-hybridization		

**Table 5.1 Representative panel of a starting FISH protocol.** The initial FISH protocol was used to optimize MyTag oligo-probes hybridization with *T. aestivum* ‘Chinese Spring’ sub-genomes.

**Pre-hybridization:** Before carrying out FISH, chromosome preparations were meticulously evaluated for their morphological integrity and permeability conditions under a phase-contrast microscope. In case of excess of cytoplasm, slides were first treated with 200 µl of 100 µg/ml DNase-free RNase A (Roche) in 2X SSC (1X SSC is 0.15M NaCl, 0.0015M sodium citrate, pH 7.4), covered with a plastic cover slip (24 x 40 mm) and incubated in humid chamber at 37°C for 60 minutes to remove any extraneous RNA which could interfere with probes. After that, slides were washed in 0.01M hydrochloric acid for 1 minute at RT, treated with 200 µl of 0.5 µg/ml pepsin solution and incubated in humid chamber at 37°C for 5 minutes. The reaction was stopped by washing the slides in distilled water for 1 minute followed by a wash in 2X SSC at RT for 5 minutes. After acid wash, slides were post-fixed in freshly depolymerized 4% (w/v) paraformaldehyde in water for 10 min and then dehydrated in a Coplin jar containing 50 ml of 70%, 80%, 96% ethanol series for 2 minutes each. The slides were air-dried in vertical position before denaturation.

**Hybridization:** The selection and concentration of the reagents to add into the denaturation mixture were conveniently adjusted based on stringency conditions. For optimization purposes, four alternative concentrations of formamide (70%, 50%, 30% or

0%) and three different concentrations of buffer SSC (2X, 4X or 6X), were tested. DNA competitors, such as 1 µg/µl salmon sperm ssDNA (Abcam) and 10% dextran sulfate (Sigma-Aldrich) were also included to the denaturation mixture to increase the binding efficiency. The use of 10% sodium dodecyl sulfate (SDS), 10 mM EDTA and/or 1X Q5 enhancer for PCR reaction (NEB) were also tested. As probe concentration, 10-15 pmol of each MyTag (as recommended by the Company) and 50 ng of each control (repetitive rDNA) probe were used. Chromosomes were denatured in three different ways: 1) by dropping 40 µl of denaturation mixture onto the preparation, subsequently covered with a 24 x 30 mm plastic coverslip and incubated on a PCR machine equipped with a metal plate from 62 to 85°C for 3 to 10 minutes; 2) by heating the slides alone at the intended temperature, without pre-treatment with the denaturation mix; 3) non-denaturing, in which chromosome preparations were incubated with 30 µl of hybridization buffer containing 10 pmol of each probe (individually) in 2X SSC at RT in a humidity chamber for 2 hours. Except for non-denaturing FISH, DNA reannealing were prevented by immediately transferring the slides in a Coplin jar containing 50 ml of ice-cold 2X SSC or autoclaved ice-cold distilled water for 4 minutes and the plastic coverslip was gently removed. After that, 40 µl of probe solution containing probes, dextran sulfate and SSC buffer (when pretreat the slide with formamide) or probes, dextran sulfate, SSC buffer and formamide (if slides were denatured alone), were dropped onto the chromosome spread, covered with a 24 x 30 mm plastic coverslip. The hybridization occurred in a humid chamber at 37° or 42°C for 2 hours or overnight.

**Post-hybridization treatment:** The detention followed the stringency washes. Both high and low stringency conditions were tested for the post-hybridization washes. Slides were initially agitated three times in Coplin jars for 5 min with formamide (50 - 25 - 0%) in SSC (0.1X) 40°C, or SSC (4X or 2X) at RT. The slides were then rinsed for 5 min in 4X SSC/0.2% Tween 20 at RT. Before staining the chromosomal DNA with 4', 6-diamidino-2-phenylindole (DAPI), slides were lastly rinsed twice for 2 to 5 min in 0.1X SSC/0.2% Tween20 at RT, or (2 - 4)X SSC /0.2% Tween 20 at RT. Finally, slides were air-dried and mounted in antifade solution (Vectashield), covered with a 24 x 40 mm cover glass. In ND-FISH conditions (S. Tang et al., 2018), after the hybridization, slides were immersed in 4X SSC/0.2% Tween 20 and agitated for 10 min at RT, 37° or 42°C. The detection of the probes was undertaken as described in the paragraph below.

**Fluorescence microscopy and imaging:** For FISH experiments, slides containing the best five metaphases were examined within 24 h of hybridization using a Nikon Ni-E fluorescence microscope equipped with appropriate filters. The selection of filter depends on the fluorochrome used for probe labelling. Images were captured and processed for optimal contrast and brightness adjustments using NIS elements software.

## 5.3 Results

### 5.3.1 Comparative analysis of chromosome dispersion methodologies in tetraploid and hexaploid *Triticum*

To allow efficient probe penetration, a good chromosome spread needs to be prepared. A workflow for optimising the Oligo-FISH experiments is depicted in Figure 5.3.

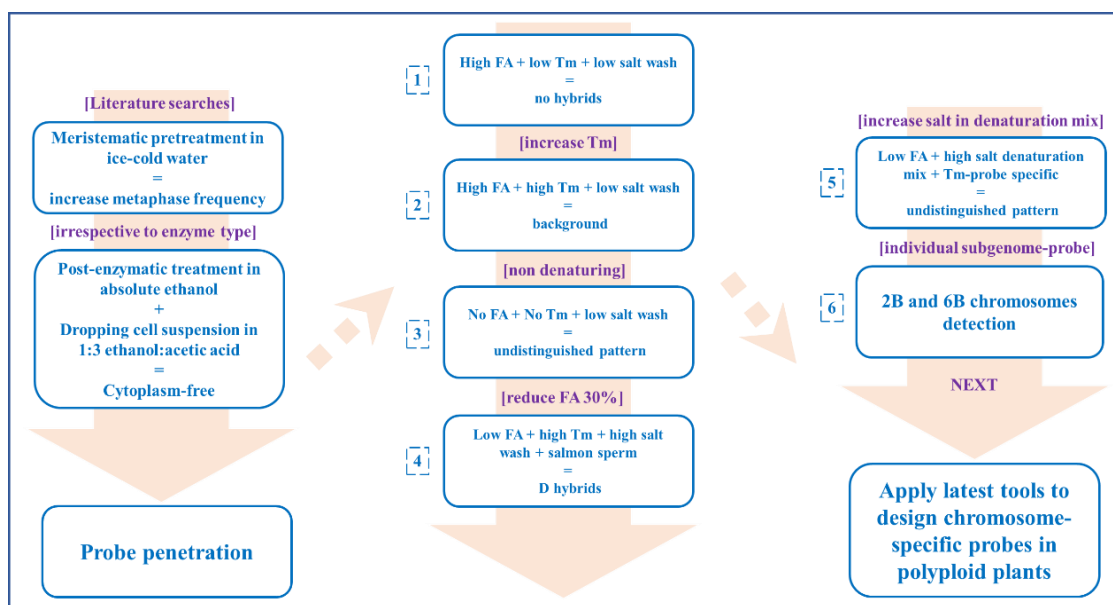


**Figure 5.3 Workflow of the entire procedure used for testing *de novo* MyTag oligo probes in mitotic chromosomes of *T. aestivum* ‘Chinese Spring’.** The preconditions for achieve full probe penetration, the modifications during the development of various FISH protocols and the future improvements in oligo probe design approach are illustrated. Square brackets report the starting points of the consecutive steps. FA = formamide, T<sub>m</sub> = melting temperature.

Chromosome spreads and FISH assays were carried out on hexaploid *T. aestivum* ‘Chinese Spring’ as the MyTag probes were designed using its genomic sequence. Based upon the phenotypes observed, a significantly greater chromosome preparation for

Chinese Spring was obtained using dropping technique than that produced by squashing and streaming methods (Figure 5.4 b). The procedure used to drop the cell suspension produced more than five mitotic metaphases with high quality chromosome morphology, without any trace of cytoplasm within the cell and widely dispersed chromosomes (see ‘Phenotype 4’ in Figure 5.4 a), in 50% of cases out of 50 slides analyzed (Figure 5.4), enabling easy chromosome counting. Only 20% of phenotype 4 was observed with streaming method and none with squashing. The full datasets of this analysis is stored in Appendix (Table S13).

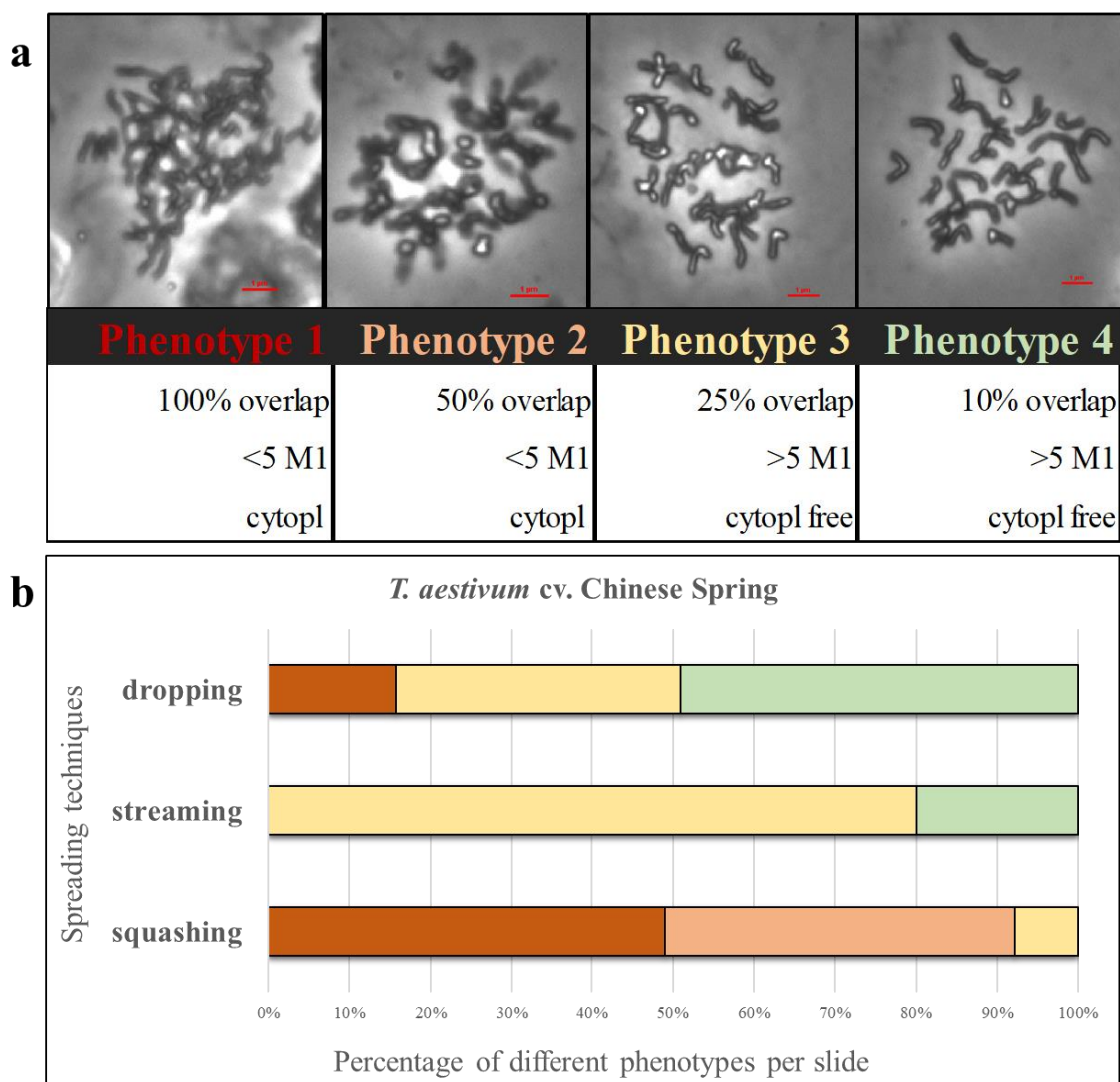


**Figure 5.4 Qualitative evaluation of three spreading techniques (dropping, streaming, squashing) tested on mitotic chromosomes of *T. aestivum* ‘Chinese Spring’.** a) Phenotypes detected and descriptions. b) Bar chart illustrates the percentage of the phenotypes detected per slides ( $n = 150$ , of which 50 for each spreading technique). Referred to Figure 5.1 in paragraph 5.2.4 for the phenotype descriptions. Scale bar = 1  $\mu\text{m}$ .

Simultaneously, a series of physical and chemical variables influencing chromosome dispersion and morphological integrity were experimentally tested according to the ploidy level of the species. From the analysis emerged that the duration of enzyme treatment was species-dependent (65 min in Kronos, 70 min in Cadenza and 75 min in Chinese Spring) and also relied on the time span of root fixation in ethanol/acetic acid and the size of the roots: the longer the roots were stored in the fixative (at 4 °C), the longer it takes to be digested. Moreover, insufficiently digested root material was usually arduous and time-consuming to disintegrate following the enzyme treatment, resulting most of time in waste of materials. In this respect, the best chromosome preparation was achieved with the use of 96% ethanol during the post-enzymatic treatment step. The final protocol is summarized in Table 5.2. An extensive discussion about these and other findings is in paragraph 5.4.

<i>T. aestivum</i> cultivars (ploidy)	Enzyme treatment	Incubation temperature (°C)	Incubation time (min)	Post-enzyme treatment	Spreading method
Kronos (4n)	2% CO + 1% PY	37	65	96% EtOH	dropping
Cadenza (6n)		37	72		
Chinese Spring (6n)		37	75		

**Table 5.2 Final protocol for mitotic chromosome preparation from meristematic tissue of three polyploid wheat genotypes.** Enzyme mixture, post-enzyme treatment and spreading technique are reported. CO = Cellulose Onozura R-10, PY = Pectolyase Y-23.

### 5.3.2 Optimization of FISH protocol for MyTag oligo-probes

In the present study, a series of FISH protocols were developed using MyTag oligo-probes applied on mitotic chromosomes of *T. aestivum* ‘Chinese Spring’, prepared with the dropping technique as described above. The signal patterns of repetitive rDNA probes (Oligo-pSc119.2-2, Oligo-pTa794-1 and Oligo-pTa71-2) were separately used as reference for the recognition of individual wheat chromosomes. The corresponding results from each optimized FISH protocol are described below.

FISH conditions evaluated for Protocol 1 are summarized in Figure 5.5 a. Pre-treated mitotic wheat chromosomes in pepsin used to digest residual cytoplasm from the meristematic protoplasts was effective at a final concentration of 0.5 µg/ml for 10 minutes. Chromosomes denaturation occurred at 65°C for 4 minutes treating the slides

with 70% formamide. A high concentration of formamide along with a low denaturation temperature and duration were sufficient for denaturing control chromosomes and enabling recognition with repetitive DNA probes, detected under the highest stringency conditions (Figure 5.5 b1). However, this was not enough for MyTag oligo-probes (Figure 5.5 b2), as suggested by the total absence of hybrids in sample treated with MyTag subjected to equal conditions. This initial attempt led to contemplate the option of increasing the temperature necessary for chromosome denaturation (Figure 5.5 a).

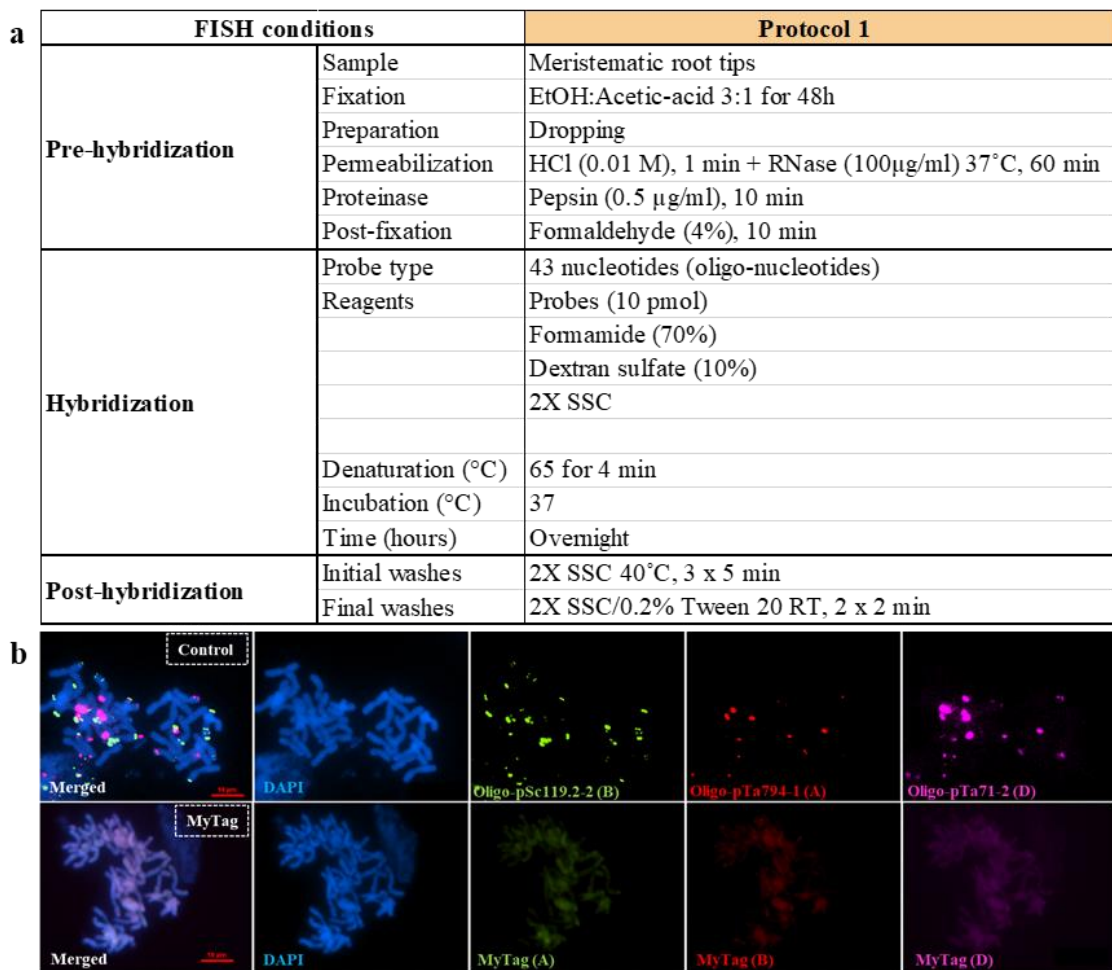


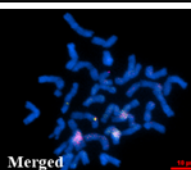
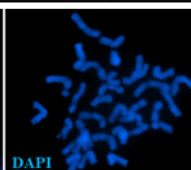
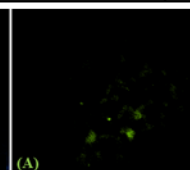
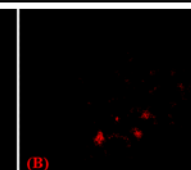
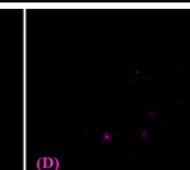
**Figure 5.5 FISH-Protocol 1 for detecting *T. aestivum* ‘ Chinese Spring’ homoeologous chromosomes from meristematic tissue using labeled synthetic oligo-probes.** a) summary of FISH conditions tested. b) FISH results: upper panel, first image on the left = merged fluorescent signals of control (repetitive rDNA) oligo probes; lower panel, first image on the left = merged fluorescent signals of MyTag oligo-probes. Oligo-pSc119.2 (green) and MyTag (B) (red) mark B genome; Oligo-pTa794-1 (red) and MyTag (A) (green) mark A genome; Oligo-pTa71-2 (magenta) and MyTag (D) (magenta) mark D genome. Chromosomal DNA is counter-stained in DAPI (blue). Scale bar = 10 µm.

Results derived from FISH conditions selected for Protocol 2 are recapitulated in Figure 5.6 a. Similar to protocol 1, hybridization was successfully achieved in control sample (Figure 5.6 b1), despite the rise of denaturation temperature, but it failed in sample subjected to MyTag oligo-probes (Figure 5.6 b2). Under these conditions, hybridization was possibly nonspecific, as indicated from the background visible in DAPI stained image (Figure 5.6 b2). Thus, the consecutive adjustment still entailed the denaturation step and focused exclusively on MyTag oligo probes requirements. ND-FISH approach in wheat was early evaluated and positively correlated to the wheat genome (Fu et al., 2015; Tang et al., 2018; Xin et al., 2020), therefore, it was decided to test the latest protocol for non-denaturing hybridization (Tang et al., 2018) applied in the same hexaploid wheat genotype (Chinese Spring) used in this work.

FISH conditions		Protocol 2
Pre-hybridization	Sample	Meristematic root tips
	Fixation	EtOH:Acetic-acid 3:1 for 48h
	Preparation	Dropping
Hybridization	Probe type	43 nucleotides (oligo-nucleotides)
	Reagents	Probes (10 pmol) Formamide (70%) Dextran sulfate (10%)
		2X SSC
	Denaturation (°C)	75 for 4 min
	Incubation (°C)	37
Post-hybridization	Time (hours)	Overnight
	Initial washes	2X SSC 40°C, 3 x 5 min
	Final washes	2X SSC/0.2% Tween 20 RT, 2 x 2 min
<b>b</b>		
<b>Figure 5.6 FISH-Protocol 2 for detecting <i>T. aestivum</i> ‘Chinese Spring’ homoeologous chromosomes from meristematic tissue using labeled synthetic oligo-probes.</b> a) summary of FISH conditions tested. b) FISH results: upper panel, first image on the left = merged fluorescent signals of control (repetitive rDNA) oligo probes; lower panel, first image on the left = merged fluorescent signals of MyTag oligo-probes. Oligo-pSc119.2 (green) and MyTag (B) (red) mark		

B genome; Oligo-pTa794-1 (red) and MyTag (A) (green) mark A genome; Oligo-pTa71-2 (magenta) and MyTag (D) (magenta) mark D genome. Chromosomal DNA is counter-stained in DAPI (blue). Scale bar = 10 µm.

The outcomes derived from ND-FISH Protocol 3 differed from the previous study, despite identical procedure and species were utilized (Figure 5.7 a). In absence of denaturation, hybridization temperature and salt concentration were re-adjusted to create the favorable hybridization conditions with enough stringency to exclude non-specific labeling. Typically, short oligonucleotide probes (20–50 nucleotides) require lower hybridization temperatures, e.g. 37°C (Fontenete et al., 2016; Young et al., 2020). Nevertheless, no sign of hybridization was observed at this temperature. Higher hybridization temperature (42°C) and high stringent condition were later performed to prevent subgenome specific-oligo probes from hybridizing with non-related genome chromosomes (e.g. MyTag A would not bind on B or D genomes). In this context, few, nonspecific hybrids were detected, perhaps non genuine, since the presence of overlapped background among the fluorescent signals (Figure 5.7 b), suggesting that these conditions were not suitable to ensure all short MyTag probes to completely occupy available targets.

a	FISH conditions	Protocol 3 (Tang et al., 2018)
Pre-hybridization	Sample	Meristematic root tips
	Fixation	EtOH:Acetic-acid 3:1 for 48h
	Preparation	Dropping
Hybridization	Probe type	43 nucleotides (oligo-nucleotides)
	Reagents	Probes (10 pmol) 2X SSC
	Denaturation (°C)	
Post-hybridization	Incubation (°C)	42
	Time (hours)	2h or overnight
Post-hybridization	Initial washes	2X SSC 42°C, 3 x 5 min
	Final washes	2X SSC/0.2% Tween 20 RT, 2 x 2 min
b		Merged
		DAPI
		(A)
		(B)
		(D)

**Figure 5.7 FISH-Protocol 3 for detecting *T. aestivum* ‘Chinese Spring’ homoeologous chromosomes from meristematic tissue using labeled synthetic oligo-probes.** a) summary of FISH conditions tested. b) FISH results. First image on the left = merged fluorescent signals of MyTag oligo-probes. MyTag (A) (green) mark A genome, MyTag (B) (red) mark B genome,

MyTag (D) (magenta) mark D genome. Chromosomal DNA is counter-stained in DAPI (blue). Scale bar = 10  $\mu$ m.

Taking in account that minor differences were observed in absence of DNA stabilizer (formamide) and kinetic energy (temperature), the subsequent modifications were addressed to the component of the denaturation mixture. It is widely known that the inclusion of DNA competitors, such as salmon sperm DNA, and chelating agent, like ethylenediaminetetraacetic acid (EDTA) and SDS in the hybridization buffer, saturates nonspecific binding sites for probes, hence reduces signal-to-noise ratio caused by the non-specific adsorption of fluorescent oligonucleotide probes (reviewed by Young et al., 2020). Moreover, chromosomes, instead of being pre-treated with formamide (except with ND-FISH protocol), now reduced to 30%, were heated alone at high temperature (75°C), while MyTag oligo-probes were incorporated to the denaturation mixture and denatured at 90°C, added 4 minutes later the starting of the heat treatment. Consequently, post-hybridization washes occurred at low stringency.

Irrespective of probe denaturation at 90°C or not (thought to abolish the formation of secondary structure), reagents and conditions established in Protocol 4 allowed to detect MyTag oligo-probes on D genome chromosomes for the first time (Figure 5.8 b), suggesting that post-hybridization washing in 4X SSC/0.2% Tween 20 at RT effectively promoted the dissociation of most of D probes from non-specific targets, without increasing the background (Figure 5.8 b), yet it was not possible to discriminate a clear fluorescent patterns of chromosomes. Simultaneously, there were fewer, if any, oligo-probes signals on A genome (Figure 5.8 b). Therefore, the use of 4X SSC/0.2% Tween 20 at RT as post-hybridization washes was maintained in the next protocol, while the range of denaturing temperature was reviewed. Additionally, assuming that high temperature may have dissociated the short oligo probes during the washing, an alternative option to ensure that only the specific and stable hybrids remain at the end of washing may be increasing the salt concentration within the denaturation buffer. Hence, regarding the loss of A oligo probe binding under Protocol 4 conditions, the hypothesis of selective hybridization (temperature-specific) of the individual probes was also examined in Protocol 5 (Figure 5.9 a).

FISH conditions		Protocol 4
Pre-hybridization	Sample	Meristematic root tips
	Fixation	EtOH:Acetic-acid 3:1 for 48h
	Preparation	Dropping
Hybridization	Probe type	43 nucleotides (oligo-nucleotides)
	Reagents	Probes (10 pmol)
		Formamide (30%)
		Dextran sulfate (10%)
		Salmon sperm DNA (1 µg/µl)
		10mM EDTA
		10% SDS
		2X SSC
	Denaturation (°C)	90 (probes) and 75 (chromosomes) for 4 min
Post-hybridization	Incubation (°C)	37
	Time (hours)	16 - 24
Post-hybridization	Initial washes	4X SSC/0.2% Tween 20 RT, 2 x 10 min
	Final washes	or formamide (50 or 25%)/0.1X SSC 42°C, 2 x 10 min

b

**Figure 5.8 FISH-Protocol 4 for detecting *T. aestivum* ‘Chinese Spring’ homoeologous chromosomes from meristematic tissue using labeled synthetic oligo-probes.** a) summary of FISH conditions tested. b) FISH results. First image on the left = merged fluorescent signals of MyTag oligo-probes. MyTag (A) (green) mark A genome, MyTag (B) (red) mark B genome, MyTag (D) (magenta) mark D genome. Chromosomal DNA is counter-stained in DAPI (blue). Scale bar = 10 µm.

Results derived from FISH conditions selected for Protocol 5 are summarized in Figure 5.9 a. Two denaturation temperatures (65°C for A probe and 85°C for B and D probes) were tested both sequentially (same sample) and in separate samples, to verify the specificity with each probe (Figure 5.9 b). Three different salt concentrations in hybridization buffer was tested (SSC 4X, 5X and 6X), however, neither of them improved the final results. Larger amount of probe concentration (15 pmol) or longer incubation also did not result in any improvement (Figure 5.9 b). Alternatively, excluding the washing steps as responsible of the probe instability, the propensity to form intramolecular secondary structure was hypothesized being the major influencer of hybridization sensitivity. It may be the case that parts of the target sequences are likely to be inaccessible to intermolecular hybridization due to the formation of stable secondary structure in the probes. To overcome this possible scenario, the idea was to add the Q5

Enhancer buffer to the hybridization buffer, a component typically used for PCR reactions (NEB) to improve specificity and/or yield in particularly difficult or high GC amplicons ( $\geq 65\%$ ). However, in this study, the supplementary use of Q5 Enhancer buffer in the hybridization mix did not significantly change the probe penetration, as shown from the increasing background (Figure 5.9).

**a**

FISH conditions		Protocol 5
Pre-hybridization	Sample	Meristematic root tips
	Fixation	EtOH:Acetic-acid 3:1 for 48h
	Preparation	Dropping
Hybridization	Probe type	43 nucleotides (oligo-nucleotides)
	Reagents	Probes (15 pmol) Dextran sulfate (10%) Formamide (30%) Salmon sperm DNA (1 $\mu\text{g}/\mu\text{l}$ )
		4X SSC Q5 enhancer
	Denaturation ( $^{\circ}\text{C}$ )	65 and 85 (chromosomes) for 4 min
	Incubation ( $^{\circ}\text{C}$ )	37
	Time (hours)	16 - 24
	Initial washes	4X SSC 37 $^{\circ}\text{C}$ , 3 x 5 min; 2X SSC RT, 5 min
	Final washes	2X SSC/0.1% Tween 20 RT, 2 x 5 min
<b>b</b>	65 $^{\circ}\text{C}$	(A) (green) (B) (red) (D) (magenta)
	Merged DAPI	
85 $^{\circ}\text{C}$	(A) (green) (B) (red) (D) (magenta)	
	Merged DAPI	

**Figure 5.9 FISH-Protocol 5 for detecting *T. aestivum* ‘Chinese Spring’ homoeologous chromosomes from meristematic tissue using labeled synthetic oligo-probes.** a) summary of FISH conditions tested. b) FISH results: upper panel, denaturation of MyTag (A) probe at 65 $^{\circ}\text{C}$ ; lower panel, denaturation of MyTag (B) and (D) probe at 85 $^{\circ}\text{C}$ . In both panels, first image on the left = merged fluorescent signals of MyTag oligo-probes. MyTag (A) (green) mark A genome, MyTag (B) (red) mark B genome, MyTag (D) (magenta) mark D genome. Chromosomal DNA is counter-stained in DAPI (blue). Scale bar = 10  $\mu\text{m}$ .

As conclusive attempt, MyTag A, B and D oligo probes were tested individually for their specific binding to the corresponding genome chromosomes (Figure 5.10). In all cases, Protocol 4 was likewise used, with minor modifications. Figure 5.9 a-a2 reported the

result for MyTag (A) probe when chromosomes were heated at 65°C, as described above in this paragraph. Unexpectedly, MyTag (A) failed to recognize the predicted chromosome regions and the signal appeared nonspecific, as indicated by the background (Figure 5.10 a2). Diversely, MyTag (B) probe seemed to work well. For this probe, chromosomes were denatured at 85°C, accompanied by post-hybridization washing in 4X SSC/0.2% Tween 20 at RT, which effectively promoted the dissociation of the probes from non-specific targets, despite a slight increase of background was observed.

Taking in account the previous results with Protocol 4, these last results support the unambiguous identification of chromosomes 2B and 6B (Figure 5.10 b, arrows). Lastly, as for MyTag (A) probe, MyTag (D) failed to bind the intended chromosome segments when chromosomes were denatured at their hypothesized optimal  $T_m$  equal to 85°C (Figure 5.10 d).

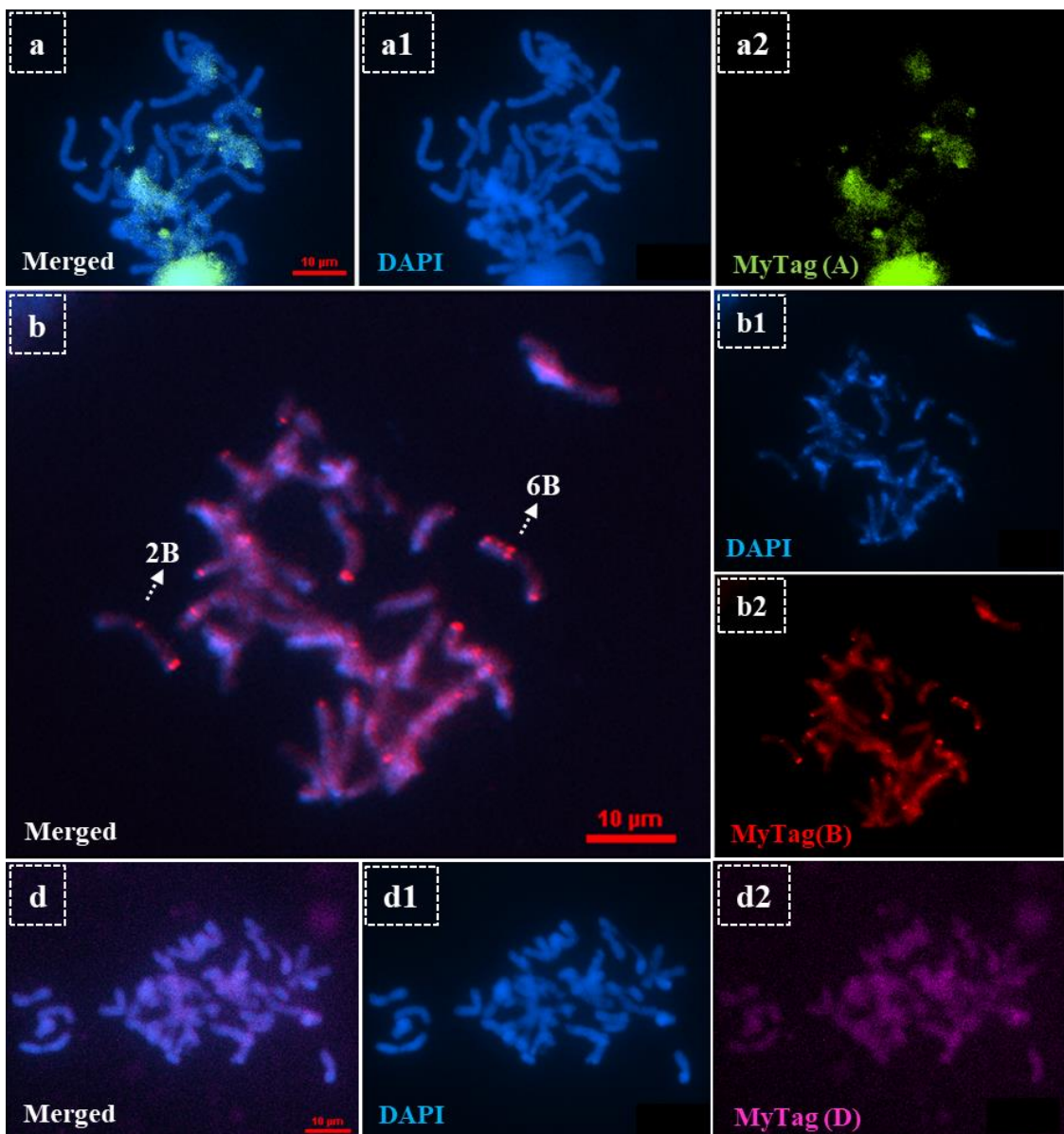


**Figure 5.10 FISH result of individual MyTag oligo marking homoeologous chromosomes of *T. aestivum* ‘Chinese Spring’.** a, b, c) merged probe signals; a1, b1, d1) DAPI-stained (blue) of chromosomes a2) MyTag (A) targeting nonspecific region of A chromosome (green signal); b2) MyTag (B) targeting specific B chromosome-segments (red signal), particularly chromosomes 2B and 6B are pointed with white arrows; d2) MyTag (D) targeting nonspecific region of D chromosome (magenta signal), with visible background. Scale bar = 10  $\mu\text{m}$ .

Lastly, when individual MyTag oligo probes were tested with their corresponding repetitive rDNA probe controls, no hybrids were formed. In Figure 5.11, the example of MyTag (B) with control probe Oligo-Sc119.2-2 (B) is reported.

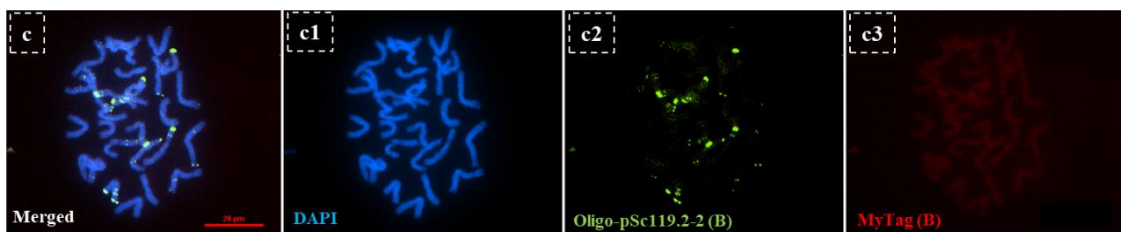


**Figure 5.11 FISH result of repetitive rDNA and MyTag oligo probes marking B chromosome in *T. aestivum* 'Chinese Spring' genome.** c) merged probe signals, c1) chromosome stained in blue-DAPI c2), Oligo pSc119.2-2 in green, c3. MyTag (B) in red. Scale bar = 20  $\mu$ m.

## 5.4 Discussion

### 5.4.1 Acetic acid clears the cytoplasm and improves chromosome dispersion in tetraploid and hexaploid *T. aestivum*

The preparation of high quality chromosome spread is a prerequisite to successfully develop a novel FISH protocol. In plants, the main difficulty relies on the presence of a rigid cell wall, which complicates chromosome separation, and the presence of abundant cytoplasm, which may interfere with probe hybridization and detection.

In this project, the preliminary approach consisted in the analytical definition of the parameters influencing the quality of the chromosome preparation and the qualitative comparison of three spreading procedures. The comparative analysis of three spreading techniques was used in this study to improve the chromosome dispersion in polyploidy *Triticum*. While producing the slides for each spreading technique and in view of the results of this analysis it was possible to determine the two major factors influencing the optimal hromosome preparation in hexaploid *T. aestivum* landrace Chinese Spring: meristematic pre-treatment and post-enzymatic treatment.

The choice of the ice-cold water as the only meristematic pre-treatment to perform for wheat with multiple and large chromosomes was deduced for exclusion, after a critical survey of relevant manuscripts (Aliyeva-Schnorr et al., 2015; Cuadrado et al., 2009; Cuadrado & Jouve, 2010; Rodríguez-Domínguez et al., 2017; King et al., 2018). The alternative use of arresting agents, such as carbamates, were excluded since their metabolites are known to induce over-condensation in species owing numerous and large

chromosomes ( $\geq 8\text{--}10 \mu\text{m}$ ), which results in chromosome overlapping (Mann & Storey, 1966). Few attempts of root tips exposed to a solution of 2 mM 8-hydroxyquinoline for 48 h at 4° C resulted in total chromosomes disintegration (data not shown). Hypotonic solution frequently used for preparing good quality chromosome spreads for human and animal cytogenetics (Claussen et al., 2002), was also ruled out due to differences in cell osmotic pressure between animal and plant cells, and for the presence of an additional cell wall in plants (Evol, 2021). Moreover, the use of hypotonic shock treatment failed to contribute to chromosomal dispersion in plant species with large and numerous chromosomes ( $2n = 120$ ) (Rodríguez-Domínguez et al., 2017). Nitrous oxygen pressure was not explored for this analysis (King et al., 2018).

Conversely, there is evidence that cold treatment stops DNA synthesis and mitotic activity (Olszewska et al., 1988) and simultaneously inhibits microtubule assemblage (Pan et al., 1993). In addition, low temperature facilitates chromosome condensation in species with large chromosomes (Schwarzacher & Leitch, 1994; Bukhari, 1997). This is true for *T. aestivum*, as demonstrated with all three genotypes considered in this work. Notably, in Kronos, Cadenza and Chinese Spring, chromosome condensation occurred after 20, 24 and 25 hours respectively, within a specific range of root length (0.8-1.0, 1.0-1.5, 0.8-2.5, respectively), which is consistent with the different duration of mitosis among tetraploid and hexaploid *Triticum* species (Kaltsikes, 1972). Evidently, the incubation of root tips in ice-cold water at variable duration (depending on the species) is the most efficient treatment utilized for synchronizing the dividing cells at metaphase stage and increasing the metaphase index in species with the naturally low rate of mitosis in root meristems.

Another crucial parameter to preserve a good chromosome morphology in the three wheat genotypes examined was the post-enzymatic treatment. The effectiveness of the absolute ethanol as solvent during the post-enzymatic washes was experimentally demonstrated and it relies on the combined use with the dropping technique. Contrarily to barley (Aliyeva-Schnorr et al., 2015), attempts with citrate buffer after the enzyme incubation produced unintended aggregates, which could not correctly hydrolyze during the later steps. The possibility of under-digested meristems was excluded, since prolonged exposure to the enzyme mix completely dissolved the cells. Furthermore, chromosome integrity was not achieved either when using water or if the proportion of acetic acid in

fixative (for example, 1:1 or 2:1) was raised during the last step. This issue also recurred during the use of stream as spreading method. Despite the relative humidity required to induce good chromosome spreading with the streaming method, this was not precisely quantified, but was only determined empirically. Other limited factors led to rule out this technique: first, it is not frequently used in wheat (Kirov et al., 2014); second, the enzymes suggested for this protocol were costly and the treatment exceeded the 2 hours of incubation; lastly, the chromosome were never morphologically intact at the end of the process. Hence, taking account the possibility to obtain a good chromosome spread regardless the type of enzyme selected, the streaming method was considered as not suitable for these wheat genotypes. Along with this method, squashing technique was the least efficient (Figure 5.4), primarily due to the lack of cytoplasm hydrolysis in the samples analyzed. If metaphase chromosomes remain embedded into cytoplasm, the latter could compromise the probe penetration during the FISH experiment. Over-digestion would not be a viable option, since it could damage the chromosome structure, thus the hybridization with the FISH-probes.

Strictly correlated to the above evidence, failure during the post-enzymatic treatment can also be evaluated from the persistence of cytoplasm. What was fundamental in order to achieve a full cytoplasm hydrolysis in meristematic protoplasts of hexaploid Chinese Spring was the preparation of sample as cell suspension, rather than pressure due to squashing. Between the protoplast suspension derived from streaming and that come from dropping method, the latter was the most effective. It can be argued that the reasons behind this achievement could be ascribable to two major elements: 1) the use of absolute ethanol (as stated above) while centrifuging and re-suspending the protoplasts followed the enzyme incubation; 2) the exceeding proportion of acetic acid over the ethanol (1:3 ethanol:acetic acid) to fix the chromosomes onto the slides joined with the vertically inflated air from the hood. In the first case, once protoplasts were mechanically broken via centrifuge/re-suspension steps to release the chromosomes, the addition of ethanol was essential to remove any trace of enzyme while preserving the integrity of the chromosomal DNA. In the second case, too high acid concentration destroyed the chromosomes, whereas too low did not dissolve the cytoplasm. The correction in three part of acetic acid and one part of ethanol for the protoplast suspension was sufficient to reduce the excess of cytoplasm, avoiding to damage the morphology of the chromosomes. At the time of the cell suspension dropping onto the slide, the minor amount of ethanol

evaporates rapidly, allowing the acetic acid, which is highly hygroscopic, to react with water from the environment and with cellular proteins and produce cell swelling. Additionally, the fast action of the inflated air from the laminar hood, prevented any influence of the humidity in slowing the drying process, thereby allowing additional chromosome spreading. In line with this statement, previous comparative study between *T. aestivum* and species with small chromosomes showed that the relative humidity altered negatively most of chromosome spread in *T. aestivum* (85%), proving that wheat chromosomes are strictly sensitive to the humidity rate (Kirov et al., 2015). The rapid drying time of the sample achieved with this method limited the occurrence of chromosome overlapping, consistent with earlier reports (Spurbeck et al., 1996; Kirov et al., 2015). Indeed, evaporation period of fixative solution was also reported to be crucial for ensuring high quality of chromosome dispersion. These findings clearly helped to enhance the quality of metaphases in the genotypes object of this study.

#### 5.4.2 MyTag chromosome-specific oligo-probes likely form secondary structures in *T. aestivum* ‘Chinese Spring’

The most challenging part of this study was attempting to establish an effective FISH protocol adapted to the new and non-conventional probe types, MyTag oligos, which were designed with the aim to specifically discriminate individual *T. aestivum* ‘Chinese Spring’ sub-genomes according to their fluorescent pattern. The complexity of this task was mainly due to the current existence of a massive number of published reagents and detection methods to evaluate for this purpose. The fact that published manuscripts rarely specified which components were essential and which were the original elements maintained from previous protocols, led to a tremendous workload to face, expanding significantly the timeframe scheduled for this analysis.

In comparison with the control probes, whose single sequence are designed to potentially anneal with multiple repetitive regions, the action mechanism of the pool of MyTag probes is based upon the recognition of a precise chromosome segment for each cluster of probe sequence, which presumes high accuracy in homology search to the target sequence, achieving under specific thermodynamic state.

Overall, from the attempts to develop a FISH protocol for MyTag oligo-probes emerged a prevalence of partial MyTag probe hybridizations observed in most of the chromosome preparations. Theoretically, probes with the highest  $T_m$  would require the most stringent post-wash conditions. Nonetheless, it seemed that higher temperature during the denaturation process, alongside the use of 30% of formamide in the hybridization buffer and least stringency condition after hybridization (4X SSC/0.2%), improved the specificity between oligo-probes and target B and D genomes, but reduced the capability to discriminate target DNA in A genome. Possibly, in presence of low concentration of formamide, which slightly reduces the rate of annealing, dextran sulfate and DNA competitor were not sufficient to associate MyTag (A) probe on the complementary A genome. However, neither increasing the formamide to 70% nor rising the probe concentration to 15 pmol improved the rate of reaction. Besides, it is worth to note that when salt concentration was adjusted during later steps of the hybridization process (post-hybridization washes), wash progression finishing with a high ionic condition (or at a lower temperature) less likely may have denatured and removed nonspecific hybrids, rather, it may have preserved greater intensity of specific labeling. In this situation, signals observed on B and D genomes may be considered valid.

Nonetheless, contrarily to what suggested by the contrasting patterns of MyTag (A) with (B) and (D), the outcomes from the experiment involving the individual MyTag oligo probes in the same hybridization mix with their corresponding repetitive rDNA probe controls, revealed no selective hybridization, possibly due to cross-hybridization between probes for identical chromosome regions.

Lastly, the explanation for which the supplementary use of Q5 Enhancer buffer in the hybridization mix failed to enhance probe penetration may be found in the PCR Troubleshooting Guide (NEB), where it is reported that Q5 enhancer buffer can also be inhibitory to high AT amplicons. Since the nucleotide sequences of the MyTag probes were not provided from the Company, further verifications about the GC contents could not be determined.

In other words, it seems that the multiple, short adjacent distribution of the MyTag oligos (as elucidated in chromosome indexing in Figure 5.2), disable the sensitivity of oligo probes to the chromosome target. In this circumstances, if probes are subjected to high

temperature and salt concentration, they alter their conformation creating secondary structure, a condition principally expected in chromosomes 3, 4, 5, 6, 7, in which the pool of probes is larger than in chromosomes 1 and 2. This may ultimately explain why in every FISH experiment, only a single region probe binding were detected. This hypothesis may find indicative evidence in literature. So far, the standard nucleic acid secondary structure prediction algorithm has demonstrated that longer-range DNA sequence interactions reduce at high temperatures, while stable local structures persist in the sequence even at high salt concentration and high temperature, creating obvious competition for binding sites (Ratushna et al., 2005; Adams et al., 2013). This frame is what it is expected during the annealing between MyTag oligo probes and their specific target sequence. Potentially, probes in altered conformation that target immediately adjacent sequences, block the other probes from binding because of the induced secondary structure. Hence, it can be argued that a way to enhance the resolution and stability of oligo probe hybridization would be mapping additional and widely distributed FISH markers on wheat chromosomes.

These results certainly proved inaccuracy during the MyTag oligo-probe design framework. As reviewed by Liu and Zhang (2021), the robustness of oligo probes, beyond that being influenced by thermodynamic proprieties (estimation of GC content,  $T_m$  and ionic conditions), is affected by its length and specificity (Liu & Zhang, 2021). In wheat, whose genomes comprise large amounts of repetitive sequences, improving the specificity of oligos in the genome must be the principal aspect to evaluate. A well-assembled reference genome, which covers a major part of the repetitive sequences as well as a complete annotation of repeat elements in the genome are also fundamental to help eliminate potential multi-copy oligos.

At present, the most commonly used strategy for single-copy oligo detection is dependent on sequence alignment. However, for plants with large genomes, such as wheat and maize, potential repetitive sequences might not be well documented. When designing oligo probes in these genomes, *de novo* repeats detection and filtering based on shotgun sequences is another approach that can be used to improve the specificity of oligos (review Liu & Zhang, 2021). Moreover, it should be noted that oligos might bind to unintended sites with minor mismatches. Therefore, oligos with multiple homologous sequences in the genome should be monitored carefully.

## 5.5 Conclusions

The protocol for dropping method optimized in this work, starting from 20 root tips and irrespective of the enzyme type, produced more than 50% of slides containing excellent metaphase chromosome preparations, free of cytoplasm and with well spread chromosomes in important tetraploid and hexaploid *T. aestivum* genotypes, enabling the access of oligo-probes for FISH experiments. Since the consistency showed in all three genotypes, this protocol can be potentially applied to other closely related wheat species, as well.

Beyond this, taking in account the results derived from FISH Protocol 4, the specific requirements to maximize the hybridization conditions of MyTag chromosome-specific probes could not be completely defined due to possible intrinsic defect(s) in probe specificity and their propensity to form intramolecular secondary structure, hypothesized to be the main limiting factors for the hybridization rate. Nevertheless, hybridization conditions and detection method setup with this study still enabled to clearly discriminate chromosomes 2 and 6 on B sub-genome in hexaploid Chinese Spring, also confirming the tangible difficulty in precisely and unambiguously identifying homoeologous chromosomes in wheat. More broadly, these findings definitely represent a good starting point for future experiments in this direction.

# **Chapter 6**

## **General conclusions**

### **6.1 Introduction**

This project first investigated the expression patterns and then the meiotic function(s) of two SC genes, *ASY1* and *ZYP1*, in polyploid *Triticum*, by implementing Sanger sequencing and cytological analysis of novel TILLING mutant lines. The molecular approach provided evidence of equal expression patterns of both SC target genes as well as uncovered *de-novo* 3' UTR spliced isoforms within reproductive tissues, to be functionally validated for their meiotic role. The cytological methodologies provided to gained preliminary evidence of *ASY1* in controlling homologous pairing and synapsis during meiotic prophase I and evidence of a conserved role of *ZYP1* in stabilising Class I CO in tetraploid wheat.

The study of the SC was further extended to the search of candidate wheat CE orthologue(s) using the latest gene co-expression network publicly available (Alabdullah et al., 2019). The newest data generated from this work and the putative meiotic gene *SWI1* identified and analysed with cytological techniques are promising and encourage future applications of *in-silico* predictive tools to explore meiotic recombination mechanisms in wheat.

Finally, the potential implementation of FISH-based single copy oligo-probes to discriminate individual wheat chromosomes was analytically evaluated, providing indications and novel directions for the improvement and development of single copy oligo-probes in crop research.

## 6.2 *ASY1* possesses a non-canonical gene expression pattern in polyploid wheat

The combined use of cloning and sequencing methods effectively revealed a non-tissue specific gene expression regulation of *TaASY1* coding region among the three diverged sub-genomes in hexaploid wheat, being expressed at similar levels in inflorescences, as initially demonstrated by Boden et al. (2007), and surprisingly in leaves. Western blot analysis showing equivalent size band of ASY1 protein extracted from leaves and anthers, further support its expression in somatic tissue (leaves). Similar expression patterns of wheat meiotic genes were also found by other two independent research works. In 2019, Alabdullah and collaborators, using RNA-seq data to create a wheat co-expression analysis, obtained evidence for a different homoeologous expression profile to the *TaZIP4* copy responsible for *Ph1* phenotype (TraesCS5B02G255100), which resulted expressed in most non-meiotic tissues (Alabdullah et al., 2019).

Analogously, the *Arabidopsis ASY1*, which encodes a protein essential for homologous chromosome synapsis, is expressed in both reproductive and non-reproductive tissues, though the protein is only detected in meiocytes (Caryl et al., 2000; Armstrong et al., 2002). Other genes in this category are *AHP2*, which encodes the *Arabidopsis* homolog of the yeast Hop2 protein involved in meiotic recombination and homologous chromosome pairing (Schommer et al., 2003), and maize *PHS1*, which encodes a protein required for homologous chromosome pairing and recombination (Pawlowski et al., 2004). In other species, transcription of meiotic genes appears to be more strictly confined to reproductive cells, although this is not without exception; for example, the rat *SCPI* gene is expressed, albeit at a low level, in the brain (Kerr et al., 1996). Thus, in wheat as in other plants, a potential obstacle to dissecting expression patterns of known meiotic genes is that the number of genes whose specific functions in meiosis are well understood is still relatively small (reviewed by Zhou & Pawlowski, 2014).

More recently, Jiang and co-workers (2022, in preparation), identified numerous transcript isoforms in their wheat meiotic transcriptome, possessing balanced expression patterns in both vegetative and reproductive tissues. Alternative spliced isoforms were in fact detected in the present project using the cloning and sequencing strategies. A putative rare splice variant was identified within the coding region of *TaASY1-5B* in Apogee

anthers, which might be included within the 0.09% frequency of minor non-canonical splice events recorded in previous work in plants (Pucker & Brockington, 2018). The same approach allowed the discovery of additional nine putative *TtASY1* 3' UTR isoforms in reproductive tissues and unmasked the presence of specific CPE regulatory regions and poly(A) composed of variable length and G-content. In other species, such as *Drosophila*, *Xenopus* and *Danio rerio*, transcripts differing in poly-A tail length are essential for meiotic and developmental processes (Eichhorn et al., 2016; Lim et al., 2016; Morgan et al., 2017). In humans and *Arabidopsis thaliana*, the guanosine percentage is associated with molecular mechanism of translational control through poly(A)-binding proteins (PABs) (Sachs et al., 1987; Deo et al., 1999; Sladic et al., 2004; Lim et al., 2018).

To recapitulate, the discovery of a balanced gene expression contribution among *TaASY1* homoeologues in meiotic and non-meiotic tissues, along with functionally unexplored alternative splicing features in both coding and untranslated regions of wheat *ASY1* may reserve a unique mechanism to regulate transcript abundance in polyploid wheat. Taken together, these data represent a fascinating starting point for future research proposals. Notably, the recent release of the wheat genome assembly and the generation of vast wheat transcriptome data will allow computational analyses to efficiently and robustly predict and screen alternative splicing events across tissue- or meiotic-stage-specific regulation of *TaASY1* alternative isoforms, and the combination of immuno-cytological staging data will provide evidence of their functionality, as previously accomplished in barley transcriptome (Barakate et al., 2020). Newly developed high-throughput sequencing technologies in model plants, such as single-cell RNA-seq (Denyer et al., 2019) and spatial transcriptomics (Giacomello et al., 2017; Chaudhary et al., 2019), will further increase the resolution of anther and meiocyte transcriptomes even at sub-cellular level, providing novel insights into the underlying mechanisms that modulate meiotic recombination in polyploidy wheat, having the ultimately goal to guarantee relevant advancements in cereal breeding programmes.

### 6.3 ASY1 is required for homology search in tetraploid wheat

In hexaploid wheat, the question related to the influence of *ASY1* on homoeologous pairing and recombination, hypothesised to be subjected to *Ph1 locus*, was first addressed

through knocking-down *ASY1* genes. Transgenic wheat mutants indeed recorded an high levels of homoeologous pairing at metaphase I, as shown in *Ph1*-deficient plants (Boden et al., 2009). Nevertheless, the mechanism behind *TaASY1* role remained elusive.

In this study, following the recent developments in genome editing technologies, cytogenetic analyses of independent TILLING (EMS-induced) mutants have provided an improved approach for characterising and validating the function of *TaASY1* in polyploid wheat. As expected, in *asy1* TILLING lines, SC assembly/synapsis was temporally disrupted; tetraploid and hexaploid *asy1* single KO mutants exhibited already an 8% increase of homoeologous interaction at diakinesis, which raised to 18% in tetraploid *asy1* hypomorphic mutant; simultaneously, the rise in homoeologous synapsis did not correspond to an increase in chiasma frequency, providing strong evidence that wheat *ASY1* is dosage-sensitive in regards to chiasma regulation, consistent with its orthologous in *Arabidopsis* (Lambing et al., 2020), and that *ASY1* is principally required for inter-homologous search and synapsis. These preliminary findings are certainly in line with those obtained by Boden and co-workers (2009), demonstrating a role of wheat *ASY1* in biasing homologous pairing, as well as with more distant *AtASY1/ScHOP1* orthologues (Sanchez-Moran et al., 2007; Carballo et al., 2008).

As anticipated in Chapter 2, chromosome pairing in tetraploid wheat appeared to be SC-dependent, therefore, if the SC is only partially formed (at least one functional copy of *ASY1*), the homologous alignment can be affected, thus random or unsynchronised chromosome sorting could generate fragments or mis-pairing. As meiosis progresses, such disorders may compromise the point of synapsis, reducing the chance to repair the DSBs. This model easily explains the gradually depletion of  $\gamma$ H2AX foci (corresponding to CO events) in *asy1 aabB* (hypomorphic) detected at pachytene stage. In all probability, if SC is completely missing (*ASY1* fully knocked-out), then there would be no possibility to concatenate the early and late events (homoeologous sorting before homologous and chromosome alignment through the axial elements, respectively). As consequence, no CO can be resolved and chromosomes are present only as univalents and sometimes monads (separated chromatids). As in yeast and mammal, it is possible that the clustering of chromosomes that occurs early during meiosis I in tetraploid wheat reflects the initiation of homoeologous associations, which has to be temporally regulated by *ASY1* to stabilise the DSBs repair mechanism as meiosis progress. Thus, the  $\gamma$ H2AX

immunolocalization assay indicates that ASY1 may be responsible for the maturation of recombination intermediates to form COs, and suggests the possibility that fragments detected at metaphase I may be originated from unrepaired meiotic DSBs, enhancing the multivalent choice. However, the DSB number reductions were not confirmed by immunolocalization of other recombination pathway proteins, such as RAD51 or MHL1, which marks DSB sites and facilitates the first step of DSB repair (Pradillo et al., 2014). Therefore, whether the observed fragments in *asy1 aabB* were caused by mispairing between true homologous chromosomes or, alternatively, they were arisen from chromosome being overstretched by meiotic tension installed during the homoeologous migration at anaphase I, remains unclear.

Intriguingly, in close relative species like barley, it has been proposed that the coordination of the appearance of the recombination foci on the chromosomes with the chromatin contraction/expansion cycles may be a contributory factor to bias the distal CO distribution (Higgins et al., 2012). In *Arabidopsis thaliana*, ASY1 acts in a dosage-dependent manner to antagonize telomere-led recombination and promotes spaced CO formation along chromosomes via interference (Lambing et al., 2020). Intriguingly, ASY1 ChIP-seq analysis of wheat landrace Chinese Spring revealed a similar pronounced distal enrichment toward the telomeres (Tock et al., 2021). Taken together with the *asy1* behaviour in this study, it could be speculated that the *TtASY1* dosage detected in these *asy1* TILLING lines may also influence CO distribution in wheat, although further investigation will be required to corroborate this supposition.

This study also hypothesised a conserved role of ASY1 in SC morphogenesis, corroborated with the investigation of ASY1-ASY3 interaction in *asy1 Aabb*. Importantly, in the hypomorphic mutant, the formation of ASY1 and ASY3 polycomplexes at diplotene were interpreted as a defective conformational state assumed by the HORMAD protein ASY1, which compromised its binding with ASY3. Typically, a conserved AAA<sup>+</sup> ATPase PCH2/TRIP13 protein ensures synapsis progression by unblocking the self-closed HORMA domain, thereby enabling the binding with the closure motifs of the linker proteins (Rosenberg & Corbett, 2015; Ye et al., 2017; West et al., 2018; Yang et al., 2020). Therefore, it was speculated that truncated ASY1 lacking its own closure motif may disrupt the progression of desynapsis process in *asy1 Aabb*, resulting in excess of unloaded proteins (polycomplexes). In future, it would be

interesting to prove this hypothesis in polyploid wheat, whose desynapsis stage is still poorly understood.

Further indication of a potential role of ASY1 during desynapsis derives from the altered localization of the cohesin SMC3 along chromosome axes at the zygotene-pachytene transition in *asy1 aabB*. Consistently, a rise of nondisjunction events at anaphase I was detected in fixed *asy1 aabB* meiocytes, and previously in *ph1*, *C. elegans him-3* and mammal *hormad1* (Zetka et al., 1999; Couteau & Zetka, 2005; Martinez-Perez & Villeneuve, 2005; Martinez-Perez et al., 2008; Boden et al., 2009; Daniel et al. 2011). According to these data, the localization of wheat ASY1 on desynapsed chromosomes supports a potential role in sister chromatid cohesion and homologous chromosome disjunction during the first meiotic division. In perspective, FISH experiment using centromere-specific probe in *asy1* meiocytes, could categorically demonstrate a supplementary function of ASY1 in chiasma junction.

Lastly, in regards to the *asy1* null mutant, metaphase I spread of fixed *asy1* full KO (null mutants) meiocytes showed asynaptic chromosomes and complete loss of the obligate CO. Presumed failure in immunostaining experiments using meiotic markers (data not recorded), were initially interpreted as technical issues. Following the cytological atlas and meticulous observation of F<sub>2</sub> segregants, more data were collected and another hypothesis was contemplated. Plants genotyped as *asy1 aabb* presented severe developmental defects, with asynchronous meiosis, rarely progressing into pachytene or diplotene. These data clearly indicate a possible activation of programmed meiotic arrest in this mutant. Literature searches further reinforced the assumption that wheat ASY1 may create a checkpoint arrest when homologous chromosomes fail to synapse, a strategy commonly observed in mammal HORMAD orthologous (Daniel et al., 2011).

With this study, it is now evident that the perturbed spatio-temporal dynamism of ASY1 within *asy1* TILLING lines monitored during the first meiotic division, correlated to a gradual reduction of DSB maturation across the *asy1* mutant genotypes, whose dosage strictly regulates normal level of CO, suggested a ASY1-dependent control in terms of homologous chromosome pairing. In future, since the presence of multiple gene copies, it may be advisable to generate a full ASY1 KO through the implementation of CRISPR/Cas9 technology, which, by targeting multiple homoeologue alleles

simultaneously, could bypass the crossing procedure and accelerate the functional gene validation process (Li et al., 2021).

To conclude, from the initial hypothesis on the suppression of intra-homologous interactions, potential supplementary functions of *TaASY1* within meiotic processes have now been speculated, suggesting a major role of this gene possibly following wheat polyploidization events, and therefore, matter of concern not only for its genome integrity and stability, but also for the oncoming breeding programmes. Future investments in *asy1* mutants will potentially unmask wider implications in research field, such as in regards to the efficiency of alien introgression in crop breeding.

## 6.4 *ZYP1* is not exclusively expressed in meiotic tissues in polyploid wheat

Analogously to what was observed in *TaASY1* and other wheat meiotic genes (Alabdullah et al., 2019; Jiang et al., 2022, in preparation), cloning and sequencing strategies unveiled a balanced expression level of *TaZYP1* among its sub-genomes, extended beyond reproductive tissues. These data clearly suggest the existence of a specific mechanism underlying the expression regulation of meiotic genes in polyploid wheat, although the mode of action remains undiscovered.

Furthermore, one predicted *TtZYP1* 3' UTR transcript and six unannotated *TtZYP1* 3' UTR transcript variants were identified in reproductive tissues through sequence analysis. In common, the 3' UTR spliced variants had two undescribed regulatory PAS sequences, but different nucleotide contents within poly(A) tail, of which 42% contained guanosine residues. The occurrence of these alternative transcripts at high frequency underlines a potential role in transcriptional efficiency (ratio between the protein abundance and the mRNA levels of that gene, and timing of transcription). This statement finds support in other independent research studies, especially in plants. Indeed, genome-wide identification of polyA motifs and PAS sequences are known to affect the mRNA stability, translation and cellular localizations to fulfil gene expression modulation in plants (Shi, 2012; Xing & Li, 2011; Zhu et al., 2020). Considering the current development of improved computational tools and databases to detect PAS sequences

(reviewed in Zhang et al., 2021), these data will accelerate the choice of the best approach for functional analysis specifically targeted in polyploid wheat, expanding the possibility to employ *ZYP1* for the development of superior wheat varieties.

## 6.5 In tetraploid wheat, SC and CO are interdependent and may rely on *ZYP1* C-terminus

In this study, the function of *ZYP1* was elucidated via the use of EMS mutagenized lines. Distinct stages of the first meiotic division investigated with cytological techniques in *zyp1* single KO lines were timely affected, and depletion of *ZYP1* compromised the exact SC elongation between the axial elements. Early effects of the individual mutation were already evident during pre-synapsis, when homologous chromosome starts to cluster in WT plants, but delayed alignment in *ZYP1*-partial-loss of function, despite axial elements appearing to be fully formed. This behaviour, already known in *S. cerevisiae zip1*, *Drosophila c(3)g* and mouse *syp1* mutants (Hall, 1972; Sym et al., 1993; Nag et al., 1995; MacQueen et al., 2002), had important consequences for progression during meiosis.

More than 15% of chromosomes at metaphase I in *zyp1* single KOs never completely synapsed and ASY1 accumulated forming polycomplexes at desynapsis sites, further increasing the number achiasmatic regions. Indeed, an immunolocalization experiment with HEI10 in *zyp1a-1* mutants unambiguously showed that 19% DSBs were not repaired at pachytene. These data are definitely comparable to the majority of mutant analyses of *ZYP1* orthologues in model organisms, including *Arabidopsis*, barley, *Drosophila* and mouse (Page et al., 2001; de Vries et al., 2005; Higgins et al., 2005; Barakate et al 2014), demonstrating that *ZYP1*, and more widely, SC may rule homologous synapsis in tetraploid wheat. Similarly, the alluvial diagram created in this study from the previous wheat co-expression data (Alabdullah et al., 2019) also reported association between *TaZYP1* and wheat orthologues of characterized genes known to be involved in the control of meiotic CO pathways in several model organisms (see Chapter 5), which further support our hypotheses in wheat.

Importantly, evidence of chromosome interlocks, together with HEI10 foci spatially closer each other and the slight increase of centromeric COs in *zyp1 Aabb-1*, may suppose

a more central role of wheat ZYP1 in meiotic recombination distribution. Shortly, the growing implementation of super resolution microscopy for the study of SC components may shed light on the multiple mechanisms of CO control evolved in polyploid wheat, also prerogative of related plant species, particularly *Poaceae* family, for years being the centre of interest in several breeding programmes.

To summarise, wheat ZYP1 fulfils essential roles in Class I CO control and homologous synapsis, representing a fascinating and useful achievement in our knowledge of wheat meiosis.

## **6.6 A novel meiotic gene candidate *SWI1* was identified in polyploid wheat with bioinformatics tools**

The utilization of a pre-existing wheat gene co-expression network built to discover putative meiotic genes, here opened up new routes to identify wheat meiotic candidates. Whilst not showing any evidence on the presence of central elements in wheat, the co-expression sub-network allowed a preliminary characterization of wheat candidate *SWI1* mainly involved in CO pathway, as demonstrated by provisional cytological analysis of a single EMS mutant line. The emergence of more improved and accurate *in silico* prediction tools, will contribute to a better assessment of regulatory genes, particularly as the process of identifying and screening homozygous mutants *in vivo* is labour and time intensive, hence widening application beyond research (e.g., industry).

## **6.7 An improved FISH-based oligo-probes protocol to discriminate individual sub-genomes in polyploid wheat**

The attempts to develop an effective FISH protocol for novel wheat chromosome-specific oligo-probes represented a good starting point to lessen the selection of reagents and experimental conditions to be evaluated for targeting future progress in FISH methodology applied on polyploid wheat chromosomes.

In parallel with the emergence of modern oligo-probes tailored to plant species, improvements in probe design tools and in genomic shotgun sequencing of polyploid species, will accelerate the entire workflow in wheat. A comprehensive review describing

and comparing the latest sophisticated tools for genome-scaled oligo probe design is already available to guide choosing the most suitable strategy to use. OligoMiner and Chorus2 softwares are suitable for users who do not have high performance computers. OligoMiner is preferred for mammals and Chorus2 is preferred for plants (Liu & Zhang, 2021).

In perspective, this methodology can be applied to unveil the genetic mechanism underlying the behaviour of homoeologous chromosomes following wheat diploidization and for chromosome engineering. As shown and discussed in Chapter 2, the meiotic gene ASY1 is likely to be involved in chromosome partner choice in tetraploid and hexaploid wheat. The functional validation via FISH assay using oligo probes will enable accurate labelling of the diverged chromosomes. Furthermore, the identification of specific chromosomal segments may provide indications about wheat evolutionary history, especially regarding the degree of colinearity between wheat and alien chromosomes, still estimated as the major bottleneck to introgressive hybridizations in crop breeding.

## 6.8 Research implication in Food Security

In the 21st century, the Food system is being subjected to unprecedeted events that are more uncertain and volatile. There is an ongoing debate about which strategies are being developed to achieve the right balance between improved food production and sustainable use and management of resources, while facing climate changes. Multiple trends (demographic, cultural, ecological, technological, economic, and political) demand continuous research investments to transform crop species for guaranteeing future global food security.

For the improvement of polyploid species, especially wheat, it is necessary to understand the allelic diversity and homoeologous genes that control phenotype. Taking advantage of the recent release of wheat genome assembly and the generation of vast wheat transcriptome data, this thesis has already proven that: 1) molecular and computational analyses can predict and screen putative/target meiotic genes and transcript isoforms; 2) mutagenesis and immuno-cytological methods are reliable and sensitive for functional analysis in wheat. Specifically, the main findings of this thesis can be highlighted and summarised as follows:

- Complete understanding of wheat ASY1 and ZYP1 gene expression regulation and transcriptome complexity may offer unexplored opportunities to manipulate meiotic recombination rate, accelerating the development of superior germplasm for crop breeding.
- Future investments in *asy1* mutants may potentially establish an improved protocol for achieving efficient alien introgression and increasing the likelihood of relevant advancements in cereal breeding programmes.
- The application of chromosome-specific oligonucleotide probes for FISH karyotyping in polyploid wheat represents a useful tool for evolutionary studies (e.g. polyploidization).
- The identification of wheat ZYP1 as a regulator of crossover formation will provide better opportunities to target ZYP1 for manipulating crossover frequency and develop superior wheat varieties.

## References

- Able, J. A., Crismani, W., & Boden, S. A. (2009). Goldacre Paper: Understanding meiosis and the implications for crop improvement. *Functional Plant Biology*, 36(7), 575–588. <https://doi.org/10.1071/FP09068>
- Acquino, P., Carrion, F., & Kosina, P. (2009). Selected Wheat Statistics. In *Wheat Facts and Futures 2009*.
- Adamski, N. M., Borrill, P., Brinton, J., Harrington, S. A., Marchal, C., Bentley, A. R., Bovill, W. D., Cattivelli, L., Cockram, J., Contreras-Moreira, B., Ford, B., Ghosh, S., Harwood, W., Hassani-Pak, K., Hayta, S., Hickey, L. T., Kanyuka, K., King, J., Maccaferri, M., ... Uauy, C. (2020). A roadmap for gene functional characterisation in crops with large genomes: Lessons from polyploid wheat. *eLife*, 9, 1–30. <https://doi.org/10.7554/eLife.55646>
- Aguilar, M., & Prieto, P. (2021). Telomeres and Subtelomeres Dynamics in the Context of Early Chromosome Interactions During Meiosis and Their Implications in Plant Breeding. In *Frontiers in Plant Science* (Vol. 12, p. 1024). <https://www.frontiersin.org/article/10.3389/fpls.2021.672489>
- Alabdullah, A. K., Borrill, P., Martin, A. C., Ramirez-Gonzalez, R. H., Hassani-Pak, K., Uauy, C., Shaw, P., & Moore, G. (2019). A Co-Expression Network in Hexaploid Wheat Reveals Mostly Balanced Expression and Lack of Significant Gene Loss of Homeologous Meiotic Genes Upon Polyploidization. *Frontiers in Plant Science*, 10, 1325. <https://doi.org/10.3389/fpls.2019.01325>
- Albert, P. S., Zhang, T., Semrau, K., Rouillard, J.-M., Kao, Y.-H., Wang, C.-J. R., Danilova, T. V., Jiang, J., & Birchler, J. A. (2019). Whole-chromosome paints in maize reveal rearrangements, nuclear domains, and chromosomal relationships. *Proceedings of the National Academy of Sciences of the United States of America*, 116(5), 1679–1685. <https://doi.org/10.1073/pnas.1813957116>
- Alexander, M. P. (1969). Differential Staining of Aborted and Nonaborted Pollen. *Stain Technology*, 44(3), 117–122. <https://doi.org/10.3109/10520296909063335>
- Alix, K., Gérard, P. R., Schwarzacher, T., & Heslop-Harrison, J. S. P. (2017). Polyploidy and interspecific hybridization: Partners for adaptation, speciation and evolution in plants. *Annals of Botany*, 120(2), 183–194. <https://doi.org/10.1093/aob/mcx079>
- Aliyeva-Schnorr, L., Ma, L., & Houben, A. (2015). A fast air-dry dropping chromosome preparation method suitable for FISH in plants. *Journal of Visualized Experiments*, 2015(106), 1–5. <https://doi.org/10.3791/53470>
- Al-Kaff, N., Knight, E., Bertin, I., Foote, T., Hart, N., Griffiths, S., & Moore, G. (2008). Detailed dissection of the chromosomal region containing the *Ph1* locus in wheat *Triticum aestivum*: with deletion mutants and expression profiling. *Annals of*

*Botany*, 101(6), 863–872. <https://doi.org/10.1093/aob/mcm252>

Allers, T., & Lichten, M. (2001). Differential timing and control of noncrossover and crossover recombination during meiosis. *Cell*, 106(1), 47–57. [https://doi.org/10.1016/s0092-8674\(01\)00416-0](https://doi.org/10.1016/s0092-8674(01)00416-0)

Anderson, H. J., Vonarx, E. J., Pastushok, L., Nakagawa, M., Katafuchi, A., Gruz, P., Di Rubbo, A., Grice, D. M., Osmond, M. J., Sakamoto, A. N., Nohmi, T., Xiao, W., & Kunz, B. A. (2008). *Arabidopsis thaliana* Y-family DNA polymerase  $\eta$  catalyses translesion synthesis and interacts functionally with PCNA2. *Plant Journal*, 55(6), 895–908. <https://doi.org/10.1111/j.1365-313X.2008.03562.x>

Anderson, L. K., Royer, S. M., Page, S. L., McKim, K. S., Lai, A., Lilly, M. A., & Hawley, R. S. (2005). Juxtaposition of C(2)M and the transverse filament protein C(3)G within the central region of *Drosophila* synaptonemal complex. *Proceedings of the National Academy of Sciences of the United States of America*, 102(12), 4482–4487. <https://doi.org/10.1073/pnas.0500172102>

Anuradha, S., & Muniyappa, K. (2005). Molecular Aspects of Meiotic Chromosome Synapsis and Recombination. *Progress in Nucleic Acid Research and Molecular Biology*, 79(04), 49–132. [https://doi.org/10.1016/S0079-6603\(04\)79002-9](https://doi.org/10.1016/S0079-6603(04)79002-9)

Appels, R., Eversole, K., Feuillet, C., Keller, B., Rogers, J., Stein, N., Pozniak, C. J., Choulet, F., Distelfeld, A., Poland, J., Ronen, G., Barad, O., Baruch, K., Keeble-Gagnère, G., Mascher, M., Ben-Zvi, G., Josselin, A. A., Himmelbach, A., Balfourier, F., ... Wang, L. (2018). Shifting the limits in wheat research and breeding using a fully annotated reference genome. *Science*, 361(6403). <https://doi.org/10.1126/science.aar7191>

Aravind, L., & Koonin, E. V. (1998). The HORMA domain: a common structural denominator in mitotic checkpoints, chromosome synapsis and DNA repair. *Trends in Biochemical Sciences*, 23(8), 284–286. [https://doi.org/10.1016/S0968-0004\(98\)01257-2](https://doi.org/10.1016/S0968-0004(98)01257-2)

Armstrong, S. J., Caryl, A. P., Jones, G. H., & Franklin, F. C. H. (2002). Asy1, a protein required for meiotic chromosome synapsis, localizes to axis-associated chromatin in *Arabidopsis* and *Brassica*. *Journal of Cell Science*, 115(Pt 18), 3645–3655. <https://doi.org/10.1242/jcs.00048>

Badaeva, E. D., Friebel, B., & Gill, B. S. (1996). Genome differentiation in *Aegilops*. 2. Physical mapping of 5S and 18S–26S ribosomal RNA gene families in diploid species. *Genome*, 39(6), 1150–1158. <https://doi.org/10.1139/g96-145>

Balboni, M., Yang, C., Komaki, S., Brun, J., & Schnittger, A. (2020). COMET Functions as a PCH2 Cofactor in Regulating the HORMA Domain Protein ASY1. *Current Biology : CB*, 30(21), 4113-4127.e6. <https://doi.org/10.1016/j.cub.2020.07.089>

Barakate, A., Higgins, J. D., Vivera, S., Stephens, J., Perry, R. M., Ramsay, L., Colas, I., Oakey, H., Waugh, R., Franklin, F. C. H., Armstrong, S. J., & Halpin, C. (2014).

- The synaptonemal complex protein ZYP1 is required for imposition of meiotic crossovers in barley. *Plant Cell*, 26(2), 729–740. <https://doi.org/10.1105/tpc.113.121269>
- Bass, H. W., Riera-Lizarazu, O., Ananiev, E. V., Bordoli, S. J., Rines, H. W., Phillips, R. L., Sedat, J. W., Agard, D. A., & Cande, W. Z. (2000). Evidence for the coincident initiation of homolog pairing and synapsis during the telomere-clustering (bouquet) stage of meiotic prophase. *Journal of Cell Science*, 113 ( Pt 6), 1033–1042.
- Bennett, M. D. (1979). CENTROMERE ARRANGEMENTS IN TRITICUM-AESTIVUM AND THEIR RELATION TO SYNAPSIS. *Heredity*, 43(AUG), 157.
- Berchowitz, L. E., Francis, K. E., Bey, A. L., & Copenhaver, G. P. (2007). The Role of AtMUS81 in Interference-Insensitive Crossovers in *A. thaliana*. *PLOS Genetics*, 3(8), e132. <https://doi.org/10.1371/journal.pgen.0030132>
- Berger, F., & Twell, D. (2011). Germline specification and function in plants. *Annual Review of Plant Biology*, 62, 461–484. <https://doi.org/10.1146/annurev-arplant-042110-103824>
- Bergerat, A., de Massy, B., Gadelle, D., Varoutas, P. C., Nicolas, A., & Forterre, P. (1997). An atypical topoisomerase II from Archaea with implications for meiotic recombination. *Nature*, 386(6623), 414–417. <https://doi.org/10.1038/386414a0>
- Bhullar, R., Nagarajan, R., Bennypaul, H., Sidhu, G. K., Sidhu, G., Rustgi, S., Von Wettstein, D., & Gill, K. S. (2014). Silencing of a metaphase I-specific gene results in a phenotype similar to that of the Pairing homeologous 1 (*Ph1*) gene mutations. *Proceedings of the National Academy of Sciences of the United States of America*, 111(39), 14187–14192. <https://doi.org/10.1073/pnas.1416241111>
- Bishop, D. K., Park, D., Xu, L., & Kleckner, N. (1992). DMC1: a meiosis-specific yeast homolog of *E. coli* recA required for recombination, synaptonemal complex formation, and cell cycle progression. *Cell*, 69(3), 439–456. [https://doi.org/10.1016/0092-8674\(92\)90446-j](https://doi.org/10.1016/0092-8674(92)90446-j)
- Blary, A., & Jenczewski, E. (2019). Manipulation of crossover frequency and distribution for plant breeding. *Theoretical and Applied Genetics*, 132(3), 575–592. <https://doi.org/10.1007/s00122-018-3240-1>
- Boden, S. A., Langridge, P., Spangenberg, G., & Able, J. A. (2009). TaASY1 promotes homologous chromosome interactions and is affected by deletion of *Ph1*. *Plant Journal*, 57(3), 487–497. <https://doi.org/10.1111/j.1365-313X.2008.03701.x>
- Boden, S. A., Shadiac, N., Tucker, E. J., Langridge, P., & Able, J. A. (2007). Expression and functional analysis of TaASY1 during meiosis of bread wheat (*Triticum aestivum*). *BMC Molecular Biology*, 8, 1–14. <https://doi.org/10.1186/1471-2199-8-65>
- Bolcun-Filas, E., Costa, Y., Speed, R., Taggart, M., Benavente, R., De Rooij, D. G., & Cooke, H. J. (2007). SYCE2 is required for synaptonemal complex assembly,

- double strand break repair, and homologous recombination. *Journal of Cell Biology*, 176(6), 741–747. <https://doi.org/10.1083/jcb.200610027>
- Bolcun-Filas, E., Speed, R., Taggart, M., Grey, C., De Massy, B., Benavente, R., & Cooke, H. J. (2009). Mutation of the mouse *Syce1* gene disrupts synapsis and suggests a link between synaptonemal complex structural components and DNA repair. *PLoS Genetics*, 5(2). <https://doi.org/10.1371/journal.pgen.1000393>
- Bollig, F., Winzen, R., Gaestel, M., Kostka, S., Resch, K., & Holtmann, H. (2003). Affinity purification of ARE-binding proteins identifies poly(A)-binding protein 1 as a potential substrate in MK2-induced mRNA stabilization. *Biochemical and Biophysical Research Communications*, 301(3), 665–670. [https://doi.org/https://doi.org/10.1016/S0006-291X\(03\)00015-9](https://doi.org/https://doi.org/10.1016/S0006-291X(03)00015-9)
- Bomblies, K., Higgins, J. D., & Yant, L. (2015). Meiosis evolves: Adaptation to external and internal environments. *New Phytologist*, 208(2), 306–323. <https://doi.org/10.1111/nph.13499>
- Borde, V., & de Massy, B. (2013). Programmed induction of DNA double strand breaks during meiosis: setting up communication between DNA and the chromosome structure. *Current Opinion in Genetics & Development*, 23(2), 147–155. <https://doi.org/10.1016/j.gde.2012.12.002>
- Börner, G. V., Kleckner, N., & Hunter, N. (2004). Crossover/noncrossover differentiation, synaptonemal complex formation, and regulatory surveillance at the leptotene/zygotene transition of meiosis. *Cell*, 117(1), 29–45. [https://doi.org/10.1016/s0092-8674\(04\)00292-2](https://doi.org/10.1016/s0092-8674(04)00292-2)
- Borrill, P., Harrington, S. A., & Uauy, C. (2019). Applying the latest advances in genomics and phenomics for trait discovery in polyploid wheat. *Plant Journal*, 97(1), 56–72. <https://doi.org/10.1111/tpj.14150>
- Borrill, P., Ramirez-Gonzalez, R., & Uauy, C. (2016). expVIP: a Customizable RNA-seq Data Analysis and Visualization Platform. *Plant Physiology*, 170(4), 2172–2186. <https://doi.org/10.1104/pp.15.01667>
- Braz, G. T., do Vale Martins, L., Zhang, T., Albert, P. S., Birchler, J. A., & Jiang, J. (2020). A universal chromosome identification system for maize and wild *Zea* species. *Chromosome Research*, 28(2), 183–194. <https://doi.org/10.1007/s10577-020-09630-5>
- Braz, G. T., He, L., Zhao, H., Zhang, T., Semrau, K., Rouillard, J.-M., Torres, G. A., & Jiang, J. (2018). Comparative Oligo-FISH Mapping: An Efficient and Powerful Methodology To Reveal Karyotypic and Chromosomal Evolution. *Genetics*, 208(2), 513–523. <https://doi.org/10.1534/genetics.117.300344>
- Bukhari, Y. M. (1997). A simple method of chromosome preparation for *Acacia* and *Prosopis* (Mimosaceae). *Hereditas*, 126(2), 195–197. <https://doi.org/10.1111/j.1601-5223.1997.00195.x>

- Burset, M., Seledtsov, I. A., & Solovyev, V. V. (2000). Analysis of canonical and non-canonical splice sites in mammalian genomes. *Nucleic Acids Research*, 28(21), 4364–4375. <https://doi.org/10.1093/nar/28.21.4364>
- Cannavo, E., Sanchez, A., Anand, R., Ranjha, L., Hugener, J., Adam, C., Acharya, A., Weyland, N., Aran-Guiu, X., Charbonnier, J.-B., Hoffmann, E. R., Borde, V., Matos, J., & Cejka, P. (2020). Regulation of the MLH1-MLH3 endonuclease in meiosis. *Nature*, 586(7830), 618–622. <https://doi.org/10.1038/s41586-020-2592-2>
- Capilla-Pérez, L., Durand, S., Hurel, A., Lian, Q., Chambon, A., Taochy, C., Solier, V., Grelon, M., & Mercier, R. (2021). The synaptonemal complex imposes crossover interference and heterochiasmy in *Arabidopsis*. *Proceedings of the National Academy of Sciences of the United States of America*, 118(12), 1–11. <https://doi.org/10.1073/pnas.2023613118>
- Carballo, J. A., Johnson, A. L., Sedgwick, S. G., & Cha, R. S. (2008). Phosphorylation of the Axial Element Protein Hop1 by Mec1/Tel1 Ensures Meiotic Interhomolog Recombination. *Cell*, 132(5), 758–770. <https://doi.org/10.1016/j.cell.2008.01.035>
- Caryl, A. P., Armstrong, S. J., Jones, G. H., & Franklin, F. C. (2000). A homologue of the yeast HOP1 gene is inactivated in the *Arabidopsis* meiotic mutant *asy1*. *Chromosoma*, 109(1–2), 62–71. <https://doi.org/10.1007/s004120050413>
- Caryl, A. P., Jones, G. H., & Franklin, F. C. H. (2003). Dissecting plant meiosis using *Arabidopsis thaliana* mutants. *Journal of Experimental Botany*, 54(380), 25–38. <https://doi.org/10.1093/jxb/erg041>
- Chakraborty, P., Pankajam, A. V., Lin, G., Dutta, A., Krishnaprasad, N. G., Tekkedil, M. M., Shinohara, A., Steinmetz, L. M., & Nishant, K. T. (2017). Modulating Crossover Frequency and Interference for Obligate Crossovers in *Saccharomyces cerevisiae* Meiosis. *G3 (Bethesda, Md.)*, 7(5), 1511–1524. <https://doi.org/10.1534/g3.117.040071>
- Challinor, A. J., Watson, J., Lobell, D. B., Howden, S. M., Smith, D. R., & Chhetri, N. (2014). A meta-analysis of crop yield under climate change and adaptation. *Nature Climate Change*, 4(4), 287–291. <https://doi.org/10.1038/nclimate2153>
- Chaudhary, S., Khokhar, W., Jabre, I., Reddy, A. S. N., Byrne, L. J., Wilson, C. M., & Syed, N. H. (2019). Alternative Splicing and Protein Diversity: Plants Versus Animals. *Frontiers in Plant Science*, 10, 708. <https://doi.org/10.3389/fpls.2019.00708>
- Chelysheva, L., Vezon, D., Chambon, A., Gendrot, G., Pereira, L., Lemhemdi, A., Vrielynck, N., Le Guin, S., Novatchkova, M., & Grelon, M. (2012). The *Arabidopsis* HEI10 Is a New ZMM Protein Related to Zip3. *PLOS Genetics*, 8(7), 1–17. <https://doi.org/10.1371/journal.pgen.1002799>
- Chen, L., Huang, L., Min, D., Phillips, A., Wang, S., Madgwick, P. J., Parry, M. A. J., & Hu, Y.-G. (2012). Development and characterization of a new TILLING population

- of common bread wheat (*Triticum aestivum* L.). *PLoS One*, 7(7), e41570–e41570. <https://doi.org/10.1371/journal.pone.0041570>
- Chen, S. Y., Tsubouchi, T., Rockmill, B., Sandler, J. S., Richards, D. R., Vader, G., Hochwagen, A., Roeder, G. S., & Fung, J. C. (2008). Global analysis of the meiotic crossover landscape. *Developmental Cell*, 15(3), 401–415. <https://doi.org/10.1016/j.devcel.2008.07.006>
- Chen, X., Suhandynata, R. T., Sandhu, R., Rockmill, B., Mohibullah, N., Niu, H., Liang, J., Lo, H. C., Miller, D. E., Zhou, H., Börner, G. V., & Hollingsworth, N. M. (2015). Phosphorylation of the Synaptonemal Complex Protein Zip1 Regulates the Crossover/Noncrossover Decision during Yeast Meiosis. *PLoS Biology*, 13(12), 1–35. <https://doi.org/10.1371/journal.pbio.1002329>
- Cheng, Z., Otto, G. M., Powers, E. N., Keskin, A., Mertins, P., Carr, S. A., Jovanovic, M., & Brar, G. A. (2018). Pervasive, Coordinated Protein-Level Changes Driven by Transcript Isoform Switching during Meiosis. *Cell*, 172(5), 910–923.e16. <https://doi.org/10.1016/j.cell.2018.01.035>
- Choi, K., Zhao, X., Tock, A. J., Lambing, C., Underwood, C. J., Hardcastle, T. J., Serra, H., Kim, J., Cho, H. S., Kim, J., Ziolkowski, P. A., Yelina, N. E., Hwang, I., Martienssen, R. A., & Henderson, I. R. (2018). Nucleosomes and DNA methylation shape meiotic DSB frequency in *Arabidopsis thaliana* transposons and gene regulatory regions. *Genome Research*, 28(4), 532–546. <https://doi.org/10.1101/gr.225599.117>
- Claussen, U., Michel, S., Mühlig, P., Westermann, M., Grummt, U.-W., Kromeyer-Hauschild, K., & Liehr, T. (2002). Demystifying chromosome preparation and the implications for the concept of chromosome condensation during mitosis. *Cytogenetic and Genome Research*, 98(2–3), 136–146. <https://doi.org/10.1159/000069817>
- Colaiácovo, M. P., MacQueen, A. J., Martinez-Perez, E., McDonald, K., Adamo, A., La Volpe, A., & Villeneuve, A. M. (2003). Synaptonemal complex assembly in *C. elegans* is dispensable for loading strand-exchange proteins but critical for proper completion of recombination. *Developmental Cell*, 5(3), 463–474. [https://doi.org/10.1016/s1534-5807\(03\)00232-6](https://doi.org/10.1016/s1534-5807(03)00232-6)
- Colas, I. (2008). “A study of the mechanisms of meiosis in wheat” X The world of the Ph1 Locus W By Isabelle Colas.
- Colas, I., Darrier, B., Arrieta, M., Mittmann, S. U., Ramsay, L., Sourdille, P., & Waugh, R. (2017). Observation of extensive chromosome axis remodeling during the “Diffuse-phase” of Meiosis in large genome cereals. *Frontiers in Plant Science*, 8(July), 1–9. <https://doi.org/10.3389/fpls.2017.01235>
- Collins, K. A., Unruh, J. R., Slaughter, B. D., Yu, Z., Lake, C. M., Nielsen, R. J., Box, K. S., Miller, D. E., Blumenstiel, J. P., Perera, A. G., Malanowski, K. E., & Hawley, R. S. (2014). Corolla is a novel protein that contributes to the architecture of the

- synaptonemal complex of *Drosophila*. *Genetics*, 198(1), 219–228. <https://doi.org/10.1534/genetics.114.165290>
- Comai, L. (2005). The advantages and disadvantages of being polyploid. *Nature Reviews Genetics*, 6(11), 836–846. <https://doi.org/10.1038/nrg1711>
- Costa, Y., Speed, R., Ollinger, R., Alsheimer, M., Semple, C. A., Gautier, P., Maratou, K., Novak, I., Höög, C., Benavente, R., & Cooke, H. J. (2005). Two novel proteins recruited by synaptonemal complex protein 1 (SYCP1) are at the centre of meiosis. *Journal of Cell Science*, 118(Pt 12), 2755–2762. <https://doi.org/10.1242/jcs.02402>
- Coulton, A., Burridge, A. J., & Edwards, K. J. (2020). Examining the Effects of Temperature on Recombination in Wheat . In *Frontiers in Plant Science* (Vol. 11, p. 230). <https://www.frontiersin.org/article/10.3389/fpls.2020.00230>
- Couteau, F., & Zetka, M. (2005). HTP-1 coordinates synaptonemal complex assembly with homolog alignment during meiosis in *C. elegans*. *Genes & Development*, 19(22), 2744–2756. <https://doi.org/10.1101/gad.1348205>
- Couteau, F., Belzile, F., Horlow, C., Grandjean, O., Vezon, D., Doutriaux, M., The, S., Cell, P., & Sep, N. (1999). *Random Chromosome Segregation without Meiotic Arrest in Both Male and Female Meiocytes of a dmc1 Mutant of Arabidopsis* Published by: American Society of Plant Biologists (ASPB) Linked references are available on JSTOR for this article: 11(9), 1623–1634.
- Crismani, W., Girard, C., Froger, N., Pradillo, M., Santos, J. L., Chelysheva, L., Copenhaver, G. P., Horlow, C., & Mercier, R. (2012). FANCM limits meiotic crossovers. *Science (New York, N.Y.)*, 336(6088), 1588–1590. <https://doi.org/10.1126/science.1220381>
- Cuacos, M., Lambing, C., Pachon-Penalba, M., Osman, K., Armstrong, S. J., Henderson, I. R., Sanchez-Moran, E., Franklin, F. C. H., & Heckmann, S. (2021). Meiotic chromosome axis remodelling is critical for meiotic recombination in *Brassica rapa*. *Journal of Experimental Botany*, 72(8), 3012–3027. <https://doi.org/10.1093/jxb/erab035>
- Cuadrado, Á., & Jouve, N. (2010). Chromosomal detection of simple sequence repeats (SSRs) using nondenaturing FISH (ND-FISH). *Chromosoma*, 119(5), 495–503. <https://doi.org/10.1007/s00412-010-0273-x>
- Cuadrado, Á., Golczyk, H., & Jouve, N. (2009). A novel, simple and rapid nondenaturing FISH (ND-FISH) technique for the detection of plant telomeres. Potential used and possible target structures detected. *Chromosome Research*, 17(6), 755–762. <https://doi.org/10.1007/s10577-009-9060-z>
- Daniel, K., Lange, J., Hached, K., Fu, J., Anastassiadis, K., Roig, I., Cooke, H. J., Stewart, A. F., Wassmann, K., Jasen, M., Keeney, S., & Tóth, A. (2011). Meiotic homologue alignment and its quality surveillance are controlled by mouse HORMAD1. *Nature Cell Biology*, 13(5), 599–610. <https://doi.org/10.1038/ncb2213>

- Danilova, T. V., Friebel, B., & Gill, B. S. (2014). Development of a wheat single gene FISH map for analyzing homoeologous relationship and chromosomal rearrangements within the Triticeae. *TAG. Theoretical and Applied Genetics. Theoretische Und Angewandte Genetik*, 127(3), 715–730. <https://doi.org/10.1007/s00122-013-2253-z>
- Database resources of the National Center for Biotechnology Information. (2018). Nucleic Acids Research, 46(D1), D8–D13. <https://doi.org/10.1093/nar/gkx1095>
- De Muyt, A., Pereira, L., Vezon, D., Chelysheva, L., Gendrot, G., Chambon, A., Lainé-Choinard, S., Pelletier, G., Mercier, R., Nogué, F., & Grelon, M. (2009). A High Throughput Genetic Screen Identifies New Early Meiotic Recombination Functions in *Arabidopsis thaliana*. *PLOS Genetics*, 5(9), e1000654. <https://doi.org/10.1371/journal.pgen.1000654>
- De Muyt, A., Zhang, L., Piolot, T., Kleckner, N., Espagne, E., & Zickler, D. (2014). E3 ligase Hei10: a multifaceted structure-based signaling molecule with roles within and beyond meiosis. *Genes & Development*, 28(10), 1111–1123. <https://doi.org/10.1101/gad.240408.114>
- de Vries, F. A. T., de Boer, E., van den Bosch, M., Baarens, W. M., Ooms, M., Yuan, L., Liu, J.-G., van Zeeland, A. A., Heyting, C., & Pastink, A. (2005). Mouse Sycp1 functions in synaptonemal complex assembly, meiotic recombination, and XY body formation. *Genes & Development*, 19(11), 1376–1389. <https://doi.org/10.1101/gad.329705>
- Delgado, A., Carvalho, A., Martín, A. C., Martín, A., & Lima-Brito, J. (2017). Genomic reshuffling in advanced lines of hexaploid tritordeum. *Genetic Resources and Crop Evolution*, 64(6), 1331–1353. <https://doi.org/10.1007/s10722-016-0439-3>
- Demirci, S., van Dijk, A. D. J., Sanchez Perez, G., Aflitos, S. A., de Ridder, D., & Peters, S. A. (2017). Distribution, position and genomic characteristics of crossovers in tomato recombinant inbred lines derived from an interspecific cross between *Solanum lycopersicum* and *Solanum pimpinellifolium*. *The Plant Journal: For Cell and Molecular Biology*, 89(3), 554–564. <https://doi.org/10.1111/tpj.13406>
- Deo, R. C., Bonanno, J. B., Sonenberg, N., & Burley, S. K. (1999). Recognition of polyadenylate RNA by the poly(A)-binding protein. *Cell*, 98(6), 835–845. [https://doi.org/10.1016/s0092-8674\(00\)81517-2](https://doi.org/10.1016/s0092-8674(00)81517-2)
- Desjardins, S. D., Ogle, D. E., Ayoub, M. A., Heckmann, S., Henderson, I. R., Edwards, K. J., & Higgins, J. D. (2020a). MutS homologue 4 and MutS homologue 5 maintain the obligate crossover in wheat despite stepwise gene loss following polyploidization1[CC-BY]. *Plant Physiology*, 183(4), 1545–1558. <https://doi.org/10.1104/pp.20.00534>
- Desjardins, S., Kanyuka, K., & Higgins, J. D. (2020b). A Cytological Analysis of Wheat Meiosis Targeted by Virus-Induced Gene Silencing (VIGS). *Methods in Molecular Biology*, 2061(2393175), 319–330. [https://doi.org/10.1007/978-1-4939-9818-0\\_22](https://doi.org/10.1007/978-1-4939-9818-0_22)

- Deutsch, C. A., Tewksbury, J. J., Tigchelaar, M., Battisti, D. S., Merrill, S. C., Huey, R. B., & Naylor, R. L. (2018). Increase in crop losses to insect pests in a warming climate. *Science (New York, N.Y.)*, 361(6405), 916–919. <https://doi.org/10.1126/science.aat3466>
- Devisetty, U. K., Mayes, K., & Mayes, S. (2010). The RAD51 and DMC1 homoeologous genes of bread wheat: cloning, molecular characterization and expression analysis. *BMC Research Notes*, 3(1), 245. <https://doi.org/10.1186/1756-0500-3-245>
- Dhaliwal, H. S., Gill, B. S., & Waines, J. G. (1977). Analysis of induced homoeologous pairing in a ph mutant wheat X rye hybrid. *Journal of Heredity*, 68(4), 207–209. <https://doi.org/10.1093/oxfordjournals.jhered.a108815>
- do Vale Martins, L., Yu, F., Zhao, H., Dennison, T., Lauter, N., Wang, H., Deng, Z., Thompson, A., Semrau, K., Rouillard, J. M., Birchler, J. A., & Jiang, J. (2019). Meiotic crossovers characterized by haplotype-specific chromosome painting in maize. *Nature Communications*, 10(1), 1–10. <https://doi.org/10.1038/s41467-019-12646-z>
- Dobson, M. J., Pearlman, R. E., Karaiskakis, A., Spyropoulos, B., & Moens, P. B. (1994). Synaptonemal complex proteins: occurrence, epitope mapping and chromosome disjunction. *Journal of Cell Science*, 107 ( Pt 1), 2749–2760.
- Dong, H., & Roeder, G. S. (2000). Organization of the yeast Zip1 protein within the central region of the synaptonemal complex. *The Journal of Cell Biology*, 148(3), 417–426. <https://doi.org/10.1083/jcb.148.3.417>
- Draeger, T., C. Martin, A., Alabdullah, A. K., Pendle, A., Rey, M. D., Shaw, P., & Moore, G. (2020). Dmc1 is a candidate for temperature tolerance during wheat meiosis. *Theoretical and Applied Genetics*, 133(3), 809–828. <https://doi.org/10.1007/s00122-019-03508-9>
- Drechsel, G., Kahles, A., Kesarwani, A. K., Stauffer, E., Behr, J., Drewe, P., Rätsch, G., & Wachter, A. (2013). Nonsense-mediated decay of alternative precursor mRNA splicing variants is a major determinant of the *Arabidopsis* steady state transcriptome. *The Plant Cell*, 25(10), 3726–3742. <https://doi.org/10.1105/tpc.113.115485>
- Driscoll, C. J. (1972). GENETIC SUPPRESSION OF HOMOEOLOGOUS CHROMOSOME PAIRING IN HEXAPLOID WHEAT. *Canadian Journal of Genetics and Cytology*, 14(1), 39–42. <https://doi.org/10.1139/g72-004>
- Drozdetskiy, A., Cole, C., Procter, J., & Barton, G. J. (2015). JPred4: a protein secondary structure prediction server. *Nucleic Acids Research*, 43(W1), W389–W394. <https://doi.org/10.1093/nar/gkv332>
- Dubcovsky, J., & Dvorak, J. (2007). Genome plasticity a key factor in the success of polyploid wheat under domestication. *Science (New York, N.Y.)*, 316(5833), 1862–1866. <https://doi.org/10.1126/science.1143986>

- Eichhorn, S. W., Subtelny, A. O., Kronja, I., Kwasnieski, J. C., Orr-Weaver, T. L., & Bartel, D. P. (2016). mRNA poly(A)-tail changes specified by deadenylation broadly reshape translation in *Drosophila* oocytes and early embryos. *ELife*, 5. <https://doi.org/10.7554/eLife.16955>
- Espagne, E., Vasnier, C., Storlazzi, A., Kleckner, N. E., Silar, P., Zickler, D., & Malagnac, F. (2011). Sme4 coiled-coil protein mediates synaptonemal complex assembly, recombinosome relocalization, and spindle pole body morphogenesis. *Proceedings of the National Academy of Sciences of the United States of America*, 108(26), 10614–10619. <https://doi.org/10.1073/pnas.1107272108>
- Evol, P. S. (2021). Cytochemical heterochromatin differentiation in Sinapis. 158(2), 97–106.
- FAOSTAT, (2021) <http://www.fao.org/faostat/en/#data/QC>
- Feldman, M., & Levy, A. A. (2005). Allopolyploidy--a shaping force in the evolution of wheat genomes. *Cytogenetic and Genome Research*, 109(1–3), 250–258. <https://doi.org/10.1159/000082407>
- Ferdous, M., Higgins, J. D., Osman, K., Lambing, C., Roitinger, E., Mechtler, K., Armstrong, S. J., Perry, R., Pradillo, M., Cuñado, N., & Franklin, F. C. H. (2012). Inter-homolog crossing-over and synapsis in arabidopsis meiosis are dependent on the chromosome axis protein *atasy3*. *PLoS Genetics*, 8(2). <https://doi.org/10.1371/journal.pgen.1002507>
- Fontenete, S., Guimarães, N., Wengel, J., & Azevedo, N. F. (2016). Prediction of melting temperatures in fluorescence in situ hybridization (FISH) procedures using thermodynamic models. *Critical Reviews in Biotechnology*, 36(3), 566–577. <https://doi.org/10.3109/07388551.2014.993589>
- France, M. G., Enderle, J., Röhrig, S., Puchta, H., Franklin, F. C. H., & Higgins, J. D. (2021). ZYP1 is required for obligate cross-over formation and cross-over interference in *Arabidopsis*. *Proceedings of the National Academy of Sciences of the United States of America*, 118(14), 1–11. <https://doi.org/10.1073/pnas.2021671118>
- Frédéric, C., Adriana, A., Sébastien, T., Natasha, G., Valérie, B., Josquin, D., Lise, P., Pierre, S., Arnaud, C., Etienne, P., Philippe, L., Sophie, M., Nicolas, G., Jacques, L. G., Francois, B., Michael, A., Véronique, J., Julie, P., Céline, D., ... Catherine, F. (2014). Structural and functional partitioning of bread wheat chromosome 3B. *Science*, 345(6194), 1249721. <https://doi.org/10.1126/science.1249721>
- Fu, S., Chen, L., Wang, Y., Li, M., Yang, Z., Qiu, L., Yan, B., Ren, Z., & Tang, Z. (2015). Oligonucleotide probes for ND-FISH analysis to identify rye and wheat chromosomes. *Scientific Reports*, 5, 1–7. <https://doi.org/10.1038/srep10552>
- Fukuda, T., Pratto, F., Schimenti, J. C., Turner, J. M. A., Camerini-Otero, R. D., & Höög, C. (2012). Phosphorylation of chromosome core components may serve as axis

- marks for the status of chromosomal events during mammalian meiosis. *PLoS Genetics*, 8(2), e1002485. <https://doi.org/10.1371/journal.pgen.1002485>
- Fukui, K., Ohmido, N., & Khush, G. S. (1994). Variability in rDNA loci in the genus *Oryza* detected through fluorescence in situ hybridization. *Theoretical and Applied Genetics: International Journal of Plant Breeding Research*, 87(8), 893–899. <https://doi.org/10.1007/BF00225782>
- Fussell, C. P. (1987). *The Rabl orientation: A prelude to synapsis*.
- Gaeta, R. T., & Chris Pires, J. (2010). Homoeologous recombination in allopolyploids: the polyploid ratchet. *The New Phytologist*, 186(1), 18–28. <https://doi.org/10.1111/j.1469-8137.2009.03089.x>
- Gao, J., & Colaiácovo, M. P. (2018). Zipping and Unzipping: Protein Modifications Regulating Synaptonemal Complex Dynamics. *Trends in Genetics*, 34(3), 232–245. <https://doi.org/10.1016/j.tig.2017.12.001>
- Gao, J., Barroso, C., Zhang, P., Kim, H.-M., Li, S., Labrador, L., Lightfoot, J., Gerashchenko, M. V., Labunskyy, V. M., Dong, M.-Q., Martinez-Perez, E., & Colaiácovo, M. P. (2016). N-terminal acetylation promotes synaptonemal complex assembly in *C. elegans*. *Genes & Development*, 30(21), 2404–2416. <https://doi.org/10.1101/gad.277350.116>
- Gao, P., Quilichini, T. D., Zhai, C., Qin, L., Nilsen, K. T., Li, Q., Sharpe, A. G., Kochian, L. V., Zou, J., Reddy, A. S. N., Wei, Y., Pozniak, C., Patterson, N., Gillmor, C. S., Datla, R., & Xiang, D. (2021). Alternative splicing dynamics and evolutionary divergence during embryogenesis in wheat species. *Plant Biotechnology Journal*, 19(8), 1624–1643. <https://doi.org/10.1111/pbi.13579>
- Gaudet, P., Livstone, M. S., Lewis, S. E., & Thomas, P. D. (2011). Phylogenetic-based propagation of functional annotations within the Gene Ontology consortium. *Briefings in Bioinformatics*, 12(5), 449–462. <https://doi.org/10.1093/bib/bbr042>
- Gauthier, F. M., & McGinnis, R. C. (1968). THE MEIOTIC BEHAVIOUR OF A NULLI-HAPLOID PLANT IN AVENA SATIVA L. *Canadian Journal of Genetics and Cytology*, 10(1), 186–189. <https://doi.org/10.1139/g68-025>
- Gerlach, W. L., & Bedbrook, J. R. (1979). Cloning and characterization of ribosomal RNA genes from wheat and barley. *Nucleic Acids Research*, 7(7), 1869–1885. <https://doi.org/10.1093/nar/7.7.1869>
- Gerlach, W. L., & Dyer, T. A. (1980). Sequence organization of the repeating units in the nucleus of wheat which contain 5S rRNA genes. *Nucleic Acids Research*, 8(21), 4851–4865. <https://doi.org/10.1093/nar/8.21.4851>
- Girard, C., Crismani, W., Froger, N., Mazel, J., Lemhemdi, A., Horlow, C., & Mercier, R. (2014). FANCM-associated proteins MHF1 and MHF2, but not the other Fanconi anemia factors, limit meiotic crossovers. *Nucleic Acids Research*, 42(14), 9087–9095. <https://doi.org/10.1093/nar/gku614>

- Goodyer, W., Kaitna, S., Couteau, F., Ward, J. D., Boulton, S. J., & Zetka, M. (2008). HTP-3 links DSB formation with homolog pairing and crossing over during *C. elegans* meiosis. *Developmental Cell*, 14(2), 263–274. <https://doi.org/10.1016/j.devcel.2007.11.016>
- Greer, E., Martín, A. C., Pendle, A., Colas, I., Jones, A. M. E., Moore, G., & Shawa, P. (2012). The *Ph1* locus suppresses *Cdk2*-type activity during premeiosis and meiosis in wheat. *Plant Cell*, 24(1), 152–162. <https://doi.org/10.1105/tpc.111.094771>
- Griffiths, S., Sharp, R., Foote, T. N., Bertin, I., Wanous, M., Reader, S., Colas, I., & Moore, G. (2006). Molecular characterization of *Ph1* as a major chromosome pairing locus in polyploid wheat. *Nature*, 439(7077), 749–752. <https://doi.org/10.1038/nature04434>
- Grishaeva, T. M., & Bogdanov, Y. F. (2014). Conservation and Variability of Synaptonemal Complex Proteins in Phylogenesis of Eukaryotes. *International Journal of Evolutionary Biology*, 2014, 1–16. <https://doi.org/10.1155/2014/856230>
- Hall, J. C. (1972). Chromosome segregation influenced by two alleles of the meiotic mutant c(3)G in *Drosophila melanogaster*. *Genetics*, 71(3), 367–400. <https://doi.org/10.1093/genetics/71.3.367>
- Hamer, G., Gell, K., Kouznetsova, A., Novak, I., Benavente, R., & Höög, C. (2006). Characterization of a novel meiosis-specific protein within the central element of the synaptonemal complex. *Journal of Cell Science*, 119(Pt 19), 4025–4032. <https://doi.org/10.1242/jcs.03182>
- Hamer, G., Wang, H., Bolcun-Filas, E., Cooke, H. J., Benavente, R., & Höög, C. (2008). Progression of meiotic recombination requires structural maturation of the central element of the synaptonemal complex. *Journal of Cell Science*, 121(Pt 15), 2445–2451. <https://doi.org/10.1242/jcs.033233>
- Han, Y. F., Dou, K., Ma, Z. Y., Zhang, S. W., Huang, H. W., Li, L., Cai, T., Chen, S., Zhu, J. K., & He, X. J. (2014). SUVR2 is involved in transcriptional gene silencing by associating with SNF2-related chromatin-remodeling proteins in *Arabidopsis*. *Cell Research*, 24(12), 1445–1465. <https://doi.org/10.1038/cr.2014.156>
- Han, Y., Zhang, T., Thammapichai, P., Weng, Y., & Jiang, J. (2015). Chromosome-Specific Painting in *Cucumis* Species Using Bulked Oligonucleotides. *Genetics*, 200(3), 771–779. <https://doi.org/10.1534/genetics.115.177642>
- Harper, L., Golubovskaya, I., & Cande, W. Z. (2004). A bouquet of chromosomes. *Journal of Cell Science*, 117(18), 4025–4032. <https://doi.org/10.1242/jcs.01363>
- Hassani-Pak, K., Singh, A., Brandizi, M., Hearnshaw, J., Parsons, J. D., Amberkar, S., Phillips, A. L., Doonan, J. H., & Rawlings, C. (2021). KnetMiner: a comprehensive approach for supporting evidence-based gene discovery and complex trait analysis across species. *Plant Biotechnology Journal*, 1–9. <https://doi.org/10.1111/pbi.13583>

- Hernández-Hernández, A., Masich, S., Fukuda, T., Kouznetsova, A., Sandin, S., Daneholt, B., & Höög, C. (2016). The central element of the synaptonemal complex in mice is organized as a bilayered junction structure. *Journal of Cell Science*, 129(11), 2239–2249. <https://doi.org/10.1242/jcs.182477>
- Hesse, S., Zelkowski, M., Mikhailova, E. I., Keijzer, C. J., Houben, A., & Schubert, V. (2019). Ultrastructure and dynamics of synaptonemal complex components during meiotic pairing and synapsis of standard (A) and accessory (B) rye chromosomes. *Frontiers in Plant Science*, 10(June), 1–20. <https://doi.org/10.3389/fpls.2019.00773>
- Higgins, J. D., Buckling, E. F., Franklin, F. C. H., & Jones, G. H. (2008). Expression and functional analysis of AtMUS81 in *Arabidopsis* meiosis reveals a role in the second pathway of crossing-over. *The Plant Journal: For Cell and Molecular Biology*, 54(1), 152–162. <https://doi.org/10.1111/j.1365-313X.2008.03403.x>
- Higgins, J. D., Osman, K., Jones, G. H., & Franklin, F. C. H. (2014). Factors underlying restricted crossover localization in barley meiosis. *Annual Review of Genetics*, 48, 29–47. <https://doi.org/10.1146/annurev-genet-120213-092509>
- Higgins, J. D., Perry, R. M., Barakate, A., Ramsay, L., Waugh, R., Halpin, C., Armstrong, S. J., & Franklin, F. C. H. (2012). Spatiotemporal asymmetry of the meiotic program underlies the predominantly distal distribution of meiotic crossovers in barley. *The Plant Cell*, 24(10), 4096–4109. <https://doi.org/10.1105/tpc.112.102483>
- Higgins, J. D., Sanchez-Moran, E., Armstrong, S. J., Jones, G. H., & Franklin, F. C. H. (2005). The *Arabidopsis* synaptonemal complex protein ZYP1 is required for chromosome synapsis and normal fidelity of crossing over. *Genes and Development*, 19(20), 2488–2500. <https://doi.org/10.1101/gad.354705>
- Hobolth, P. (1981). Chromosome pairing in allohexaploid wheat var. Chinese Spring. Transformation of multivalents into bivalents, a mechanism for exclusive bivalent formation. *Carlsberg Research Communications*, 46(3), 129. <https://doi.org/10.1007/BF02910465>
- Hollingsworth, N. M., & Byers, B. (1989). HOP1: a yeast meiotic pairing gene. *Genetics*, 121(3), 445–462. <https://doi.org/10.1093/genetics/121.3.445>
- Hollingsworth, N. M., Goetsch, L., & Byers, B. (1990). The HOP1 gene encodes a meiosis-specific component of yeast chromosomes. *Cell*, 61(1), 73–84. [https://doi.org/10.1016/0092-8674\(90\)90216-2](https://doi.org/10.1016/0092-8674(90)90216-2)
- Holm, P. B. (1986). Chromosome pairing and chiasma formation in allohexaploid wheat, *Triticum aestivum* analyzed by spreading of meiotic nuclei. *Carlsberg Research Communications*, 51(4), 239. <https://doi.org/10.1007/BF02906837>
- Holm, P. B., & Wang, X. (1988). The effect of chromosome 5B on synapsis and chiasma formation in wheat, *Triticum aestivum* cv. Chinese Spring. *Carlsberg Research Communications*, 53(2), 191. <https://doi.org/10.1007/BF02907179>

- Howe, K. L., Contreras-Moreira, B., De Silva, N., Maslen, G., Akanni, W., Allen, J., Alvarez-Jarreta, J., Barba, M., Bolser, D. M., Cambell, L., Carbajo, M., Chakiachvili, M., Christensen, M., Cummins, C., Cuzick, A., Davis, P., Fexova, S., Gall, A., George, N., ... Flieck, P. (2020). Ensembl Genomes 2020-enabling non-vertebrate genomic research. *Nucleic Acids Research*, 48(D1), D689–D695. <https://doi.org/10.1093/nar/gkz890>
- Humphries, N., Leung, W.-K., Argunhan, B., Terentyev, Y., Dvorackova, M., & Tsubouchi, H. (2013). The Ecm11-Gmc2 complex promotes synaptonemal complex formation through assembly of transverse filaments in budding yeast. *PLoS Genetics*, 9(1), e1003194–e1003194. <https://doi.org/10.1371/journal.pgen.1003194>
- Hunter, N., & Borts, R. H. (1997). Mlh1 is unique among mismatch repair proteins in its ability to promote crossing-over during meiosis. *Genes and Development*, 11(12), 1573–1582. <https://doi.org/10.1101/gad.11.12.1573>
- Hurlock, M. E., Čavka, I., Kursel, L. E., Haversat, J., Wooten, M., Nizami, Z., Turniansky, R., Hoess, P., Ries, J., Gall, J. G., Rog, O., Köhler, S., & Kim, Y. (2020). Identification of novel synaptonemal complex components in *C. Elegans*. *Journal of Cell Biology*, 219(5). <https://doi.org/10.1083/jcb.201910043>
- Imai, Y., Saito, K., Takemoto, K., Velilla, F., Kawasaki, T., Ishiguro, K. I., & Sakai, N. (2021). Sycp1 Is Not Required for Subtelomeric DNA Double-Strand Breaks but Is Required for Homologous Alignment in Zebrafish Spermatocytes. *Frontiers in Cell and Developmental Biology*, 9(March), 1–19. <https://doi.org/10.3389/fcell.2021.664377>
- Irshad, A., Guo, H., Ur Rehman, S., Wang, X., Gu, J., Xiong, H., Xie, Y., Zhao, L., Zhao, S., Wang, C., & Liu, L. (2021). Identification of Single Nucleotide Polymorphism in TaSBEIII and Development of KASP Marker Associated With Grain Weight in Wheat. *Frontiers in Genetics*, 12(July), 1–10. <https://doi.org/10.3389/fgene.2021.697294>
- Jackson, S., & Chen, Z. J. (2010). Genomic and expression plasticity of polyploidy. *Current Opinion in Plant Biology*, 13(2), 153–159. <https://doi.org/10.1016/j.pbi.2009.11.004>
- Janda, J., Šafář, J., Kubaláková, M., Bartoš, J., Kovářová, P., Suchánková, P., Pateyron, S., Číhalíková, J., Sourdille, P., Šimková, H., Faivre-Rampant, P., Hřibová, E., Bernard, M., Lukaszewski, A., Doležel, J., & Chalhoub, B. (2006). Advanced resources for plant genomics: A BAC library specific for the short arm of wheat chromosome 1B. *Plant Journal*, 47(6), 977–986. <https://doi.org/10.1111/j.1365-313X.2006.02840.x>
- Jauhar, P. P. (1975). Genetic control of diploid-like meiosis in hexaploid tall fescue. *Nature*, 254(5501), 595–597. <https://doi.org/10.1038/254595a0>
- Jenczewski, E., & Alix, K. (2004). From Diploids to Allopolyploids: The Emergence of

- Efficient Pairing Control Genes in Plants. *Critical Reviews in Plant Sciences*, 23(1), 21–45. <https://doi.org/10.1080/07352680490273239>
- Jenczewski, E., Eber, F., Grimaud, A., Huet, S., Lucas, M. O., Monod, H., & Chèvre, A. M. (2003). PrBn, a Major Gene Controlling Homeologous Pairing in Oilseed Rape (*Brassica napus*) Haploids. *Genetics*, 164(2), 645–653. <https://doi.org/10.1093/genetics/164.2.645>
- Jenkins, G., & Rees, H. (1991). Strategies of bivalent formation in allopolyploid plants. *Proceedings of the Royal Society B: Biological Sciences*, 243(1308), 209–214. <https://doi.org/10.1098/rspb.1991.0033>
- Jeon, J.-S., Chung, Y.-Y., Lee, S., Yi, G.-H., Oh, B.-G., & An, G. (1999). Isolation and characterization of an anther-specific gene, RA8, from rice (*Oryza sativa L.*). *Plant Molecular Biology*, 39(1), 35–44. <https://doi.org/10.1023/A:1006157603096>
- Ji, J., Tang, D., Shen, Y., Xue, Z., Wang, H., Shi, W., Zhang, C., Du, G., Li, Y., & Cheng, Z. (2016). P31comet, a member of the synaptonemal complex, participates in meiotic DSB formation in rice. *Proceedings of the National Academy of Sciences of the United States of America*, 113(38), 10577–10582. <https://doi.org/10.1073/pnas.1607334113>
- Jiang, J. (2019). Fluorescence in situ hybridization in plants: recent developments and future applications. *Chromosome Research*, 27(3), 153–165. <https://doi.org/10.1007/s10577-019-09607-z>
- Jiang, W., Jiang, C., Yuan, W., Zhang, M., Fang, Z., Li, Y., Li, G., Jia, J., & Yang, Z. (2021). A universal karyotypic system for hexaploid and diploid *Avena* species brings oat cytogenetics into the genomics era. *BMC Plant Biology*, 21(1), 1–15. <https://doi.org/10.1186/s12870-021-02999-3>
- Jiao, Y., Wickett, N. J., Ayyampalayam, S., Chanderbali, A. S., Landherr, L., Ralph, P. E., Tomsho, L. P., Hu, Y., Liang, H., Soltis, P. S., Soltis, D. E., Clifton, S. W., Schlarbaum, S. E., Schuster, S. C., Ma, H., Leebens-Mack, J., & dePamphilis, C. W. (2011). Ancestral polyploidy in seed plants and angiosperms. *Nature*, 473(7345), 97–100. <https://doi.org/10.1038/nature09916>
- Jones, G. H., & Franklin, F. C. H. (2006). Meiotic Crossing-over: Obligation and Interference. *Cell*, 126(2), 246–248. <https://doi.org/https://doi.org/10.1016/j.cell.2006.07.010>
- Jordan, P. W., Karppinen, J., & Handel, M. A. (2012). Polo-like kinase is required for synaptonemal complex disassembly and phosphorylation in mouse spermatocytes. *Journal of Cell Science*, 125(Pt 21), 5061–5072. <https://doi.org/10.1242/jcs.105015>
- Kaltsikes, P. J. (1972). Duration of the mitotic cycle in triticale. *Caryologia*, 25(4), 437–542. <https://doi.org/10.1080/00087114.1972.10796507>
- Kashtwari, M., Wani, A. A., & Rather, R. N. (2019). TILLING: an alternative path for crop improvement. *Journal of Crop Improvement*, 33(1), 83–109.

<https://doi.org/10.1080/15427528.2018.1544954>

- Kato, A., Lamb, J. C., & Birchler, J. A. (2004). Chromosome painting using repetitive DNA sequences as probes for somatic chromosome identification in maize. *Proceedings of the National Academy of Sciences of the United States of America*, 101(37), 13554–13559. <https://doi.org/10.1073/pnas.0403659101>
- Keeney, S. (2008). Spo11 and the Formation of DNA Double-Strand Breaks in Meiosis. *Genome Dynamics and Stability*, 2, 81–123. [https://doi.org/10.1007/7050\\_2007\\_026](https://doi.org/10.1007/7050_2007_026)
- Kerr, S. M., Taggart, M. H., Lee, M., & Cooke, H. J. (1996). Ott, a mouse X-linked multigene family expressed specifically during meiosis. *Human Molecular Genetics*, 5(8), 1139–1148. <https://doi.org/10.1093/hmg/5.8.1139>
- Khoo, K. H. P., Able, A. J., & Able, J. A. (2012). The isolation and characterisation of the wheat molecular ZIPper i homologue, TaZYP1. *BMC Research Notes*, 5, 1–13. <https://doi.org/10.1186/1756-0500-5-106>
- Kim, E., Magen, A., & Ast, G. (2007). Different levels of alternative splicing among eukaryotes. *Nucleic Acids Research*, 35(1), 125–131. <https://doi.org/10.1093/nar/gkl924>
- Kim, Y., Rosenberg, S. C., Kugel, C. L., Kostow, N., Rog, O., Davydov, V., Su, T. Y., Dernburg, A. F., & Corbett, K. D. (2014). The chromosome axis controls meiotic events through a hierarchical assembly of HORMA domain proteins. *Developmental Cell*, 31(4), 487–502. <https://doi.org/10.1016/j.devcel.2014.09.013>
- King, J., Grewal, S., Yang, C. Y., Hubbart, S., Scholefield, D., Ashling, S., Edwards, K. J., Allen, A. M., Burridge, A., Bloor, C., Davassi, A., da Silva, G. J., Chalmers, K., & King, I. P. (2017). A step change in the transfer of interspecific variation into wheat from *Amblyopyrum muticum*. *Plant Biotechnology Journal*, 15(2), 217–226. <https://doi.org/10.1111/pbi.12606>
- King, J., Grewal, S., Yang, C., Hubbart Edwards, S., Scholefield, D., Ashling, S., Harper, J. A., Allen, A. M., Edwards, K. J., Burridge, A. J., & King, I. P. (2018). Introgression of *Aegilops speltoides* segments in *Triticum aestivum* and the effect of the gametocidal genes. *Annals of Botany*, 121(2), 229–240. <https://doi.org/10.1093/aob/mcx149>
- Kirov, I., Divashuk, M., Van Laere, K., Soloviev, A., & Khrustaleva, L. (2014). An easy “steamDrop” method for high quality plant chromosome preparation. *Molecular Cytogenetics*, 7(1), 1–10. <https://doi.org/10.1186/1755-8166-7-21>
- Kleckner, N. (1996). Meiosis: How could it Work? *Proceedings of the National Academy of Sciences of the United States of America*, 93(16), 8167–8174. <http://www.jstor.org/stable/39832>
- Kleckner, N., Zickler, D., Jones, G. H., Dekker, J., Padmore, R., Henle, J., & Hutchinson, J. (2004). A mechanical basis for chromosome function. *Proceedings of the*

National Academy of Sciences, 101(34), 12592–12597.  
<https://doi.org/10.1073/PNAS.0402724101>

Knoll, A., Higgins, J. D., Seeliger, K., Reha, S. J., Dangel, N. J., Bauknecht, M., Schröpfer, S., Franklin, F. C. H., & Puchta, H. (2012). The Fanconi Anemia Ortholog FANCM Ensures Ordered Homologous Recombination in Both Somatic and Meiotic Cells in *Arabidopsis*. *The Plant Cell*, 24(4), 1448–1464.  
<https://doi.org/10.1105/tpc.112.096644>

Komuro, S., Endo, R., Shikata, K., & Kato, A. (2013). Genomic and chromosomal distribution patterns of various repeated DNA sequences in wheat revealed by a fluorescence in situ hybridization procedure. *Genome*, 56(3), 131–137.  
<https://doi.org/10.1139/gen-2013-0003>

Krasileva, K. V., Vasquez-Gross, H. A., Howell, T., Bailey, P., Paraiso, F., Clissold, L., Simmonds, J., Ramirez-Gonzalez, R. H., Wang, X., Borrill, P., Fosker, C., Ayling, S., Phillips, A. L., Uauy, C., & Dubcovsky, J. (2017). Uncovering hidden variation in polyploid wheat. *Proceedings of the National Academy of Sciences*, 114(6), E913 LP-E921. <https://doi.org/10.1073/pnas.1619268114>

Kulkarni, D. S., Owens, S. N., Honda, M., Ito, M., Yang, Y., Corrigan, M. W., Chen, L., Quan, A. L., & Hunter, N. (2020). PCNA activates the MutL $\gamma$  endonuclease to promote meiotic crossing over. *Nature*, 586(7830), 623–627.  
<https://doi.org/10.1038/s41586-020-2645-6>

Kuo, P., Da Ines, O., & Lambing, C. (2021). Rewiring Meiosis for Crop Improvement. *Frontiers in Plant Science*, 12, 708948. <https://doi.org/10.3389/fpls.2021.708948>

Kupfer, D. M., Drabenstot, S. D., Buchanan, K. L., Lai, H., Zhu, H., Dyer, D. W., Roe, B. A., & Murphy, J. W. (2004). Introns and splicing elements of five diverse fungi. *Eukaryotic Cell*, 3(5), 1088–1100. <https://doi.org/10.1128/EC.3.5.1088-1100.2004>

Lambing, C., Franklin, F. C. H., & Wang, C. J. R. (2017). Understanding and manipulating meiotic recombination in plants. *Plant Physiology*, 173(3), 1530–1542. <https://doi.org/10.1104/pp.16.01530>

Lambing, C., Kuo, P. C., Tock, A. J., Topp, S. D., & Henderson, I. R. (2020). ASY1 acts as a dosage-dependent antagonist of telomere-led recombination and mediates crossover interference in *Arabidopsis*. *Proceedings of the National Academy of Sciences of the United States of America*, 117(24), 13647–13658.  
<https://doi.org/10.1073/pnas.1921055117>

Lambing, C., Osman, K., Nuntasontorn, K., West, A., Higgins, J. D., Copenhaver, G. P., Yang, J., Armstrong, S. J., Mechtler, K., Roitinger, E., & Franklin, F. C. H. (2015). *Arabidopsis* PCH2 Mediates Meiotic Chromosome Remodeling and Maturation of Crossovers. *PLOS Genetics*, 11(7), 1–27.  
<https://doi.org/10.1371/journal.pgen.1005372>

Langfelder, P., & Horvath, S. (2008). WGCNA: an R package for weighted correlation

- network analysis. *BMC Bioinformatics*, 9(1), 559. <https://doi.org/10.1186/1471-2105-9-559>
- Latypov, V., Rothenberg, M., Lorenz, A., Octobre, G., Csutak, O., Lehmann, E., Loidl, J., & Kohli, J. (2010). Roles of Hop1 and Mek1 in meiotic chromosome pairing and recombination partner choice in *Schizosaccharomyces pombe*. *Molecular and Cellular Biology*, 30(7), 1570–1581. <https://doi.org/10.1128/MCB.00919-09>
- Lenormand, T., Engelstädter, J., Johnston, S. E., Wijnker, E., & Haag, C. R. (2016). Evolutionary mysteries in meiosis. *Philosophical Transactions of the Royal Society B: Biological Sciences*, 371(1706). <https://doi.org/10.1098/rstb.2016.0001>
- Leung, W. K., Humphryes, N., Afshar, N., Argunhan, B., Terentyev, Y., Tsubouchi, T., & Tsubouchi, H. (2015). The synaptonemal complex is assembled by a polySUMOylation-driven feedback mechanism in yeast. *Journal of Cell Biology*, 211(4), 785–793. <https://doi.org/10.1083/jcb.201506103>
- Li, J., Li, Y., & Ma, L. (2021). Recent advances in CRISPR/Cas9 and applications for wheat functional genomics and breeding. *ABIOTECH*. <https://doi.org/10.1007/s42994-021-00042-5>
- Libuda, D. E., Uzawa, S., Meyer, B. J., & Villeneuve, A. M. (2013). Meiotic chromosome structures constrain and respond to designation of crossover sites. *Nature*, 502(7473), 703–706. <https://doi.org/10.1038/nature12577>
- Lim, J., Kim, D., Lee, Y.-S., Ha, M., Lee, M., Yeo, J., Chang, H., Song, J., Ahn, K., & Kim, V. N. (2018). Mixed tailing by TENT4A and TENT4B shields mRNA from rapid deadenylation. *Science (New York, N.Y.)*, 361(6403), 701–704. <https://doi.org/10.1126/science.aam5794>
- Lim, J., Lee, M., Son, A., Chang, H., & Kim, V. N. (2016). mTAIL-seq reveals dynamic poly(A) tail regulation in oocyte-to-embryo development. *Genes & Development*, 30(14), 1671–1682. <https://doi.org/10.1101/gad.284802.116>
- Liu, C.-X., Zhang, H., Yan, B., Qi, X.-L., Frauenheim, T., Dai, X., Fang, Z., & Zhang, S.-C. (2010). Oscillatory crossover from two-dimensional to three-dimensional topological insulators. *Physical Review B*, 81(4), 041307. <https://doi.org/10.1103/PhysRevB.81.041307>
- Liu, G., & Zhang, T. (2021). Single copy oligonucleotide fluorescence in situ hybridization probe design platforms: Development, application and evaluation. *International Journal of Molecular Sciences*, 22(13). <https://doi.org/10.3390/ijms22137124>
- Liu, J. G., Yuan, L., Brundell, E., Björkroth, B., Daneholt, B., & Höög, C. (1996). Localization of the N-terminus of SCP1 to the central element of the synaptonemal complex and evidence for direct interactions between the N-termini of SCP1 molecules organized head-to-head. *Experimental Cell Research*, 226(1), 11–19. <https://doi.org/10.1006/excr.1996.0197>

- Liu, S., Liu, Y., Yang, X., Tong, C., Edwards, D., Parkin, I. A. P., Zhao, M., Ma, J., Yu, J., Huang, S., Wang, X., Wang, J., Lu, K., Fang, Z., Bancroft, I., Yang, T.-J., Hu, Q., Wang, X., Yue, Z., ... Paterson, A. H. (2014). The *Brassica oleracea* genome reveals the asymmetrical evolution of polyploid genomes. *Nature Communications*, 5(1), 3930. <https://doi.org/10.1038/ncomms4930>
- Liu, X., Sun, S., Wu, Y., Zhou, Y., Gu, S., Yu, H., Yi, C., Gu, M., Jiang, J., Liu, B., Zhang, T., & Gong, Z. (2020). Dual-color oligo-FISH can reveal chromosomal variations and evolution in *Oryza* species. *Plant Journal*, 101(1), 112–121. <https://doi.org/10.1111/tpj.14522>
- Loidl, J., Klein, F., & Scherthan, H. (1994). Homologous pairing is reduced but not abolished in asynaptic mutants of yeast. *The Journal of Cell Biology*, 125(6), 1191–1200. <https://doi.org/10.1083/jcb.125.6.1191>
- Luo, M.-C., Gu, Y. Q., Puiu, D., Wang, H., Twardziok, S. O., Deal, K. R., Huo, N., Zhu, T., Wang, L., Wang, Y., McGuire, P. E., Liu, S., Long, H., Ramasamy, R. K., Rodriguez, J. C., Van, S. L., Yuan, L., Wang, Z., Xia, Z., ... Dvořák, J. (2017). Genome sequence of the progenitor of the wheat D genome *Aegilops tauschii*. *Nature*, 551(7681), 498–502. <https://doi.org/10.1038/nature24486>
- Lysak, M. A., Fransz, P. F., Ali, H. B., & Schubert, I. (2001). Chromosome painting in *Arabidopsis thaliana*. *The Plant Journal : For Cell and Molecular Biology*, 28(6), 689–697. <https://doi.org/10.1046/j.1365-313x.2001.01194.x>
- MacQueen, A. J., Colaiácovo, M. P., McDonald, K., & Villeneuve, A. M. (2002). Synapsis-dependent and -independent mechanisms stabilize homolog pairing during meiotic prophase in *C. elegans*. *Genes & Development*, 16(18), 2428–2442. <https://doi.org/10.1101/gad.1011602>
- Maestra, B., Hans de Jong, J., Shepherd, K., & Naranjo, T. (2002). Chromosome arrangement and behaviour of two rye homologous telosomes at the onset of meiosis in disomic wheat-5RL addition lines with and without the Ph1 locus. *Chromosome Research : An International Journal on the Molecular, Supramolecular and Evolutionary Aspects of Chromosome Biology*, 10(8), 655–667. <https://doi.org/10.1023/a:1021564327226>
- Mahadevaiah, S. K., Turner, J. M., Baudat, F., Rogakou, E. P., de Boer, P., Blanco-Rodríguez, J., Jasin, M., Keeney, S., Bonner, W. M., & Burgoyne, P. S. (2001). Recombinational DNA double-strand breaks in mice precede synapsis. *Nature Genetics*, 27(3), 271–276. <https://doi.org/10.1038/85830>
- Mahesh, S., Bethaju, K., Nalli, A., Frank, K., & Siddiqi, I. (2021). Functional analysis of a conserved domain in SWITCH1 reveals a role in commitment to female meiocyte differentiation in *Arabidopsis*. *Biochemical and Biophysical Research Communications*, 551, 121–126. <https://doi.org/10.1016/j.bbrc.2021.03.007>
- Mankouri, H. W., & Hickson, I. D. (2007). The RecQ helicase-topoisomerase III-Rmi1 complex: a DNA structure-specific “dissolvosome”? *Trends in Biochemical Sciences*, 32(10), 479–486. <https://doi.org/10.1016/j.tibs.2007.08.007>

- Sciences*, 32(12), 538–546. <https://doi.org/10.1016/j.tibs.2007.09.009>
- Mann, J. D., & Storey, W. B. (1966). Rapid Action of Carbamate Herbicides Upon Plant Cell Nuclei. *Cytologia*, 31(2), 203–207. <https://doi.org/10.1508/cytologia.31.203>
- Marcussen, T., Sandve, S. R., Heier, L., Spannagl, M., Pfeifer, M., Jakobsen, K. S., Wulff, B. B. H., Steuernagel, B., Mayer, K. F. X., & Olsen, O.-A. (2014). Ancient hybridizations among the ancestral genomes of bread wheat. *Science* (New York, N.Y.), 345(6194), 1250092. <https://doi.org/10.1126/science.1250092>
- Martín, A. C., Rey, M. D., Shaw, P., & Moore, G. (2017). Dual effect of the wheat Ph1 locus on chromosome synapsis and crossover. *Chromosoma*, 126(6), 669–680. <https://doi.org/10.1007/s00412-017-0630-0>
- Martín, Azahara C., Rey, M. D., Shaw, P., & Moore, G. (2017a). Dual effect of the wheat *Ph1* locus on chromosome synapsis and crossover. *Chromosoma*, 126(6), 669–680. <https://doi.org/10.1007/s00412-017-0630-0>
- Martín, Azahara C., Shaw, P., Phillips, D., Reader, S., & Moore, G. (2014). Licensing MLH1 sites for crossover during meiosis. *Nature Communications*, 5, 1–5. <https://doi.org/10.1038/ncomms5580>
- Martín, Azahara Carmen, Borrill, P., Higgins, J., Alabdullah, A., Ramírez-González, R. H., Swarbreck, D., Uauy, C., Shaw, P., & Moore, G. (2018). Genome-wide transcription during early wheat meiosis is independent of synapsis, ploidy level, and the Ph1 locus. *Frontiers in Plant Science*, 871(December), 1–19. <https://doi.org/10.3389/fpls.2018.01791>
- Martinez-Perez, E., & Villeneuve, A. M. (2005). HTP-1-dependent constraints coordinate homolog pairing and synapsis and promote chiasma formation during *C. elegans* meiosis. *Genes & Development*, 19(22), 2727–2743. <https://doi.org/10.1101/gad.1338505>
- Martinez-Perez, E., Schvarzstein, M., Barroso, C., Lightfoot, J., Dernburg, A. F., & Villeneuve, A. M. (2008). Crossovers trigger a remodeling of meiotic chromosome axis composition that is linked to two-step loss of sister chromatid cohesion. *Genes and Development*, 22(20), 2886–2901. <https://doi.org/10.1101/gad.1694108>
- Martinez-Perez, E., Shaw, P. J., & Moore, G. (2000). Polyploidy induces centromere association. *Journal of Cell Biology*, 148(2), 233–238. <https://doi.org/10.1083/jcb.148.2.233>
- Martinez-Perez, E., Shaw, P., Aragon-Alcaide, L., & Moore, G. (2003). Chromosomes form into seven groups in hexaploid and tetraploid wheat as a prelude to meiosis. *Plant Journal*, 36(1), 21–29. <https://doi.org/10.1046/j.1365-313X.2003.01853.x>
- Martínez-Pérez, E., Shaw, P., Reader, S., Aragón-Alcaide, L., Miller, T., & Moore, G. (1999). Homologous chromosome pairing in wheat. *Journal of Cell Science*, 112(11), 1761–1769.

- Martini, E., Diaz, R. L., Hunter, N., & Keeney, S. (2006). Crossover homeostasis in yeast meiosis. *Cell*, 126(2), 285–295. <https://doi.org/10.1016/j.cell.2006.05.044>
- Mason, A. S., & Wendel, J. F. (2020). Homoeologous Exchanges, Segmental Allopolyploidy, and Polyploid Genome Evolution . In *Frontiers in Genetics* (Vol. 11, p. 1014). <https://www.frontiersin.org/article/10.3389/fgene.2020.01014>
- Matsuoka, Y. (2011). Evolution of Polyploid Triticum Wheats under Cultivation: The Role of Domestication, Natural Hybridization and Allopolyploid Speciation in their Diversification. *Plant and Cell Physiology*, 52(5), 750–764. <https://doi.org/10.1093/pcp/pcr018>
- McGlincy, N. J., & Smith, C. W. J. (2008). Alternative splicing resulting in nonsense-mediated mRNA decay: what is the meaning of nonsense? *Trends in Biochemical Sciences*, 33(8), 385–393. <https://doi.org/10.1016/j.tibs.2008.06.001>
- Mello-Sampayo, T. (1971). Genetic regulation of meiotic chromosome pairing by chromosome 3D of *Triticum aestivum*. *Nature: New Biology*, 230(1), 22–23. <https://doi.org/10.1038/newbio230022a0>
- Meng, Z., Zhang, Z., Yan, T., Lin, Q., Wang, Y., Huang, W., Huang, Y., Li, Z., Yu, Q., Wang, J., & Wang, K. (2018). Comprehensively Characterizing the Cytological Features of *Saccharum spontaneum* by the Development of a Complete Set of Chromosome-Specific Oligo Probes. *Frontiers in Plant Science*, 9, 1624. <https://doi.org/10.3389/fpls.2018.01624>
- Mercier, R., Mézard, C., Jenczewski, E., Macaisne, N., & Grelon, M. (2015). The Molecular Biology of Meiosis in Plants. *Annual Review of Plant Biology*, 66(1), 297–327. <https://doi.org/10.1146/annurev-arplant-050213-035923>
- Meuwissen, R. L. J., Offenberg, H. H., Dietrich, A. J. J., Riesewijk, A., Van Iersel, M., & Heyting, C. (1992). A coiled-coil related protein specific for synapsed regions of meiotic prophase chromosomes. *EMBO Journal*, 11(13), 5091–5100. <https://doi.org/10.1002/j.1460-2075.1992.tb05616.x>
- Miao, C., Tang, D., Zhang, H., Wang, M., Li, Y., Tang, S., Yu, H., Gu, M., & Cheng, Z. (2013). Central region component1, a novel synaptonemal complex component, is essential for meiotic recombination initiation in rice. *The Plant Cell*, 25(8), 2998–3009. <https://doi.org/10.1105/tpc.113.113175>
- Miller, C. E. (Chuck). (2010). IDRC 2010 Report. *NIR News*, 21(7), 4–5. <https://doi.org/10.1255/nirn.1204>
- Mirzaghaderi, G., Houben, A., & Badaeva, E. D. (2014). Molecular-cytogenetic analysis of *Aegilops triuncialis* and identification of its chromosomes in the background of wheat. *Molecular Cytogenetics*, 7(1), 91. <https://doi.org/10.1186/s13039-014-0091-6>
- Mlynarczyk-Evans, S., & Villeneuve, A. M. (2017). Time-course analysis of early meiotic prophase events informs mechanisms of homolog pairing and synapsis in

*caenorhabditis elegans.* Genetics, 207(1), 103–114.  
<https://doi.org/10.1534/genetics.117.204172>

Moens, P. B. (1984). The synaptonemal complex in higher plants. *Critical Reviews in Plant Sciences*, 2(2), 81–116. <https://doi.org/10.1080/07352688409382191>

Morgan, M., Much, C., DiGiacomo, M., Azzi, C., Ivanova, I., Vitsios, D. M., Pistolic, J., Collier, P., Moreira, P. N., Benes, V., Enright, A. J., & O'Carroll, D. (2017). mRNA 3' uridylation and poly(A) tail length sculpt the mammalian maternal transcriptome. *Nature*, 548(7667), 347–351. <https://doi.org/10.1038/nature23318>

Mukai, Y., Nakahara, Y., & Yamamoto, M. (1993). Simultaneous discrimination of the three genomes in hexaploid wheat by multicolor fluorescence in situ hybridization using total genomic and highly repeated DNA probes. *Genome*, 36(3), 489–494. <https://doi.org/10.1139/g93-067>

Nadarajan, S., Lambert, T. J., Altendorfer, E., Gao, J., Blower, M. D., Waters, J. C., & Colaiácovo, M. P. (2017). Polo-like kinase-dependent phosphorylation of the synaptonemal complex protein SYP-4 regulates double-strand break formation through a negative feedback loop. *eLife*, 6. <https://doi.org/10.7554/eLife.23437>

Nag, D. K., Scherthan, H., Rockmill, B., Bhargava, J., & Roeder, G. S. (1995). Heteroduplex DNA formation and homolog pairing in yeast meiotic mutants. *Genetics*, 141(1), 75 LP – 86. <http://www.genetics.org/content/141/1/75.abstract>

Nakai, K., & Horton, P. (1999). PSORT: a program for detecting sorting signals in proteins and predicting their subcellular localization. *Trends in Biochemical Sciences*, 24(1), 34–36. [https://doi.org/10.1016/s0968-0004\(98\)01336-x](https://doi.org/10.1016/s0968-0004(98)01336-x)

Nan, G. L., Ronceret, A., Wang, R. C., Fernandes, J. F., Cande, W. Z., & Walbot, V. (2011). Global transcriptome analysis of two *ameiotic1* alleles in maize anthers: Defining steps in meiotic entry and progression through prophase I. *BMC Plant Biology*, 11, 1–20. <https://doi.org/10.1186/1471-2229-11-120>

Naro, C., Jolly, A., Di Persio, S., Bielli, P., Setterblad, N., Alberdi, A. J., Vicini, E., Geremia, R., De la Grange, P., & Sette, C. (2017). An Orchestrated Intron Retention Program in Meiosis Controls Timely Usage of Transcripts during Germ Cell Differentiation. *Developmental Cell*, 41(1), 82-93.e4. <https://doi.org/10.1016/j.devcel.2017.03.003>

Neale, M. J., Pan, J., & Keeney, S. (2005). Endonucleolytic processing of covalent protein-linked DNA double-strand breaks. *Nature*, 436(7053), 1053–1057. <https://doi.org/10.1038/nature03872>

Newton, W. C. F., & Darlington, C. D. (1929). Meiosis in polyploids. *Journal of Genetics*, 21(1), 1–15. <https://doi.org/10.1007/BF02983355>

Nilsen, T. W., & Graveley, B. R. (2010). Expansion of the eukaryotic proteome by alternative splicing. *Nature*, 463(7280), 457–463. <https://doi.org/10.1038/nature08909>

- Niu, H., Wan, L., Baumgartner, B., Schaefer, D., Loidl, J., & NM, H. (2005). Partner choice during meiosis is regulated by Hop1-promoted dimerization of Mek1. *Molecular Biology of the Cell*, 16(12), 5804–5818.
- Nonomura, K. I., Nakano, M., Eiguchi, M., Suzuki, T., & Kurata, N. (2006). PAIR2 is essential for homologous chromosome synapsis in rice meiosis I. *Journal of Cell Science*, 119(2), 217–225. <https://doi.org/10.1242/jcs.02736>
- Nonomura, K. I., Nakano, M., Eiguchi, M., Suzuki, T., & Kurata, N. (2006). PAIR2 is essential for homologous chromosome synapsis in rice meiosis I. *Journal of Cell Science*, 119(2), 217–225. <https://doi.org/10.1242/jcs.02736>
- Nonomura, K.-I., Nakano, M., Fukuda, T., Eiguchi, M., Miyao, A., Hirochika, H., & Kurata, N. (2004). The novel gene HOMOLOGOUS PAIRING ABERRATION IN RICE MEIOSIS1 of rice encodes a putative coiled-coil protein required for homologous chromosome pairing in meiosis. *The Plant Cell*, 16(4), 1008–1020. <https://doi.org/10.1105/tpc.020701>
- Okamoto, M. (1957). Asynaptic effect of chromosome V. *Wheat Inf. Serv.*, 5, 6.
- Olszewska, M. J., Kuran, H., & Marciniak, K. (1988). Relationship between resumption of rRNA transport into cytoplasm after cold treatment and progression through the cell cycle in root meristem cells. 28(4), 375–380.
- Osman, K., Algopishi, U., Higgins, J. D., Henderson, I. R., Edwards, K. J., Franklin, F. C. H., & Sanchez-Moran, E. (2021). Distal Bias of Meiotic Crossovers in Hexaploid Bread Wheat Reflects Spatio-Temporal Asymmetry of the Meiotic Program. *Frontiers in Plant Science*, 12(February), 1–20. <https://doi.org/10.3389/fpls.2021.631323>
- Osman, K., Higgins, J. D., Sanchez-Moran, E., Armstrong, S. J., & Franklin, F. C. H. (2011). Pathways to meiotic recombination in *Arabidopsis thaliana*. *The New Phytologist*, 190(3), 523–544. <https://doi.org/10.1111/j.1469-8137.2011.03665.x>
- Osman, K., Sanchez-Moran, E., Higgins, J. D., Jones, G. H., & Franklin, F. C. H. (2006). Chromosome synapsis in *Arabidopsis*: analysis of the transverse filament protein ZYP1 reveals novel functions for the synaptonemal complex. *Chromosoma*, 115(3), 212. <https://doi.org/10.1007/s00412-005-0042-4>
- Osman, K., Yang, J., Roitinger, E., Lambing, C., Heckmann, S., Howell, E., Cuacos, M., Imre, R., Dürnberger, G., Mechtler, K., Armstrong, S., & Franklin, F. C. H. (2018). Affinity proteomics reveals extensive phosphorylation of the *Brassica* chromosome axis protein ASY1 and a network of associated proteins at prophase I of meiosis. *Plant Journal*, 93(1), 17–33. <https://doi.org/10.1111/tpj.13752>
- Osman, K., Yang, J., Roitinger, E., Lambing, C., Heckmann, S., Howell, E., Cuacos, M., Imre, R., Dürnberger, G., Mechtler, K., Armstrong, S., & Franklin, F. C. H. (2018). Affinity proteomics reveals extensive phosphorylation of the *Brassica* chromosome axis protein ASY1 and a network of associated proteins at prophase I of meiosis.

Plant Journal, 93(1), 17–33. <https://doi.org/10.1111/tpj.13752>

- Page, S L, & Hawley, R. S. (2001). *c(3)G* encodes a *Drosophila* synaptonemal complex protein. *Genes & Development*, 15(23), 3130–3143. <https://doi.org/10.1101/gad.935001>
- Page, S. L., Khetani, R. S., Lake, C. M., Nielsen, R. J., Jeffress, J. K., Warren, W. D., Bickel, S. E., & Hawley, R. S. (2008). Corona is required for higher-order assembly of transverse filaments into full-length synaptonemal complex in *Drosophila* oocytes. *PLoS Genetics*, 4(9), e1000194. <https://doi.org/10.1371/journal.pgen.1000194>
- Page, Scott L., & Hawley, R. S. (2004). the Genetics and Molecular Biology of the Synaptonemal Complex. *Annual Review of Cell and Developmental Biology*, 20(1), 525–558. <https://doi.org/10.1146/annurev.cellbio.19.111301.155141>
- Pan, Q., Shai, O., Lee, L. J., Frey, B. J., & Blencowe, B. J. (2008). Deep surveying of alternative splicing complexity in the human transcriptome by high-throughput sequencing. *Nature Genetics*, 40(12), 1413–1415. <https://doi.org/10.1038/ng.259>
- Pan, W. H., Houben, A., & Schlegel, R. (1993). Highly effective cell synchronization in plant roots by hydroxyurea and amiprophos-methyl or colchicine. *Genome*, 36(2), 387–390. <https://doi.org/10.1139/g93-053>
- Pawlowski, W. P., Golubovskaya, I. N., Timofejeva, L., Meeley, R. B., Sheridan, W. F., & Cande, W. Z. (2004). Coordination of meiotic recombination, pairing, and synapsis by PHS1. *Science (New York, N.Y.)*, 303(5654), 89–92. <https://doi.org/10.1126/science.1091110>
- Pearce, S., Vazquez-Gross, H., Herin, S. Y., Hane, D., Wang, Y., Gu, Y. Q., & Dubcovsky, J. (2015). WheatExp: an RNA-seq expression database for polyploid wheat. *BMC Plant Biology*, 15(1), 299. <https://doi.org/10.1186/s12870-015-0692-1>
- Penkina, M. V., Karpova, O. I., & Bogdanov, I. F. (2002). Synaptonemal complex proteins: specific proteins of meiotic chromosomes. *Molekularnaia Biologija*, 36(3), 397–407.
- Pernickova, K., Linc, G., Gaal, E., Kopecky, D., Samajova, O., & Lukaszewski, A. J. (2019). Out-of-position telomeres in meiotic leptotene appear responsible for chiasmate pairing in an inversion heterozygote in wheat (*Triticum aestivum* L.). *Chromosoma*, 128(1), 31–39. <https://doi.org/10.1007/s00412-018-0686-5>
- Petrillo, E., Kalyna, M., Mandadi, K. K., Tu, S.-L., & Simpson, C. G. (2020). Editorial: Alternative Splicing Regulation in Plants. *Frontiers in Plant Science*, 11, 913. <https://doi.org/10.3389/fpls.2020.00913>
- Phillips, D., Wnetrzak, J., Nibau, C., Barakate, A., Ramsay, L., Wright, F., Higgins, J. D., Perry, R. M., & Jenkins, G. (2013). Quantitative high resolution mapping of HvMLH3 foci in barley pachytene nuclei reveals a strong distal bias and weak

- interference. *Journal of Experimental Botany*, 64(8), 2139–2154. <https://doi.org/10.1093/jxb/ert079>
- Pradillo, M., López, E., Linacero, R., Romero, C., Cuñado, N., Sánchez-Morán, E., & Santos, J. L. (2012). Together yes, but not coupled: new insights into the roles of RAD51 and DMC1 in plant meiotic recombination. *The Plant Journal*, 69(6), 921–933. <https://doi.org/https://doi.org/10.1111/j.1365-313X.2011.04845.x>
- Pradillo, M., Varas, J., Oliver, C., & Santos, J. (2014). On the role of AtDMC1, AtRAD51 and its paralogs during *Arabidopsis* meiosis. *Frontiers in Plant Science*, 5, 23. <https://doi.org/10.3389/fpls.2014.00023>
- Prieto, P., Moore, G., & Reader, S. (2005). Control of conformation changes associated with homologue recognition during meiosis. *Theoretical and Applied Genetics*, 111(3), 505–510. <https://doi.org/10.1007/s00122-005-2040-6>
- Prieto, P., Moore, G., & Reader, S. (2005). Control of conformation changes associated with homologue recognition during meiosis. *Theoretical and Applied Genetics*, 111(3), 505–510. <https://doi.org/10.1007/s00122-005-2040-6>
- Pucker, B., & Brockington, S. F. (2018). Genome-wide analyses supported by RNA-Seq reveal non-canonical splice sites in plant genomes. *BMC Genomics*, 19(1), 1–13. <https://doi.org/10.1186/s12864-018-5360-z>
- Punzo, P., Ruggiero, A., Grillo, S., & Batelli, G. (2018). TIP41 network analysis and mutant phenotypes predict interactions between the TOR and ABA pathways. *Plant Signaling and Behavior*, 13(12), 1–4. <https://doi.org/10.1080/15592324.2018.1537698>
- Pyatnitskaya, A., Borde, V., & De Muyt, A. (2019). Crossing and zipping: molecular duties of the ZMM proteins in meiosis. *Chromosoma*, 128(3), 181–198. <https://doi.org/10.1007/s00412-019-00714-8>
- Qian, M., Wang, D., Watkins, W. E., Gebski, V., Yan, Y. Q., Li, M., & Chen, Z. P. (2005). The effects of iodine on intelligence in children: A meta-analysis of studies conducted in China. *Asia Pacific Journal of Clinical Nutrition*, 14(1), 32–42.
- Qiao, H., Chen, J. K., Reynolds, A., Höög, C., Paddy, M., & Hunter, N. (2012). Interplay between Synaptonemal Complex, Homologous Recombination, and Centromeres during Mammalian Meiosis. *PLOS Genetics*, 8(6), e1002790. <https://doi.org/10.1371/journal.pgen.1002790>
- Qu, M., Li, K., Han, Y., Chen, L., Li, Z., & Han, Y. (2017). Integrated Karyotyping of Woodland Strawberry (*Fragaria vesca*) with Oligopaint FISH Probes. *Cytogenetic and Genome Research*, 153(3), 158–164. <https://doi.org/10.1159/000485283>
- Ramírez-González, R. H., Borrill, P., Lang, D., Harrington, S. A., Brinton, J., Venturini, L., Davey, M., Jacobs, J., van Ex, F., Pasha, A., Khedikar, Y., Robinson, S. J., Cory, A. T., Florio, T., Concia, L., Juery, C., Schoonbeek, H., Steuernagel, B., Xiang, D., ... Uauy, C. (2018). The transcriptional landscape of polyploid wheat. *Science*

- (New York, N.Y.), 361(6403). <https://doi.org/10.1126/science.aar6089>
- Ratushna, V. G., Weller, J. W., & Gibas, C. J. (2005). Secondary structure in the target as a confounding factor in synthetic oligomer microarray design. *BMC Genomics*, 6(June). <https://doi.org/10.1186/1471-2164-6-31>
- Raz, A., Dahan-Meir, T., Melamed-Bessudo, C., Leshkowitz, D., & Levy, A. A. (2021). Redistribution of Meiotic Crossovers Along Wheat Chromosomes by Virus-Induced Gene Silencing . In *Frontiers in Plant Science* (Vol. 11, p. 2332). <https://www.frontiersin.org/article/10.3389/fpls.2020.635139>
- Reddy, A. S. N., Marquez, Y., Kalyna, M., & Barta, A. (2013). Complexity of the alternative splicing landscape in plants. *Plant Cell*, 25(10), 3657–3683. <https://doi.org/10.1105/tpc.113.117523>
- Rees, H. (1976). Chromosome configurations at meiosis. *Nature*, 262(5564), 159. <https://doi.org/10.1038/262159b0>
- Renaut, S., & Rieseberg, L. H. (2015). The Accumulation of Deleterious Mutations as a Consequence of Domestication and Improvement in Sunflowers and Other Compositae Crops. *Molecular Biology and Evolution*, 32(9), 2273–2283. <https://doi.org/10.1093/molbev/msv106>
- Rey, M. D., Martín, A. C., Higgins, J., Swarbreck, D., Uauy, C., Shaw, P., & Moore, G. (2017). Exploiting the ZIP4 homologue within the wheat Ph1 locus has identified two lines exhibiting homoeologous crossover in wheat-wild relative hybrids. *Molecular Breeding*, 37(8). <https://doi.org/10.1007/s11032-017-0700-2>
- Rey, M. D., Martín, A. C., Smedley, M., Hayta, S., Harwood, W., Shaw, P., & Moore, G. (2018). Magnesium increases homoeologous crossover frequency during meiosis in ZIP4 (Ph1 gene) mutant wheat-wild relative hybrids. *Frontiers in Plant Science*, 9(April), 1–12. <https://doi.org/10.3389/fpls.2018.00509>
- Riley, r., & Chapman, V. (1958). Genetic Control of the Cytologically Diploid Behaviour of Hexaploid Wheat. *Nature*, 182(4637), 713–715. <https://doi.org/10.1038/182713a0>
- Rinaldi, V. D., Bolcun-Filas, E., Kogo, H., Kurahashi, H., & Schimenti, J. C. (2017). The DNA Damage Checkpoint Eliminates Mouse Oocytes with Chromosome Synapsis Failure. *Molecular Cell*, 67(6), 1026-1036.e2. <https://doi.org/10.1016/j.molcel.2017.07.027>
- Roberts, M. A., Reader, S. M., Dalgliesh, C., Miller, T. E., Foote, T. N., Fish, L. J., Snape, J. W., & Moore, G. (1999). Induction and Characterization of Ph1 Wheat Mutants. *Genetics*, 153(4), 1909–1918. <https://doi.org/10.1093/genetics/153.4.1909>
- Rodgers-Melnick, E., Bradbury, P. J., Elshire, R. J., Glaubitz, J. C., Acharya, C. B., Mitchell, S. E., Li, C., Li, Y., & Buckler, E. S. (2015). Recombination in diverse maize is stable, predictable, and associated with genetic load. *Proceedings of the National Academy of Sciences*, 112(12), 3823 LP – 3828.

<https://doi.org/10.1073/pnas.1413864112>

Rodríguez-Domínguez, J. M., Ríos-Lara, L. L., Tapia-Campos, E., & Barba-Gonzalez, R. (2017). An improved technique for obtaining well-spread metaphases from plants with numerous large chromosomes. *Biotechnic and Histochemistry*, 92(3), 159–166. <https://doi.org/10.1080/10520295.2017.1288927>

*Rome Declaration on World Food Security and World Food Summit Plan of Action: World Food Summit, 13-17 November 1996, Rome, Italy.* (1996). FAO, PP - Rome

Rosenberg, S. C., & Corbett, K. D. (2015). The multifaceted roles of the HOR MA domain in cellular signaling. *Journal of Cell Biology*, 211(4), 745–755. <https://doi.org/10.1083/jcb.201509076>

Sachs, A. B., Davis, R. W., & Kornberg, R. D. (1987). A single domain of yeast poly(A)-binding protein is necessary and sufficient for RNA binding and cell viability. *Molecular and Cellular Biology*, 7(9), 3268–3276. <https://doi.org/10.1128/mcb.7.9.3268-3276.1987>

Saintenac, C., Falque, M., Martin, O. C., Paux, E., Feuillet, C., & Sourdille, P. (2009). Detailed recombination studies along chromosome 3B provide new insights on crossover distribution in wheat (*Triticum aestivum* L.). *Genetics*, 181(2), 393–403. <https://doi.org/10.1534/genetics.108.097469>

Salman-Minkov, A., Sabath, N., & Mayrose, I. (2016). Whole-genome duplication as a key factor in crop domestication. *Nature Plants*, 2(8), 1–4. <https://doi.org/10.1038/NPLANTS.2016.115>

Sanchez-Moran, E., Santos, J. L., Jones, G. H., & Franklin, F. C. H. (2007). ASY1 mediates *AtDMC1*-dependent interhomolog recombination during meiosis in *Arabidopsis*. *Genes and Development*, 21(17), 2220–2233. <https://doi.org/10.1101/gad.439007>

Sato-Carlton, A., Nakamura-Tabuchi, C., Chartrand, S. K., Uchino, T., & Carlton, P. M. (2018). Phosphorylation of the synaptonemal complex protein SYP-1 promotes meiotic chromosome segregation. *Journal of Cell Biology*, 217(2), 555–570. <https://doi.org/10.1083/jcb.201707161>

Schild-Prüfert, K., Saito, T. T., Smolikov, S., Gu, Y., Hincapie, M., Hill, D. E., Vidal, M., McDonald, K., & Colaiáco, M. P. (2011). Organization of the synaptonemal complex during meiosis in *Caenorhabditis elegans*. *Genetics*, 189(2), 411–421. <https://doi.org/10.1534/genetics.111.132431>

Schild-Prüfert, K., Saito, T. T., Smolikov, S., Gu, Y., Hincapie, M., Hill, D. E., Vidal, M., McDonald, K., & Colaiáco, M. P. (2011). Organization of the synaptonemal complex during meiosis in *Caenorhabditis elegans*. *Genetics*, 189(2), 411–421. <https://doi.org/10.1534/genetics.111.132431>

Schmekel, K., Meuwissen, R. L., Dietrich, A. J., Vink, A. C., van Marle, J., van Veen,

- H., & Heyting, C. (1996). Organization of SCP1 protein molecules within synaptonemal complexes of the rat. *Experimental Cell Research*, 226(1), 20–30. <https://doi.org/10.1006/excr.1996.0198>
- Schommer, C., Beven, A., Lawrenson, T., Shaw, P., & Sablowski, R. (2003). AHP2 is required for bivalent formation and for segregation of homologous chromosomes in *Arabidopsis* meiosis. *Plant Journal*, 36(1), 1–11. <https://doi.org/10.1046/j.1365-313X.2003.01850.x>
- Schramm, S., Fraune, J., Naumann, R., Hernandez-Hernandez, A., Höög, C., Cooke, H. J., Alsheimer, M., & Benavente, R. (2011). A novel mouse synaptonemal complex protein is essential for loading of central element proteins, recombination, and fertility. *PLoS Genetics*, 7(5), e1002088–e1002088. <https://doi.org/10.1371/journal.pgen.1002088>
- Schücker, K., Holm, T., Franke, C., Sauer, M., & Benavente, R. (2015). Elucidation of synaptonemal complex organization by super-resolution imaging with isotropic resolution. *Proceedings of the National Academy of Sciences of the United States of America*, 112(7), 2029–2033. <https://doi.org/10.1073/pnas.1414814112>
- Schwartz, E. K., & Heyer, W.-D. (2011). Processing of joint molecule intermediates by structure-selective endonucleases during homologous recombination in eukaryotes. *Chromosoma*, 120(2), 109–127. <https://doi.org/10.1007/s00412-010-0304-7>
- Schwarzacher, T. (2003). Meiosis, recombination and chromosomes: a review of gene isolation and fluorescent in situ hybridization data in plants. *Journal of Experimental Botany*, 54(380), 11–23. <https://doi.org/10.1093/jxb/erg042>
- Schwarzacher, T., & Leitch, A. R. (1994). Enzymatic treatment of plant material to spread chromosomes for in situ hybridization. Methods in Molecular Biology (Clifton, N.J.), 28, 153–160. <https://doi.org/10.1385/0-89603-254-x:153>
- Sears, E. R. (1958). Intergenomic chromosome relationships in hexaploid wheat. *Proc. Int. Congress Genet.*, 2, 258–259.
- Sears, E. R. (1977). Genetics society of Canada award of excellence lecture an induced mutant with homoeologous pairing in common wheat. *Canadian Journal of Genetics and Cytology*, 19(4), 585–593. <https://doi.org/10.1139/g77-063>
- Séguéla-Arnaud, M., Crismani, W., Larchevêque, C., Mazel, J., Froger, N., Choinard, S., Lemhemdi, A., Macaisne, N., Van Leene, J., Gevaert, K., De Jaeger, G., Chelysheva, L., & Mercier, R. (2015). Multiple mechanisms limit meiotic crossovers: TOP3 $\alpha$  and two BLM homologs antagonize crossovers in parallel to FANCM. *Proceedings of the National Academy of Sciences*, 112(15), 4713 LP – 4718. <https://doi.org/10.1073/pnas.1423107112>
- Semagn, K., Babu, R., Hearne, S., & Olsen, M. (2014). Single nucleotide polymorphism genotyping using Kompetitive Allele Specific PCR (KASP): Overview of the

- technology and its application in crop improvement. *Molecular Breeding*, 33(1), 1–14. <https://doi.org/10.1007/s11032-013-9917-x>
- Sepsi, A., Higgins, J. D., Heslop-Harrison, J. S. P., & Schwarzacher, T. (2017). CENH3 morphogenesis reveals dynamic centromere associations during synaptonemal complex formation and the progression through male meiosis in hexaploid wheat. *Plant Journal*, 89(2), 235–249. <https://doi.org/10.1111/tpj.13379>
- Serin, E. A. R., Nijveen, H., Hilhorst, H. W. M., & Ligterink, W. (2016). Learning from Co-expression Networks: Possibilities and Challenges. *Frontiers in Plant Science*, 7, 444. <https://doi.org/10.3389/fpls.2016.00444>
- Serra, H., Svačina, R., Baumann, U., Whitford, R., Sutton, T., Bartoš, J., & Sourville, P. (2021). Ph2 encodes the mismatch repair protein MSH7-3D that inhibits wheat homoeologous recombination. *Nature Communications*, 12(1), 1–10. <https://doi.org/10.1038/s41467-021-21127-1>
- Severson, A. F., Ling, L., van Zuylen, V., & Meyer, B. J. (2009). The axial element protein HTP-3 promotes cohesin loading and meiotic axis assembly in *C. elegans* to implement the meiotic program of chromosome segregation. *Genes & Development*, 23(15), 1763–1778. <https://doi.org/10.1101/gad.1808809>
- Shaked, H., Avivi-Ragolsky, N., & Levy, A. A. (2006). Involvement of the arabidopsis SWI2/SNF2 chromatin remodeling gene family in DNA damage response and recombination. *Genetics*, 173(2), 985–994. <https://doi.org/10.1534/genetics.105.051664>
- Shannon, P., Markiel, A., Ozier, O., Baliga, N. S., Wang, J. T., Ramage, D., Amin, N., Schwikowski, B., & Ideker, T. (2003). Cytoscape: a software environment for integrated models of biomolecular interaction networks. *Genome Research*, 13(11), 2498–2504. <https://doi.org/10.1101/gr.1239303>
- Sheets, M. D., Fox, C. A., Hunt, T., Vande Woude, & Wickens, M. (1994). The 3'-untranslated regions of c-mos and cyclin mRNAs stimulate translation by regulating cytoplasmic polyadenylation. *Genes and Development*, 8(8), 926–938. <https://doi.org/10.1101/gad.8.8.926>
- Shi, Y. (2012). Alternative polyadenylation: new insights from global analyses. *RNA (New York, N.Y.)*, 18(12), 2105–2117. <https://doi.org/10.1261/rna.035899.112>
- Shiferaw, B., Prasanna, B. M., Hellin, J., & Bänziger, M. (2011). Crops that feed the world 6. Past successes and future challenges to the role played by maize in global food security. *Food Security*, 3(3), 307. <https://doi.org/10.1007/s12571-011-0140-5>
- Shin, Y.-H., Choi, Y., Erdin, S. U., Yatsenko, S. A., Kloc, M., Yang, F., Wang, P. J., Meistrich, M. L., & Rajkovic, A. (2010). Hormad1 mutation disrupts synaptonemal complex formation, recombination, and chromosome segregation in mammalian meiosis. *PLoS Genetics*, 6(11), e1001190.

<https://doi.org/10.1371/journal.pgen.1001190>

- Shunmugam, A. S. K., Bollina, V., Dukowic-Schulze, S., Bhowmik, P. K., Ambrose, C., Higgins, J. D., Pozniak, C., Sharpe, A. G., Rozwadowski, K., & Kagale, S. (2018). MeioCapture: an efficient method for staging and isolation of meiocytes in the prophase I sub-stages of meiosis in wheat. *BMC Plant Biology*, 18(1), 293. <https://doi.org/10.1186/s12870-018-1514-z>
- Sidhu, G. K., Fang, C., Olson, M. A., Falque, M., Martin, O. C., & Pawlowski, W. P. (2015). Recombination patterns in maize reveal limits to crossover homeostasis. *Proceedings of the National Academy of Sciences of the United States of America*, 112(52), 15982–15987. <https://doi.org/10.1073/pnas.1514265112>
- Šimoníková, D., Němečková, A., Karafiátová, M., Uwimana, B., Swennen, R., Doležel, J., & Hřibová, E. (2019). Chromosome Painting Facilitates Anchoring Reference Genome Sequence to Chromosomes In Situ and Integrated Karyotyping in Banana (*Musa Spp.*). *Frontiers in Plant Science*, 10, 1503. <https://doi.org/10.3389/fpls.2019.01503>
- Sims, J., Schlögelhofer, P., & Kurzbauer, M.-T. (2021). From Microscopy to Nanoscopy: Defining an *Arabidopsis thaliana* Meiotic Atlas at the Nanometer Scale. *Frontiers in Plant Science*, 12, 954. <https://doi.org/10.3389/fpls.2021.672914>
- Sladic, R. T., Lagnado, C. A., Bagley, C. J., & Goodall, G. J. (2004). Human PABP binds AU-rich RNA via RNA-binding domains 3 and 4. *European Journal of Biochemistry*, 271(2), 450–457. <https://doi.org/10.1046/j.1432-1033.2003.03945.x>
- Smolikov, S., Eizinger, A., Schild-Prufert, K., Hurlburt, A., McDonald, K., Engebrecht, J., Villeneuve, A. M., & Colaiácovo, M. P. (2007). SYP-3 Restricts Synaptonemal Complex Assembly to Bridge Paired Chromosome Axes During Meiosis in *Caenorhabditis elegans*. *Genetics*, 176(4), 2015–2025. <https://doi.org/10.1534/genetics.107.072413>
- Smolikov, S., Schild-Prüfert, K., & Colaiácovo, M. P. (2009). A Yeast Two-Hybrid Screen for SYP-3 Interactors Identifies SYP-4, a Component Required for Synaptonemal Complex Assembly and Chiasma Formation in *Caenorhabditis elegans* Meiosis. *PLOS Genetics*, 5(10), e1000669. <https://doi.org/10.1371/journal.pgen.1000669>
- Song, L., Langfelder, P., & Horvath, S. (2012). Comparison of co-expression measures: mutual information, correlation, and model based indices. *BMC Bioinformatics*, 13, 328. <https://doi.org/10.1186/1471-2105-13-328>
- Song, X., Song, R., Zhou, J., Yan, W., Zhang, T., Sun, H., Xiao, J., Wu, Y., Xi, M., Lou, Q., Wang, H., & Wang, X. (2020). Development and application of oligonucleotide-based chromosome painting for chromosome 4D of *Triticum aestivum* L. *Chromosome Research: An International Journal on the Molecular, Supramolecular and Evolutionary Aspects of Chromosome Biology*, 28(2), 171–182. <https://doi.org/10.1007/s10577-020-09627-0>

- Spurbeck, J. L., Zinsmeister, A. R., Meyer, K. J., & Jalal, S. M. (1996). Dynamics of chromosome spreading. *American Journal of Medical Genetics*, 61(4), 387–393. [https://doi.org/10.1002/\(SICI\)1096-8628\(19960202\)61:4<387::AID-AJMG15>3.0.CO;2-O](https://doi.org/10.1002/(SICI)1096-8628(19960202)61:4<387::AID-AJMG15>3.0.CO;2-O)
- Sridhar, V. V., Kapoor, A., Zhang, K., Zhu, J., Zhou, T., Hasegawa, P. M., Bressan, R. A., & Zhu, J. K. (2007). Control of DNA methylation and heterochromatic silencing by histone H2B deubiquitination. *Nature*, 447(7145), 735–738. <https://doi.org/10.1038/nature05864>
- Srivastava, A. K., Lu, Y., Zinta, G., Lang, Z., & Zhu, J. K. (2018). UTR-Dependent Control of Gene Expression in Plants. *Trends in Plant Science*, 23(3), 248–259. <https://doi.org/10.1016/j.tplants.2017.11.003>
- Stack, S. M., & Anderson, L. K. (2001). A model for chromosome structure during the mitotic and meiotic cell cycles. *Chromosome Research : An International Journal on the Molecular, Supramolecular and Evolutionary Aspects of Chromosome Biology*, 9(3), 175–198. <https://doi.org/10.1023/a:1016690802570>
- Stapley, J., Feulner, P. G. D., Johnston, S. E., Santure, A. W., & Smadja, C. M. (2017). Variation in recombination frequency and distribution across eukaryotes: Patterns and processes. *Philosophical Transactions of the Royal Society B: Biological Sciences*, 372(1736). <https://doi.org/10.1098/rstb.2016.0455>
- Stemmer, C., Leeming, D. J., Franssen, L., Grimm, R., & Grasser, K. D. (2003). Phosphorylation of maize and *Arabidopsis* HMGB proteins by protein kinase CK2alpha. *Biochemistry*, 42(12), 3503–3508. <https://doi.org/10.1021/bi027350d>
- Suzuki, G., Ogaki, Y., Hokimoto, N., Xiao, L., Kikuchi-Taura, A., Harada, C., Okayama, R., Tsuru, A., Onishi, M., Saito, N., Do, G. S., Lee, S. H., Ito, T., Kanno, A., Yamamoto, M., & Mukai, Y. (2012). Random BAC FISH of monocot plants reveals differential distribution of repetitive DNA elements in small and large chromosome species. *Plant Cell Reports*, 31(4), 621–628. <https://doi.org/10.1007/s00299-011-1178-8>
- Svačina, R., Sourdille, P., Kopecký, D., & Bartoš, J. (2020). Chromosome Pairing in Polyploid Grasses. *Frontiers in Plant Science*, 11(July), 1–17. <https://doi.org/10.3389/fpls.2020.01056>
- Sybenga, J. (2012). *Meiotic configurations: a source of information for estimating genetic parameters* (Vol. 1). Springer Science & Business Media.
- Sym, M., Engebrecht, J., & Roeder, G. S. (1993). ZIP1 is a synaptonemal complex protein required for meiotic chromosome synapsis. *Cell*, 72(3), 365–378. [https://doi.org/https://doi.org/10.1016/0092-8674\(93\)90114-6](https://doi.org/https://doi.org/10.1016/0092-8674(93)90114-6)
- Szathmáry, E., & Smith, J. M. (1995). The major evolutionary transitions. *Nature*, 374(6519), 227–232. <https://doi.org/10.1038/374227a0>
- Takahashi, N., Quimbaya, M., Schubert, V., Lammens, T., Vandepoele, K., Schubert, I.,

- Matsui, M., Inzé, D., Berx, G., & De Veylder, L. (2010). The MCM-binding protein ETG1 aids sister chromatid cohesion required for postreplicative homologous recombination repair. *PLoS Genetics*, 6(1). <https://doi.org/10.1371/journal.pgen.1000817>
- Tang, S., Tang, Z., Qiu, L., Yang, Z., Li, G., Lang, T., Zhu, W., Zhang, J., & Fu, S. (2018). Developing new oligo probes to distinguish specific chromosomal segments and the A, B, D genomes of wheat (*Triticum aestivum* L.) using ND-FISH. *Frontiers in Plant Science*, 9(July), 1–10. <https://doi.org/10.3389/fpls.2018.01104>
- Tang, Z., Li, M., Chen, L., Wang, Y., Ren, Z., & Fu, S. (2014). New types of wheat chromosomal structural variations in derivatives of wheat-rye hybrids. *PLoS ONE*, 9(10), 1–7. <https://doi.org/10.1371/journal.pone.0110282>
- Tian, B., & Manley, J. L. (2017). Alternative polyadenylation of mRNA precursors. *Nature Reviews Molecular Cell Biology*, 18(1), 18–30. <https://doi.org/10.1038/nrm.2016.116>
- Tiwari, V. K., Wang, S., Sehgal, S., Vrána, J., Fribe, B., Kubaláková, M., Chhuneja, P., Doležel, J., Akhunov, E., Kalia, B., Sabir, J., & Gill, B. S. (2014). SNP Discovery for mapping alien introgressions in wheat. *BMC Genomics*, 15(1), 1–11. <https://doi.org/10.1186/1471-2164-15-273>
- Tock, A. J., Holland, D. M., Jiang, W., Osman, K., Sanchez-Moran, E., Higgins, J. D., Edwards, K. J., Uauy, C., Franklin, F. C. H., & Henderson, I. R. (2021). Crossover-active regions of the wheat genome are distinguished by DMC1, the chromosome axis, H3K27me3, and signatures of adaptation. *Genome Research*, 31(9), 1614–1628. <https://doi.org/10.1101/gr.273672.120>
- Tripathi, P., Pal, D., & Muniyappa, K. (2007). *Saccharomyces cerevisiae* Hop1 protein zinc finger motif binds to the Holliday junction and distorts the DNA structure: implications for holliday junction migration. *Biochemistry*, 46(44), 12530–12542.
- Tung, K.-S., & Roeder, G. S. (1998). Meiotic Chromosome Morphology and Behavior in zip1 Mutants of *Saccharomyces cerevisiae*. *Genetics*, 149(2), 817–832. <https://doi.org/10.1093/genetics/149.2.817>
- Uauy, C., Paraiso, F., Colasuonno, P., Tran, R. K., Tsai, H., Berardi, S., Comai, L., & Dubcovsky, J. (2009). A modified TILLING approach to detect induced mutations in tetraploid and hexaploid wheat. *BMC Plant Biology*, 9(1), 115. <https://doi.org/10.1186/1471-2229-9-115>
- Underwood, C. J., Choi, K., Lambing, C., Zhao, X., Serra, H., Borges, F., Simorowski, J., Ernst, E., Jacob, Y., Henderson, I. R., & Martienssen, R. A. (2018). Epigenetic activation of meiotic recombination near *Arabidopsis thaliana* centromeres via loss of H3K9me2 and non-CG DNA methylation. *Genome Research*, 28(4), 519–531. <https://doi.org/10.1101/gr.227116.117>
- UniProt: the universal protein knowledgebase in 2021. (2021). *Nucleic Acids Research*,

- 49(D1), D480–D489. <https://doi.org/10.1093/nar/gkaa1100>
- van Dam, S., Võsa, U., van der Graaf, A., Franke, L., & de Magalhães, J. P. (2018). Gene co-expression analysis for functional classification and gene-disease predictions. *Briefings in Bioinformatics*, 19(4), 575–592. <https://doi.org/10.1093/bib/bbw139>
- Vincenten, N., Kuhl, L.-M., Lam, I., Oke, A., Kerr, A. R., Hochwagen, A., Fung, J., Keeney, S., Vader, G., & Marston, A. L. (2015). The kinetochore prevents centromere-proximal crossover recombination during meiosis. *eLife*, 4. <https://doi.org/10.7554/eLife.10850>
- Voelkel-Meiman, K., Cheng, S. Y., Morehouse, S. J., & Macqueen, A. J. (2016). Synaptonemal complex proteins of budding yeast define reciprocal roles in MutS $\gamma$ -mediated crossover formation. *Genetics*, 203(3), 1091–1103. <https://doi.org/10.1534/genetics.115.182923>
- Wang, E. T., Sandberg, R., Luo, S., Khrebtukova, I., Zhang, L., Mayr, C., Kingsmore, S. F., Schroth, G. P., & Burge, C. B. (2008). Alternative isoform regulation in human tissue transcriptomes. *Nature*, 456(7221), 470–476. <https://doi.org/10.1038/nature07509>
- Wang, K., Wang, C., Liu, Q., Liu, W., & Fu, Y. (2015). Increasing the Genetic Recombination Frequency by Partial Loss of Function of the Synaptonemal Complex in Rice. In *Molecular plant* (Vol. 8, Issue 8, pp. 1295–1298). <https://doi.org/10.1016/j.molp.2015.04.011>
- Wang, M., Wang, K., Tang, D., Wei, C., Li, M., Shen, Y., Chi, Z., Gu, M., & Cheng, Z. (2010). The central element protein ZEP1 of the synaptonemal complex regulates the number of crossovers during meiosis in rice. *Plant Cell*, 22(2), 417–430. <https://doi.org/10.1105/tpc.109.070789>
- Wang, Y., Zhang, X., Zhang, H., Lu, Y., Huang, H., Dong, X., Chen, J., Dong, J., Yang, X., Hang, H., & Jiang, T. (2012). Coiled-coil networking shapes cell molecular machinery. *Molecular Biology of the Cell*, 23(19), 3911–3922.
- Wang, Yazhong, van Rengs, W. M. J., Zaidan, M. W. A. M., & Underwood, C. J. (2021). Meiosis in crops: from genes to genomes. *Journal of Experimental Botany*, 72(18), 6091–6109. <https://doi.org/10.1093/jxb/erab217>
- Wang, Yingxiang, & Copenhaver, G. P. (2018). Meiotic Recombination: Mixing It Up in Plants. *Annual Review of Plant Biology*, 69(1), 577–609. <https://doi.org/10.1146/annurev-arplant-042817-040431>
- Watson, A., Ghosh, S., Williams, M. J., Cuddy, W. S., Simmonds, J., Rey, M.-D., Asyraf Md Hatta, M., Hinchliffe, A., Steed, A., Reynolds, D., Adamski, N. M., Breakspear, A., Korolev, A., Rayner, T., Dixon, L. E., Riaz, A., Martin, W., Ryan, M., Edwards, D., ... Hickey, L. T. (2018). Speed breeding is a powerful tool to accelerate crop research and breeding. *Nature Plants*, 4(1), 23–29. <https://doi.org/10.1038/s41477-017-0083-8>

- West, A. M. V., Komives, E. A., & Corbett, K. D. (2018). Conformational dynamics of the Hop1 HORMA domain reveal a common mechanism with the spindle checkpoint protein Mad2. *Nucleic Acids Research*, 46(1), 279–292. <https://doi.org/10.1093/nar/gkx1196>
- Wojtasz, L., Daniel, K., Roig, I., Bolcun-Filas, E., Xu, H., Boonsanay, V., Eckmann, C. R., Cooke, H. J., Jasin, M., Keeney, S., McKay, M. J., & Toth, A. (2009). Mouse HORMAD1 and HORMAD2, two conserved meiotic chromosomal proteins, are depleted from synapsed chromosome axes with the help of TRIP13 AAA-ATPase. *PLoS Genetics*, 5(10), e1000702. <https://doi.org/10.1371/journal.pgen.1000702>
- Wu, S. Y., Culligan, K., Lamers, M., & Hays, J. (2003). Dissimilar mispair-recognition spectra of Arabidopsis DNA-mismatch-repair proteins MSH2·MSH6 (*MutS $\alpha$* ) and MSH2·MSH7 (*MutS $\gamma$* ). *Nucleic Acids Research*, 31(20), 6027–6034. <https://doi.org/10.1093/nar/gkg780>
- Wu, Z., Ji, J., Tang, D., Wang, H., Shen, Y., Shi, W., Li, Y., Tan, X., Cheng, Z., & Luo, Q. (2015). *OsSDS* is essential for DSB formation in rice meiosis. *Frontiers in Plant Science*, 6, 21. <https://doi.org/10.3389/fpls.2015.00021>
- Xin, H., Zhang, T., Wu, Y., Zhang, W., Zhang, P., Xi, M., & Jiang, J. (2020). An extraordinarily stable karyotype of the woody *Populus* species revealed by chromosome painting. *The Plant Journal: For Cell and Molecular Biology*, 101(2), 253–264. <https://doi.org/10.1111/tpj.14536>
- Xing, D., & Li, Q. Q. (2011). Alternative polyadenylation and gene expression regulation in plants. *Wiley Interdisciplinary Reviews. RNA*, 2(3), 445–458. <https://doi.org/10.1002/wrna.59>
- Yang, C., Hamamura, Y., Sofroni, K., Böwer, F., Stolze, S. C., Nakagami, H., & Schnittger, A. (2019). SWITCH 1/DYAD is a WINGS APART-LIKE antagonist that maintains sister chromatid cohesion in meiosis. *Nature Communications*, 10(1), 1755. <https://doi.org/10.1038/s41467-019-09759-w>
- Yang, C., Hu, B., Portheine, S. M., Chuenban, P., & Schnittger, A. (2020). State changes of the HORMA protein ASY1 are mediated by an interplay between its closure motif and PCH2. *Nucleic Acids Research*, 48(20), 11521–11535. <https://doi.org/10.1093/nar/gkaa527>
- Yang, F., De La Fuente, R., Leu, N. A., Baumann, C., McLaughlin, K. J., & Wang, P. J. (2006). Mouse SYCP2 is required for synaptonemal complex assembly and chromosomal synapsis during male meiosis. *The Journal of Cell Biology*, 173(4), 497–507. <https://doi.org/10.1083/jcb.200603063>
- Yang, F., Wang, W., Cetinbas, M., Sadreyev, R. I., & Blower, M. D. (2020). Genome-wide analysis identifies cis-acting elements regulating mRNA polyadenylation and translation during vertebrate oocyte maturation. *RNA (New York, N.Y.)*, 26(3), 324–344. <https://doi.org/10.1261/rna.073247.119>

- Ye, Q., Kim, D. H., Dereli, I., Rosenberg, S. C., Hagemann, G., Herzog, F., Tóth, A., Cleveland, D. W., & Corbett, K. D. (2017). The AAA+ ATPase TRIP13 remodels HORMA domains through N-terminal engagement and unfolding. *The EMBO Journal*, 36(16), 2419–2434. <https://doi.org/10.15252/embj.201797291>
- Yelagandula, R., Stroud, H., Holec, S., Zhou, K., Feng, S., Zhong, X., Muthurajan, U. M., Nie, X., Kawashima, T., Groth, M., Luger, K., Jacobsen, S. E., & Berger, F. (2014). The histone variant H2A.W defines heterochromatin and promotes chromatin condensation in arabidopsis. *Cell*, 158(1), 98–109. <https://doi.org/10.1016/j.cell.2014.06.006>
- Yoo, M.-J., Szadkowski, E., & Wendel, J. F. (2013). Homoeolog expression bias and expression level dominance in allopolyploid cotton. *Heredity*, 110(2), 171–180. <https://doi.org/10.1038/hdy.2012.94>
- Young, A. P., Jackson, D. J., & Wyeth, R. C. (2020). A technical review and guide to RNA fluorescence in situ hybridization. *PeerJ*, 8, 1–27. <https://doi.org/10.7717/peerj.8806>
- Yuan, L., Liu, J. G., Zhao, J., Brundell, E., Daneholt, B., & Höög, C. (2000). The murine SCP3 gene is required for synaptonemal complex assembly, chromosome synapsis, and male fertility. *Molecular Cell*, 5(1), 73–83. [https://doi.org/10.1016/s1097-2765\(00\)80404-9](https://doi.org/10.1016/s1097-2765(00)80404-9)
- Zetka, M. C., Kawasaki, I., Strome, S., & Müller, F. (1999). Synapsis and chiasma formation in *Caenorhabditis elegans* require HIM-3, a meiotic chromosome core component that functions in chromosome segregation. *Genes & Development*, 13(17), 2258–2270. <https://doi.org/10.1101/gad.13.17.2258>
- Zhang, B., & Horvath, S. (2005). A general framework for weighted gene co-expression network analysis. *Statistical Applications in Genetics and Molecular Biology*, 4, Article17. <https://doi.org/10.2202/1544-6115.1128>
- Zhang, L., AG, F., Cheung, V., Winston, F., & LA, S. (2008). Spn1 regulates the recruitment of Spt6 and the Swi/Snf complex during transcriptional activation by RNA polymerase II. *Molecular and Cellular Biology*, 28(4), 1393–1403.
- Zhang, L., Wang, S., Yin, S., Hong, S., Kim, K. P., & Kleckner, N. (2014). Topoisomerase II mediates meiotic crossover interference. *Nature*, 511(7511), 551–556. <https://doi.org/10.1038/nature13442>
- Zhang, P., Li, W., Friebel, B., & Gill, B. S. (2004). Simultaneous painting of three genomes in hexaploid wheat by BAC-FISH. *Genome*, 47(5), 979–987. <https://doi.org/10.1139/G04-042>
- Zhang, W., Zhu, X., Zhang, M., Chao, S., Xu, S., & Cai, X. (2018). Meiotic homoeologous recombination-based mapping of wheat chromosome 2B and its homoeologues in *Aegilops speltoides* and *Thinopyrum elongatum*. *Theoretical and Applied Genetics*, 131(11), 2381–2395. <https://doi.org/10.1007/s00122-018-3160>

- Zhang, Y., Fan, C., Chen, Y., Wang, R. R. C., Zhang, X., Han, F., & Hu, Z. (2021). Genome evolution during bread wheat formation unveiled by the distribution dynamics of SSR sequences on chromosomes using FISH. *BMC Genomics*, 22(1), 1–15. <https://doi.org/10.1186/s12864-020-07364-6>
- Zhang, Z., Xie, S., Wang, R., Guo, S., Zhao, Q., Nie, H., Liu, Y., Zhang, F., Chen, M., Liu, L., Meng, X., Liu, M., Zhao, L., Colaiácovo, M. P., Zhou, J., & Gao, J. (2020). Multivalent weak interactions between assembly units drive synaptonemal complex formation. *Journal of Cell Biology*, 219(5), e201910086. <https://doi.org/10.1083/jcb.201910086>
- Zhao, T., Huan, Q., Sun, J., Liu, C., Hou, X., Yu, X., Silverman, I. M., Zhang, Y., Gregory, B. D., Liu, C.-M., Qian, W., & Cao, X. (2019). Impact of poly(A)-tail G-content on Arabidopsis PAB binding and their role in enhancing translational efficiency. *Genome Biology*, 20(1), 189. <https://doi.org/10.1186/s13059-019-1799-8>
- Zhou, A., & Pawlowski, W. P. (2014). Regulation of meiotic gene expression in plants. *Frontiers in Plant Science*, 5, 413. <https://doi.org/10.3389/fpls.2014.00413>
- Zhou, L., Han, J., Chen, Y., Wang, Y., & Liu, Y.-G. (2017). Bivalent Formation 1, a plant-conserved gene, encodes an OmpH/coiled-coil motif-containing protein required for meiotic recombination in rice. *Journal of Experimental Botany*, 68(9), 2163–2174. <https://doi.org/10.1093/jxb/erx077>
- Zhu, S., Ye, W., Ye, L., Fu, H., Ye, C., Xiao, X., Ji, Y., Lin, W., Ji, G., & Wu, X. (2020). PlantAPAdb: A Comprehensive Database for Alternative Polyadenylation Sites in Plants. *Plant Physiology*, 182(1), 228–242. <https://doi.org/10.1104/pp.19.00943>
- Zickler, D., & Kleckner, N. (1999). Meiotic chromosomes: integrating structure and function. *Annual Review of Genetics*, 33, 603–754. <https://doi.org/10.1146/annurev.genet.33.1.603>

## Appendices

**Table S1: *TtASY1* 3' UTR sequences**

B sub-genome clones are highlighted in yellow. Poly(A) tails and reference sequences are indicated.

>ASY1K.M31F

TTCAGTGAGGCGGCACGGAATCGCAAGGAGCCTCAGCGCAACTAACCGTAGG  
TCAGCGAAGAACGAGAAATACCCCTAGTCGGTACTACTTCAGTCGTTCAGGTGCTTGA  
AACTTGTGAAGATAGCGACAGAGCACCCCTCCGGCAGATGTAGATCCTTGTCCCTAGCC  
CTATCCTTGGTAGCAAAACGTAACGAGAGAGACTTGTGCCCCCTGAGACGTGTTGTT  
TATGATGTTGTTCACTGGAGACTGCACCGAGGCCACTTTCGCTGAATGCTGAAACGT  
AGCAATGTTGGTTGCTTC AAAA

>**ASY1K.M33F**

TTCAGTTGGGCGGCACGGAATCGCAAGGAGCCTCAGCGCAACTAACCTCGCAG  
GTCAGCGAAGAACGAGAAATACCCCTAGTCGGTACTACTTCAGTCGTTCAGGTGCTTGA  
AAACTTGTGAAGATAGCGACAGAGCACCCCTCCGGCAGATGTAGATCCTTGTCCCTAGC  
CCTATCCTTGGTAGCAAAACGTAACGAGAGAGACTTGTGCCCCCTGAGACGTGTTGTT  
TATGATGTTGTTCACTGGAGACTGCACCGAGGCCACTTTCGCTGAATGCTGAAACGT  
TAGCAATGTTGGTTGCTTCACGCCATGGTTTAATGATGTATCTATTGAACTTCTGTA  
AAAA

>ASY1K.M34F

TTCAGTGAGGCGGCACGGAATCGCAAGGAGCCTCAGCGCAACTAACCGTAGG  
GTCAGCGAAGAACGAGAAATACCCCTAGTCGGTACTACTTCAGTCGTTCAGGTGCTTGA  
AAACTTGTGAAGATAGCGACAGAGCACCCCTCCGGCAGATGTAGATCCTTGTCCCTAGC  
CCTATCCTTGGTAGCAAAACGTAACGAGAGAGACTTGTGCCCCCTGAGACGTGTTGTT  
TATGATGTTGTTCACTGGAGACTGCACCGAGGCCACTTTCGCTGAATGCTGAAACGT  
TAGCAATGTTGGTTGCTTCACGCCATGGTTTAATGATGTATCTATTGAACTTCTGTA  
CTGAGCAGCGAT AAAA

>ASY1K.M35F

TTCAGTGAGGCGGCACGGAATCGCAAGGAGCCTCAGCGCAACTAACCGTAGG  
TCAGCGAAGAACGAGAAATACCCCTAGTCGGTACTACTTCAGTCGTTCAGGTGCTTGA  
AACTTGTGAAGATAGCGACAGAGCACCCCTCCGGCAGATGTAGATCCTTGTCCCTAGCC  
CTATCCTTGGTAGCAAAACGTAACGAGAGAGACTTGTGCCCCCTGAGACGTGTTGTT  
TATGATGTTGTTCACTGGAGACTGCACCGAGGCCACTTTCGCTGAATGCTGAAACGT  
AGCAATGTTGGTTGCTTCACGCCATGGTTTAATGATGTATCTATTGAACTTC  
AAAA

>ASY1K.M36F

TTCAGTGAGGCGGCACGGAATCGCAAGGAGCCTCAGCGCAACTAACCGTAG  
GGTCAGCGAAGAACGAGAAATACCCCTAGTCGGTACTACTTCAGTCGTTCAGGTGCTT  
GAAACTTGTGAAGATAGCGACAGAGCACCCCTCCGGCAGATGTAGATCCTTGTCCCTAG  
CCCTATCCTTGGTAGCAAAACGTAACGAGAGAGACTTGTGCCCCCTGAGACGTGTTG  
TTATGATGTTGTTCACTGGAGACTGCACCGAGGCCACTTTCGCTGAATGCTGAAAC  
GTAGCAATGTTGGTTGCTTCACGCCATGGTTTAATGATGTATCTATTGAACTTC  
AAAA

>ASY1K.M38F

TTCAGTGAGGCGGCACGGAATCGCAAGGAGCCTCAGCGCAACTAACCGTAG  
GGTCAGCGAAGAACGAGAAATACCCCTAGTCGGTACTACTTCAGTCGTTCAGGTGCTT  
GAAACTTGTGAAGATAGCGACAGAGCACCCCTCCGGCAGATGTAGATCCTTGTCCCTAG  
CCCTATCCTTGGTAGCAAAACGTAACGAGAGAGACTTGTGCCCCCTGAGACGTGTTG

TTTATGATGTTGTTCACTGGAGACTGCACCGAGGCCACTTGCCTGAATGCTGAAAC  
GTAGCAATGTTGGTTGCTCACGCCATGGTTAATGATGTATCTATTGAACCTTC  
AAAAAAAAAAAAAAA

>ASY1K.M311F  
TTCAGTGAGGCGGCACGGAATCGCAAGGAGCCTCAGCGCAACTAACACGTA  
GGTCAGCGAAGAAGCAGAATACCCCTAGTCGGTACTACTTCAGTCAGGTGCTT  
GAAACTTGTGAAGATAGCGACAGAGCACCCCTCCGGCAGATGTAGATCCTGTCCTAG  
CCCTATCCTGGTAGCAAAACGTAACGAGAGAGACTTGTGCCCCCTGAGACGTGTTG  
TTTATGATGTTGTTCACTGGAGACTGCACCGAGGCCACTTGCCTGAATGCTGAAAC  
GTAGCAATGTTGGTTGCTCACGCCATGGTTAATGATGTATCTATTG  
AAAAAAAAAAAAAAA

>ASY1K.M312F  
TTCAGTGAGGCGGCACGGAATCGCAAGGAGCCTCAGCGCAACTAACACGTA  
TCAGCGAAGAAGCAGAATACCCCTAGTCGGTACTACTTCAGTCAGGTGCTTGA  
AACTTGTGAAGATAGCGACAGAGCACCCCTCCGGCAGATGTAGATCCTGTCCTAG  
CTATCCTGGTAGCAAAACGTAACGAGAGAGACTTGTGCCCCCTGAGACGTGTTG  
TATGATGTTGTTCACTGGAGACTGCACCGAGGCCACTTGCCTGAATGCTGAAAC  
AGCAATGTTGGTTGCTC AAA

>ASY1K.M316F  
TTCAGTGAGGCGGCACGGAATCGCAAGGAGCCTCAGCGCAACTAACACGTA  
TCAGCGAAGAAGCAGAATACCCCTAGTCGGTACTACTTCAGTCAGGTGCTTGA  
AACTTGTGAAGATAGCGACAGAGCACCCCTCCGGCAGATGTAGATCCTGTCCTAG  
CTATCCTGGTAGCAAAACGTAACGAGAGAGACTTGTGCCCCCTGAGACGTGTTG  
TATGATGTTGTTCACTGGAGACTGCACCGAGGTCACTTGCCTGAATGCTGAAAC  
AGCAATGTTGGTTGCT AAA

>ASY1K.M317F  
TTCAGTGAGGCGGCACGGAATCGCAAGGAGCCTCAGCGCAACTAACACGTA  
GGTCAGCGAGGAAGCAGAATACCCCTAGTCGGTACTACTTCAGTCAGGTGCTT  
GAAACTTGTGAAGATAGCGACAGAGCACCCCTCCGGCAGATGTAGATCCTGTCCTAG  
CCCTATCCTGGTAGCAAAACGTAACGAGAGAGACTTGTGCCCCCTGAGACGTGTTG  
TTTATGATGTTGTTCACTGGAGACTGCACCGAGGCCACTTGCCTGAATGCTGAAAC  
GTAGCAATGTTGGTTGCTCACGCCATGGTTAATGATGTATCTATTGAACCTCTG  
CTGAGCAGCGATGATCGCG AAA

>ASY1K.M318F  
TTCAGTGAGGCGGCACGGAATCGCAAGGAGCCTCAGCGCAACTAACACG  
AGGTCAAGCGAAGAAGCAGAATACCCCTAGTCGGTACTACTTCAGTCAGGTGCT  
TGAAACTTGTGAAGATAGCGACAGAGCACCCCTCCGGCAGATGTAGATCCTGTCCTA  
GCCCTATCCTGGTAGCAAAACGTAACGAGAGAGACTTGTGCCCCCTGAGACGTGTT  
GTTTATGATGTTGTTCACTGGAGACTGCACCGAGGCCACTTGCCTGAATGCTGAAA  
CGTAGCAATGTTGGTTGCTCACGCCATGGTTAATGATGTATCTATTGA  
AAAAAAAAAAAAAAA

>ASY1K.M319F  
TTCAGTTGGGGCGGCACGGAATCGCAAGGAGCCTCAGCGCAACTAACCTCGTA  
GGCCAGGTGAAGAAGCAGAATACCCCTAGTCAGTCAGTCAGGTGCTTGA  
ACTTGTGAAGATAGCGACAGAGCACCCCTCCGGCAGATGTAGATCCTGTCCTAG  
ATCCTGGTAGCAAAACGTAACGAGAGAGACTTGTGCCCCCTGAGACGTGTTGTT  
ATGATGTTGTTCACTGGAGACTGTACTGTGAGGCCACTTGCCTGAATGATGAAAC  
TAACAATGTTGATAACATGATGATCATCGTTGGTTGCTCACGCAATGACGGTC  
GGCGC AAA

>ASY1K.M320F  
TTCAGTGAGGCGGCACGGAATCGCAAGGAGCCTCAGCGCAACTAACACGTA  
AGGCGAAGAAGCAGAATACCCCTAGTCGGTACTACTTCAGTCAGTCAGGTGCTTGA  
CTTGTGAAGATAGCGACAGAGCACCCCTCCGGCAGATGTAGATCCTGTCCTAG  
ATCCTGGTAGCAAAACGTAACGAGAGAGACTTGTGCCCCCTGAGACGTGTTG  
TGATGTTGTTCACTGGAGACTGCACCGAGGCCACTTGCCTGAATGCTGAAAC  
GTAG

CAATGTTGGITGCTTCACGCCATGGTTTAATGATGT AAAAAAAAAAAAAAAA

>ASY1K.M321F

TTCAGTGAGGCCGCACCGAATCGCAAGGAGCCTCAGCGCAACTAACACGT  
AGGTCAAGCGAAGAACGACAATACCCCTAGTCGGTACTACTTCAGTCAGTCAGGTGCT  
TGAAACTTGTGAAGATAGCGACAGAGCACCCCTCCGGCAGATGTAGATCCTGTCCCTA  
GCCCTATCCTTGGTAGCAAACGTAAACGAGAGAGACTTGTGCCCCCTGAGACGTGTT  
GTTTATGATGTTGTTCACTGGAGACTGCACCGAGGCCACTTTCAGCTGAATGCTGAAA  
CGTAGCAATGTTGGITGCTTCACGCCATGGTTTAATGATGTATCTATTGAACCTC  
AAAAAAAAAAAAAAA

>ASY1K.F31F

TTCAGTGAGGCCGCACCGAATCGCAAGGAGCCTCAGCGCAACTAACACGTA  
GGTCAGCGAAGAACGACAATACCCCTAGTCGGTACTACTTCAGTCAGTCAGGTGCT  
GAAACTTGTGAAGATAGCGACAGAGCACCCCTCCGGCAGATGTAGATCCTGTCCCTA  
CCCTATCCTTGGTAGCAAACGTAAACGAGAGAGACTTGTGCCCCCTGAGACGTGTTG  
TTTATGATGTTGTTCACTGGAGACTGCACCGAGGCCACTTTCAGCTGAATGCTGAAAC  
GTAGCAATGTTGGITGCTTC AAAAAAAAAAAAAAAA

>ASY1K.F32F

TTCAGTGAGGCCGCACCGAATCGCAAGGAGCCTCAGCGCAACTAACACGTAG  
GTCAGCGAAGAACGACAATACCCCTAGTCGGTACTACTTCAGTCAGTCAGGTGCTTG  
AAACTTGTGAAGATAGCGACAGAGCACCCCTCCGGCAGATGTAGATCCTGTCCCTAGC  
CCTATCCTTGGTAGCAAACGTAAACGAGAGAGACTTGTGCCCCCTGAGACGTGTTGT  
TTATGATGTTGTTCACTGGAGACTGCACCGAGGCCACTTTCAGCTGAATGCTGAAACG  
TAGCAATGTTGGITGCTTCACGCCATGGTTTAATGATGTATCTATTGAACCTC  
AAAAAAAAAAAAAAA

>ASY1K.F33F

TTCAGTGAGGCCGCACCGAATCGCAAGGAGCCTCAGCGCAACTAACACGTA  
GTCAGCGAAGAACGACAATACCCCTAGTCGGTACTACTTCAGTCAGTCAGGTGCTTG  
AAACTTGTGAAGATAGCGACAGAGCACCCCTCCGGCAGATGTAGATCCTGTCCCTAAC  
CCTATCCTTGGTAGCAAACGTAAACGAGAGAGACTCGTGCCCCCTGAGACGTGTTGT  
TTATGATGTTGTTCACTGGAGACTGCACCGAGGCCACTTTCAGCTGAATGCTGAAACG  
TAGCAATGTTGGITGCTTCACGCCATGGTTTAATGATGTATCTATTGAACCTC  
AAAAAAAAAAAAAAA

>ASY1K.F34F

TTCAGTGAGGCCGCACCGAATCGCAAGGAGCCTCAGCGCAACTAACACGT  
AGGTCAAGCGAAGAACGACAATACCCCTAGTCGGTACTACTTCAGTCAGTCAGGTGCT  
TGAAACTTGTGAAGATAGCGACAGAGCACCCCTCCGGCAGATGTAGATCCTGTCCCTA  
GCCCTATCCTTGGTAGCAAACGTAAACGAGAGAGACTTGTGCCCCCTGAGACGTGTT  
GTTTATGATGTTGTTCACTGGAGACTGCACCGAGGCCACTTTCAGCTGAATGCTGAAA  
CGTAGCAATGTTGGITGCTTCACGCC AAAAAAAAAAAA

>ASY1K.F35F

TTCAGTGAGGCCGCACCGAATCGCAAGGAGCCTCAGCGCAACTAACACGTAGGTC  
AGCGAAGAACGACAATACCCCTAGTCGGTACTACTTCAGTCAGTCAGGTGCTTGAAA  
CTTGTGAAGATAGCGACAGAGCACCCCTCCGGCAGATGTAGATCCTGTCCCTAGCCCT  
ATCCTTGGTAGCAAACGTAAACGAGAGAGACTTGTGCCCCCTGAGACGTGTTGTTA  
TGATGTTGTTCACTGGAGACTGCACCGAGGCCACTTTCAGCTGAATGCTGAAACGTA  
CAATGTTGGITGCTTC AAAAAAAAAAAAAAAA

>ASY1K.F36F

TTCAGTTGGGCCGCACCGAATCGCAAGGAGCCTCAGCGCAACTAACCTCGTAGG  
CCAGGTGAAGAACGAGATAACCCCTAGTCAGTACGTAGTCAGTCAGGTGCTTGAAAC  
TTGTGAAGATAGCGACAGAGCACCCCTCCGGCAGATGTAGATCCTGTCCCTAGCCGTAT  
CCTTGGTAGCAAACGTAAACGAGAGAGACTTGTGCCCCCTGAGACGTGTTGTTGTTA  
GATGTTGTTCACTGGAGACTGTACTGTGAGGCCACTTTCAGCTGAATGATGAAACGTA  
ACAATGTTGTATACAATGATGATCATCGTTGGITGCTTC AAAAAAAAAAAAAAAA

>ASY1K.F37F

TTCAGTTGGGCCGCACCGAATCGCAAGGAGCCTCAGCGCAACTAACCTCGTAG

GCCAGGTGAAGAAGCAGATACCCCCTAGTTCACTACGTCAGTCAGTCAGGTGCTTGA  
AACTTGTAAGATAGCGACAGAGCACCCCCCAGGCAGATGTAGATCCTGTCCTAGCC  
TCCTTGGTAGCAAAACGTAACGAGAGAGACTTGTCCCCCTGAGACGTGTTGTTCA  
TGATGTTGTTCACTGGAGACTGTACTGTGAGGCCACTTGCCTGAATGATGAAACGT  
AACAAATGTTGTTATAC AAAAAAAAAAAAAAAAAAAAAAAA

>ASY1K.F38F

TTCAGTGGGGCGGCACCGAATCGCAAGGAGCCTCAGCGCAACTAACACGTAGG  
TCAGCGAAGAAGCAGAAATACCCCTAGTTCACTACGTCAGTCAGTCAGGTGCTTGA  
AACTTGTAAGATAGCGACAGAGCACCCCTCCGGCAGATGTAGATCCTGTCCTAGCC  
CTATCCTTGGTAGCAAAACGTAACGAGAGAGACTTGTCCCCCTGAGACGTGTTGTT  
TATGATGTTGTTCACTGGAGACTGTGACCGAGGCCACTTGCCTGAATGCTGAAACGT  
AGCAATGTTGGTTGCTTC AAAAAAAAAAAAAAAAAAAAAAAA

>ASY1K.F39F

TTCAGTTGGGGCGGCACCGAATCGCAAGGAGCCTCAGCGCAACTAACCTCG  
TAGGCCAGGTGAAGAAGCAGATAACCCCTAGTTCACTACGTCAGTCAGTCAGGTGCTTGA  
AACTTGTAAGATAGCGACAGAGCACCCCTCCGGCAGATGTAGATCCTGTCCTAGCC  
GTATCCTTGGTAGCAAAACGTAACGAGAGAGACTTGTCCCCCTGAGACGTGTTGTT  
TCATGATGTTGTTCACTGGAGACTGTACTGTGAGGCCACTTGCCTGAATGATGAAA  
CGTAACAATGTTGTTATAC AAAAAAAAAAAAAA**G**AAAAAAA

>ASY1K.F312F

TTCAGTGAGGCGGCACCGAATCGCAAGGAGCCTCAGCGCAACTAACACGTAGG  
TCAGCGAAGAAGCAGAAATACCCCTAGTTCACTACGTCAGTCAGTCAGTCAGGTGCTTGA  
AACTTGTAAGATAGCGACAGAGCACCCCTCCGGCAGATGTAGATCCTGTCCTAGCC  
CTATCCTTGGTAGCAAAACGTAACGAGAGAGACTTGTCCCCCTGAGACGTGTTGTT  
TATGATGTTGTTCACTGGAGACTGTGACCGAGGCCACTTGCCTGAATGCTGAAACGT  
AGCAATGTTGGTTGCTTCACGCCATGGTTAATGATGTATCTATTGAACCTC  
AAAAAAAAAAAAAAA

>TRIAE\_CS42\_5AL\_TGACv1.1

TTCAGTGAGGCGGCACCGAATCGCAAGGAGCCTCAGCGCAACTAACACGTAGGTAGGC  
GAAGAACGAGAAATACCCCTAGTTCACTACGTCAGTCAGTCAGTCAGGTGCTTGA  
TGAAGATAGCGACAGAGCACCCCTCCGGCAGATGTAGATCCTGTCCTAGCC  
TTGGTAGCAAAACGTAACGAGAGAGACTTGTGCCCCCTGAGACGTGTTGTTATGAT  
GTTGTTCACTGGAGACTGTGACCGAGGCCACTTGCCTGAATGCTGAAACGTAGCAAT  
GTTGTTGCTTCACGCCATGGTTAATGATGTATCTATTGAACCTCTGACTGAGCAG  
CGATGATCGGCG

>TRIAE\_CS42\_5BL\_TGACv1.1

TTCAGTTGGGGCGGCACCGAATCGCAAGGAGCCTCAGCGCAACTAACCTCGTAGGCCAGG  
TGAAGAACGAGATAACCCCTAGTTCACTACGTCAGTCAGTCAGTCAGGTGCTTGA  
AAGATAGCGACAGAGCACCCCTCCGGCAGATGTAGATCCTGTCCTAGCC  
GTAGCAAAACGTAACGAGAGAGACTTGTCCCCCTGAGACGTGTTGTT

**Table S2: Chiasmata counts for *asy1* single knock-outs, including Kronos WT control**

Univalents, Rod Bivalents, Ring Bivalents, Multivalents, Fragments, Chiasmata Frequency and CO location (interstitial, distal, centromeric) are recorded.

Image ID	Univalents	Bivalent (rod)	Bivalent (ring)	Multivalents	Fragments	Chiasmata Frequency	Interstitial CO	Distal CO	Centromeric CO
Kronos wt 01	0	3	11	0	0	25	11	13	1
Kronos wt 02	0	2	12	0	0	26	6	17	3
Kronos wt 03	0	5	9	0	0	23	4	12	7
Kronos wt 04	0	7	7	0	0	21	7	13	1
Kronos wt 05	0	4	10	0	0	24	6	18	0
Kronos wt 06	0	1	13	0	0	28	11	16	1
Kronos wt 07	0	0	14	0	0	29	10	17	2
Kronos wt 08	1	2	11	0	0	24	14	10	0
Kronos wt 09	0	4	10	0	0	24	3	18	3
Kronos wt 10	0	2	12	0	0	26	14	11	1
Kronos wt 11	0	4	10	0	0	27	11	10	6
Kronos wt 12	0	0	14	0	0	29	7	18	4
Kronos wt 13	1	3	10	0	0	23	4	18	1
Kronos wt 14	0	6	8	0	0	29	15	12	2
Kronos wt 15	1	2	11	0	0	24	4	17	3
Kronos wt 16	0	3	11	0	0	26	10	11	5
Kronos wt 17	0	0	14	0	0	29	9	17	3
Kronos wt 18	0	4	10	0	0	24	8	13	3
Kronos wt 19	0	1	13	0	0	29	11	12	6
Kronos wt 20	0	1	13	0	0	27	2	19	6
Kronos wt 21	0	3	11	0	0	25	2	16	7
Kronos wt 22	0	0	14	0	0	30	9	18	3
Kronos wt 23	0	3	11	0	0	30	12	14	4
Kronos wt 24	0	2	12	0	0	28	9	15	4
Kronos wt 25	0	2	12	0	0	27	11	16	0
Kronos wt 26	0	4	10	0	0	26	12	11	3
Kronos wt 27	0	4	10	0	0	28	14	11	3
Kronos wt 28	1	3	10	0	0	28	12	13	3
Kronos wt 29	0	1	13	0	0	28	11	15	2
Kronos wt 30	0	1	13	0	0	29	12	13	4
Kronos wt 31	0	1	13	0	0	27	7	14	6
Kronos wt 32	0	2	12	0	0	26	6	12	8
Kronos wt 33	0	3	11	0	0	26	5	17	4
Kronos wt 34	0	2	12	0	0	26	5	20	1
Kronos wt 35	0	3	11	0	0	26	10	13	3
Kronos wt 36	0	2	12	0	0	27	7	17	3
Kronos wt 37	0	3	11	0	0	28	11	14	3
Kronos wt 38	1	2	11	0	0	24	5	15	4
Kronos wt 39	0	0	14	0	0	28	2	21	5
Kronos wt 40	0	4	10	0	0	24	7	14	3
Kronos wt 41	1	2	11	0	0	26	11	9	6
Kronos wt 42	0	2	12	0	0	26	4	21	1
Kronos wt 43	0	7	7	0	0	21	8	11	2
Kronos wt 44	0	5	9	0	0	23	7	12	4
Kronos wt 45	1	1	12	0	0	26	7	17	2
Kronos wt 46	0	3	11	0	0	25	2	22	1
Kronos wt 47	0	4	10	0	0	26	11	15	0
Kronos wt 48	1	2	11	0	0	24	4	19	1
Kronos wt 49	0	3	11	0	0	25	1	22	2
Kronos wt 50	0	2	12	0	0	27	13	13	1
<b>Sum</b>	<b>8</b>	<b>130</b>	<b>562</b>	<b>0</b>	<b>0</b>	<b>1307</b>	<b>404</b>	<b>752</b>	<b>151</b>
<b>Average</b>	<b>0.16</b>	<b>2.6</b>	<b>11.24</b>	<b>0</b>	<b>0</b>	<b>26.14</b>	<b>8.08</b>	<b>15.04</b>	<b>3.02</b>
<b>SD</b>	<b>0.37032804</b>	<b>1.665986256</b>	<b>1.660587553</b>	<b>0</b>	<b>0</b>	<b>2.176028961</b>	<b>3.740784595</b>	<b>3.337847284</b>	<b>2.015146726</b>

Image ID	Univalents	Bivalent (rod)	Bivalent (ring)	*Tetravalents	Fragments	Chiasmata Frequency	Interstitial CO	Distal CO	Centromeric CO
asy1 aaBB 01	1	0	13	0	0	26	13	6	7
asy1 aaBB 02	0	1	13	0	0	27	12	10	5
asy1 aaBB 03	3	1	10	0	0	21	8	10	3
asy1 aaBB 04	2	3	9	0	0	21	9	9	3
asy1 aaBB 05	4	4	6	0	0	16	7	6	3
asy1 aaBB 06	1	2	11	0	0	24	11	5	8
asy1 aaBB 07	1	2	11	0	0	24	7	11	6
asy1 aaBB 08	0	6	8	0	0	22	10	9	3
asy1 aaBB 09	0	3	11	0	0	25	4	16	5
asy1 aaBB 10	2	4	8	0	0	20	8	8	4
asy1 aaBB 11	0	2	10	1	1	24	5	12	7
asy1 aaBB 12	1	6	7	0	0	20	8	10	2
asy1 aaBB 13	2	3	9	0	0	21	8	9	4
asy1 aaBB 14	1	7	6	0	0	19	5	10	4
asy1 aaBB 15	1	2	11	0	0	24	11	11	2
asy1 aaBB 16	1	5	8	0	0	21	6	11	4
asy1 aaBB 17	1	0	13	0	0	26	11	12	3
asy1 aaBB 18	0	8	4	1	0	24	3	19	2
asy1 aaBB 19	0	6	8	0	0	22	5	16	1
asy1 aaBB 20	2	4	8	0	0	20	6	11	3
asy1 aaBB 21	0	5	9	0	0	23	14	9	0
asy1 aaBB 22	2	6	6	0	0	18	11	6	1
asy1 aaBB 23	0	3	11	0	0	25	9	16	0
asy1 aaBB 24	1	1	12	0	0	25	14	6	5
asy1 aaBB 25	0	1	11	1	0	26	14	11	1
asy1 aaBB 26	1	5	8	0	0	21	9	12	0
asy1 aaBB 27	1	5	9	0	0	22	13	8	1
asy1 aaBB 28	1	8	5	0	0	21	8	12	1
asy1 aaBB 29	0	3	11	0	0	25	4	14	7
asy1 aaBB 30	0	6	8	0	0	22	9	13	0
asy1 aaBB 31	1	7	5	1	0	20	10	7	3
asy1 aaBB 32	0	2	12	0	0	26	4	19	3
asy1 aaBB 33	2	2	10	0	0	22	7	11	4
asy1 aaBB 34	1	7	6	0	0	19	3	15	1
asy1 aaBB 35	3	5	6	0	0	17	3	12	2
asy1 aaBB 36	2	1	11	0	0	24	4	17	3
asy1 aaBB 37	0	6	8	0	0	22	9	11	2
asy1 aaBB 38	1	4	9	0	0	22	6	12	4
asy1 aaBB 39	0	6	8	0	0	22	12	10	0
asy1 aaBB 40	1	6	7	0	0	20	6	13	1
asy1 aaBB 41	0	2	12	0	0	26	6	20	0
asy1 aaBB 42	0	2	12	0	0	26	6	15	5
asy1 aaBB 43	0	4	10	0	0	24	7	16	1
asy1 aaBB 44	0	4	10	0	0	24	4	17	3
asy1 aaBB 45	1	5	8	0	0	21	6	15	0
asy1 aaBB 46	0	1	13	0	0	27	17	9	1
asy1 aaBB 47	2	2	10	0	0	22	5	13	4
asy1 aaBB 48	1	0	13	0	0	26	6	13	7
asy1 aaBB 49	0	7	7	0	0	21	9	10	2
asy1 aaBB 50	3	6	5	0	0	16	6	9	1
Sum	47	191	456	4	1	1122	398	582	142
Average	0.94	3.82	9.12	0.08	0.02	22.44	7.96	11.64	2.84
SD	0.998161575	2.264995382	2.446488529	0.274047516	0.1414214	2.785970684	3.356139668	3.612676096	2.160498809

\*multivalents also include clumping chromosomes

Image ID	Univalents	Bivalent (rod)	Bivalent (ring)	*Multivalents	Fragments	Chiasmata Frequency	Interstitial CO	Distal CO	Centromeric CO
asy1 AAbb-1 01	2	1	11	0	0	23	5	17	1
asy1 AAbb-1 02	2	6	6	0	0	18	1	13	4
asy1 AAbb-1 03	0	1	13	0	0	27	4	19	4
asy1 AAbb-1 04	0	6	8	0	0	22	5	12	5
asy1 AAbb-1 05	2	3	9	0	0	21	1	17	3
asy1 AAbb-1 06	1	3	10	0	0	23	5	10	8
asy1 AAbb-1 07	0	2	12	0	0	26	10	15	1
asy1 AAbb-1 08	3	2	9	0	0	20	5	12	3
asy1 AAbb-1 09	0	4	10	0	0	24	8	14	2
asy1 AAbb-1 10	1	0	13	0	0	26	9	13	4
asy1 AAbb-1 11	0	1	11	1	0	26	11	14	1
asy1 AAbb-1 12	0	2	12	0	0	26	8	10	8
asy1 AAbb-1 13	1	1	13	0	0	25	6	16	3
asy1 AAbb-1 14	0	2	12	0	0	26	8	16	2
asy1 AAbb-1 15	0	3	11	0	0	25	6	16	3
asy1 AAbb-1 16	1	4	9	0	0	22	4	11	7
asy1 AAbb-1 17	0	2	12	0	0	26	6	17	3
asy1 AAbb-1 18	2	4	8	0	0	20	4	12	4
asy1 AAbb-1 19	1	2	11	0	0	24	4	16	4
asy1 AAbb-1 20	0	6	8	0	0	22	6	9	7
asy1 AAbb-1 21	0	2	12	0	0	26	11	12	3
asy1 AAbb-1 22	2	3	9	0	0	21	8	8	5
asy1 AAbb-1 23	2	1	9	1	0	22	10	12	2
asy1 AAbb-1 24	0	5	9	0	0	23	8	11	4
asy1 AAbb-1 25	2	5	7	0	0	19	4	4	1
asy1 AAbb-1 26	0	7	7	0	0	21	4	13	4
asy1 AAbb-1 27	1	4	7	1	0	21	7	7	7
asy1 AAbb-1 28	2	4	8	0	0	20	3	11	6
asy1 AAbb-1 29	0	5	9	0	0	23	5	14	4
asy1 AAbb-1 30	1	4	9	0	0	22	6	11	5
asy1 AAbb-1 31	1	8	5	0	0	18	8	9	1
asy1 AAbb-1 32	0	0	14	0	0	28	3	17	8
asy1 AAbb-1 33	0	5	9	0	0	23	6	16	1
asy1 AAbb-1 34	1	4	9	0	0	22	4	12	7
asy1 AAbb-1 35	1	3	10	0	0	23	10	9	4
asy1 AAbb-1 36	1	7	6	0	0	19	12	4	3
asy1 AAbb-1 37	1	2	11	0	0	24	13	7	4
asy1 AAbb-1 38	0	3	11	0	0	25	10	11	4
asy1 AAbb-1 39	0	9	5	0	0	19	5	14	3
asy1 AAbb-1 40	2	6	6	0	0	18	5	6	7
asy1 AAbb-1 41	3	3	8	0	0	19	6	9	4
asy1 AAbb-1 42	2	0	12	0	0	24	10	14	0
asy1 AAbb-1 43	4	3	7	0	1	17	9	6	2
asy1 AAbb-1 44	0	5	9	0	0	23	13	10	0
asy1 AAbb-1 45	2	7	5	0	0	17	7	9	1
asy1 AAbb-1 46	2	4	8	0	0	20	9	10	1
asy1 AAbb-1 47	2	1	11	0	0	23	13	7	3
asy1 AAbb-1 48	0	5	9	0	0	23	15	6	2
asy1 AAbb-1 49	1	3	10	0	0	23	10	13	0
asy1 AAbb-1 50	0	2	12	0	0	26	6	18	2
<b>Sum</b>	<b>49</b>	<b>175</b>	<b>471</b>	<b>3</b>	<b>1</b>	<b>1124</b>	<b>356</b>	<b>589</b>	<b>175</b>
<b>Average</b>	<b>0.98</b>	<b>3.5</b>	<b>9.42</b>	<b>0.06</b>	<b>0.02</b>	<b>22.48</b>	<b>7.12</b>	<b>11.78</b>	<b>3.5</b>
<b>SD</b>	<b>1.020004002</b>	<b>2.140474866</b>	<b>2.286517716</b>	<b>0.239897937</b>	<b>0.14142136</b>	<b>2.801165938</b>	<b>3.204843274</b>	<b>3.748686845</b>	<b>2.215437488</b>

\*multivalents also include clumping chromosomes

Image ID	Univalents	Bivalent (rod)	Bivalent (ring)	*Multivalents	Fragments	Chiasmata Frequency	Interstitial CO	Distal CO	Centromeric CO
asy1 AAbb-2 01	1	2	11	0	0	24	10	12	2
asy1 AAbb-2 02	1	3	10	0	0	23	8	15	0
asy1 AAbb-2 03	1	3	10	0	0	23	8	15	0
asy1 AAbb-2 04	1	4	9	0	0	22	12	9	1
asy1 AAbb-2 05	1	5	8	0	0	21	12	9	0
asy1 AAbb-2 06	1	6	7	0	0	20	9	11	0
asy1 AAbb-2 07	0	3	11	0	0	26	13	11	2
asy1 AAbb-2 08	1	4	9	0	0	23	7	10	6
asy1 AAbb-2 09	0	7	7	0	0	21	10	6	5
asy1 AAbb-2 10	1	2	11	0	0	24	12	10	2
asy1 AAbb-2 11	0	5	9	0	0	23	9	11	3
asy1 AAbb-2 12	0	6	8	0	0	22	9	8	5
asy1 AAbb-2 13	0	1	13	0	0	29	17	9	3
asy1 AAbb-2 14	0	6	8	0	0	20	9	9	2
asy1 AAbb-2 15	2	3	9	0	0	21	8	12	1
asy1 AAbb-2 16	1	6	6	0	0	19	5	8	5
asy1 AAbb-2 17	0	2	12	0	0	26	16	9	1
asy1 AAbb-2 18	0	2	12	0	0	26	6	15	5
asy1 AAbb-2 19	0	2	12	0	0	26	7	13	6
asy1 AAbb-2 20	1	2	11	0	0	23	4	11	8
asy1 AAbb-2 21	1	4	9	0	0	22	7	11	4
asy1 AAbb-2 22	2	4	8	0	0	20	6	10	4
asy1 AAbb-2 23	2	7	3	1	0	16	8	4	4
asy1 AAbb-2 24	1	3	10	0	0	23	8	14	1
asy1 AAbb-2 25	0	4	10	0	0	24	11	12	1
asy1 AAbb-2 26	2	4	8	0	0	20	10	9	1
asy1 AAbb-2 27	0	0	14	0	0	28	8	14	6
asy1 AAbb-2 28	0	4	10	0	0	24	11	9	4
asy1 AAbb-2 29	0	2	12	0	0	26	9	16	1
asy1 AAbb-2 30	0	5	9	0	0	23	5	14	4
asy1 AAbb-2 31	1	4	9	0	0	22	16	3	3
asy1 AAbb-2 32	1	5	8	0	0	21	9	6	6
asy1 AAbb-2 33	0	5	9	0	0	23	10	7	6
asy1 AAbb-2 34	0	4	10	0	0	24	12	12	2
asy1 AAbb-2 35	2	4	8	0	0	20	10	6	4
asy1 AAbb-2 36	0	5	9	0	0	23	9	7	7
asy1 AAbb-2 37	1	4	9	0	0	22	6	12	4
asy1 AAbb-2 38	2	2	8	1	0	21	3	14	4
asy1 AAbb-2 39	3	4	7	0	2	18	7	7	4
asy1 AAbb-2 40	0	4	10	0	0	24	9	13	2
asy1 AAbb-2 41	0	5	9	0	0	23	10	10	3
asy1 AAbb-2 42	0	4	10	0	0	24	7	9	8
asy1 AAbb-2 43	0	5	7	1	0	22	9	8	5
asy1 AAbb-2 44	1	4	9	0	0	22	8	11	4
asy1 AAbb-2 45	2	2	10	0	0	22	8	7	7
asy1 AAbb-2 46	2	3	9	0	0	21	1	15	5
asy1 AAbb-2 47	1	0	11	1	0	25	4	21	4
asy1 AAbb-2 48	1	4	9	0	0	22	9	5	8
asy1 AAbb-2 49	1	3	10	0	0	23	5	12	6
asy1 AAbb-2 50	2	5	7	0	0	19	9	5	5
Sum	40	187	464	4	2	1129	435	516	184
Average	0.8	3.74	9.28	0.08	0.04	22.58	8.7	10.32	3.68
SD	0.808122036	1.588350447	1.895644847	0.274047516	0.282842712	2.441896219	3.118411422	3.507659258	2.244630782

**Table S3: Chi square ( $\chi^2$ ) analysis of the *asy1* K0157 F<sub>2</sub> segregants**

The expected genotypes were predicted from the results of the Punnett square (n = 16). The calculated  $\chi^2$  was tested for its significance with the value associated to the degree of freedom (Df = 9 – 1 = 8) referring to the  $\chi^2$  distribution table. In this case ( $\chi^2 = 3.92E-23$ , n = 68), the closest *p*-value is about 0.95, which means that there is more than 95% probability that any deviation from expected results is due to chance only. Based on the confidence interval  $\alpha > 0.05$ , this is within the range of acceptable deviation, hence, the observed  $\chi^2$  is not significantly different from the expected values. The observed numbers are consistent with those expected under Mendel's law.

TILLING line	F <sub>2</sub> Genotypes	Observed (n=68)	Expected (n=16)	$\chi^2 = 3.92E-23$							
K0157_F2	AABB	1	1								
K0157_F2	AABb	8	2								
K0157_F2	AaBB	5	2								
K0157_F2	AaBb	29	4								
K0157_F2	AAAb	0	1								
K0157_F2	Aabb	3	2								
K0157_F2	aaBB	5	1								
K0157_F2	aaBb	13	2								
K0157_F2	aabb	2	1								
Df		$\chi^2$									
1	0.004	0.02	0.06	0.15	0.46	1.07	1.64	2.71	3.84	6.63	10.83
2	0.10	0.21	0.45	0.71	1.39	2.41	3.22	4.61	5.99	9.21	13.82
3	0.35	0.58	1.01	1.42	2.37	3.66	4.64	6.25	7.81	11.34	16.27
4	0.71	1.06	1.65	2.20	3.36	4.88	5.99	7.78	9.49	13.28	18.47
5	1.14	1.61	2.34	3.00	4.35	6.06	7.29	9.24	11.07	15.09	20.52
6	1.63	2.20	3.07	3.83	5.35	7.23	8.56	10.64	12.59	16.81	22.46
7	2.17	2.83	3.82	4.67	6.35	8.38	9.80	12.02	14.07	18.48	24.32
<b>8</b>	2.73	3.49	4.59	5.53	7.34	9.52	11.03	13.36	<b>15.51</b>	20.09	26.12
9	3.32	4.17	5.38	6.39	8.34	10.66	12.24	14.68	16.92	21.67	27.88
10	3.94	4.87	6.18	7.27	9.34	11.78	13.44	15.99	18.31	23.21	29.59
<b>p-value</b>	0.95	0.90	0.80	0.70	0.50	0.30	0.20	0.10	<b>0.05</b>	0.01	0.001

**Table S4: Chiasmata counts for *asy1 Aabb*, *aabB* and *aabb* genotypes**

Univalents, Rod Bivalents, Ring Bivalents, Multivalents, Fragments, Chiasmata Frequency and CO localization (interstitial, distal, centromeric) are reported.

Image ID	Univalents	Bivalent (rod)	Bivalent (ring)	Trivalents	Tetravalents	Pentavalents	Chiasmata Frequency	*Multivalents	Fragments	Interstitial CO	Distal CO	Centromeric CO
asy1 Aabb 01	1	1	12	0	0	0	25	0	0	1	22	2
asy1 Aabb 02	10	0	0	0	1	1	7	2	0	0	7	0
asy1 Aabb 03	0	4	10	0	0	0	24	0	0	2	20	2
asy1 Aabb 04	11	3	0	0	0	0	3	0	0	0	0	0
asy1 Aabb 05	13	1	0	0	0	0	1	0	0	0	1	0
asy1 Aabb 06	0	5	9	0	0	0	23	0	0	3	20	0
asy1 Aabb 07	0	6	6	0	1	0	21	1	0	6	10	5
asy1 Aabb 08	0	12	2	0	0	0	16	0	0	0	16	0
asy1 Aabb 09	0	12	2	0	0	0	16	0	0	3	11	2
asy1 Aabb 10	0	10	4	0	0	0	18	0	0	3	14	1
asy1 Aabb 11	0	12	2	0	0	0	16	0	0	2	13	1
asy1 Aabb 12	0	8	4	0	0	1	28	1	1	0	28	0
asy1 Aabb 13	0	10	4	0	0	0	18	0	0	4	10	4
asy1 Aabb 14	0	9	5	0	0	0	19	0	0	8	8	3
asy1 Aabb 15	0	2	12	0	0	0	26	0	0	8	11	7
asy1 Aabb 16	0	12	2	0	0	0	16	0	0	0	16	0
asy1 Aabb 17	0	9	5	0	0	0	19	0	0	2	17	0
asy1 Aabb 18	0	9	5	0	0	0	19	0	0	1	18	0
asy1 Aabb 19	11	1	0	1	0	0	3	0	1	0	3	0
asy1 Aabb 20	0	11	3	0	0	0	17	0	0	1	15	1
asy1 Aabb 21	0	6	8	0	0	0	22	0	1	2	20	0
asy1 Aabb 22	14	0	0	0	0	0	0	0	0	0	0	0
asy1 Aabb 23	14	0	0	0	0	0	0	0	0	0	0	0
asy1 Aabb 24	0	12	2	0	0	0	26	0	0	2	23	1
asy1 Aabb 25	8	4	0	1	0	0	6	1	0	0	6	0
asy1 Aabb 26	12	2	0	0	0	0	2	0	0	0	2	0
asy1 Aabb 27	14	0	0	0	0	0	0	0	0	0	0	0
asy1 Aabb 28	0	10	4	0	0	0	18	0	0	0	18	0
asy1 Aabb 29	4	4	6	0	0	0	16	0	0	0	16	0
asy1 Aabb 30	12	1	0	1	0	0	3	1	1	0	3	0
asy1 Aabb 31	0	3	11	0	0	0	25	0	0	4	17	2
asy1 Aabb 32	14	0	0	0	0	0	0	0	0	0	0	0
asy1 Aabb 33	0	9	5	0	0	0	19	0	0	0	19	0
asy1 Aabb 34	0	4	10	0	0	0	24	0	0	2	20	2
asy1 Aabb 35	0	12	2	0	0	0	16	0	0	5	11	0
asy1 Aabb 36	0	6	8	0	0	0	22	0	1	0	22	0
asy1 Aabb 37	5	5	4	0	0	0	13	0	0	0	13	0
asy1 Aabb 38	2	7	5	0	0	0	17	0	0	0	17	0
asy1 Aabb 39	0	11	3	0	0	0	17	0	0	0	16	1
asy1 Aabb 40	0	11	3	0	0	0	17	0	0	0	17	0
asy1 Aabb 41	0	9	5	0	0	0	19	0	0	0	19	0
asy1 Aabb 42	0	3	11	0	0	0	25	0	0	4	17	2
asy1 Aabb 43	7	5	2	0	0	0	9	0	0	2	6	1
asy1 Aabb 44	0	10	4	0	0	0	18	0	0	0	15	3
asy1 Aabb 45	0	6	4	0	2	0	20	2	0	0	20	0
asy1 Aabb 46	13	1	0	0	0	0	1	0	0	0	1	0
asy1 Aabb 47	1	1	12	0	0	0	25	0	0	1	22	2
asy1 Aabb 48	0	14	0	0	0	0	14	1	0	0	12	2
asy1 Aabb 49	0	11	3	0	0	0	17	0	0	5	10	2
asy1 Aabb 50	6	5	3	0	0	0	11	0	0	0	11	0
<b>Sum</b>	<b>172</b>	<b>309</b>	<b>202</b>	<b>3</b>	<b>4</b>	<b>2</b>	<b>757</b>	<b>9</b>	<b>5</b>	<b>71</b>	<b>633</b>	<b>46</b>
<b>Average</b>	<b>3.44</b>	<b>6.18</b>	<b>4.04</b>	<b>0.06</b>	<b>0.08</b>	<b>0.04</b>	<b>15.14</b>	<b>0.18</b>	<b>0.1</b>	<b>1.42</b>	<b>12.66</b>	<b>0.92</b>
<b>SD</b>	<b>5.2611786</b>	<b>4.288998741</b>	<b>3.708567026</b>	<b>0.2398979</b>	<b>0.340467865</b>	<b>0.197948664</b>	<b>8.369063537</b>	<b>0.481917937</b>	<b>0.3030458</b>	<b>2.119780505</b>	<b>7.438482</b>	<b>1.482413917</b>

\*multivalents also include clumping chromosomes

Image ID	Univalents	Bivalent (rod)	Bivalent (ring)	Trivalents	Tetravalents	Pentavalents	Chiasmata	Frequency	*Multivalents	Fragments	Interstitial CO	Distal CO	Centromeric CO
asy1 aaBb 01	0	11	3	0	0	0	17	0	0	0	1	15	1
asy1 aaBb 02	0	9	5	0	0	0	19	0	0	0	2	17	0
asy1 aaBb 03	4	4	6	0	0	0	16	0	0	0	0	16	0
asy1 aaBb 04	0	11	3	0	0	0	17	0	0	3	13	1	
asy1 aaBb 05	0	6	8	0	0	0	22	0	1	0	0	22	0
asy1 aaBb 06	7	7	0	0	0	0	7	0	0	4	3	0	
asy1 aaBb 07	14	0	0	0	0	0	0	0	0	0	0	0	0
asy1 aaBb 08	8	4	0	1	0	0	6	1	0	0	6	0	
asy1 aaBb 09	1	1	12	0	0	0	25	0	0	1	22	2	
asy1 aaBb 10	0	3	11	0	0	0	25	0	0	4	17	2	
asy1 aaBb 11	14	0	0	0	0	0	0	0	0	0	0	0	
asy1 aaBb 12	12	1	0	1	0	0	3	1	1	0	3	0	
asy1 aaBb 13	13	1	0	0	0	0	1	0	0	0	0	1	0
asy1 aaBb 14	0	3	11	0	0	0	25	0	0	4	17	2	
asy1 aaBb 15	0	9	5	0	0	0	19	0	0	0	0	19	0
asy1 aaBb 16	2	7	5	0	0	0	17	0	0	0	0	17	0
asy1 aaBb 17	11	1	0	1	0	0	3	0	1	0	3	0	
asy1 aaBb 18	0	9	5	0	0	0	19	0	0	1	18	0	
asy1 aaBb 19	0	9	5	0	0	0	19	0	0	0	0	19	0
asy1 aaBb 20	0	10	4	0	0	0	18	0	0	0	0	15	3
asy1 aaBb 21	0	12	2	0	0	0	16	0	0	5	11	0	
asy1 aaBb 22	0	6	4	0	2	0	20	2	0	0	0	20	0
asy1 aaBb 23	0	5	9	0	0	0	23	0	0	3	20	0	
asy1 aaBb 24	6	5	3	0	0	0	11	0	0	0	0	11	0
asy1 aaBb 25	0	12	2	0	0	0	16	0	0	0	0	16	0
asy1 aaBb 26	0	11	3	0	0	0	17	0	0	0	0	16	1
asy1 aaBb 27	7	5	2	0	0	0	9	0	0	2	6	1	
asy1 aaBb 28	11	3	0	0	0	0	3	0	0	0	0	0	
asy1 aaBb 29	0	4	10	0	0	0	24	0	0	2	20	2	
asy1 aaBb 30	0	8	4	0	0	1	28	1	1	0	0	28	0
asy1 aaBb 31	0	10	4	0	0	0	18	0	0	3	14	1	
asy1 aaBb 32	0	12	2	0	0	0	16	0	0	0	0	16	0
asy1 aaBb 33	13	1	0	0	0	0	1	0	0	0	0	1	0
asy1 aaBb 34	0	14	0	0	0	0	14	1	0	0	0	12	2
asy1 aaBb 35	10	0	0	0	1	1	7	2	0	0	0	7	0
asy1 aaBb 36	0	6	8	0	0	0	22	0	1	2	20	0	
asy1 aaBb 37	0	10	4	0	0	0	18	0	0	4	10	4	
asy1 aaBb 38	0	12	2	0	0	0	16	0	0	0	0	16	0
asy1 aaBb 39	14	0	0	0	0	0	0	0	0	0	0	0	
asy1 aaBb 40	0	12	2	0	0	0	16	0	0	3	11	2	
asy1 aaBb 41	0	2	12	0	0	0	26	0	0	8	11	7	
asy1 aaBb 42	0	11	3	0	0	0	17	0	0	5	10	2	
asy1 aaBb 43	0	10	4	0	0	0	18	0	0	0	0	18	0
asy1 aaBb 44	0	6	6	0	1	0	21	1	0	6	10	5	
asy1 aaBb 45	0	12	2	0	0	0	16	0	0	2	13	1	
asy1 aaBb 46	5	5	4	0	0	0	13	0	0	0	0	13	0
asy1 aaBb 47	12	2	0	0	0	0	2	0	0	0	0	2	0
asy1 aaBb 48	0	4	10	0	0	0	24	0	0	2	20	2	
asy1 aaBb 49	0	9	5	0	0	0	19	0	0	8	8	3	
asy1 aaBb 50	14	0	0	0	0	0	0	0	0	0	0	0	
<b>Sum</b>	<b>178</b>	<b>315</b>	<b>190</b>	<b>3</b>	<b>4</b>	<b>2</b>	<b>729</b>	<b>9</b>	<b>5</b>	<b>75</b>	<b>603</b>	<b>44</b>	
Average	3.56	6.3	3.8	0.06	0.08	0.04	14.58	0.18	0.1	1.5	12.06	0.88	
SD	5.2728028	4.224563738	3.568570285	0.2398979	0.340467865	0.197948664	8.166856863	0.481917937	0.3030458	2.159459494	7.263018	1.479657986	

\*multivalents also include clumping chromosomes

Image ID	Univalents	Bivalent (rod)	Bivalent (ring)	Trivalents	Tetravalents	Pentavalents	Chiasmata Frequency	Multivalents	Fragments	Interstitial CO	Distal CO	Centromeric CO
asy1 aabb 01	28	0	0	0	0	0	0	0	0	0	0	0
asy1 aabb 02	28	0	0	0	0	0	0	0	0	0	0	0
asy1 aabb 03	28	0	0	0	0	0	0	0	0	0	0	0
asy1 aabb 04	28	0	0	0	0	0	0	0	0	0	0	0
asy1 aabb 05	28	0	0	0	0	0	0	0	0	0	0	0
asy1 aabb 06	28	0	0	0	0	0	0	0	0	0	0	0
asy1 aabb 07	28	0	0	0	0	0	0	0	0	0	0	0
asy1 aabb 08	28	0	0	0	0	0	0	0	0	0	0	0
asy1 aabb 09	28	0	0	0	0	0	0	0	0	0	0	0
asy1 aabb 10	28	0	0	0	0	0	0	0	0	0	0	0
asy1 aabb 11	28	0	0	0	0	0	0	0	1	0	0	0
asy1 aabb 12	28	0	0	0	0	0	0	0	0	0	0	0
asy1 aabb 13	28	0	0	0	0	0	0	0	0	0	0	0
asy1 aabb 14	28	0	0	0	0	0	0	0	0	0	0	0
asy1 aabb 15	28	0	0	0	0	0	0	0	0	0	0	0
asy1 aabb 16	28	0	0	0	0	0	0	0	0	0	0	0
asy1 aabb 17	28	0	0	0	0	0	0	0	0	0	0	0
asy1 aabb 18	28	0	0	0	0	0	0	0	0	0	0	0
asy1 aabb 19	28	0	0	0	0	0	0	0	0	0	0	0
asy1 aabb 20	28	0	0	0	0	0	0	0	0	0	0	0
asy1 aabb 21	28	0	0	0	0	0	0	0	0	0	0	0
asy1 aabb 22	28	0	0	0	0	0	0	0	0	0	0	0
asy1 aabb 23	28	0	0	0	0	0	0	0	0	0	0	0
asy1 aabb 24	28	0	0	0	0	0	0	0	0	0	0	0
asy1 aabb 25	28	0	0	0	0	0	0	0	0	0	0	0
asy1 aabb 26	28	0	0	0	0	0	0	0	0	0	0	0
asy1 aabb 27	28	0	0	0	0	0	0	0	0	0	0	0
asy1 aabb 28	28	0	0	0	0	0	0	0	1	0	0	0
asy1 aabb 29	28	0	0	0	0	0	0	0	0	0	0	0
asy1 aabb 30	28	0	0	0	0	0	0	0	0	0	0	0
asy1 aabb 31	28	0	0	0	0	0	0	0	0	0	0	0
asy1 aabb 32	28	0	0	0	0	0	0	0	0	0	0	0
asy1 aabb 33	28	0	0	0	0	0	0	0	0	0	0	0
asy1 aabb 34	28	0	0	0	0	0	0	0	0	0	0	0
asy1 aabb 35	28	0	0	0	0	0	0	0	0	0	0	0
asy1 aabb 36	28	0	0	0	0	0	0	0	0	0	0	0
asy1 aabb 37	28	0	0	0	0	0	0	0	0	0	0	0
asy1 aabb 38	28	0	0	0	0	0	0	0	0	0	0	0
asy1 aabb 39	28	0	0	0	0	0	0	0	0	0	0	0
asy1 aabb 40	28	0	0	0	0	0	0	0	0	0	0	0
asy1 aabb 41	28	0	0	0	0	0	0	0	0	0	0	0
asy1 aabb 42	28	0	0	0	0	0	0	0	0	0	0	0
asy1 aabb 43	28	0	0	0	0	0	0	0	0	0	0	0
asy1 aabb 44	28	0	0	0	0	0	0	0	0	0	0	0
asy1 aabb 45	28	0	0	0	0	0	0	0	0	0	0	0
asy1 aabb 46	28	0	0	0	0	0	0	0	0	0	0	0
asy1 aabb 47	28	0	0	0	0	0	0	0	0	0	0	0
asy1 aabb 48	28	0	0	0	0	0	0	0	0	0	0	0
asy1 aabb 49	28	0	0	0	0	0	0	0	0	0	0	0
asy1 aabb 50	28	0	0	0	0	0	0	0	0	0	0	0
<b>Sum</b>	<b>1400</b>	<b>0</b>	<b>0</b>	<b>0</b>	<b>0</b>	<b>0</b>	<b>0</b>	<b>0</b>	<b>2</b>	<b>0</b>	<b>0</b>	<b>0</b>
<b>Average</b>	<b>28</b>	<b>0</b>	<b>0</b>	<b>0</b>	<b>0</b>	<b>0</b>	<b>0</b>	<b>0</b>	<b>0.04</b>	<b>0</b>	<b>0</b>	<b>0</b>
<b>SD</b>	<b>0</b>	<b>0</b>	<b>0</b>	<b>0</b>	<b>0</b>	<b>0</b>	<b>0</b>	<b>0</b>	<b>0.1979487</b>	<b>0</b>	<b>0</b>	<b>0</b>

**Table S5: H2AX foci counts for *asy1 aabB*, including Kronos WT control**

Data sets were used in this format for statistical calculation in R programming.

Genotypes	H2AX Foci
WT	1387
WT	1320
WT	1328
WT	1348
WT	1363
WT	1328
WT	1341
WT	1359
WT	1353
WT	1331
WT	1351
WT	1313
WT	1308
WT	1347
WT	1327
WT	1355
WT	1312
WT	1337
WT	1341
WT	1372
asy1 aabB	716
asy1 aabB	707
asy1 aabB	718
asy1 aabB	745
asy1 aabB	720
asy1 aabB	738
asy1 aabB	697
asy1 aabB	734
asy1 aabB	714
asy1 aabB	696
asy1 aabB	705
asy1 aabB	709
asy1 aabB	741
asy1 aabB	700
asy1 aabB	728
asy1 aabB	713
asy1 aabB	712
asy1 aabB	718
asy1 aabB	733
asy1 aabB	704

**Table S6: Chiasmata counts for *asy1 AAbbDD*, including Cadenza WT control**

Univalents, Rod Bivalents, Ring Bivalents, Multivalents, Fragments and Chiasmata Frequency are reported.

<b>Image ID</b>	<b>Univalents</b>	<b>Bivalent (ring)</b>	<b>Bivalent (rod)</b>	<b>Multivalents</b>	<b>Fragments</b>	<b>Chiasmata Frequency</b>
Cadenza wt 01	0	20	1	0	0	41
Cadenza wt 02	0	21	0	0	0	42
Cadenza wt 03	0	19	2	0	0	40
Cadenza wt 04	0	21	0	0	0	42
Cadenza wt 05	0	20	1	0	0	41
Cadenza wt 06	0	20	1	0	0	41
Cadenza wt 07	0	20	1	0	0	41
Cadenza wt 08	0	19	2	0	0	40
Cadenza wt 09	0	21	0	0	0	42
Cadenza wt 10	0	20	1	0	0	41
Cadenza wt 11	0	18	3	0	0	39
Cadenza wt 12	0	20	1	0	0	41
Cadenza wt 13	0	20	1	0	0	41
Cadenza wt 14	0	21	0	0	0	42
Cadenza wt 15	0	19	2	0	0	40
Cadenza wt 16	0	19	2	0	0	40
Cadenza wt 17	0	19	2	0	0	40
Cadenza wt 18	0	19	2	0	0	40
Cadenza wt 19	0	18	3	0	0	39
Cadenza wt 20	1	14	6	0	0	36
Cadenza wt 21	0	19	2	0	0	40
Cadenza wt 22	0	20	1	0	0	41
Cadenza wt 23	0	19	2	0	0	40
Cadenza wt 24	0	19	2	0	0	40
Cadenza wt 25	0	19	2	0	0	40
Cadenza wt 26	0	18	3	0	0	39
Cadenza wt 27	0	18	3	0	0	39
Cadenza wt 28	0	18	3	0	0	39
Cadenza wt 29	0	19	2	0	0	40
Cadenza wt 30	0	18	3	0	0	39
Cadenza wt 31	0	18	3	0	0	39
Cadenza wt 32	0	18	3	0	0	39
Cadenza wt 33	0	20	1	0	0	41
Cadenza wt 34	0	18	3	0	0	39
Cadenza wt 35	0	18	3	0	0	39
Cadenza wt 36	0	18	3	0	0	39
Cadenza wt 37	0	18	3	0	0	39
Cadenza wt 38	2	13	6	0	0	35
Cadenza wt 39	0	18	3	0	0	39
Cadenza wt 40	0	18	3	0	0	39
Cadenza wt 41	0	18	3	0	0	39
Cadenza wt 42	0	17	4	0	0	38
Cadenza wt 43	0	17	4	0	0	38
Cadenza wt 44	0	17	4	0	0	38
Cadenza wt 45	1	17	3	0	0	38
Cadenza wt 46	1	16	4	0	0	37
Cadenza wt 47	1	16	4	0	0	37
Cadenza wt 48	1	14	6	0	0	36
Cadenza wt 49	0	19	2	0	0	40
Cadenza wt 50	0	18	3	0	0	39
<b>Sum</b>	<b>7</b>	<b>921</b>	<b>122</b>	<b>0</b>	<b>0</b>	<b>1974</b>
<b>Average</b>	<b>0.14</b>	<b>18.42</b>	<b>2.44</b>	<b>0</b>	<b>0</b>	<b>39.48</b>
<b>SD</b>	<b>0.40</b>	<b>1.72</b>	<b>1.43</b>	<b>0</b>	<b>0</b>	<b>1.55</b>

<b>Image ID</b>	<b>Univalents</b>	<b>Bivalent (ring)</b>	<b>Bivalent (rod)</b>	<b>Trivalents</b>	<b>Tetravalents</b>	<b>Chiasmata Frequency</b>	<b>Fragments</b>	<b>Multivalents</b>
asy1 AAbbDD 01	1	15	5	0	0	35	0	0
asy1 AAbbDD 02	2	14	5	0	0	33	0	0
asy1 AAbbDD 03	2	14	5	0	0	33	0	0
asy1 AAbbDD 04	0	18	3	0	0	39	0	0
asy1 AAbbDD 05	2	16	3	0	0	35	0	0
asy1 AAbbDD 06	0	21	0	0	0	42	0	0
asy1 AAbbDD 07	1	16	4	0	0	36	0	0
asy1 AAbbDD 08	1	18	2	0	0	38	0	0
asy1 AAbbDD 09	1	18	2	0	0	38	0	0
asy1 AAbbDD 10	4	13	4	0	0	30	0	0
asy1 AAbbDD 11	2	14	5	0	0	33	0	0
asy1 AAbbDD 12	0	17	4	0	0	38	0	0
asy1 AAbbDD 13	0	16	5	0	0	37	0	0
asy1 AAbbDD 14	2	15	4	0	0	34	0	0
asy1 AAbbDD 15	0	21	0	0	0	42	0	0
asy1 AAbbDD 16	1	15	5	0	0	35	0	0
asy1 AAbbDD 17	0	19	2	0	0	40	0	0
asy1 AAbbDD 18	2	5	14	0	0	24	0	0
asy1 AAbbDD 19	0	21	0	0	0	42	0	0
asy1 AAbbDD 20	1	17	3	0	0	37	0	0
asy1 AAbbDD 21	2	15	4	0	1	37	0	1
asy1 AAbbDD 22	0	21	0	0	0	42	0	0
asy1 AAbbDD 23	2	16	3	0	0	35	0	0
asy1 AAbbDD 24	0	20	1	0	0	41	0	0
asy1 AAbbDD 25	1	15	5	0	0	35	0	0
asy1 AAbbDD 26	0	17	2	0	1	42	0	1
asy1 AAbbDD 27	0	18	3	0	0	39	0	0
asy1 AAbbDD 28	2	16	3	0	0	35	0	0
asy1 AAbbDD 29	0	19	2	0	0	40	0	0
asy1 AAbbDD 30	0	15	4	0	1	36	0	1
asy1 AAbbDD 31	0	17	4	0	0	39	0	0
asy1 AAbbDD 32	1	16	4	0	0	37	0	0
asy1 AAbbDD 33	1	18	2	0	0	38	0	0
asy1 AAbbDD 34	0	21	0	0	0	42	0	0
asy1 AAbbDD 35	2	15	4	0	0	34	0	0
asy1 AAbbDD 36	1	17	3	0	0	37	0	0
asy1 AAbbDD 37	0	21	0	0	0	42	0	0
asy1 AAbbDD 38	1	16	4	0	0	36	0	0
asy1 AAbbDD 39	1	17	3	0	0	37	0	0
asy1 AAbbDD 40	2	16	3	0	0	35	0	0
asy1 AAbbDD 41	0	17	4	0	0	39	0	0
asy1 AAbbDD 42	0	20	1	0	0	41	0	0
asy1 AAbbDD 43	0	19	2	0	0	40	0	0
asy1 AAbbDD 44	2	17	2	0	0	36	0	0
asy1 AAbbDD 45	0	20	1	0	0	41	0	0
asy1 AAbbDD 46	0	17	4	0	0	38	0	0
asy1 AAbbDD 47	1	17	3	0	0	37	0	0
asy1 AAbbDD 48	0	21	0	0	0	42	0	0
asy1 AAbbDD 49	0	18	3	0	0	39	0	0
asy1 AAbbDD 50	0	19	2	0	0	40	0	0
<b>Sum</b>	<b>41</b>	<b>854</b>	<b>151</b>	<b>0</b>	<b>3</b>	<b>1873</b>	<b>0</b>	<b>3</b>
<b>Average</b>	<b>0.82</b>	<b>17.08</b>	<b>3.02</b>	<b>0.00</b>	<b>0.06</b>	<b>37.46</b>	<b>0</b>	<b>0.06</b>
<b>SD</b>	<b>0.94</b>	<b>2.80</b>	<b>2.24</b>	<b>0.00</b>	<b>0.24</b>	<b>3.54</b>	<b>0</b>	<b>0.24</b>

**Table S7: *TtZYP1* 3' UTR sequences**

B sub-genome clones are highlighted in yellow. Poly(A) tails and reference sequences are indicated.

>ZYP1.F31

CAAGGATGTAA  
CAAAAACAAGAAAGGTTGTCAGGATCCCGTCCCCATCCTGCCAATATTGGTGAATTAT  
TTTCTGAGGGCTCCTGAATCCATATGCTGATGACCCCTATGCATTGGCTAGAAGCTCA  
CGTCTATTGGTCTGATCTTAAGAACGATGGAAACGTAATCTGGATTGCATAATTCCCTG  
CTGCCGCCAGGTCTAACGATGATTTGCTGCCCTGGTCATGATATCCGATCATCC  
CAGTGTTCATATGACTGTTAACACCGTGCCTGGTGTCTGGAACATTCTATGATGAG  
CACTGTGAGTGGTTATCTGTACGCTGGTGCCTGTGAAATAAACCGACCTCGTCATC  
TATGGAATAGAGAACAGG AAAAAAAAAAAAAAAA

>ZYP1.F32

CAAGGATGTAA  
ACAAAAACAAGAAAGGTTGTCAGGATCCCGTCCCCATCCTGCCAATATTGGTGAATT  
TTTCTGAGGGCTCCTGAATCCATATGCTGATGACCCCTATGCATTGGCTAGAAGCTC  
ACGCTCTATTGGTCTGATCTTAAGAACGATGGAAACGTAATCTGGATTGCATAATTCCCT  
GCTGCCGCCAGGTCTAACGATGATTTGCTGCCCTGGTCATGATATCCGATCATC  
CCAGTGTTCATATGACTGTTAACACCGTGCCTGGTGTCTGGAACATTCTATGATGA  
GCACTGTGAGTGGTTATCTGTACGCTGGTGCCTGTGAAATAAACCGACCTCGTCAT  
CTATGGAATAGAGAACAGG AAAAAA**GGGGGGGG**AAAAAAAAAA

>ZYP1.F33

CAAGGATGTCA  
CAAAAACAAGAAAGGTTGTCAGGATCCCGTCCCCATCCTGCCAATATCGGTGAATTAT  
TTTCTGAGGGCTCCTGAATCCATATGCTGATGACCCCTATGCATTGGCTAGAAGCTCA  
CGTCTATTGATGCTGATCTTAAGAACGATGGAAACGTAATCTGATTGCATAATTCCCTG  
CTGCCGCCAGGTCTAACGATGATGGTTTGCTGCCCTGGTCATGATATCCAATCATTCCAG  
TGTTCTGATGACTGTTAACACCGTGCCTGGTGTCTGGAACATTCTACGATGAACA  
CTGCGAGTGTATTCTTGACCGCAGGTGTGCTGTGAAATAAACCGACCTCTCAACT  
ATGGAATGGAGAACAGAGAAAATTACCGCC AAAAAAAAAAAAAAAA

>ZYP1.F34

CAAGGATGTCACA  
AAAACAAGAAAGGTTGTCAGGATCCCGTCCCCATCCTGCCAATATCGGTGAATTATTT  
TCTGAGGGCTCCTGAATCCATATGCTGATGACCCCTATGCATTGGCTAGAAGCTCACG  
TCTATTGATGCTGATCTTAAGAACGATGGAAACGTAATCTGATTGCATAATTCCCTGCT  
GCCGCCAGGTCTAACGATGATGGTTTGCTGCCCTGGTCATGATATCCAATCATTCCAGTG  
TTCGTATGACTGTTAACACCGTGTGGTGTCTGGAACATTCTACGATGAACACT  
GCGAGTGTATTCTTGACCGCAGGTGTGCTGTGAAATAAACCGACCTCTCAACTAT  
GGAATAGAGAACAGAGAAAATTACCGCCAACCGTCTGATACCTTTGGATTTC  
TCTTGAAAGGCTGAAAGATACCGTGTGCTGCTGCCGTATTAGGCAGCGCTTGGAA  
TTGACTGATCATTGCGCATGAACCTGTTGTGTATAATGCAAGTAGATGCCCTCGA  
TAGGGAAGTGTAAATCCTGTGTGTTCCATTGGTCATGAGCTGTGAGCCCAGTATT  
GTCTTGCTGC AAAAAAAAAAAA**GGGGGG**AAAAAAAAAAAAAAA

>ZYP1.F35

CAAGGATGT  
TACAAAAACAAGAAAGGTTGTCAGGATCCCGTCCCCATCCTGCCAATATTGGTGAATT  
ATTTCCTGAGGGCTCCTGAATCCATATGCTGATGACCCCTATGCATTGGCTAGAAGCT  
CACGCTATTGGTCTGATCTTAAGAACGATGGAAACGTAATCTGGATTGCATAATTCCC  
TGCTGCCGCCAGGTCTAACGATGATGGTTTGCTGCCCTGGTCATGATATCCGATCAT  
CCCAGTGTTCATATGACTGTTAACACCGTGCCTGGTGTCTGGAACATTCTATGATG  
AGCACTGTGAGTGGTTATCTGTACGCTGGTGTGCTGTGAAATAAACCGACCTCGTC  
TCTATGGAATAGAGAACAGGAAATTACTGCCAACCGTCTGATACCTTTGGAA  
CTGCTCTTGTAGAAGGCTGAAAGATACTGTGCTGCTGCCATATTAGGCTTAGTCGC  
TTTGGAGTTGCCTGATCGTTACCCACGAACCCGTGTTGTGATAATGCAAGTAGATG  
CCTCGATGGGGAAAGTGTAAATTCAAGTGTGTTCCATTGGTCATGAGCTGCATGAAA

TCTC AAAAAAAAAAAAAA

>ZYP1.F36

CAAGGATGT

CACAAAAACAAGAAAGGTTGTCAGGATCCCGCCCCATCCTGCCAATATCGGTGAATT  
ATTTCTGAGGGCTCCTGAATCCATATGCTGATGACCCTTATGCATTGGTTAGAAGCT  
CACGCTATTGATGCTGATCTTAAGAACGATGGAAACGTAATCTGATTGCATAATTCCC  
TGCTGCCGCCAGGTCTAACGATGGTTTGCCTGCCCTGGTCATGATATCCAATCATTCC  
AGTGGTCTGATGACTGTTAACAACGCTGTGTTGGTGTCTGGAACATTCTACGATGAA  
CACTGCGAGTGATTATCTGCACGCAGGTGTGCTGTGAAATAAAACCGACCTCTCAA  
CTATGGAATAGAGAATTCAACAGAGAAAATTACCGCC AAAAAAAAAAAAAA

>ZYP1.F37

CAAGGATGTCA

CAAAACAAGAAAGGTTGTCAGGATCCCGCCCCATCCTGCCAATATCGGTGAATTAT  
TTCTGAGGGCTCCTGAATCCATATGCTGATGACCCTTATGCATTGGTTAGAAGCTCA  
CGTCTATTGATGCTGATCTTAAGAACGATGGAAACGCAATCTGATTGCATAATTCCCTG  
CTGCCGCCAGGTCTAACGATGGTTTGCCTGCCCTGGTCATGATATCCAATCATTCCAG  
TGTTCTGATGACTGTTAACAACGCTGTGTTGGTGTCTGGAACATTCTACGATGAA  
CTGCGAGTGATTATCTGCACGCAGGTGTGCTGTGAAATAAAACCGACCTCTCAA  
ATGGAATAGAGAATTCAACAGAGAAAATTACCGCC AAAAAAAAAAAAAA

>ZYP1.F38

CAAGGATGTCACA

AAAACAAGAAAGGTTGTCAGGATCCCGCCCCATCCTGCCAATATCGGTGAATTATT  
TCTGAGGGCTCCTGAATCCATATGCTGATGACCCTTATGCATTGGCTAGAAGCTCAC  
TCTATTGATGCTGATCTTAAGAACGATGGAAACGTAATCTGATTGCATAATTCCCTG  
GCCGCCAGGTCTAACGATGGTTTGCCTGCCCTGGTCATGATATCCAATCATTCCAGTG  
TTCGTATGACTGTTAACACGCTGTGTTGGTGTCTGGAACATTCTACGATGAA  
GCGAGTGATTATCTGCACGCAGGTGTGCTGTGAAATAAAACCGACCTCTCAA  
GGAATAGAGAATTCAACAGAGAAAATTACCGCC AAAAAAAAAA**GGG**AAAAAAA

>ZYP1.F39

CAAGGATGTTAC

AAAACAAGAAAGGTTGTCAGGATCCCGCCCCATCCTGCCAATATTGGTGAATTATT  
TTCTGAGGGCTCCTGAATCCATATGCTGATGACCCTTATGCATTGGCTAGAAGCTCAC  
GTCTATTGGTCTGATCTTAAGAACGATGGAAACGTAATCTGATTGCATAATTCCCTG  
TGCCGCCAGGTCTAACGATGGTTTGCCTGCCCTGGTCATGATATCCGATCATCCC  
AGTGGTCTGATGACTGTTAACACGTCGCTGGTGTCTGGAACATTCTATGATGAGC  
ACTGTGAGTGTTATCTGTACGCTGGTGCCTGTGAAATAAAACCGACCTCGTCATCT  
ATGGAATAGAGAATTCAACAGG AAAAAAAAAA**GAAGG**AAAAAAA

>ZYP1.F310

CAAGG

ATGTTACAAAACAAGAAAGGTTGTCAGGATCCCGCCCCATCCTGCCAATATTGGT  
AATTATTTCTGAGGGCTCCTGAATCCATATGCTGATGACCCTTATGCATTGGCTAGA  
AGCTCACGTCTATTGGTCTGATCTTAAGAACGATGGAAACGTAATCTGATTGCATAAT  
TCCCTGCTGCCGCCAGGTCTAACGATGGTTTGCCTGCCCTGGTCATGATATCCGA  
TCATCCCAGTGTCTGATGACTGTTAACACGTCGCTGGTGTCTGGAACATTCTAT  
GATGAGCACTGTGAGTGTTATCTGTACGCTGGTGCCTGTGAAATAAAACCGACCTC  
GTCATCTATGGAATAGAGAATTCAACAGG AAAAAAAAAA**GGG**AAAAAAA

>ZYP1.M31

CAAGGATGTTACA

AAAACAAGAAAGGTTGTCAGGATCCCGCCCCATCCTGCCAATATTGGTGAATTATT  
TCTGAGGGCTCCTGAATCCATATGCTGATGACCCTTATGCATTGGCTAGAAGCTCAC  
TCTATTGGTCTGATCTTAAGAACGATGGAAACGTAATCTGATTGCATAATTCCCTG  
GCCGCCAGGTCTAACGATGGTTTGCCTGCCCTGGTCATGATATCCGATCATCCC  
GTGTTCTGATGACTGTTAACACGTCGCTGGTGTCTGGAACATTCTATGATGAGC  
CTGTGAGTGTTATCTGTACGCTGGTGCCTGTGAAATAAAACCGACCTCGTCATCTA  
TGGAAATAGAGAATTCAACAGG AAAAAAAAAA**GGGGAG**AAAAA**C**AAA

>ZYP1.M32

AAGCTCACGT  
CTATTGATGCTGACCTTAAGAAGCATGGAAACGTAATCTTGATTGCATAATTCCCTGCTG  
CCGCCAGGTCTAACGATGGTTTGCCTGCCCTGGTCATGATATCCAATCATTCCAGTGT  
TCGTATGACTGTTAACAAACGCTGTGTTGGTGTCTGGAACATTCTACGATGAACACTG  
CGGGTGAATTATCTGCGCGCAGGTGTGCTTGTAAATAAAACCGACCTCTCAACT  
AAAAAAAAAAAAAAA

>ZYP1.M33

AAGCTCACGT  
CTATTGATGCTGACCTTAAGAAGCATGGAAACGTAATCTTGATTGCATAATTCCCTGCTG  
CCGCCAGGTCTAACGATGGTTTGCCTGCCCTGGTCATGATATCCAATCATTCCAGTGT  
TCGTATGACTGTTAACAAACGCTGTGTTGGTGTCTGGAACATTCTACGATGAACACTG  
CGGGTGAATTATCTGCGCGCAGGTGTGCTTGTAAATAAAACCGACCTCTCAACT  
AAAAAAAAAAAAA**GAGGAAGG**AAAAAAAAAAAAAA

>ZYP1.M34

CAAGGATGTTACAA  
AAACAAGAAAGGTTGTCAGGATCCCGTCCCCATCCTGCCAATATTGGTGAATTATTT  
CTGAGGGCTCCTGAATCCATATGCTGATGACCCCTATGCATTGGCTAGAACGTCACGT  
CTATTGGTCTGATCTAACGATGGAAACGTAATCTGGATTGCATAATTCCCTGCTG  
CCGCCAGGTCTAACGATGGATTGGCTGCCCTGGTCATGATATCCGATCATCCCAG  
TGTCATATGACTGTTAACAAACGTCGTTGGTGTCTGGAACATTCTATGAGGAC  
TGTGAGTGGTTATCTGTACGCTGGTGCCTGTGAAATAAAACCGACCTCATCATCTAT  
GGAATAGAGAATTCAACAGG AAAAAAAAAAAAAAAA

>ZYP1.M35

CAAGGATGTTACA  
AAAACAAGAAAGGTTGTCAGGATCCCGTCCCCATCCTGCCAATATTGGTGAATTATTT  
TCTGAGGGCTCCTGAATCCATATGCTGATGACCCCTATGCATTGGCTAGAACGTCACGT  
TCTATTGGTCTGATCTAACGATGGAAACGTAATCTGGATTGCATAATTCCCTGCTG  
GCCGCCAGGTCTAACGATGGATTGGCTGCCCTGGTCATGATATCCGATCATCCCAG  
GTGTCATATGACTGTTAACAAACGTCGTTGGTGTCTGGAACATTCTATGAGGAC  
CTGTGAGTGGTTATCTGTACGCTGGTGCCTGTGAAATAAAACCGACCTCATCATCTA  
TGAATAGAGAATTCAACAGG AAAAAAA**GAG**AAAAAAAAAA

>ZY1P.M37

CAAGGATGTTA  
CAAAACAAGAAAGGTTGTCAGGATCCCGTCCCCATCCTGCCAATATTGGTGAATTAT  
TTCTGAGGGCTCCTGAATCCATATGCTGATGACCCCTATGCATTGGCTAGAACGTCACGT  
CGTCTATTGGTCTGATCTAACGATGGAAACGTAATCTGGATTGCATAATTCCCTGCTG  
CTGCCGCCAGGTCTAACGATGGATTGGCTGCCCTGGTCATGATATCCGATCATCCCAG  
CAGTGTTCATATGACTGTTAACAAACGTCGTTGGTGTCTGGAACATTCTATGAGGAC  
CACTGTGAGTGGTTATCTGTACGCTGGTGCCTGTGAAATAAAACCGACCTCGTCATC  
TATGGAATAGAGAATTCAACAGG AAAAAAAAAAAAAAAA

>ZYP1.M38

CAAGGATGTTA  
CAAAACAAGAAAGGTTGTCAGGATCCCGTCCCCATCCTGCCAATATTGGTGAATTAT  
TTCTGAGGGCTCCTGAATCCATATGCTGATGACCCCTATGCATTGGCTAGAACGTCACGT  
CGTCTATTGGTCTGATCTAACGATGGAAACGTAATCTGGATTGCATAATTCCCTGCTG  
CTGCCGCCAGGTCTAACGATGGATTGGCTGCCCTGGTCATGATATCCGATCATCCCAG  
CAGTGTTCATATGACTGTTAACAAACGTCGTTGGTGTCTGGAACATTCTATGAGGAC  
CACTGTGAGTGGTTATCTGTACGCTGGTGCCTGTGAAATAAAACCGACCTCGTCATC  
TATGGAATAGAGAATTCAACAGG AAAAAAA**GAAG**AAAAAAAAAAAAAA

>ZYP1.M39

CAAGGAT  
GTCACAAAAACAAGAAAGGTTGTCAGGATCCCGTCCCCATCCTGCCAATATCGGTGAA  
TTATTCTGAGGGCTCCTGAATCCATATGCTGATGACCCCTATGCATTGGTAGAAG  
CTCGCTCTATTGATGCTGATCTAACGATGGAAACGTAATCTTGATTGCATAATT  
CCTGCTGCCGCCAGGTCTAACGATGGTTTGCCTGCCCTGGTCATGATATCCAATCATT

CCAGTGTTCGTATGACTGTTAACACGCTGTGGTGTCTGGAACATTCTACGATG  
AACACTGCGAGTGATTATCTGCACCGCAGGTGTGCTGTAAATAAACCACCTCTC  
AACTATGGAATAGAGAATTCAACAGAGAAAATTACGCCAACGTCCTGATACCTTTG  
G AAAAAAAAAAAAAAA**GAAGAAG**

>ZYP1.M310

CAAGGATGTTA  
CAAAAACAAGAAAGGTTGTCAGGATCCGCCCCATCCTGCCAATATTGGTAATTAT  
TTTCTGAGGGCTCCTGAATCCATATGCTGATGACCCCTATGCATTGGCTAGAAGCTCA  
CGTCTATTGGTGTGATCTTAAGAACGATGGAAACGTAATCTGGATTGCATAATTCCCTG  
CTGCCGCCAGGTCTAATCGATGTTGCTGCCCTGGTCATGATATCCGATCATCC  
CAGTGTTCATATGACTGTTAACACGTCGTTGGTGTCTGGAACATTCTATGAG  
CACTGTGAGTGGTTATCTGTACGCTGGTGCCTGTAAATAAACGACCTCGTCATC  
TATGGAATAGAGAATTCAACAGGAGATTACTGCCAACGTC AAAAAAAAAAAAAAA

>TraesCS2A02G340400.1\_utr3

CAAGGATGTTACAAAACAAGAAAGGTTGTCAGGATCCGCCCCATCCTGCCAATAT  
TGGTGAATTATTTCTGAGGGCTCCTGAATCCATATGCTGATGACCCCTATGCATTGG  
CTAGAACGCTACGTCTATTGGTGTGATCTTAAGAACGATGGAAACGTAATCTGGATTGC  
ATAATTCCCTGCTGCCGCCAGGTCTAATCGATGATTGCTGCCCTGGTCATGATA  
TCCGATCATCCCAGTGTCTATGACTGTTAACACGTCGTTGGTGTCTGGAACATT  
TCTATGATGAGCACTGTGAGTGGTTATCTGTACGCTGGTGCCTGTGTAATAAACCG  
ACCTCGTCATCTATGGAATAGAGAATTCAACAGGAAATTACTGCCAACGTCCTGATAC  
CTTTTGGACTGCTCTTGTAGAAGGCTGAAAGATACTGTGCTGCTGCCATATTAGG  
CTTAGTCGCTTGGAGTTGCGCTGATCGTTAACCCACGAACCCCTGTTGTATAAATG  
CAGTAGATGCCCGATGGGGAAAGTATGTTAAATTCAAG

>TraesCS2A02G340400.2\_utr3

AAGCTCACGCTATTGGTGTGATCTTAAGAACGATGGAAACGTAATCTGGATTGCATAA  
TTCCCTGCTGCCGCCAGGTCTAATCGATGATTGCTGCCCTGGTCATGATATCCG  
ATCATCCCAGTGTCTATGACTGTTAACACGTCGTTGGTGTCTGGAACATTCTA  
TGATGAGCACTGTGAGTGGTTATCTGTACGCTGGTGCCTGTGTAATAAACCGACCT  
CGTCATCTATGGAATAGAGAATTCAACAGGAAATTACTGCCAACGTCCTGATACCTT  
TTGGACTGCTCTTGTAGAAGGCTGAAAGATACTGTGCTGCTGCCATATTAGGCTTA  
GTCGCTTGGAGTTGCGCTGATCGTTAACCCACGAACCCCTGTTGTATAAATGCA  
AGATGCCCTCGATGGGGAAAGTATGTTAAATTCAAG

>TraesCS2B02G338300.3\_utr3

AAGGTCTAACGCTGTGTTGGCTGCCCTGGTCATGATATCCAATCATTCCAGTGTTCGT  
ATGACTGTTAACACGCTGTGTTGGTGTCTGGAACATTCTACGATGAACACTGCGAG  
TGATTATCTGCACGCAGGTGTGCTGTGTAATAAACCGACCTCTTCAACTATGGAAT  
AGAGAATTCAACAGAGAAAATTACCGCCAACGTCCTGATACCTTTGGATTCTCTT  
GTAAAAGGCTGAAAGATAACCGTGTGCTGCCGTATTAGGCGACGCTTGGAAATTGAC  
TGATCATTATGCGCATGAACCCCTGTTGTGTTAAATGCAAGTAGATGCCCTCGATAGGG  
AAGTATGTTAAATCCTGTGTTCCATTGGTCATGAGCTGTGAGCCCATGATTGTCT

>TraesCS2B02G338300.4\_utr3

AAGGTCTAACGCTGTGTTGGCTGCCCTGGTCATGATATCCAATCATTCCAGTGTTCGT  
ATGACTGTTAACACGCTGTGTTGGTGTCTGGAACATTCTACGATGAACACTGCGAG  
TGATTATCTGCACGCAGGTGTGCTGTGTAATAAACCGACCTCTTCAACTATGGAAT  
AGAGAATTCAACAGAGAAAATTACCGCCAACGTCCTGATACCTTTGGATTCTCTT  
GTAAAAGGCTGAAAGATAACCGTGTGCTGCCGTATTAGGCGACGCTTGGAAATTGAC  
TGATCATTATGCGCATGAACCCCTGTTGTGTTAAATGCAAGTAGATGCCCTCGATAGGG  
AAGTATGTTAAATCCTGTGTTCCATTGGTCATGAGCTGTGAGCCCATGATTGTCT

**Table S8: Chiasmata counts for *zyp1* single knock-outs, including Kronos WT control**

Univalents, Rod Bivalents, Ring Bivalents, Multivalents, Fragments, Chiasmata Frequency and CO localization (interstitial, distal, centromeric) are indicated.

Image ID	Univalents	Bivalent (rod)	Bivalent (ring)	Multivalents	Fragments	Chiasmata Frequency	Interstitial CO	Distal CO	Centromeric CO
Kronos wt 01	0	3	11	0	0	25	11	13	1
Kronos wt 02	0	2	12	0	0	26	6	17	3
Kronos wt 03	0	5	9	0	0	23	4	12	7
Kronos wt 04	0	7	7	0	0	21	7	13	1
Kronos wt 05	0	4	10	0	0	24	6	18	0
Kronos wt 06	0	1	13	0	0	28	11	16	1
Kronos wt 07	0	0	14	0	0	29	10	17	2
Kronos wt 08	1	2	11	0	0	24	14	10	0
Kronos wt 09	0	4	10	0	0	24	3	18	3
Kronos wt 10	0	2	12	0	0	26	14	11	1
Kronos wt 11	0	4	10	0	0	27	11	10	6
Kronos wt 12	0	0	14	0	0	29	7	18	4
Kronos wt 13	1	3	10	0	0	23	4	18	1
Kronos wt 14	0	6	8	0	0	29	15	12	2
Kronos wt 15	1	2	11	0	0	24	4	17	3
Kronos wt 16	0	3	11	0	0	26	10	11	5
Kronos wt 17	0	0	14	0	0	29	9	17	3
Kronos wt 18	0	4	10	0	0	24	8	13	3
Kronos wt 19	0	1	13	0	0	29	11	12	6
Kronos wt 20	0	1	13	0	0	27	2	19	6
Kronos wt 21	0	3	11	0	0	25	2	16	7
Kronos wt 22	0	0	14	0	0	30	9	18	3
Kronos wt 23	0	3	11	0	0	30	12	14	4
Kronos wt 24	0	2	12	0	0	28	9	15	4
Kronos wt 25	0	2	12	0	0	27	11	16	0
Kronos wt 26	0	4	10	0	0	26	12	11	3
Kronos wt 27	0	4	10	0	0	28	14	11	3
Kronos wt 28	1	3	10	0	0	28	12	13	3
Kronos wt 29	0	1	13	0	0	28	11	15	2
Kronos wt 30	0	1	13	0	0	29	12	13	4
Kronos wt 31	0	1	13	0	0	27	7	14	6
Kronos wt 32	0	2	12	0	0	26	6	12	8
Kronos wt 33	0	3	11	0	0	26	5	17	4
Kronos wt 34	0	2	12	0	0	26	5	20	1
Kronos wt 35	0	3	11	0	0	26	10	13	3
Kronos wt 36	0	2	12	0	0	27	7	17	3
Kronos wt 37	0	3	11	0	0	28	11	14	3
Kronos wt 38	1	2	11	0	0	24	5	15	4
Kronos wt 39	0	0	14	0	0	28	2	21	5
Kronos wt 40	0	4	10	0	0	24	7	14	3
Kronos wt 41	1	2	11	0	0	26	11	9	6
Kronos wt 42	0	2	12	0	0	26	4	21	1
Kronos wt 43	0	7	7	0	0	21	8	11	2
Kronos wt 44	0	5	9	0	0	23	7	12	4
Kronos wt 45	1	1	12	0	0	26	7	17	2
Kronos wt 46	0	3	11	0	0	25	2	22	1
Kronos wt 47	0	4	10	0	0	26	11	15	0
Kronos wt 48	1	2	11	0	0	24	4	19	1
Kronos wt 49	0	3	11	0	0	25	1	22	2
Kronos wt 50	0	2	12	0	0	27	13	13	1
<b>Sum</b>	<b>8</b>	<b>130</b>	<b>562</b>	<b>0</b>	<b>0</b>	<b>1307</b>	<b>404</b>	<b>752</b>	<b>151</b>
<b>Average</b>	<b>0.16</b>	<b>2.6</b>	<b>11.24</b>	<b>0</b>	<b>0</b>	<b>26.14</b>	<b>8.08</b>	<b>15.04</b>	<b>3.02</b>
<b>SD</b>	<b>0.37032804</b>	<b>1.665986256</b>	<b>1.660587553</b>	<b>0</b>	<b>0</b>	<b>2.176028961</b>	<b>3.740784595</b>	<b>3.337847284</b>	<b>2.015146726</b>

<b>Image ID</b>	<b>Univalents</b>	<b>Bivalent (rod)</b>	<b>Bivalent (ring)</b>	<b>*Multivalents</b>	<b>Fragments</b>	<b>Chiasmata Frequency</b>	<b>Interstitial CO</b>	<b>Distal CO</b>	<b>Centromeric CO</b>
zyp1 aaBB-1 01	3	7	4	0	0	15	4	6	5
zyp1 aaBB-1 02	0	3	11	0	0	25	8	14	3
zyp1 aaBB-1 03	1	4	9	0	0	22	6	9	7
zyp1 aaBB-1 04	3	3	8	0	0	19	6	9	4
zyp1 aaBB-1 05	0	4	10	0	0	24	7	11	6
zyp1 aaBB-1 06	0	4	10	0	0	24	8	11	5
zyp1 aaBB-1 07	2	5	7	0	0	19	4	12	3
zyp1 aaBB-1 08	0	2	12	0	0	26	8	11	7
zyp1 aaBB-1 09	1	3	10	0	0	23	5	16	2
zyp1 aaBB-1 10	1	6	7	0	0	20	5	12	3
zyp1 aaBB-1 11	0	4	10	0	0	24	9	15	0
zyp1 aaBB-1 12	0	0	14	0	0	28	6	20	2
zyp1 aaBB-1 13	3	2	9	0	0	20	9	10	1
zyp1 aaBB-1 14	2	5	7	1	0	19	3	14	2
zyp1 aaBB-1 15	1	5	8	0	0	21	7	13	1
zyp1 aaBB-1 16	0	3	11	0	0	25	7	12	6
zyp1 aaBB-1 17	1	3	10	0	0	23	5	16	2
zyp1 aaBB-1 18	1	2	11	0	0	24	7	15	2
zyp1 aaBB-1 19	2	4	8	0	0	20	6	11	3
zyp1 aaBB-1 20	1	5	8	0	0	21	3	17	1
zyp1 aaBB-1 21	1	4	9	0	0	22	1	18	3
zyp1 aaBB-1 22	0	3	11	0	0	25	3	21	1
zyp1 aaBB-1 23	1	3	10	0	0	23	7	14	2
zyp1 aaBB-1 24	0	1	13	0	0	27	6	19	2
zyp1 aaBB-1 25	0	6	8	0	0	22	4	15	3
zyp1 aaBB-1 26	1	5	8	0	0	21	5	15	1
zyp1 aaBB-1 27	1	4	9	1	0	22	3	17	2
zyp1 aaBB-1 28	1	5	8	0	0	21	10	9	2
zyp1 aaBB-1 29	0	5	9	0	0	23	7	13	3
zyp1 aaBB-1 30	0	7	7	0	0	21	6	12	3
zyp1 aaBB-1 31	0	5	9	0	0	23	9	12	2
zyp1 aaBB-1 32	2	4	8	0	0	20	6	11	3
zyp1 aaBB-1 33	2	6	6	0	0	18	4	10	4
zyp1 aaBB-1 34	0	5	9	0	0	23	3	13	7
zyp1 aaBB-1 35	1	6	7	0	0	20	6	14	0
zyp1 aaBB-1 36	0	4	10	0	0	24	2	13	9
zyp1 aaBB-1 37	1	7	6	0	0	19	4	14	1
zyp1 aaBB-1 38	0	4	10	0	0	24	9	15	0
zyp1 aaBB-1 39	1	3	11	0	0	23	2	20	1
zyp1 aaBB-1 40	2	3	9	0	0	21	4	15	2
zyp1 aaBB-1 41	1	5	8	0	0	21	7	13	1
zyp1 aaBB-1 42	0	4	10	0	0	24	5	16	3
zyp1 aaBB-1 43	1	5	8	0	0	21	2	16	3
zyp1 aaBB-1 44	0	6	8	0	1	22	7	11	4
zyp1 aaBB-1 45	0	8	6	0	0	20	7	10	3
zyp1 aaBB-1 46	0	3	11	0	0	25	4	19	2
zyp1 aaBB-1 47	1	1	12	0	0	25	8	15	2
zyp1 aaBB-1 48	1	3	10	0	0	23	3	17	3
zyp1 aaBB-1 49	2	2	10	0	0	22	7	13	2
zyp1 aaBB-1 50	0	0	14	0	0	28	8	17	3
<b>Sum</b>	<b>42</b>	<b>201</b>	<b>458</b>	<b>2</b>	<b>1</b>	<b>1115</b>	<b>282</b>	<b>691</b>	<b>142</b>
<b>Average</b>	<b>0.84</b>	<b>4.02</b>	<b>9.16</b>	<b>0.04</b>	<b>0.02</b>	<b>22.3</b>	<b>5.64</b>	<b>13.82</b>	<b>2.84</b>
<b>SD</b>	<b>0.888934239</b>	<b>1.755341702</b>	<b>2.023938371</b>	<b>0.141421356</b>	<b>0.1414214</b>	<b>2.565469285</b>	<b>2.192380125</b>	<b>3.230530379</b>	<b>1.941596229</b>

\*multivalents also include clumping chromosomes

Image ID	Univalents	Bivalent (rod)	Bivalent (ring)	*Multivalents	Fragments	Chiasmata Frequency	Interstitial CO	Distal CO	Centromeric CO
zyp1 aaBB-2 01	2	3	9	0	0	21	6	10	5
zyp1 aaBB-2 02	2	4	8	0	0	20	5	13	2
zyp1 aaBB-2 03	0	6	8	0	0	22	8	9	5
zyp1 aaBB-2 04	2	4	8	0	0	20	6	11	3
zyp1 aaBB-2 05	1	3	10	0	0	23	12	10	1
zyp1 aaBB-2 06	0	4	10	0	0	24	6	15	3
zyp1 aaBB-2 07	0	1	13	0	0	27	5	19	3
zyp1 aaBB-2 08	0	6	8	0	0	22	3	13	6
zyp1 aaBB-2 09	1	4	9	0	0	22	3	18	1
zyp1 aaBB-2 10	0	4	10	0	0	24	8	12	4
zyp1 aaBB-2 11	3	5	6	0	0	17	2	14	1
zyp1 aaBB-2 12	3	5	6	0	0	17	2	13	1
zyp1 aaBB-2 13	2	5	7	1	0	19	1	15	3
zyp1 aaBB-2 14	0	3	11	0	0	25	8	14	2
zyp1 aaBB-2 15	1	4	9	0	0	22	2	16	4
zyp1 aaBB-2 16	2	3	9	0	0	21	4	13	4
zyp1 aaBB-2 17	2	2	10	0	0	22	3	14	5
zyp1 aaBB-2 18	0	4	10	0	0	24	5	15	4
zyp1 aaBB-2 19	0	1	13	0	0	27	4	21	2
zyp1 aaBB-2 20	0	2	12	0	0	26	3	21	2
zyp1 aaBB-2 21	2	2	10	0	0	22	6	15	1
zyp1 aaBB-2 22	0	5	9	0	0	23	0	21	2
zyp1 aaBB-2 23	1	6	7	0	0	20	2	17	1
zyp1 aaBB-2 24	1	3	10	0	0	23	3	18	2
zyp1 aaBB-2 25	0	4	10	0	0	24	5	19	0
zyp1 aaBB-2 26	1	5	8	0	0	21	3	10	8
zyp1 aaBB-2 27	0	6	8	0	0	22	1	18	3
zyp1 aaBB-2 28	1	9	4	0	0	17	7	7	3
zyp1 aaBB-2 29	2	4	8	0	0	20	4	9	7
zyp1 aaBB-2 30	1	5	8	2	0	21	4	11	6
zyp1 aaBB-2 31	2	6	6	0	0	18	3	12	3
zyp1 aaBB-2 32	3	3	8	0	0	19	6	11	2
zyp1 aaBB-2 33	6	3	5	0	0	13	8	5	0
zyp1 aaBB-2 34	1	6	7	0	0	20	7	9	4
zyp1 aaBB-2 35	3	3	8	0	0	19	6	11	2
zyp1 aaBB-2 36	1	7	6	0	1	19	3	15	1
zyp1 aaBB-2 37	2	6	6	0	0	18	10	7	1
zyp1 aaBB-2 38	1	6	7	0	0	20	5	15	0
zyp1 aaBB-2 39	4	4	6	0	0	16	3	13	0
zyp1 aaBB-2 40	4	4	6	0	0	16	4	12	0
zyp1 aaBB-2 41	2	4	8	0	0	20	5	14	1
zyp1 aaBB-2 42	1	5	8	0	1	21	1	16	4
zyp1 aaBB-2 43	2	2	10	0	0	22	3	18	1
zyp1 aaBB-2 44	3	7	4	0	0	15	4	8	3
zyp1 aaBB-2 45	0	6	8	0	0	22	4	12	6
zyp1 aaBB-2 46	0	5	9	0	0	23	4	15	4
zyp1 aaBB-2 47	1	5	8	0	0	21	6	10	5
zyp1 aaBB-2 48	0	6	8	0	0	22	5	10	7
zyp1 aaBB-2 49	0	6	8	0	0	22	0	20	2
zyp1 aaBB-2 50	0	8	6	0	0	20	3	13	4
<b>Sum</b>	<b>66</b>	<b>224</b>	<b>410</b>	<b>3</b>	<b>2</b>	<b>1044</b>	<b>221</b>	<b>677</b>	<b>144</b>
<b>Average</b>	<b>1.32</b>	<b>4.48</b>	<b>8.2</b>	<b>1.5</b>	<b>0.04</b>	<b>20.88</b>	<b>4.42</b>	<b>13.54</b>	<b>2.88</b>
<b>SD</b>	<b>1.331563451</b>	<b>1.705214093</b>	<b>1.979486637</b>	<b>0.707106781</b>	<b>0.1414214</b>	<b>2.911202851</b>	<b>2.450239472</b>	<b>3.881983503</b>	<b>2.026759754</b>

\*multivalents also include clumping chromosomes

Image ID	Univalents	Bivalent (rod)	Bivalent (ring)	*Multivalents	Fragments	Chiasmata Frequency	Interstitial CO	Distal CO	Centromeric CO
zyp1 AAbb 01	2	5	7	0	0	19	6	7	6
zyp1 AAbb 02	1	1	12	0	0	25	8	17	0
zyp1 AAbb 03	0	3	11	0	0	25	2	15	8
zyp1 AAbb 04	1	8	5	0	0	18	3	4	1
zyp1 AAbb 05	2	3	9	0	0	21	7	10	4
zyp1 AAbb 06	1	5	8	0	0	21	11	9	1
zyp1 AAbb 07	0	4	10	0	0	24	5	16	3
zyp1 AAbb 08	1	7	6	0	0	19	6	13	0
zyp1 AAbb 09	0	3	11	0	0	25	9	15	1
zyp1 AAbb 10	0	2	12	0	0	26	6	15	5
zyp1 AAbb 11	0	2	12	0	0	26	4	16	6
zyp1 AAbb 12	0	5	9	0	0	23	9	13	1
zyp1 AAbb 13	1	1	12	0	0	25	6	18	1
zyp1 AAbb 14	0	3	11	0	0	25	9	16	0
zyp1 AAbb 15	0	1	13	0	0	27	11	16	0
zyp1 AAbb 16	1	3	10	0	0	23	7	16	0
zyp1 AAbb 17	2	2	10	0	0	22	7	15	0
zyp1 AAbb 18	1	1	12	0	0	25	13	8	4
zyp1 AAbb 19	1	3	10	0	0	23	5	15	3
zyp1 AAbb 20	0	3	11	0	0	25	11	14	0
zyp1 AAbb 21	0	6	8	0	0	22	9	13	0
zyp1 AAbb 22	0	3	11	0	0	25	7	16	2
zyp1 AAbb 23	0	5	9	0	0	23	14	9	0
zyp1 AAbb 24	0	2	12	0	0	26	7	17	2
zyp1 AAbb 25	0	2	12	0	0	26	5	19	2
zyp1 AAbb 26	2	4	8	2	0	20	11	8	1
zyp1 AAbb 27	0	2	12	0	0	26	8	18	0
zyp1 AAbb 28	1	2	11	0	0	24	6	17	1
zyp1 AAbb 29	0	1	13	0	0	27	6	18	3
zyp1 AAbb 30	0	3	11	0	1	25	8	15	2
zyp1 AAbb 31	1	3	10	0	0	23	1	19	3
zyp1 AAbb 32	0	4	10	0	0	24	9	8	7
zyp1 AAbb 33	0	3	11	0	0	25	9	13	3
zyp1 AAbb 34	0	3	11	0	0	25	6	19	0
zyp1 AAbb 35	2	1	11	0	0	23	4	18	1
zyp1 AAbb 36	0	3	11	0	0	25	4	17	4
zyp1 AAbb 37	0	5	9	0	0	23	3	20	0
zyp1 AAbb 38	0	2	12	0	0	26	9	15	2
zyp1 AAbb 39	1	5	8	0	0	21	6	12	3
zyp1 AAbb 40	1	7	6	0	0	19	4	12	3
zyp1 AAbb 41	1	6	7	0	0	20	3	16	1
zyp1 AAbb 42	2	6	6	0	0	18	6	10	2
zyp1 AAbb 43	0	4	10	0	0	24	9	14	1
zyp1 AAbb 44	0	3	11	0	0	25	7	16	2
zyp1 AAbb 45	0	3	11	0	0	25	6	18	1
zyp1 AAbb 46	1	4	9	0	0	22	4	18	0
zyp1 AAbb 47	1	3	10	0	0	23	10	11	2
zyp1 AAbb 48	0	5	9	0	0	23	6	14	3
zyp1 AAbb 49	0	3	11	0	0	25	6	15	4
zyp1 AAbb 50	1	2	11	1	0	24	9	13	2
<b>Sum</b>	<b>28</b>	<b>170</b>	<b>502</b>	<b>3</b>	<b>1</b>	<b>1174</b>	<b>347</b>	<b>716</b>	<b>101</b>
<b>Average</b>	<b>0.56</b>	<b>3.4</b>	<b>10.04</b>	<b>1.5</b>	<b>0.02</b>	<b>23.48</b>	<b>6.94</b>	<b>14.32</b>	<b>2.02</b>
<b>SD</b>	<b>0.704504457</b>	<b>1.702339327</b>	<b>1.926824606</b>	<b>0.707106781</b>	<b>0.1414214</b>	<b>2.349468025</b>	<b>2.765752656</b>	<b>3.610867949</b>	<b>1.963857096</b>

\*multivalents also include clumping chromosomes

**Table S9: The chi square ( $\chi^2$ ) analysis of the *zyp1* K3331 F<sub>2</sub> segregants**

The expected genotypes were predicted from the results of the Punnett square (n = 16). The calculated  $\chi^2$  was tested for its significance with the value associated to the degree of freedom (Df = 9 – 1 = 8) referring to the  $\chi^2$  distribution table. In this case ( $\chi^2 = 1.09E-68$ , n = 40), the closest p-value is about 0.95, which means that there is a 95% probability that any deviation from expected results is due to chance only. Based on the confidence interval  $\alpha > 0.05$ , this is within the range of acceptable deviation, hence, the observed  $\chi^2$  is not significantly different from the expected values. The observed numbers are consistent with those expected under Mendel's law.

TILLING line	Genotypes	Observed (n=40)	Expected (n=16)	$\chi^2 = 1.09E-68$							
K3331_BC_F2	AABB	15	1								
K3331_BC_F2	AABb	1	2								
K3331_BC_F2	AaBB	8	2								
K3331_BC_F2	AaBb	3	4								
K3331_BC_F2	AA <sup>b</sup> b	0	1								
K3331_BC_F2	Aabb	0	2								
K3331_BC_F2	aaBB	12	1								
K3331_BC_F2	aaBb	1	2								
K3331_BC_F2	aabb	0	1								
Df	$\chi^2$										
1	0.004	0.02	0.06	0.15	0.46	1.07	1.64	2.71	3.84	6.63	10.83
2	0.10	0.21	0.45	0.71	1.39	2.41	3.22	4.61	5.99	9.21	13.82
3	0.35	0.58	1.01	1.42	2.37	3.66	4.64	6.25	7.81	11.34	16.27
4	0.71	1.06	1.65	2.20	3.36	4.88	5.99	7.78	9.49	13.28	18.47
5	1.14	1.61	2.34	3.00	4.35	6.06	7.29	9.24	11.07	15.09	20.52
6	1.63	2.20	3.07	3.83	5.35	7.23	8.56	10.64	12.59	16.81	22.46
7	2.17	2.83	3.82	4.67	6.35	8.38	9.80	12.02	14.07	18.48	24.32
<b>8</b>	<b>2.73</b>	<b>3.49</b>	<b>4.59</b>	<b>5.53</b>	<b>7.34</b>	<b>9.52</b>	<b>11.03</b>	<b>13.36</b>	<b>15.51</b>	<b>20.09</b>	<b>26.12</b>
9	3.32	4.17	5.38	6.39	8.34	10.66	12.24	14.68	16.92	21.67	27.88
10	3.94	4.87	6.18	7.27	9.34	11.78	13.44	15.99	18.31	23.21	29.59
<b>p-value</b>	0.95	0.90	0.80	0.70	0.50	0.30	0.20	0.10	<b>0.05</b>	0.01	0.001

**Table S10: CO localization (interstitial, distal, centromeric) scores for *zyp1a-1*, *zyp1a-2*, *zyp1b* and *zyp1 Aabb-1*, including Kronos WT control**

Data sets were used in this format for statistical calculation in R programming.

Genotypes	Distribution	Values
Kronos WT	Interstitial	8.08
Kronos WT	Distal	15.04
Kronos WT	Centromeric	3.02
<i>zyp1a-1</i>	Interstitial	5.64
<i>zyp1a-1</i>	Distal	13.82
<i>zyp1a-1</i>	Centromeric	2.84
<i>zyp1a-2</i>	Interstitial	4.42
<i>zyp1a-2</i>	Distal	13.54
<i>zyp1a-2</i>	Centromeric	2.88
<i>zyp1b</i>	Interstitial	6.94
<i>zyp1b</i>	Distal	14.32
<i>zyp1b</i>	Centromeric	2.02
<i>zyp1 Aabb-1</i>	Interstitial	1.63
<i>zyp1 Aabb-1</i>	Distal	9.23
<i>zyp1 Aabb-1</i>	Centromeric	4.83

**Table S11: HEI10 foci counts for *zyp1a-1*, including Kronos WT control**

Data sets were used in this format for statistical calculation in R programming.

Genotypes	HEI10 Foci	Genotype	HEI10 Foci
Kronos_WT	24	<i>zyp1a-1</i>	17
Kronos_WT	24	<i>zyp1a-1</i>	17
Kronos_WT	25	<i>zyp1a-1</i>	18
Kronos_WT	25	<i>zyp1a-1</i>	20
Kronos_WT	27	<i>zyp1a-1</i>	20
Kronos_WT	27	<i>zyp1a-1</i>	20
Kronos_WT	27	<i>zyp1a-1</i>	20
Kronos_WT	28	<i>zyp1a-1</i>	21
Kronos_WT	28	<i>zyp1a-1</i>	21
Kronos_WT	28	<i>zyp1a-1</i>	22
Kronos_WT	28	<i>zyp1a-1</i>	23
Kronos_WT	28	<i>zyp1a-1</i>	23
Kronos_WT	28	<i>zyp1a-1</i>	23
Kronos_WT	28	<i>zyp1a-1</i>	23
Kronos_WT	28	<i>zyp1a-1</i>	23
Kronos_WT	29	<i>zyp1a-1</i>	23
Kronos_WT	29	<i>zyp1a-1</i>	24
Kronos_WT	29	<i>zyp1a-1</i>	24
Kronos_WT	29	<i>zyp1a-1</i>	25
Kronos_WT	30	<i>zyp1a-1</i>	25
Kronos_WT	30	<i>zyp1a-1</i>	25
Kronos_WT	30	<i>zyp1a-1</i>	25
Kronos_WT	31	<i>zyp1a-1</i>	27
Kronos_WT	32	<i>zyp1a-1</i>	27
Kronos_WT	32	<i>zyp1a-1</i>	27
Kronos_WT	36	<i>zyp1a-1</i>	27
Kronos_WT	34	<i>zyp1a-1</i>	28
Kronos_WT	34	<i>zyp1a-1</i>	28

**Table S12: Chiasmata counts for CE candidates *cc1*, *cc2* and *cc3* single knock-outs, including Kronos WT control**

Univalents, Rod Bivalents, Ring Bivalents, and Chiasmata Frequency are reported.

Image ID	Univalents	Bivalent (rod)	Bivalent (ring)	Chiasmata Frequency
Kronos WT 01	1	1	12	25
Kronos WT 02	0	1	13	27
Kronos WT 03	0	0	14	28
Kronos WT 04	0	0	14	28
Kronos WT 05	0	0	14	28
Kronos WT 06	0	1	13	27
Kronos WT 07	1	1	12	25
Kronos WT 08	0	2	12	26
Kronos WT 09	0	2	12	26
Kronos WT 10	0	5	9	23
Kronos WT 11	0	0	14	28
Kronos WT 12	0	1	13	27
Kronos WT 13	0	0	14	28
Kronos WT 14	0	4	10	24
Kronos WT 15	0	0	14	28
Kronos WT 16	0	4	10	24
Kronos WT 17	0	2	12	26
Kronos WT 18	0	1	13	27
Kronos WT 19	1	0	13	26
Kronos WT 20	0	2	12	26
Kronos WT 21	0	1	13	27
Kronos WT 22	0	0	14	28
Kronos WT 23	0	0	14	28
Kronos WT 24	0	1	13	27
Kronos WT 25	0	0	14	28
Kronos WT 26	0	1	13	27
Kronos WT 27	0	2	12	26
Kronos WT 28	0	0	14	28
Kronos WT 29	0	2	12	26
Kronos WT 30	0	1	13	27
Kronos WT 31	0	0	14	28
Kronos WT 32	0	1	13	27
Kronos WT 33	0	0	14	28
Kronos WT 34	0	0	14	28
Kronos WT 35	0	1	13	27
Kronos WT 36	0	0	14	28
Kronos WT 37	0	0	14	28
Kronos WT 38	0	2	12	26
Kronos WT 39	0	0	14	28
Kronos WT 40	0	5	9	23
Kronos WT 41	0	4	10	24
Kronos WT 42	0	0	14	28
Kronos WT 43	0	2	12	26
Kronos WT 44	0	2	12	26
Kronos WT 45	0	3	11	25
Kronos WT 46	0	1	13	27
Kronos WT 47	0	1	13	27
Kronos WT 48	0	1	13	27
Kronos WT 49	1	0	13	26
Kronos WT 50	0	1	13	27
Kronos WT 51	0	3	11	25
Kronos WT 52	0	3	11	25
Kronos WT 53	1	1	12	25
sum	4	64	632	1328
average	0.08	1.28	12.64	26.56
SD	0.274047516	1.385640646	1.366658371	1.402039331

<b>Image ID</b>	<b>Univalents</b>	<b>Bivalent (rod)</b>	<b>Bivalent (ring)</b>	<b>Chiasmata Frequency</b>
cc1 01	0	1	13	27
cc1 02	1	4	9	22
cc1 03	0	1	13	27
cc1 04	0	5	9	23
cc1 05	0	1	13	27
cc1 06	0	3	11	25
cc1 07	0	4	10	24
cc1 08	0	1	13	27
cc1 09	1	5	8	21
cc1 10	0	4	10	24
cc1 11	0	3	11	25
cc1 12	2	4	8	20
cc1 13	0	2	12	26
cc1 14	1	2	11	24
cc1 15	0	1	13	27
cc1 16	0	0	14	28
cc1 17	0	0	14	28
cc1 18	0	1	13	27
cc1 19	0	2	12	26
cc1 20	0	1	13	27
cc1 21	0	1	13	27
cc1 22	0	3	11	25
cc1 23	0	0	14	28
cc1 24	0	0	14	28
cc1 25	0	1	13	27
cc1 26	0	2	12	26
cc1 27	0	1	13	27
cc1 28	0	2	12	26
cc1 29	0	1	13	27
cc1 30	1	0	13	26
cc1 31	0	0	14	28
cc1 32	0	1	13	27
cc1 33	0	1	13	27
cc1 34	0	1	13	27
cc1 35	1	0	13	26
cc1 36	0	0	14	28
cc1 37	0	2	12	26
cc1 38	0	1	13	27
cc1 39	0	2	12	26
cc1 40	0	0	14	28
cc1 41	0	0	14	28
cc1 42	0	0	14	28
cc1 43	0	2	12	26
cc1 44	0	3	11	25
cc1 45	0	2	12	26
cc1 46	0	0	14	28
cc1 47	0	0	14	28
cc1 48	0	3	11	25
cc1 49	0	0	14	28
cc1 50	0	0	14	28
<b>sum</b>	<b>7</b>	<b>74</b>	<b>619</b>	<b>1312</b>
<b>average</b>	<b>0.14</b>	<b>1.48</b>	<b>12.38</b>	<b>26.24</b>
<b>SD</b>	<b>0.404565779</b>	<b>1.431995896</b>	<b>1.6021669</b>	<b>1.846784298</b>

<b>Image ID</b>	<b>Univalents</b>	<b>Bivalent (rod)</b>	<b>Bivalent (ring)</b>	<b>Chiasmata Frequency</b>
cc2 01	1	0	13	26
cc2 02	1	0	13	26
cc2 03	0	1	13	27
cc2 04	0	3	11	25
cc2 05	0	2	12	26
cc2 06	0	1	13	27
cc2 07	0	2	12	26
cc2 08	0	3	11	25
cc2 09	0	3	11	25
cc2 10	0	2	12	26
cc2 11	0	2	12	26
cc2 12	0	1	13	27
cc2 13	0	5	9	23
cc2 14	0	1	13	27
cc2 15	0	0	14	28
cc2 16	0	2	12	26
cc2 17	0	1	13	27
cc2 18	0	5	9	23
cc2 19	0	1	13	27
cc2 20	0	2	12	26
cc2 21	0	0	14	28
cc2 22	0	3	11	25
cc2 23	0	3	11	25
cc2 24	1	1	12	25
cc2 25	0	3	11	25
cc2 26	1	1	12	25
cc2 27	1	1	12	25
cc2 28	0	1	13	27
cc2 29	0	4	10	24
cc2 30	0	0	14	28
cc2 31	0	2	12	26
cc2 32	1	1	12	25
cc2 33	1	5	8	21
cc2 34	0	0	14	28
cc2 35	0	1	13	27
cc2 36	0	4	10	24
cc2 37	0	5	9	23
cc2 38	0	3	11	25
cc2 39	0	3	11	25
cc2 40	0	3	11	25
cc2 41	0	2	12	26
cc2 42	0	4	10	24
cc2 43	0	1	13	27
cc2 44	0	3	11	25
cc2 45	0	2	12	26
cc2 46	0	1	13	27
cc2 47	0	2	12	26
cc2 48	0	3	11	25
cc2 49	0	3	11	25
cc2 50	1	2	11	24
<b>sum</b>	<b>8</b>	<b>104</b>	<b>588</b>	<b>1280</b>
<b>average</b>	<b>0.16</b>	<b>2.08</b>	<b>11.76</b>	<b>25.6</b>
<b>SD</b>	<b>0.37032804</b>	<b>1.411902754</b>	<b>1.378552924</b>	<b>1.44278642</b>

<b>Image ID</b>	<b>Univalents</b>	<b>Bivalent (rod)</b>	<b>Bivalent (ring)</b>	<b>Chiasmata Frequency</b>
cc3 01	1	2	11	24
cc3 02	0	0	14	28
cc3 03	0	2	12	26
cc3 04	1	1	12	25
cc3 05	1	3	10	23
cc3 06	1	1	12	25
cc3 07	0	2	12	26
cc3 08	0	2	12	26
cc3 09	0	3	11	25
cc3 10	0	2	12	26
cc3 11	0	3	11	25
cc3 12	0	1	13	27
cc3 13	1	3	10	23
cc3 14	0	1	13	27
cc3 15	0	2	12	26
cc3 16	0	1	13	27
cc3 17	0	1	13	27
cc3 18	0	1	13	27
cc3 19	1	0	13	26
cc3 20	0	2	12	26
cc3 21	0	3	11	25
cc3 22	0	2	12	26
cc3 23	0	1	13	27
cc3 24	0	3	11	25
cc3 25	0	0	14	28
cc3 26	0	2	12	26
cc3 27	0	1	13	27
cc3 28	0	1	13	27
cc3 29	0	4	10	24
cc3 30	1	1	12	25
cc3 31	0	1	13	27
cc3 32	0	0	14	28
cc3 33	1	2	11	24
cc3 34	1	2	11	24
cc3 35	1	3	10	23
cc3 36	0	4	10	24
cc3 37	1	1	12	25
cc3 38	1	2	11	24
cc3 39	0	5	9	23
cc3 40	1	1	12	25
cc3 41	0	3	11	25
cc3 42	1	2	11	24
cc3 43	0	0	14	28
cc3 44	0	3	11	25
cc3 45	1	3	10	23
cc3 46	0	4	10	24
cc3 47	0	0	14	28
cc3 48	0	4	10	24
cc3 49	0	4	10	24
cc3 50	0	1	13	27
<b>sum</b>	<b>15</b>	<b>96</b>	<b>589</b>	<b>1274</b>
<b>average</b>	<b>0.3</b>	<b>1.92</b>	<b>11.78</b>	<b>25.48</b>
<b>SD</b>	<b>0.46291005</b>	<b>1.259089402</b>	<b>1.313819793</b>	<b>1.515094124</b>

**Table S13: Datasets of distinct phenotypes collected from the optimization of three spreading techniques (dropping, streaming, squashing) executed on mitotic chromosomes of *T. aestivum* ‘Chinese Spring’**

Slides	squash	Slides	stream	Slides	dropping
CS_1	Phenotype 1	CS_51	Phenotype 3	CS_101	Phenotype 1
CS_2	Phenotype 1	CS_52	Phenotype 3	CS_102	Phenotype 1
CS_3	Phenotype 1	CS_53	Phenotype 3	CS_103	Phenotype 1
CS_4	Phenotype 1	CS_54	Phenotype 3	CS_104	Phenotype 1
CS_5	Phenotype 1	CS_55	Phenotype 3	CS_105	Phenotype 1
CS_6	Phenotype 1	CS_56	Phenotype 3	CS_106	Phenotype 1
CS_7	Phenotype 1	CS_57	Phenotype 3	CS_107	Phenotype 1
CS_8	Phenotype 1	CS_58	Phenotype 3	CS_108	Phenotype 1
CS_9	Phenotype 1	CS_59	Phenotype 3	CS_109	Phenotype 4
CS_10	Phenotype 1	CS_60	Phenotype 3	CS_110	Phenotype 4
CS_11	Phenotype 1	CS_61	Phenotype 3	CS_111	Phenotype 4
CS_12	Phenotype 1	CS_62	Phenotype 3	CS_112	Phenotype 4
CS_13	Phenotype 1	CS_63	Phenotype 3	CS_113	Phenotype 4
CS_14	Phenotype 1	CS_64	Phenotype 3	CS_114	Phenotype 4
CS_15	Phenotype 1	CS_65	Phenotype 3	CS_115	Phenotype 4
CS_16	Phenotype 1	CS_66	Phenotype 3	CS_116	Phenotype 4
CS_17	Phenotype 1	CS_67	Phenotype 3	CS_117	Phenotype 4
CS_18	Phenotype 2	CS_68	Phenotype 3	CS_118	Phenotype 4
CS_19	Phenotype 2	CS_69	Phenotype 3	CS_119	Phenotype 4
CS_20	Phenotype 2	CS_70	Phenotype 3	CS_120	Phenotype 4
CS_21	Phenotype 2	CS_71	Phenotype 3	CS_121	Phenotype 4
CS_22	Phenotype 2	CS_72	Phenotype 3	CS_122	Phenotype 4
CS_23	Phenotype 2	CS_73	Phenotype 3	CS_123	Phenotype 4
CS_24	Phenotype 2	CS_74	Phenotype 3	CS_124	Phenotype 4
CS_25	Phenotype 2	CS_75	Phenotype 3	CS_125	Phenotype 4
CS_26	Phenotype 2	CS_76	Phenotype 3	CS_126	Phenotype 4
CS_27	Phenotype 2	CS_77	Phenotype 3	CS_127	Phenotype 4
CS_28	Phenotype 2	CS_78	Phenotype 3	CS_128	Phenotype 4
CS_29	Phenotype 2	CS_79	Phenotype 3	CS_129	Phenotype 4
CS_30	Phenotype 2	CS_80	Phenotype 4	CS_130	Phenotype 3
CS_31	Phenotype 2	CS_81	Phenotype 4	CS_131	Phenotype 3
CS_32	Phenotype 2	CS_82	Phenotype 4	CS_132	Phenotype 3
CS_33	Phenotype 2	CS_83	Phenotype 4	CS_133	Phenotype 3
CS_34	Phenotype 2	CS_84	Phenotype 4	CS_134	Phenotype 3
CS_35	Phenotype 2	CS_85	Phenotype 4	CS_135	Phenotype 3
CS_36	Phenotype 2	CS_86	Phenotype 4	CS_136	Phenotype 3
CS_37	Phenotype 2	CS_87	Phenotype 4	CS_137	Phenotype 3
CS_38	Phenotype 2	CS_88	Phenotype 4	CS_138	Phenotype 3
CS_39	Phenotype 2	CS_89	Phenotype 4	CS_139	Phenotype 3
CS_40	Phenotype 1	CS_90	Phenotype 3	CS_140	Phenotype 3
CS_41	Phenotype 1	CS_91	Phenotype 3	CS_141	Phenotype 3
CS_42	Phenotype 1	CS_92	Phenotype 3	CS_142	Phenotype 3
CS_43	Phenotype 1	CS_93	Phenotype 3	CS_143	Phenotype 3
CS_44	Phenotype 1	CS_94	Phenotype 3	CS_144	Phenotype 3
CS_45	Phenotype 1	CS_95	Phenotype 3	CS_145	Phenotype 3
CS_46	Phenotype 1	CS_96	Phenotype 3	CS_146	Phenotype 3
CS_47	Phenotype 3	CS_97	Phenotype 3	CS_147	Phenotype 3
CS_48	Phenotype 3	CS_98	Phenotype 3	CS_148	Phenotype 3
CS_49	Phenotype 3	CS_99	Phenotype 3	CS_149	Phenotype 3
CS_50	Phenotype 3	CS_100	Phenotype 3	CS_150	Phenotype 3